Transport of Nonlinearly Adsorbing Compounds between Stream Water and Sediment Bed in a Laboratory Flume

by

Selena M. Forman

Project Supervisors:

Norman H. Brooks
James J. Morgan

Supported by:

National Science Foundation
Grant Nos. BCS-9105965 and BES-9421491

W. M. Keck Laboratory of Hydraulics and Water Resources
Division of Engineering and Applied Science
California Institute of Technology
Pasadena, California 91125

Report No. KH-R-58

May 1998

This report is same as the thesis of the same title submitted by the writer on May 26, 1998, to the California Institute of Technology, in partial fulfillment of the requirements for the degree of Doctor of Philosophy in Environmental Engineering Science.

Disclaimer

This material is based upon work supported by the National Science Foundation under Awards BCS-9105965 and BES-9421491. Any opinions, findings, and conclusions or recommendations expressed in this publication are those of the author and do not necessarily reflect the views of the National Science Foundation.

ACKNOWLEDGEMENTS

My years as a Caltech graduate student have been challenging and rewarding both professionally and personally. This thesis would not have been completed without the assistance and support of many people.

First and foremost I want to thank my advisor, Professor Norman Brooks, for his guidance, understanding and support. He has been an inspirational mentor who has shown me what it means to be a teacher. I would also like to thank him for giving me the freedom to pursue my outside interests, which at times distracted me from my research. I want to thank my co-advisor, Professor Jim Morgan, for helping me understand and appreciate aquatic chemistry, for providing invaluable insight into my research project, and for keeping me on my toes during our discussions. Thanks to Michael Hoffmann, Fred Raichlen and George Rossman for serving as members of my thesis examination committee and to John List for serving as a member of my candidacy committee. Thanks also to Joel Franklin for making me enjoy mathematics again.

The major financial support for this research was provided by the National Science Foundation through grant BES-9421491. I greatly appreciate the funding provided by the Walter L. and Reta Mae Moore Fellowship, which supported the final stages of this thesis.

I could not have completed my experiments without the help and patience of Rich Eastvedt, Hai Vu, Russ Green and Peter Green. Thanks to Fran Matzen for keeping things on track and for being there to listen when I needed to chat. Thanks also to Linda Scott, Rayma Harrison and Susan Leising for providing help, assistance and cheer. I would also like to thank Nathan Lee for assisting with laboratory work.

Thanks to all of my friends at Caltech. Susan Paulsen, Edye Udell and Kim Mislick have helped me stay sane and have always provided support and encouragement when I needed it the

most. Tom Lloyd has been a good friend and provided invaluable assistance with chemical techniques and problems. Hinrich Eylers fostered my interest in my research topic and has been like a big brother to me. Bruce Nairn has not only assisted me with my research but has been a good friend. I'm glad we were able to write our theses together. I couldn't have done it without him. Nicole Peill was one of the first graduate students I met at Caltech and has become my best friend. Thanks for all of your support and for encouraging me to live life to the fullest. Thanks to Lisa Anderson for the great dinners, the sympathetic ear and the career advice. You are my role model. I'd also like to thank my fellow classmates Pat, Jim, Denis, Linda and Veronica. Finally, I'd like to thank Arden Albee for helping make Caltech a better place for graduate students.

Many people outside of Caltech have been there for me during the last five years. I thank the IMPACT gang – Lisa, Johnny, Heidi and Jeff – not only for teaching me how to fight but also for being great friends and getting me involved with IMPACT. It has truly been a life altering experience. I want to thank Sylvia Deilly and Mary Miller for helping me open-up and become the person I am today.

Thanks to the gang at 24-Hour Fitness – Sam, Roseanne and Kerri Anne – for keeping me in shape and for the good humor. I'd also like to thank Roseanne for being a great friend and for taking care of my cats and me while I was writing my thesis.

Finally, I want to thank my family. Words cannot express the way I feel and the way I want to thank you for loving me and supporting me, but I am going to try. Manny and Cata Arrieta have been a never-ending source of unconditional love and support. I always smile when I hear your voices. I can't wait until I am your daughter-in-law.

My brother Richard "Junior" has become one of my best friends. He has always been there to listen, somehow knowing when I needed space and when I needed assistance.

I can't remember what my life was like before I met Rich Arrieta – my friend, partner and fiancé. First, I want to thank him for providing the drawings included in this thesis. Rich has been patient, understanding and encouraging while I have been writing, even when I wasn't the

nicest person to be around. I hope I can make it up to you while we spend the rest of our lives together. There are not enough words to express what I feel for you and how you have made my life complete. I love you. I cherish you, and I treasure every minute we spend together. Thank you for unconditionally loving me and for supporting my life and my dreams.

Last, but not least, I'd like to thank my parents who have made it possible for me to accomplish what I have. When I was young and you told me that I would go to college, I bet you didn't think I would be there eleven years. Thanks for inspiring me and making me realize my potential. I admire and love you both.

I dedicate this thesis to my parents, Richard and Marcia Forman, and to Richard Arrieta.

I hope my achievements in life shall be these --

that I will have fought for what was right and fair,

that I will have risked for that which mattered,

that I will have given help to those who were in need ...

that I will leave the earth a better place for what I have done and who I have been.

C. Hoppe

ABSTRACT

The exchange of nonlinearly adsorbing compounds between stream water and sediment beds covered with stationary bedforms was investigated in laboratory experiments. The dominant physical exchange process is advective pumping caused by dynamic pressure variations over dunes on the bed. Observations of net mass exchange of cationic surfactants in a 5-meter long recirculating flume were used to validate the exchange model, which is based on the hydraulics of advective pumping and nonlinear adsorption isotherms derived from batch experiments.

The flume experiments were conducted under steady, uniform flow conditions. The pH and ionic strength of the flume water was controlled by adding sodium chloride and sodium bicarbonate to deionized water. The sand was washed prior to every experiment. The mass exchange of cationic surfactants and bromide was determined by measuring the depletion of these compounds in the overlying water column as it mixed with the clean porewater from the bed. Porewater concentration profiles were acquired to monitor the penetration depth of the compounds in the bed. Bromide was used as a conservative tracer to observe the hydraulics of water exchange between the bed and the overlying water. Garnet sand was used as the model sediment because it had heterogeneous properties similar to natural sediments.

The net mass exchange with a bed covered with stationary bedforms was greater than the exchange with a flat bed. The mass exchange of the cationic surfactants versus time observed in the flume experiments could not be modeled using linear adsorption; however, linear approximations provided upper and lower limits on the exchange. The total mass transfer of the cationic surfactants to the bed increased with their hydrocarbon chain lengths.

The model for the exchange of nonlinearly adsorbing compounds solves the advection equation to track the transport of the compounds within the bed and computes the net mass flux

through the bed surface. Nonlinear adsorption was modeled by the means of four different isotherm equations fitted to the batch adsorption data. The effect of the choice of isotherm on the exchange models for the flume experiments was found to be very small. The model generally predicted the flume results well without calibration. Additional model simulations were performed to provide a sensitivity analysis for the model inputs.

TABLE OF CONTENTS

LIST OF TABLES

LIST OF FIGURES

NOTATION

A_b - plan area of the sediment bed

A_s - cross-sectional area of a streamtube normal to s

b - width of sediment bed

C - aqueous chemical concentration

C_0 - initial chemical concentration in solution

C_b - chemical concentration in the porewater

C_w - chemical concentration in the water column

d - average water depth in the channel

d' - effective water depth in the flume = V/A_b

d* - normalized effective water depth = kd'

d_b - depth of sediment bed

d_g - geometric mean sand grain diameter

d_q - equivalent concentration front penetration depth in the bed

d_q^* - normalized equivalent concentration front penetration depth = kd_q

D - diffusion coefficient

f - Darcy-Weisbach friction factor

f_a - fraction of chemical adsorbed to the sand surface

f_b - bed friction factor

f_w - wall friction factor

f(C) - functional representation of an isotherm equation

F - Faraday constant = 96,485 C/mole

$\mathbf{F_r}$ - Froude number = $U/\sqrt{gd}$

g - gravitational acceleration

$G(C)$ - column isotherm (Equation 3.79)

h - piezometric head

h_m - amplitude of piezometric head at bed surface (Equation 3.3)

$h_{m,c}$ - corrected/calibrated value for the amplitude of the piezometric head at the bed surface

H - average bedform height (crest to trough)

k - bedform wavenumber = $2\pi/\lambda$

k_B - Boltzmann's constant = 1.3085×10^{-23} J/K

k_L - linear mass transfer coefficient used in box models to describe the exchange of pollutants between the water and bed compartments (units of velocity)

K - hydraulic conductivity

K_d - solid-water distribution ratio used in linear adsorption isotherm

K_F - Freundlich sorption coefficient

K_L - Langmuir sorption coefficient

K_{LF} - Langmuir-Freundlich sorption coefficient

K_T - Tóth sorption coefficient

L - length of a streamtube or column

L^* - normalized streamtube length = kL

L_b - length of sediment bed

m - accumulated mass transfer into the sediment bed divided by C_0 (units of length)

m^* - normalized m; $m^* = km = 2\pi m/\lambda$

m_s - mass of sand in batch adsorption experiments

N_{Pe} - Peclet number (Equation 2.2)

q - mass flux into the bed surface divided by C (units of velocity)

q^* - normalized q; $q^* = q/u_m$

$\overline{q}$ - q averaged over the bed surface

$\overline{q}^*$ - normalized $\overline{q}$; $\overline{q}^* = \overline{q}/u_m$

Q - water flow rate

Q_s - flow rate in a streamtube per unit width

r_h - hydraulic radius = bd/(b+2d)

R - retardation coefficient (Equation 3.37)

Re - Reynolds number = $4Ur_h/v$

R_{eff} - effective retardation coefficient defined at a point on a nonlinear isotherm (Equation 3.118)

R_T - residence time function which equals the probability that a solute molecule which enters the bed at time t_0 and position x_0 remains in the bed at later time t

$\overline{R}_T$ - flux-weighted mean value of R_T (Equation 3.22)

s - coordinate along a streamline

s* - normalized streamline coordinate = ks

s_{ad} - association degree of adsorbed surfactant

s_e - slope of energy grade line

S - sorbed chemical concentration on the solid

S_A - specific surface area of sand

S_T - maximum sorbed concentration on the solid

t - time

t* - normalized time = ku_mt

t_{ads} - adsorption time scale

t_{pump} - characteristic porewater advection time scale = $1/(ku_m)$

T_{avg} - average temperature

u - horizontal Darcy velocity

u* - normalized horizontal Darcy velocity = u/u_m

u_{ep} - electrophoretic mobility

u_m - maximum Darcy velocity = kKh_m

U - average flow velocity in the channel

U_* - shear velocity

U_b - bedform propagation velocity

U_b^* - normalized bedform propagation velocity = $\theta U_b/u_m$

v - vertical Darcy velocity

$\overline{v}$ - average vertical Darcy velocity

v^* - normalized vertical Darcy velocity = v/u_m

v_{shock} - velocity of a concentration shock front (Equation 3.61)

V - volume of water in the flume excluding porewater but including water in the return system

V_s - solution volume in batch adsorption experiments

w - magnitude of the Darcy velocity at a point s on a streamline

w^* - normalized Darcy velocity at s* on a streamline = w/u_m

w_s - constant seepage velocity in a column

x - horizontal coordinate

x^* - normalized horizontal coordinate = kx

X^* - normalized horizontal coordinate on a streamline

X_0 - horizontal coordinate where the inward flowing streamline intersects the bed surface

X_0^* - normalized horizontal coordinate where the inward flowing streamline intersects the bed surface = kX_0

y - vertical coordinate

y^* - normalized vertical coordinate = ky

Y^* - normalized vertical coordinate on a streamline

GREEK SYMBOLS:

α - exponent in Freundlich, Tóth and Langmuir-Freundlich isotherms

α_c - correction factor for h_m

ε_0 - permittivity of free space = 8.854×10^{-12} J^{-1} C^2 m^{-1}

ε - relative dielectric constant of water = 78.5 at 25°C

ϕ - energy required to remove one CH_2 group from water to an environment saturated with hydrocarbon chains

Γ_p - ratio of time scales for adsorption and porewater advection (t_{ads}/t_{pump})

η - dynamic viscosity

κ - Debye parameter (Equation 2.7)

λ - average bedform wavelength

ν - kinematic viscosity

θ - porosity of the sediment bed

ρ_b - bulk density of the sediment bed

ρ_s - particle density

$\sigma(C)$ - $1 + (\rho_b/\theta)f'(C)$

$\tilde{\sigma}(C_l, C_r)$ - jump condition across a shock where C_l is the concentration on the left and C_r the concentration on the right (Equation 3.61)

σ_g - geometric standard deviation of the sand grain diameters

σ_H - standard deviation of bedform heights

σ_λ - standard deviation of bedform wavelengths

τ - time

Ψ_0 - surface potential

ζ - zeta potential

1. INTRODUCTION

Riverbeds are sources and sinks of contaminants and therefore influence the transport and fate of pollutants in river systems. Contaminants in the water column can be transported into the riverbed, stored there and then released slowly back into the stream. Contaminated sediments can be significant pollutant sources that may cause water quality degradation to persist even when other pollutant sources are terminated. Therefore, it is important to develop predictive models of the bed/stream exchange that can be used to help develop remediation strategies for contaminated rivers and to assess the duration and exposure from accidental chemical spills to drinking water supplies and aquatic organisms.

Both physical and chemical processes contribute to the capture and release of contaminants in a riverbed: flow of solutes into and out of the bed or banks of the stream, molecular diffusion, net infiltration and exfiltration between the stream and groundwater, adsorption onto particulates and subsequent deposition, chemical conversions, and uptake and degradation by biological processes. Current pollutant transport models for rivers account for the transfer of pollutants between the water column and riverbed by calibrating an appropriate linear exchange coefficient using field data. Models based on the actual physical and chemical exchange processes need to be developed.

Detailed mathematical bed/stream exchange models for nonsorbing (Elliott, 1990) compounds, linearly adsorbing compounds (Eylers, 1994), and colloidal clay (Packman, 1997) have been developed in three previous Caltech Ph.D. theses. The purpose of the work presented in this thesis is to build upon the work of Elliott and Eylers to develop a model that predicts the bed/stream exchange of nonlinearly adsorbing compounds with a sediment bed covered with

stationary bedforms. Nonlinear adsorption isotherms are often encountered for polar organic and inorganic pollutants such as pesticides and heavy metals.

Bedforms are wave-like deformations of the bed surface, such as dunes and ripples, that are created when water flows over a moveable, cohesionless sediment bed. The nature of the interactions between the bed and fluid and the resulting bedform configuration depend on the depth and flow velocity and the properties of the sediment and fluid. The bedforms are the result of an orderly pattern of scour and deposition caused by a systematic perturbation of the gross forward transport of bed material (Kennedy, 1963). The bedforms considered in this thesis are classified as ripples and dunes. Smaller bedforms having wavelengths less than 30 cm are usually called ripples and the larger bedforms are dunes (ASCE, 1975). Ripples and dunes have a roughly triangular shape with a gentle upstream slope that is slightly convex upward and a steep downstream slope. In the experiments, stationary bedforms, which were formed at higher flows, are used. Moving bedforms, moving flat beds, sand bars and anti-dunes are not considered.

When the bedforms are stationary, the acceleration of the flow over the bedforms and the separation of the flow at the crest of the bedforms cause pressure variations over the bed surface. This pressure disturbance (departure from hydrostatic) induces flow through the sediment bed. The terms used to refer to this exchange process are porewater advection or 'pumping'. This thesis focuses on the bed/stream exchange of nonlinearly adsorbing compounds by pumping.

The bed/stream exchange model for nonlinearly adsorbing compounds, which is developed in this thesis, incorporates nonlinear adsorption isotherms developed from batch adsorption experiments into a pumping transport model. Flume experiments were conducted to verify the model. Cationic surfactants were used as the nonlinearly adsorbing compounds, bromide as a conservative tracer, and garnet sand as the model sediment.

Flume experiments were conducted in a 5-meter-long tilting recirculating flume under controlled hydraulic and chemical conditions. The flume had a rectangular channel with straight, impermeable walls and bottom. The slope of the flume was adjusted to establish uniform flow.

The experiments were conducted in deionized water with salts and buffers added to control the ionic strength and pH. The water was recirculated from the downstream to upstream end of the flume through recirculation pipes. Bedforms were created at higher flow rates; then the flow rate was reduced until the bedforms were stationary. To begin the exchange experiment, the conservative and adsorbing compounds were added to the flowing flume water. After the initial mixing period of one to five minutes, the recirculation and longitudinal dispersion eliminated longitudinal concentration gradients in the flowing water.

The mass exchange of the compounds was determined by measuring the depletion of the compound in the overlying water column. Because the water in the flume was recirculated, the small net flux of the compounds into the bed led to measurable concentration changes in the overlying water with time. In addition to measuring the mass exchange, porewater concentration profiles were acquired to monitor the penetration depth of the compounds in the bed.

A model was developed to predict the exchange of nonsorbing compounds due to pumping. The model is based on Elliott's pumping model, which was then modified to account for nonlinear adsorption. The model inputs are either directly measured or derived from measured parameters. This feature eliminates the need for calibration and allows the model to be applied in various situations. The results of the model calculations are presented in non-dimensional form so that the exchange for arbitrary flow conditions and bedform dimensions can be calculated.

Chapter 2 contains the background and related literature that form the foundation for the work presented in this thesis. First, the general framework of models that simulate pollutant transport and fate in rivers is presented. Then the field and laboratory observations of porewater advection (i.e., pumping) are discussed. The transport of solutes into a bed by pumping was found to be significantly greater than transport by molecular diffusion. Porewater advection models have been used to predict the exchange of linearly adsorbing compounds. However, the bed/stream exchange of nonlinearly adsorbing compounds due to pumping has not been

previously studied or reported as far as the writer can ascertain. However, the transport of nonlinearly adsorbing compounds in groundwater systems has been studied extensively. The general purpose nonlinear isotherms used in groundwater transport models are presented, and then the implications of nonlinear adsorption in groundwater systems are discussed. The stream/bed exchange of selected cationic surfactants is presented in this thesis. Cationic surfactants have a wide range of industrial and commercial applications. Traces of these compounds are found in surface waters and groundwater near population centers. Therefore, knowledge of their fate in the aquatic environment is important.

The models developed in this study are presented in Chapter 3. First, previous models of the pumping exchange of nonsorbing and linearly adsorbing compounds are reviewed. Then a detailed model that simulates the exchange of nonlinearly adsorbing compounds with a bed covered with stationary bedforms is developed. The theory that describes the transport of nonlinearly adsorbing compounds in porous media is used to model the transport within the bed. The pumping model is used to determine the flux through the surface of the bed and to simulate the flow field within the bed. Approximate models, which require significantly less computational effort, are presented at the end of the chapter.

The apparatus, materials and experimental methods are described in Chapter 4. The results of the batch adsorption experiments and the flume experiments are presented in Chapter 5. The model predictions for the individual flume runs are discussed in detail. Chapter 6 contains further discussions and implications for the stream/bed exchange of nonlinearly adsorbing compounds. Comparisons are made between the exchange with a stationary flat bed and the exchange with a bed covered with stationary bedforms. The differences in the exchange of linearly and nonlinearly adsorbing compounds are examined. Additional model simulations are presented to illustrate the sensitivity of the stream/bed exchange of nonlinearly adsorbing compounds to the hydraulic, bed and chemical parameters. A comparison of the results from the approximate models to the detailed model is presented in Sections 6.10 and 6.12. The

applications of the new bed/stream exchange models to natural streams are explained with examples at the end of Chapter 6 in Section 6.12.

Chapter 7 gives an overall summary and lists the principal conclusions. Suggestions for future studies are also made. Five appendices provide additional experimental and modeling details.

2. BACKGROUND & RELATED RESEARCH

Since river basins are the center of agricultural, commercial and industrial development, the rivers are prone to pollution. The polluted river water poses human health threats, endangers drinking water supplies, and destroys aquatic ecosystems. Mathematical models are needed to 1) gain a better understanding of the fate and transport of pollutants, 2) assess the effects of the pollutants by determining chemical exposure concentrations to humans and aquatic organisms, and 3) to predict future chemical concentrations under various loading scenarios to develop management and remediation strategies (Schnoor, 1996). The riverbeds act as sources and sinks for contaminants. Examples of riverbed contamination are the transport of radionuclides in the Pariyar River in India (Paul & Pillai, 1991); DDD, DDE and DDT in the San Jaoquin River in California (Gillion and Clifton, 1990); PCB's in the Em River system in Sweden (Larsson et al., 1990); and kepone in the James River Estuary (Nichols, 1990).

Since contaminated sediments pose a health risk to both humans and aquatic organisms, the river pollutant fate-and-transport models need to simulate the exchange of the pollutants with the riverbed. Descriptions of the stream/bed exchange submodels currently used in the larger river pollutant fate-and-transport models are included in Section 2.1. Physical bed/stream exchange processes are described in Section 2.2. Porewater advection field and laboratory studies are discussed in Sections 2.2.1 through 2.2.4. The exchange of nonlinearly adsorbing compounds by porewater advection, which is the focus of this thesis, has not been previously studied or reported as far as the writer can ascertain. However, the transport of nonlinearly adsorbing compounds has been investigated extensively for groundwater systems. Section 2.3 contains 1) descriptions of adsorption processes and nonlinear adsorption isotherms and 2) reviews the transport models developed for nonlinearly adsorbing compounds in porous media.

Cationic surfactants are used in this work to observe the bed/stream exchange of nonlinearly adsorbing compounds. The adsorption characteristics of cationic surfactants on negatively-charged oxides and natural aquifer material are discussed in Section 2.4.

2.1. MODELING THE FATE OF CHEMICALS IN STREAMS AND RIVERS

The pollutant fate and transport river models use a mass balance modeling approach. The fate of chemicals in a river is determined by two factors: the reactivity of the chemical and its physical transport in the river. In order to minimize computational effort, many of the models that have been developed to describe pollutant transport and fate in rivers are compartment or 'box' models (Onishi, 1981; Di Toro et al., 1982; Burns et al., 1982; O'Connor et al., 1983; Ambrose et al., 1983; Connolly and Winfield, 1984; Burns and Cline, 1985; Basmadjian and Quan, 1987; O'Connor, 1988; Halfon and Brueggemann, 1990; Bencala et al., 1990; Schnoor, 1996). In compartment models, the river is divided into completely mixed boxes of known volume and interchange (Figure 2.1). The models assume that the chemicals are mixed laterally and vertically and are transported downstream by advection (current velocity) and longitudinal dispersion. The assumption of complete mixing reduces the set of partial differential equations in time and space to a set of ordinary differential equations in time only.

The river is divided in water and sediment compartments (compartments 1 and 2 in Figure 2.1). The transport between the water compartments (1,3,5 and 7 in Figure 2.1) occurs by advection and longitudinal dispersion. It is assumed that there is no longitudinal transport between the sediment compartments (2, 4, 6 and 8 in Figure 2.1). The exchange between the water and sediment compartments (1 and 2 in Figure 2.1) is generally modeled by an overall mass transfer coefficient k_L.

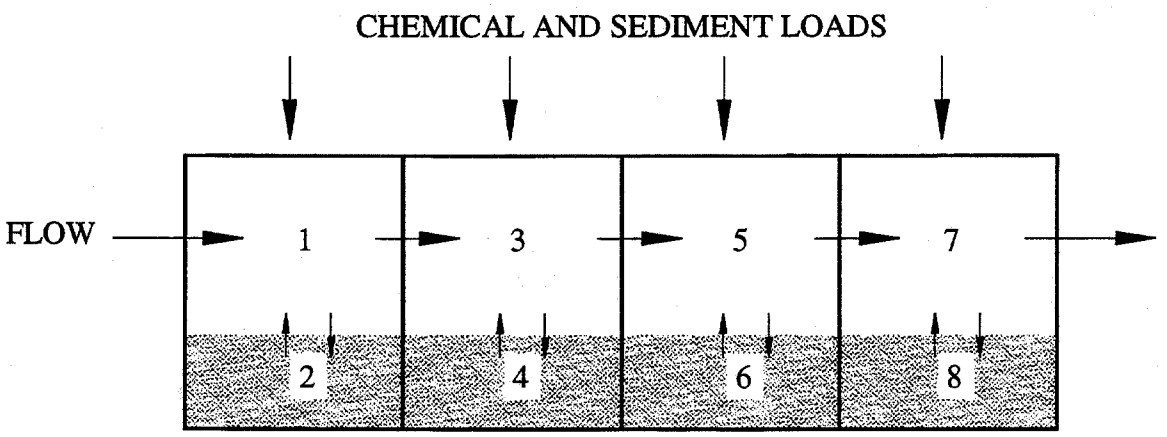

Figure 2.1. Compartmentalized river (Ambrose et al., 1983).

The overall mass transfer coefficient k_L, which has units of velocity, is the ratio of the mass flux to concentration difference. Once the chemical has been transported through the interface, it is assumed to be mixed vertically with the remainder of the chemical in the water or sediment compartment. The depth of the sediment layer is adjusted so that the well-mixed assumption is valid. The flux from the water to sediment compartments is given by

$$k_L \left(C_{porewater} - C_{overlying\ water}\right) \tag{2.1}$$

The parameters k_L and the depth of the sediment bed are determined by calibrating the model to field data.

The exchange between the water and sediment compartments is similar mathematically in the models but differ in exchanges processes they are intended to represent. Schnoor (1996) suggests that k_L represents the velocity at which the chemical moves by molecular diffusion while O'Connor (1988) suggests that the exchange coefficient should be that for the boundary layer resistance in the flow above the bed. The exchange coefficient of Bencala et al. (1990) is an empirical lumped parameter that describes the net effect of many exchange processes. O'Connor et al. (1983) assume the sediment compartment represents a 10-cm 'active' layer mixed by

bioturbation or shear, while Onishi (1981) models the exchange with the top sediment grains only.

In some models, a layered bed is used to model the vertical variations within the bed. O'Connor et al. (1983) has an active and a deep bed layer and Burns et al. (1982) has an arbitrary number of bed layers. Other modelers have simulated the vertical transport of solute within the bed using one-dimensional advection and diffusion (Holloran, 1982; Jackman et al., 1984; Gschwend et al., 1986; Richardson and Parr, 1988; Cerling et al., 1990; Nagaoki and Ohgaki, 1990). Holloran (1982) used a molecular diffusion coefficient. Jackman et al. (1984) and Cerling et al. (1990) determined the value of an effective diffusion coefficient by calibrating their results to field data. The values of the diffusion coefficient used by Richardson and Parr (1988) and Nagaoki and Ohgaki (1990) were fit to exchange data from hydraulic models.

The exchange parameters used in the models described in this section are not related to actual physical exchange mechanisms. Furthermore, the exchange parameters are usually obtained by calibration for one stream and cannot be applied to other rivers. The models that describe the fate and transport of pollutants in rivers could be improved by incorporating exchange submodels that are based on the physical and chemical characteristics of the system and that do not require calibration.

2.2. Bed Exchange Processes

Pollutant exchange between stream water and streambeds occurs through a variety of processes such as advective pumping, bedform turnover, molecular diffusion, net infiltration and exfiltration between the stream and groundwater, resuspension, pressure fluctuations due to stream turbulence, flow into and out of the banks of the stream, and diurnal and seasonal changes in the thermal convective motions. The results of the physical exchange processes may be

strongly modified by chemical and biological interactions. The research presented in this work investigates the exchange of nonlinearly adsorbing compounds between the stream water and sediment bed by porewater advection.

Porewater advection, also referred to as pumping, refers to the movement of porewater into and out of a streambed due to flows induced by dynamic pressure variations over bedforms. Bedforms are wave-like deformations of the bed surface that arise of instability of the flat erodible bed interacting with the turbulent flow. The bedforms considered in this thesis are classified as ripples and dunes and these terms will be used interchangeably. The exchange of fluid across interfaces due to porewater advection has been studied both in the laboratory and in the field.

2.2.1. Porewater advection field observations

The advection of interstitial fluid has been observed in riverbeds, ocean beds and snow dunes. Bencala (1984) and Bencala et al. (1984) observed significant transport between the free water and the water within a "storage zone" in the bed of a small mountain stream. They speculated that the transport resulted from turbulence generated by bottom irregularities and flow obstructions consisting of cobbles, small boulders and vegetation that protruded in the flow. Flow into, out of, and through the coarse gravel and cobble bed was also mentioned. Boyle (1984) observed similar behavior in several streams and noted the effect of flow in the permeable bed on biochemical reaction rates. Grimm and Fisher (1984) used dye injection to observe the exchange surface water and porewater in a shallow creek. They recorded distance of travel and travel time of the dye injected into the streambed.

Webb and Theodor (1972) studied the wave-induced transport of dye into sand ripples on the ocean floor. The porewater velocities were controlled by the height of the water surface waves and the permeability of the sand.

Colbeck (1989) presented an idealized model for the airflow patterns that arise within snowpack because of wind pumping. Airflow through the snow occurred in response to pressure gradients at the surface that arose from the surface topography. Clarke and Waddington (1991) investigated wind pumping of air through permeable snow surfaces on glaciers. They developed a three-dimensional model that simulated the penetration of the pressure fluctuations into the firn.

2.2.2. Porewater advection laboratory observations

The flow of water over mobile, non-cohesive bed material such as silt, sand and gravel usually produces a series of sediment sandwaves called bedforms. These bedforms have been observed on the bottom of many aquatic environments where active water flow occurs over the bed material. The stream flow over a ripple or dune (often with streamline separation at the crest) produces a dynamic pressure differential between the long upstream face and the downstream steep face and trough area. The magnitude of this pressure variation has been measured by Vittal et al. (1977), Fehlman (1985) and Shen et al. (1990). The dynamic pressure variation over the bedform induces flow in the bed; this process is referred to as porewater advection. These flows, which are depicted in Figure 2.2, have been observed in laboratory flumes by Thibodeaux and Boyle (1987), Savant et al. (1987), Elliott (1990), and Elliott and Brooks (1997b). These researchers found that the transport of solutes in the bed by porewater advection was significantly greater than transport by molecular diffusion.

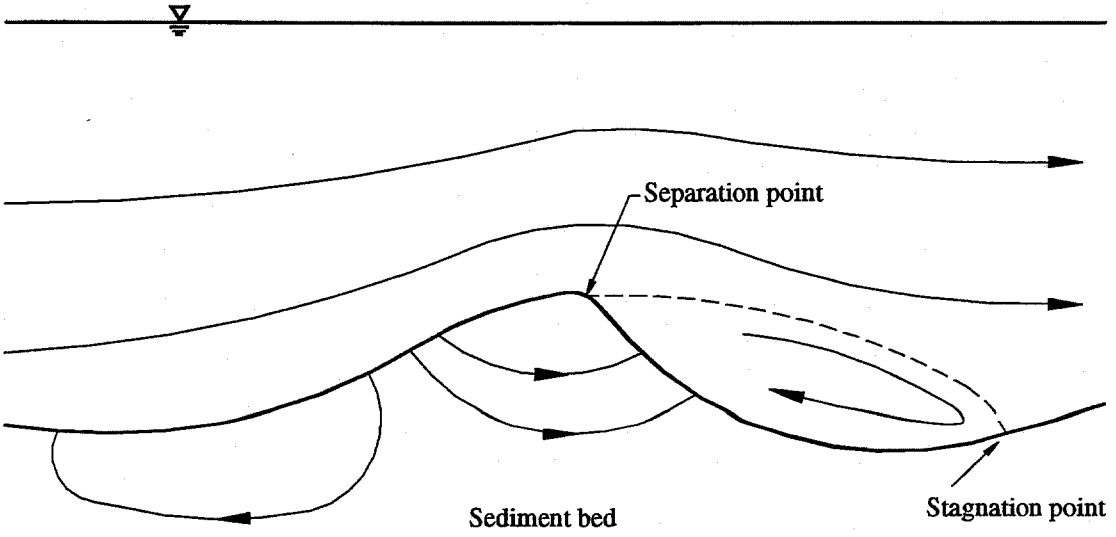

Figure 2.2. Flow patterns induced by porewater advection (pumping) over and through a bedform.

Thibodeaux and Boyle (1987) conducted a series of flume experiments using a sediment bed of coarse gravel with a mean diameter of 8 mm. A series of two-dimensional bedforms were created by hand to cover the entire bed surface. The large waves were 5 cm high and 55 cm long; the smaller waves were 2.5 cm high and 25 cm long. Dye traces were used to observe the flow into the bed. Porewater velocities were measured by timing the dye front movement over a known distance. The porewater velocity was within 1-2 orders of magnitude lower than the free stream velocity and persisted to as much as 3-5 wave heights into the bed. Thibodeaux and Boyle (1987) developed an algorithm for predicting the bed velocity and Peclet number based on stream and bed parameters. The model was based on Darcy's law coupled with the piezometric head measurements by Vittal et al. (1977).

Savant et al. (1987) performed flume experiments similar to those of Thibodeaux and Boyle (1987) using Mississippi River sand having a mean diameter of 0.37 mm. The sand was artificially shaped into dunes 50.8 cm in length and 5.08 cm high. The streamlines observed in

the sand bed were of the same general shape as those measured by Thibodeaux and Boyle (1987) in their gravel bed. The porewater velocities were 4-5 orders of magnitude smaller than the overlying free stream velocity. Savant et al. (1987) developed a numerical model using boundary element methods to simulate the flow induced within the sediment by both dynamic and static pressures. The model solved the Laplace equation, derived from Darcy's law and the continuity equation, using the piezometric head measurements from Vittal et al. (1977). The model simulations were in good agreement with the observed porewater trajectories. The model was used to estimate the porewater velocities and Peclet numbers for the Nile, Mississippi and Red rivers. The Peclet number was defined as

$$N_{Pe} = \frac{vH}{D} \tag{2.2}$$

where v is the porewater velocity, H is the height of the bedform and D is the typical value for molecular diffusion (10^{-5} cm^2/s). The Peclet numbers from the river simulations were all of the order of 100 or greater. The predicted porewater velocities in these rivers were 5-7 orders of magnitude less than the stream velocity, but the Peclet numbers indicated that the convective transport was much more rapid than the interstitial diffusive transport. Savant et al. (1987) did not calculate the solute exchange that would result from the porewater flows into and out of the bed.

Reible and Savant-Malhiet (1993) developed a model that compared contaminant transport across the sediment-water interface for the following processes: molecular diffusion, colloidal diffusion, porewater advection between the stream and associated aquifer, porewater advection due to bedforms, and sediment movement. The results showed that porewater advection induced by the bedforms should normally be the dominant mechanism in stationary sediments and in movable beds experiencing sediment transport and advancing bedforms. Molecular diffusion appeared to be unimportant except in very low-permeability sediment beds.

Elliott (1990) conducted extensive flume experiments to study the stream/bed exchange of non-adsorbing tracers into sediment beds having stationary and moving bedforms. The porewater flow patterns were observed using dye injection similar to Thibodeaux and Boyle (1987) and Savant et al. (1987). The dye fronts from a run with stationary natural bedforms are illustrated in Figure 2.3. Porewater flows and solute exchange was measured for both artificially-molded and naturally-created bedforms. Two silica sands, one medium (0.47 mm) and one fine (0.13 mm), were used in the experiments. The bedform wavelengths were 9 to 30 cm; the heights were 0.75 to 2.5 cm. Elliott and Brooks (1997ab) developed models that simulated the porewater flow in the bed and calculated the magnitude of the corresponding solute exchange. The porewater flow model solved the continuity equation using Darcy's law and Fehlman's (1985) piezometric head measurements. Elliott and Brooks (1997ab) developed a simplified model that used a sinusoidal pressure variation over the bedform. This model incorporated the porewater advection process by calculating the average flux into the sediment bed and then utilizing a residence time approach. The results of this model did not differ greatly from those using Fehlman's measurements. Elliott and Brooks (1997ab) found that molecular diffusion was a significant exchange mechanism only when the porewater velocities were extremely small. They showed that longitudinal dispersion did not affect the exchange. However, lateral dispersion could increase the exchange for long times.

Unlike the models discussed in Section 2.1, the models developed by Elliott and Brooks (1997ab) were based on the detailed description of the flows in the bed and descriptions of bedform movement. The models did not require calibration, only measurement of stream and bed properties. The porewater advection model developed by Elliott and Brooks (1997ab) is the starting point for this work and is explained in Chapter 3, Sections 3.1 and 3.2.

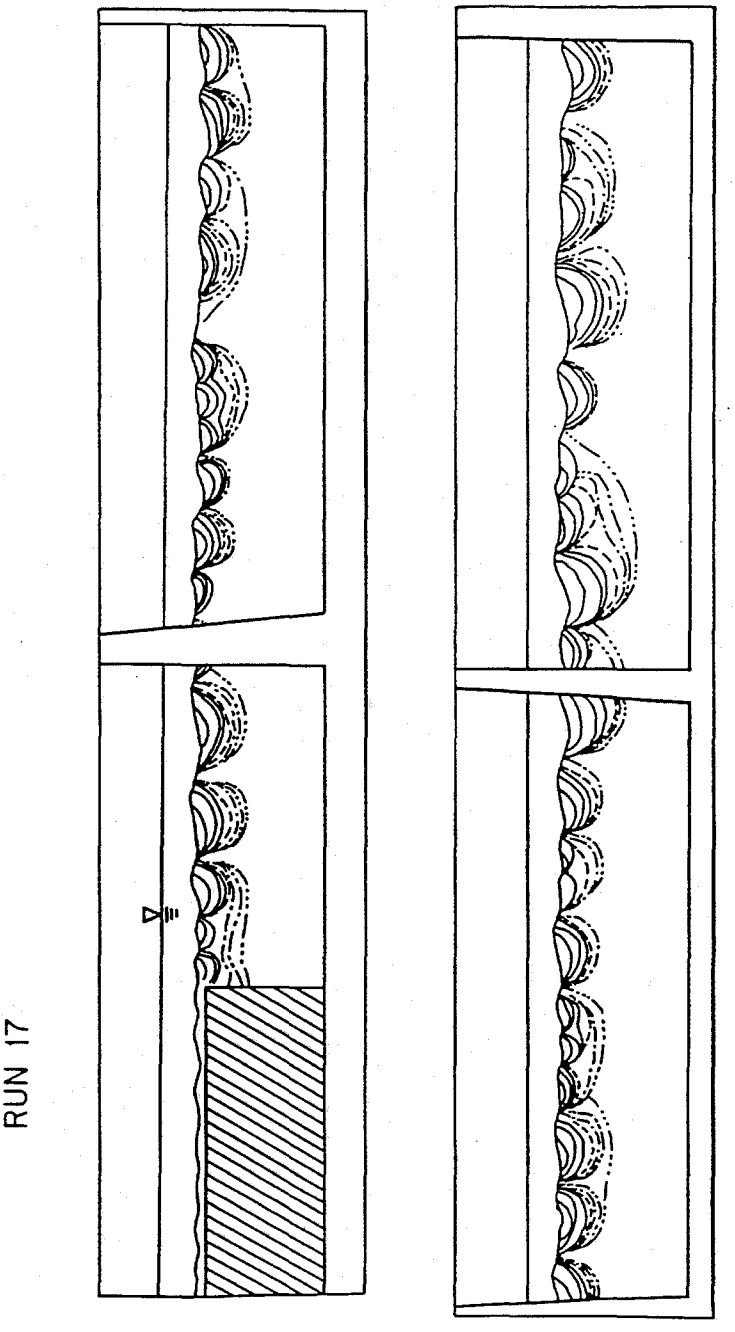

Figure 2.3. Dye fronts from Elliott (1990) Run 17 with stationary natural bed forms at 5 hr, 23 hr, 49 hr, 101 hr (dash, 4 days), 167 hr (double dash, 7 days), 240 hr (triple dash, 10 days) and 336 hr (quadruple dash, 14 days). The inlet box of the flume is shown at the left of the upper section of the figure. The lower part of the figure shows the downstream half of the bed.

2.2.3. Exchange of reactive compounds

Only a few researchers have studied the stream/bed exchange of reactive compounds by porewater advection. The transport of linearly adsorbing compounds has been studied by Reible and Savant-Malhiet (1993), Eylers (1994) and Eylers et al. (1995). The exchange of nonlinearly adsorbing compounds has apparently not been investigated heretofore.

Reible and Savant-Malhiet (1993) modeled the transport of linearly adsorbing compounds across the sediment water interface by molecular diffusion, porewater advection, and sediment movement. The model predicted that in stable sediments porewater advection is the dominant transport process. In unstable sediments, sediment movement was predicted to be the dominant transport process.

Rutherford et al. (1995) used the porewater advection model developed by Elliott (1990) and Elliott and Brooks (1997ab) to estimate the contribution porewater pumping makes to the benthic oxygen uptake rate in a polluted river. The model predicted that pumping made a significant contribution to deoxygenation in the Waiotapu River, New Zealand, where the gravel bed is highly permeable and biological activity is high, but not in the sand-bed Tarawera River.

Eylers (1994) conducted a series of flume experiments to study the exchange of metal ions (lithium copper, zinc, magnesium, and calcium) between stream water and a silica sand bed covered with bedforms. Lithium was used as a nonsorbing tracer. Copper, zinc, magnesium and calcium ions adsorbed linearly to the sand. The partition coefficients for the metals were determined by conducting batch adsorption experiments. The advective flux into the bed was not affected by the adsorption of the metals to the sand surface. However, partitioning did effect the net mass exchange between the overlying water and the sediment bed. Eylers (1994) observed that the stronger the partitioning of the pollutant, the larger the mass transfer into the bed and the smaller the penetration depth into the bed. Eylers (1994) modified the pumping model developed by Elliott and Brooks (1997ab) to account for the additional mass exchange. The time

scale for the residence time function was divided by a constant retardation coefficient, which was calculated from the partition coefficient determined in the batch experiments. The model simulations agreed with the observed mass transfer in the flume. Eylers (1994) determined that the assumption of equilibrium adsorption was valid when the adsorption time scale was short compared to the porewater pumping time scale. Eylers' model is explained in more detail in Chapter 3, Section 3.3.

2.2.4. Exchange of colloidal particles

Packman (1997) conducted flume experiments to study the transport of kaolinite clay into a silica sand bed by porewater advection and bedform turnover. Packman (1997) modified the models developed by Elliott and Brooks (1997ab) to account for particle filtration and settling. The models were successful in reproducing the experimental results. For stationary bedforms, the kaolinite particles were transported into the bed by porewater advection. Due to filtration and settling, the particles were generally completely trapped in the bed and were not returned to the overlying stream water.

2.3. TRANSPORT OF NONLINEARLY ADSORBING COMPOUNDS IN POROUS MEDIA

Nonlinear isotherms are often encountered for polar organic chemicals such as pesticides and for inorganic compounds such as heavy metals. Although the bed/stream exchange of nonlinearly adsorbing compounds has not been studied, the transport of these compounds in groundwater systems has been investigated. Adsorption processes and nonlinear adsorption isotherms are reviewed in Sections 2.3.1 and 2.3.2. Literature pertaining to the transport of nonlinearly adsorbing compounds in porous media is discussed in Section 2.3.3.

2.3.1. Adsorption processes

Adsorption is defined as the accumulation of matter at the solid-water interface (Stumm and Morgan, 1996). The adsorption reactions that are important in waters, sediments and soils are chemical interactions with the surface (surface hydrolysis, complexation, ligand exchange and hydrogen bond formation), electrical interactions with the surface, and interactions with the solvent (hydrophobic expulsion) (Stumm, 1992). In natural soils and sediments, the adsorption of organic compounds is enhanced in the presence of natural organic matter. At the mineral surface, ions may be in the diffuse swarm of the double layer, associate with the surface as an outer-sphere complex (ion pair) or form an inner-sphere complex ("chemical bond").

The extent of adsorption resulting from coulombic interactions can be calculated using the method developed by Stone et al. (1993). An estimation of the electrical potential at the surface is required for the calculation. The fraction a monovalent cation adsorbed in the diffuse swarm can be calculated by

$$(f_a)_{coul} = \frac{INTEG - 1}{INTEG} \tag{2.3}$$

where

$$INTEG = 1 + \frac{1}{\kappa}\left(\frac{4IJ\left(1 - J\exp\left(-\kappa V_s/S_{AT}\right)\right)}{\left(I - J\right)\left(I - J\exp\left(-\kappa V_s/S_{AT}\right)\right)}\right) \tag{2.4}$$

$$I = \exp\left(-\frac{F\Psi_0}{2RT}\right) + 1 \tag{2.5}$$

$$J = \exp\left(-\frac{F\Psi_0}{2RT}\right) - 1 \tag{2.6}$$

and κ is the Debye parameters defined by Equation (2.7), V_s is the suspension volume in cm^3, S_{AT} is the total surface area of the solid in cm^2, F is the Faraday constant, R is the gas constant, T is temperature in K, and Ψ_0 is the electric potential at the solid surface. The Debye parameter in m^{-1} is given by

$$\kappa = \left(\frac{2F^2 I_s \times 10^3}{\varepsilon \varepsilon_0 RT} \right)^{1/2} \tag{2.7}$$

where I_s is the ionic strength in (M), ε is the relative dielectric constant of water (78.5 at 25°C) and ε_0 is the permittivity of free space (8.854×10^{-12} C V^{-1} m^{-1}).

The surface potential is not accessible by direct measurement, but it can be calculated from experimentally determined surface charges. The zeta potential ζ, which is calculated from electrophoretic measurements, is defined as the potential drop across the mobile part of the double layer (Stumm, 1992). The zeta potential is typically lower than the surface potential.

2.3.2. Adsorption Isotherms

In pollutant transport models, the partitioning of contaminants between aqueous solution and sorbed phases is commonly described as an equilibrium process and modeled by an empirical sorption isotherm, which shows the relationship between the aqueous concentration of the compound to the amount adsorbed at a fixed temperature. Linear equilibrium reactions are often assumed, but nonlinear effects appear to be significant in many situations (Weber et al., 1991). The results of a transport model based on different isotherms can be quite different (Hinz et al., 1994) and careful choice of the isotherm model is sometimes critical. A description of some of the most common isotherm models and their ranges of applicability follows.

The isotherms considered in this thesis are convex upward (Figure 2.4). The most commonly used nonlinear adsorption models are the Langmuir and Freundlich isotherms. The frequent application of these isotherms reflects their ability to fit a variety of adsorption data, but can also be attributed to the simplicity of the isotherm equations and ease of the associated parameter estimation. In some cases, closer examination of the data reveals systematic underestimation or overestimation from the fitted isotherms (Kinniburgh, 1986). Kinniburgh (1986) suggested a number of more complicated isotherm equations that are suitable for

describing nonlinear adsorption on heterogeneous surfaces and that provide improved flexibility and ability to fit a wide variety of adsorption data. The Langmuir-Freundlich and the Tóth isotherms are described below.

The assumptions associated with the conceptual developments of the isotherm models are rarely satisfied in natural systems. The fact that an isotherm model may fit adsorption data well should not be taken as a verification of the concept or mechanisms upon which the isotherm is based.

2.3.2.1. Linear Adsorption

In order to simplify computational effort, the linear isotherm has been used in many transport models. The linear isotherm is given by Equation (2.8), where K_d is the solid-water distribution ratio.

$$S = K_d C \tag{2.8}$$

Linear isotherms are usually observed for the sorption of hydrophobic organic chemicals on organic or organically coated particles (Stumm and Morgan, 1996). Otherwise, this isotherm is generally valid over small concentration ranges at a given pH and temperature. In some instances, it can describe adsorption at very low aqueous concentrations and for solids of low sorption potential (Weber et al., 1991).

a) Linear scale

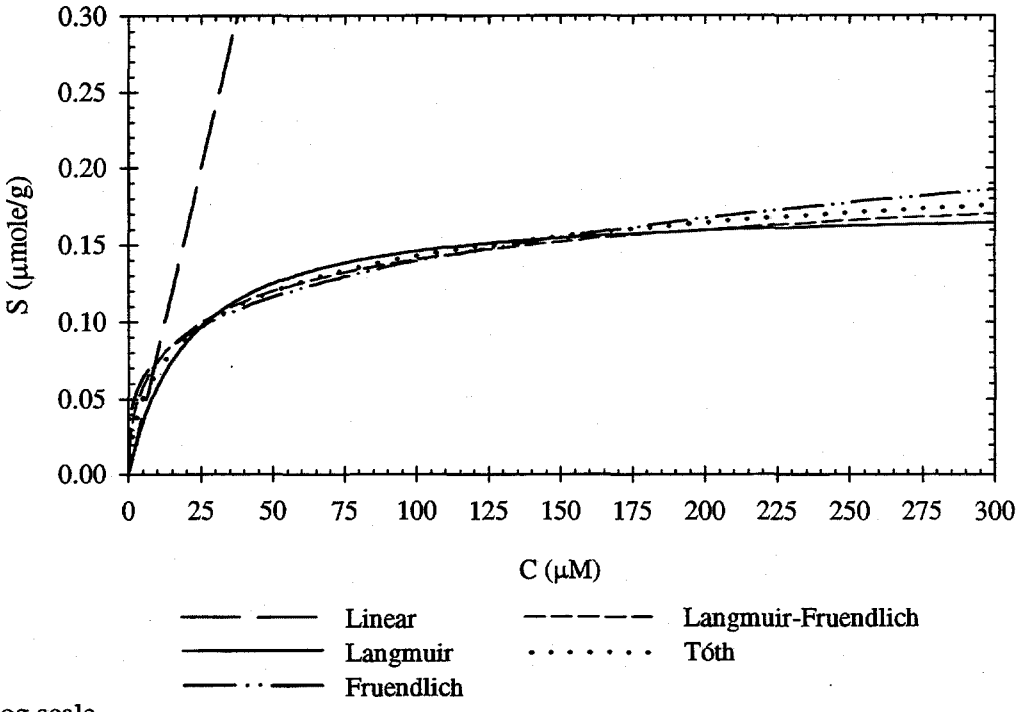

b) Log scale

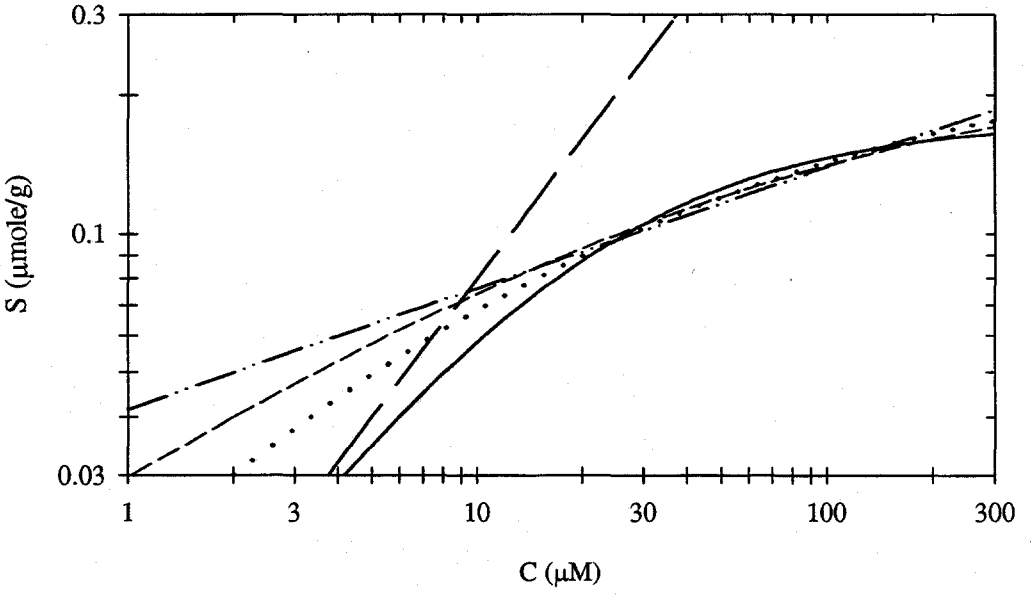

Figure 2.4. Comparison of linear, Langmuir, Fruendlich, Tóth and Langmuir-Freundlich isotherms. The Langmuir, Freundlich and Tóth parameters are based on the dodecyltrimethylammonium bromide adsorption data presented in Chapter 5, Table 5.4. The Langmuir-Freundlich parameters are adjusted to exaggerate the difference from the Tóth isotherm. The value of K_d for the linear isotherm is 0.008 liters/gram.

2.3.2.2. Langmuir Isotherm

The Langmuir model was developed originally for systems in which sorption leads to the formation of a monolayer of sorbate on the surface of a sorbent. Equation (2.9) represents the Langmuir isotherm, where S_T is the sorbed concentration on the solid corresponding to complete monolayer coverage and K_L is the sorption coefficient.

$$S = \frac{S_T K_L C}{1 + K_L C} \tag{2.9}$$

The Langmuir isotherm is valid for the following conditions:

1. The sorbed concentration does not exceed monolayer coverage.
2. The energy of sorption for each molecule is the same and independent of surface coverage.
3. Sorption occurs only on localized sites and involves no interactions between sorbed molecules.

The Langmuir equation reduces to a linear isotherm at low concentrations.

2.3.2.3. Freundlich Isotherm

The Freundlich isotherm has the form:

$$S = K_F C^{\alpha} \tag{2.10}$$

The parameter K_F is the Freundlich sorption coefficient and α is the measure of nonlinearity. This equation applies to solids with heterogeneous surface properties and soils consisting of a mixture of different minerals. Sposito (1984) showed that Equation (2.10) could be derived by integrating over a continuum of Langmuir equations. At high concentrations, the Freundlich isotherm does not exhibit an upper limit and has an infinite slope as the aqueous concentration approaches zero.

2.3.2.4. Langmuir-Freundlich Isotherm

Sips (1950) derived the general Langmuir-Freundlich isotherm given in Equation (2.11), where K_{LF} is the sorption coefficient and $0 < \alpha < 1$. The Langmuir-Freundlich isotherm is essentially the Freundlich isotherm for low concentrations and reduces to the Langmuir isotherm when α equals one. An adsorption maximum is reached at high concentrations, but the slope of the isotherm becomes infinite as the aqueous concentration approaches zero.

$$S = \frac{S_T (K_{LF} C)^{\alpha}}{1 + (K_{LF} C)^{\alpha}} \tag{2.11}$$

2.3.2.5. Tóth Isotherm

The Tóth isotherm (Tóth et al., 1974) is given by

$$S = \frac{S_T K_T C}{\left(1 + (K_T C)^{\alpha}\right)^{1/\alpha}} \tag{2.12}$$

where K_T is the sorption coefficient and $0 < \alpha < 1$. At low concentrations, the Tóth isotherm approaches the linear isotherm; and an adsorption maximum is reached at high aqueous concentrations. On a log S-log C plot, the Tóth isotherm gives a continuous smooth curve over the intermediate concentration range. The Tóth isotherm reduces to the Langmuir isotherm when α equals one.

2.3.3. Porous media contaminant transport models

The advection-dispersion equation describes the transport of dissolved contaminants in porous media. For one-dimensional transport in the positive x-direction with steady-state flow, the advection-dispersion equation is

$$\theta\frac{\partial C}{\partial t} + \rho_b\frac{\partial S}{\partial t} + u\frac{\partial C}{\partial x} = \theta D\frac{\partial^2 C}{\partial x^2} \qquad (2.13)$$

where θ is the porosity, ρ_b is the bulk density, u is the Darcy flow velocity in the x-direction, D is the pore-scale dispersion coefficient, C in the concentration of the chemical in the fluid and S is the sorbed concentration of the chemical on the solid.

For one-dimensional transport in porous media, analytical solutions of the advection-dispersion equation have been developed for non-reactive solutes and linearly adsorbing compounds. Van Genuchten and Alves (1982) compiled solutions for transport with linear equilibrium adsorption and zeroth and first-order production and decay. Other analytical solutions include reversible linear sorption having first-order kinetics (Van Genuchten et al., 1974), kinetic two-site linear adsorption (Selim et al., 1976; Cameron and Klute, 1977), and linear adsorption in a dual porosity medium (Van Genuchten and Wierenga, 1976).

Charbeneau (1981) and Rhee et al. (1986) neglected dispersion and developed solutions of the advective equation with nonlinear adsorption using the method of characteristics. Charbeneau (1981) used the Freundlich adsorption isotherm and cation exchange. Rhee et al. (1986) presented solutions for the cases of Langmuir, Freundlich and BET adsorption.

Analytical solutions of the advection-dispersion equation for nonlinear adsorption-desorption reactions have been developed by van der Zee (1990), van Duijn and Knabner (1992), and Bosma and van der Zee (1993). These solutions focus on the development of a traveling wave, which may form when the boundary and initial conditions are such that the injected concentration exceeds the initial concentration and the isotherm is convex upward. A traveling wave is approached asymptotically when a self-sharpening wave propagates in the presence of pore-scale dispersion.

With continuous injection of a nonlinearly adsorbing compound, Bosma and van der Zee (1993) showed that the concentration front moves at the same velocity as a linearly adsorbing compound with the same effective retardation coefficient. However, an instantaneously injected

plume of the nonlinearly adsorbing compound (with a convex upward isotherm) moves with a decreasing average velocity (Bosma et al., 1994), whereas a linearly adsorbing compound moves with a constant velocity. In pump-and-treat remediation of aquifers, nonlinear sorption effects may lead to enhanced tailing in mass arrival at extraction wells (Cvetkovic and Dagan, 1994; Rabideau and Miller, 1994; Berglund, 1995).

Hinz et al. (1994) used the advection-dispersion equation to model the breakthrough curves resulting from different adsorption isotherms. There were significant differences in the breakthrough curves resulting from simulations with different sorption isotherms fitted to the same data. Berglund and Cvetkovic (1996) studied the effect of the different adsorption isotherms on the predicted cleanup time for an aquifer contaminated by a nonlinearly adsorbing compound. They found that the Freundlich and Langmuir-Freundlich isotherms resulted in infinitely long cleanup times. They concluded that the choice of isotherm in a particular situation should be based on the ability of the different candidate isotherms to fit the sorption data. For remediation applications in which very low concentrations are encountered, the asymptotic behavior of the isotherm must be consistent with the data.

2.4. CATIONIC SURFACTANTS

The sorbate used in the flume experiments had to be relatively non-toxic in order to permit disposal of the large volume of wastewater generated in the flume experiments (83 liters). The compound also had to be non-volatile, exhibit nonlinear adsorption behavior and behave conservatively in the absence of sediment in the flume. Cationic surfactants satisfied these criteria.

A surfactant is a surface-active substance, which has both hydrophilic and hydrophobic structural groups, that decreases interfacial tension. A cationic surfactant has a positively charged hydrophilic head group with a hydrophobic tail.

The use of surfactants throughout the world is increasing at a rate in excess of population growth (Myers, 1988). Many surface waters and ground waters near large population centers or at sites of contamination have concentrations of surfactants below their respective critical micelle concentrations (A. D. Little Co., 1977; Thurman et al., 1986; Lewis, 1991; Edwards et al., 1992). Quaternary ammonium compounds, which are studied in this research, are a class of cationic surfactants that have a wide range of industrial and commercial applications. They can be found as components of drilling mud, fabric softeners, hair conditioners, emulsifiers and disinfectants (Hayes et al., 1995). Quaternary ammonium compounds are potent germicides (Lawrence, 1970) and are toxic in the mg/ℓ range and lower to a wide variety of aquatic organisms including algae, fish, molluscs, barnacles, rotifers, starfish, shrimp and others (Boethling, 1984).

Cationic surfactants adsorb strongly from aqueous solutions onto soil, sediments, and suspended particles because of favorable hydrophobic and electrostatic interactions with negatively charged surfaces of natural materials. The transport, fate and biological effects of these compounds are greatly affected by adsorption and by association with suspended and dissolved organic matter (Lewis and Wee, 1983; Boethling, 1984). Cationic surfactants can also influence the behavior of other pollutants in surface water and groundwater. Adsorbed cationic surfactants can displace adsorbed metal ions (Beveridge and Pickering, 1983; Bouchard et al., 1988) and increase the affinity of sorbents for hydrophobic organic compounds (Bouchard et al., 1988; Lee et al., 1989; Smith et al., 1990; Burris and Antworth, 1992; Wagner et al.; 1994, Brown and Burris, 1996).

2.4.1. Cationic surfactant adsorption on negatively-charged oxides

An extensive amount of research has been conducted to investigate the adsorption of cationic surfactants onto pure mineral oxides. The oxides studied include quartz (Gaudin and Fuerstenau, 1955; Fuerstenau, 1956; Somasundaran et al., 1964; Takeda and Usui (1987);

Schwarz et al., 1988; Hayes et al., 1995), silica (Bijsterbosch 1974; Esumi et al., 1991; Favoriti et al., 1996; Esumi et al., 1996), rutile (Koopal et al., 1995; Lee and Koopal, 1996; Favoriti et al., 1996; Vanjara and Dixit, 1996), and alumina (Huang et al., 1996; Favoriti et al., 1996). The flotation data presented by Cases (1970) demonstrate that both anionic and cationic surfactants interact strongly with a garnet surface, even in the pH range where the sign of the surface charge is the same as the ion.

A schematic of a typical adsorption isotherm for cationic surfactants on negatively charged oxides is shown in Figure 2.5. The isotherm can be divided into four distinct regions defined by Somasundaran and Fuerstenau (1966). In Region I, adsorption results primarily from electrostatic forces with simple ion exchange occurring between the adsorbed counterions of the supporting electrolyte in the double layer and the surfactant ions. The electrical characteristics of the surface remain unchanged (Fuerstenau, 1956; Somasundaran et al., 1964). For compounds having an alkyl chain length greater than nine, there are slight alkyl chain-surface interactions in Region I (Wakamatsu and Fuerstenau, 1968).

The Region I-II transition occurs at the critical hemimicelle/admicelle concentration. At this point, the associative van der Waals forces among the hydrocarbon chains are supplemented and reinforced by the coulombic forces of attraction between the surfactant ions and the surface. The adsorbed ions associate in tight patches with their tails sticking out into the solution, thus minimizing the surface area of the hydrocarbon chain in contact with the water. Monolayer patches are defined as hemimicelles (Gaudin and Fuerstenau, 1955) and bilayer patches are admicelles (Harwell et al., 1985). The critical concentration decreases as the alkyl chain length increases. The van der Waals cohesive energy which is responsible for hemi-micelle formation has been found to be 1.0 k_BT per CH_2 group (Fuerstenau et al., 1964; Somasundaran et al., 1964), where k_B is Boltzmann's constant and T is absolute temperature.

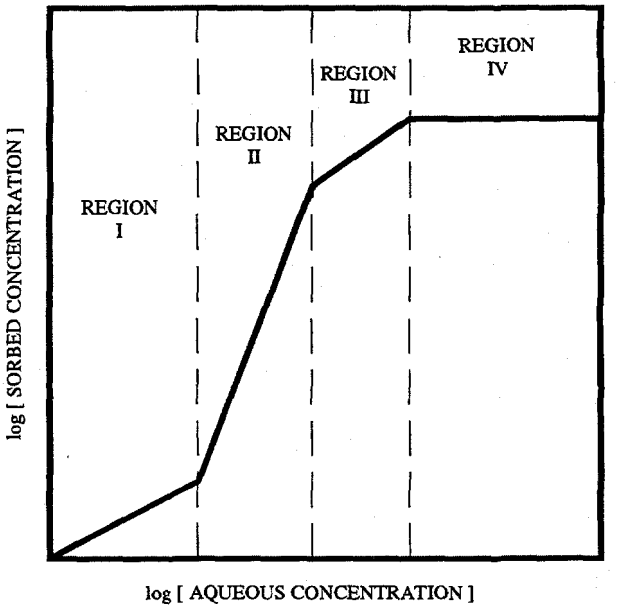

Figure 2.5. Schematic of a typical adsorption isotherm for cationic surfactant adsorption on negatively-charged metal oxides.

In Region II, adsorption increases rapidly as hemimicelles and/or admicelles form on the surface. This adsorption is accompanied by a sharp increase in the zeta-potential (Gaudin and Fuerstenau, 1955; Fuerstenau, 1956; Somasundaran et al., 1964; Vanjara and Dixit, 1996). There is a net increase in the surface charge. The slope of the isotherm in Region II increases with alkyl chain length.

Generally, the surface charge is neutralized at or near the transition between Regions II and III. Further adsorption proceeds slowly primarily through hydrophobic interactions between the tails of the adsorbed ions and those in the bulk solution. The exact mechanism is under debate by researchers. As adsorption proceeds, the surface charge is reversed. This is demonstrated by a reversal in the zeta potential (Gaudin and Fuerstenau, 1955; Fuerstenau, 1956; Somasundaran et al., 1964; Vanjara and Dixit, 1996).

In Region IV, the adsorption isotherm plateaus near the critical micelle concentration. Researchers disagree on the mechanism causing this adsorption maximum.

A number of thermodynamic adsorption models have been developed for the adsorption of ionic surfactants onto oxide surfaces. There are two different approaches to the modeling. The first approach includes the work of Ottewill and Rastogi (1960), Somasundaran et al. (1964), Somasundaran and Fuerstenau (1966), Wilson and Moffat (1979), Kiefer and Wilson (1980), Chander et al. (1983), and Böhmer and Koopal (1992abc). The adsorbing surface is generally treated as homogeneous. These workers assume the hydrocarbon chains associate with the surface at a critical concentration. In the earlier models, single-layered, two-dimensional aggregates – the hemi-micelles – are assumed to form on the surface. In these models, the adsorption is described by the Stern-Langmuir equation (Ottewill and Rastogi, 1960; Chander et al., 1983), the Stern-Grahame equation (Somasundaran et al., 1964; Somasundaran and Fuerstenau, 1966), or the Frumkin-Fowler-Guggenheim equation (Wilson and Moffat, 1979). In later models, Kiefer and Wilson (1980) and Böhmer and Koopal (1992abc) have allowed for the formation of bilayered structures – admicelles – at high surfactant concentrations. Wängnerud and Jönsson (1994) have calculated that bilayered structures will form instantaneously at the critical concentration without prior monolayer formation.

The second modeling approach is assumed by Scamehorn et al. (1982), Harwell et al. (1985), Yeskie and Harwell (1988), Cases and Villieras (1992), and Hankins et al. (1996). In these models, it is assumed that adsorption proceeds on local patches of the surface either sparsely or as a result of spontaneous thermodynamic phase transitions resulting in a local monolayer (hemimicelle), a local bilayer (admicelle), or an intermediate structure.

All of the adsorption models mentioned above attempt to explain the fine structure of the adsorption isotherm (Figure 2.5). The models differ in their interpretations of the transition between Regions II and III. Somasundaran and Fuerstenau (1966) assume that the transition occurs when the surface charge is neutralized and further adsorption proceeds by hydrophobic interactions between the hydrocarbon tails. Böhmer and Koopal (1992a) interpret the transition in terms of a change in the favored primary aggregate from head-on monolayer to bilayer and do

not believe it necessarily coincides with the oxide's isoelectric point. Scamehorn et al. (1982), Harwell et al. (1985), Yeskie and Harwell (1988), Cases and Villieras (1992), and Hankins et al. (1996) interpret the transition in terms of sorption to less favorable adsorption sites that have a wider distribution of energies.

2.4.2. Cationic surfactant adsorption onto natural materials

It is not practical to use the thermodynamic adsorption models, which require detailed solid surface data, to describe cationic surfactant adsorption on heterogeneous porous media that are composed of a variety of minerals. An empirical isotherm should be derived from batch adsorption experiments. The empirical isotherm cannot be used to determine intrinsic adsorption energies or adsorption mechanisms (Brownawell et al., 1990). The adsorption isotherms of cationic surfactants on natural materials are highly nonlinear and L-shaped (Lee et al., 1989; Brownawell et al., 1990; Burris and Antworth, 1992; Wagner et al., 1994; and Brown and Burris, 1996). The adsorption plateaus corresponded closely with the cation exchange capacity of the materials.

Brownawell et al. (1990) and Wagner et al. (1994) fit a Freundlich isotherm to the adsorption data for surface coverages less than 20 percent. A multisite, competitive Langmuir adsorption model was also developed. The nonlinearity of the isotherm was attributed to the heterogeneity of the solid surface sites because hemimicelle formation was not observed.

Brown and Burris (1996) fit a Langmuir isotherm to their adsorption data. The Langmuir adsorption constant was derived from the equilibrium constant of the ion exchange reaction. The model underestimated the adsorption plateau.

Hayworth and Burris (1996) investigated the transport and partitioning behavior of a cationic surfactant in columns filled with aquifer material. Simulations for transport with equilibrium Langmuir partitioning and transport with kinetic Langmuir partitioning were

performed. The advection-dispersion equation was solved numerically. The equilibrium model fit the data well for low porewater velocities and the kinetic model for high porewater velocities.

2.5. CLOSURE

The models that describe the fate and transport of pollutants in rivers could be improved by incorporating bed/stream exchange submodels that are based on the physical and chemical characteristics of the system and that do not require calibration. Detailed models for the exchange of nonsorbing and linearly adsorbing compounds by porewater advection have been developed by Elliott and Brooks (1997ab) and Eylers (1994), respectively. An exchange model for the exchange of nonlinearly adsorbing compounds is developed in this thesis. The model incorporates measurable hydraulic and bed parameters and sorption coefficients derived from batch adsorption experiments. The model does not require calibration and provides predictions that can be tested against experimental data.

3. MODELING

The models developed in this chapter predict the mass transfer of nonsorbing and adsorbing pollutants into a sediment bed covered with stationary bedforms (dunes or ripples). Porewater advection ('pumping') is assumed to be the dominant physical bed/stream exchange process when bedforms do not move. Pore scale dispersion and molecular diffusion at the bed/water interface are neglected because Elliott (1990) found that these processes do not significantly contribute to the mass exchange compared to porewater advection.

The interstitial velocity field and the streamlines in the sediment bed are simulated using Elliott's pumping model, which is described in Section 3.1. The bed exchange models which predict the mass transfer of either nonsorbing or adsorbing compounds to the sediment bed utilize the pumping model to determine the flux through the bed surface and to track the contaminants within the bed. The bed exchange model developed by Elliott for nonsorbing tracers is outlined in Section 3.2.

Both the pumping model and an adsorption model are coupled to predict the bed exchange for adsorbing compounds. The bed exchange model developed by Eylers (1994), which is described in Section 3.3, assumes equilibrium linear adsorption. Eylers' criterion that is used to evaluate the validity of the equilibrium assumption is also presented.

In Section 3.4, a model that simulates the bed exchange of nonlinearly adsorbing compounds is developed. The theory that describes the transport of nonlinearly adsorbing compounds in porous media is used to model the transport within the sediment bed. The partitioning of the contaminant between the porewater and the sediment is assumed to be an equilibrium process and is modeled using an empirical adsorption isotherm. The Langmuir, Freundlich, Langmuir-Freundlich and Tóth isotherms, which are presented in Chapter 2 (Section 2.3.2), can be used in the models.

Approximate bed exchange models, which require significantly less computational effort, are presented in Sections 3.5 and 3.6. Their mass transfer predictions for nonsorbing and adsorbing compounds are compared to the simulations from the detailed models.

The coordinate system and relevant variables used in the exchange models are depicted in Figure 3.1.

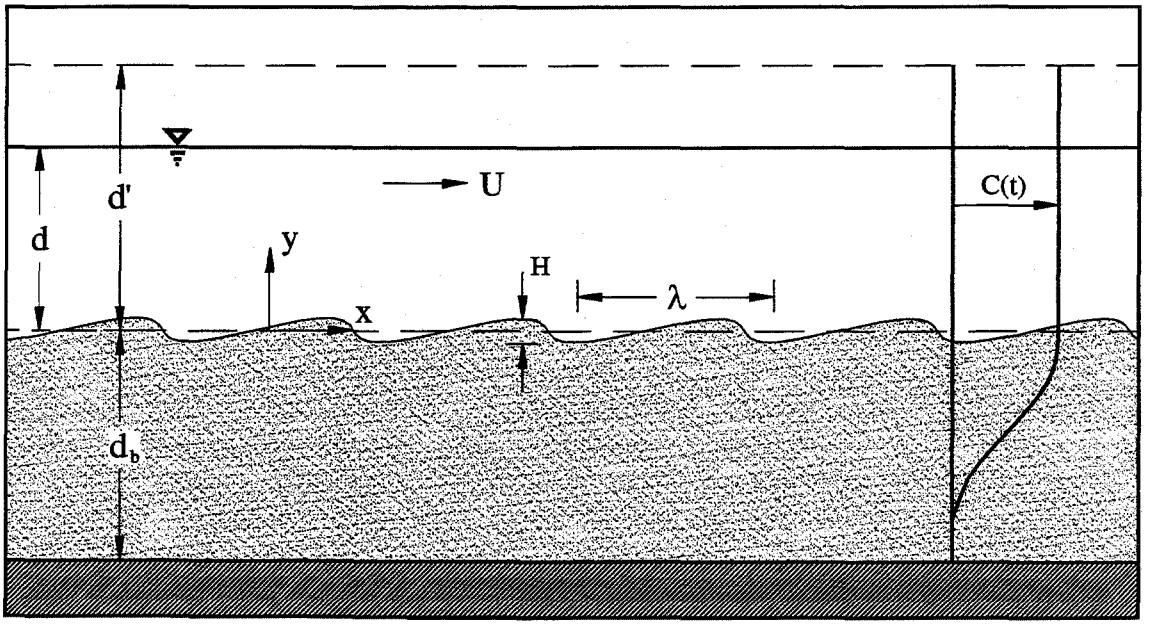

Figure 3.1. Definition of variables used in the bed exchange models.

The notation used in Figure 3.1 is listed below:

- x - horizontal coordinate
- y - vertical coordinate (positive up)
- d - average water depth in the channel
- d' - effective water depth (to account for water in the recirculation system of the flume)
- d_b - depth of sediment bed
- U - average flow velocity in stream channel

λ - average bedform wavelength

H - average bedform height

C - chemical concentration in stream water or porewater

t - time from beginning of experiment

3.1. PUMPING MODEL FOR STATIONARY BEDFORMS

For stationary bedforms, Elliott (1990, 1997a) developed a simple pumping model that applies a sinusoidal pressure variation over an infinitely deep flat bed. Elliott (1990) showed that the piezometric head variations over a triangular bedform that were measured by Fehlman (1985) could be approximated by a sine function (Figure 3.2a). The flat bed approximation is valid for the following reasons:

1. With the application of a sinusoidal pressure variation, the vertical flow into and out of the bed is retained when the bed is assumed flat.
2. Since the height of the bedforms is small compared to the bed depth, the flow patterns within the "flat bed" (assuming the sinusoidal pressure variation) do not differ significantly from those in the full solution (Rutherford et al., 1995).

A more detailed discussion of the minor errors that result from these approximations is presented by Elliott (1990). The infinite bed depth assumption is valid when the bed depth is greater than the bedform wavelength. Packman (1997) developed a pumping model for a finite bed; but for the range of bedform wavelengths in the experiments considered in this thesis, the infinite bed assumption is valid. Elliott's model also assumes that the bed is homogeneous and isotropic and that the bedforms are two-dimensional and periodic with wavelength λ.

The piezometric head at the surface is given by

$$h\big|_{y=0} = h_m \sin(kx) \tag{3.1}$$

where h_m is the amplitude of the pressure head and k is the wavenumber of the pressure variation

$$k = \frac{2\pi}{\lambda} \tag{3.2}$$

By using Fehlman's (1985) pressure measurements and correlation for the form drag coefficient, Elliott derived the following expression for the amplitude of the piezometric head variation

$$h_m = 0.28 \frac{U^2}{2g} \begin{cases} \left(\frac{H/d}{0.34}\right)^{3/8} & H/d \le 0.34 \\ \left(\frac{H/d}{0.34}\right)^{3/2} & H/d \ge 0.34 \end{cases} \tag{3.3}$$

where U is the mean stream velocity, g is gravitational acceleration, H is the height of the bedform and d is mean water depth.

Equation (3.4) gives the piezometric head h in the bed, which is found by applying Darcy's law to the equation of continuity and solving in the semi-infinite domain $y \le 0$.

$$h = h_m \sin(kx) e^{ky} \tag{3.4}$$

The Darcy velocities in the bed are then

$$u = -u_m \cos(kx) e^{ky} \tag{3.5}$$

$$v = -u_m \sin(kx) e^{ky} \tag{3.6}$$

The parameter u_m is the maximum Darcy velocity given by

$$u_m = K k h_m \tag{3.7}$$

where K is the hydraulic conductivity.

Length, velocity, and time are normalized as follows:

$$x^* = kx \tag{3.8}$$

$$y^* = ky \tag{3.9}$$

$$u^* = \frac{u}{u_m} \tag{3.10}$$

$$v^* = \frac{v}{u_m} \tag{3.11}$$

$$\frac{t^*}{\theta} = k u_m \frac{t}{\theta} \tag{3.12}$$

where θ is the porosity of the bed material. After a time $t^*/\theta = 1$, a fluid particle traveling at the maximum porewater velocity u_m/θ will travel a distance $k^{-1} = \lambda/2\pi$. The space variables are normalized with respect to this distance.

The normalized Darcy velocities are

$$u^* = -\cos(x^*)e^{y^*} \tag{3.13}$$

$$v^* = -\sin(x^*)e^{y^*} \tag{3.14}$$

The streamlines are described by the relation $Y^*(X^*, X_0^*)$, where X_0^* is the point where the inward flowing streamline intersects the bed surface. The streamline positions can be found from

$$\frac{dY^*}{dX^*} = \frac{v^*}{u^*} = \tan(X^*) \tag{3.15}$$

which yields

$$Y^* = -\ln\left(\frac{\cos(X^*)}{\cos(X_0^*)}\right) \tag{3.16}$$

Typical streamlines are shown in Figure 3.2b.

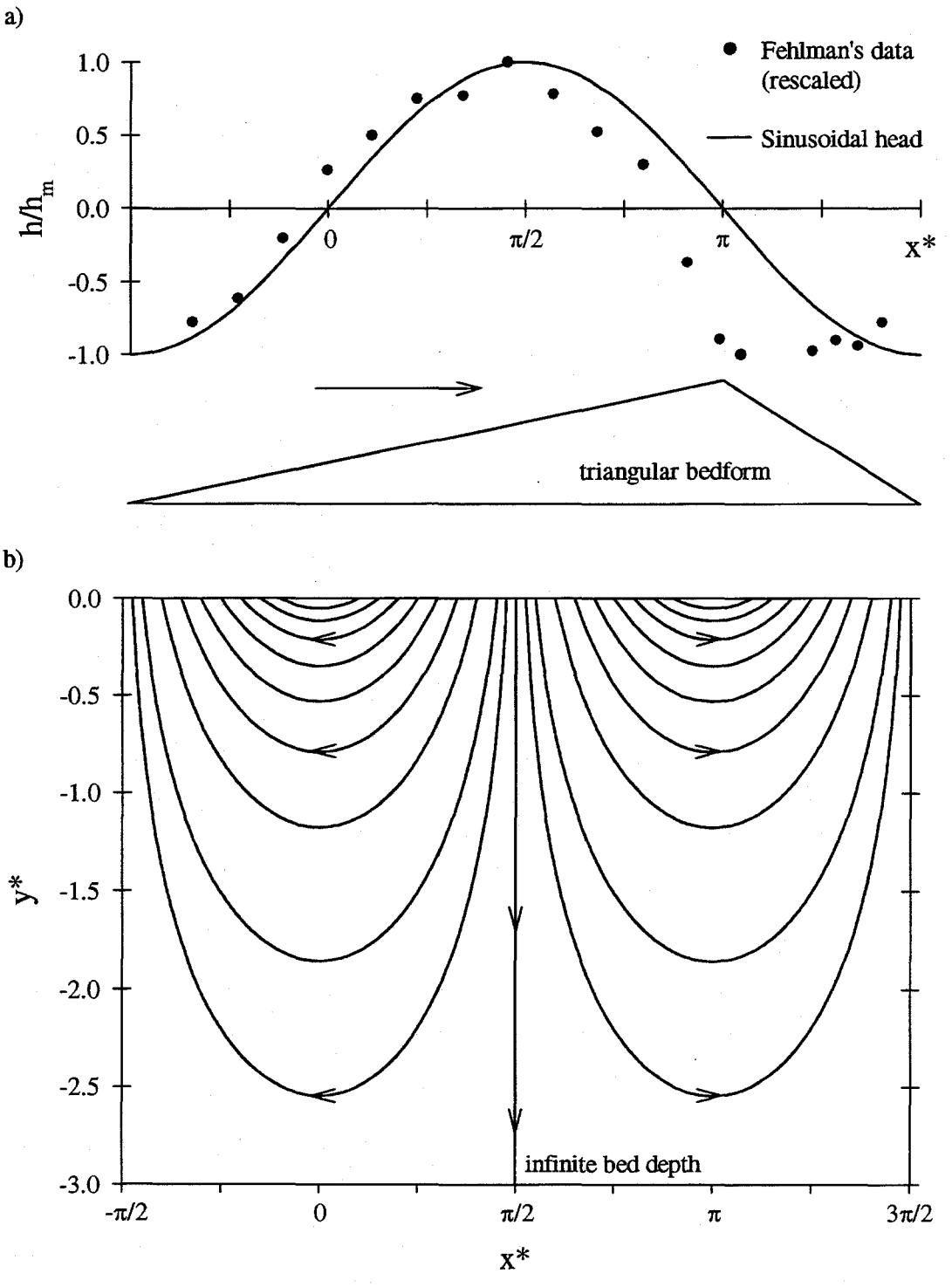

Figure 3.2. (a) Comparison of measured pressure variations over a triangular bedform to the sinusoidal approximation; (b) streamlines for sinusoidal head model with an infinitely deep bed (vertical scale is exaggerated two times the horizontal scale).

3.2. BED EXCHANGE MODEL FOR NONSORBING SOLUTES

In this section, Elliott's model that predicts the mass transfer of a nonsorbing solute into a streambed due to porewater advection is presented. Pore scale dispersion is neglected because it does not significantly affect the mass exchange (Chapter 2, Section 2.2.2). The net flux of solute into the bed is determined using a residence time function approach. In order to calculate the interfacial flux and the residence time function, the sinusoidal head pumping model is used to simulate the flow into, within and out of the bed.

The residence time function, $R_T(t,t_0,x_0)$, is the probability that a solute molecule which enters the bed at time t_0 and position x_0 remains in the bed at a later time t. Generally, for a nonsorbing solute, R_T does not depend on the time that the solute entered the bed, and the function reduces to $R_T(\tau,x_0)$ where $\tau = t-t_0$.

The inward flux of solute at a point on the bed surface is denoted by qC, where C is the concentration of the solute in the water column and q is the flow into the bed

$$q = \begin{cases} \vec{v}\cdot\vec{n} & \vec{v}\cdot\vec{n} > 0 \\ 0 & \vec{v}\cdot\vec{n} < 0 \end{cases} \tag{3.17}$$

where $\vec{v}$ is the Darcy velocity vector at the bed surface and $\vec{n}$ is the unit normal vector into the bed surface. For the sinusoidal pumping model with a flat bed, q is given by

$$q = \begin{cases} u_m \sin(kx) & 0 < x < \lambda/2 \\ 0 & \text{otherwise} \end{cases} \tag{3.18}$$

Since q is a velocity, it is normalized by u_m as follows:

$$q^* = \frac{q}{u_m} = \begin{cases} \sin(x^*) & 0 < x^* < \pi \\ 0 & \text{otherwise} \end{cases} \tag{3.19}$$

The sinusoidal pumping model is based on the assumption that the bedforms are two-dimensional and periodic. The average value of the flow into the bed ($\overline{q}$) is determined by integrating q over the bedform wavelength λ.

$$\overline{q} = \frac{1}{\lambda}\int_0^{\lambda/2} q\,dx = \frac{1}{\lambda}\int_0^{\lambda/2} u_m \sin(kx)\,dx = \frac{u_m}{\pi} \tag{3.20}$$

$$\overline{q}^* = \frac{\overline{q}}{u_m} = \frac{1}{\pi} \tag{3.21}$$

It is assumed that the bed surface is "flat" (see Section 3.1).

The spatially averaged residence time function $\overline{R}_T(\tau)$ represents the fraction of solute which enters the bed at time t_0 and remains in the bed at time $t_0+\tau$. Since the flux of the solute into the surface varies with position x_0, $R_T(x_0,\tau)$ must be weighted by q to determine $\overline{R}_T(\tau)$. The appropriate formula for averaging (assuming a "flat" bed) is

$$\overline{R}_T(\tau) = \frac{\overline{qR_T}}{\overline{q}} = \frac{\frac{1}{\lambda}\int_0^{\lambda/2} q(x)\,R_T(\tau,x)\,dx}{\overline{q}} \tag{3.22}$$

For Elliott's sinusoidal pumping model, an implicit relation for $\overline{R}_T$ is given by

$$\frac{\tau^*}{\theta} = \frac{2\cos^{-1}\overline{R}_T}{\overline{R}_T} \tag{3.23}$$

Figure 3.3 shows the residence time function for the sinusoidal pumping model.

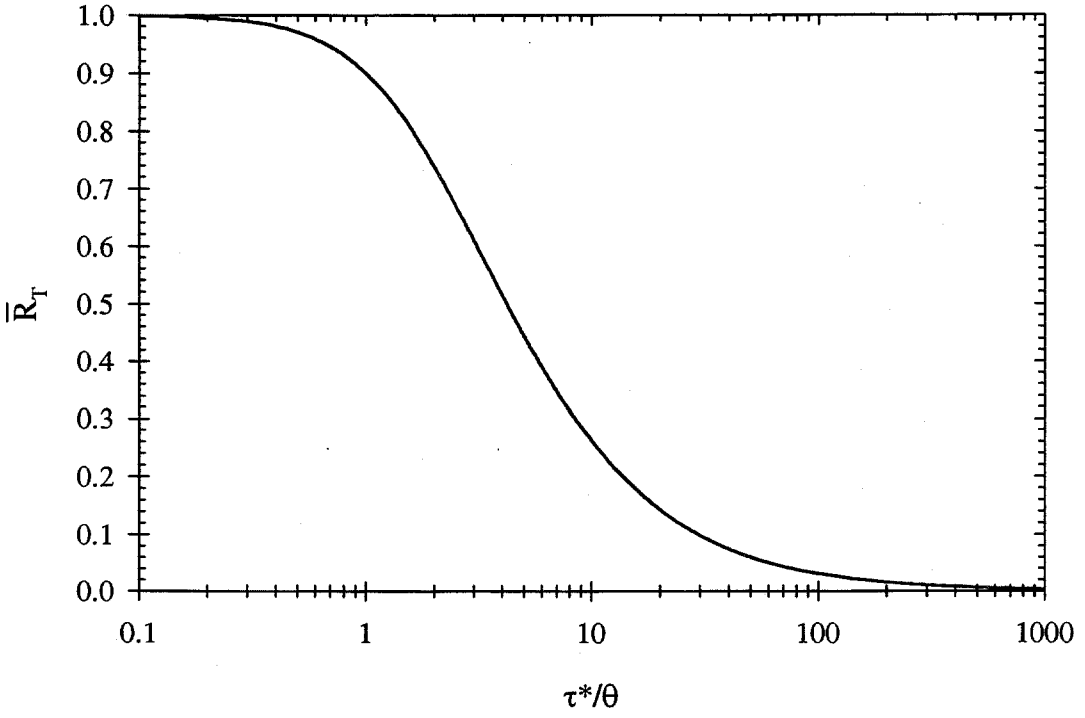

Figure 3.3. Residence time function for nonsorbing solute using the sinusoidal pumping model.

Once $\overline{R}_T$ has been determined, the mass transfer into the bed can be calculated. The mass of solute which entered the bed over a small time increment $d\tau$ at a past time $t-\tau$ is $\overline{q}\, C(t-\tau)\, d\tau$ per unit plan area of the bed. At time t, a fraction $\overline{R}_T(\tau)$ of this mass remains in the bed. The incremental contribution to the mass at time t from flux into the bed at a past time $(t-\tau)$ is

$$\overline{q}\, \overline{R}_T(\tau)\, C(t-\tau)\, d\tau \tag{3.24}$$

The accumulated mass transfer from all elapsed time τ is

$$m(t)C_0 = \overline{q} \int_0^\infty \overline{R}_T(\tau)\, C(t-\tau)\, d\tau \tag{3.25}$$

where m is the accumulated mass per unit plan area of the bed divided by the initial concentration C_0. The parameters m and C are normalized as follows:

$$m^* = km \tag{3.26}$$

$$C^* = \frac{C}{C_0} \tag{3.27}$$

Elliott used a different normalization for m [$m^* = (2\pi k/\theta)m$]. Since the quantity m has the dimensions of length, m is normalized here in the same manner as other variables having length dimensions. The normalized form of Equation (3.25) is

$$m^*\left(\frac{t^*}{\theta}\right) = \frac{\theta}{\pi}\int_0^{\infty} \overline{R}_T\left(\frac{\tau^*}{\theta}\right) C^*\left(\frac{t^*}{\theta} - \frac{\tau^*}{\theta}\right) d\left(\frac{\tau^*}{\theta}\right) \tag{3.28}$$

In order to evaluate Equation (3.28), the time history of the concentration in the water column must be known. In the special case when there is no solute in the bed at t = 0, Equation (3.28) can be simplified to

$$m^*\left(\frac{t^*}{\theta}\right) = \frac{\theta}{\pi}\int_0^{t^*/\theta} \overline{R}_T\left(\frac{\tau^*}{\theta}\right) C^*\left(\frac{t^*}{\theta} - \frac{\tau^*}{\theta}\right) d\left(\frac{\tau^*}{\theta}\right) \tag{3.29}$$

3.2.1. Application to a closed system

In the recirculating flume, there are no losses of a conservative solute apart from those to the bed. The increase of the solute mass in the bed equals the decrease in the water column, which can be expressed by

$$\frac{dm}{dt} = -d'\frac{dC^*}{dt} \tag{3.30}$$

where d' is an effective water depth in the flume defined as the ratio

$$d' = \frac{V}{A_b} \tag{3.31}$$

where V is the total volume of water in the flume system excluding porewater and A_b is the plan area of the sediment bed. With the initial conditions m(0) = 0 and C*(0) = 1, the solution to Equation (3.30) is

$$C^*(t) = 1 - \frac{m(t)}{d'} \tag{3.32}$$

The normalized form of Equation (3.32) is given by

$$C^*\left(\frac{t^*}{\theta}\right) = 1 - \frac{m^*\left(t^*/\theta\right)}{d^*} \tag{3.33}$$

where d* is the normalized effective water depth equal to kd'.

The system of two coupled Equations (3.29) and (3.33) must be solved to predict the mass transfer in the recirculating flume.

3.3. Bed Exchange for Linearly Adsorbing Compounds

Eylers (1994) modified Elliott's residence time model to incorporate equilibrium linear adsorption of a chemical to the sediment. Eylers observed that equilibrium adsorption retards the concentration front in the sediment bed similar to that observed for chemical transport in groundwater. The advection-dispersion equations for a unit volume of sediment along a streamline is

$$\theta \frac{\partial C}{\partial t} + w \frac{\partial C}{\partial s} = \theta D \frac{\partial^2 C}{\partial s^2} - \rho_b \frac{\partial S}{\partial t} \tag{3.34}$$

where s is the coordinate along the streamline, w is the Darcy velocity in the s-direction, C is the aqueous concentration of the contaminant, S is the concentration of the contaminant on the solid, ρ_b is the dry bulk density of the sediment and D is the dispersion coefficient.

Equilibrium linear adsorption is represented by

$$S = K_d C \tag{3.35}$$

where K_d is the partition coefficient. With linear adsorption, the advection-dispersion equation becomes

$$\left(1+\frac{\rho_b}{\theta}K_d\right)\frac{\partial C}{\partial t} + \frac{w}{\theta}\frac{\partial C}{\partial s} = D\frac{\partial^2 C}{\partial s^2} \tag{3.36}$$

The retardation coefficient is defined as

$$R = 1 + \frac{\rho_b}{\theta}K_d \tag{3.37}$$

The total mass of the chemical per unit bulk volume of the sediment increases by a factor of R. The velocity of the concentration front for the linearly adsorbing compound is reduced by a factor of R compared to the seepage velocity; and therefore, the linearly adsorbing compound has a longer residence time in the sediment bed when compared to a nonsorbing solute.

Eylers concluded that the flux-weighted mean residence time function $\overline{R}_T$ for a linearly adsorbing chemical can be calculated by changing τ^*/θ in Equation (3.23) to $\tau^*/\theta R$:

$$\frac{\tau^*}{\theta R} = \frac{2\cos^{-1}\overline{R}_T}{\overline{R}_T} \tag{3.38}$$

Figure 3.4 compares the residence time function $\overline{R}_T$ for nonsorbing solutes (R = 1) and linearly adsorbing compounds having retardation coefficients of 5, 20 and 50.

The coupled equations that must be used to solve the mass exchange of a linearly adsorbing chemical in the recirculating flume are

$$m^*\left(\frac{t^*}{\theta}\right) = \frac{\theta}{\pi}\int_0^{t^*/\theta}\overline{R}_T\left(\frac{\tau^*}{\theta}, R\right)C^*\left(\frac{t^*}{\theta}-\frac{\tau^*}{\theta}\right)d\left(\frac{\tau^*}{\theta}\right) \tag{3.39}$$

$$C^*\left(\frac{t^*}{\theta}\right) = 1 - \frac{m^*\left(t^*/\theta\right)}{d^*} \tag{3.40}$$

where $\overline{R}_T$ is now calculated according to Equation (3.38), which includes the retardation coefficient. Thus, the only change in modeling from the nonsorbing case is the inclusion of the retardation coefficient R in the equation for the residence time function $\overline{R}_T$, but not anywhere else.

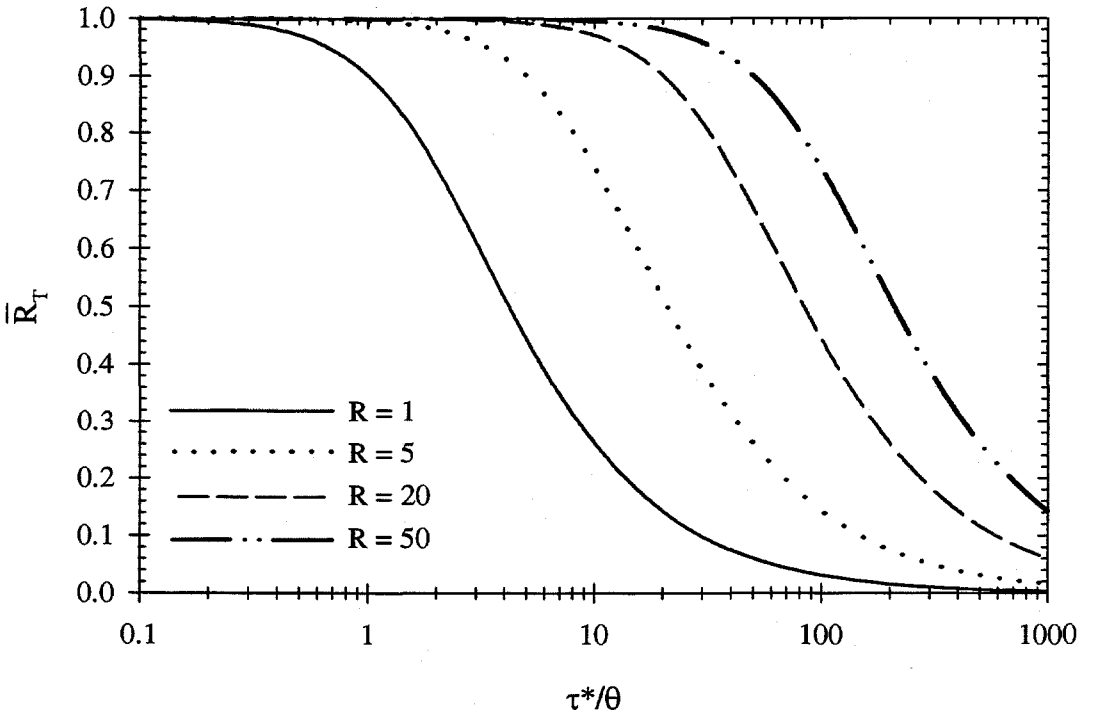

Figure 3.4. Residence time function for different retardation factors.

3.3.1. Validity of equilibrium adsorption assumption in pumping model

Equilibrium adsorption can be assumed if the characteristic advection time in the bed (t_{pump}) is long compared to the adsorption time scale (t_{ads}). Eylers (1994) formulated a non-dimensional number Γ_p that can be used to determine the validity of the equilibrium adsorption assumption in the pumping model:

$$\Gamma_p = \frac{t_{ads}}{t_{pump}} \tag{3.41}$$

The characteristic advection time can be approximated by the time at which the non-dimensional time t* equals one (i.e., $t_{pump} = 1/ku_m$). Then Γ_p becomes

$$\Gamma_p = (ku_m)\, t_{ads} \tag{3.42}$$

where t_{ads} is determined experimentally. The equilibrium assumption holds when t_{pump} is large compared to t_{ads}:

$$\begin{aligned} \Gamma_p << 1 \quad &\Rightarrow \quad \text{equilibrium adsorption} \\ \Gamma_p >> 1 \quad &\Rightarrow \quad \text{non} - \text{equilibrium} \end{aligned} \tag{3.43}$$

This criterion does not necessarily imply local equilibrium at every point in the bed.

3.4. BED EXCHANGE FOR NONLINEARLY ADSORBING COMPOUNDS

For nonlinearly adsorbing compounds, the residence time of the chemical in the sediment bed depends upon its concentration history in the bed. This fact makes it very difficult to formulate a generalized residence time function for a bed exchange model. A different modeling approach is required.

In this section, a detailed model that simulates the bed exchange of a nonlinearly adsorbing compound is presented. First, the relevant transport equations are developed for nonlinearly adsorbing compounds in porous media. Then the conditions for which the transport of linearly and nonlinearly adsorbing compounds differs significantly are discussed. The bed exchange model is then formulated. The model solves the advection equation (neglecting dispersion and molecular diffusion) for the transport of nonlinearly adsorbing compounds through a series of streamtubes in the sediment bed and then calculates the resulting flux of the compound into and out of the bed surface. Examples that illustrate the effects of nonlinear adsorption upon the bed/stream exchange of chemicals will be presented.

3.4.1. Advection equation for the transport of contaminants in the bed

The transport of pollutants in porous media is described by the advection-dispersion equation. In the bed exchange model, it is assumed that the dispersive transport is negligible. This assumption is supported by the following:

1. The adsorption isotherms used in the models exhibit a convex shape with respect to the aqueous concentration (see Figure 2.4 in Chapter 2). When the concentration in the overlying water column exceeds the initial concentration in the bed, such isotherms produce self-sharpening concentration fronts, which counter the effects of dispersion (Bosma and van der Zee, 1993). However, at small concentrations where the slope of the nonlinear isotherm is steep, dispersive transport may become important (Berglund and Cvetkovic, 1996). The concentrations in the flume experiments are large enough to justify neglecting pore scale dispersion.

2. Elliott's model studies demonstrate that longitudinal dispersion has a minor effect on the predicted mass exchange of a nonsorbing tracer when $\lambda/d_g \geq 180$. This criterion will be satisfied for the situations in which the model will be applied.

Since dispersion is neglected, the advection equation is used to model transport of a nonlinearly adsorbing compound in the sediment bed. The sediment bed is divided into a series of two-dimensional streamtubes bounded by streamlines (as in Figure 3.2c), which start at equal intervals along the x-axis. The properties of the streamtubes are discussed in Section 3.4.3. The advection equation in a streamtube is

$$\theta\frac{\partial(A_s C)}{\partial t} + \frac{\partial(Q_s C)}{\partial s} + \rho_b\frac{\partial(A_s S)}{\partial t} = 0 \tag{3.44}$$

where s is the coordinate along the streamtube, A_s is the cross-sectional area of the streamtube normal to s and Q_s is the Darcy flow rate in the tube. Steady flow is assumed and, therefore, Q_s is constant in each streamtube and A_s does not depend on time. Equation (3.44) reduces to

$$\frac{\partial C}{\partial t} + \frac{w(s)}{\theta}\frac{\partial C}{\partial s} + \frac{\rho_b}{\theta}\frac{\partial S}{\partial t} = 0 \tag{3.45}$$

where ρ_b is the bulk density of the dry sediment and w(s) is

$$w(s) = \frac{Q_s}{A_s(s)} \tag{3.46}$$

3.4.2. General transport behavior of nonlinearly adsorbing compounds in porous media

Analytical solutions of the advection equation will be presented for the transport of nonlinearly adsorbing compounds in a one-dimensional column with constant cross-sectional area and steady flow rate. These solutions demonstrate the general transport behavior of nonlinearly adsorbing compounds in porous media, and will be adapted later into the detailed bed/stream exchange model.

For equilibrium adsorption,

$$S = f(C) \tag{3.47}$$

$$\frac{\partial S}{\partial t} = \frac{dS}{dC}\frac{\partial C}{\partial t} = f'(C)\frac{\partial C}{\partial t} \tag{3.48}$$

where f(C) is the equation for the adsorption isotherm and f'(C) is its derivative with respect to C. In this case, the advection equation, which is given by Equation (3.45), becomes

$$\sigma(C)\frac{\partial C}{\partial t} + w_s\frac{\partial C}{\partial s} = 0 \tag{3.49}$$

where w_s is a constant seepage velocity (w/θ) and σ (C) is

$$\sigma(C) = 1 + \frac{\rho_b}{\theta} f'(C) \tag{3.50}$$

Table 3.1 lists the functions f(C) and σ(C) for different adsorption isotherms (see Section 2.3.2 in Chapter 2).

Table 3.1. Functions used in the advection equation for different adsorption isotherms.

Isotherm	f (C)	σ (C)
No adsorption	0	1
Linear	$K_d C$	$R = 1 + \frac{\rho_b}{\theta} K_d$
Langmuir	$\frac{S_T K_L C}{1 + K_L C}$	$1 + \frac{\rho_b}{\theta} \frac{S_T K_L}{(1 + K_L C)^2}$
Freundlich $0 < \alpha < 1$	$K_F C^{\alpha}$	$1 + \frac{\rho_b}{\theta} \frac{\alpha K_F}{C^{1-\alpha}}$
Langmuir-Freundlich $0 < \alpha < 1$	$\frac{S_T (K_{LF} C)^{\alpha}}{1 + (K_{LF} C)^{\alpha}}$	$1 + \frac{\rho_b}{\theta} \frac{\alpha S_T (K_{LF} C)^{\alpha}}{C \left(1 + (K_{LF} C)^{\alpha}\right)^2}$
Tóth $0 < \alpha < 1$	$\frac{S_T K_T C}{\left(1 + (K_T C)^{\alpha}\right)^{1/\alpha}}$	$1 + \frac{\rho_b}{\theta} \frac{S_T K_T}{\left(1 + (K_T C)^{\alpha}\right)^{\frac{\alpha+1}{\alpha}}}$

The initial and boundary conditions are taken as

$$C(s,0) = h(s), \qquad 0 \le s \le L \tag{3.51}$$

$$C(0,t) = g(t), \qquad 0 \le t \tag{3.52}$$

where L is the length of the column.

The concentration profiles for nonsorbing solutes travel unperturbed with the same velocity as the fluid. The solution to Equation (3.49) for nonsorbing compounds is

$$C(s,t) = \begin{cases} h(s - w_s t), & t < \dfrac{s}{w_s} \\ g\left(t - \dfrac{s}{w_s}\right), & t \geq \dfrac{s}{w_s} \end{cases} \tag{3.53}$$

For each position s and time t, Equation (3.53) simply states that the initial distribution in the column is pushed out as a slug and replaced with the boundary values at a earlier time s/w_s.

The concentration profiles for linearly adsorbing compounds are also unperturbed but travel at a slower velocity equal to w_s/R, where R is the retardation coefficient defined in Equation (3.37) ($R > 1$). This phenomenon is referred to as retardation because the speed of replacement of the initial concentration profile is reduced by the factor R. With retardation, the solution to Equation (3.49) for a linearly adsorbing compound is

$$C(s,t) = \begin{cases} h\left(s - \dfrac{w_s t}{R}\right), & t < \dfrac{Rs}{w_s} \\ g\left(t - \dfrac{Rs}{w_s}\right), & t \geq \dfrac{Rs}{w_s} \end{cases} \tag{3.54}$$

For the various cases of nonlinear adsorption, Equation (3.49) can be solved using the method of characteristics. The characteristic differential equations are given by

$$\frac{dt}{dT} = \sigma(C) \tag{3.55}$$

$$\frac{ds}{dT} = w_s \tag{3.56}$$

$$\frac{dC}{dT} = 0 \tag{3.57}$$

where T is the characteristic parameter than runs along the characteristic curves. Equation (3.57) implies that the aqueous concentration C is constant along the characteristic curves. The characteristic direction in the (s, t)-plane is

$$\frac{dt}{ds} = \frac{\sigma(C)}{w_s} \tag{3.58}$$

Since C is constant along the characteristics, the characteristic curves are straight lines with slopes in the (s,t)-plane defined by Equation (3.58). The solution can be constructed by tracing the characteristics from points along the initial curves defined by Equations (3.51) and (3.52). Solutions to Equation (3.49) will be illustrated for two cases having different initial and boundary conditions. These cases will identify the circumstances for which the transport of nonlinearly adsorbing compounds differs significantly from that for linearly adsorbing compounds.

3.4.2.1. Case 1: Step increase in concentration

In the first case, there is a step increase in the concentration at the inlet of an initially clean column. Under this condition, it will be shown that the transport of linearly and nonlinearly adsorbing compounds is essentially the same.

The initial and boundary conditions are

$$C(s,0) = 0, \qquad 0 \le s \le L \tag{3.59}$$

$$C(0,t) = C_0, \qquad 0 \le t \tag{3.60}$$

where $C_0 > 0$. The general shape of the characteristic curves for the Langmuir and Tóth isotherms are shown in Figure 3.5a, and those for the Freundlich and Langmuir-Freundlich isotherms in Figure 3.5b. The plots of the characteristic solutions for the Freundlich and Langmuir-Freundlich isotherms are distinguished from the plots for the Langmuir and Tóth isotherms because when C=0 the slope of the characteristics for the Freundlich and Langmuir-Freundlich isotherms is infinite.

(a) Langmuir and Tóth isotherms

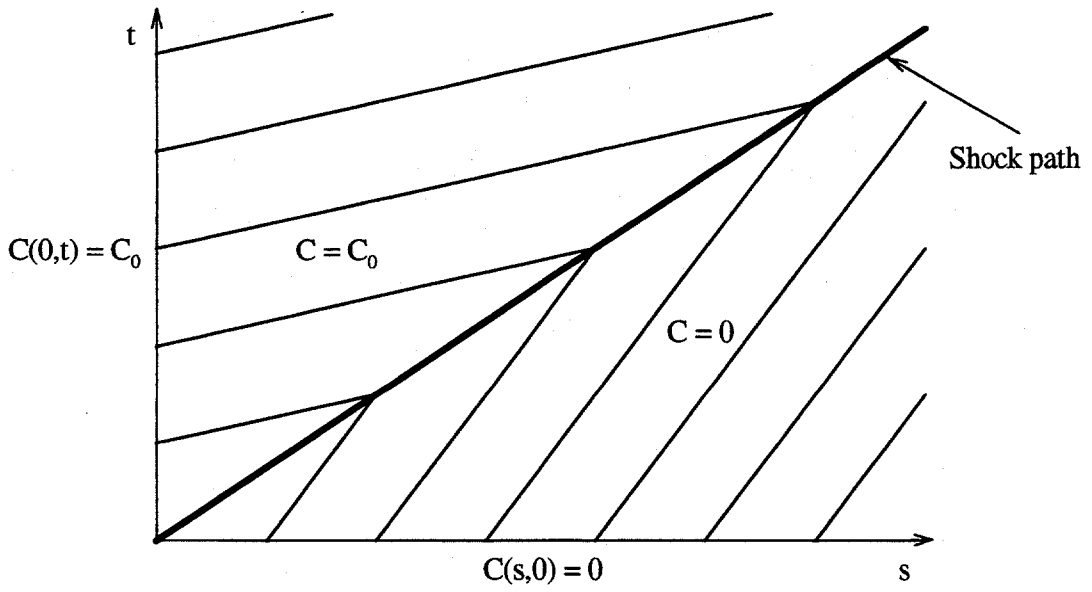

(b) Freundlich and Langmuir-Freundlich isotherms

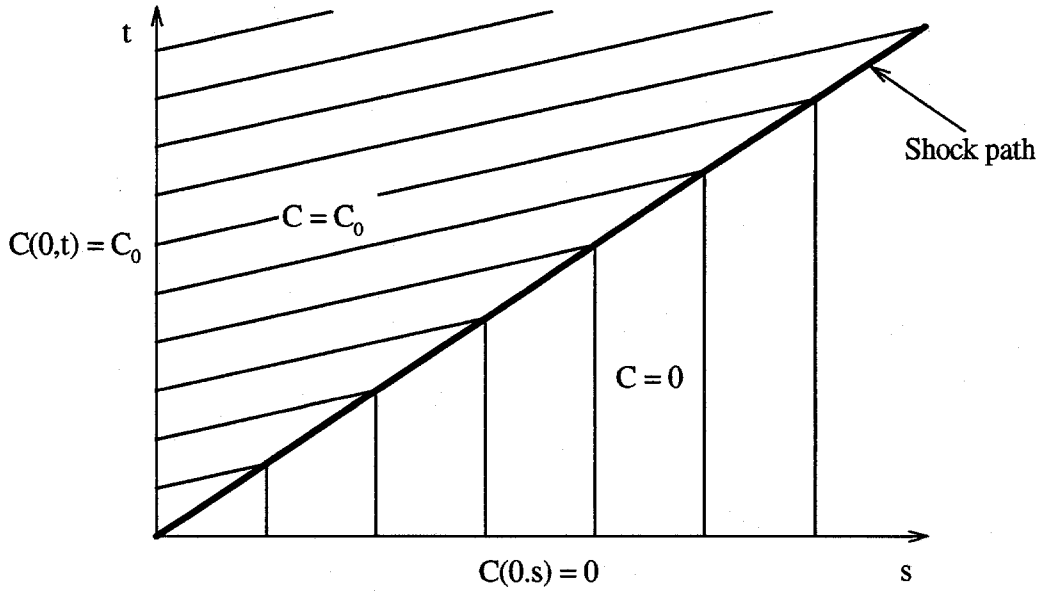

Figure 3.5. Representative characteristic curves resulting from a step increase in the feed concentration of a column for Langmuir, Tóth, Freundlich and Langmuir-Freundlich isotherms for an initially clean column.

At the inlet of the column, the boundary condition defined by Equation (3.60) creates a discontinuity. Since $\sigma(C_0) < \sigma(0)$ for all of the nonlinear isotherms considered, a genuine shock forms at the origin and propagates through the column (Rhee et al., 1986). The slope of the shock path (i.e., the jump condition) is

$$\left.\frac{dt}{ds}\right|_{shock} = \frac{1}{w_s}\left(1 + \frac{\rho_b}{\theta}\frac{f(C_0) - f(0)}{C_0}\right) = \frac{\tilde{\sigma}(C_0,0)}{w_s} \tag{3.61}$$

The shock travels with speed v_{shock} given by

$$v_{shock} = \frac{w_s}{\tilde{\sigma}(C_0,0)} \tag{3.62}$$

where "0" in Equations (3.61) and (3.62) may be replaced by any other concentration value less than C_0. For $C = 0$, we expect $f(0) = 0$.

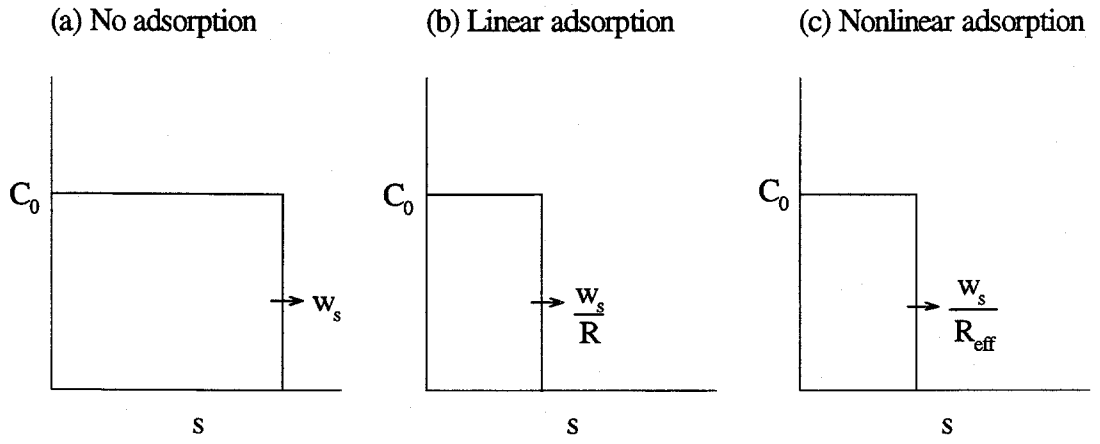

Figure 3.6. Concentration profiles at $t > 0$ for a step increase in the feed concentration for an initially clean column.

Figure 3.6 illustrates the resulting concentration profiles for (a) nonsorbing, (b) linearly adsorbing and (c) nonlinearly adsorbing tracers. The nonlinearly adsorbing compound acts the same as a linearly adsorbing compound having an effective retardation coefficient R_{eff} equal to $\tilde{\sigma}(C_0,0)$. The formulas for $\tilde{\sigma}(C_0,0)$ are listed in

Table 3.2. A simple way to visualize the result is to observe that in this case only the isotherm values at the end points matter (i.e., f(0) and $f(C_0)$) and that R_{eff} is simply based on the slope of the chord connecting these points on the isotherm graph (i.e., $f(C_0)/C_0$) (see Figure 3.7).

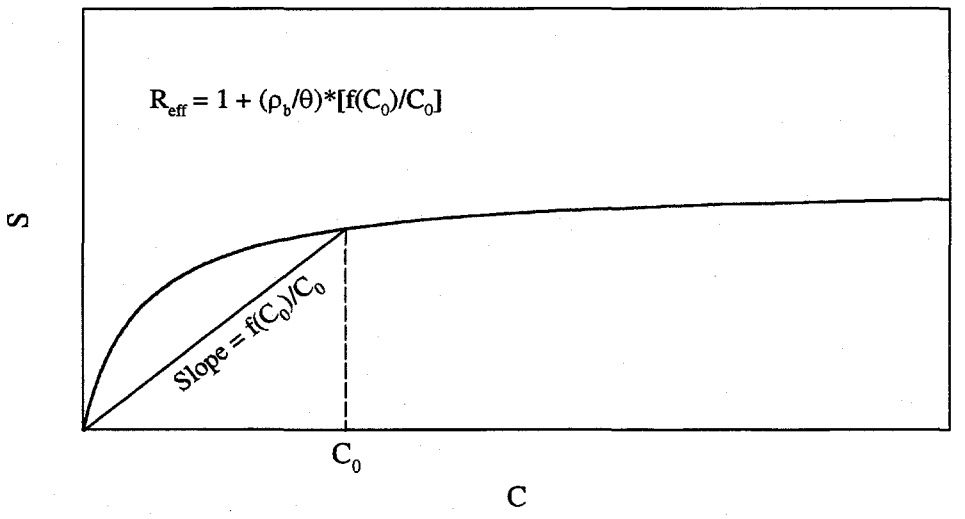

Figure 3.7. Definition of the effective retardation coefficient R_{eff}. R_{eff} is related to the slope of the chord from the origin to a point on the isotherm.

Table 3.2. Formulas $R_{eff} = \tilde{\sigma}(C_0,0)$ for a step increase in the feed concentration of a column.

Isotherm	$R_{eff} = \tilde{\sigma}(C_0,0)$
Langmuir	$1 + \frac{\rho_b}{\theta}\frac{S_T K_L}{1+K_L C_0}$
Freundlich	$1 + \frac{\rho_b}{\theta}\frac{K_F}{C_0^{1-\alpha}}$
Langmuir-Freundlich	$1 + \frac{\rho_b}{\theta}\frac{S_T (K_{LF}C_0)^{\alpha}}{C_0\left(1+(K_{LF}C_0)^{\alpha}\right)}$
Tóth	$1 + \frac{\rho_b}{\theta}\frac{S_T K_T}{\left(1+(K_T C_0)^{\alpha}\right)^{1/\alpha}}$

3.4.2.2. Case 2: Pulse change in concentration

For this case, a pulse of a pollutant is injected into the column during the interval $0 < t < t_1$. It will be demonstrated that the transport of nonlinearly adsorbing compounds, which are characterized by the isotherms listed in Table 3.1, differs significantly from linearly adsorbing compounds.

The initial and boundary conditions are

$$C(s,0) = 0, \qquad 0 \le s \le L \tag{3.63}$$

$$C(0,t) = \begin{cases} C_0, & 0 \le t \le t_1 \\ 0, & t_1 < t \end{cases} \tag{3.64}$$

The representative characteristic curves for the nonlinearly adsorbing compounds are illustrated in Figure 3.8. For $t < t_1$, the solution is the same as Case 1. When the injection is stopped at $t = t_1$, another discontinuity appears at the inlet of the column. All of the concentrations between $C = 0$ and $C = C_0$ are present, and the characteristics fan out to give a centered, simple wave which expands with time.

The forward edge of the simple wave is bounded by the characteristic bearing the maximum concentration C_0. The speed at which the front edge of this wave travels is $w_s/\sigma(C_0)$. Because of the convexity of the isotherm, $\sigma(C_0) < \tilde{\sigma}(C_0,0)$; and the simple wave travels faster than the initial shock and catches up with it at $t = t_A$ (see Figure 3.8).

For $t > t_A$, the simple wave continuously overtakes the shock. The concentration on the left side of the shock constantly decreases while the concentration on the right side remains zero. The velocity of the shock also decreases because $\tilde{\sigma}(C,0)$ increases as C decreases.

(a) Langmuir and Tóth isotherms

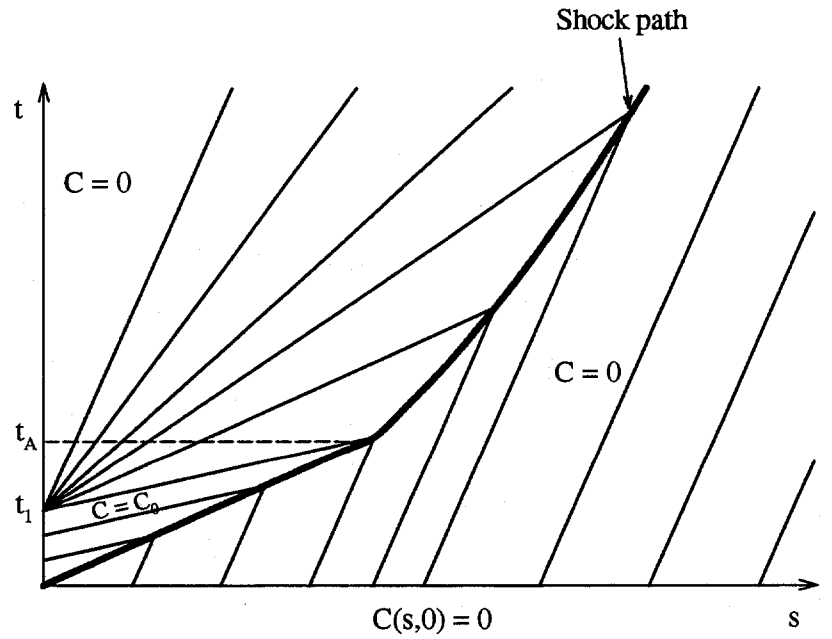

(b) Freundlich and Langmuir-Freundlich isotherms

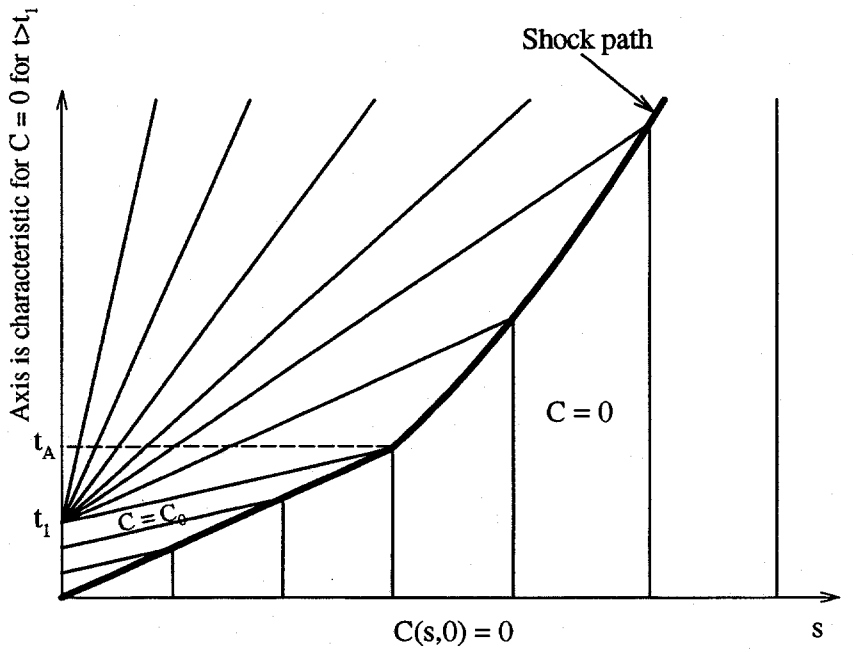

Figure 3.8. Representative characteristics for a pulse injection of a nonlinearly adsorbing compound into an initially clean column.

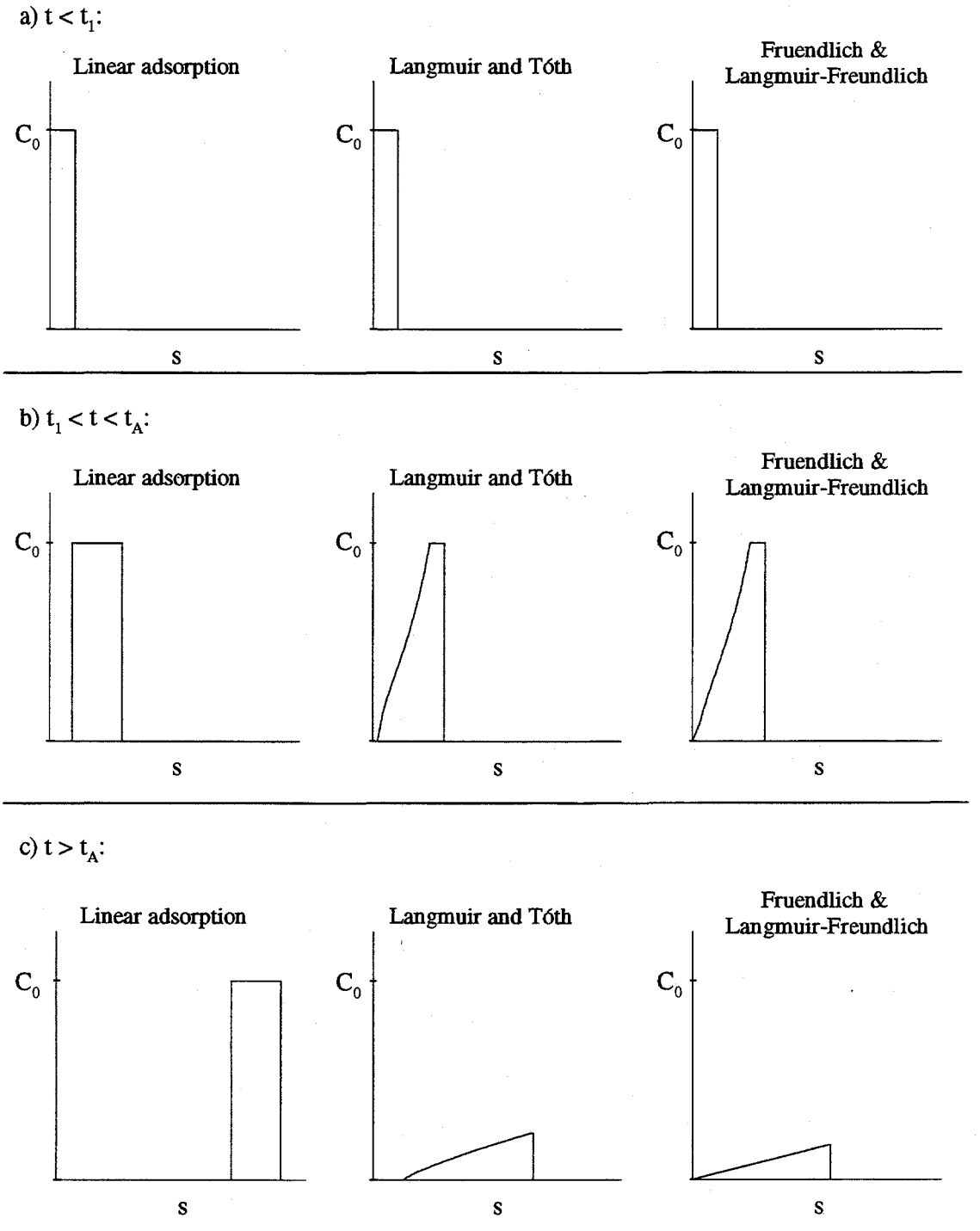

Figure 3.9. Comparison of representative concentration profiles at different times for a pulse injection of linearly and nonlinearly adsorbing compounds into an initially clean column.

Representative concentration profiles for linearly adsorbing and nonlinearly adsorbing compounds in the column are depicted in Figure 3.9. For a linearly adsorbing compound, all concentrations travel with the same velocity w_s/R and the square shape of the concentration pulse is preserved. Conversely, for nonlinearly adsorbing compounds, different concentrations move with different velocities. For the isotherms considered here, high concentrations travel faster than small concentrations. Consequently, the concentration pulse for the nonlinearly adsorbing compounds expands along the length of the column with a corresponding decrease in the aqueous concentration. The resulting breakthrough curves exhibit extensive tailing. The value of $\sigma(0)$ is finite for the Langmuir and Tóth isotherms and infinite for the Freundlich and Langmuir-Freundlich isotherms. Therefore, the tailing is more notable for the Freundlich and Langmuir-Freundlich isotherms.

When the pollutant concentration in the overlying water column is fairly constant, the solution to Case 1 implies that the mass transfer of a nonlinearly adsorbing compound can be modeled using Eylers' model, which applies the modified residence time function, with an appropriate choice of the retardation coefficient. However, when the concentration in the overlying water column is variable, the magnitude of the nonlinear effects should be considered.

3.4.3. Detailed model for the bed exchange of nonlinearly adsorbing compounds

The mass transfer of nonlinearly adsorbing compounds between the stream water and the sediment bed is calculated as follows:

1. The initial values are specified for the following: the total mass of the pollutant in the bed, the concentration distribution of the pollutant in the streamtubes, and the concentration of the pollutant in the overlying water column.

2. During a small time dt, the flux of pollutant and resulting change of pollutant mass in the bed is calculated.
3. The concentration profile of the pollutant along each streamtube is determined by solving the advection equation.
4. For the closed system, the pollutant concentration in the overlying water column at t+dt is computed.
5. Steps 2 through 4 are repeated for the next time step.

Figure 3.10 depicts a streamtube within the sediment bed. The streamtube is bounded by two streamlines separated by a small distance dX_0 at the bed surface. The coordinate s follows a streamline that begins X_0, which is the x-coordinate at the mid-point of the streamtube inlet.

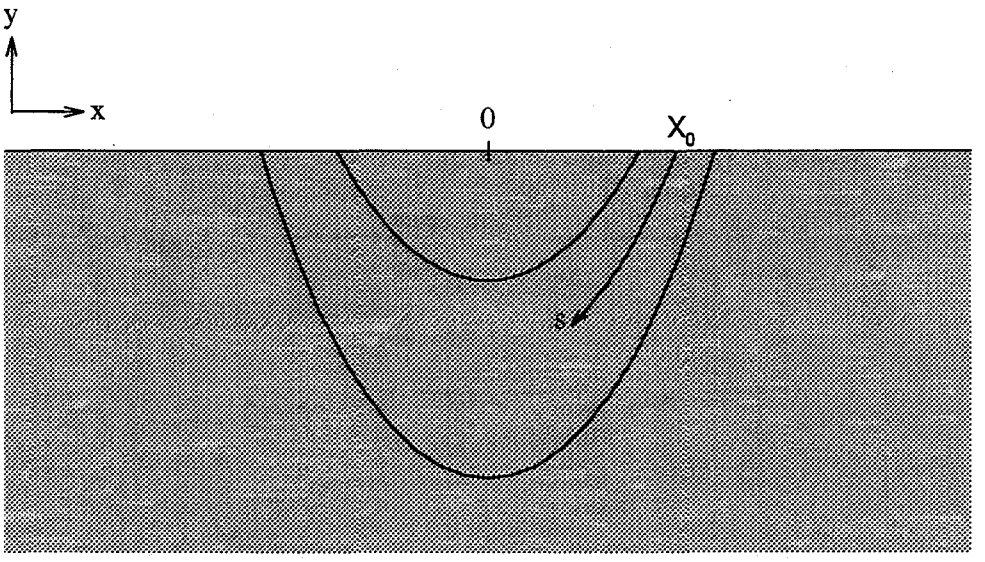

Figure 3.10. Diagram of streamtube in sediment bed. The diagram is **not** to scale. The size of the streamtube is exaggerated for illustrative purposes.

Elliott's pumping model presented in Section 3.1 is used to calculate coordinates of the streamlines and the flow within the tube. Equation (3.65) defines the coordinate s in terms of the rectangular coordinates (X,Y):

$$\begin{aligned} s &= \int ds \\ &= \int \sqrt{dx^2 + dy^2} \\ &= \int_{X}^{X_0} \sec(kx)\, dx \\ &= \frac{1}{k} \ln\left[\frac{\tan\left(\frac{\pi}{4} + \frac{kX_0}{2}\right)}{\tan\left(\frac{\pi}{4} + \frac{kX}{2}\right)} \right] \end{aligned} \tag{3.65}$$

where $-X_0 < X < X_0$ and $0 < X_0 < \lambda/4$. The non-dimensional form with $s^* = ks$ is given by

$$s^* = \ln\left[\frac{\tan\left(\frac{\pi}{4} + \frac{X_0^*}{2}\right)}{\tan\left(\frac{\pi}{4} + \frac{X^*}{2}\right)} \right] \tag{3.66}$$

where $-\pi/2 < X^* < X_0^*$ and $0 < X_0^* < \pi/2$. The total length of a streamtube is

$$L = \frac{1}{k} \ln\left[\frac{\tan\left(\frac{\pi}{4} + \frac{kX_0}{2}\right)}{\tan\left(\frac{\pi}{4} - \frac{kX_0}{2}\right)} \right] \tag{3.67}$$

$$L^* = \ln\left[\frac{\tan\left(\frac{\pi}{4} + \frac{X_0^*}{2}\right)}{\tan\left(\frac{\pi}{4} - \frac{X_0^*}{2}\right)} \right] \tag{3.68}$$

The magnitude of the Darcy velocity at s is

$$\begin{aligned} w(s(X,Y)) &= \left(u^2 + v^2\right)^{1/2} \\ &= u_m\, e^{kY} \\ &= u_m \left(\frac{\cos(kX_0)}{\cos(kX)}\right) \end{aligned} \tag{3.69}$$

By using Equations (3.5), (3.6) and (3.16), the formula for w in terms of s is

$$w(s) = u_m \cos(kX_0)\left\{\cos\left[2\tan^{-1}\left(e^{-ks}\tan\left(\frac{\pi}{4}+\frac{kX_0}{2}\right)\right) - \frac{\pi}{2}\right]\right\}^{-1} \tag{3.70}$$

The velocity w is normalized by u_m and is expressed as

$$w^*(s^*) = \cos(X_0^*)\left\{\cos\left[2\tan^{-1}\left(e^{-s^*}\tan\left(\frac{\pi}{4}+\frac{X_0^*}{2}\right)\right) - \frac{\pi}{2}\right]\right\}^{-1} \tag{3.71}$$

The mass exchange with the bed is determined by calculating the flux of chemical into and out of each streamtube. There are two identical sets of streamtubes associated with each bedform (see Figure 3.2). The flux is computed for the streamtubes starting in the interval $0 < X_0^* < \pi/2$ and then multiplied by two. The mass transfer over the entire bed is calculated by multiplying the result for one bedform by the number of bedforms on the bed. The mass exchange with the bed during a small time Δt is

$$\begin{aligned} \Delta(\text{mass in bed}) &= (\text{No. of bedforms}) \cdot 2 \cdot \sum_j (\text{mass added} - \text{mass removed})_{\text{tube } j} \\ &= \left(\frac{L_b}{\lambda}\right) 2 \sum_{j=1}^{N} q(X_{0,j})\left(C_{b,j}(0) - C_{b,j}(L_j)\right) dX_{0,j}\, b\, \Delta t \end{aligned} \tag{3.72}$$

where

L_b = length of bed

λ = average bedform wavelength

N = number of streamtubes

qdX_{0j} = Darcy flow into tube *j* given by Equation (3.18) at $x=X_0$

X_{0j} = value of x at the centerline of the *j*th streamtube at the inlet on the bed surface

$C_{b,j}(0)$ = concentration of chemical at inlet of *j*th streamtube which equals C_w

C_w = concentration of chemical in overlying water column

$C_{b,j}(L_j)$ = concentration of chemical at outlet of streamtube *j* computed by solving the advection equation along the streamtube

L_j = length of *j*th streamtube

$dX_{0,j}$ = width of inlet for streamtube *j* at bed surface

Δt = time interval used for calculation

b = width of bed

Equation (3.72) reduces to an expression for the mass in the bed per unit plan area of the bed:

$$C_0 \Delta m = \frac{2}{\lambda} \sum_{j=1}^{N} u_m \sin(kX_{0,j}) \left(C_w(t) - C_{b,j}(L_j, t)\right) dX_{0,j} \Delta t \tag{3.73}$$

The non-dimensional form is

$$\Delta m^* = \frac{\theta}{\pi} \sum_{j=1}^{N} \sin(X^*_{0,j}) \left(C^*_w\left(\frac{t^*}{\theta}\right) - C^*_{b,j}\left(L^*_j, \frac{t^*}{\theta}\right)\right) dX^*_{0,j} \Delta\left(\frac{t^*}{\theta}\right) \tag{3.74}$$

where L^*_j equals kL_j. In the closed system, the concentration in the overlying water column is given by

$$C^*_w\left(\frac{t^*}{\theta} + \Delta\left(\frac{t^*}{\theta}\right)\right) = \frac{C^*_w\left(t^*/\theta\right) d^* - \Delta m^*}{d^*} \tag{3.75}$$

where the normalized effective water depth d* equals kd', with d' representing the effective water depth in the flume.

3.4.3.1. Numerical solution of the advection equation in a streamtube

By Equation (3.49), the advection equation with generalized equilibrium adsorption for a streamtube is

$$\sigma(C_b)\frac{\partial C_b}{\partial t} + \frac{w(s)}{\theta}\frac{\partial C_b}{\partial s} = 0 \tag{3.76}$$

where $C_b(s,t)$ is the concentration of the pollutant in the porewater of the bed. The slope of the characteristic curves is not constant because w(s) changes with position.

$$\frac{dt}{ds} = \frac{\theta\sigma(C_b)}{w(s)} = \theta\sigma(C_b)\frac{\cos\left[2\tan^{-1}\left(e^{-ks}\tan\left(\frac{\pi}{4}+\frac{kX_0}{2}\right)\right)-\frac{\pi}{2}\right]}{u_m\cos(kX_0)} \tag{3.77}$$

The characteristics are not straight lines and a closed form solution for $C_b(s,t)$ cannot be derived. Consequently, the advection equation is solved numerically using a finite difference method with flux-corrected transport as outlined by Finlayson (1992). The advection equation can be written as

$$\frac{\partial G}{\partial t} + \frac{w(s)}{\theta}\frac{\partial C_b}{\partial s} = 0 \tag{3.78}$$

where G is defined as the column isotherm given by

$$G = C_b + \frac{\rho_b}{\theta}f(C_b) \tag{3.79}$$

This form of the advection equation is used in order to obtain meaningful physical results (Poulain and Finlayson, 1993). Equation (3.78) is normalized below

$$\frac{\partial G}{\partial(t^*/\theta)} + w^*(s^*)\frac{\partial C_b}{\partial s^*} = 0 \tag{3.80}$$

Since the isotherms are nonlinear functions of $C_{b,,}$ neither G nor C_b can be normalized.

The numerical method (Finlayson, 1992) for the model is described below. In the algorithm, the low-order solution for G is calculated and then adjusted using the flux-limited flows. The flux correction preserves the steep concentration front (shock) and prevents oscillations that are artifacts of the finite difference method. The flux correction method averages two kinds of numerical fluxes: (1) high-order fluxes from finite difference schemes that can keep the front steep but oscillate and (2) low-order fluxes from methods that do not oscillate but

smooth the front excessively. The upstream finite difference method is used to calculate the low-order terms and the MacCormack method the high-order terms. The Fortran code for the bed/stream exchange model with Langmuir adsorption is included in Appendix C.

The values of G and C in the streamtube at a position s* and at time t*/θ are denoted by

$$G_i^n = G\left(s_i^*, \left(\frac{t^*}{\theta}\right)_n\right) = G\left(i\Delta s^*, n\Delta\left(\frac{t^*}{\theta}\right)\right) \tag{3.81}$$

$$C_{b,i}^n = C_b\left(s_i^*, \left(\frac{t^*}{\theta}\right)_n\right) = C_b\left(i\,\Delta s^*, n\,\Delta\left(\frac{t^*}{\theta}\right)\right) \tag{3.82}$$

The values of G_i^{n+1} and C_i^{n+1} for all s_i^* are computed from the values at $(t^*/\theta)_n$ as follows:

1. Evaluate the low-order flows, F^L.

$$F_{i+1/2}^L = \frac{\Delta\left(t^*/\theta\right)}{\Delta s^*} w_i^* C_{b,i}^n \tag{3.83}$$

$$F_{i-1/2}^L = \frac{\Delta\left(t^*/\theta\right)}{\Delta s^*} w_i^* C_{b,i-1}^n \tag{3.84}$$

2. Evaluate the high-order flows, F^H.

$$\tilde{G}_i^{n+1} = G_i^n - \frac{\Delta\left(t^*/\theta\right)}{\Delta s^*} w_i^* \left(C_{b,i+1}^n - C_{b,i}^n\right) \tag{3.85}$$

$$\tilde{C}_{b,i}^{n+1} = G^{-1}\left(\tilde{G}_i^{n+1}\right) \tag{3.86}$$

$$F_{i+1/2}^H = \frac{\Delta\left(t^*/\theta\right)}{2\Delta s^*} w_i^* \left(C_{b,i+1}^n + \tilde{C}_{b,i}^{n+1}\right) \tag{3.87}$$

$$F_{i-1/2}^H = \frac{\Delta\left(t^*/\theta\right)}{2\Delta s^*} w_i^* \left(C_{b,i}^n + \tilde{C}_{b,i-1}^{n+1}\right) \tag{3.88}$$

3. Define the anti-diffusion terms:

$$\begin{aligned} A_{i+1/2} &= F^H_{i+1/2} - F^L_{i+1/2} \\ A_{i-1/2} &= F^H_{i-1/2} - F^L_{i-1/2} \end{aligned} \tag{3.89}$$

4. Calculate the low order solution.

$$G^L_i = G^n_i - \left(F^L_{i+1/2} - F^L_{i-1/2}\right) \tag{3.90}$$

5. Use the following algorithm to find the anti-diffusion correction factors.

$$\begin{aligned} G^a_i &= \max\left(G^n_i, G^L_i\right) \\ G^b_i &= \min\left(G^n_i, G^L_i\right) \\ G^{max}_i &= \max\left(G^a_{i-1}, G^a_{i+1}, G^a_i\right) \\ G^{min}_i &= \min\left(G^b_{i-1}, G^b_{i+1}, G^b_i\right) \end{aligned} \tag{3.91}$$

$$\begin{aligned} P^+_i &= \max\left(0, A_{i-1/2}\right) - \min\left(0, A_{i+1/2}\right) \\ Q^+_i &= G^{max}_i - G^L_i \\ R^+_i &= \begin{cases} \min\left(1, Q^+_i / P^+_i\right), & \text{if } P^+_i > 0 \\ 0 & \text{if } P^+_i = 0 \end{cases} \end{aligned} \tag{3.92}$$

$$\begin{aligned} P^-_i &= \max\left(0, A_{i+1/2}\right) - \min\left(0, A_{i-1/2}\right) \\ Q^-_i &= G^L_i - G^{min}_i \\ R^-_i &= \begin{cases} \min\left(1, Q^-_i / P^-_i\right), & \text{if } P^-_i > 0 \\ 0 & \text{if } P^-_i = 0 \end{cases} \end{aligned} \tag{3.93}$$

$$Z_{i+1/2} = \begin{cases} \min\left(R^-_{i+1}, R^+_i\right), & A_{i+1/2} < 0 \\ \min\left(R^-_i, R^+_{i+1}\right), & A_{i+1/2} \geq 0 \end{cases} \tag{3.94}$$

$$Z_{i-1/2} = \begin{cases} \min\left(R^-_i, R^+_{i-1}\right), & A_{i-1/2} < 0 \\ \min\left(R^-_{i-1}, R^+_i\right), & A_{i-1/2} \geq 0 \end{cases} \tag{3.95}$$

$$A^c_{i+1/2} = Z_{i+1/2} A_{i+1/2}$$
$$A^c_{i-1/2} = Z_{i-1/2} A_{i-1/2} \qquad (3.96)$$

6. Compute the final solution as a correction or limitation to the low order solution computed in Step 4.

$$G_i^{n+1} = G_i^L - \left(A^c_{i+1/2} - A^c_{i-1/2}\right) \qquad (3.97)$$

$$C_{b,i}^{n+1} = G^{-1}\left(G_i^{n+1}\right) \qquad (3.98)$$

Table 3.3 lists the formulas for G corresponding to the Langmuir, Freundlich, Langmuir-Freundlich and Tóth isotherms. The function G is invertible only for the Langmuir isotherm. Otherwise, C_b is determined for a known G by finding the root of G–G(C_b) using the bisection method (Press et al., 1989), which drastically increases the computation time. The average computation time for the exchange model using the Langmuir isotherm is 2 hours whereas the models with the Freundlich, Tóth, and Langmuir-Freundlich isotherms ran 24 hours.

Table 3.3. Expressions for the column isotherms $G(C_b)$.

Isotherm	$G(C_b)$
Langmuir	$G = C_b\left(1 + \frac{\rho_b}{\theta}\frac{S_T K_L}{1+K_L C_b}\right)$
Freundlich	$G = C_b + \frac{\rho_b}{\theta} K_F C_b^{\alpha}$
Langmuir-Freundlich	$G = C_b + \frac{\rho_b}{\theta}\frac{S_T (K_{LF} C_b)^{\alpha}}{1 + (K_{LF} C_b)^{\alpha}}$
Tóth	$G = C_b\left(1 + \frac{\rho_b}{\theta}\frac{S_T K_T}{\left(1+(K_T C_b)^{\alpha}\right)^{1/\alpha}}\right)$

The finite difference method is stable as long as the Courant number is less than or equal to one:

$$\frac{\Delta\left(t^*/\theta\right) w^*}{\Delta s^*} \leq 1 \tag{3.99}$$

Since the maximum value of w* is one, the condition is restated as

$$\frac{\Delta\left(t^*/\theta\right)}{\Delta s^*} \leq 1 \tag{3.100}$$

In the model, 65 or more streamtubes were chosen with inlets between $X_0^* = 0$ and $X_0^* = \pi/2$, each having equal width dX_0^* on the bed surface. The largest time step $\Delta(t^*/\theta)$ is 0.01, and Δs^* is at a value such that the ratio in Equation (3.100) is less than 0.90. The value Δs^* is constant for each streamtube. The shorter tubes have at least 3 nodes for s* and the longer tubes have a maximum of 200 nodes. Porewater concentration profiles for several of the streamtubes are illustrated in Appendix D.

For an initially clean column with a pulse injection of a contaminant, the numerical solution to the advection equation using the Langmuir isotherm is compared to the analytical solution in Appendix C, Figure C.1. The differences between the numerical and analytical solutions are small and decrease with time. Appendix C also contains a comparison of the predictions from Eylers' exchange model, which uses a modified residence time function (Section 3.3), for linearly adsorbing compounds, and the numerical exchange model, which has been developed in this section, using a linear isotherm. The bed/stream exchange predictions are the same for both models. Therefore, the numerical method used to solve the advection equation in the streamtubes does not introduce significant errors into the bed/stream exchange calculations.

3.4.3.2. Illustrative model results

To illustrate the effects of nonlinear adsorption on the mass exchange between stream water and a sediment bed, two simple examples will be presented. In the first example, the mass exchange in an open system with a pulse change in the contaminant concentration is examined. In a river, this situation corresponds to a chemical spill. The system is contaminated, then the input ceases and the system recovers. In this example, the concentration jumps from zero to C_0 at $t = 0$ and then drops back to zero at time $t = T$. The normalized mass exchange for nonsorbing, linearly adsorbing and nonlinearly adsorbing compounds is shown in Figure 3.11. The sorption parameters for dodecyltrimethylammonium bromide on garnet sand (Table 5.4, Chapter 5) are used in the models; and the initial concentration is 200 μM.

While $t < T$, the exchange model simulations based on the linear and nonlinear isotherms are approximately the same. When $t > T$, it takes longer for the system to recover when the compound adsorbs nonlinearly to the sediment. The recovery time differs significantly among the models using the different nonlinear adsorption isotherms. The retardation for the Freundlich and Langmuir-Freundlich isotherms approach infinity as the concentration tends to zero, and, therefore, they exhibit more tailing than the Langmuir and Tóth isotherms. At small concentrations where the asymptotic behavior of the nonlinear isotherms becomes important, the bed/stream exchange predictions are sensitive to the choice of the isotherm. Therefore, the choice of isotherm should be based on the ability of the isotherms to fit the sorption data in the concentration range of interest; and caution should be exercised when the Freundlich and Langmuir-Freundlich isotherms are used to model adsorption at small concentrations.

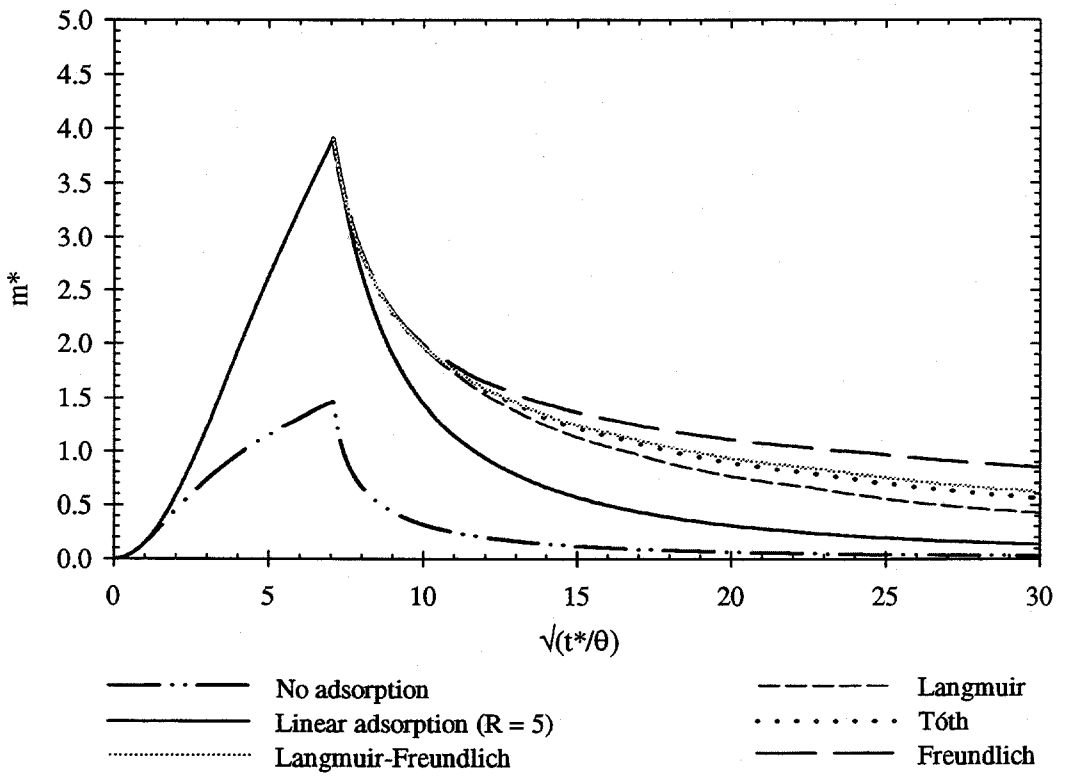

Figure 3.11. Comparison of mass exchange for nonsorbing and adsorbing compounds resulting from a pulse change in concentration in an open system. The normalized pulse duration is $T^*/\theta = 50$ and $C_0 = 200$ μM.

In the second example, the mass transfer in a closed system, similar to the laboratory flume setup, is investigated. At t = 0, a known mass of contaminant is added to the system and the concentration jumps to C_0. The bed is initially uncontaminated. Figure 3.12 illustrates the difference in the mass exchange for nonsorbing, linearly adsorbing and nonlinearly adsorbing compounds. The models are based on the hydraulic and bed parameters from Flume Run 2 (Chapter 5, Tables 5.10 through 5.12). The nonlinear exchange model uses the Langmuir sorption parameters for dodecyltrimethylammonium bromide on garnet given in Chapter 5, Table 5.4. The sensitivity of the bed/stream exchange model for a closed system to the choice of the nonlinear isotherm is discussed in Chapter 6, Section 6.9.

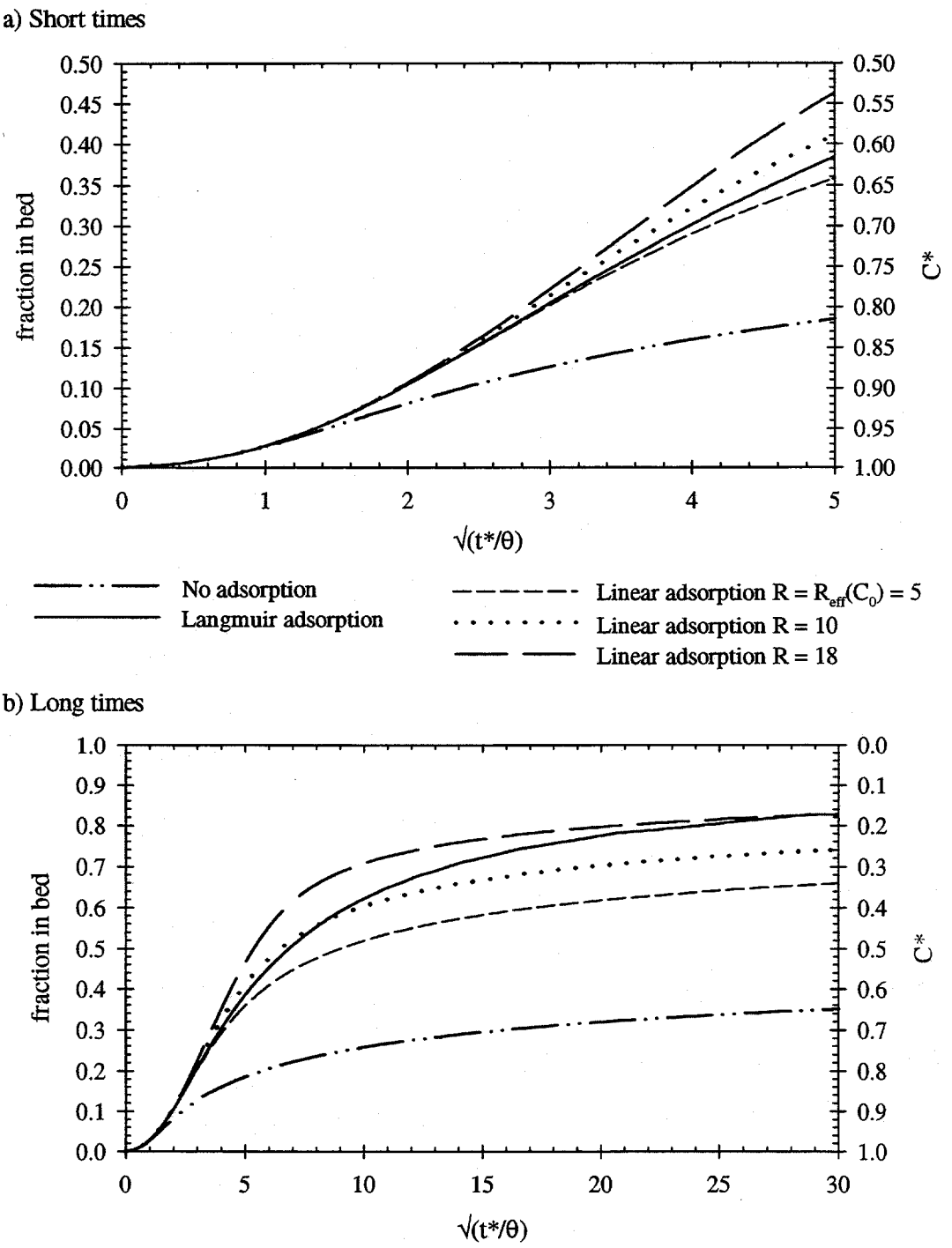

Figure 3.12. Comparison of mass transfer to sediment bed in a closed system for nonsorbing, linearly adsorbing and nonlinearly adsorbing compounds (d* = 5.3). The hydraulic and bed parameters are based on Flume Run 2 (Chapter 5, Tables 5.10 through 5.12). The Langmuir sorption parameters from Chapter 5, Table 5.4 are used by the nonlinear model. The initial concentration is 200 μM.

Initially ($t^*/\theta < 1$), the advective flux into the bed dominates and the mass exchange is the same for all of the compounds. While $t^*/(\theta R_{eff}(C_0)) < 1$, the mass transfer of the nonlinearly adsorbing compound is the same as that for a linearly adsorbing compound with a retardation coefficient equal to $R_{eff}(C_0)$ (see Table 3.2). The effective retardation coefficient (see Figure 3.7) for a given aqueous concentration C is defined by

$$R_{eff}(C) = 1 + \frac{\rho_b}{\theta}\frac{f(C)}{C} \tag{3.101}$$

where ρ_b is the dry bulk density of the sediment and f(C) is the equation for the isotherm. As time proceeds, the concentration of the compound in the overlying water column decreases. For nonlinearly adsorbing compounds, smaller concentrations travel slower than higher concentrations, causing the rate of contaminant release from the bed to decrease. Therefore, more of the nonlinearly adsorbing compound is retained in the bed compared to the linearly adsorbing compound having a retardation of $R_{eff}(C_0)$.

For early times in Figure 3.12, the mass transfer of linearly adsorbing compounds having retardation coefficients (10 and 18) greater than $R_{eff}(C_0) = 5$ exceeds that of the nonlinearly adsorbing compound. However, at a time when the concentration in the overlying water column equals a value such that $R_{eff}(C)$ equals the retardation coefficient of the linearly adsorbing compound (i.e., in Figure 3.12b, when the nonlinear model equals the linear model for R = 10 at $t^*/\theta = 76$, $C^* = 0.42$, C = 84 μM and $R_{eff}(84\mu M) = 10$), the amount of compound contained on the bed is equal. The linear adsorption model can be used to provide upper and lower bounds on the mass transfer of a nonlinearly adsorbing compound by using retardation coefficients $R_{eff}(C_{minimum})$ and $R_{eff}(C_0)$, respectively (i.e., in Figure 3.12b, R equals 18 and 5, respectively).

Both of the examples discussed in this section demonstrate that the approximation of linear adsorption can lead to significant errors in the predicted mass exchange of a nonlinearly adsorbing compound when the overlying water concentration is variable. The magnitude of the errors depends upon the choice of the retardation coefficient in the linear model and on the

amount of variability in the parameter $R_{eff}(C)$, calculated using the concentration extremes in the overlying water column.

3.5. Approximate Bed Exchange Model — The Well-Mixed Assumption

Because the detailed bed/stream exchange model developed in Section 3.4 for nonlinearly adsorbing compounds is computationally intensive, it would be too costly to include the detailed model into a larger river transport model. A simpler model for nonsorbing and adsorbing tracers is developed. The model is based on the assumption that the bed, down to a certain depth, is well-mixed with the overlying water column. The mass transfer to the bed is modeled by assuming a front of well-mixed pollutant is driven down into the bed by pumping. The well-mixed modeling approach was proposed by Packman (1997). The concepts of the model are depicted in Figure 3.13. The well-mixed assumption is valid in situations where 1) the sediment bed is initially uncontaminated and 2) the concentration in the stream water changes gradually (i.e., when dC/dt is small).

First, the well-mixed approximate model for the exchange of nonsorbing solutes will be developed. Then the appropriate modifications for linear and nonlinear adsorption will be incorporated. The predicted mass transfer will be compared to the results from the detailed models developed in Sections 3.2 and 3.3.

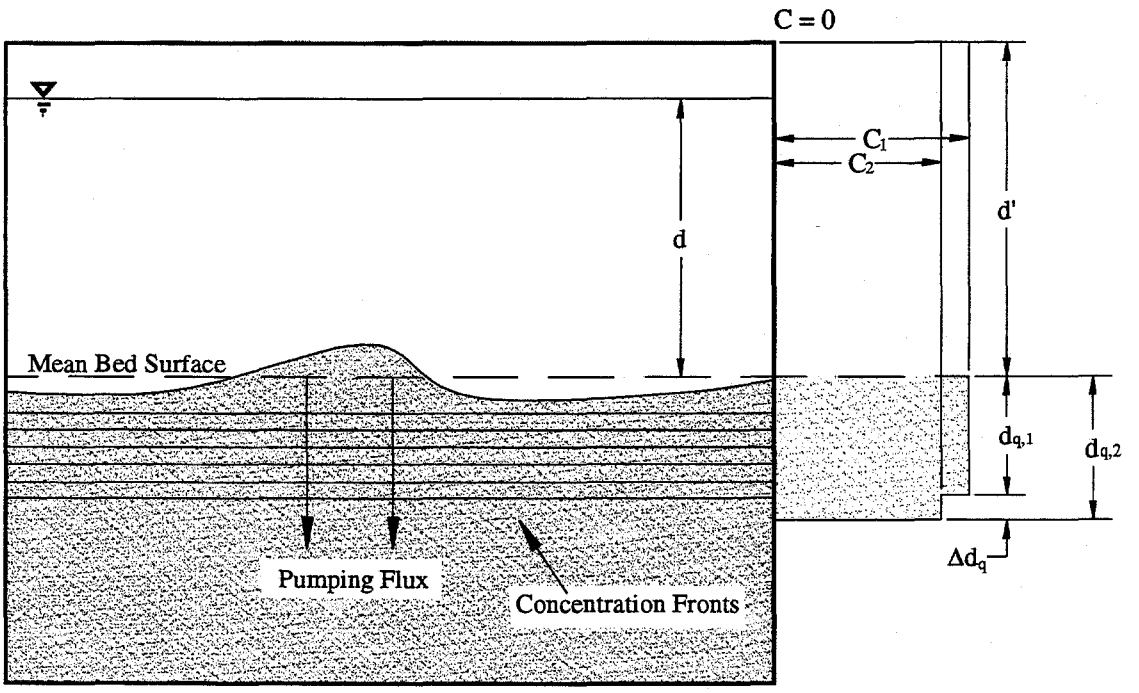

Figure 3.13. Schematic showing the concepts of the well-mixed bed exchange model.

3.5.1. Well-mixed exchange model for nonsorbing solutes

The front of the well-mixed layer moves downward at the rate equal to the mean magnitude of the downward velocity denoted by $\overline{v}(d_q)$ divided by the porosity θ to convert from the Darcy to the seepage velocity:

$$\frac{\Delta d_q}{\Delta t} = \frac{\overline{v}(d_q)}{\theta} \tag{3.102}$$

where d_q is the front depth. The front velocity $\overline{v}(d_q)$ is calculated by averaging the magnitude of the downward vertical velocity at a bed depth d_q over one wavelength λ, while neglecting the upward velocity:

$$\begin{aligned}\bar{v}(d_q) &= -\frac{1}{\lambda}\int_0^{\lambda} v(x,d_q)\,dx \\ &= \frac{1}{\lambda}\int_0^{\lambda/2} u_m \sin(kx)\, e^{-kd_q}\,dx \\ &= \frac{u_m}{\pi} e^{-kd_q}\end{aligned} \tag{3.103}$$

A formula for d_q as a function of time can be derived by rearranging Equation (3.102) and integrating. The result is

$$d_q(t) = \frac{1}{k}\ln\left(1+\frac{ku_m}{\pi}\left(\frac{t}{\theta}\right)\right) \tag{3.104}$$

The total mass of the contaminant per unit area of the bed at a time t is

$$C_0 m(t) = \theta C(t) d_q(t) \tag{3.105}$$

Therefore,

$$m(t) = \frac{\theta}{k} C^*(t) \ln\left(1+\frac{ku_m}{\pi}\left(\frac{t}{\theta}\right)\right) \tag{3.106}$$

$$m^*\left(\frac{t^*}{\theta}\right) = \theta C^*\left(\frac{t^*}{\theta}\right) \ln\left(1+\frac{1}{\pi}\left(\frac{t^*}{\theta}\right)\right) \tag{3.107}$$

In a closed system, conservation of mass requires

$$\frac{C(t)}{C_0} = \frac{d'}{d' + \theta d_q(t)} \tag{3.108}$$

and

$$C^*\left(\frac{t^*}{\theta}\right) = \frac{d^*}{d^* + \theta \ln\left(1+\frac{1}{\pi}\left(\frac{t^*}{\theta}\right)\right)} \tag{3.109}$$

a) Comparison of model results for a nonsorbing solute

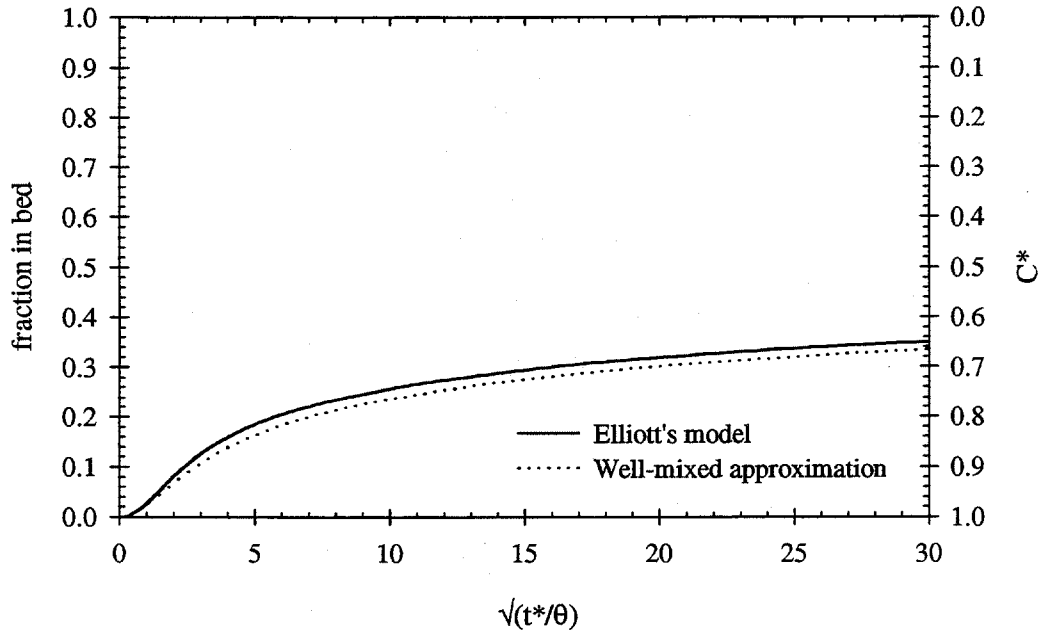

b) Difference between Elliott's model and the well-mixed approximation

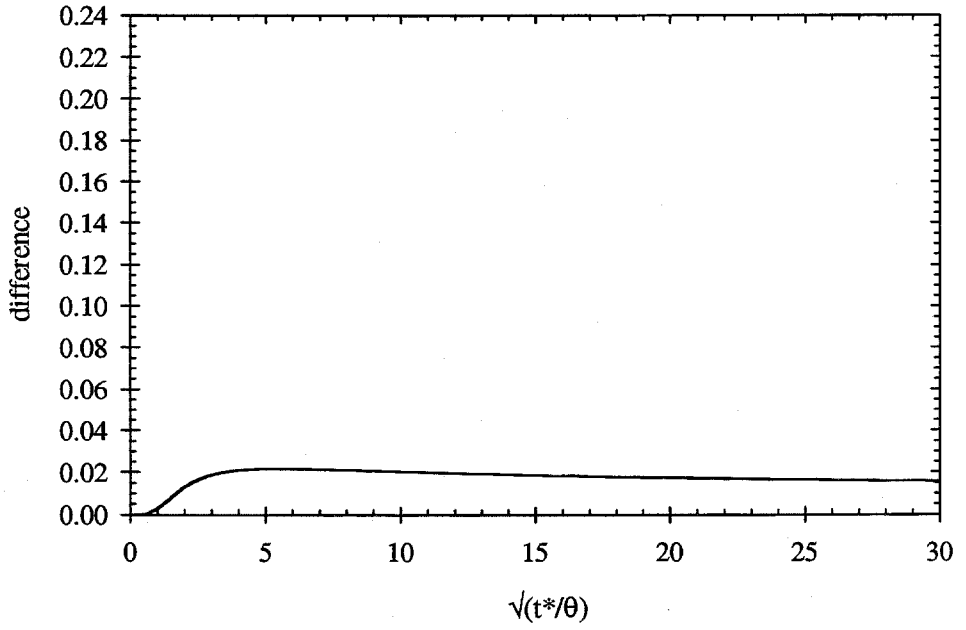

Figure 3.14. Effect of the well-mixed approximation in the mass transfer of a nonsorbing solute in a closed system with d* = 5.3.

The error introduced by the well-mixed approximation to the mass transfer of a nonsorbing solute is examined for a closed system. At t = 0, the a known mass of the solute is added to the system and the concentration jumps to C_0. The differences in the mass transfer predictions of a nonsorbing solute using Elliott's model in Section 3.2 and that from the well-mixed model are depicted in Figure 3.14. The latter slightly underestimates the fraction of the solute contained in the bed (and overestimates C*) when dC/dt is large. The maximum difference in the predicted value of C* equals 0.022 when d* is 5.3 (the value of the normalized effective depth for most of the flume experiments presented in Chapter 5) and 0.012 when d* is 10.6 (not shown). In the flume, larger values of d* correspond to larger volumes of water (excluding porewater). Therefore, as d* increases, the impact of the mass transfer to the bed upon the overlying water concentration is reduced, thus, resulting in a smaller value for dC/dt. For large values of d*, dC/dt is small and the magnitude of the error in C* for the well-mixed bed exchange model is reduced.

3.5.2. Well-mixed exchange model with linear adsorption

The mass of a linearly adsorbing compound per unit area of the bed between y = 0 and y = y_b is

$$\begin{aligned} \text{mass per unit area} &= (\theta C + \rho_b S) y_b \\ &= \theta\left(1 + \frac{\rho_b}{\theta}\frac{S}{C}\right) C y_b \\ &= \theta\left(1 + \frac{\rho_b}{\theta} K_d\right) C y_b \\ &= \theta R C y_b \end{aligned} \tag{3.110}$$

where C_s is the concentration on the solid (mass chemical/mass solid). For a linearly adsorbing compound, the increase in the depth of the well-mixed layer during a small time Δt is

$$\Delta d_q = \frac{\bar{v}(d_q)}{\theta R}\Delta t \tag{3.111}$$

The equivalent bed depth d_q for a linearly adsorbing compound, derived from the integration of Equation (3.111), is

$$d_q(t) = \frac{1}{k}\ln\left(1+\frac{ku_m}{\pi R}\left(\frac{t}{\theta}\right)\right) \tag{3.112}$$

Equation (3.112) is equivalent to replacing u_m by u_m/R in Equation (3.104), the corresponding expression for the front depth of a nonsorbing solute.

The total mass of contaminant per unit area of the bed at time t is then

$$C_0 m(t) = \theta R C(t) d_q(t) \tag{3.113}$$

Therefore,

$$m(t) = \frac{\theta}{k} R C^*(t) \ln\left(1+\frac{ku_m}{\pi R}\left(\frac{t}{\theta}\right)\right) \tag{3.114}$$

and

$$m^*\left(\frac{t^*}{\theta}\right) = \theta R C^*\left(\frac{t^*}{\theta}\right) \ln\left(1+\frac{1}{\pi R}\left(\frac{t^*}{\theta}\right)\right) \tag{3.115}$$

By applying conservation of mass in a closed system, the concentration in the overlying water column is related to d_q as follows:

$$\frac{C(t)}{C_0} = \frac{d'}{d'+\theta R d_q(t)} \tag{3.116}$$

$$C^*\left(\frac{t^*}{\theta}\right) = \frac{d^*}{d^*+\theta R \ln\left(1+\frac{1}{\pi R}\left(\frac{t^*}{\theta}\right)\right)} \tag{3.117}$$

The predicted mass transfer using the well-mixed approximation is compared to the results of Eylers' detailed model, which is based on a modified residence time function presented in Section 3.3 for compounds having retardation coefficients of 2 (Figure 3.15), 10 (Figure 3.16) and 50 (Figure 3.17).

a) Comparison of model results for a linearly adsorbing compound

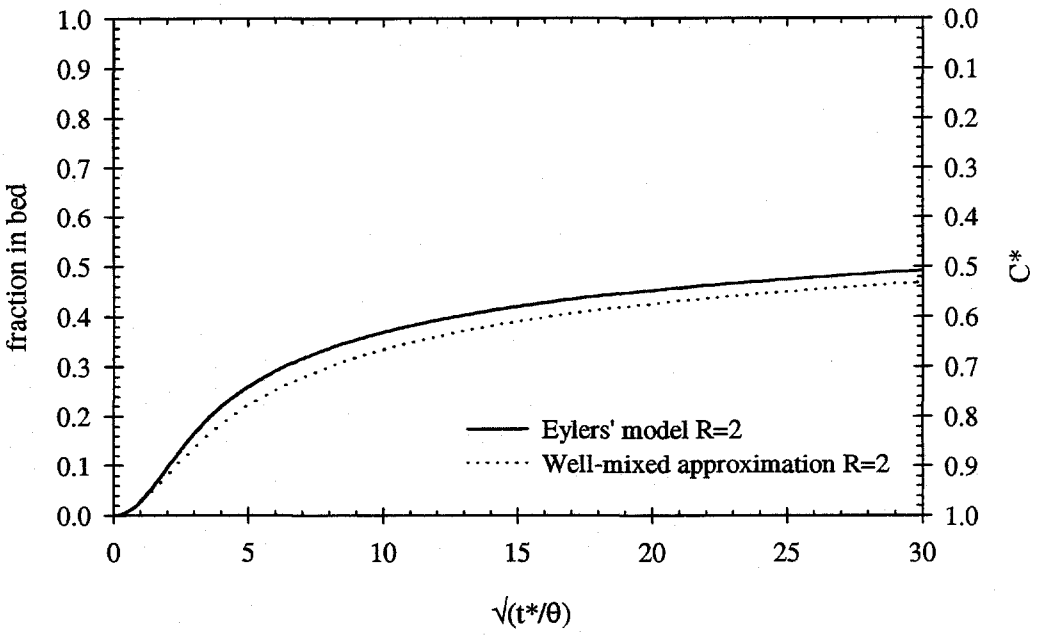

b) Difference between Eylers' model and the well-mixed approximation

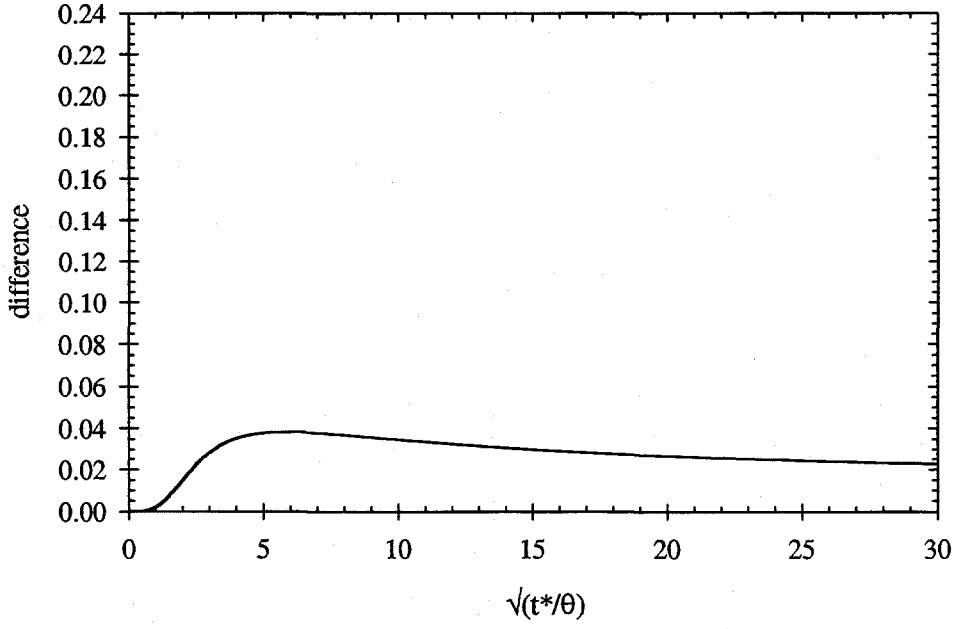

Figure 3.15. Effect of the well-mixed approximation in the mass transfer of a linearly adsorbing compound with R = 2 in a closed system where d* = 5.3.

a) Comparison of model results for a linearly adsorbing compound

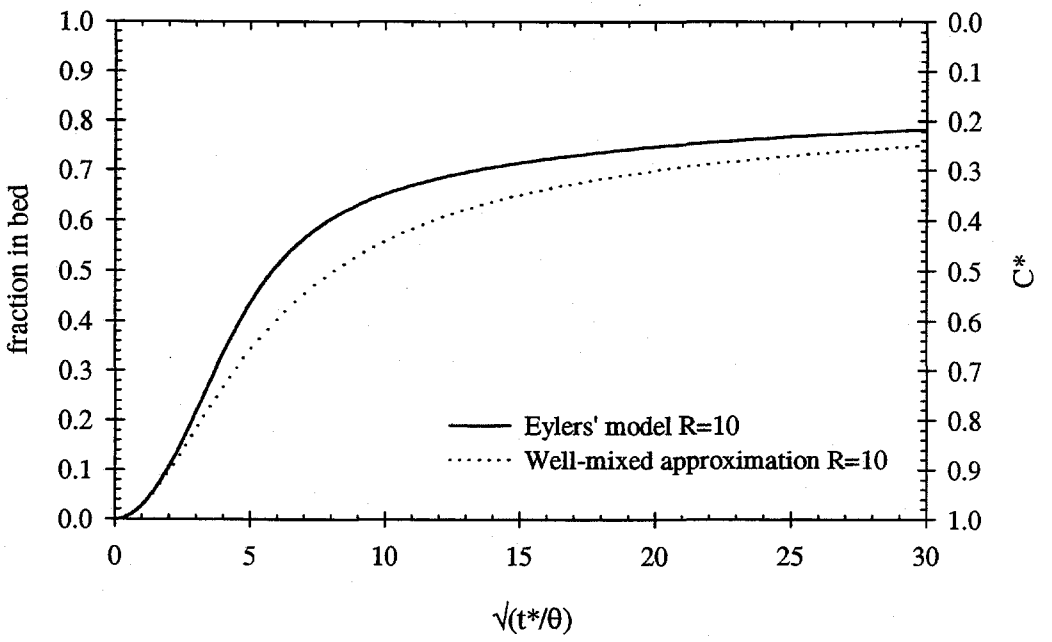

b) Difference between Eylers' model and the well-mixed approximation

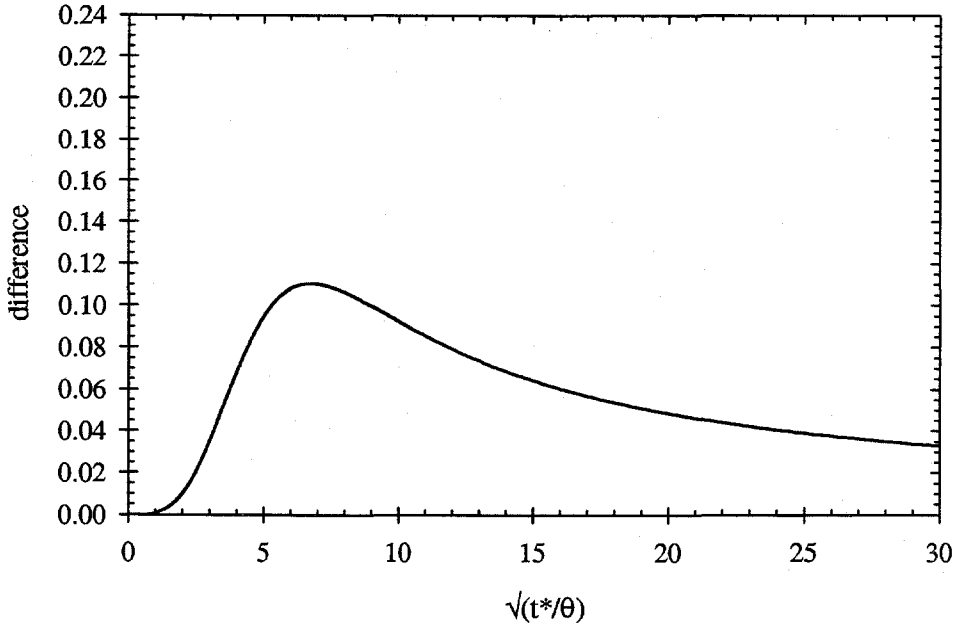

Figure 3.16. Effect of the well-mixed approximation in the mass transfer of a linearly adsorbing compound with R = 10 in a closed system where d* = 5.3.

a) Comparison of model results for a linearly adsorbing compound

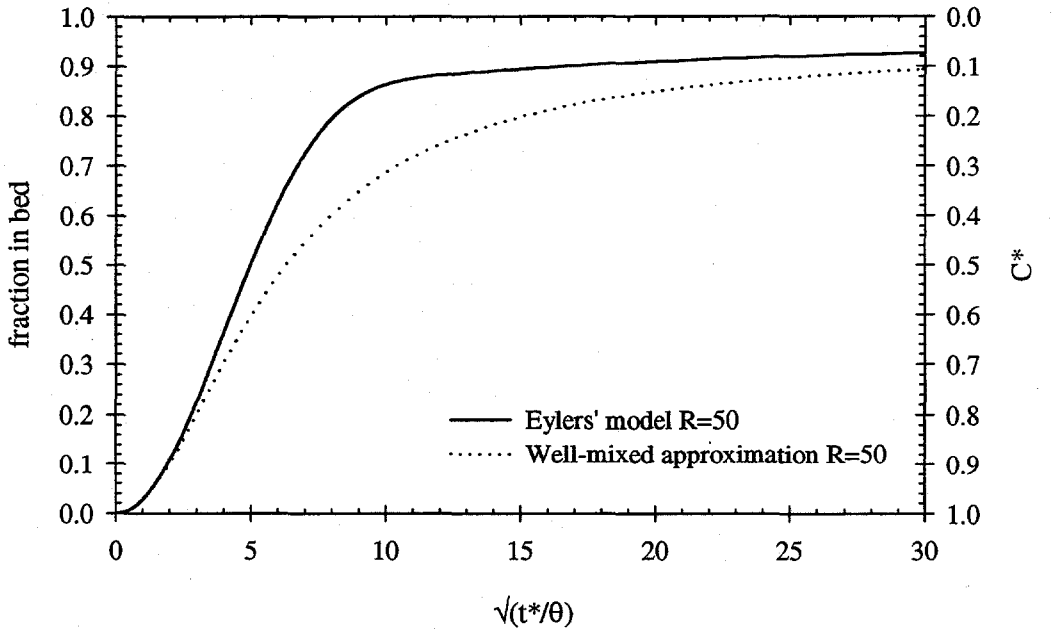

b) Difference between Eylers' model and the well-mixed approximation

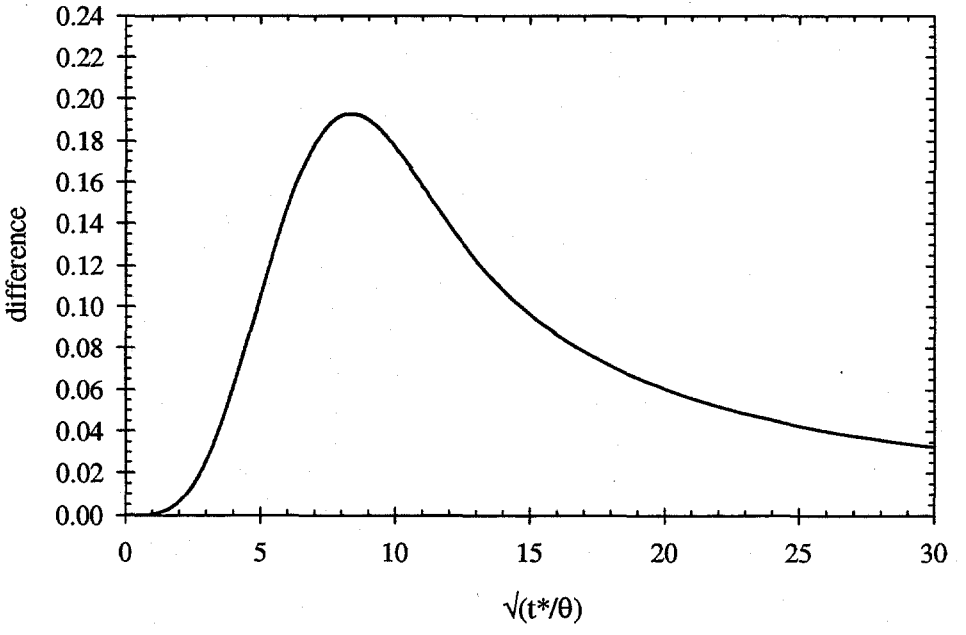

Figure 3.17. Effect of the well-mixed approximation in the mass transfer of a linearly adsorbing compound with R = 50 in a closed system where d* = 5.3.

For a linearly adsorbing compound, the error introduced by the well-mixed approximation increases with the value of R because more mass is transferred to the bed, which causes an increase in dC/dt. For strongly adsorbing compounds, the well-mixed approximation should not be used to predict the mass transfer for short times. The well-mixed model is valid for linearly adsorbing compounds for all t^*/θ when $R < 2$, for $t^*/\theta > 300$ when $R = 10$, and for $t^*/\theta > 500$ when $R = 50$. Therefore, the well-mixed model can be used to estimate the long-term mass transfer with considerably less computational effort than required by the detailed bed/stream exchange models.

3.5.3. Well-mixed exchange model with nonlinear adsorption

The accumulated mass exchange of a nonlinearly adsorbing compound per unit area of the bed can be computed using Equation (3.110) with an appropriate choice of the retardation coefficient. The constant retardation coefficient R is replaced by an "effective retardation coefficient" R_{eff} defined by

$$R_{eff}(C) = 1 + \frac{\rho_b}{\theta}\frac{f(C)}{C} \tag{3.118}$$

The formulas for $R_{eff}(C)$ associated with the nonlinear isotherms under consideration are listed in Table 3.2.

The advance of a the well-mixed layer is given by

$$\Delta d_q = \frac{\bar{v}(d_q)}{\theta R_{eff}(C)}\Delta t \tag{3.119}$$

which is the same as Equation (3.111) with R replaced by R_{eff}. Therefore,

$$\int_0^{d_q}\frac{dy}{\bar{v}(y)} = \frac{1}{\theta}\int_0^{t}\frac{d\tau}{R_{eff}(C(\tau))} \tag{3.120}$$

and the resulting expression for the front depth d_q is

$$d_q(t) = \frac{1}{k}\ln\left(1 + \frac{ku_m}{\pi\theta}\int_0^t \frac{d\tau}{R_{eff}(C(\tau))}\right) \tag{3.121}$$

The accumulated mass transfer to the bed divided by C_0 is

$$m(t) = \theta R_{eff}(C(t))\, C^*(t) d_q(t) \tag{3.122}$$

and the non-dimensional expression is

$$m^*\left(\frac{t^*}{\theta}\right) = \theta R_{eff}(C_0 C^*(t))\, C^*(t) d_q^*\left(\frac{t^*}{\theta}\right) \tag{3.123}$$

where $d_q^* = kd_q$.

In a closed system, the mass transfer is calculated by solving the coupled system of equations for d_q^* and C*:

$$d_q^*\left(\frac{t^*}{\theta}\right) = \ln\left(1 + \frac{1}{\pi}\int_0^{t^*/\theta} \frac{1}{R_{eff}(C_0 C^*(\tau^*/\theta))}\, d\left(\frac{\tau^*}{\theta}\right)\right) \tag{3.124}$$

$$C^*\left(\frac{t^*}{\theta}\right) = \frac{d^*}{d^* + \theta R_{eff}(C_0 C^*(t^*/\theta))\, d_q^*(t^*/\theta)} \tag{3.125}$$

The numerical solution to the coupled system is described below:

1. In order to start the calculations, the concentration in the water column at t_0^* and $t_1^* = t_0^* + \Delta t^*$ is set to the initial value (C* = 1).
2. For $t_i^* > t_1^*$, the front depth is found from Equation (3.124) using concentrations from previous time ($t_0^*, \ldots, t_{i-1}^*$). The integral is evaluated using the extended trapezoid rule (Press et al., 1989):

$$\int_0^{t_{i-1}^*/\theta} \frac{1}{R_{eff}(C_0 C^*(\tau^*/\theta))}\, d\left(\frac{\tau^*}{\theta}\right) = \Delta\left(\frac{t^*}{\theta}\right)\left(\frac{1}{2R_{eff}(C_0)} + \sum_{j=1}^{i-2}\frac{1}{R_{eff}(C_0 C^*(t_j^*/\theta))} + \frac{1}{2R_{eff}(C_0 C^*(t_{i-1}^*/\theta))}\right) \tag{3.126}$$

3. The concentration $C^*\left(t_i^*/\theta\right)$ is calculated from Equation (3.125) using $d_q^*\left(t_i^*/\theta\right)$ and $R_{eff}\left(C_0 C^*\left(t_{i-1}^*/\theta\right)\right)$.

The error in the predicted mass transfer for nonlinearly adsorbing compound using the well-mixed approximation increases with the adsorption affinity of the chemical. The well-mixed model is restricted to a step increase from zero and to situations in which the overlying water concentration varies gradually. The validity of the well-mixed approximation for nonlinearly adsorbing compounds will be examined in Chapter 6, Section 6.10.

3.6. Approximate Bed Exchange Model for Complete Capture

At small times, almost all of the chemical which enters the bed remains in the bed; this process is referred to as "complete capture". The mass transfer to the bed can be approximated by determining the mass flux of chemical through the bed surface. The total mass of pollutant per unit area of the bed after a time t is

$$C_0 m(t) = \int_0^t \bar{v}(0) C(\tau)\, d\tau = \frac{u_m}{\pi} \int_0^t C(\tau)\, d\tau \tag{3.127}$$

where $\bar{v}(0)$ is determined from Equation (3.103) with d_q equal to zero. The normalized expression is

$$m^*(t) = \frac{\theta}{\pi} \int_0^{t^*/\theta} C^*\left(\frac{\tau^*}{\theta}\right) d\left(\frac{\tau^*}{\theta}\right) \tag{3.128}$$

In a closed system, the mass removed from the water column during a small time Δt equals the flux of chemical through the bed surface

$$d'\Delta C = -\bar{v}(0) C \Delta t \tag{3.129}$$

An expression for C can be derived by integrating Equation (3.129) as follows:

$$\int_{C_0}^{C} \frac{dC}{C} = -\frac{u_m}{\pi d'} \int_0^t d\tau \tag{3.130}$$

The evaluation of Equation (3.130) gives

$$C(t) = C_0 \exp\left(-\frac{u_m}{\pi d'} t\right) \tag{3.131}$$

and

$$C^*\left(\frac{t^*}{\theta}\right) = \exp\left(-\frac{\theta}{\pi d^*}\left(\frac{t^*}{\theta}\right)\right) \tag{3.132}$$

The mass transfer prediction using the small time approximation is compared to the exact solution for nonsorbing and linearly adsorbing (R = 10) compounds in Figure 3.18. The approximation is valid for nonsorbing solutes when $t^*/\theta < 1$, for linearly adsorbing compounds when $t^*/\theta < R$, and for nonlinearly adsorbing compounds when $t^*/\theta < R_{eff}$ (C_0). Thus, although the retardation coefficients R and R_{eff} do not appear in the approximate model Equations (3.131) and (3.132), adsorption extends the time of validity of the approximation in direct proportion to the retardation.

a) Nonsorbing solute

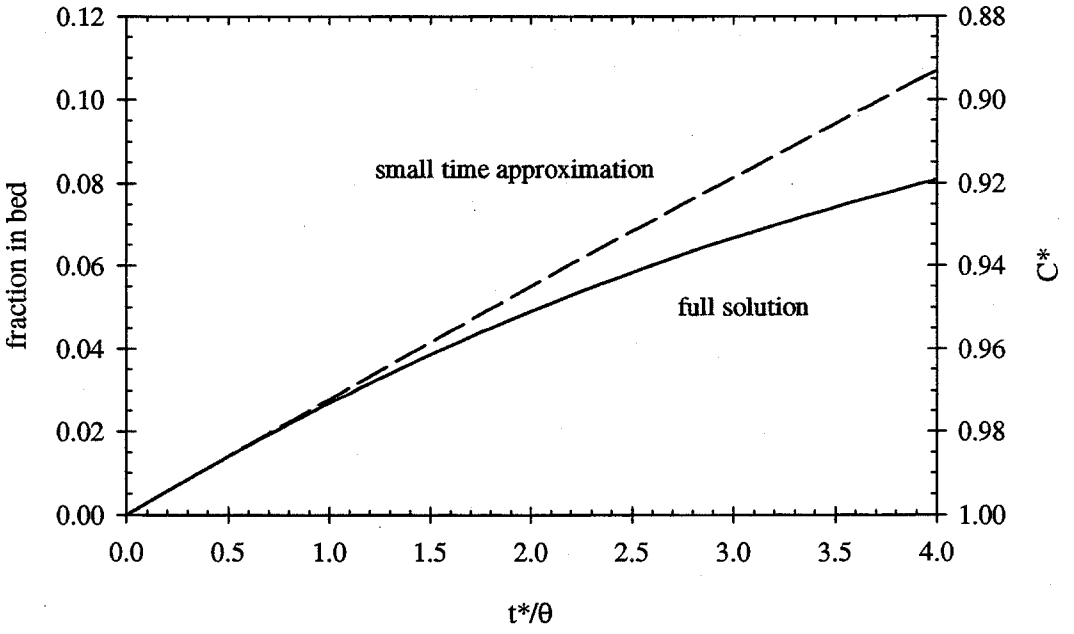

b) Linear adsorption with R = 10

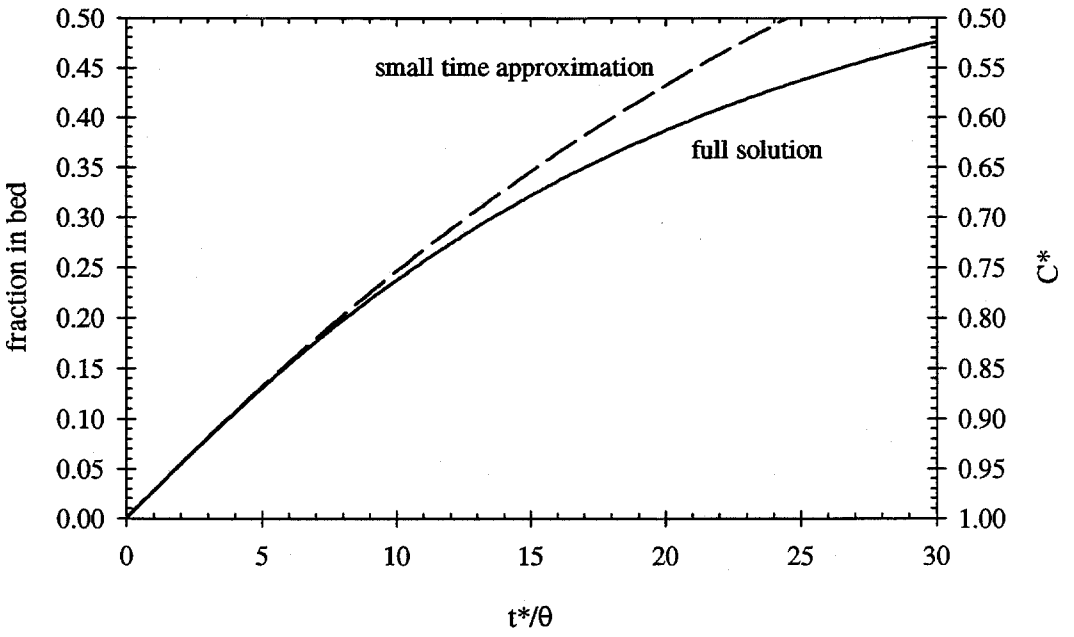

Figure 3.18. Comparison of bed exchange between the detailed model and the small-time approximate model for (a) nonsorbing solutes and (b) linearly adsorbing compounds with R = 10 in a closed system where d* = 5.3.

4. APPARATUS AND PROCEDURES

A series of small chemical batch experiments and large-scale flume experiments were conducted to characterize the modeling variables and to observe the transport of adsorbing compounds into a sediment bed. The important experimental components were:

- batch equilibrium and kinetic experiments to quantify adsorption behavior in the sediment bed;
- use of garnet sand which permitted a variety of hydraulic and chemical conditions;
- use of a recirculating flume for bed/stream exchange experiments;
- use of naturally-created bedforms;
- controlled, well-defined chemical conditions in the flume;
- use of a conservative tracer to verify the hydraulics of exchange between the stream and the bed.

4.1. FLUME DESCRIPTION

A tilting, recirculating flume having a total length of 551 cm, a width of 15.25 cm, and a depth of 50 cm was used in all bed/stream exchange experiments (Figure 4.1 and Figure 4.2). The rectangular channel had straight impermeable walls, a length of 431 cm and a depth of 50 cm. Except for the pump and orifice meter, the entire flume was constructed out of clear lucite and polyvinyl chloride. A stainless steel centrifugal pump, driven by an AC motor with a continuously-variable speed controller, recirculated the flow and suspended sediment. To determine the flow rate, a standard orifice meter constructed of stainless steel and lucite was installed about one meter upstream of the diverging section and was connected to a mercury manometer. The orifice diameter was 2.83 cm (0.700 times the pipe inner diameter).

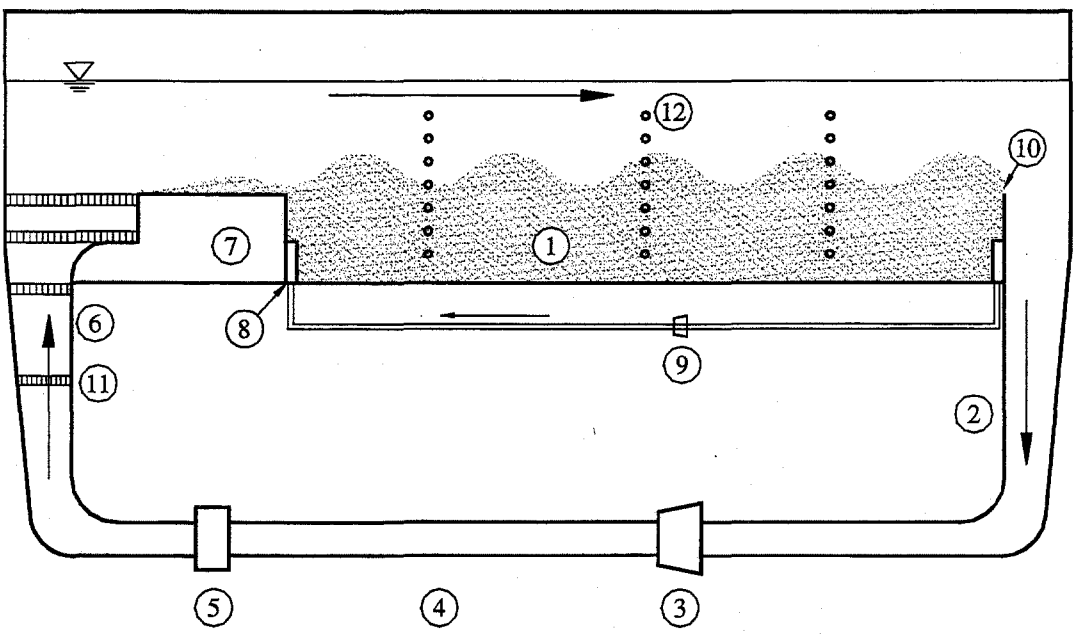

1) Sand bed with ripples
2) Converging section
3) Centrifugal pump with speed controller
4) Clear pipe section (4.04 cm id)
5) Orifice meter
6) Diverging section
7) Inlet box
8) Pump discharge for subsurface flow
9) Peristaltic pump for subsurface flow
10) Impermeable end plate
11) Baffle
12) Sampling ports

Figure 4.1. Schematic of flume. Drawing is not to scale.

Figure 4.2. Photograph of flume.

In order to minimize the volume of water and sediment buildup in the return system, the return pipe had a diameter of 4.04 cm. The entire recirculation system (return pipe and diverging sections) contained a total volume of 28 liters.

One advantage of the recirculating design was that the same body of water was passed over the bed many times. Consequently, apart from evaporation, the flume as a whole (bed, channel, pipes and water column) behaved similar to a closed system for water mass. With time, the small fluxes of contaminant into and out of the bed resulted in measurable contaminant concentration changes in the overlying water column. The observable mass exchange between the water column and sediment bed allowed for a detailed study of the exchange process.

The circulation time of the total volume of water in the flume was on the order of one to two minutes. Since the characteristic time for the bed exchange is on the order of hours, the flume water was essentially well-mixed and longitudinal variations of contaminant concentration

were insignificant. However, the flume was long enough so that there was a sufficient number of bedforms (15 to 25) to allow averaging of possible local concentration differences in the bed. Since the sidewalls of the channel were high (50 cm), the sediment bed was sufficiently deep (23 cm) to inhibit transport of contaminants close to the bottom of the flume. As a result, the bed depth was assumed infinite in the predictive bed exchange models.

Baffles were placed in the diverging portion of the return to help make the velocity distribution at the inlet of the channel more uniform and to reduce the scale of turbulence generated in the return pipe. The inlet section of the flume consisted of a curved block and a 70-cm long sealed lucite box that allowed the flow to adjust to conditions approximating those in the rest of the channel. The top of the box was 1 to 2 cm below the mean sand bed level and minimized the bed/stream exchange in that section. This box also provided an impermeable boundary at the upstream end of the sand bed. The downstream end of the sand bed was sealed by a vertical plate. These boundaries ensured that mass transport into and out of the bed occurred only through the top surface of the bed and not through the vertical faces at the end.

The impermeable ends for the sand bed did not provide acceptable end conditions because longitudinal porewater flow was induced by the hydraulic gradient down the flume. Because of the impermeable barriers at the ends of the sediment bed, flow entered the bed at the upstream end to supply the longitudinal flow further down the bed. The flow was then diverted upward and out of the bed at the downstream end (Figure 4.3a). This could result in a significant amount of additional contaminant transport into the bed. To prevent this additional exchange, a subsurface recirculation system, driven by a peristaltic pump, was used to establish a small longitudinal flow of porewater through the sediment bed adjusted to the same hydraulic gradient as the stream flow (Figure 4.3b).

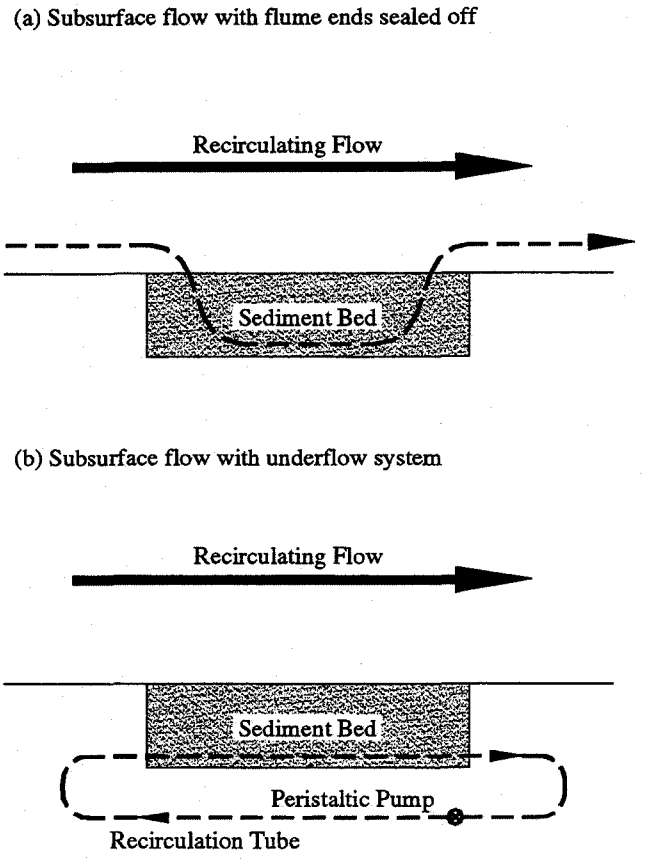

Figure 4.3. Underflow of porewater in flume (a) without and (b) with underflow system.

Porewater samples were drawn from three vertical arrays of sampling ports at three different locations along the sidewall of the flume. The ports were spaced at 1-cm intervals and were covered by silicone rubber septum.

The flume was equipped with adjustable rails that ran along the flume parallel to the flume bottom. Instrument carriages for point gauges and laser sensors were mounted on the rails. The flume was constructed of flat lucite sheets and polyvinyl chloride pipe to permit observation of the bedforms in the flume, to prevent adsorption of chemical compounds to the flume walls and piping, and to observe the flow of sediment through the return pipe.

4.2. Bed and Water Surface Elevation Measurements

Both the still and flowing water surface elevations were measured manually using a point gauge mounted on an instrument carriage. The point gauge was a stainless steel needle connected to a level detector that generated a square wave having value of 5 volts when the probe contacted the water and zero in air. This signal was filtered to get the average value and then displayed on an analog scale.

For still water surface elevation measurements, the position of the point gauge was recorded when the detector's output was 5 volts. These elevation measurements were accurate to 0.01 cm. Measurements were taken every 25 cm down the centerline of the flume. If the flowing water surface was smooth and glassy, the point gauge elevation was determined in the same manner.

With small ripples or waves in the flowing water surface, the point gauge was adjusted until the probe contacted the water slightly more than half of the time because the meniscus, once formed, would not break until the point gauge was a few tenths of a millimeter above the surface. The position of the point gauge was recorded when the output of the detector was 2.8 volts. The accuracy of the measurements depended on the size of the ripples in the water surface. The maximum error was 0.05 cm. Measurements were taken every 20 cm down the centerline of the flume.

Measurement of the bed surface elevation was automated using a computer-controlled motorized instrument carriage that held a laser displacement sensor (Keyence LB-70/LB-11). The apparatus is shown in Figure 4.4. A stepper motor mounted on the carriage was connected to a spur gear that traveled along a 32-pitch gear rack attached to one of the flume rails. The number of steps moved was linearly related to the distance traveled. The motor advanced 100.19 steps per centimeter.

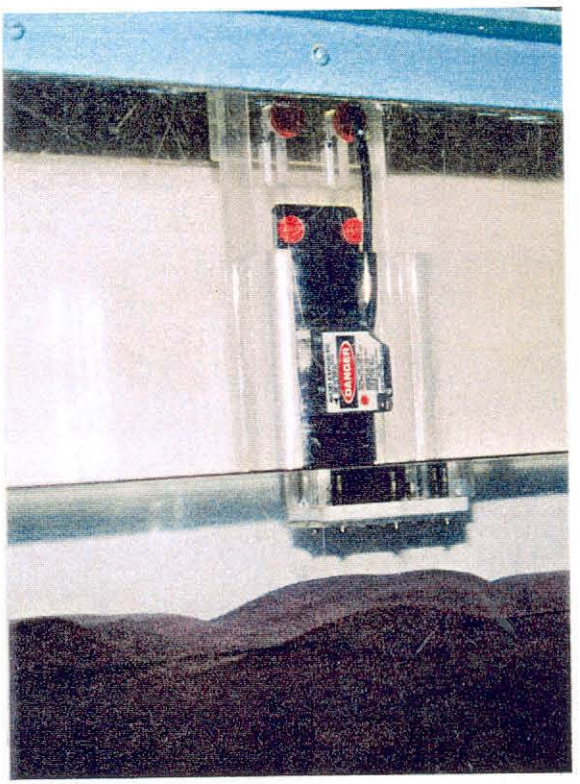

Figure 4.4. Photograph of laser sensor apparatus.

The laser displacement sensor emitted a laser beam, measured the reflected light intensity from the bed and then produced an output signal in volts. The laser spot diameter was 1.0 x 2.0 mm. The sensor had a measurement range of 6 to 14 cm in both air and water, a specified accuracy of 10 μm on white paper and an observed accuracy of 30 μm on the sand bed. The laser was housed in a waterproof lucite box with a glass bottom, which provided a constant interface between air and water. The laser was mounted 4 cm above the bottom of the box. The box was attached to the motorized instrument carriage and lowered into the water column until the sensor was 10 cm above the mean bed level. The bed profiles were acquired in still water rather than flowing water because the box would disturb the flow and scour the bed.

(a) Calibration of distance versus laser voltage in the mid-range

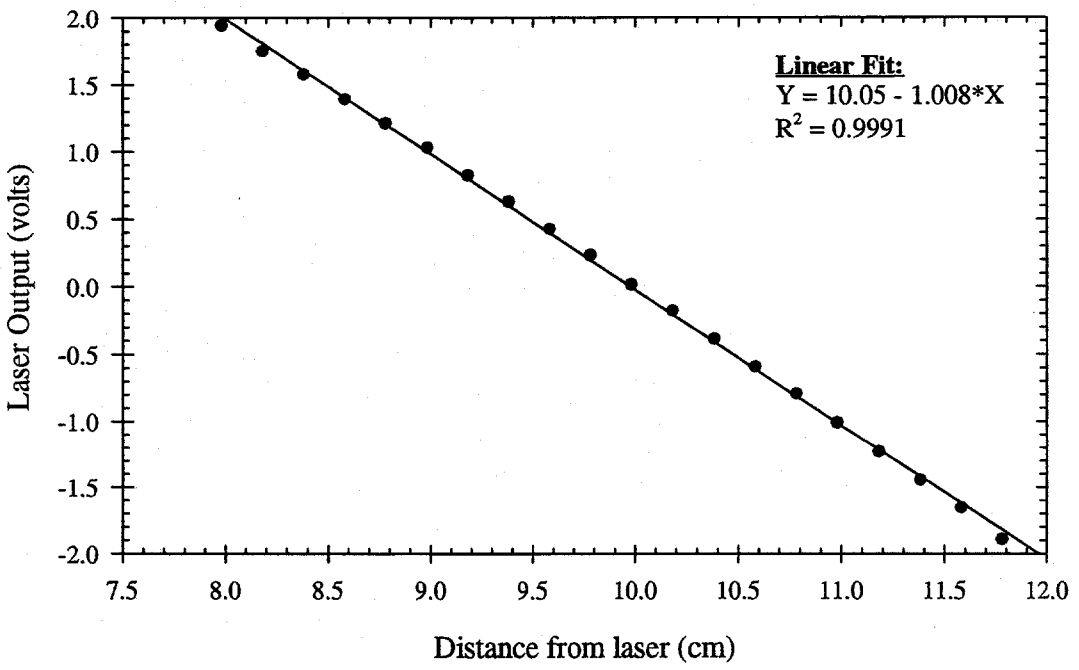

(b) Calibration of distance versus laser voltage over the full range

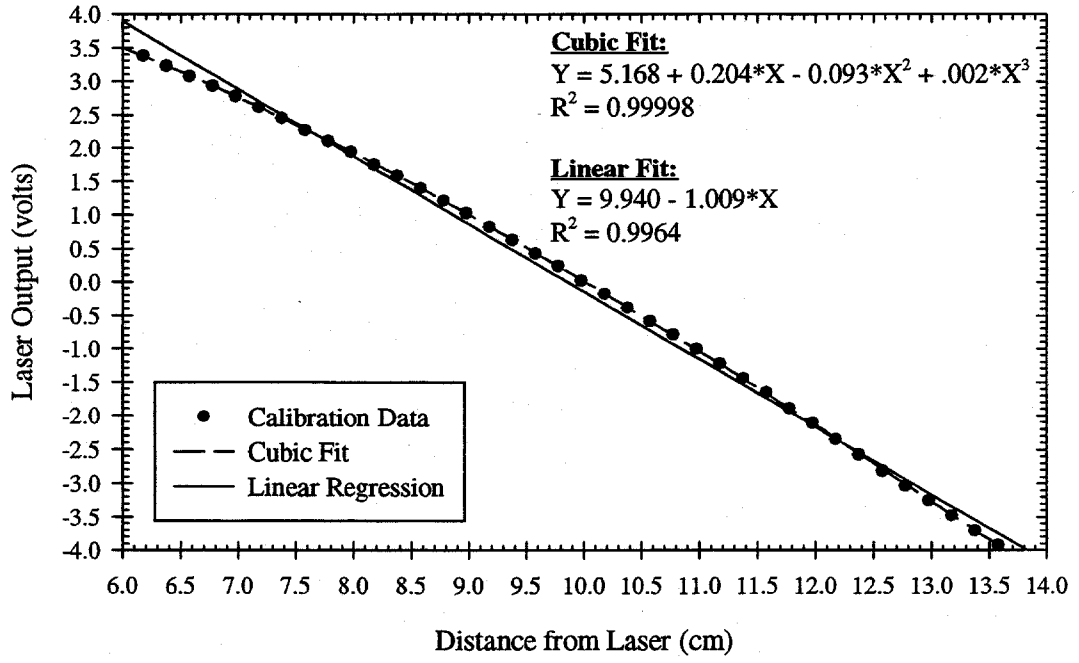

Figure 4.5. Sample calibration curves for laser displacement sensor (Keyence LB70/LB-11) as installed for flume measurements (partly through water).

The laser's voltage output was calibrated to distance by taking measurements on a stationary reddish-purple plastic target (the same color as the garnet sand) attached to a point gauge which was accurate to 0.01 cm. The point gauge readings were then converted into equivalent positions that corresponded to those from the water surface gauge. The voltage and distance were linearly related in the mid-range of the sensor (8-12 cm, see Figure 4.5a), but were better fit by a cubic equation for data that spanned the entire measurement range (Figure 4.5b).

The input and output signals for the stepper motor and the voltage signal from the laser were connected to a 12-bit analog and digital I/O board Data Translation model DT2811 in a PC. A QuickBasic program was written to control movement of the stepper motor and to acquire the bed surface elevations. Bed surface elevations were measured every 4 mm down the centerline of the flume. Bed and water surface profiles for each flume experiment are included in Appendix A.

4.3. SEDIMENT CHARACTERISTICS

Emerald Creek garnet sand was used in all of the flume experiments. Garnet is a common orthosilicate mineral in which the SiO_4 tetrahedra are isolated and bound to each other only by ionic bonds from interstitial cations. The atomic packing is generally dense, causing the minerals of this group to have a relatively high specific gravity and hardness. The angular fractures and high hardness of the garnets make them desirable for a variety of abrasive purposes including garnet sand paper.

4.3.1. Composition

The composition of the sand grains was analyzed by Paul Carpenter using scanning electron microprobe analysis. Approximately 70 percent of the sand grains were almandine garnet; and 30 percent of the grains were staurolite. Many of the sand grains contained quartz inclusions. A few grains of quartz, ilmenite ($FeTiO_3$) and amphibole were present.

The average composition of the almandine garnet sand grains was

$$(Fe_{2.4},Mg_{0.3},Mn_{0.2},Ca_{0.1})Al_2(SiO_4)_3$$

Almandine garnet is a common garnet found in metamorphic rocks, resulting from the regional metamorphism of argillaceous sediments. Almandine garnet is also a widespread detrital garnet in sedimentary rocks.

The average composition of the staurolite grains was $(Fe_{1.7},Mg_{0.3})Al_9O_6(SiO_4)_4(O,OH)_2$. Staurolite is often associated with almandine garnet in metamorphic rocks.

4.3.2. Shape

Larger chunks of almandine garnet were crushed and sieved by the supplier to produce the sand used in the flume experiments. The garnet broke in angular fragments as illustrated in Figure 4.6. The sand grains exhibited sub-conchoidal and uneven (Figure 4.7). The specific surface area (S_A) of the grains determined by dye adsorption (Iler, 1955; Giles and Trivedi, 1969) was 0.12 ± 0.02 m^2/g.

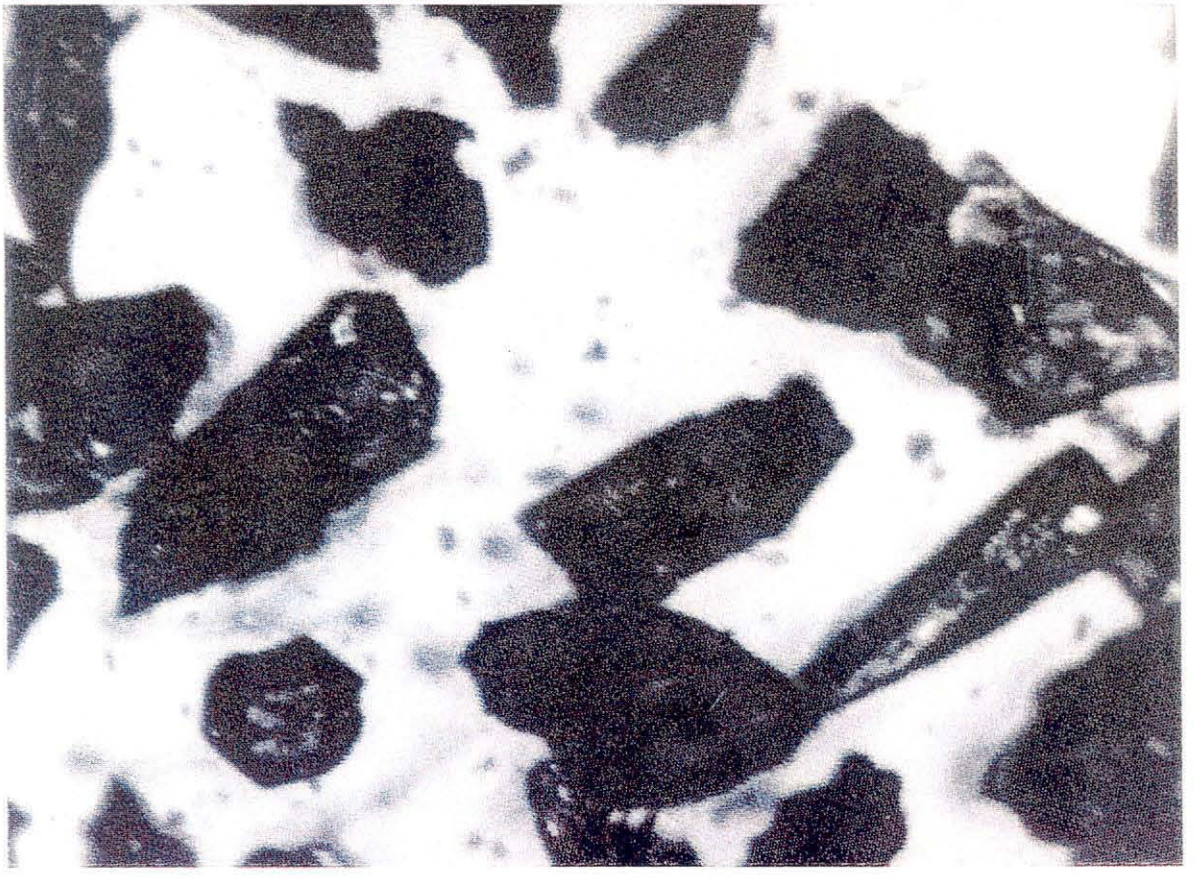

Figure 4.6. Photograph of garnet sand grains.

Figure 4.7. Blow-up of garnet sand grains.

4.3.3. Size

Sieve analyses of the garnet sand were performed using standard sieves in a shaker for five minutes. The results are shown in Figure 4.8. The sand was lognormally distributed with a geometric mean diameter (d_g) of 279 μm and a geometric standard deviation (σ_g) of 1.27.

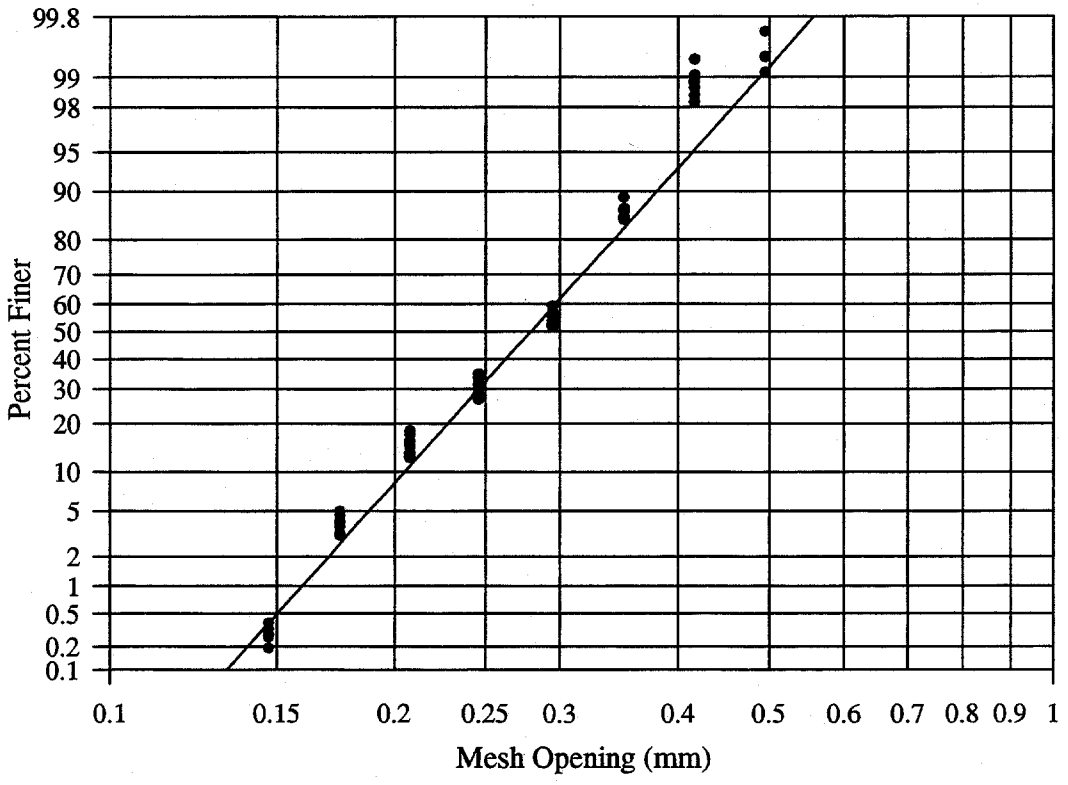

Figure 4.8. Sieve analyses of garnet sand (d_g = 279 μm, σ_g = 1.27).

4.3.4. Particle density

The particle density of the sand was calculated by determining the mass and volume of a sample of sand following the procedure of Blake (1965). The mass was determined by weighing an oven-dried sample (baked at 110°C for 6 to 12 hours) of the sand and by measuring the volume of water displaced by the sample. A mean particle density (ρ_s) of 4.1 g/cm^3 and a standard deviation of 0.1 g/cm^3 was determined from the analysis of eight different samples.

4.3.5. Properties in sediment bed

The hydraulic conductivity (K) of the sand was measured using a falling head permeameter (Bear, 1972). The permeameter consisted of a 14-cm diameter lucite tube with sand

packed to a depth of 15 cm between two permeable plates and polypropylene cloth. The measured hydraulic conductivity of the sand was 0.065 cm/s with a standard deviation of 0.009 cm/s.

The hydraulic conductivity can be estimated using Equation (4.1) (Bear, 1972).

$$K = 6.5 \times 10^{-4} \frac{d_g^2 g}{\nu} \tag{4.1}$$

Using a temperature of 25°C, a kinematic viscosity ν equal to 0.00893 cm^2/s and $d_g = 0.279$ mm, this equation yields a value of 0.056 cm/s for the hydraulic conductivity, which is in good agreement with the measured value. A value of 0.06 cm/s is used for all calculations.

The porosity (θ) was determined by measuring the volume of water required to fill the voids in 1.5 kg of oven dried sand. The dried sand was placed in a 1-liter glass graduated cylinder, and then water was added in measured amounts until the sand was saturated. The sand/water mixture was shaken and stirred to remove air bubbles, then the sand was consolidated by tapping on the side of the cylinder. The porosity was calculated by dividing the volume of water required to fill the voids by the bulk volume of the mixture. The measured porosity was 0.47 ± 0.01. The porosity depends on the packing of the grains, their shape, arrangement and size distribution. The porosity for uniform sand varies from 0.30 to 0.40 (Bear, 1972). The higher porosity value for the garnet sand can probably be attributed to the angularity of its grains.

4.3.6. Microparticle electrophoresis

The surface of a silicate mineral, when immersed in water, tends to behave as if it were the surface of a composite oxides made up of SiO_2 and M_xO_y, with H^+ and OH^- functioning as potential-determining ions (Fuerstenau and Raghavan, 1978). The surface contains broken -Si-O and -M-O bonds that chemisorb water to cover the surface with hydroxyl groups. These hydroxyl groups can adsorb/dissociate hydrogen ions, giving rise to a positive or negative charge at the surface, depending on the pH of the medium (Figure 4.9).

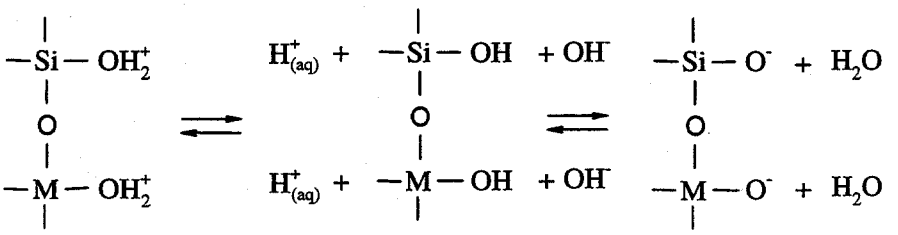

Figure 4.9. Schematic representation of silicate charged surface.

The pH at which the number of positive and negative sites is equal and the surface is uncharged is referred to as the pH of the point of zero charge (pH_{pzc}) or the isoelectric point. It is the condition where particles do not move in an applied electric field.

The pH_{pzc} of the garnet sand was determined by finding the pH at which the electrophoretic mobility of the garnet particles was zero. Garnet particle mobilities were investigated using a Mark II particle microelectrophoresis apparatus (Rank Brothers, London) with a flat cell 1mm thick and 10 mm high. The cell was cleaned by soaking in 2M HCl and then rinsed in 18.2 MΩ-cm Milli-Q water.

Small garnet particles (1-20 μm) required for mobility measurements were obtained by crushing clean sand grains in a shatterbox. The particles were equilibrated with a solution of desired ionic strength and pH for 24 hours before their mobilities were measured. In each measurement, at least 10 particles were timed in each direction of movement. The electric field was between 2 and 10 Volt/cm, and the particles traveled at least 250 μm. All measurements were taken at the solvent's stationary level where the observed particle velocity equals its own electrophoretic velocity. The temperature was maintained at 25°C.

a) Mobility

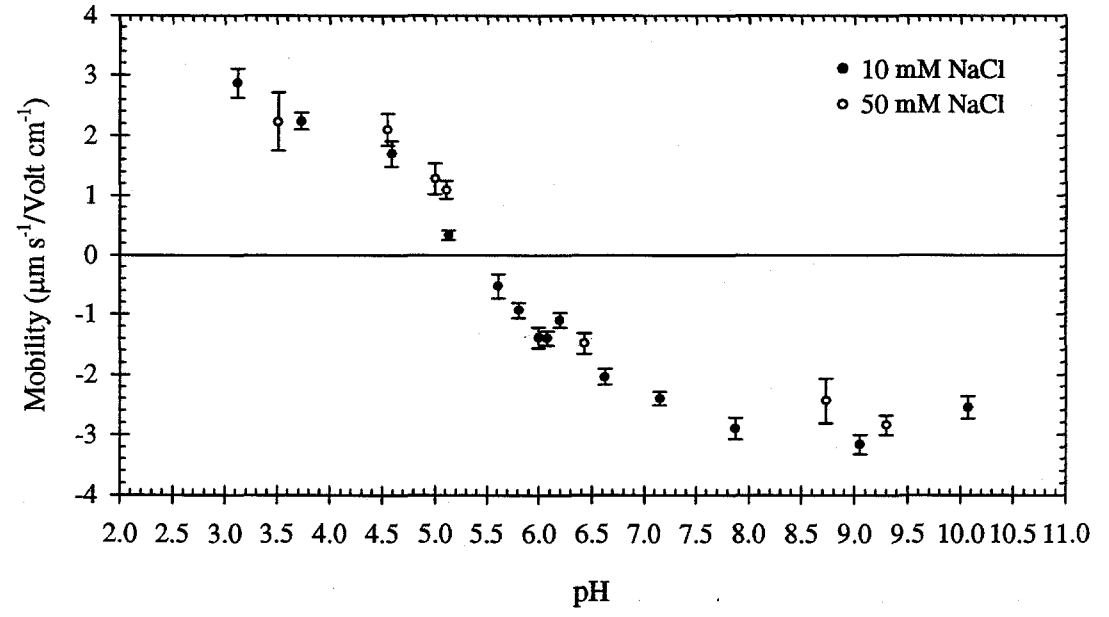

b) Zeta potential

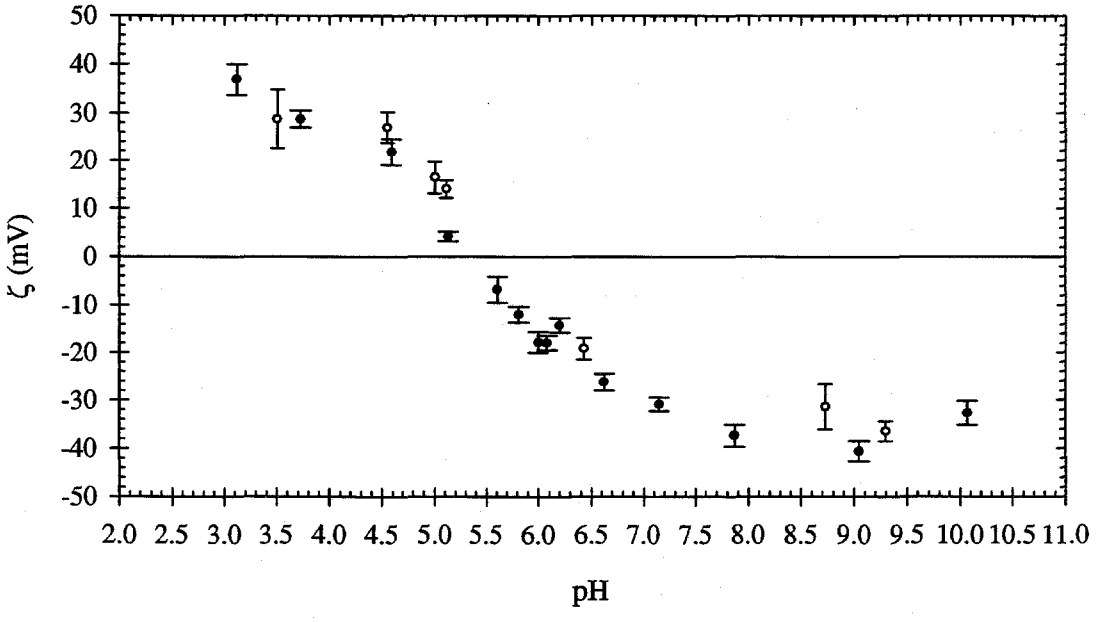

Figure 4.10. Electrophoretic mobility (a) and zeta potential (b) of garnet plotted as a function of pH at 25°C. The ionic strength is adjusted by NaCl.

The effect of pH on the mobility of garnet at constant ionic strength is illustrated in Figure 4.10. The mobility of garnet was investigated at two different ionic strengths of 0.01 M and 0.05 M NaCl. Since $\kappa d_p > 200$ (κ is the Debye parameter and d_p is the diameter of the particles), the zeta potential ζ was calculated using the Smoluchowski equation

$$\zeta = \frac{\eta}{\varepsilon_r \varepsilon_0} u_{ep} \tag{4.2}$$

where u_{ep} is the measured mobility, η is the dynamic viscosity of water at (0.894×10^3 N·s/m^2 at 25°C), ε_r is the relative dielectric constant of water (78.5 at 25°C), and ε_0 is the permittivity of free space (8.854 x 10-12 C/V·m). The measurements indicate that the pH_{pzc} of the garnet sand is 5.4 ± 0.1, which is close to the measured pH_{pzc} of 5.8 for almandine garnet (Lai, 1970).

4.3.7. Choice of sediment

Because of their availability and chemical purity, Ottawa and other silica sands have been used in bed/stream exchange research at Caltech (Elliot, 1990; Elliott and Brooks, 1997b; Eylers 1994; Packman, 1997). Natural river sediments are generally coated with iron, aluminum and manganese oxides. In an effort to more closely simulate natural river bed sediments, iron oxide coating of the silica sand was considered (Edwards and Benjamin, 1989; Stahl and James, 1991; Scheidegger et al., 1993). Due to the inability to collect developing acid fumes while heating the sand to 100°C, it was not technologically feasible to reproducibly coat the large amount of silica sand (~250 kg) required in the flume experiments. Because of the extremely difficult in creating reproducible iron oxide coatings on silica sand, garnet sand, which has a high iron and aluminum content, was chosen as an alternative. The properties of the garnet sand are summarized in Table 4.1.

Table 4.1. Summary of garnet sand properties.

Property	Symbol	Value
Mean grain diameter	d_g	279 μm
Geometric standard deviation	σ_g	1.27
Particle density	ρ_s	4.1 g/cm^3
Specific surface area	S_A	0.12 m^2/g
Hydraulic conductivity	K	0.06 cm/s
Porosity	θ	0.47
pH at point of zero charge	pH_{zpc}	5.4

The garnet sand has several advantages over silica sand in the study of stream/bed exchange in the flume. Garnet sand is more dense than silica sand (specific gravities of 4.1 and 2.65, respectively). Consequently, sediment motion for the garnet sand grains occurs at higher fluid velocities compared to those necessary for silica sand motion. The magnitude of advective pumping is proportional to the square of the average fluid velocity in the channel, so higher flows have higher pumping rates. A broader range of advective pumping rates can be used for stationary bedform experiments with the garnet sand than with silica sand.

The pH_{pzc}'s for garnet and silica sands are 5.4 and 2, respectively. In the pH range of natural waters (5-8), the garnet surface can be positively charged, neutral or negatively charged, whereas the silica sand surface is highly negative. When using garnet sand, a larger variety of chemical compounds (anionic, cationic and neutral) can be used to study stream/bed exchange coupled with adsorption.

4.4. Conservative Tracers

Conservative tracers (i.e., non-reactive tracers) were used in the flume experiments to measure the exchange of solution between the water column and the sediment bed and to verify the hydraulic parameters used in the model. Previous researchers (Eylers, 1994; Packman, 1997)

used the lithium ion as a conservative tracer. However, after five flume experiments, lithium adsorption to garnet sand was discovered. Bromide was used as the conservative tracer in the remaining flume runs.

LiCl crystals (E. M. Science Guaranteed Reagent) were dissolved into solution for both batch adsorption and flume experiments. Bromide was associated with the surfactant salts.

4.5. CATIONIC SURFACTANTS

The sorbate used in the flume experiments had to be relatively non-toxic in order to permit disposal of the large volume of wastewater generated in the flume experiments (~85 ℓ). The sorbate also had to be non-volatile, exhibit nonlinear adsorption, and behave conservatively in the flume. Cationic surfactants satisfied these criteria.

A series of alkyltrimethylammonium compounds, which had varying hydrocarbon chain lengths and exhibiting weak to strong adsorption, were used. Figure 4.11 illustrates the structure of these compounds.

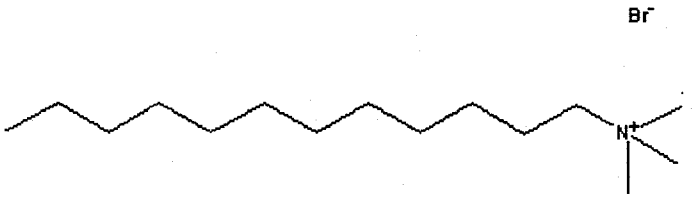

Figure 4.11. Chemical structure of alkyltrimethylammonium-bromide salts.

Their properties are listed in Table 4.2. All of the compounds have pK_a's greater than 10 (Streitwieser and Heathcock, 1981).

Table 4.2. Properties of alkyltrimethylammonium compounds used in experiments.

Compound (Abbreviation) *(CAS Registry Number)*	Chemical Formula	Critical Micelle Concentration*	Supplier
Nonyltrimethylammonium bromide (NTMA) *(1943-11-9)*	$CH_3(CH_2)_8N(CH_3)_3Br$	140 mM	J. T. Baker
Dodecyltrimethylammonium bromide (DTMA) *(1119-97-4)*	$CH_3(CH_2)_{11}N(CH_3)_3Br$	10 mM	Aldrich 99% pure
Myristyltrimethylammonium bromide (MTMA) *(1119-97-7)*	$CH_3(CH_2)_{13}N(CH_3)_3Br$	1 mM	Aldrich 99% pure
Octadecyltrimethylammonium bromide (OTMA) *(1120-02-1)*	$CH_3(CH_2)_{17}N(CH_3)_3Br$	0.3 mM	Aldrich

*Mukerjee and Mysels (1970)

4.6. Batch Adsorption Experiments

Batch experiments were conducted to develop equilibrium adsorption isotherms at fixed pH and ionic strength, to study adsorption kinetics and to investigate adsorption as a function of pH. Each batch experiment consisted of garnet sand, an adsorbing compound, the supporting electrolyte and Milli-Q water (18.2 MΩ-cm). The extent of adsorption was determined by measuring the loss of the adsorbing compound from solution and applying a mass balance equation to calculate the amount of the compound adsorbed.

The cleaning procedure for all plastic and glassware included three different washes: detergent, acid and methanol. The washing steps are outlined below:

1. Soak overnight in a 1% solution of Extran 300 general purpose liquid detergent used to remove routine laboratory contamination as well as soil, grit, oil, grease and low-level radioactive and protein contamination.
2. Rinse in deionized water (plastics five times and glass seven times).
3. Soak in heated 10% nitric acid (E.M. Science Tracepur) bath 12 to 24 hours to desorb trace metals.
4. Rinse four times in deionized water.
5. Soak overnight in methanol to remove any remaining detergent residues.
6. Rinse two times in deionized water and bake at 90°C for 6 to 12 hours to remove methanol residue.

All solutions were mixed and stored in polypropylene beakers, cylinders and flasks. pH measurements were conducted using a Corning High Performance Combination Electrode (Catalog No. 476390) and a Corning pH meter (Model 345). The batch experiments were conducted in 50-mℓ Corning polypropylene centrifuge tubes. A measured amount of sand and 30 ml of a solution containing a known concentration of the adsorbing compound, supporting electrolyte (NaCl) and H^+ was added to the tube and shaken by hand. The tube was then placed on a Thermolyne Labquake rotator that revolved at a speed of 8 rpm. The pH was measured periodically and small amounts of acid (HCl) or base (NaOH) were added to adjust the pH as needed.

For the kinetic studies, 250 μℓ of the liquid phase was removed at several different time intervals. For equilibrium adsorption experiments, the sand/water mixture was allowed to equilibrate for 24 hours and then the liquid and solid phases were separated. Concentrations in the liquid phase were measured.

4.7. ANALYSIS METHODS

4.7.1. Inductively coupled plasma mass spectrometry (ICP-MS)

An ion coupled plasma mass spectrometer (Perkin-Elmer Elan 5000) was used to measure lithium and bromide ion concentrations. The samples were prepared in 2.5 percent nitric acid (E. M. Science Tracepur) and stored in 15-mℓ Corning polypropylene centrifuge tubes. Reference concentration solutions were prepared from commercial standards (J. T. Baker ICP-MS 1000 ppm Li^+ Standard in 5 percent HNO_3 and VWR Scientific 1000 ppm NaBr Standard). The lower detection limit of the ICP-MS was 4 ppb (0.6 μM) for lithium and 10 ppb (0.1 μM) for bromide. The maximum bromide concentration that could be analyzed without affecting the background concentration levels was 200 ppb (2.5 μM). Instrument drift was monitored by reanalyzing the standards once every hour.

4.7.2. Capillary electrophoresis

Capillary electrophoresis (Hewlett-Packard 3D CE G1600) with indirect UV detection was used to analyze surfactant concentrations greater than 50 μM. The separation method was based on the procedure developed by Weiss et al. (1992). The buffer consisted of 60 percent tetrahydrafuran (J. T. Baker Stabilized, HPLC Grade) and 40 percent Milli-Q water, 3 mM benzyldimethyldodecylammonium bromide (Aldrich, 97% pure), 3 mM of sodium dodecyl sulfate (Aldrich, 98% pure) and 10 mM sodium phosphate, monobasic monohydrate (E. M. Science Guaranteed Reagent, 99% pure). The buffer was prepared by first mixing the appropriate volumes of tetrahydrafuran (THF) and water. This mixture was vacuum filtered through a Gelman Science Type A/E glass fiber filter (1 μm). The salts were added to the THF-water solution, and the mixture was vacuum filtered and degassed. The concentrations of THF and

water reported reflect the volume percentages of the original amounts of THF and water that were actually mixed. Some THF was lost during filtration.

The capillary (Supelco P175) was composed of bare fused silica with a neutral hydrophilic coating that reduced sample and capillary wall interactions. The capillary had an inner diameter of 75 μm and an effective length of 56 cm. The capillary was pre-conditioned by rinsing with the buffer for one hour and then running three baselines. Post-conditioning included methanol and water flushes. The applied electric field strength was 36 kV/m. The samples were injected by pressure.

250 μℓ of standard solutions and samples were mixed with 250 μℓ of methanol. Standard solutions were analyzed at the beginning and end of each run. Each sample was analyzed twice. The time required for peak separation averaged 30 minutes. The peak areas of the standards were calibrated to their known concentrations. The measured concentrations were accurate to 10 percent. Nonyltrimethylammonium ion concentrations could not analyzed using capillary electrophoresis.

4.7.3. Dye extraction

Samples having cationic surfactant concentrations less than 60 μM were measured using the Orange II dye extraction method developed by Few and Ottewill (1956). Samples having concentrations greater than 60 μM could be analyzed by this method if they were diluted. A 250-μM Orange II (Aldrich, 98% pure) solution was prepared with 0.1 M NaCl. A solution composed of 5 mℓ of chloroform (E. M. Science Omnisolv), 1 mℓ of the dye mixture, 0.5 mℓ of 2N HCl and 3.5 mℓ of the sample was mixed in a glass test-tube sealed with a teflon coated cap. The tubes were shaken 50 times and then allowed to settle overnight. The cationic surfactant formed a complex with the anionic dye. The complex was insoluble in the aqueous phase and transferred

into the chloroform phase. The uncomplexed dye was insoluble in chloroform and remained in the aqueous phase.

The aqueous phase was extracted and its absorbance was measured in a glass cell (1-cm path length) at 484 nm by a Hewlett-Packard UV/Vis Spectrophotometer 8450A. The absorbance of a blank solution, prepared according to the method described above with 3.5 mℓ of Milli-Q water, was measured to determine the initial dye concentration. Reference solutions with known surfactant concentrations were used to develop calibration curves relating the measured absorbance of the aqueous phase to the surfactant concentration. The measurements were accurate to 10 percent for surfactant concentrations less than 10 μM and 5 percent for concentrations between 10 and 60 μM. Dodecyltrimethylammonium, myristyltrimethyl-ammonium and octadecyltrimethylammonium had a complexation ratio of 1:1 with the dye, whereas nonyltrimethylammonium had a ratio of 2:1.

4.8. SEDIMENT PREPARATION

4.8.1. Sand washing apparatus

The sand was washed in the apparatus shown in Figure 4.12 and Figure 4.13 (after Elliott, 1990). Lucite tubes, having an inner diameter of 20 cm and a height of 180 cm, were filled with sand to a depth of 70 cm; the sand was held by a stainless steel screen. The washing solution was pumped from the polyethylene reservoir, through a spun-polypropylene sediment cartridge (Amtek Model P5 5μm), then upward through the washing tubes fluidizing the sand (Figure 4.14) and returned via an overflow outlet at the top of the washing tube to the reservoir through polypropylene hoses.

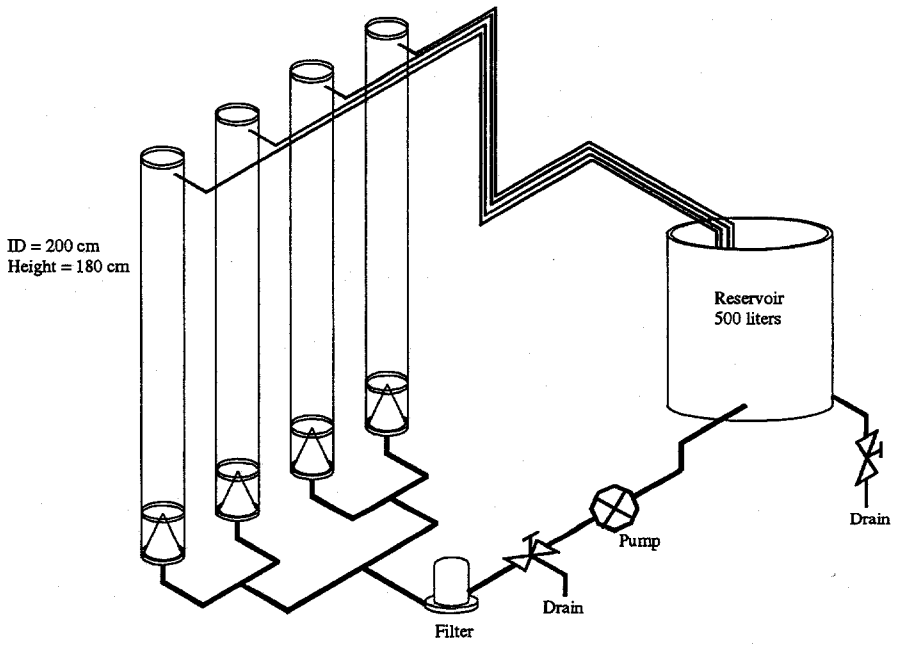

Figure 4.12. Diagram of washing system.

Polypropylene pipe, ball valves and gate valves were used in the system. Flow straightening cones installed at the base of each washing tube inhibited the development of preferential flow patterns and ensured uniform fluidization of the sand. Gate valves installed in the manifold regulated the flow rate into the tubes. The flow was adjusted until the sand column expanded 100 percent. The top of the fluidized sand was kept below the tube outlets. 500 liters of washing solution was used to clean 190 kg of garnet sand (half of the amount required for flume experiments). A total of 570 kg of garnet sand was in use, so that some of the washing could be done concurrently with the flume experiments.

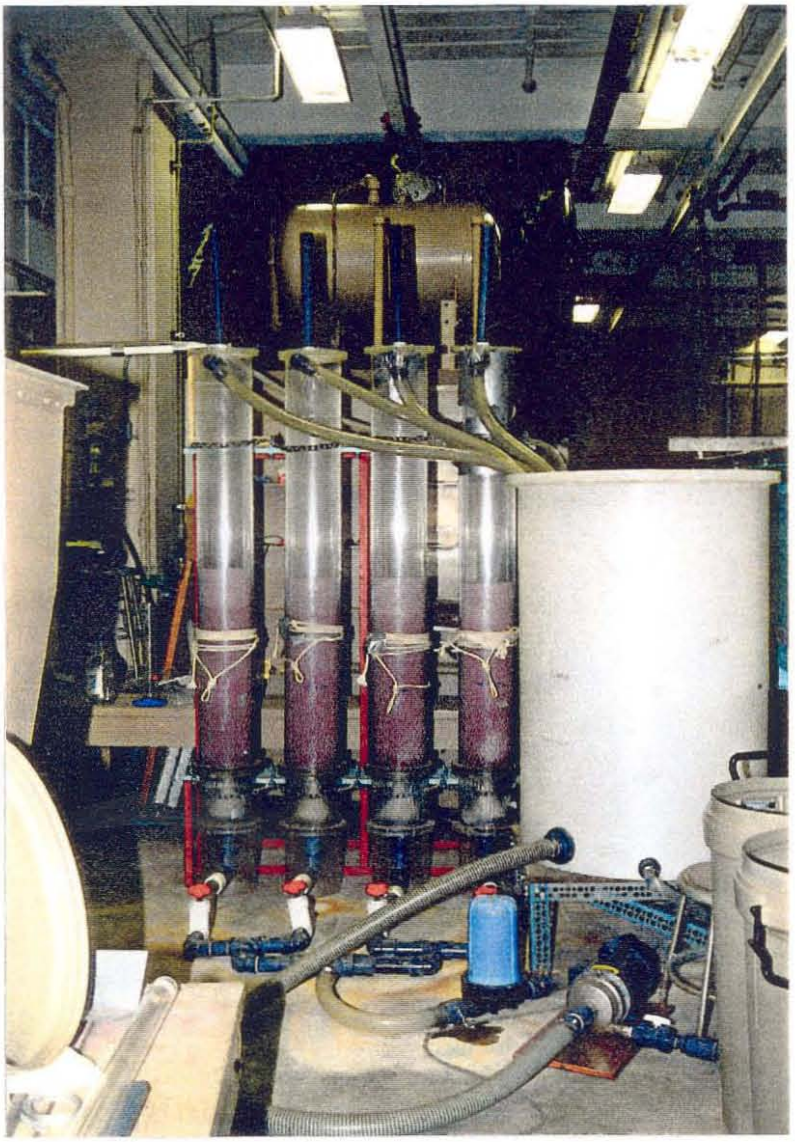

Figure 4.13. Photograph of washing system.

4.8.2. Sand pre-treatment

New sand (direct from the supplier) contained a significant amount of iron oxides and other fine particles (Figure 4.14).

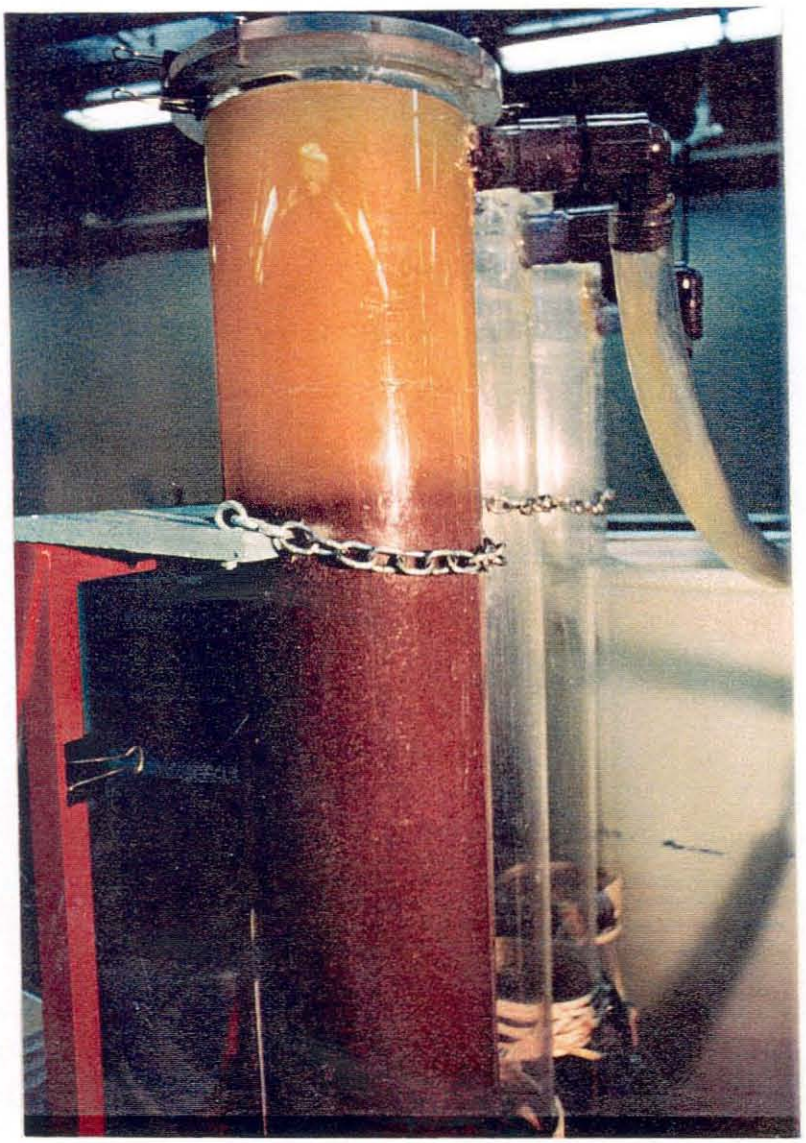

Figure 4.14. Photograph of new sand being washed in the fluidized bed in the washing system.

The sand was rinsed with deionized water until the solution was clear (5 to 6 rinses). The sand required further treatment to remove noncrystalline forms of iron and aluminum, which

would skew the adsorption experiments. Batch experiments, which investigated the effectiveness of several treatment methods outlined by Ross and Wang (1993), were conducted. A 2-mM acid ammonium oxalate mixture adjusted to a pH of three was determined to be most suitable method. After six treatments, the following was removed: 0.82 mg Fe/gram of sand, 0.09 mg Al/gram of sand and 0.13 g Si/gram of sand.

After the initial deionized water rinses, the sand was treated six times using the following procedure:

1. Wash for 16 hours with 500 liters of a solution containing 2 mM oxalic acid and 2 mM ammonium oxalate.
2. Rinse with deionized water for one hour.
3. Rinse in a 2-mM sodium bicarbonate solution at pH 8 for 12 hours. This step removed trace amounts of oxalate and returned that sand surface to the condition required for the flume experiments.

4.8.3. Sand treatment between flume experiments

The sand needed to be washed between all of the flume experiments to remove the adsorbed surfactants. Batch experiments were conducted to develop an effective washing method. For pH's less than five, the garnet surface was positively charged, and there was an electrostatic repulsion between the sand surface and the cationic surfactant. However, trace amounts of surfactant ions still adsorbed to the surface via hydrophobic bonding. The batch experiments showed that a series of acid washes was required to remove all of the adsorbed surfactant ions from the sand.

The sand washing sequence is described below:

1. Wash with 500 liters of an HCl solution at pH 2.5 for 12 hours.
2. Rinse two times with deionized water.
3. Wash 8 to 12 hours with a 2-mM bicarbonate solution (pH = 8).

Sand with adsorbed nonyltrimethylammonium required two washing sequences; adsorbed dodecyltrimethylammonium required three sequences; adsorbed myristyltrimethylammonium required five sequences; and adsorbed octadecyltrimethylammonium required ten sequences. Afterwards, the sand was treated with the oxalate wash described in Section 4.8.2 in order to assure that the garnet surface had the same properties for each flume experiment. Table 4.3 lists the total time required to clean one batch of sand (190 kg) for each cationic surfactant, with the washing system in operation 24 hours a day.

Table 4.3. Sand washing time requirements.

Cationic Surfactant	Time in days
Nonyltrimethylammonium ($NTMA^+$)	4
Dodecyltrimethylammonium ($DTMA^+$)	5
Myristyltrimethylammonium ($MTMA^+$)	7
Octadecyltrimethylammonium ($OTMA^+$)	12

4.9. EXPERIMENTAL PROTOCOL

The basic approach in conducting a flume experiment is first to establish the desired experimental conditions (water chemistry, bedforms and flow); acquire a bed profile; add the

conservative tracer and cationic surfactant; take water samples over a period of several days; and measure the concentrations in the samples. The duration of each flume experiment, including flume preparation and analysis time but excluding sand washing, ranged from 13 to 20 days. The detailed experimental protocol is described below.

1. The flume was cleaned to remove surfactant residues, trace metals and bacterial growth as follows: rinse two times with deionized water to remove surfactant residues; soak with a dilute nitric acid solution to remove trace metals; rinse two times with deionized water; soak with a chlorine solution to eliminate bacterial; and rinse four times with deionized water (3 days).

2. 250 liters of deionized water was added to the flume. Sodium chloride and sodium bicarbonate were added to the water to produce final concentrations of 10 mM and 2 mM, respectively. The pH was adjusted as necessary using 2N NaOH. The system was allowed to equilibrate overnight (12 to 24 hours).

3. Clean sand was scooped into the flume. In order to remove potential air pockets, all of the sand was resuspended and recirculated in the flume at a moderate flow rate. The sand bed was compacted by lightly tapping the flume walls with a rubber mallet. The surface of the bed was flattened using a lucite plate attached to an instrument carriage (3 hours).

4. The sand experienced a small amount of mechanical abrasion during Step 3 and some fine particles were present in the water column. Since these particles would interfere with the adsorption experiment, the flume water (excluding porewater) was drained and deionized water was added to the desired depth. With the flume running slowly to allow mixing,

sodium chloride and sodium bicarbonate were added so that their concentrations were equal to those in Step 2. Air was then purged from the manometer lines (1 hour).

5. The flow rate was set high enough to induce sediment motion which created bedforms. The system ran until the bedforms had developed fully. The flow was stopped and a bed profile was acquired (1 day).

6. The flume was adjusted to a horizontal position (no slope). The still horizontal water surface was measured.

7. The hydraulic conditions (depth and flow rate) for the bed/stream exchange experiment were established. The flume slope was adjusted until uniform flow was achieved. The flow was stopped and a still water surface profile was measured. The slope of the flume (the hydraulic grade line) equaled the slope of the line fit to the differences between these still water surface measurements and those measured in Step 6 (12 to 24 hours).

8. The flow was resumed and the subsurface recirculation system was started. The speed of the peristaltic pump was set so that the subsurface flow rate equaled the product of the hydraulic conductivity, the hydraulic grade line, the bed width and ¾ of the bed depth. A flowing water surface profile was acquired.

9. The bed exchange and adsorption experiment began. One liter of flume water was removed and mixed with known amounts of the conservative tracer and the cationic surfactant. This solution was slowly added to the flume over a period equal to the time required to circulate the total volume of water in the flume (83 liters). The timer was started after this addition (defined as $t = 0$).

10. Overlying water samples were acquired by dipping 50-ml Corning polypropylene tubes into the water column. During the first ten to fifteen minutes, samples were taken every two minutes at two different locations along the flume. These samples were used to determine the initial concentration of the chemical compounds and the state of overall mixing in the flume. Samples were taken every hour for the first 10 hours, every three hours until t = 24 hours, then every four to six hours during the remainder of the experiment (3 to 7 days).

11. Porewater samples were acquired by inserting a 26-gauge Hamilton hypodermic needle through the rubber sampling ports in the flume wall. One milliliter of porewater was extracted into a plastic syringe. Porewater profiles were acquired at 12 hours and 24 hours, then once daily until the end of the experiment.

12. Flowing water surface profiles were measured periodically. Deionized water was added to the flume to compensate for evaporation losses (1 to 2.5 liters per day). The pH and water temperature was monitored throughout the experiment.

13. The samples were analyzed at the conclusion of the experiment.

14. For lithium analysis of the overlying water samples, 5 mℓ of the sample was diluted into 5 mℓ of 5% HNO_3 then analyzed on the ICP-MS. For the porewater samples, 0.5 mℓ was diluted in 5 ml of 2.5% HNO_3 (3 days).

15. Sample dilution for the ICP-MS bromide measurements was determined by calculating the sample volume required to dilute the initial Br^- concentration to 2 μM. Sample preparation and analysis time totaled three days.

16. The concentration of the cationic surfactants in all of the overlying water samples was analyzed using Orange II dye extraction method discussed in Section 4.7.3 (2 days). Overlying water samples that had surfactant concentrations greater than 100 μM were also analyzed using capillary electrophoresis (1-3 days). Due to their small volume, the surfactant concentrations in the porewater samples were analyzed using capillary electrophoresis (5 days).

5. EXPERIMENTAL RESULTS

In this chapter, the experimental and modeling results are presented and discussed. The adsorption isotherms, which were determined in batch experiments, are incorporated into the bed/stream exchange models, which predict the mass transfer of bromide ions, lithium ions and cationic surfactants into a garnet sand bed in a recirculating flume. The results of the flume experiments are used to test the models.

First, the results of the kinetic and equilibrium batch adsorption experiments are presented in Section 5.1, and then the data and modeling results for the individual flume experiments are included in Section 5.2. A detailed discussion of the modeling results and a sensitivity analysis proceed in Chapter 6.

5.1. BATCH ADSORPTION EXPERIMENTS

The partitioning of solutes between the stream water and sediment bed is modeled by an empirical sorption isotherm, which is derived from batch experiments. Equations for the Langmuir, Freundlich, Langmuir-Freundlich and the Tóth isotherms are fitted to the adsorption data. These isotherms are not used to identify adsorption mechanisms. They are used strictly to provide a mathematical function that can be incorporated into the bed/stream exchange models that include nonlinear equilibrium adsorption reactions.

The isotherm equations are fitted to the data using the Lorentzian minimization method. This fitting method reduces the effect that the outlying data points have on the fitted parameters. The following quantity is minimized in the curve fit:

$$\text{Minimize} \sum \ln\left(1 + |y_i - \hat{y}_i|^2\right) \tag{5.1}$$

where y is the y-value of a given (x, y) data pair, and $\hat{y}$ is the value computed from the curve-fit equation at this same x-value.

The adsorption of lithium, bromide and surfactant ions onto garnet sand was studied in batch experiments. The properties of the sand and the chemicals were described in Chapter 4. The experimental procedures were also outlined in Chapter 4. Most of the equilibrium adsorption experiments were conducted in 10 mM NaCl solutions at constant pH and temperature (23°C). The pH of the solution was measured periodically during the experiments, and small amounts of acid (HCl) and base (NaOH) were added as needed to adjust the pH to the desired level. The adsorption time scale was determined from kinetic adsorption studies. In order to identify the optimum pH for the flume experiments, equilibrium batch experiments were performed to study the effect of pH on adsorption. Table 5.1 summarizes the adsorption experiments presented in this section.

Table 5.1. Summary of batch adsorption experiments.

Ion	Equilibrium Adsorption	Kinetic Adsorption	pH Effects
Bromide	Yes – pH = 8	No	No
Lithium	Yes – pH = 8	No	No
Dodecyltrimethylammonium ($DTMA^+$)	Yes – pH = 7,8	Yes	Yes
Myristyltrimethylammonium ($MTMA^+$)	Yes – pH = 8	Yes	Yes
Nonyltrimethylammonium ($NTMA^+$)	Yes – pH = 8	No	No
Octadecyltrimethylammonium ($OTMA^+$)	Yes – pH = 8	No	No

The adsorption data exhibit a considerable amount of scatter. The scatter can be attributed to both analytical techniques and physical processes. The sorbed concentrations are determined by the mass depletion method using the following formula:

$$S = \frac{(C_{initial} - C_{final}) \cdot V_s}{m_s} \tag{5.2}$$

where C is the concentration in solution, S is the concentration on the solid, V_s is the solution volume and m_s is the mass of sand. The errors in V_s and m_s are small compared to the aqueous concentration measurements. The error in the sorbed concentration is calculated using

$$\Delta S = \frac{V_s}{m_s} \sqrt{(\Delta C_{initial})^2 + (\Delta C_{final})^2} \tag{5.3}$$

When the difference between the initial and final concentrations is small, a relatively large error can be carried over to the sorbed concentration and $\Delta S/S$ becomes large. Consequently, some of the scatter in the adsorption data can be attributed to the method used to calculate S.

The sand experienced some mechanical abrasion during the adsorption experiments and generated some fine particles. The amount of fine material varied with the water to sand ratio of the sample. The sorbed concentration reflects the amount adsorbed on both the bulk sand and the fines. When a considerable amount of fines was present, the amount adsorbed onto the fine particles could be significant compared to that adsorbed on the bulk sand, and thus introduced additional error into the adsorption results. This possible error has not been quantified.

The adsorption results for the individual compounds are presented in Sections 5.1.1 through 5.1.6. Since the adsorption of NTMA onto garnet sand is not studied in detail, the results of the batch adsorption experiments are presented after the results for DTMA, MTMA and OTMA. In Section 5.1.7, the adsorption results for the cationic surfactants are summarized and the effects of the hydrocarbon chain length are discussed.

5.1.1. Bromide adsorption

Bromide adsorption onto the garnet sand was studied in the presence of the cationic surfactants. The initial bromide and surfactant concentrations were equal. Within experimental error, the bromide did not adsorb to the garnet sand. Therefore, bromide can be used as a non-reactive tracer (i.e., conservative tracer) in the flume experiments.

5.1.2. Lithium adsorption

Both Eylers (1994) and Packman (1997) used the lithium ion as a conservative tracer in their bed exchange experiments with quartz sands. However, lithium adsorbed to the garnet sand. Lithium adsorption has also been observed in groundwater systems (Newman et al., 1991 and Zhang et al., 1998). Newman et al. (1991) observed that the adsorption isotherm for lithium on crushed tuff from Yucca Mountain was nonlinear. They found that the Langmuir and the Langmuir-Freundlich isotherms best represented their adsorption data.

The batch adsorption data and isotherm fits for lithium adsorption on garnet sand at pH 8 are depicted in Figure 5.1. The data are plotted on a log-log scale in Figure 5.1b to emphasize the difference in the fitted isotherms at low concentrations. The errors in the aqueous concentration measurements (C) range from 2 to 10 percent, and the errors in the sorbed concentration (S) range from 10 to 100 percent.

Since the garnet sand is negatively charged at pH 8 (see microparticle electrophoresis measurements Chapter 4, Section 4.3.6), some of the lithium ions migrate into the diffuse layer and attain an equilibrium distribution that maintains a constant electrochemical potential throughout the system (Stone et al., 1993). The fraction of lithium ions adsorbed as part of the diffuse swarm is calculated using the method given by Stone et al. (1993) (Chapter 2, Section 2.3.1). The results of this calculation for each of the lithium adsorption experiments are tabulated

in Appendix E. The zeta potential of the garnet sand at pH 8 in 10 mM NaCl is -40 mV (Chapter 4, Figure 4.10). The magnitude of the potential at the sand surface is higher than the zeta potential (Chapter 2, Section 2.3.1). Assuming a surface potential Ψ_0 of –60 mV, the fraction of lithium ions contained in the diffuse swarm $f_{a,coul}$ is 1.4×10^{-6}; if Ψ_0 = -100 mV, $f_{a,coul}$ increases to 3.7×10^{-6}. In the batch adsorption experiments, the fraction of lithium ions adsorbed onto the garnet sand ranges from 0.017 to 0.29. Therefore, the amount of lithium ions adsorbed on the garnet sand exceeds the amount expected from coulombic interactions, and the lithium ions form a surface complex. Further experiments are required to determine the adsorption mechanism and surface complexation constants.

The fitted parameters for the isotherms are listed in Table 5.2. The lithium concentrations in the flume experiments range from 25 to 100 μM. In this concentration range, the Langmuir, Tóth and Langmuir-Freundlich isotherms coincide. The Freundlich isotherm differs significantly for concentrations less than 15 μM and greater than 70 μM. The ranking of the isotherms based on the degree of freedom adjusted R^2 is:

Langmuir > Tóth > Langmuir-Freundlich > Freundlich

In the bed exchange models, the Langmuir isotherm is used to model lithium adsorption. The Tóth and Langmuir-Freundlich isotherms are not used in bed exchange models because they coincide with the Langmuir fit. The difference in the bed/stream exchange predictions using the Freundlich isotherm is considered Chapter 6, Section 6.9.

a) Linear scale

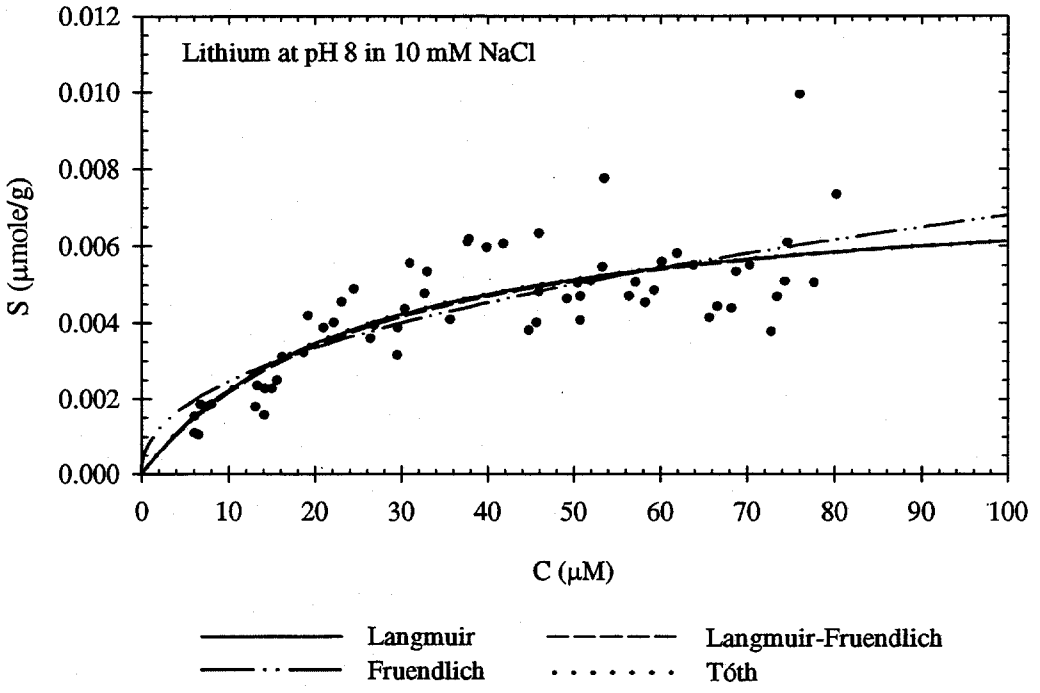

b) Log scale

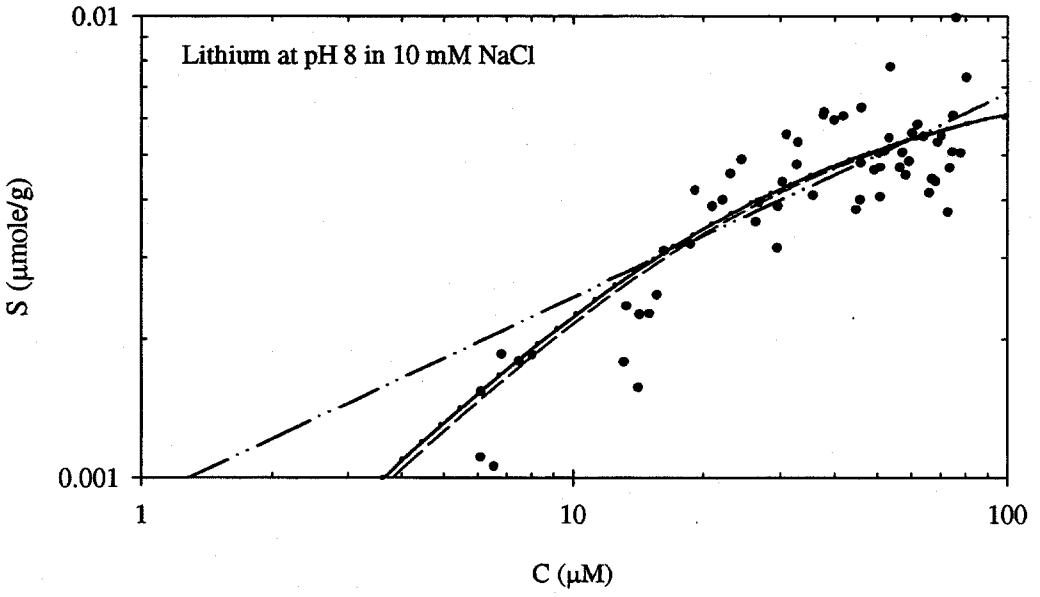

Figure 5.1. Isotherm fits and batch experiment data for lithium adsorption on garnet sand at pH 8 in 10 mM NaCl.

Table 5.2. Fitted parameters for the Langmuir, Freundlich, Tóth and Langmuir-Freundlich isotherms that describe lithium adsorption on garnet sand at pH 8 in 10 mM NaCl.

Isotherm	Parameters (Units)	Parameter Values	95% Confidence Limits	Degree of Freedom Adjusted R^2
Langmuir	K_L (μM^{-1})	0.0076	(0.0062, 0.0090)	0.621
	S_T (μmole/g)	0.0417	(0.0206, 0.0628)	
Freundlich	K_F ($\mu M^{-\alpha}$ μmole/g)	0.00089	(0.00050, 0.00129)	0.584
	α	0.440	(0.325, 0.555)	
Langmuir-Freundlich	K_{LF} (μM^{-1})	0.0077	(0.0029, 0.0124)	0.613
	S_T (μmole/g)	0.0393	(0, 0.0942)	
	α	1.000	(0.222, 1)	
Tóth	K_T (μM^{-1})	0.0076	(0.0014, 0.0137)	0.615
	S_T (μmole/g)	0.0424	(0.0133, 0.0715)	
	α	1.000	(0, 1)	

5.1.3. Dodecyltrimethylammonium bromide adsorption

Dodecyltrimethylammonium bromide (DTMA) is a cationic surfactant with the chemical formula $CH_3(CH_2)_{11}N(CH_3)_3Br$ and a critical micelle concentration (CMC) approximately 10 mM (Mukerjee and Mysels, 1970). The concentrations in the batch adsorption and flume experiments (< 400 μM) were below the CMC. Both equilibrium and kinetic batch experiments were conducted at pH's of 7 (0.5 mM $NaHCO_3$) and 8 (2 mM $NaHCO_3$). The effects of pH and ionic strength upon the extent of adsorption were also investigated.

a) DTMA short-term kinetics at pH 7 in 1 mM NaCl

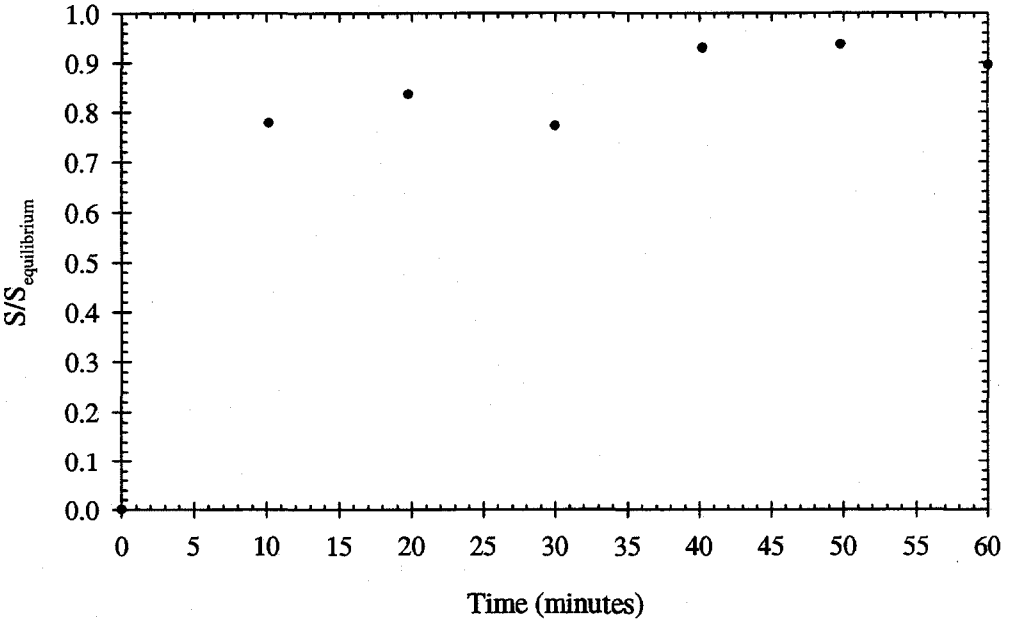

b) DTMA long-term kinetics at pH 7 in 1 mM NaCl

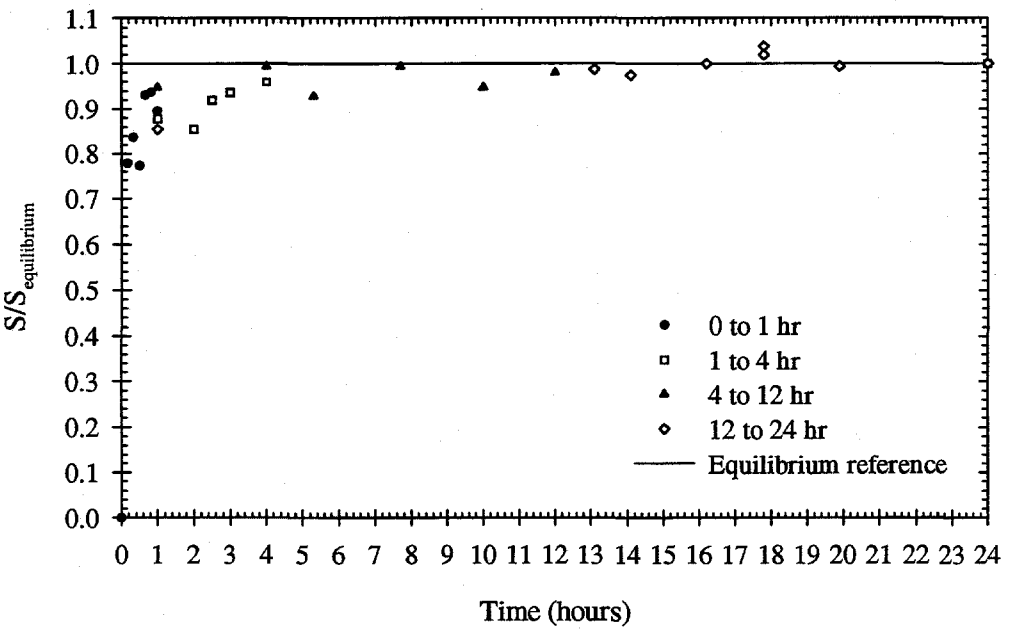

Figure 5.2. Adsorption kinetics of DTMA on garnet sand at pH 7 in 1 mM NaCl. The initial concentration was 200 μM, and 30 ml of solution was mixed with 25g of sand.

a) DTMA short-term kinetics at pH 8 in 10 mM NaCl

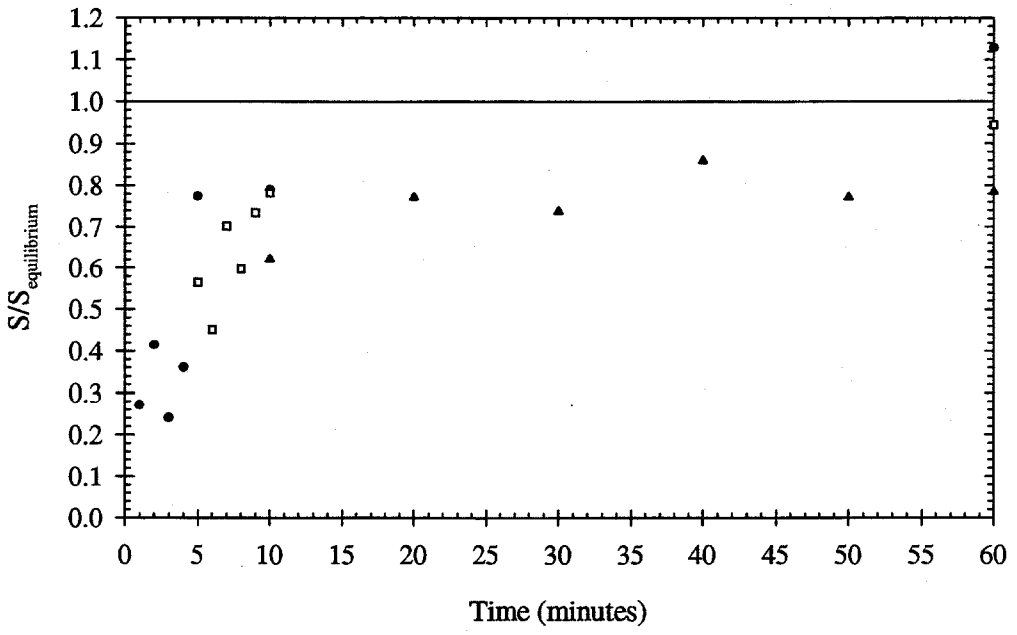

b) DTMA long-term kinetics at pH 8 in 10 mM NaCl

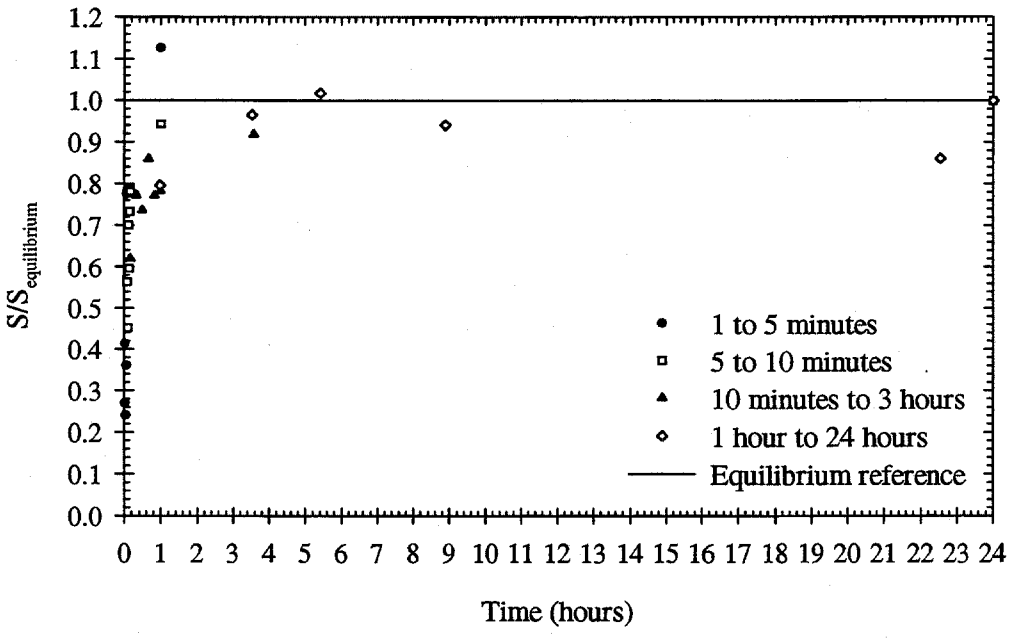

Figure 5.3. Adsorption kinetics of DTMA on garnet sand at pH 8 in 10 mM NaCl. The initial concentration was 200 μM; 30 ml of solution was mixed with 25g of sand.

5.1.3.1. DTMA kinetic adsorption

Figure 5.2 shows the adsorption kinetics for DTMA on garnet sand at pH 7 in 1 mM NaCl. Adsorption is 80 percent complete after 10 minutes and 90 percent complete after 40 minutes. Equilibrium is achieved after 4 hours. The equilibrium adsorption time scale (80 percent value) is on the order of 10 minutes. The adsorption time scale will be compared to characteristic porewater advection time scale of the flume experiments to check the validity of the equilibrium adsorption assumption.

The kinetic results for DTMA adsorption at pH 8 in 10 mM NaCl are shown in Figure 5.3. Adsorption is 80 percent complete after 10 minutes, 90 percent complete after 1 hour and 100 percent complete between 4 and 6 hours. The adsorption time scale remains at 10 minutes.

5.1.3.2. Effect of pH upon DTMA adsorption

Figure 5.4 shows the effect of pH upon the extent of DTMA adsorption on garnet sand in solutions containing 1 mM and 10 mM NaCl. Within experimental error, the results do not differ significantly for the different salt concentrations.

At low pH values, the surface is positively charged and DTMA ions experience electrostatic repulsion. However, some DTMA adsorbs to the sand by hydrophobic interactions. When pH > 5, the sorbed concentration begins to increase because the surface charge becomes negative and the DTMA ions are electrostatically attracted to the sand surface. The sorbed concentration reaches a plateau when pH > 7.

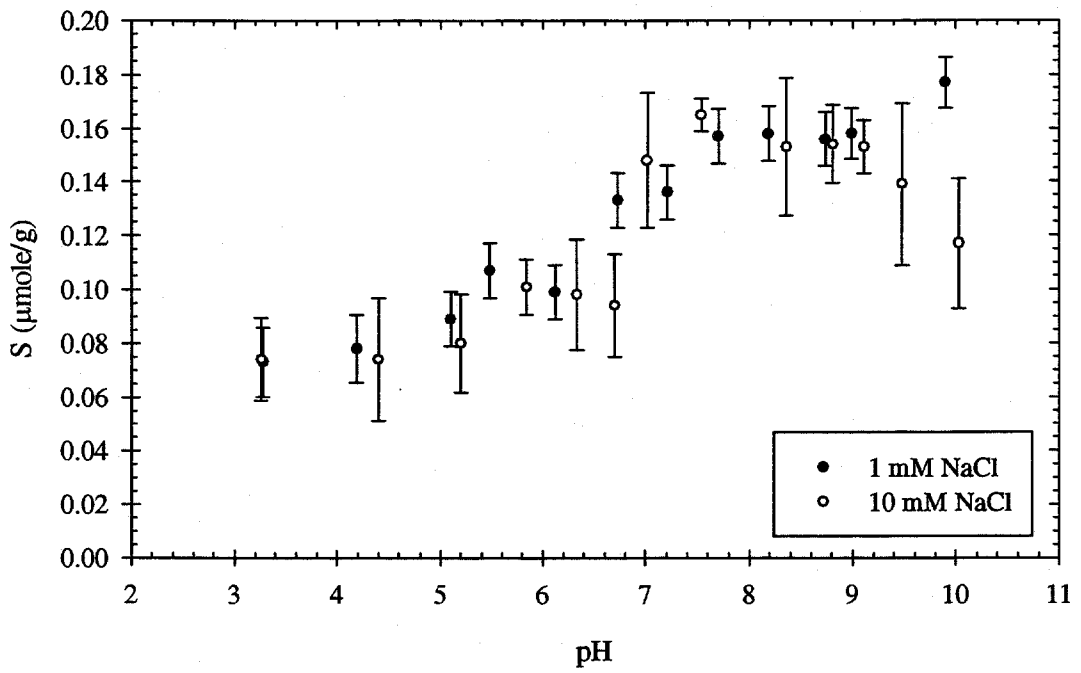

Figure 5.4. Effect of pH upon the extent of adsorption of DTMA on garnet sand in 1 mM and 10 mM NaCl solutions. The initial concentration was 200 μM and 30 ml of solution was mixed with 20g of sand.

5.1.3.3. DTMA equilibrium adsorption isotherms

Plots of the DTMA equilibrium adsorption data with error bars are included in Appendix B. The results of the equilibrium batch adsorption experiments for DTMA on garnet sand at pH 7 in 1 mM and 10 mM NaCl are compared in Figure 5.5.

For bulk DTMA concentrations less than 100 μM, the amount of DTMA adsorbed is greater at the lower salt concentration. An increase in the salt concentration causes a decrease in the coulombic attraction between the surfactant and the surface, which leads to a decrease in adsorption.

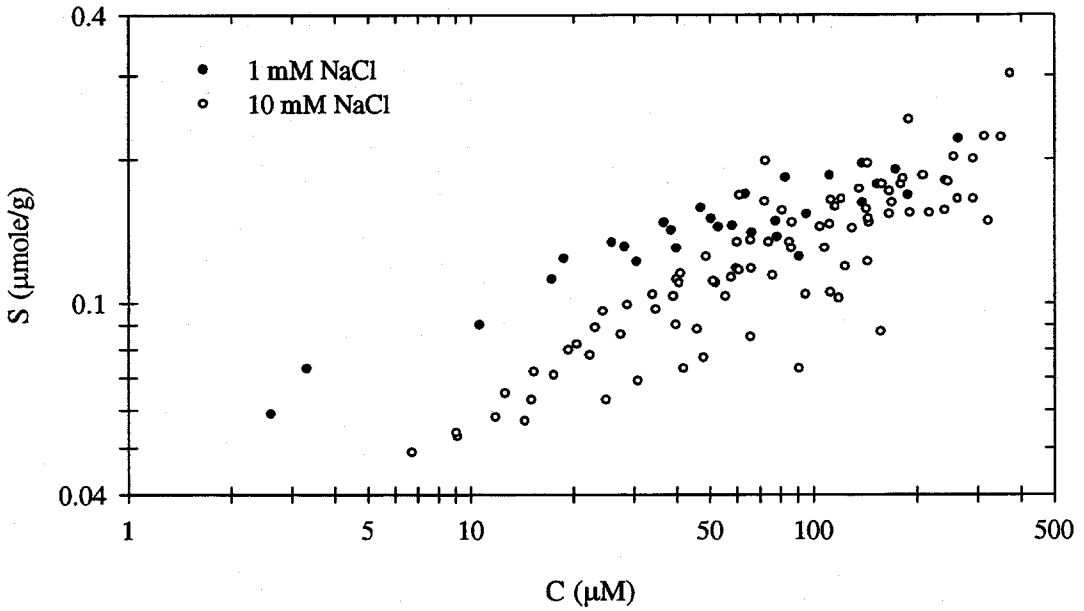

Figure 5.5. The effect of ionic strength on the adsorption of DTMA on garnet sand at pH 7.

The data merge near a DTMA bulk concentration of 200 µM. At this point, the electrostatic interaction contribution to the free energy of adsorption is small and adsorption proceeds primarily through hydrophobic interactions (Koopal et al., 1995).

Figure 5.6 compares the DTMA adsorption results on garnet sand in solutions of 10 mM NaCl at pH's 7 and 8. Within experimental error, DTMA adsorption is not affected by the pH difference. These results are consistent with those presented in Section 5.1.3.2.

Figure 5.7 compares DTMA adsorption data acquired in January 1997 and April 1998. The sand used in the later experiments had been through seven flume experiments and associated acid washes (see Chapter 4, Section 4.8.3). Over the concentration range of the batch experiments, the amount of DTMA adsorbed in the initial data set is greater than the amount in the April 1998 experiments. This indicates that the surface properties of the sand gradually changed, which probably occurred in response to the repeated acid washes.

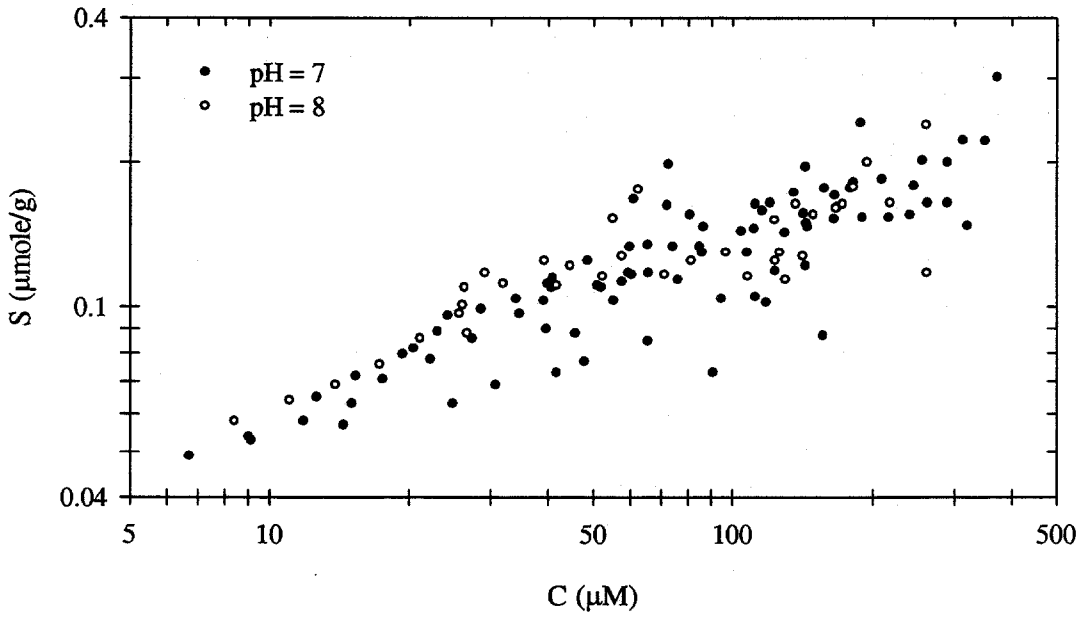

Figure 5.6. Comparison of DTMA adsorption on garnet sand at pH's 7 and 8 in solutions of 10 mM NaCl.

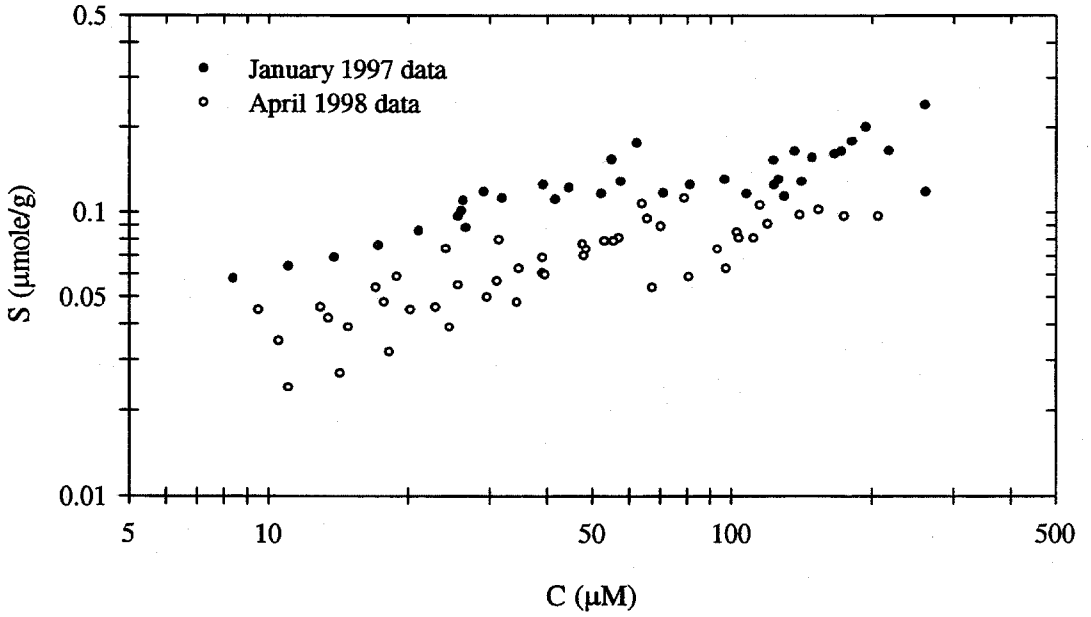

Figure 5.7. Change with time of DTMA adsorption on garnet sand at pH 8 in 10 mM NaCl.

Four flume experiments were conducted to study the bed exchange of DTMA:

Run 1:.....pH = 7 .....1 mM NaCl.....Nov. 1996

Run 2:.....pH = 8 .....10 mM NaCl.....Mar. 1997

Run 7:.....pH = 8 .....10 mM NaCl.....Nov. 1997

Run 10:.....pH = 8 .....10 mM NaCl.....Mar. 1998

The isotherm fits for the associated adsorption data are illustrated in Figure 5.8 through Figure 5.10. The values of the fitted sorption parameters are listed in Table 5.3 through Table 5.5.

The fitted isotherms are ranked according to the degree-of-freedom adjusted R^2:

pH 7, 1 mM NaCl: ..... Tóth > Langmuir-Freundlich > Freundlich > Langmuir

pH 8, 10 mM NaCl (Jan. 1997): ... Freundlich > Tóth > Langmuir-Freundlich > Langmuir

pH 8, 10 mM NaCl (Apr. 1998): .. Langmuir > Tóth > Langmuir-Freundlich > Freundlich

For the pH 7 data (1 mM NaCl), the Freundlich, Tóth and Langmuir-Freundlich isotherms coincide for the concentrations observed in Flume Run 1 (50 – 200 μM). The Tóth and Langmuir-Freundlich isotherm fits do not differ for the pH 8 data acquired in January 1997. The Langmuir, Tóth and Langmuir-Freundlich isotherm fits for the pH 8 April 1998 data agree over the range of concentrations studied in the batch experiments.

a) Linear scale

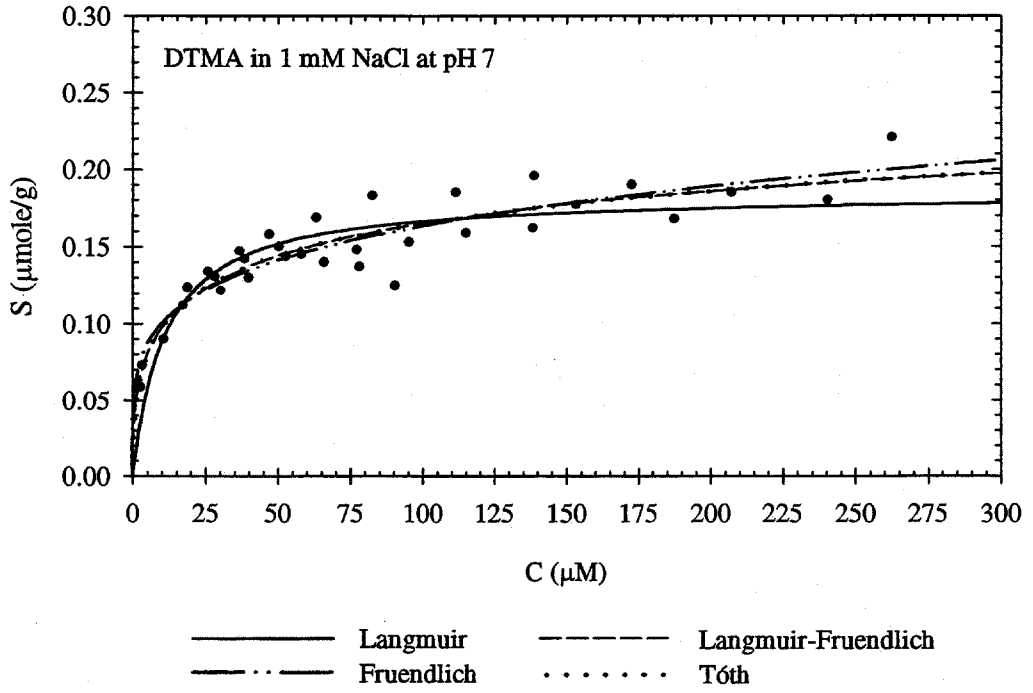

b) Log scale

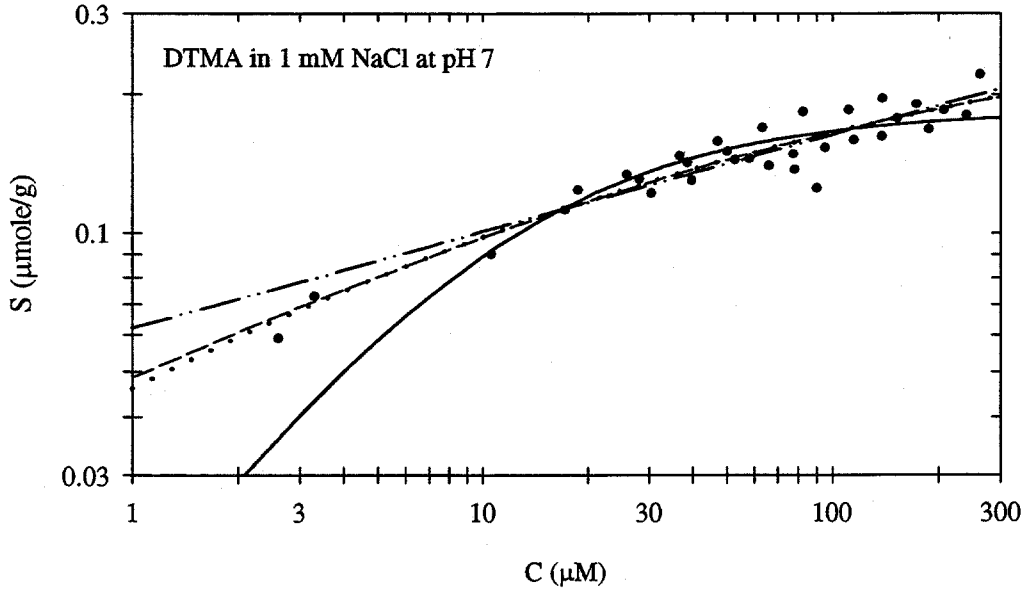

Figure 5.8. Isotherm fits for DTMA batch adsorption on garnet sand at pH 7 in 1 mM NaCl.

a) Linear scale

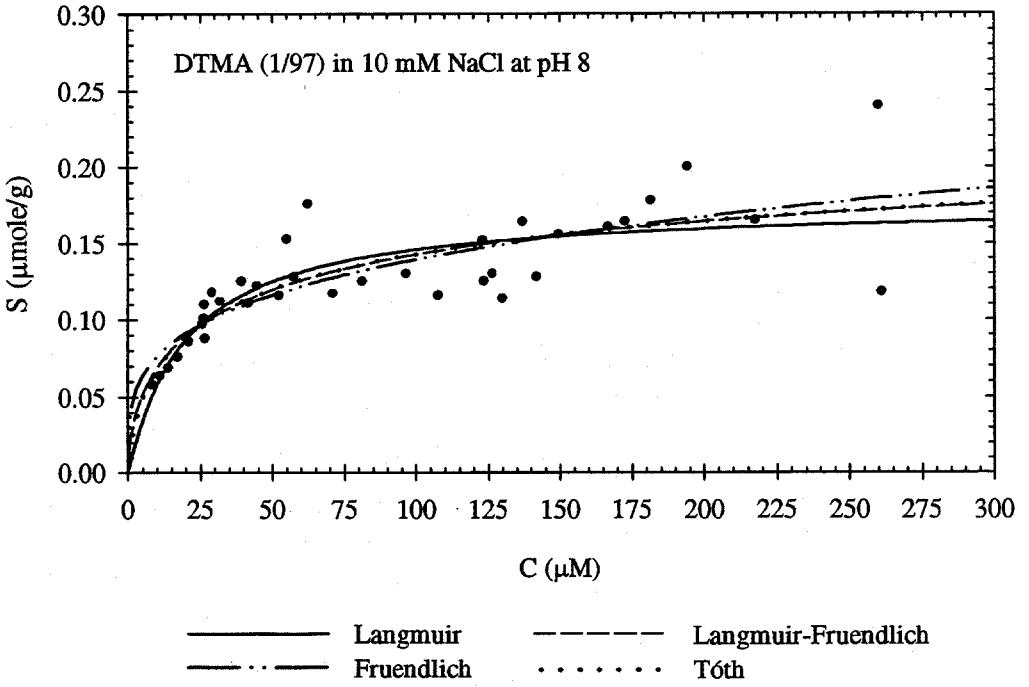

b) Log scale

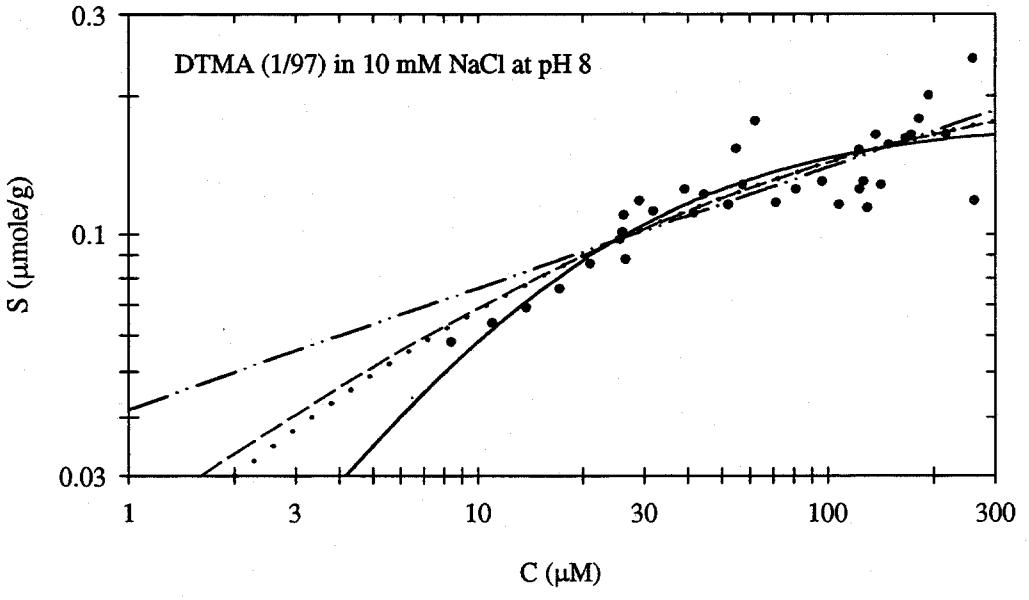

Figure 5.9. Isotherm fits for DTMA adsorption on garnet sand at pH 8 in 10 mM NaCl for data acquired January 1997.

a) Linear scale

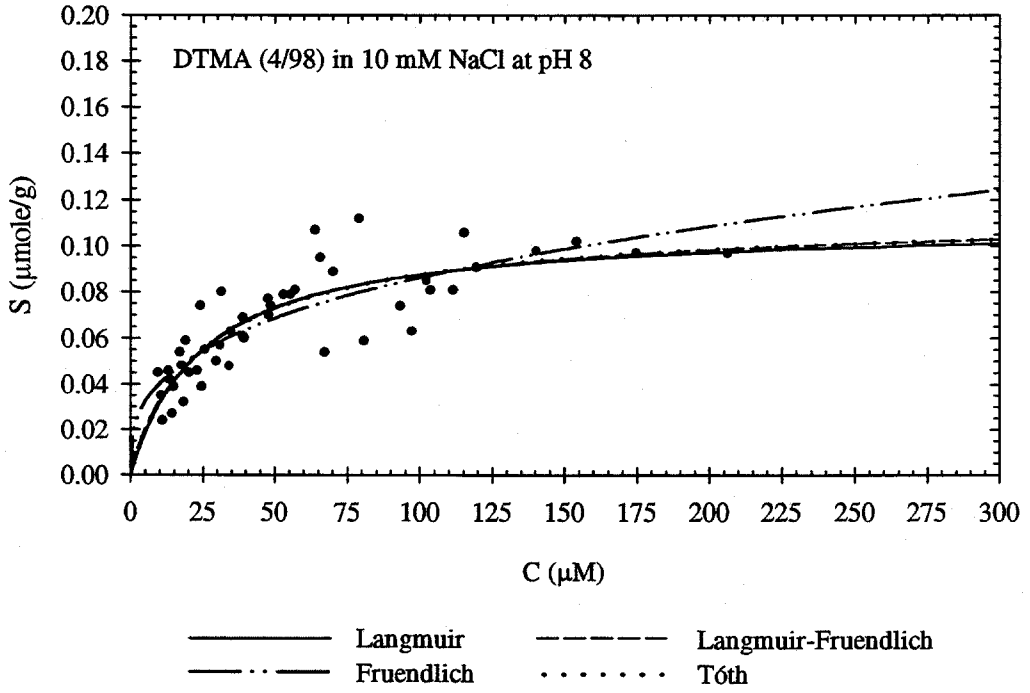

b) Log scale

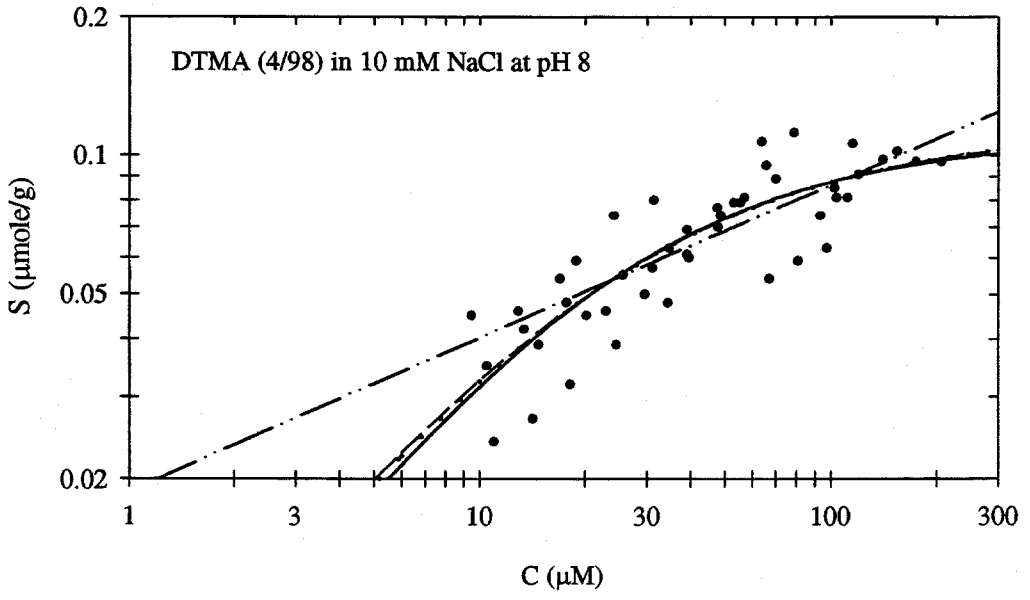

Figure 5.10. Isotherm fits for DTMA adsorption on garnet sand at pH 8 in 10 mM NaCl for data acquired April 1998.

Table 5.3. Fitted parameters for the Langmuir, Freundlich, Tóth and Langmuir-Freundlich isotherms that describe DTMA adsorption on garnet sand at pH 7 in 1 mM NaCl.

Isotherm	Parameters (Units)	Parameter Values	95% Confidence Limits	Degree of Freedom Adjusted R^2
Langmuir	K_L (μM^{-1})	0.0931	(0.0546, 0.1316)	0.742
	S_T (μmole/g)	0.185	(0.171, 0.198)	
Freundlich	K_F ($\mu M^{-\alpha}$ μmole/g)	0.0622	(0.0508, 0.0735)	0.816
	α	0.210	(0.170, 0.250)	
Langmuir-Freundlich	K_{LF} (μM^{-1})	0.0141	(0.0, 0.07525)	0.819
	S_T (μmole/g)	0.309	(0.0528, 0.5657)	
	α	0.394	(0.105, 0.683)	
Tóth	K_T (μM^{-1})	8.032	(0.0, 79.53)	0.820
	S_T (μmole/g)	0.409	(0.0, 1.592)	
	α	0.223	(0.0, 0.558)	

Table 5.4. Fitted parameters for the Langmuir, Freundlich, Tóth and Langmuir-Freundlich isotherms that describe DTMA adsorption on garnet sand at pH 8 in 10 mM NaCl for data acquired January 1997.

Isotherm	Parameters (Units)	Parameter Values	95% Confidence Limits	Degree of Freedom Adjusted R^2
Langmuir	K_L (μM^{-1})	0.0495	(0.0267, 0.0724)	0.616
	S_T (μmole/g)	0.176	(0.156, 0.195)	
Freundlich	K_F ($\mu M^{-\alpha}$ μmole/g)	0.0416	(0.0273, 0.0559)	0.620
	α	0.263	(0.188, 0.337)	
Langmuir-Freundlich	K_{LF} (μM^{-1})	0.0201	(0.0, 0.0994)	0.615
	S_T (μmole/g)	0.239	(0.0, 0.489)	
	α	0.565	(0.0, 1.0)	
Tóth	K_T (μM^{-1})	0.205	(0.0, 1.387)	0.617
	S_T (μmole/g)	0.269	(0.0, 0.713)	
	α	0.406	(0.0, 1.0)	

Table 5.5. Fitted parameters for the Langmuir, Freundlich, Tóth and Langmuir-Freundlich isotherms that describe DTMA adsorption on garnet sand at pH 8 in 10 mM NaCl for data acquired April 1998.

Isotherm	Parameters (Units)	Parameter Values	95% Confidence Limits	Degree of Freedom Adjusted R^2
Langmuir	K_L (μM^{-1})	0.0406	(0.0259, 0.0554)	0.697
	S_T (μmole/g)	0.109	(0.096, 0.122)	
Freundlich	K_F ($\mu M^{-\alpha}$ μmole/g)	0.0188	(0.0131, 0.0246)	0.665
	α	0.331	(0.259, 0.403)	
Langmuir-Freundlich	K_{LF} (μM^{-1})	0.0372	(0.0037, 0.0706)	0.690
	S_T (μmole/g)	0.114	(0.071, 0.156)	
	α	0.924	(0.335, 1.0)	
Tóth	K_T (μM^{-1})	0.0439	(0.0065, 0.0814)	0.690
	S_T (μmole/g)	0.114	(0.061, 0.168)	
	α	0.891	(0.0, 1.0)	

5.1.4. Myristyltrimethylammonium bromide

The chemical formula for myristyltrimethylammonium (MTMA) bromide is $CH_3(CH_2)_{13}N(CH_3)_3Br$, which has two more CH_2 groups in its hydrophobic tail than DTMA. The CMC is approximately 1 mM (Mukerjee and Mysels, 1970). The effect of pH upon extent of MTMA adsorption on garnet sand was studied in solutions of 10 mM NaCl. The kinetic and equilibrium adsorption experiments were conducted at pH 8 in 10 mM NaCl.

a) MTMA short-term kinetics at pH 8 in 10 mM NaCl

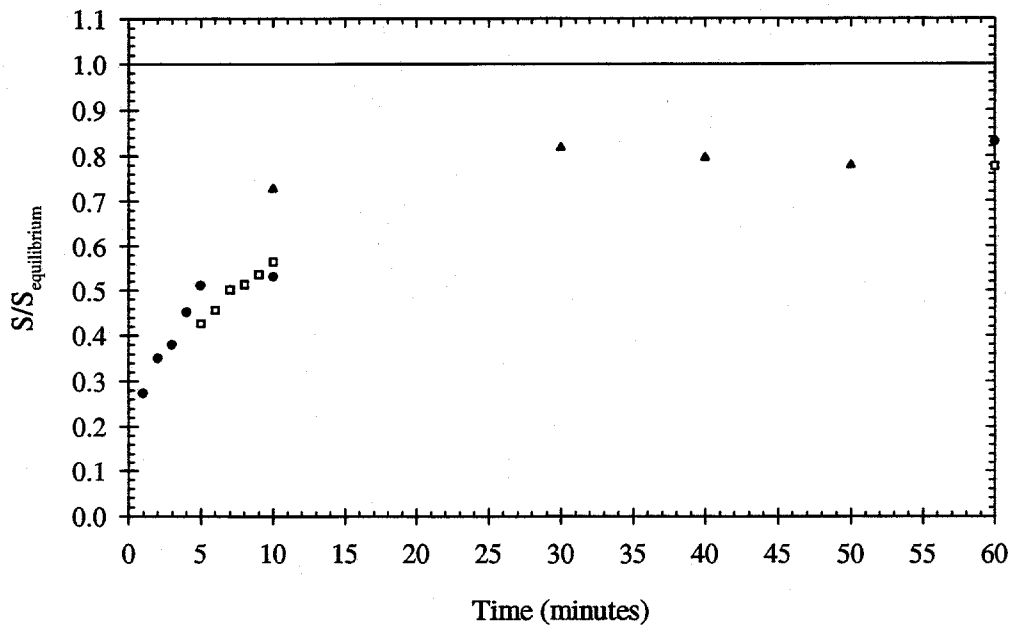

b) MTMA long-term kinetics at pH 8 in 10 mM NaCl

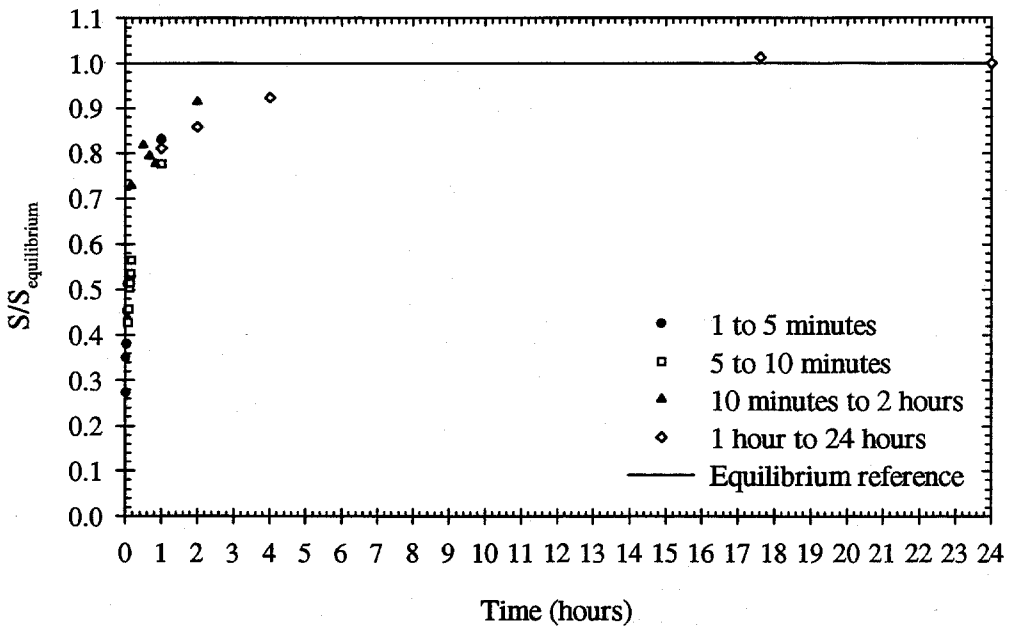

Figure 5.11. Adsorption kinetics of MTMA adsorption on garnet sand at pH 8 in 10 mM NaCl. The initial concentration was 200 μM; 30 ml of solution was mixed with 25g of sand.

5.1.4.1. MTMA kinetic adsorption

Figure 5.11 shows the short- and long-term adsorption kinetics for MTMA onto garnet sand. Adsorption is 80 percent complete after 30 minutes, 90 percent complete after 2 hours, and achieves equilibrium between 4 and 12 hours. The equilibrium adsorption time scale (80 percent value) is 30 minutes.

5.1.4.2. Effect of pH on MTMA adsorption

The effect of pH on MTMA adsorption on garnet sand in solutions of 10 mM NaCl is illustrated in Figure 5.12.

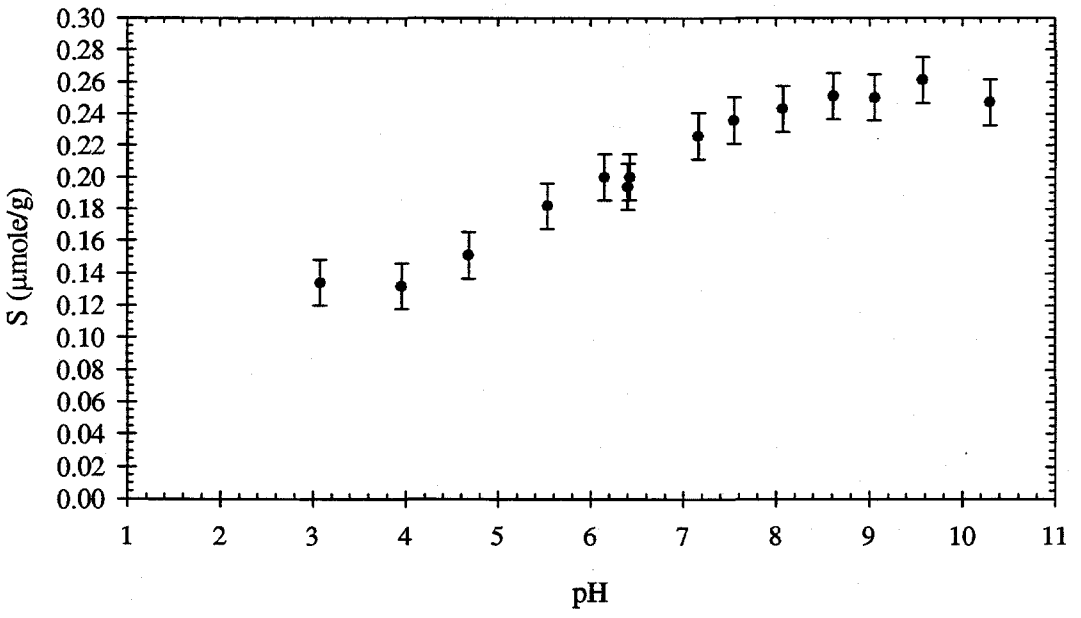

Figure 5.12. Effect of pH on the extent of MTMA adsorption on garnet sand in 10 mM NaCl. The initial concentration was 200 mM and 30 ml of solution was mixed with 20g of sand.

The overall trend is the same as for DTMA. However, at low pH when the electrostatic attraction is negligible, the MTMA sorbed concentration (0.13 µmole/g) is almost double the amount for

DTMA (0.07 μmole/g from Figure 5.4). This reflects the increase in the hydrophobic attraction to the surface that results from the additional CH_2 groups in MTMA. The sorbed MTMA concentration at the plateau is 1.5 times that for DTMA.

5.1.4.3. MTMA equilibrium adsorption isotherms

The MTMA adsorption data are plotted with error bars in Appendix B. The data were acquired over a period of six months. Multiple experiments were conducted to check the reproducibility of the experimental results. Figure 5.13 compares the adsorption results acquired at different times. The data acquired in November and December 1997 are lower than those acquired during May through August 1997. The decrease is adsorption may be a reflection of the change in the sand surface that is discussed in Section 5.1.3.3. Overall, the percent reduction in the adsorption over time is significantly less for MTMA than the decrease observed for DTMA (Figure 5.7).

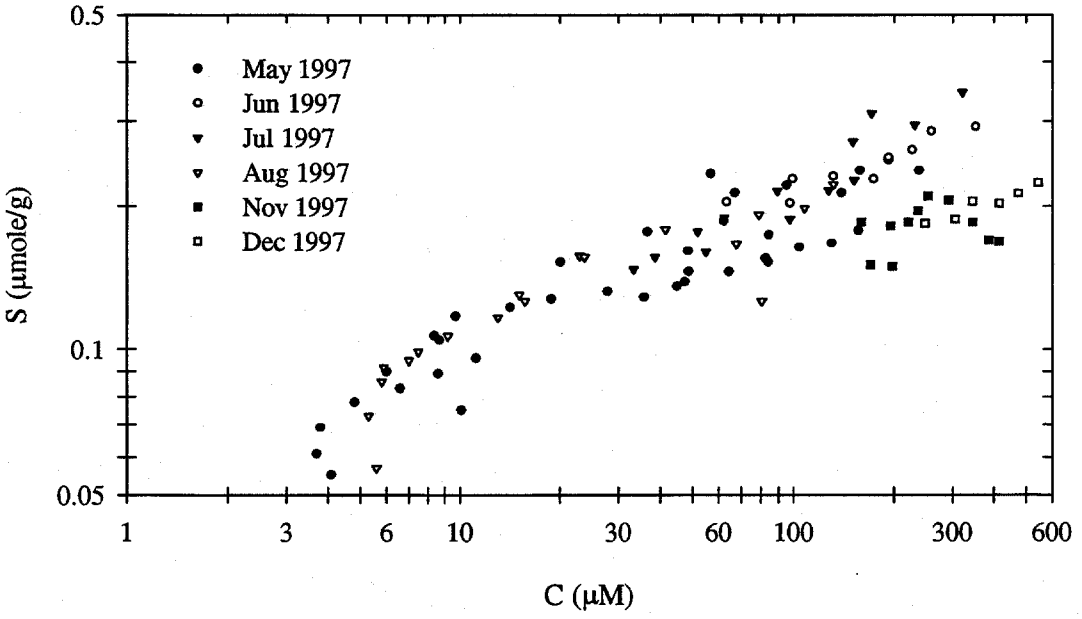

Figure 5.13. Change with time of MTMA equilibrium adsorption on garnet sand at pH 8 in 10 mM NaCl.

a) Linear scale

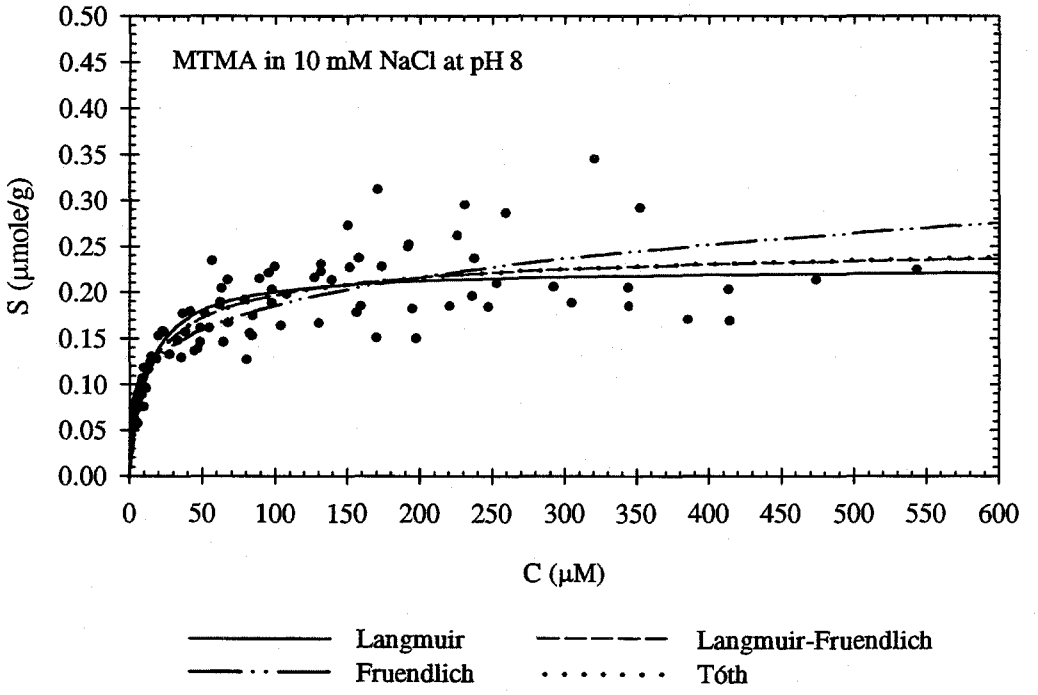

b) Log scale

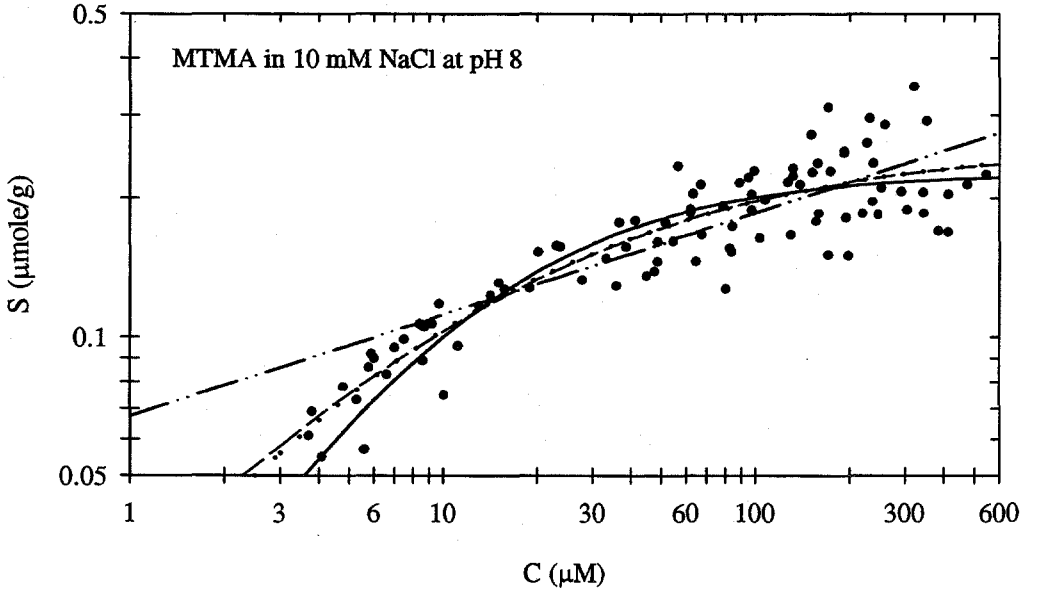

Figure 5.14. Isotherm fits for MTMA adsorption on garnet sand at pH 8 in 10 mM NaCl.

The bed exchange of MTMA was studied in four flume runs beginning in May 1997 and ending in October 1997. These experiments were conducted in solutions of 10 mM NaCl at pH 8. The isotherm fits for the adsorption data are displayed in Figure 5.14 and the fitted parameters are listed in Table 5.6. The concentrations in the flume experiments range from 15 to 400 μM. The Tóth and Langmuir-Freundlich coincide in this range while the Langmuir and Freundlich isotherms differ slightly. The ranking of the isotherms based on the degree-of-freedom adjusted R^2 is:

Tóth = Langmuir-Freundlich > Langmuir > Freundlich

Table 5.6. Fitted parameters for the Langmuir, Freundlich, Tóth and Langmuir-Freundlich isotherms that describe MTMA adsorption on garnet sand at pH 8 in 10 mM NaCl.

Isotherm	Parameters (Units)	Parameter Values	95% Confidence Limits	Degree of Freedom Adjusted R^2
Langmuir	K_L (μM^{-1}) S_T (μmole/g)	0.0793 0.226	(0.0561, 0.126) (0.213, 0.239)	0.679
Freundlich	K_F ($\mu M^{-\alpha}$ μmole/g) α	0.0674 0.220	(0.0549, 0.0800) (0.181, 0.259)	0.648
Langmuir-Freundlich	K_{LF} (μM^{-1}) S_T (μmole/g) α	0.0557 0.257 0.689	(0.0145, 0.0969) (0.204, 0.310) (0.394, 0.984)	0.690
Tóth	K_T (μM^{-1}) S_T (μmole/g) α	0.171 0.265 0.584	(0.0, 0.400) (0.192, 0.338) (0.202, 0.966)	0.690

5.1.5. Octadecyltrimethylammonium bromide

Octadecyltrimethylammonium bromide (OTMA) has the chemical formula $CH_3(CH_2)_{17}N(CH_3)_3Br$, which has six more CH_2 groups than DTMA. The CMC is 300 μM. The kinetics of OTMA adsorption were not studied because of analytical limitations. The sample

volume from the kinetic experiments had to be small enough so that the overall adsorption would not be affected by sample removal. This volume was too small to be analyzed by Orange II dye extraction. The OTMA peaks in capillary electrophoresis were not distinguishable for concentrations less than 100 μM. Consequently, the capillary electrophoresis method was not sensitive enough to analyze OTMA concentrations. The adsorption time scale for should be longer than that for MTMA because of the increase in the hydrophobicity of the surfactant (see kinetic discussion in Section 5.1.7).

The OTMA equilibrium batch adsorption data are plotted with error bars in Appendix B. The data and isotherm fits are shown in Figure 5.15, and the values of the fitted parameters are listed in Table 5.7.

Table 5.7. Fitted parameters for the Langmuir, Freundlich, Tóth and Langmuir-Freundlich isotherms that describe OTMA adsorption on garnet sand at pH 8 in 10 mM NaCl.

Isotherm	Parameters (Units)	Parameter Values	95% Confidence Limits	Degree of Freedom Adjusted R^2
Langmuir	K_L (μM^{-1})	0.132	(0.0854, 0.178)	0.760
	S_T (μmole/g)	0.420	(0.390, 0.449)	
Freundlich	K_F ($\mu M^{-\alpha}$ μmole/g)	0.151	(0.117, 0.184)	0.681
	α	0.193	(0.144, 0.241)	
Langmuir-Freundlich	K_{LF} (μM^{-1})	0.135	(0.0846, 0.186)	0.753
	S_T (μmole/g)	0.418	(0.370, 0.466)	
	α	1.000	(0.499, 1.0)	
Tóth	K_T (μM^{-1})	0.132	(0.009, 0.255)	0.753
	S_T (μmole/g)	0.420	(0.365, 0.474)	
	α	0.9999	(0.286, 1.0)	

a) Linear scale

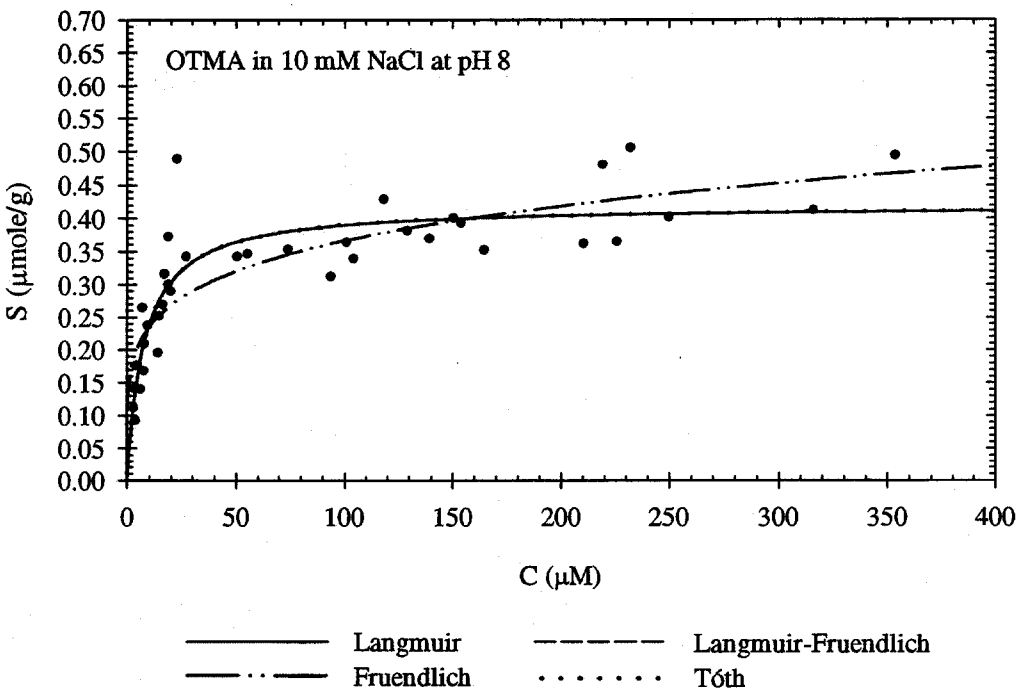

b) Log scale

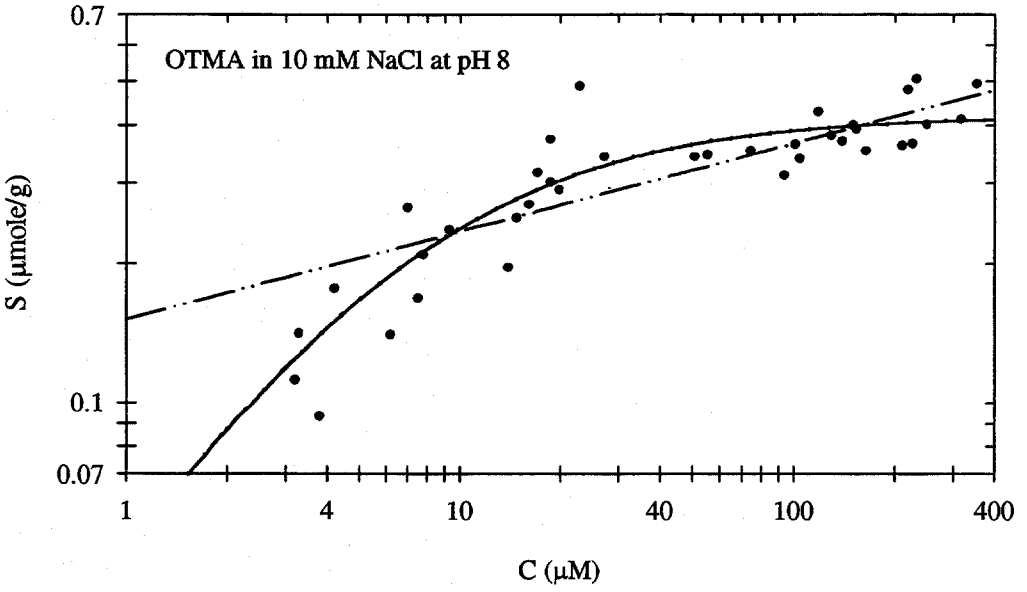

Figure 5.15. Isotherm fits for OTMA adsorption on garnet sand at pH 8 in 10 mM NaCl.

OTMA was studied in one flume experiment in which the concentrations were between 20 and 200 μM. Since the Tóth and Langmuir-Freundlich isotherms coincide with the Langmuir isotherm, there is no need to consider them separately in the bed/stream exchange models. The isotherms are ranked as follows:

Langmuir > Tóth = Langmuir-Freundlich > Freundlich

5.1.6. Nonyltrimethylammonium bromide

The chemical formula for nonyltrimethylammonium bromide (NTMA) is $CH_3(CH_2)_8N(CH_3)_3Br$, which has three less CH_2 groups than DTMA. The NTMA adsorption kinetics were not studied, but the adsorption time scale should be less than that for DTMA because NTMA is less hydrophobic. Figure 5.16 displays the NTMA adsorption data and isotherm fits. The fitted isotherm parameters are listed in Table 5.1.

Table 5.8. Fitted parameters for the Langmuir, Freundlich, Tóth and Langmuir-Freundlich isotherms that describe NTMA adsorption on garnet sand at pH 8 in 10 mM NaCl.

Isotherm	Parameters (Units)	Parameter Values	95% Confidence Limits	Degree of Freedom Adjusted R^2
Langmuir	K_L (μM^{-1})	0.00760	(0.0, 0.0160)	0.368
	S_T (μmole/g)	0.0826	(0.0229, 0.1422)	
Freundlich	K_F ($\mu M^{-\alpha}$ μmole/g)	0.00225	(0.00059, 0.00391)	0.452
	α	0.593	(0.416, 0.769)	
Langmuir-Freundlich	K_{LF} (μM^{-1})	0.000028	(0.0, 0.0037)	0.438
	S_T (μmole/g)	1.241	(0.0, 91.70)	
	α	0.604	(0.0, 1.0)	
Tóth	K_T (μM^{-1})	0.00235	(0.0, 0.0668)	0.426
	S_T (μmole/g)	6.357	(0.0, 443.3)	
	α	0.155	(0.0, 1.0)	

a) Linear scale

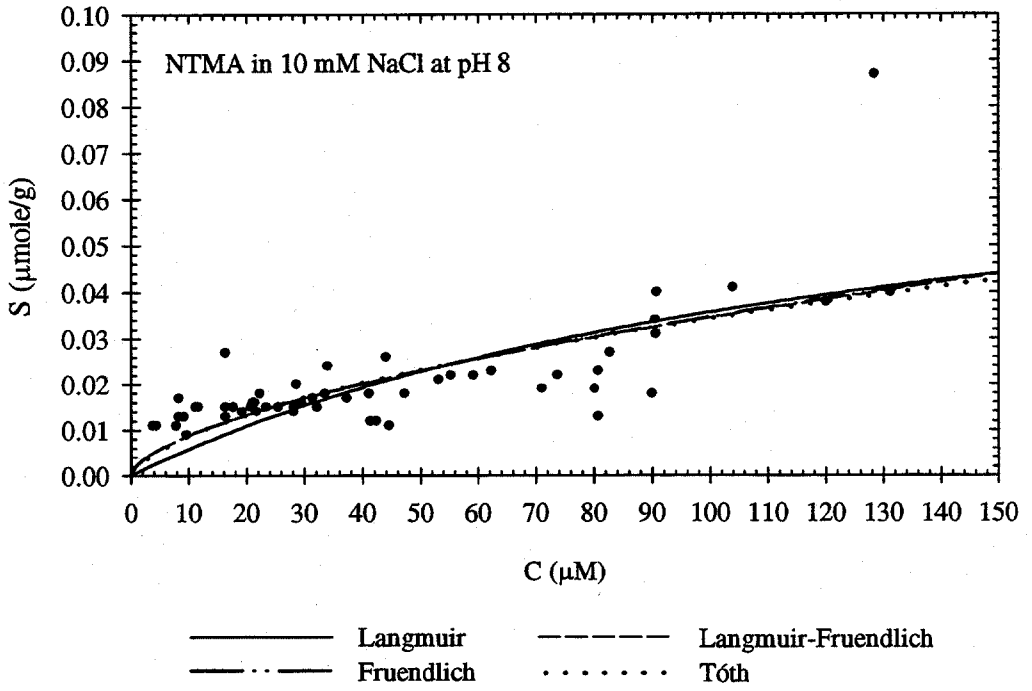

b) Log scale

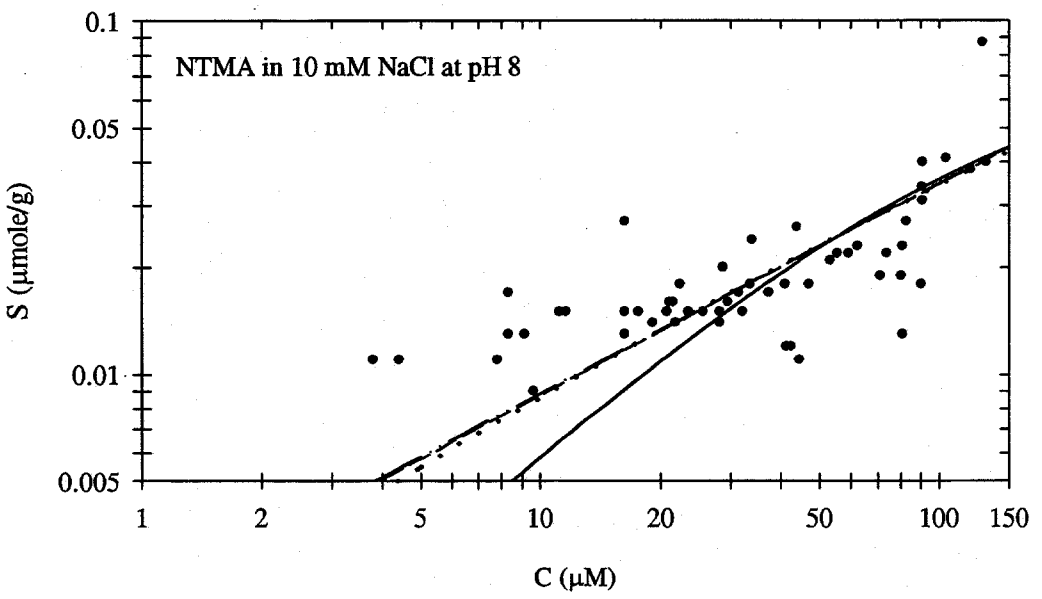

Figure 5.16. Isotherm fits for NTMA adsorption on garnet sand at pH 8 and 10 mM NaCl.

NTMA was used in one flume experiments in which the aqueous concentrations were between 20 and 100 μM. The isotherm are ranked using the degree-of-freedom adjusted R^2:

Freundlich > Langmuir-Freundlich > Tóth > Langmuir

The Tóth and Langmuir-Freundlich isotherms are not used in the bed/stream exchange models for NTMA because they coincide with the Freundlich isotherm. The adsorption data are plotted with error bars in Appendix B. The error in the NTMA sorption experiments is large compared to the amount adsorbed. None of the isotherms fit the data well, and the uncertainty in the sorption parameters for NTMA is greater than for the other cationic surfactants. Large errors in the sorption parameters cause errors in the bed/stream exchange model predictions. The sensitivity of the bed/stream exchange model to the sorption coefficients is examined in Chapter 6, Section 6.8.

5.1.7. Summary and comparison of results

The adsorption of cationic surfactants on garnet sand is studied for alkyltrimethylammonium salts having hydrocarbon chain lengths of 9 (NTMA), 12 (DTMA), 14 (MTMA) and 18 (OTMA). Cationic surfactants can adsorb to a charged mineral surface by several mechanisms: 1) electrostatic interactions, 2) exchange reactions with ligands previously bound to the solid, and 3) hydrophobic interactions. The alkyltrimethylammonium surfactants studied here do not retain any nonbonded electrons that can form bonds with components on the solid (Schwarzenbach et al., 1993) and generally sorb more as counterions. In addition to hydrophobic interactions, cationic surfactants can migrate into the diffuse swarm, undergo ion exchange and form ion pairs. The adsorption isotherms fit to the batch adsorption data represent the combination of all of the adsorption processes. A detailed discussion of the adsorption constants associated with each adsorption mechanism and their relationships to the Langmuir sorption coefficient is presented by Schwarzenbach et al. (1993).

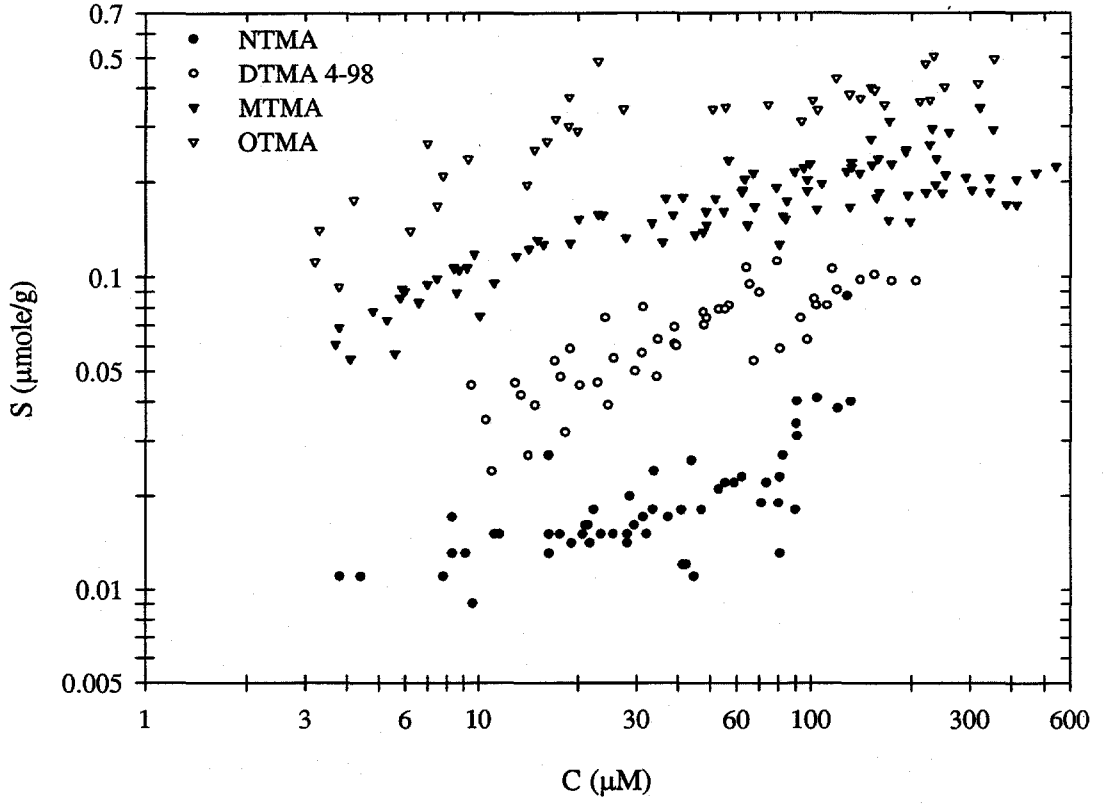

Figure 5.17. Effect of alkyl chain length on the adsorption of alkyltrimethylammonium salts on garnet sand at pH 8 in 10 mM NaCl.

The effect of the hydrocarbon chain length on adsorption is illustrated in Figure 5.17. The sorbed concentration increases with the chain length because of an increase in hydrophobic interactions. The binding energy of the hydrocarbon chains can be estimated using the Langmuir sorption coefficient K_L determined for the different surfactants at the same pH and ionic strength. To determine the binding energy of one CH_2 group in the chain, $\ln(K_L)$ is plotted against the number of CH_2 groups in the chain (n) in Figure 5.18. Because of the high uncertainty associated with the Langmuir sorption constant K_L for NTMA, the value is not included in Figure 5.18.

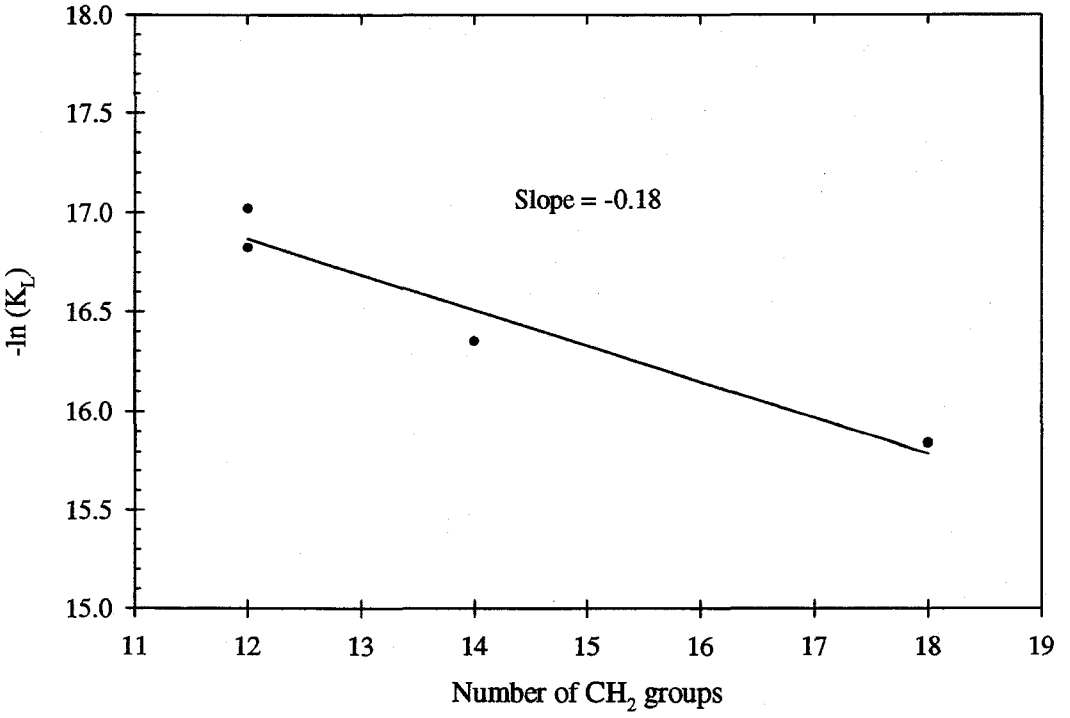

Figure 5.18. Langmuir sorption coefficient as a function of the number of CH_2 groups in the surfactant hydrocarbon chain.

The slope of the regression line in Figure 5.18 is

$$\frac{d(-\ln K_L)}{dn} = -\frac{s_{ad}\phi}{k_B T} \tag{5.4}$$

where ϕ is the energy required to completely remove one CH_2 group from the aqueous solution to an environment saturated with hydrocarbon chains (i.e., hemi-micelle formation), s_{ad} is the association degree (Dobiás, 1984), k_B is Boltzmann's constant and T is temperature. For the adsorption of N-alkylammonium chlorides on SiO_2, the values of $s_{ad}\phi$ determined from the Langmuir sorption coefficients span the range 0.31 to $1.03k_BT$ (Dobiás, 1984) and vary with the surface coverage on the solid. From the regression in Figure 5.18, $s_{ad}\phi$ is $0.18k_BT$ for the alkyltrimethylammonium bromide adsorption on the garnet sand. The small value of $s_{ad}\phi$ indicates that most of the hydrocarbon chains are in contact with the aqueous phase, and hemi-micelle formation does not occur.

The orientation of the adsorbed surfactant ions at the maximum sorption capacity is assessed using the Langmuir adsorption capacity and estimates of the cross-sectional areas of the ions. From Rosen (1989, page 81), the cross-sectional area of a surfactant ion oriented perpendicular to the surface is about 20 $Å^2$, and the cross-sectional area of one CH_2 group lying flat on the surface is about 7 $Å^2$. Then the cross-sectional area occupied by DTMA, MTMA and OTMA molecules that are lying flat on the surface is 104, 118 and 146 $Å^2$ per molecule, respectively. Assuming a specific surface area of 0.12 m^2/g for the garnet sand (Chapter 4, Section 4.3.2), the cross-sectional area of the adsorbed molecules at the Langmuir adsorption maximum is 113, 183, 88 and 47 $Å^2$ per molecule for DTMA (1/97), DTMA (4/98), MTMA and OTMA, respectively. These calculations indicate that the DTMA molecules lie flat on the surface; whereas the tails of the MTMA and OTMA point away from but are not perpendicular to the surface. Since the molecules are not perpendicular to the surface, hemi-micelles are not formed.

At pH 3, the garnet sand surface is positively charged (Chapter 4, Section 4.3.6) and the coulombic interactions with the cationic surfactants are unfavorable. However, adsorption can occur when the hydrophobic interactions of the surfactant ions are stronger than the electrostatic repulsion from the surface. The free energy of adsorption can be broken into chemical and coulombic parts

$$\Delta G^{o}_{ads} = \Delta G^{o}_{coul} + \Delta G^{o}_{chem} \tag{5.5}$$

The coulombic term is defined as

$$\Delta G^{o}_{coul} = \Delta zF\Psi \tag{5.6}$$

where z the valence of the ion, F is the Faraday constant and Ψ is the surface potential. At pH 3, the zeta potential of the garnet sand is 30 mV (Chapter 4, Figure 4.10). The surface potential is greater than the zeta potential (Chapter 2, Section 2.3.1). Assuming a surface potential of 50 mV, ΔG^{o}_{coul} is 4.8 kJ per mole. Adsorption occurs when $\Delta G^{o}_{chem} < -4.8$ kJ per mole. Assuming the

adsorption occurs by hydrophobic interactions, ΔG^{o}_{chem} equals –n0.18RT. With T equal to 25°C, ΔG^{o}_{chem} for DTMA (n = 12) and MTMA (n = 14) equals –5.3 and –6.2 kJ/mole, respectively. Therefore, some adsorption of DTMA and MTMA is expected to occur at pH 3. Adsorption of DTMA (Figure 5.4) and MTMA (Figure 5.12) at pH 3 was observed in the batch adsorption experiments, and therefore the theory and experimental results agree. The increase in adsorption with observed in the batch experiments, demonstrates that coulombic interactions do contribute to the cationic surfactant adsorption for pH's greater than the pH_{pzc} of the garnet sand.

The adsorption isotherms do not exhibit the four regions commonly observed for cationic surfactants (see Chapter 2, Figure 2.5). The adsorption data for DTMA, MTMA and OTMA show two regions. In the first region, the amount of surfactant adsorbed on the garnet sand increases with the bulk aqueous concentration; and then a plateau occurs at an aqueous concentration less than the critical micelle concentration. Adsorption occurs primarily through hydrophobic and coulombic interactions as demonstrated by the results of the pH studies conducted with DTMA and MTMA and the calculations presented earlier in this section. The calculations presented earlier in this section indicate that hemi-micelles do not form on the sand surface. Therefore, the adsorption of the cationic surfactants onto the garnet sand corresponds primarily to Region I in Figure 2.5. The adsorption may extend into Region II defined in Figure 2.5 for the longer chain compounds.

The rate of adsorption is controlled by two processes: (1) mass transfer of the sorbate to the interface and (2) the chemical reactions between the sorbate and the surface. The time necessary for transport of the sorbate to the interface can be estimated by assuming semi-infinite linear diffusion (Stumm and Morgan, 1996). The time necessary to achieve the equilibrium surface concentration can be estimated by

$$t = \frac{\pi}{4}\frac{\left(S_{eq}/S_A\right)^2}{DC^2} \qquad (5.7)$$

where S_{eq} is the equilibrium surface concentration in mole/g, D is the molecular diffusion coefficient (10^{-5} cm^2/s), S_A is the specific surface area of the solid (0.12 m^2/g for the garnet sand) and C is the bulk aqueous concentration of the sorbate. Using the data from the DTMA kinetic experiments (C = 90 μM and S_{eq} = 0.15 μmole/g), the diffusion transport time is 0.18 seconds; and for MTMA with C = 60 μM and S_{eq} = 0.18 μmole/g the time is 0.49 seconds. The kinetic adsorption experiments for these compounds showed that equilibrium was achieved after 4 to 12 hours. Therefore, the adsorption of these compounds on garnet sand is not transport limited in the batch adsorption experiments. Chain-chain interactions tend to cause rearrangement of the surfactant ions on the solid surface. These reactions have been shown to be slow (Stumm and Morgan, 1996). Since, MTMA is more hydrophobic than DTMA, there are more interactions among the MTMA chains compared to DTMA which could lead to longer equilibration times for MTMA as was shown in Sections 5.1.3.1 and 5.1.4.1.

Since the sorbed concentration is not sensitive to pH fluctuations for pH's greater than 7 (see Sections 5.1.3.2 and 5.1.4.2), the flume experiments were conducted at pH's between 7 and 8.5. The computation time required to run the detailed bed exchange model for the cationic surfactants is minimized when the Langmuir isotherm is applied (see Chapter 3, Section 3.4.3.1). Therefore, the model results presented in Section 5.2 for comparison with the flume data are based on the Langmuir isotherm. The sensitivity of the model to isotherm choice is examined in Chapter 6, Section 6.9. The differences in the mass exchange of cationic surfactants with different hydrocarbon chain lengths are presented in Chapter 6, Section 6.7.

5.2. FLUME EXPERIMENTS

A total of 10 flume experiments were conducted. One run had with lower-regime flat bed conditions (no sediment motion) and the remaining runs had naturally-created bedforms. The bedforms were generated at velocities that induced sediment motion and generated bedforms; and then the flow was reduced for exchange experiments. The bedforms were stationary in all but three of the runs where the bedforms moved slowly. When bedforms move, the turnover may affect the bed/stream exchange. Turnover is the term used to describe the capture of new porewater at the front of an advancing bedform and the release of old porewater at the backside of the bedform where erosion occurs.

Previous researchers at Caltech (Eylers, 1994; Packman, 1997) used lithium as a conservative (non-reactive) tracer to verify the hydraulics of the bed/stream exchange with a quartz sand bed. Initially, conservative behavior of lithium was assumed in the garnet sand bed, and lithium chloride was added to the first five flume runs with the intent to use it to verify the bed/stream exchange hydraulics. However, lithium adsorption onto the garnet sand was discovered. Bromide was then used as a conservative tracer in the remaining flume runs. The mass exchange of both lithium and bromide with the garnet sand bed was examined in Flume Run 6.

The measured and derived experimental parameters for the flume experiments are summarized in Section 5.2.1. Then, in Section 5.2.2, the experimental data and modeling results are presented for the individual flume runs. The observations are summarized in Section 5.2.3.

5.2.1. Measured and calculated parameters

The experimental parameters for the flume runs are summarized in Table 5.9 through Table 5.12. The chemical conditions are given in Table 5.9, the bed characteristics in Table 5.10, the hydraulic variables in Table 5.11, and the modeling parameters in Table 5.12. The common properties of the sand in the sediment bed are given in Chapter 4, Table 4.1. The notation used in the tables is defined below:

A_b - plan area of the sand bed = 6573 cm^2

b - width of channel = 15.25 cm

C_0 - initial concentration of compound in solution (mole/liter)

d - average water depth in channel

d' - effective water depth (V/A_b)

d* - normalized effective water depth = kd'

d_b - bed depth = 23 cm

$\mathbf{F_r}$ - Froude number = $U/\sqrt{gd}$, where g is gravitational acceleration

f - Darcy-Weisbach friction factor = $8(U_*/U)^2$

f_b - bed friction factor calculated by the procedure of Vanoni and Brooks (1957)

f_w - wall friction factor

h_m - predicted amplitude of piezometric head at the bed surface

$h_{m,c}$ - corrected amplitude of piezometric head at bed surface ($\alpha_c h_m$)

H - average bedform height (see Section 5.2.1.2 for further explanation)

k - bedform wavenumber ($2\pi/\lambda$)

Q - water flow rate in the flume

r_h - hydraulic radius = bd/(b+2d)

Re - Reynolds number = $4Ur_h/\nu$

s_e - slope of energy grade line

t_{ads} - adsorption time scale

t_{pump} - characteristic porewater advection time scale = $1/(ku_m)$

T_{avg} - average temperature during flume run

u_m - maximum Darcy porewater velocity = $kK(\alpha_c h_m)$

U - mean flow velocity in the channel = $Q/(d \cdot b)$

U_* - shear velocity = $\sqrt{gr_h s_e}$

U_b - bedform propagation velocity

U_b^* - normalized bedform propagation velocity = $\theta U_b/u_m$

V - volume of water in the flume excluding porewater

α_c - correction factor for h_m (see Section 5.2.1.4 for further explanation)

Γ_p - ratio of the time scales for adsorption and porewater advection = t_{ads}/t_{pump}

λ - average bedform wavelength (see Section 5.2.1.2 for further explanation)

λ/H - average bedform aspect ratio

σ_λ - standard deviation of bedform wavelengths

σ_H - standard deviation of bedform heights

ν - kinematic viscosity

Table 5.9. Chemical conditions of flume experiments.

Flume Run	T_{avg} (°C)	NaCl (mM)	$NaHCO_3$ (mM)	$pH_{initial}$	pH_{final}	Compounds	C_o (μM)
1 (11/96)	21.6	1	0.5	7.48	5.06	Li^+ $DTMA^+$	54 206
2 (3/97)	24.1	10	2	8.20	8.17	Li^+ $DTMA^+$	90 182
3 (5/97)	24.1	10	2	8.33	8.26	Li^+ $MTMA^+$	93 196
4 (7/97)	24.0	10	2	8.33	8.34	Li^+ $MTMA^+$	100 395
5 (8/97)	25.7	10	2	8.22	8.27	Li^+ $MTMA^+$	95 279
6 (10/97)	27.6	10	2	8.13	8.37	Br^- Li^+ $MTMA^+$	295 47 295
7 (11/97)	23.9	10	2	8.27	8.11	Br^- $DTMA^+$	96 96
8 (11/97)	23.8	10	2	8.13	8.05	Br^- $NTMA^+$	92 92
9 (12/97)	23.3	10	2	8.31	8.32	Br^- $OTMA^+$	182 182
10 (3/98)	23.9	10	2	8.13	8.22	Br^- $DTMA^+$	179 179

Table 5.10. Bed characteristics for flume experiments.

Flume Run	Bedforms	H (cm)	σ_H (cm)	λ (cm)	σ_λ (cm)	k (cm^{-1})	λ/H	U_b (cm/min)
1	ripples/ dunes	1.30	0.52	19.9	8.6	0.315	15.4	0.000
2	ripples/ dunes	1.41	0.46	15.3	4.0	0.411	10.8	0.000
3	ripples/ dunes	1.59	0.62	16.9	6.4	0.373	10.6	NM
4	ripples/ dunes	1.26	0.42	13.8	5.3	0.456	10.9	0.000
5	ripples/ dunes	1.53	0.62	18.2	7.5	0.346	11.9	0.100
6	ripples/ dunes	1.41	0.44	14.9	4.0	0.423	10.6	0.004
7	ripples/ dunes	1.45	0.26	15.9	3.4	0.395	11.0	0.000
8	ripples/ dunes	1.07	0.33	14.3	6.7	0.438	13.4	0.000
9	ripples/ dunes	1.19	0.34	17.9	6.4	0.350	15.1	0.000
10	flat							

NM = not measured

Table 5.11 Hydraulic parameters of the flume experiments.

Flume Run	V (ℓ)	s x 10^4	Q (cm^3/s)	d (cm)	d' (cm)	U (cm/s)	r_h (cm)
1	76	8.4	1442	5.67	11.5	16.7	3.25
2	85	7.8	1723	6.75	12.9	16.7	3.58
3	81	11.4	1714	6.29	12.3	17.9	3.45
4	83	8.0	1657	6.54	12.6	16.6	3.52
5	83	22.7	2490	6.54	12.6	25.0	3.52
6	108	10.2	3204	9.57	16.5	22.0	4.24
7	81	12.0	1701	6.34	12.4	17.6	3.46
8	81	6.9	1635	6.37	12.4	16.8	3.47
9	83	6.1	1593	6.52	12.6	16.0	3.51
10	87	2.4	1714	6.99	13.2	16.1	3.65

Flume Run	F_r	Re x 10^{-3}	U_* (cm/s)	f	f_w	f_b
1	0.22	22.5	1.64	0.077	0.032	0.111
2	0.21	26.3	1.65	0.078	0.033	0.117
3	0.23	27.0	1.96	0.096	0.032	0.149
4	0.21	25.6	1.66	0.080	0.033	0.120
5	0.31	39.9	2.80	0.101	0.030	0.162
6	0.23	44.2	2.06	0.070	0.027	0.125
7	0.22	26.6	2.02	0.105	0.033	0.165
8	0.21	25.4	1.54	0.067	0.030	0.097
9	0.20	24.3	1.45	0.066	0.030	0.096
10	0.19	25.6	0.92	0.026	0.025	0.028

Table 5.12. Model parameters for the flume experiments.

Flume Run	H/d	α_c	h_m (cm)	u_m (cm/min)	d*	U_b^*	t_{pump} (min)	t_{ads} (min)	Γ_p
1	0.23	1.00	0.034	0.039	3.63	0.00	82	10	0.12
2	0.21	1.42	0.033	0.070	5.30	0.00	35	10	0.29
3	0.25	1.47	0.041	0.081	4.58	NM	33	30	0.90
4	0.19	1.25	0.032	0.066	5.75	0.00	33	30	0.90
5	0.23	1.00	0.077	0.096	4.36	0.49	30	30	1.00
6	0.15	1.00	0.050	0.076	6.97	0.02	31	30	0.97
7	0.23	1.00	0.038	0.054	4.88	0.00	47	10	0.21
8	0.17	2.25	0.031	0.110	5.43	0.00	21	< 10	< 0.48
9	0.18	1.08	0.029	0.040	4.41	0.00	72	> 30	> 0.42
10									

NM = not measured

5.2.1.1. Determination of initial concentration C_0

The initial concentration C_0 is calculated by averaging the measured concentrations of the samples collected during the first 20 minutes of the flume run ($t^*/\theta < 1$). These samples were collected every two minutes at two different locations along the flume. However, some mass exchange occurred during this time. The value of C_0 may be underestimated by as much as 5 percent. The effect of this error on the results is discussed in Chapter 6, Section 6.6.1.

5.2.1.2. Measurement of bedform parameters

Bed surface profiles were acquired using the laser displacement sensor described in Chapter 4, Section 4.2. The centerline bed profile from Flume Run 2 is displayed in Figure 5.19. The height of a particular ripple or dune is taken as the difference in elevation between the crest and the mean of the elevations of the troughs at the ends of the bedform. The bedform wavelength is the distance between the troughs. The average height H and wavelength λ reported in Table 5.10 are the means of the individual bedform measurements taken along the centerline of the flume. The variations in the bedform heights and wavelengths are as high as ±40 percent of the average.

Photographs of typical garnet sand dunes are included in Figure 5.20 and Figure 5.21. The dunes are irregular and three-dimensional. The mean dune height varies by approximately 10 percent across the width of the channel and the average wavelength by about 5 percent. The sensitivity of the models to changes in H and λ is discussed in Chapter 6, Section 6.5.

a) Full bed profile

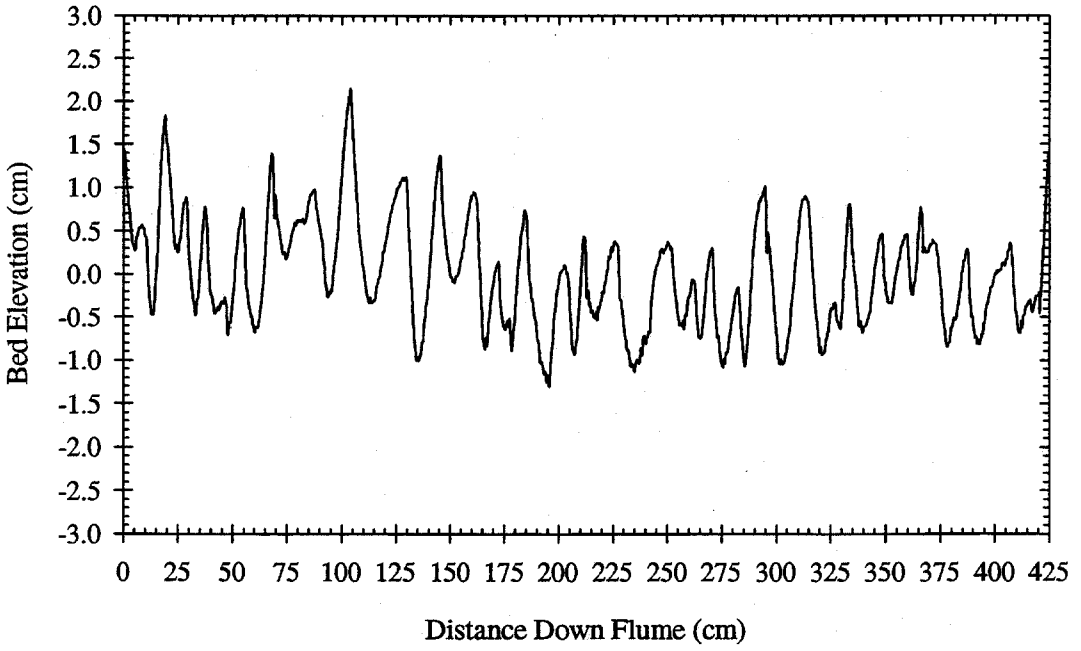

b) Section of bed profile

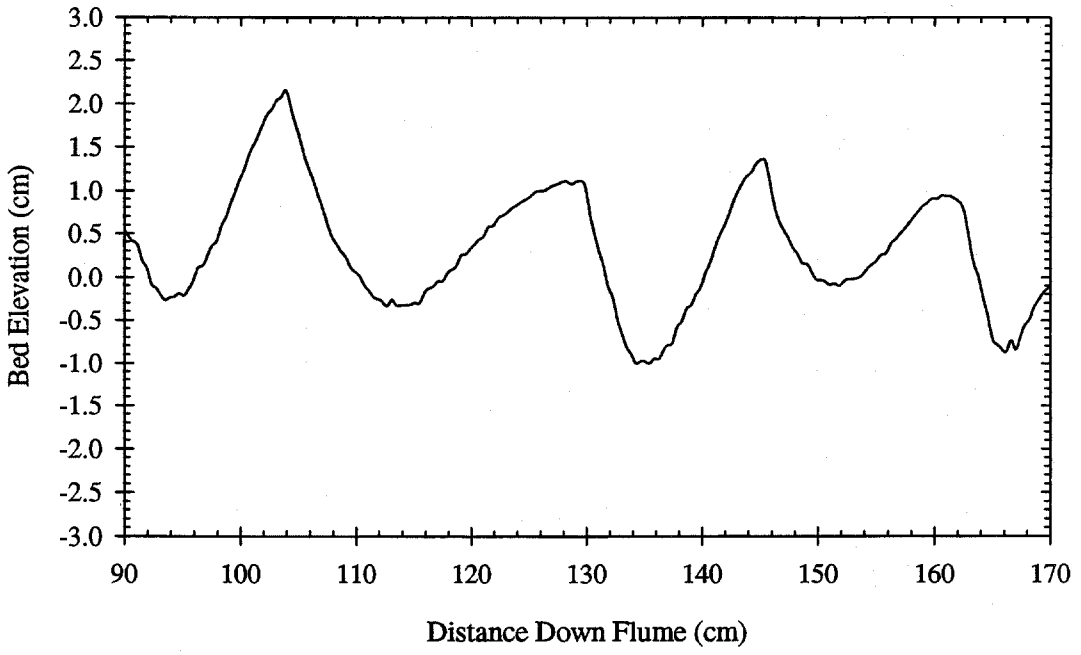

Figure 5.19. Centerline bed profile from Flume Run 2.

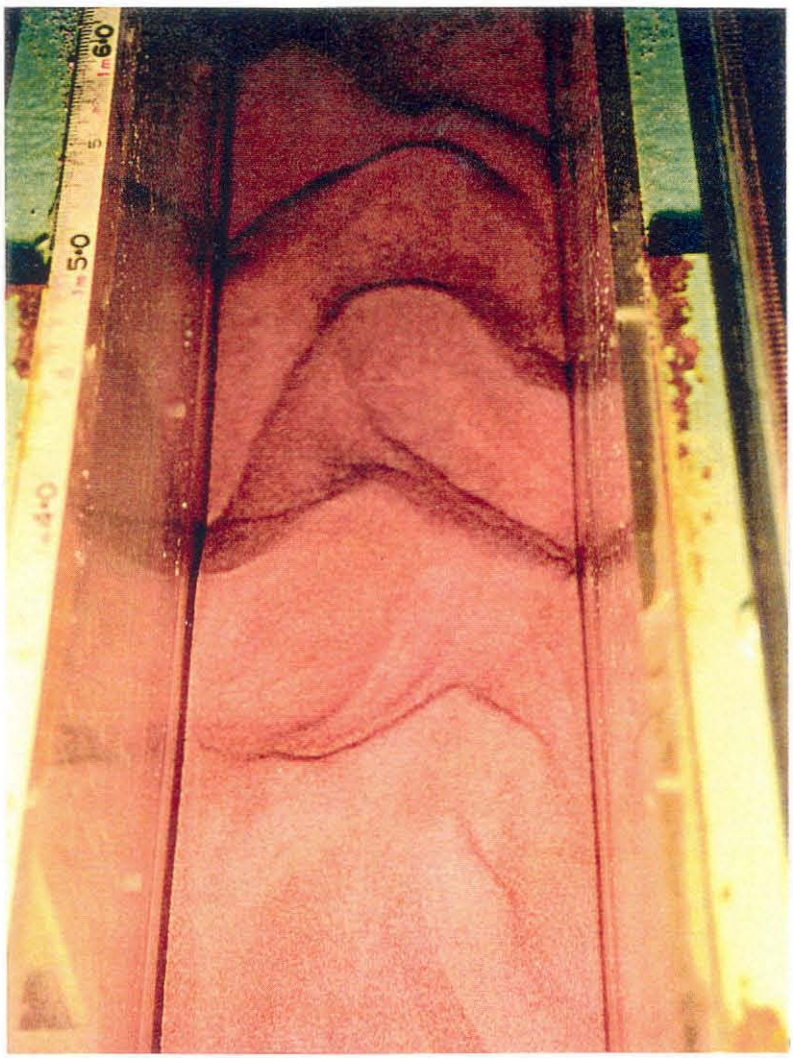

Figure 5.20. Photograph of typical garnet sand dunes - top view, looking downstream.

In order to calculate the bedform velocity, two centerline bed profiles were acquired at two different times differing by Δt. The distance that the bedforms traveled during Δt was calculated by stepping back the second profile until the correlation coefficient between the profiles was maximized. The bedform propagation velocity U_b was then calculated by dividing this distance by Δt.

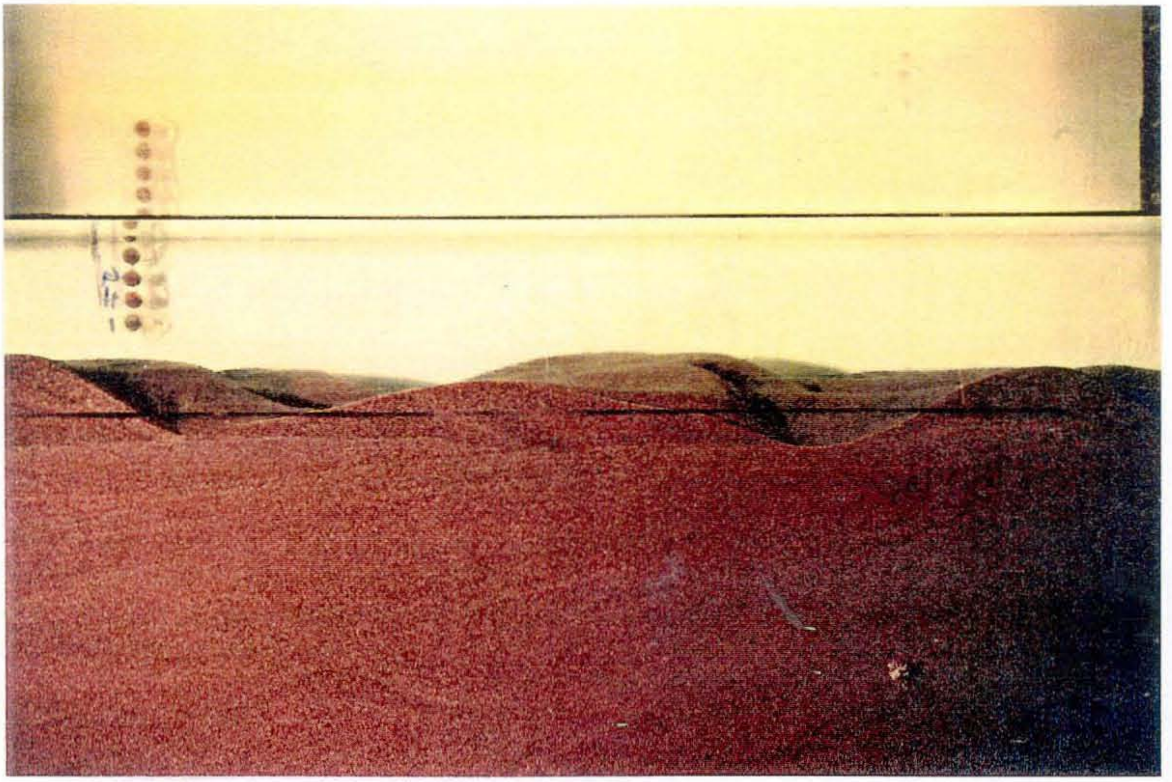

Figure 5.21. Photograph of typical garnet sand dunes - side view, flow direction from left to right.

5.2.1.3. Slope of the energy grade line

The slope of the energy grade line (s) is calculated by

$$s_e = s_f - \frac{de}{dx} \tag{5.8}$$

where s_f is the slope of the flume, x is the distance along the flume and e is the specific energy.

The specific energy is defined as

$$e = y'_s + \frac{1}{2g}\left(\frac{Q/b}{y'_s - y'_b}\right)^2 \tag{5.9}$$

where y'_s is the elevation of the flowing water surface relative to the flume rails and y'_b is the bed elevation relative to the flume rails. The flume slope s_f equals the slope of the line fitted to the difference in the point gauge readings between the still water surface when the flume is horizontal and the still water surface after the slope of the flume is adjusted. The point gauge readings acquired when the flume was at the horizontal position were used to account for deviations in the flume rails. When the bed and flowing water surfaces are parallel $s_e = s_f$.

5.2.1.4. Amplitude of piezometric head h_m

The only parameter that is not measured directly is the amplitude of the piezometric head over the bedforms (h_m). The value of h_m is estimated using Equation (5.10).

$$h_m = 0.28 \frac{U^2}{2g} \begin{cases} \left(\frac{H/d}{0.34}\right)^{3/8} & H/d \le 0.34 \\ \left(\frac{H/d}{0.34}\right)^{3/2} & H/d \ge 0.34 \end{cases} \qquad (5.10)$$

This formula was developed by Elliott (1990) (see Chapter 3, Section 3.1) using Fehlman's (1985) pressure measurements over a single, solid triangular bedform 0.14 m high, 0.91 m long and 0.61 m wide. The downstream face had a 30° incline and the upstream face an 11.5° incline.

The bedforms in the flume have different shapes and sizes. The form drag of a bedform varies with the size and shape of the bedform and is affected by the spacing and arrangement of the neighboring bedforms. Since the form drag results from pressures acting on the bedform, the pressure head should also be affected by these factors. Fehlman observed that the size of the bedform immediately upstream of the one studied had a drastic effect on the shape of the pressure distribution. The piezometric head may be affected by the wavelength-to-depth ratio and the aspect ratio. The aspect ratio for Fehlman's bedform is 6.5 whereas the average aspect ratio of the bedforms observed in the flume experiments is 11. There may be some scaling effects.

Since the piezometric head is very difficult to measure on sand dunes, the amplitude h_m was calibrated to the flume data. The correction factor α_c is defined as the ratio of the calibrated amplitude of the pressure head and the predicted value calculated using Equation (5.10). In the exchange models, conservative tracer data was used for the calibration. In the absence of a conservative tracer, the initial flux of the lithium and surfactant ions was used. The correction factor α_c varied between 1.0 and 2.25. The sensitivity of the bed exchange models to changes in h_m is examined in Chapter 6, Section 6.3.

5.2.2. Results from individual experiments

The results of the individual flume experiments are presented in this section. The following sections summarize the observations and general model results, while plots showing the bed and flowing water surface profiles and the variations of pH and water temperature with time for each experiment are included in Appendix A.

The mass transfer to the bed is illustrated on a plot that shows the fraction of the total mass of each compound contained in the bed ($1 - C/C_0$) versus $\sqrt{(t^*/\theta)}$, where t^* is the non-dimensional time ($t^* = ku_m$). The real time in hours is displayed as $\sqrt{t}$ along the top axis. The curves from the conservative (Chapter 3, Section 3.2) and nonlinear (Chapter 3, Section 3.4.3) bed/stream exchange model simulations are also included in the plot.

The porewater profiles are also presented in this section. The porewater samples were taken approximately 5 cm inward from the flume wall. The vertical rows of sampling ports were located 40 cm (Station 1), 200 cm (Station 2) and 330 cm (Station 3) from the inlet box. The ports at Stations 1 and 3 were installed after Flume Run 4. By sampling at different locations along the flume, the variability of the concentration fronts for the different compounds can be assessed and an average front depth can be calculated.

The porewater concentration profiles are fairly constant in the upper region of the bed, and then there is a sharp drop-off of concentration with depth. The shape of the porewater concentration profiles is similar to a downward-moving front, which is typical of advective mass transfer. If the transfer were due to diffusion, there would be a more gradual decay of the concentration profile with depth.

The penetration depth of the concentration fronts increases with time. Nonsorbing compounds travel deeper into the bed than sorbing compounds. The penetration depth of a sorbing compound is inversely related to the strength of the adsorption reaction.

The detailed model simulations (Chapter 3, Section 3.4.3) for lithium and the cationic surfactants utilized the Langmuir adsorption isotherm. The time required to complete one simulation on a PC with a Pentium processor averaged two hours. The computation time required for simulations with the Freundlich, Tóth and Langmuir-Freundlich isotherms averaged 24 hours (see Chapter 3 for details). The models for DTMA, MTMA and OTMA used 65 streamtubes and $\Delta(t^*/\theta)$ was 0.01. Because lithium and NTMA exhibited weak adsorption to the garnet sand, the model parameters needed to be refined. The NTMA model had 120 streamtubes and $\Delta(t^*/\theta)$ was set at 0.005. For lithium, the number of streamtubes increased to 200 and $\Delta(t^*/\theta)$ was reduced to 0.002.

5.2.2.1. Flume Run 1

In Flume Run 1, the transport of DTMA (C_0 = 206 μM) and lithium (C_0 = 54 μM) into the sediment was studied in 1 mM NaCl. Porewater samples were not taken. The initial pH was 7.5 and then dropped 2.5 pH units during the experiment as shown in Figure 5.22.

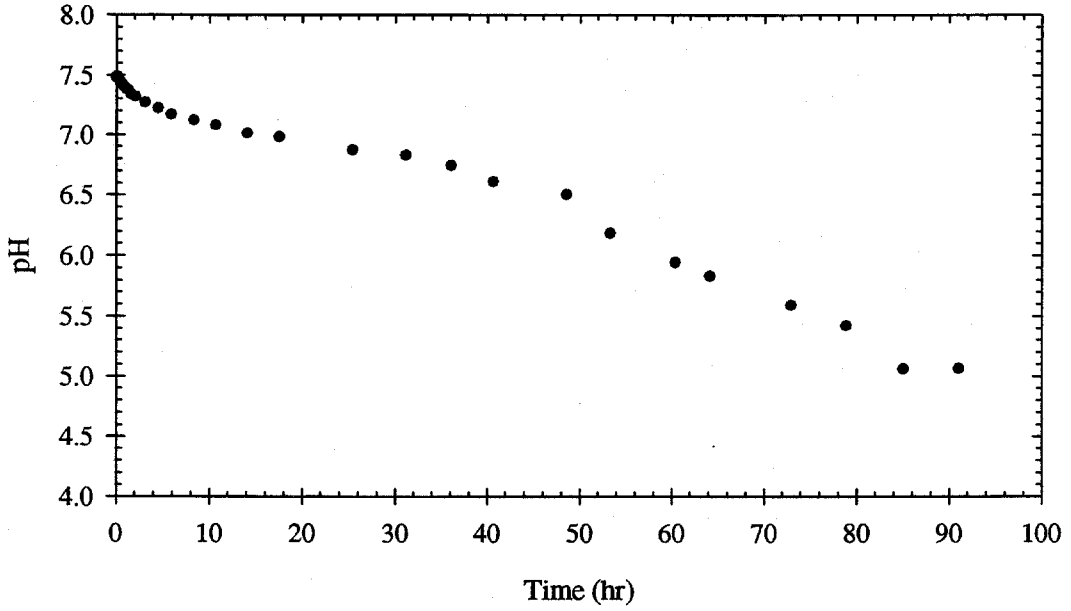

Figure 5.22. Variation of pH with time during Flume Run 1.

The experimental results and model predictions are compared in Figure 5.23. The Langmuir parameters from Table 5.3 are used in the DTMA model. The DTMA model over-predicts the mass transfer for $t^*/\theta > 25$ ($t > 20$ hours). At this point, the pH dropped below 7 and continued to decrease as the experiment proceeded. The decrease in pH caused a decrease in adsorption (see Figure 5.4). Since the model used an isotherm determined for adsorption at pH 7, it over predicted DTMA adsorption in the latter part of the experiment. The magnitude of the difference between the DTMA model and data increases with time.

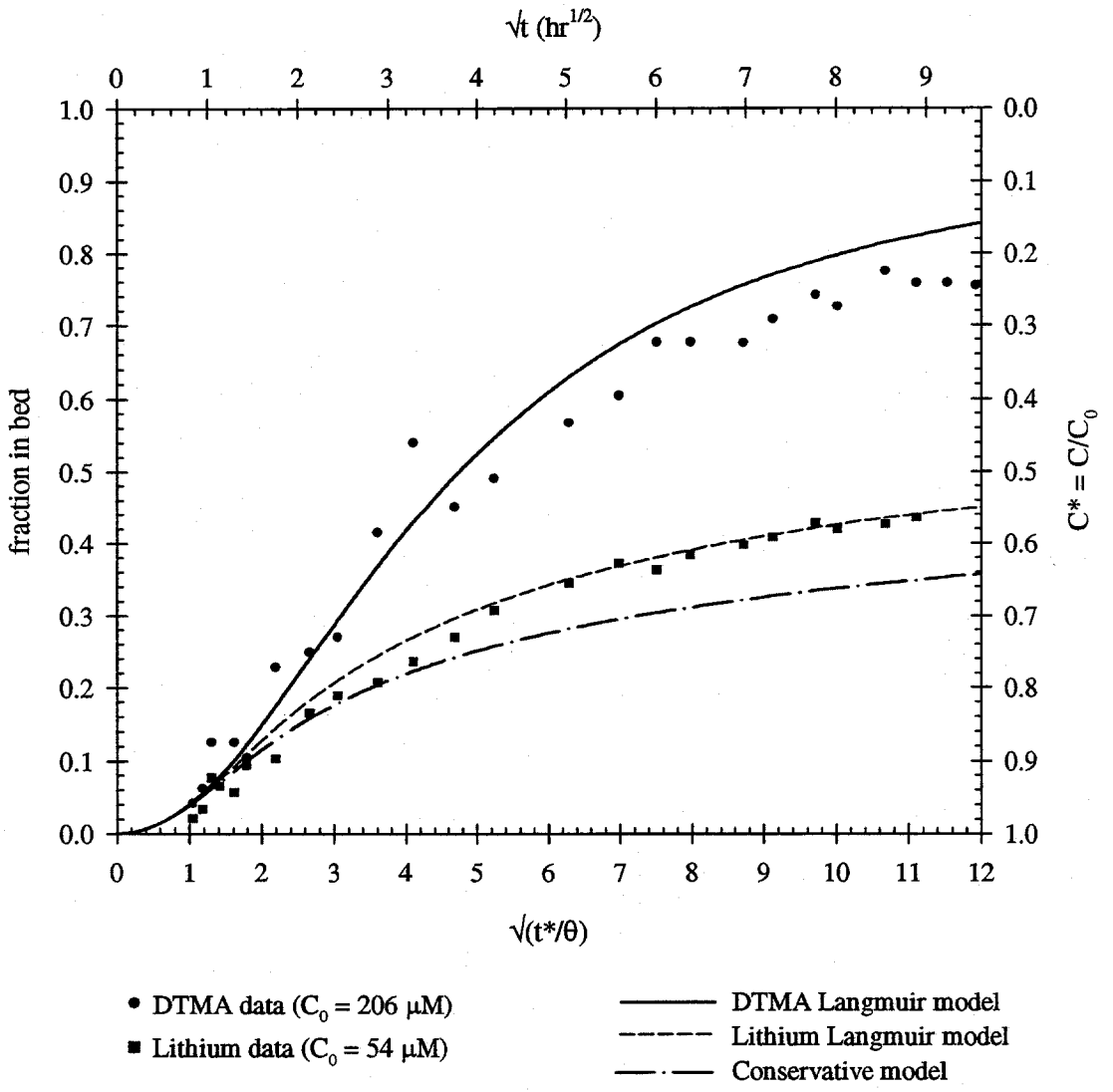

Hydraulic parameters:	d = 5.67 cm	U = 16.7 cm/s
Bed parameters:	$\lambda = 19.9 \pm 8.6$ cm	$H = 1.30 \pm 0.52$ cm
Chemical parameters:	1 mM NaCl 0.5 mM $NaHCO_3$	$pH_{initial} = 7.5$
Model parameters:	$\alpha_c = 1.00$	$h_m = 0.034$ cm

Figure 5.23. Comparison of experiment results and model predictions for Flume Run 1. The ± value represents one standard deviation.

5.2.2.2. Flume Run 2

In Flume Run 2, the transport of DTMA and lithium was studied at a higher pH (8.2) and salt concentration (10 mM NaCl) than in Flume Run 1. The initial DTMA concentration (~182 μM) was approximately the same as in Run 1 and the lithium concentration was increased by about a factor of two (to ~90 μM). The pH fluctuated between 8.1 and 8.3 during the experiment.

The porewater samples were taken at Station 2. The porewater concentration profiles at different times are displayed in Figure 5.24. The maximum penetration depths (after 191 hours) for lithium and DMTA are 18 cm and 10 cm, respectively. The height and wavelength of the individual bedform at which the samples were taken are 1.23 cm and 11.6 cm, respectively. The maximum penetration depth for lithium exceeds the individual and average bedform wavelengths. The lithium transport deep in the bed is affected by the larger bedforms in the flume. This phenomenon is discussed further in Section 5.2.3. DTMA does not travel deep enough into the bed to be influenced by the larger bedforms.

The lithium concentration at the end of the experiment is 43.5 μM (C* = 0.49). The corresponding effective retardation coefficient calculated using Equation (5.11) is 1.52 (Chapter 3, Section 3.4).

$$R_{eff}(C) = 1 + \frac{\rho_b}{\theta}\frac{S_T K_L}{1 + K_L C} \tag{5.11}$$

The Langmuir adsorption parameters for lithium are listed in Table 5.2. The equivalent penetration depth (Chapter 3, Section 3.5.3), defined by Equation (5.12), is 18.8 cm for lithium, which agrees with the observed concentration profiles.

$$d_q = \frac{d'}{\theta R_{eff}}\left(\frac{1}{C^*} - 1\right) \tag{5.12}$$

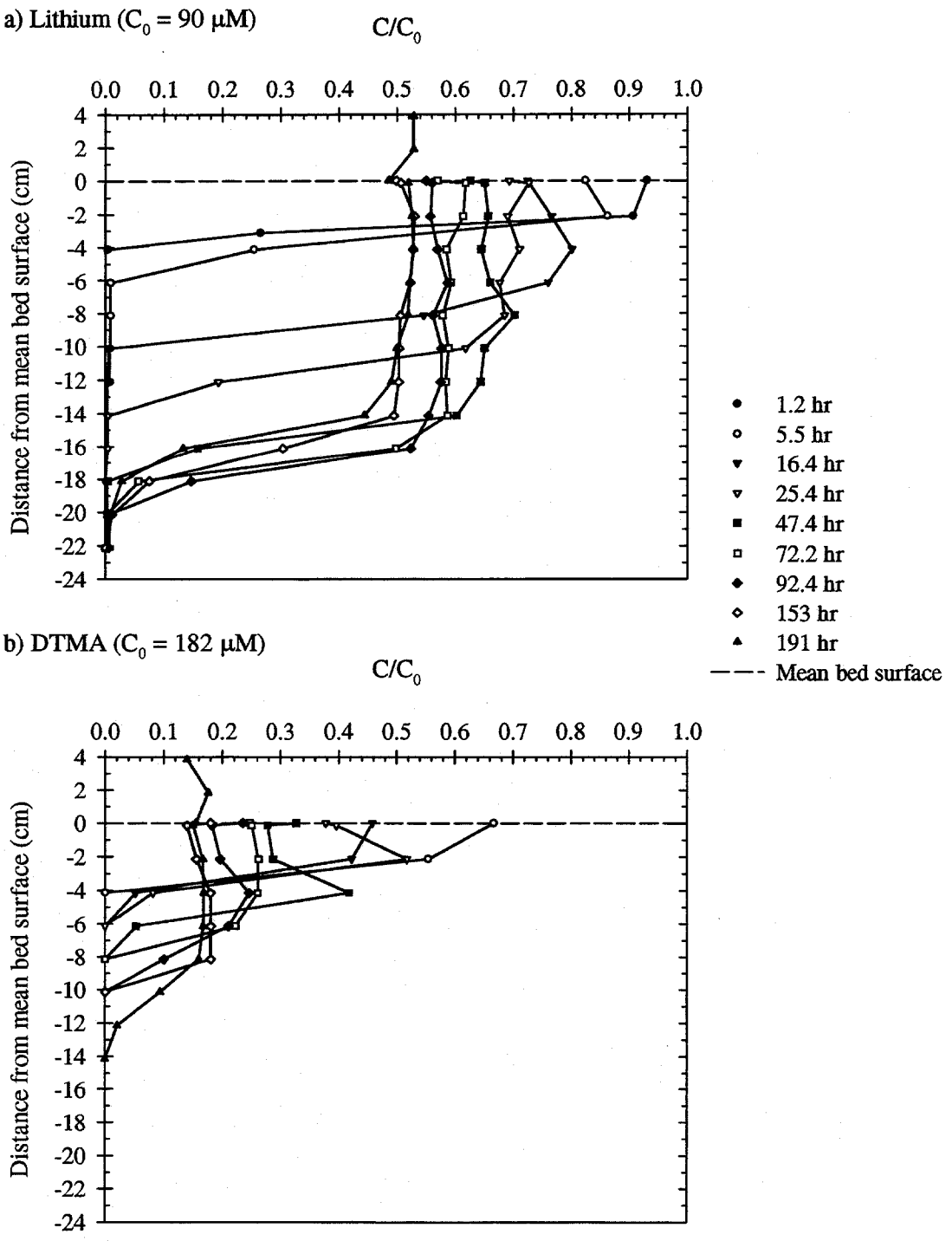

Figure 5.24. Porewater concentration profiles for (a) lithium and (b) DTMA at Station 2 in Flume Run 2.

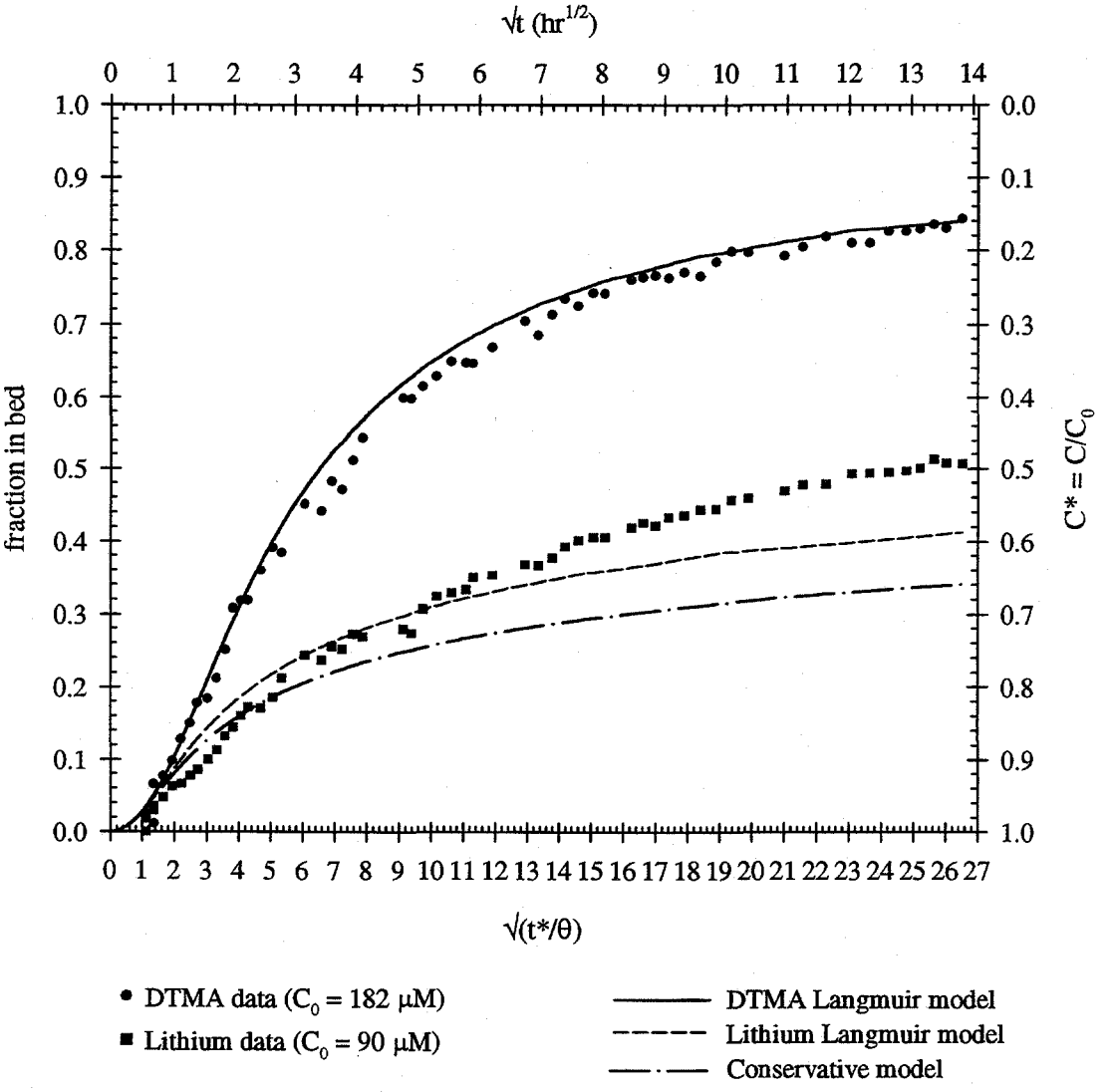

Hydraulic parameters:	d = 6.75 cm	U = 16.7 cm/s
Bed parameters:	$\lambda = 15.3 \pm 4.0$ cm	$H = 1.41 \pm 0.46$ cm
Chemical parameters:	10 mM NaCl 2 mM $NaHCO_3$	$pH_{initial} = 8.2$
Model parameters:	$\alpha_c = 1.42$	$h_m = 0.033$ cm

Figure 5.25. Comparison of experiment results and model predictions for Flume Run 2. The ± value represents one standard deviation.

Figure 5.25 compares the experimental data to the model predictions for Flume Run 2. The DTMA Langmuir sorption coefficients are listed in Table 5.4. The model simulation for DTMA agrees well with the flume data. The lithium transport into the bed is under-predicted when $t^*/\theta > 121$ ($t > 36$ hours) because the lithium transport is influenced by the larger bedforms and the model uses the average bedform wavelength (see Chapter 6, Section 6.5).

5.2.2.3. Flume Run 3

The transport of MTMA and lithium was observed in Flume Run 3. The initial concentrations and chemical conditions were the same as in Flume Run 2, while the flow velocity U in Run 3 (17.9 cm/s) was slightly faster than the velocity in Run 2 (16.7 cm/s). Sediment motion was observed, and the bedforms propagated slowly down the flume. The bedform propagation velocity was not measured, but the velocity was less than 0.1 cm/min. For bedforms that travel at low velocities, advective pumping still dominates the exchange (Elliott, 1990).

Porewater samples were taken at Station 2. Figure 5.26 displays the porewater concentration profiles for lithium and MTMA. The average bedform wavelength is 16.9 cm. The maximum penetration depths for lithium and MTMA are 18 cm and 5 cm, respectively. The effective retardation coefficient for lithium at the end of the run is 1.50, which gives an equivalent penetration depth of 17.9 cm. This value agrees with the penetration depth observed in the lithium porewater concentration profiles. The lithium penetration depth exceeds the average bedform wavelength which indicates that the lithium transport within the bed is affected by porewater flows induced by the larger bedforms.

The penetration depths for both lithium and MTMA moved up and down with time. This reflects the unsteady porewater velocity caused by the moving bedforms.

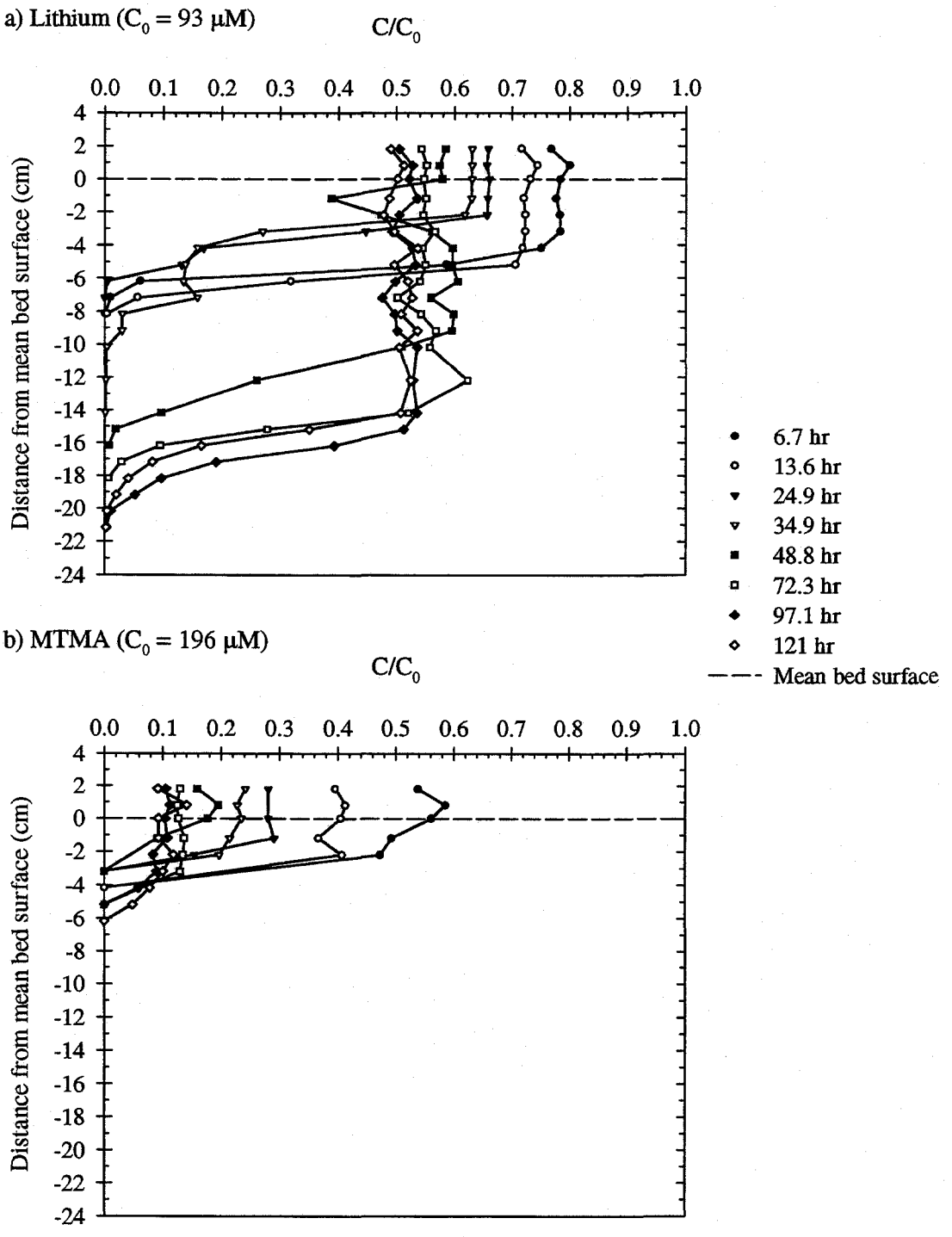

Figure 5.26. Porewater concentration profiles for (a) lithium and (b) MTMA at Station 2 in Flume Run 3.

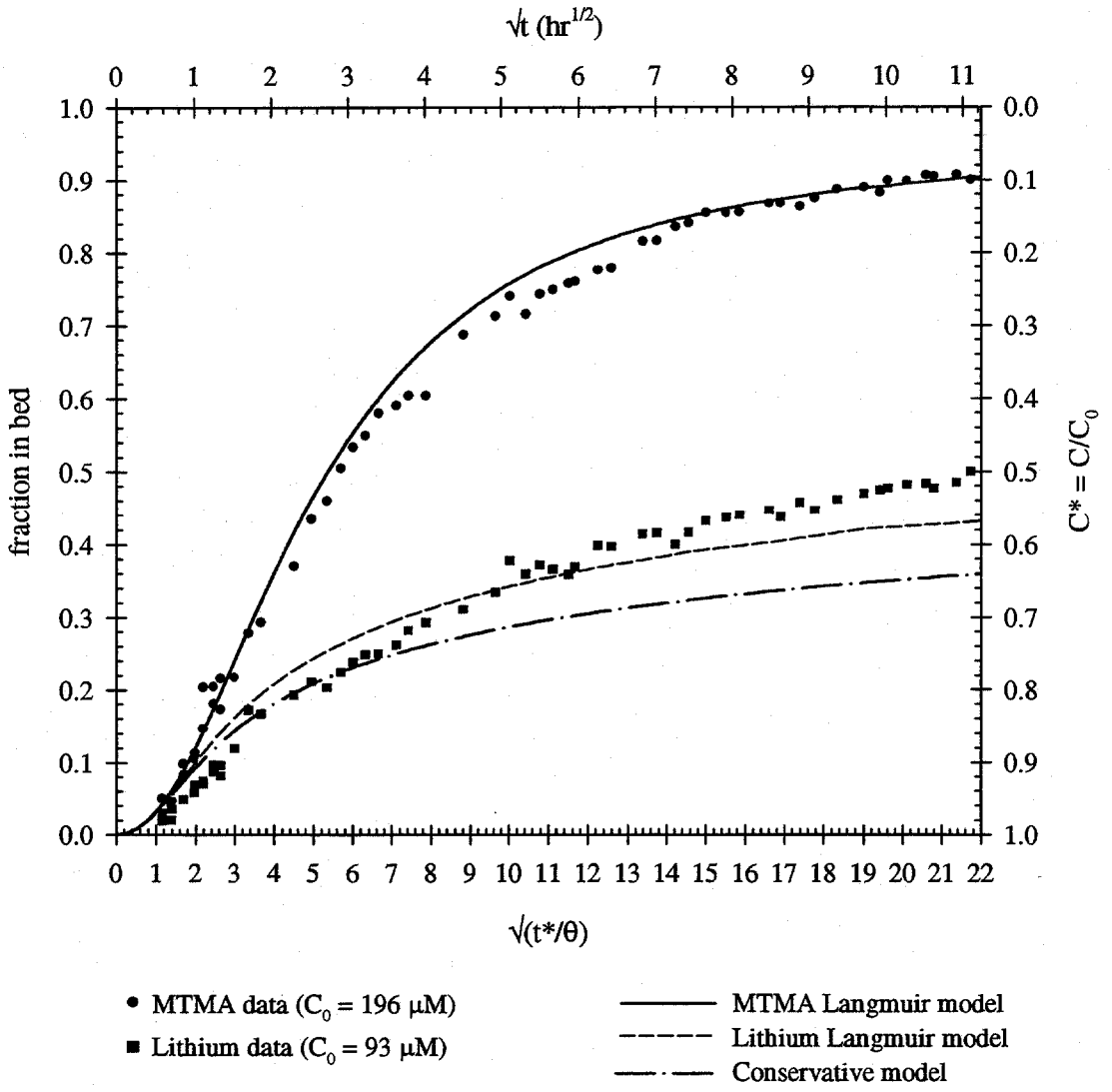

Hydraulic parameters:	d = 6.29 cm	U = 17.9 cm/s
Bed parameters:	$\lambda = 16.9 \pm 6.4$ cm	$H = 1.59 \pm 0.62$ cm
Chemical parameters:	10 mM NaCl 2 mM $NaHCO_3$	$pH_{initial} = 8.3$
Model parameters:	$\alpha_c = 1.47$	$h_m = 0.041$ cm

Figure 5.27. Comparison of experiment results and model predictions for Flume Run 3. The ± value represents one standard deviation.

The penetration depth of MTMA is half of the depth achieved by DTMA in Flume Run 2. The difference in the penetration depths reflects the difference in the effective retardation coefficients of the two surfactants. The Langmuir adsorption parameters for MTMA are listed in Table 5.6.

The experimental data and model results for Flume Run 3 are shown in Figure 5.27. The pumping model for MTMA agrees with the data although the bedforms were not stationary. The lithium model simulations fall below the lithium data when $t^*/\theta > 144$ ($t > 40$ hours).

5.2.2.4. Flume Run 4

The objective of Flume Run 4 was to investigate the effect of the initial concentration of MTMA on the bed exchange. The initial MTMA concentration in Run 4 (395 μM) was double the initial concentration in Run 3 (196 μM).

The porewater concentration profiles acquired at Station 2 are shown in Figure 5.28. The average bedform wavelength is 13.8 cm. The maximum penetration depths for lithium and MTMA are 15 cm and 7 cm, respectively. The transport of the lithium ion within the bed is affected by the longer bedforms.

Figure 5.29 shows the mass transfer results and model simulations for Flume Run 4. The MTMA model predictions match the observed mass exchange very closely, within experimental error. The lithium mass transfer is under-predicted to a somewhat greater extent than in previous flume runs.

Since the total mass available for exchange doubled from Flume Run 3 to Run 4, the total mass transfer to the bed increased. However, a smaller fraction of the total mass was retained in the bed in Flume Run 4 because a smaller fraction of the total mass adsorbed to the sand. The effect of the increase in the initial concentration on the overall MTMA mass exchange is discussed further in Chapter 6, Section 6.6.2.

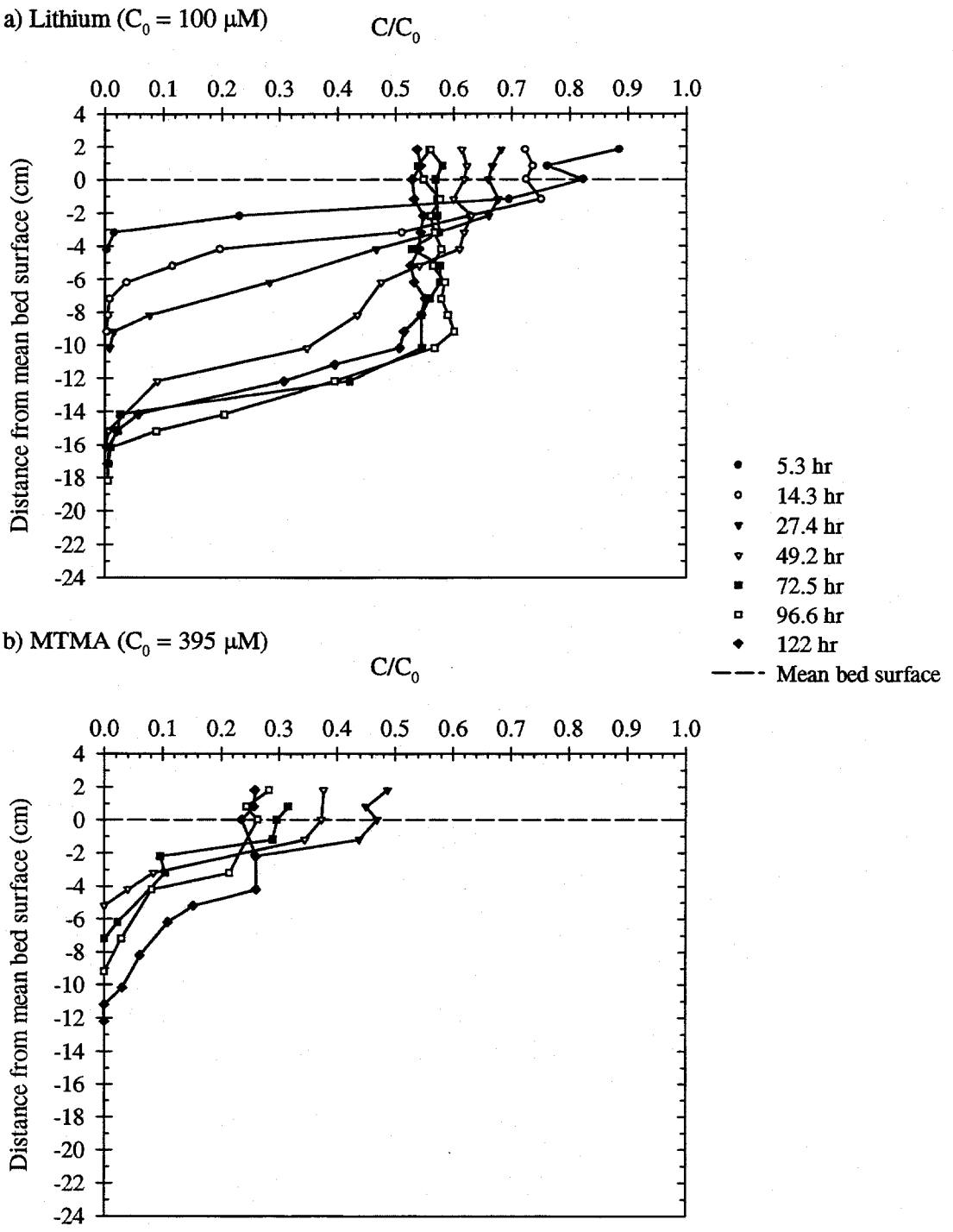

Figure 5.28. Porewater concentration profiles for (a) lithium and (b) MTMA at Station 2 in Flume Run 4.

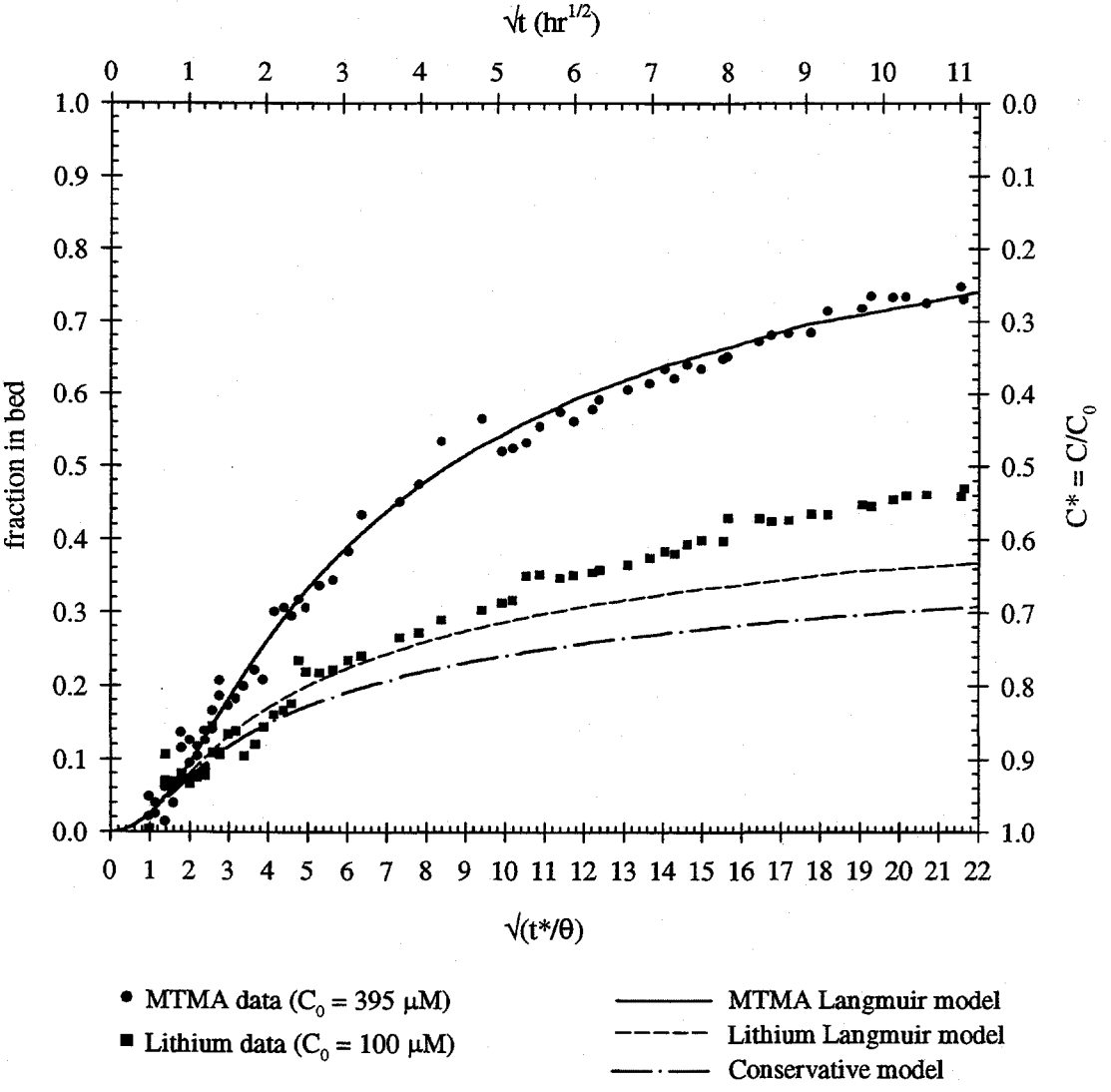

Hydraulic parameters:	d = 6.54 cm	U = 16.6 cm/s
Bed parameters:	$\lambda = 13.8 \pm 5.3$ cm	$H = 1.26 \pm 0.42$ cm
Chemical parameters:	10 mM NaCl 2 mM $NaHCO_3$	$pH_{initial} = 8.3$
Model parameters:	$\alpha_c = 1.47$	$h_m = 0.032$ cm

Figure 5.29. Comparison of experiment results and model predictions for Flume Run 4. The ± value represents one standard deviation.

5.2.2.5. Flume Run 5

In Flume Run 5, the flow velocity was increased to 25 cm/s and the initial MTMA concentration was 300 μM. The bedforms moved slowly with a velocity U_b of 0.1 cm/min. Elliott (1990) developed a parameter U_b^*, which reflects the relative importance of the turnover and pumping exchange processes:

$$U_b^* = \frac{\theta U_b}{u_m} \tag{5.13}$$

where u_m is the maximum Darcy velocity in the bed, which has a value of 0.096 cm/min in Flume Run 5. The value of U_b^* in Flume Run 5 is 0.49. Elliott found that when $U_b^* << 1$, the effect of turnover on the exchange is negligible, but turnover did affect the exchange for values of U_b^* down to 0.28. Consequently, some turnover effects are expected in the mass exchange for Flume Run 5.

Porewater samples were collected at Stations 1, 2 and 3. The concentration profiles are illustrated in Figure 5.30 through Figure 5.32. The moving bedforms create fluctuating porewater streamline patterns that cause the concentration fronts for both lithium and MTMA to move up and down with time at the fixed sampling stations. Elliott's dye experiments showed that the penetration depth of the dye was variable along the length of the flume in the presence of slowly moving bedforms. The maximum penetration depths for lithium at Stations 1, 2 and 3 are 19 cm, 13 cm and 15 cm, respectively; and for MTMA the maximum depths are 5, 7 and 9 cm at Stations 1, 2 and 3, respectively.

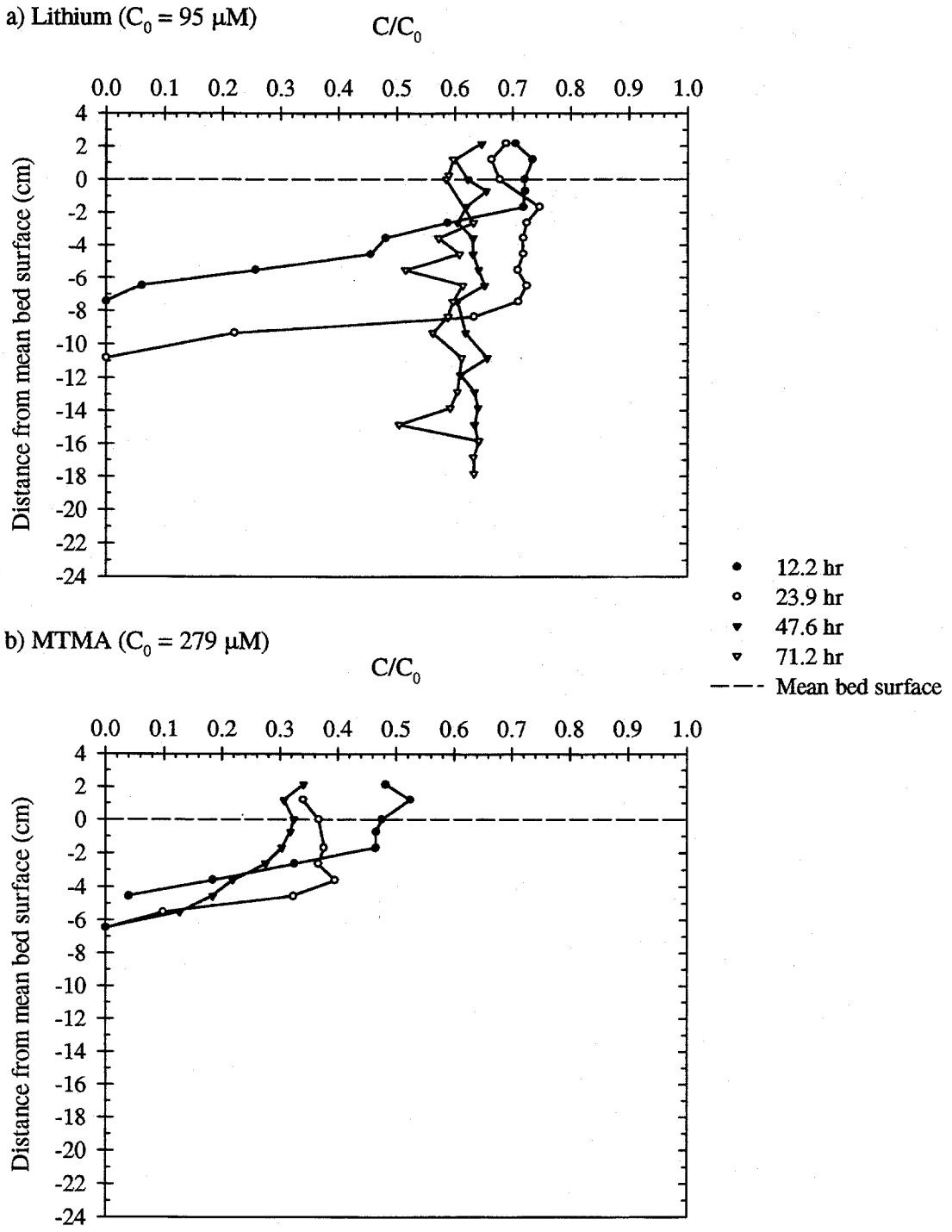

Figure 5.30. Porewater concentration profiles for (a) lithium and (b) MTMA at Station 1 in Flume Run 5.

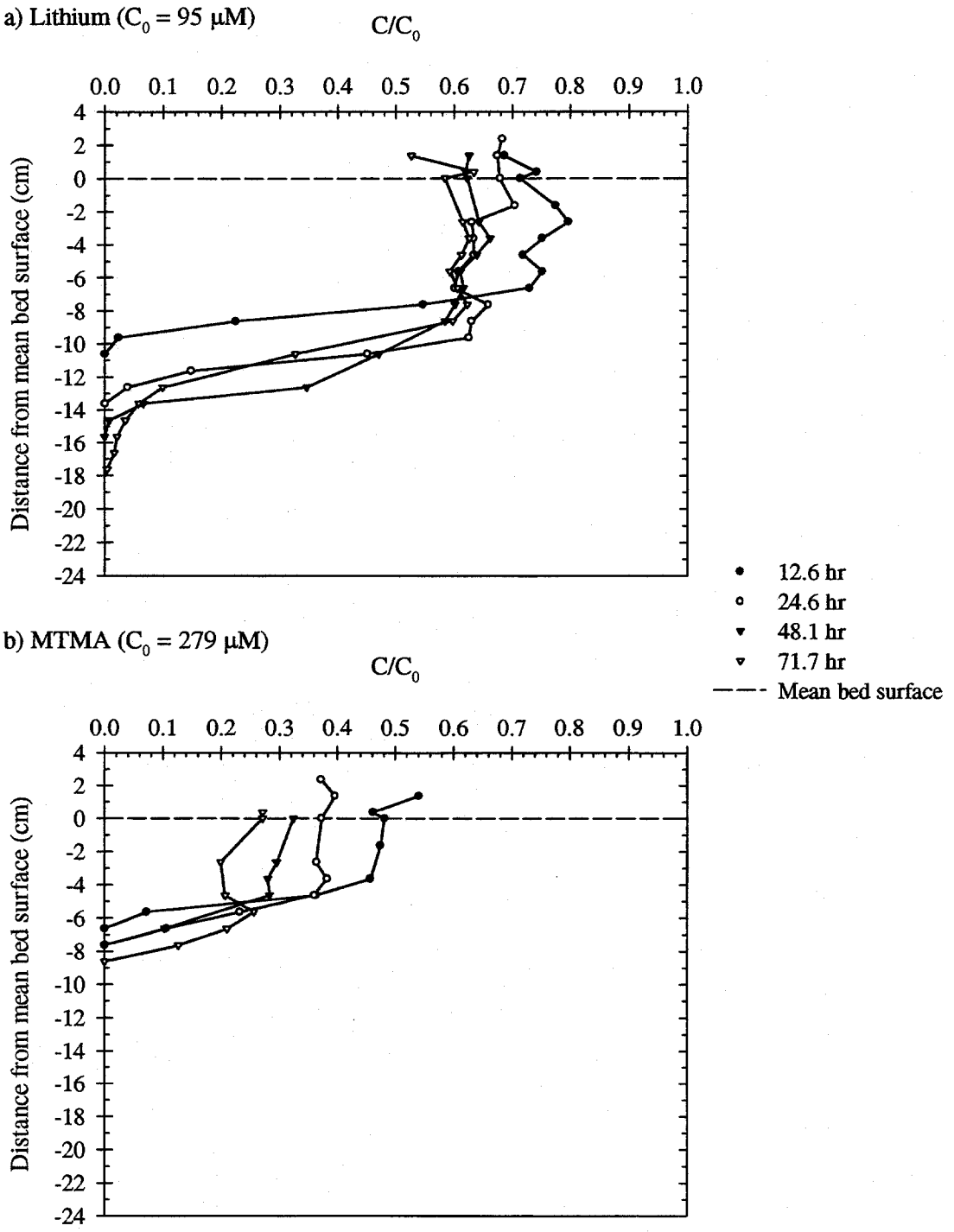

Figure 5.31. Porewater concentration profiles for (a) lithium and (b) MTMA at Station 2 in Flume Run 5.

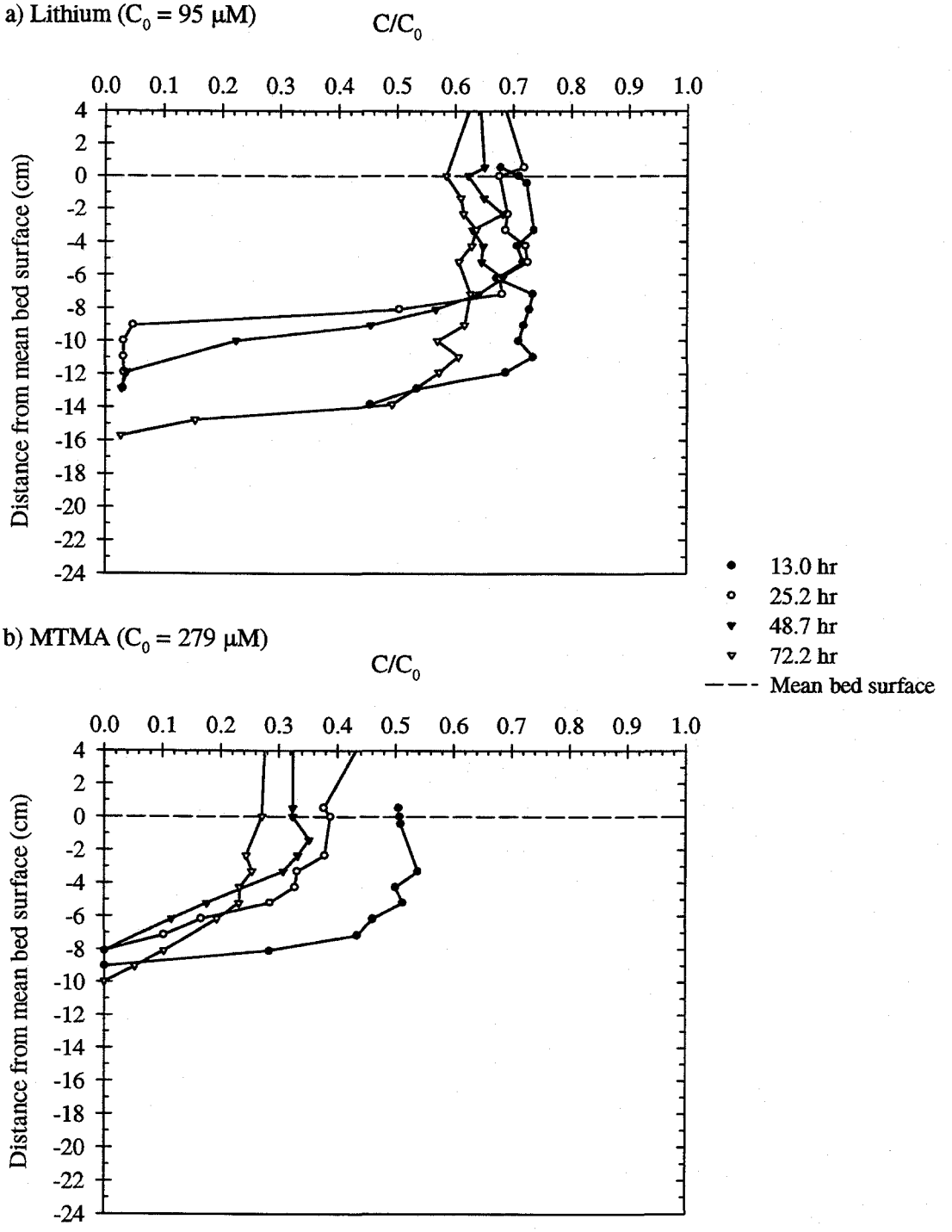

Figure 5.32. Porewater concentration profiles for (a) lithium and (b) MTMA at Station 3 in Flume Run 5.

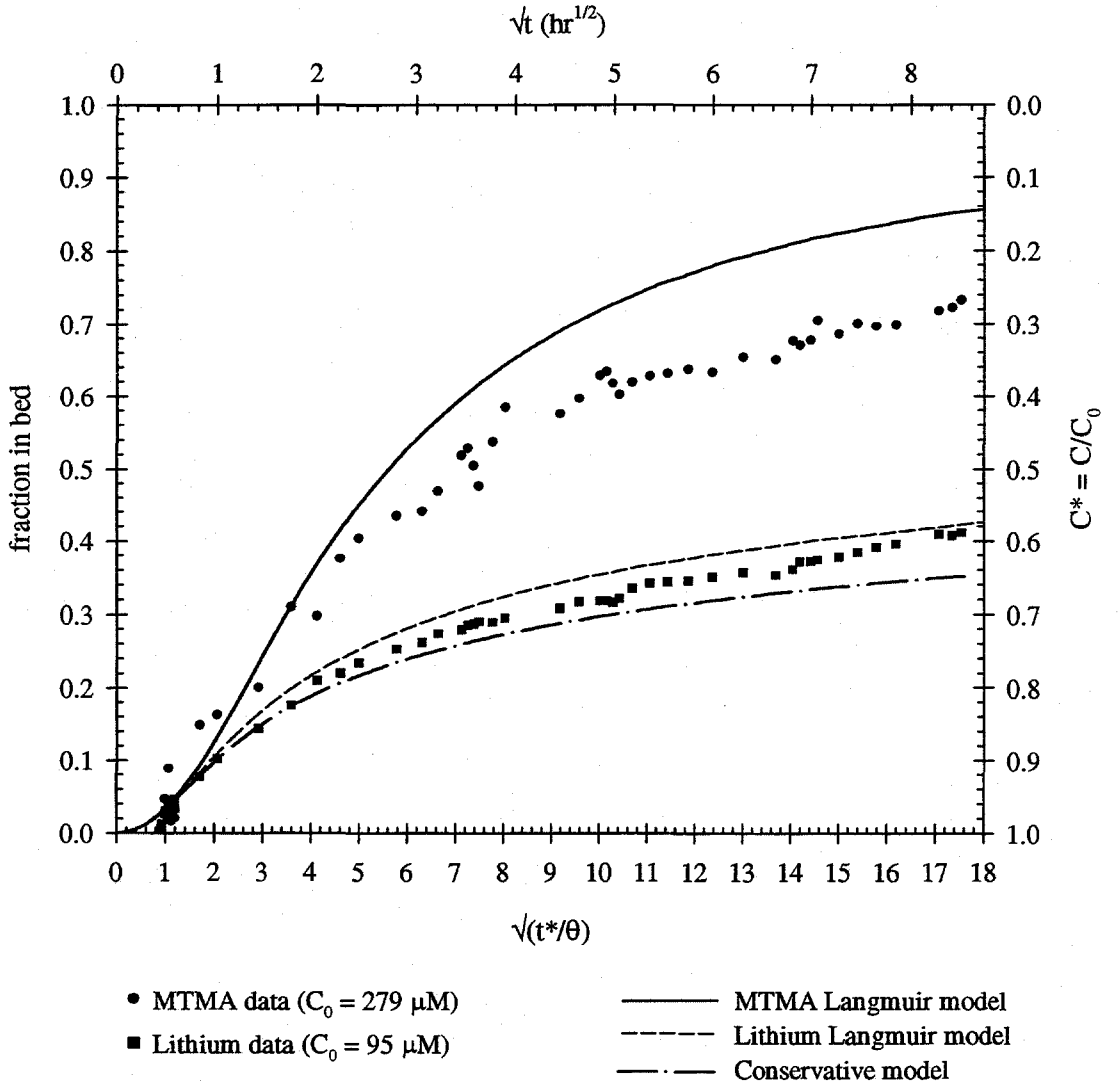

Hydraulic parameters:	d = 6.54 cm	U = 25.0 cm/s
Bed parameters:	$\lambda = 18.2 \pm 7.5$ cm $U_b = 0.1$ cm/min	$H = 1.53 \pm 0.62$ cm
Chemical parameters:	10 mM NaCl 2 mM $NaHCO_3$	$pH_{initial} = 8.2$
Model parameters:	$\alpha_c = 1.00$ $U_b^* = 0.49$	$h_m = 0.077$ cm

Figure 5.33. Comparison of experiment results and model predictions for Flume Run 5. The ± value represents one standard deviation.

Figure 5.33 compares the experimental data and pumping model prediction for Flume Run 5. The pumping model over-predicts the mass transfer for both lithium and MTMA, which agrees with Elliott's observation that turnover causes a decrease in the net exchange with respect to stationary bedforms. The magnitude of the difference between the data and the model is greater for MTMA than for lithium. The stronger MTMA adsorption magnifies the error. The effect of adsorption kinetics may also affect the deviations between the MTMA data and model because the adsorption and pumping time scales are equal.

5.2.2.6. Flume Run 6

The exchange of bromide, lithium and MTMA was studied in Flume Run 6. The water depth was increased from 6.54 cm in Run 5 to 9.57 cm in Run 6. The flow velocity was 22.0 cm/s, which is slightly less than the velocity in Run 5 (25.0 cm/s). The initial MTMA concentration remained the same but the initial lithium concentration was cut in half. The bedform velocity was 0.004 cm/min and U_b^* equaled 0.02. Therefore, the turnover exchange was negligible.

The bromide and lithium porewater concentrations were analyzed for samples acquired from all three sampling stations. MTMA porewater concentrations were measured only at Station 2. The concentration profiles at Station 1 are displayed in Figure 5.34, Station 2 in Figure 5.35 and Station 3 in Figure 5.36. In general, the bromide concentration front traveled faster than the lithium front. The penetration depths for lithium and bromide are the same at Station 1; however, the bromide penetration depth is 1 to 2 cm deeper than the penetration depth of lithium at Stations 2 and 3. The observed maximum penetration depths for bromide are 22 cm, 21 cm and 19 cm at Stations 1, 2 and 3, respectively. The calculated equivalent front depth for bromide at the end of the experiment is 19.8 cm, which agrees with the observed porewater concentrations. These calculations show that bromide behaved conservatively in the sediment bed. Since the average

bedform wavelength (14.9 cm) is less than the bromide penetration depth, the bromide transport in the bed was affected by the porewater flows induced by the larger bedforms. The transport of the lithium ions was also affected by the larger bedforms. The observed penetration depth for MTMA at Station 2 is 12 cm.

The experimental results and model predictions for Flume Run 6 are shown in Figure 5.37. The MTMA exchange is over-predicted while the bromide and lithium exchanges are under-predicted. Two factors that contribute to the deviations between the MTMA data and model results are described below. First, the adsorption and pumping time scales are almost the same and adsorption kinetics may be important. If equilibrium is not achieved, the observed adsorption would be less than the adsorption predicted by the equilibrium model. The second possible source of error stems from the change in garnet sand surface properties which is discussed in Section 5.1.3.3. Most of the data points used to derive the MTMA adsorption isotherm used in the model were acquired three months before Flume Run 6. The change in the sand surface properties may have caused a decrease in adsorption. Therefore, the model would over-predict the extent of MTMA adsorption.

Both bromide and lithium are over-predicted because their transport in the bed is affected by bedforms that have longer wavelengths than the average wavelength used in the model. The sensitivity of the model to the bedform wavelength is discussed further in Section 5.2.3 and in Chapter 6, Section 6.5.

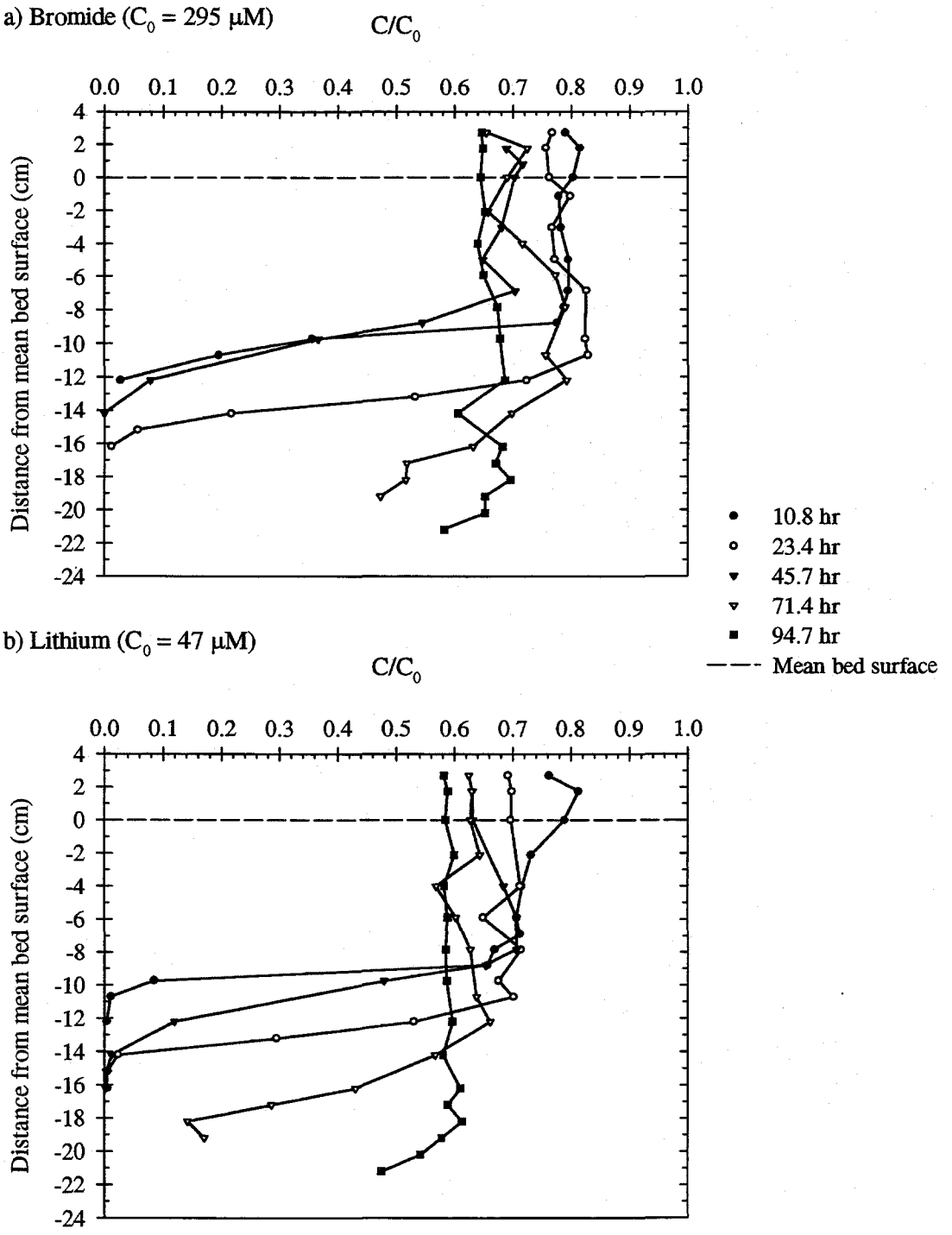

Figure 5.34. Porewater concentration profiles for (a) bromide and (b) lithium at Station 1 in Flume Run 6.

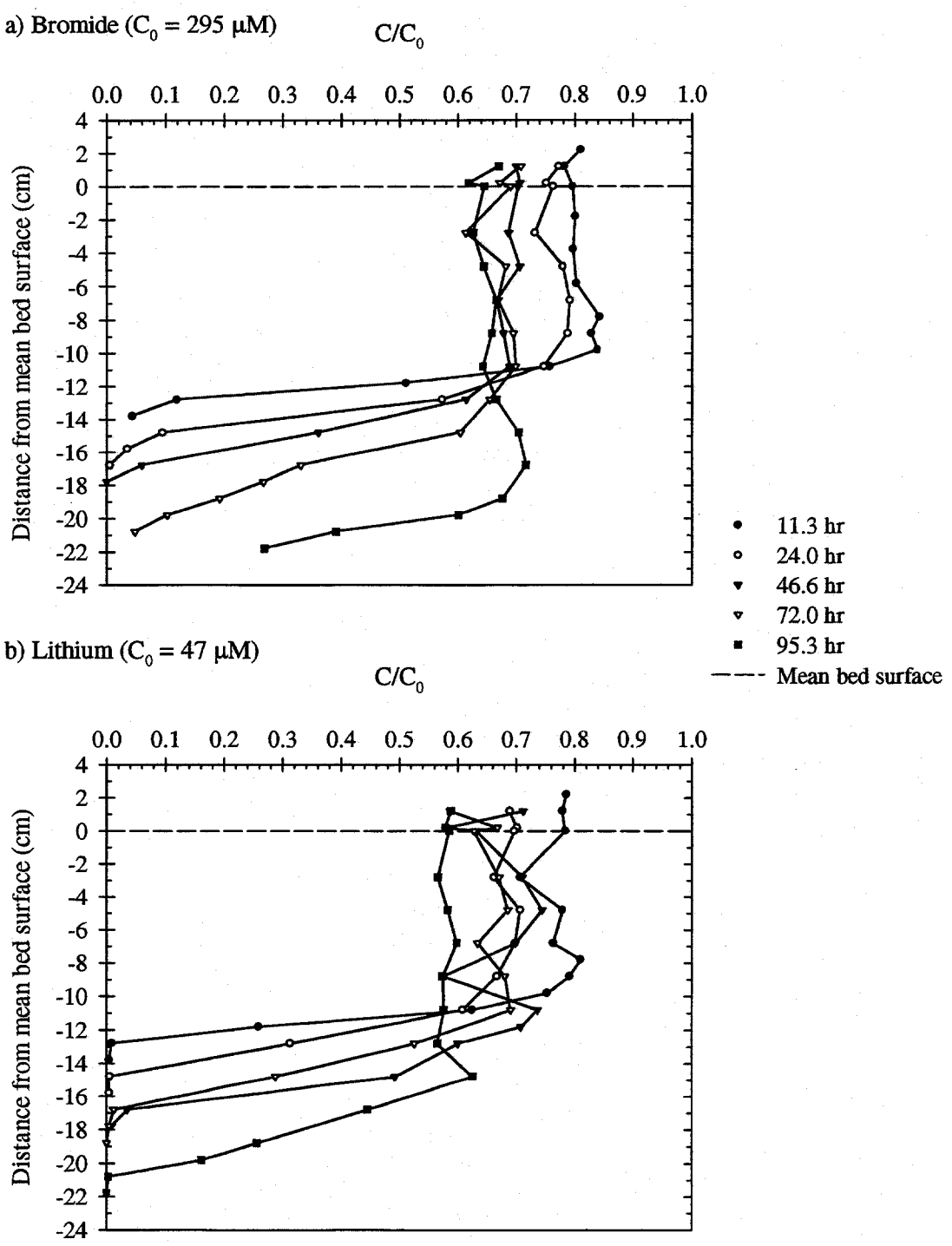

Figure 5.35. (continued on the next page) Porewater concentration profiles for (a) bromide, (b) lithium and (c) MTMA at Station 2 in Flume Run 6.

c) MTMA (C_0 = 295 μM)

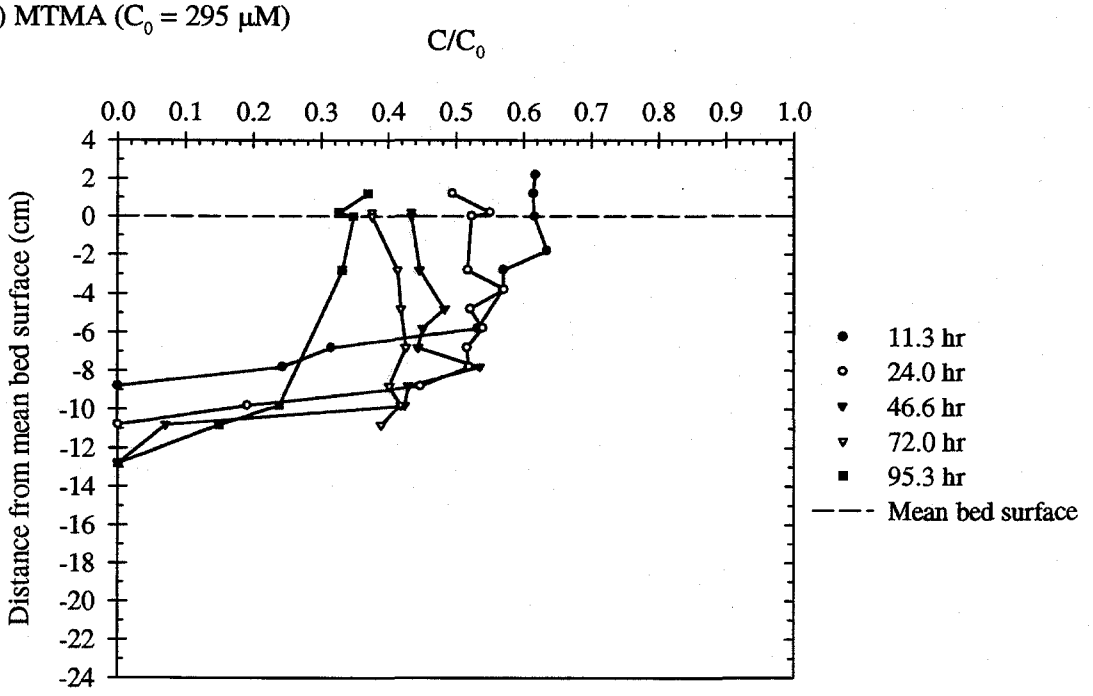

Figure 5.35 (continued) Porewater concentration profiles for (a) bromide, (b) lithium and (c) MTMA at Station 2 in Flume Run 6.

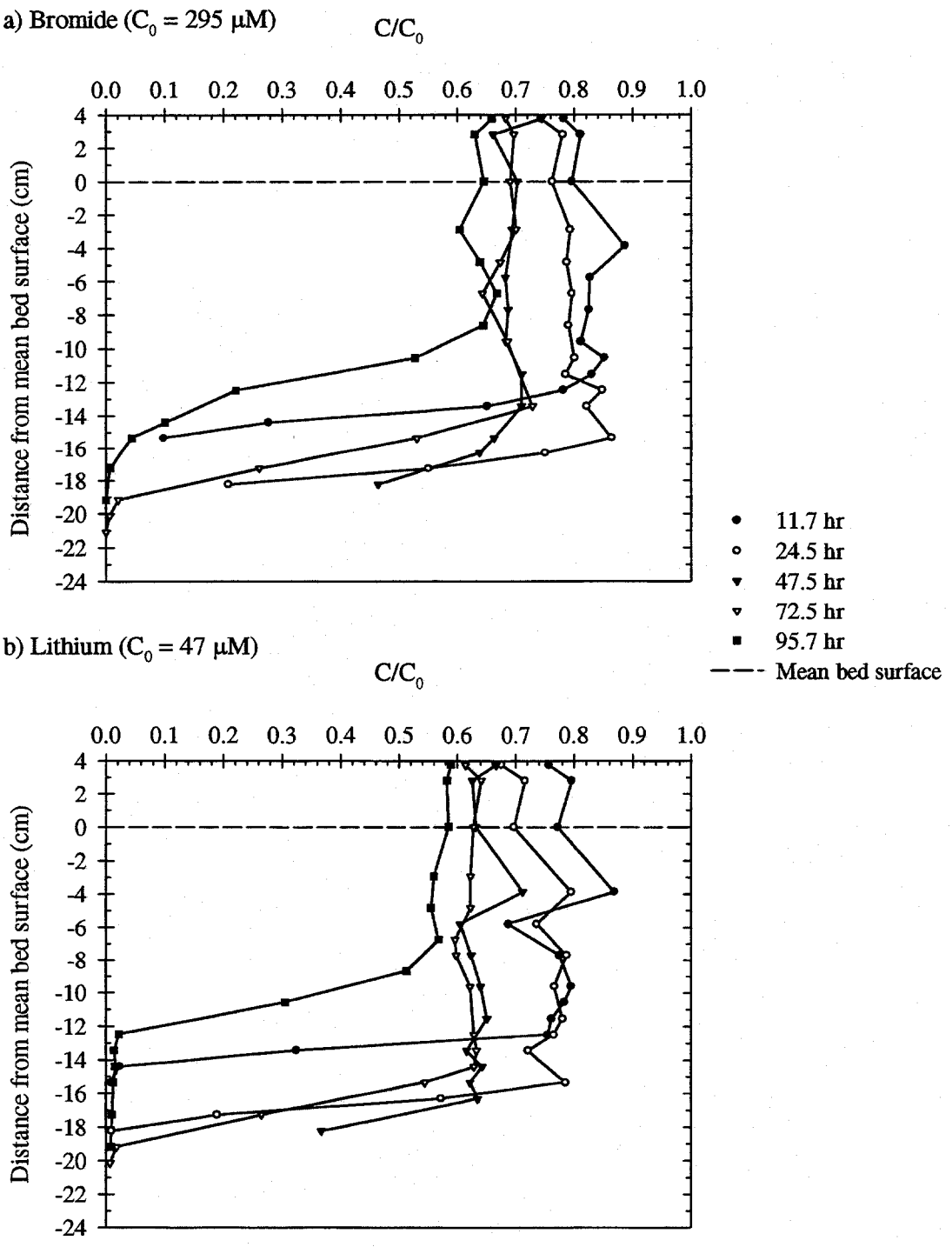

Figure 5.36. Porewater concentration profiles for (a) bromide and (b) lithium at Station 3 in Flume Run 6.

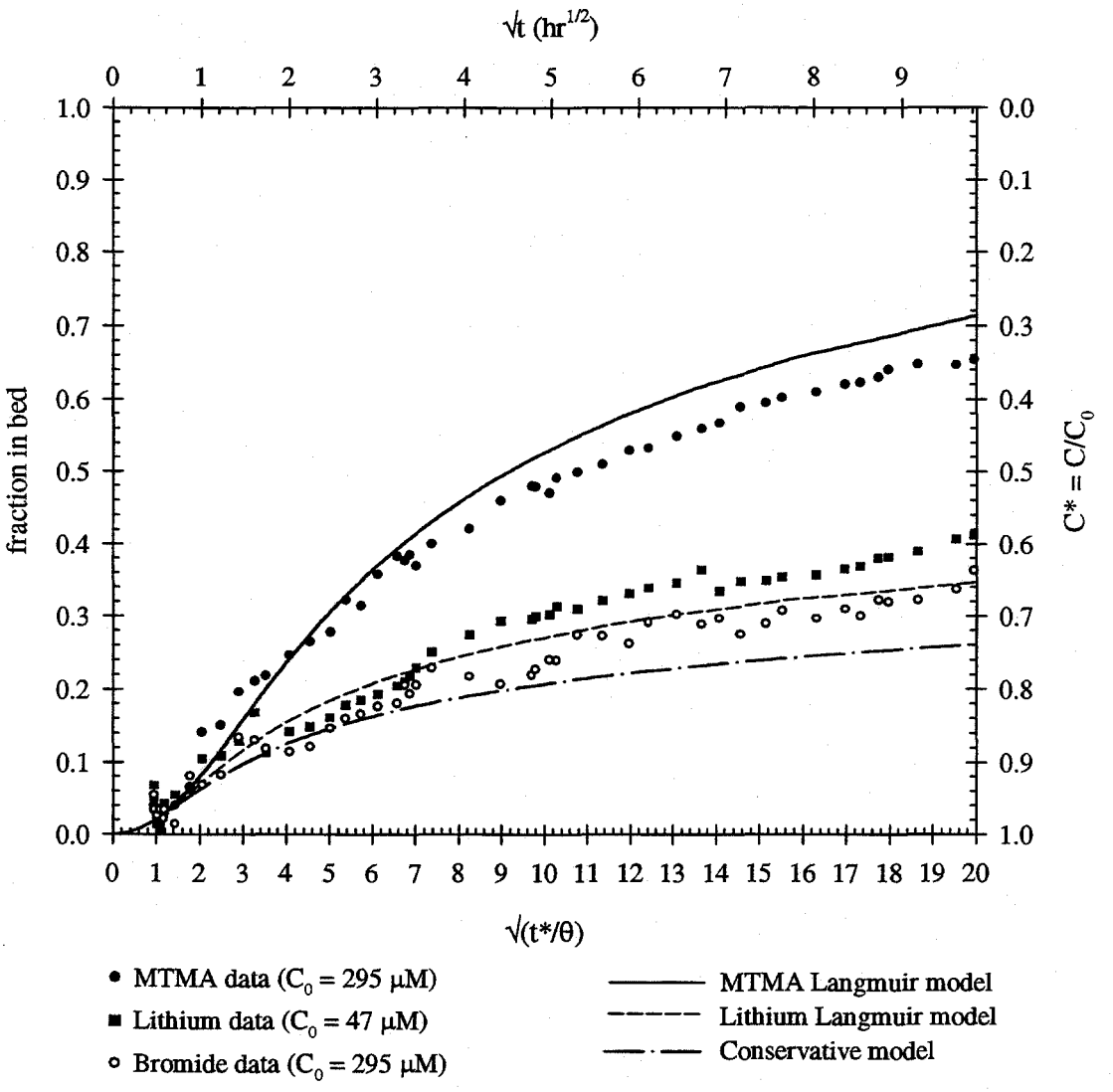

Hydraulic parameters:	d = 9.57 cm	U = 22.0 cm/s
Bed parameters:	$\lambda = 14.9 \pm 4.0$ cm $U_b = 0.004$ cm/min	$H = 1.41 \pm 0.44$ cm
Chemical parameters:	10 mM NaCl 2 mM $NaHCO_3$	$pH_{initial} = 8.1$
Model parameters:	$\alpha_c = 1.00$ $U_b^* = 0.02$	$h_m = 0.050$ cm

Figure 5.37. Comparison of experiment results and model predictions for Flume Run 6. The ± value represents one standard deviation.

5.2.2.7. Flume Run 7

The objective of Flume Run 7 was to study the effect of the initial concentration on the exchange of DTMA. The initial DTMA concentration (96 μM) was half of the initial concentration in Flume Run 2 (182 μM). However, the DTMA adsorption observed in the Run 7 did not agree with isotherm data associated with Run 2. Separate batch adsorption experiments were performed and new adsorption parameters were calculated. The Langmuir adsorption parameters used in the DTMA model for Flume Run 7 are included in Table 5.5.

The porewater concentration profiles for bromide and DTMA at Station 2 are illustrated in Figure 5.38. Porewater samples were not taken at the other sampling stations. The observed bromide penetration depth of about 17 cm is close to the average bedform wavelength of 15.9 cm.

Figure 5.39 compares the experimental data and model predictions for Flume Run 7. Elliott's residence time model (Chapter 3, Section 3.2) agrees with the bromide data. The DTMA exchange is slightly over-predicted during the latter part of the experiment. The maximum difference in C* between the DTMA data and the model is 0.06, which corresponds to only 6 μM. The error in the concentration measurements is approximately 3 μM. The remainder of the deviation may be attributed to the error associated with the adsorption parameters. The sensitivity of the model to the Langmuir sorption coefficients is examined in Chapter 6.

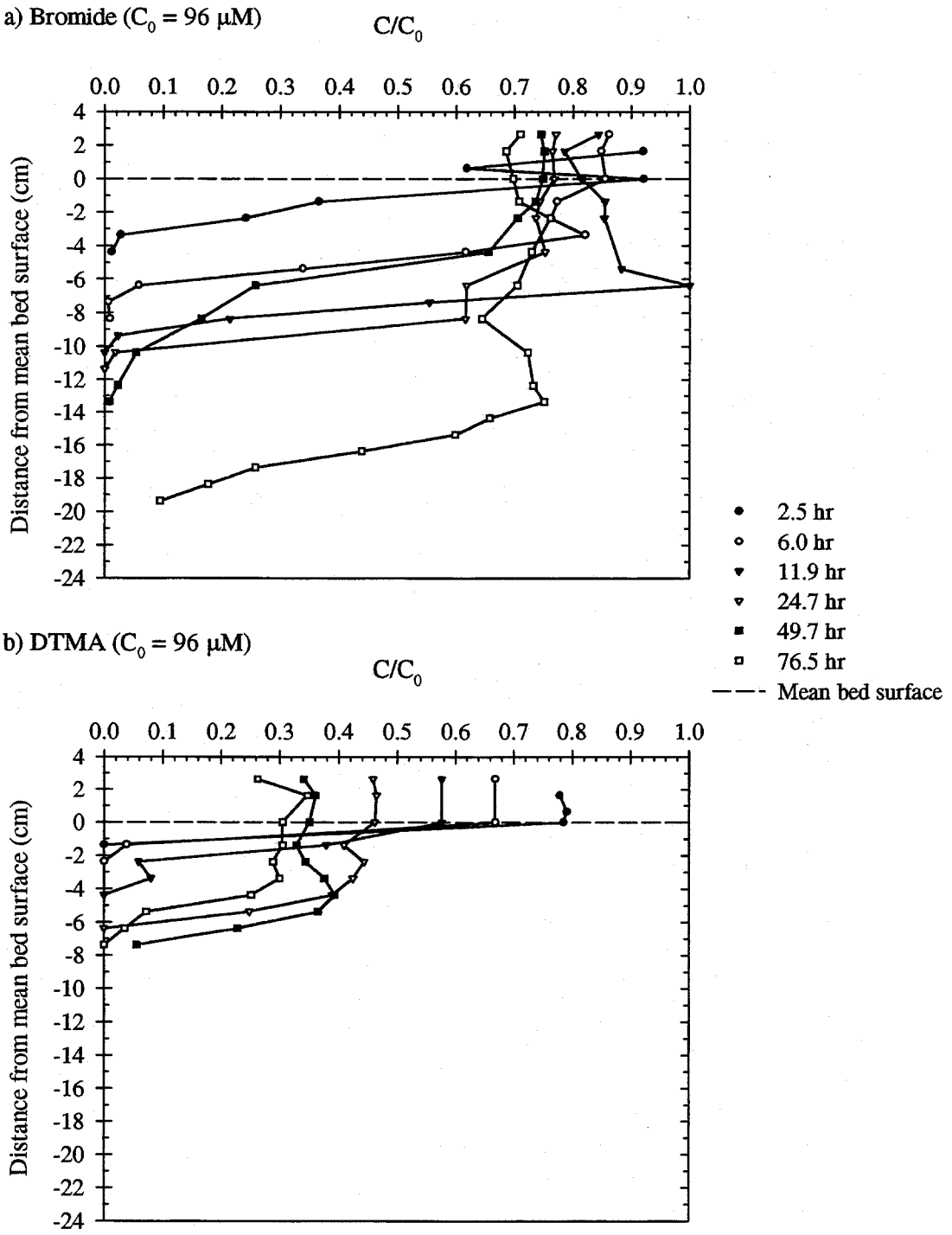

Figure 5.38. Porewater concentration profiles for (a) bromide and (b) DTMA at Station 2 in Flume Run 7.

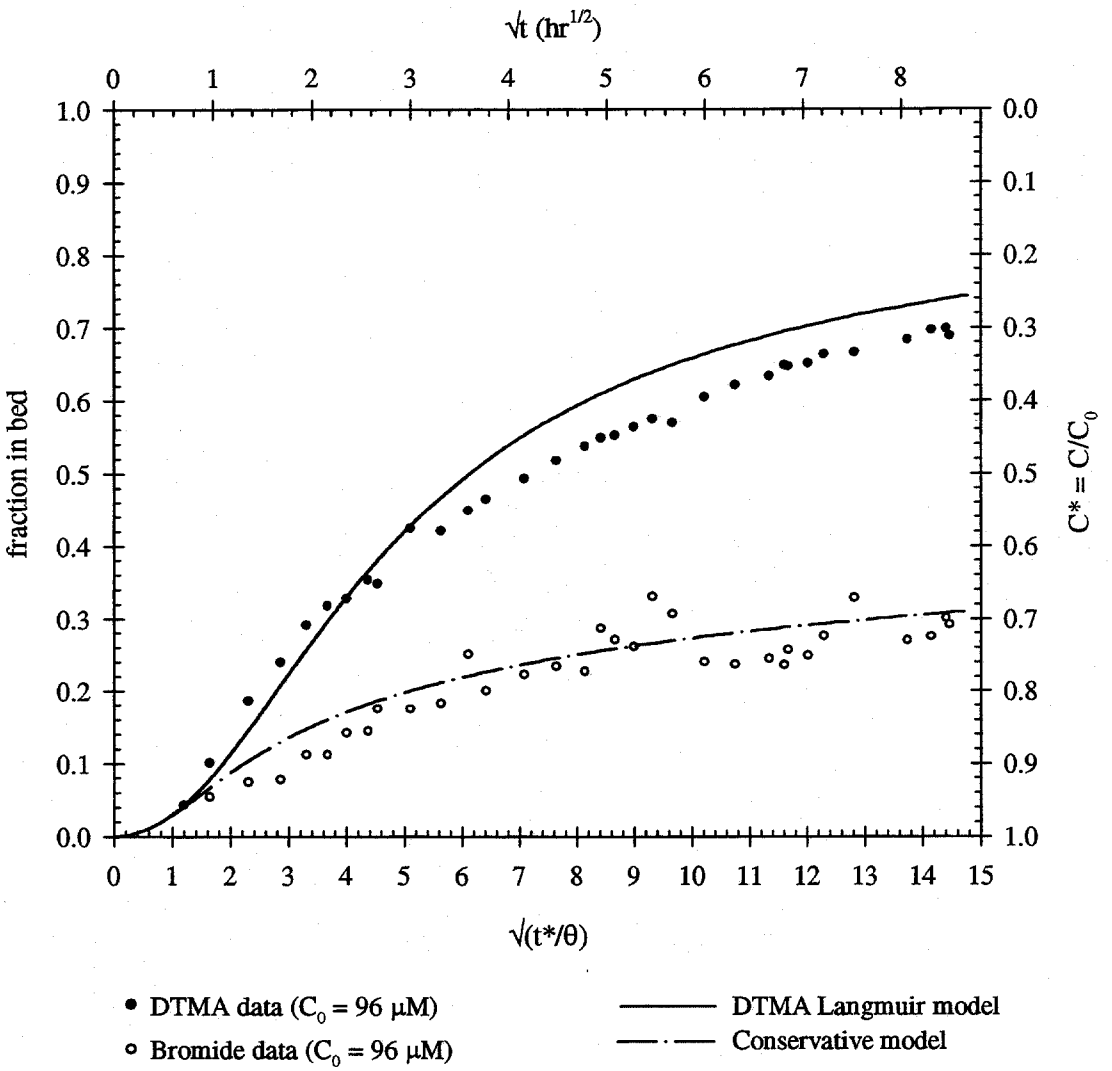

Hydraulic parameters:	d = 6.34 cm	U = 17.6 cm/s
Bed parameters:	$\lambda = 15.9 \pm 3.4$ cm	$H = 1.45 \pm 0.26$ cm
Chemical parameters:	10 mM NaCl 2 mM $NaHCO_3$	$pH_{initial} = 8.3$
Model parameters:	$\alpha_c = 1.00$	$h_m = 0.038$ cm

Figure 5.39. Comparison of experiment results and model predictions for Flume Run 7. The ± value represents one standard deviation.

5.2.2.8. Flume Run 8

The exchange of NTMA, with an initial concentration of 92 μM, was studied in Flume Run 8. The NTMA concentrations in the porewater samples were not analyzed. The porewater sample volume was 1 ml, half of which was used for the bromide analysis. The remaining 0.5 ml available for the NTMA analysis was too small for the Orange 2 dye extraction analysis. The separation of NTMA could not be achieved using capillary electrophoresis. Therefore, the NTMA porewater concentrations were not measured. The NTMA concentrations in the overlying water samples were analyzed by Orange 2 dye extraction.

Figure 5.40 shows the bromide porewater concentration profiles at Station 2. The observed bromide penetration depth at the end of the experiment was 6 cm, whereas the equivalent bromide front concentration depth was 13.6 cm. The concentration profiles vary along the length of the flume. The bromide concentration profile is shallow at Station 2 because the sampling ports are located at a low-pressure zone where the overall flow is up rather than down.

The experimental data and model results for Flume Run 8 are shown in Figure 5.41. The conservative model agrees with the bromide data, which indicates that the concentration profiles in Figure 5.40 are not representative. The difference between the NTMA data and model simulation is large. The Langmuir adsorption coefficients used in the model are listed in Table 5.8. Since the adsorption of NTMA on garnet sand is small, the error associated with the adsorption data is large (see Appendix B). The deviation between the NTMA data and model can be attributed to the uncertainty in the sorption parameters and errors in the concentration measurements. A sensitivity analysis of the NTMA model to the sorption coefficients is presented in Chapter 6, Section 6.8.4.

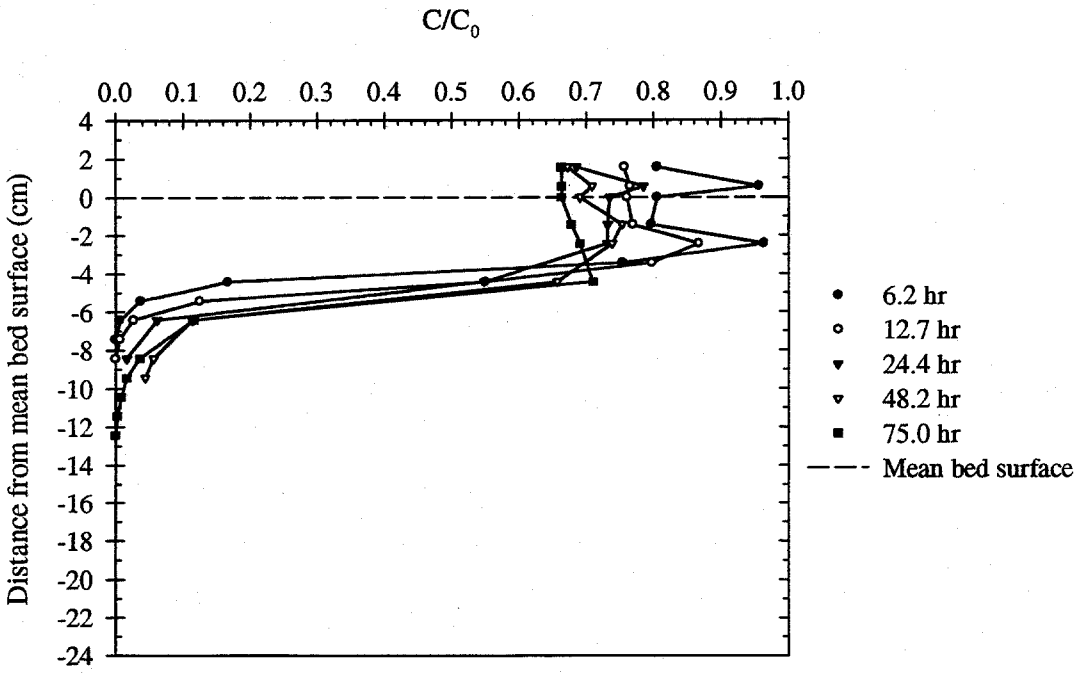

Figure 5.40. Porewater concentration profiles for bromide at Station 2 in Flume Run 8.

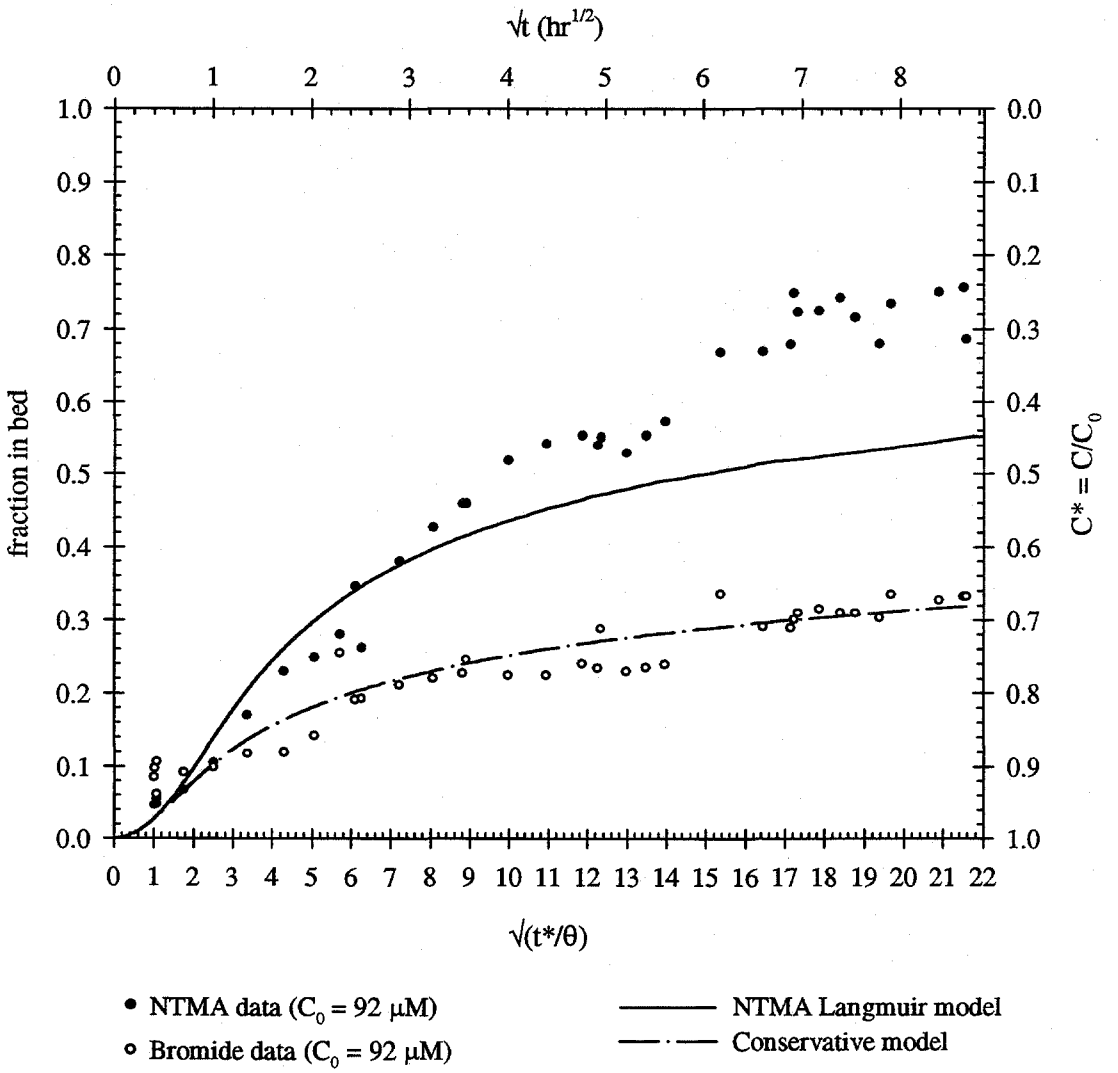

Hydraulic parameters:	d = 6.37 cm	U = 16.8 cm/s
Bed parameters:	$\lambda = 14.3 \pm 6.7$ cm	$H = 1.07 \pm 0.33$ cm
Chemical parameters:	10 mM NaCl 2 mM $NaHCO_3$	$pH_{initial} = 8.1$
Model parameters:	$\alpha_c = 2.25$	$h_m = 0.031$ cm

Figure 5.41. Comparison of experiment results and model predictions for Flume Run 8. The ± value represents one standard deviation.

5.2.2.9. Flume Run 9

The exchange of OTMA was studied in Flume Run 9. The purpose of the experiment was to compare the exchange of OTMA with the exchange of the shorter chain compounds DTMA and MTMA, under hydraulic and chemical conditions similar to the corresponding Runs 2 and 3.

Bromide porewater concentration profiles at Stations 1 and 2 are displayed in Figure 5.42. These profiles illustrate how highly variable the concentration profiles can be along the length of the flume. At the end of the experiment, the bromide penetration depths at Stations 1 and 2 are 15 and 5 cm, respectively. The OTMA concentrations in the porewater samples were too small to be detected by capillary electrophoresis.

Figure 5.43 shows the experimental results and model simulations for OTMA and bromide in Flume Run 9. Both models agree well with the data. The effect of the hydrocarbon chain length on the exchange of the different surfactants is discussed in Chapter 6, Section 6.7.

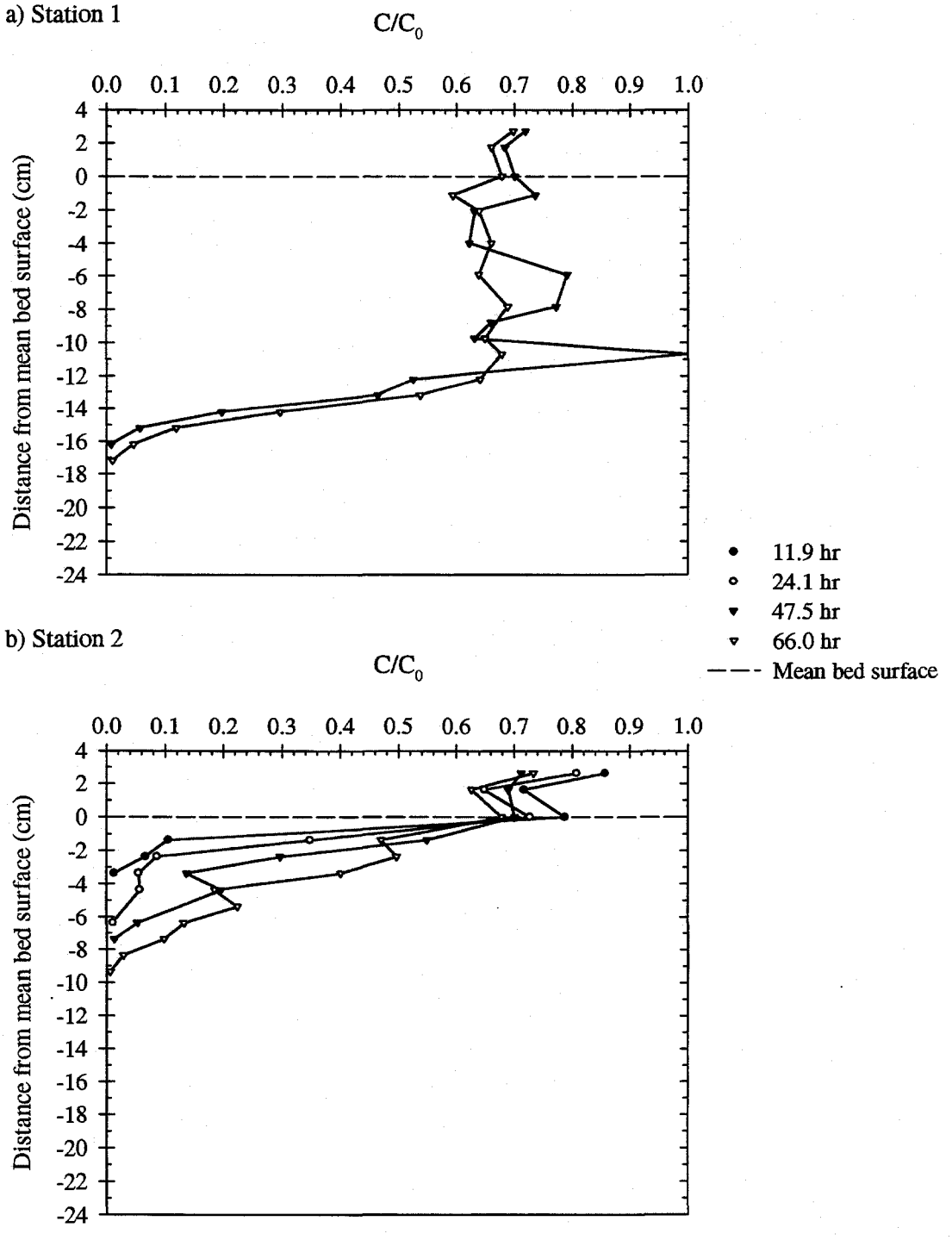

Figure 5.42. Porewater concentration profiles for bromide at Stations 1 and 2 for Flume Run 9.

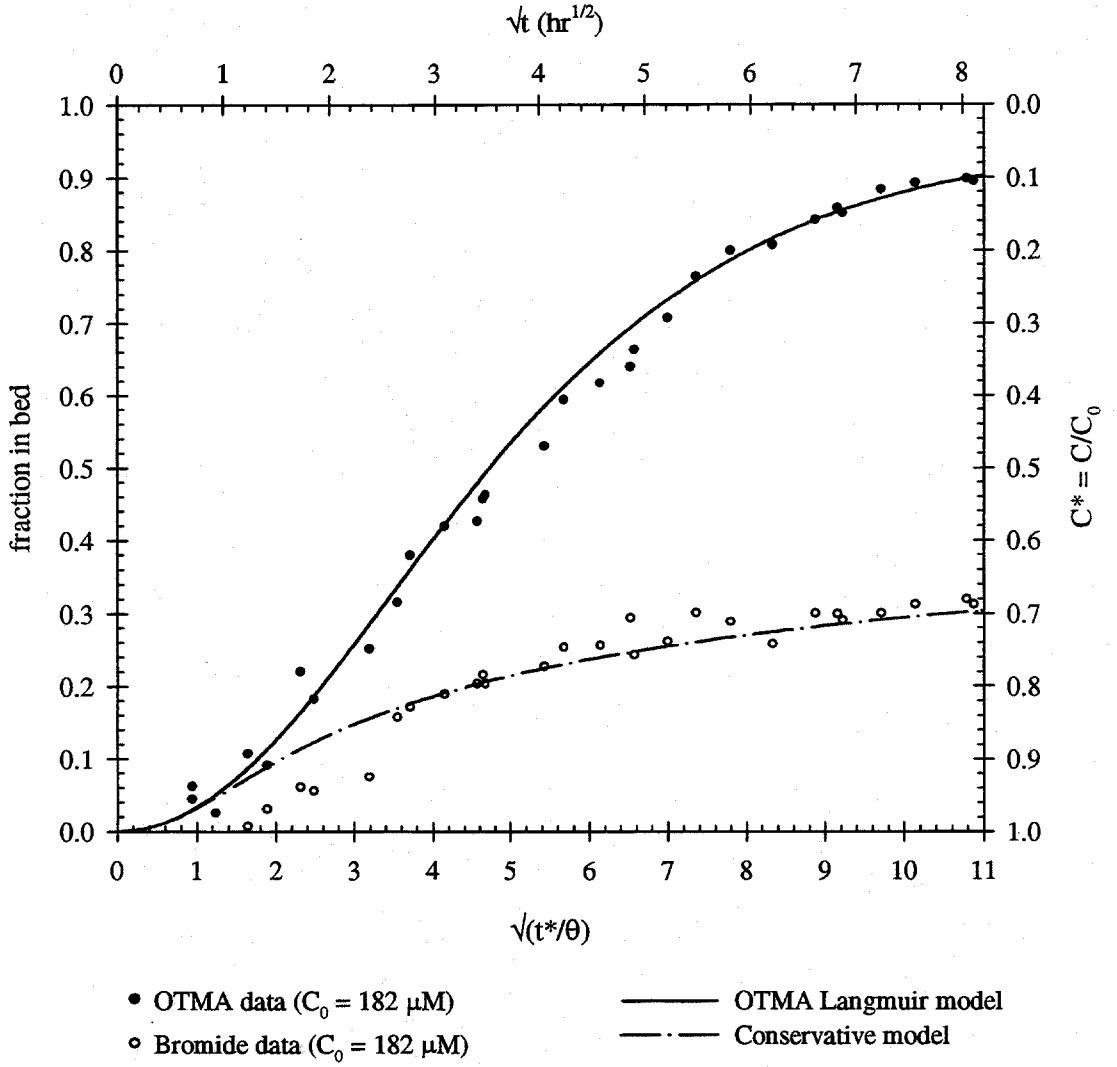

Hydraulic parameters:	d = 6.52 cm	U = 16.0 cm/s
Bed parameters:	$\lambda = 17.9 \pm 6.4$ cm	$H = 1.19 \pm 0.34$ cm
Chemical parameters:	10 mM NaCl 2 mM $NaHCO_3$	$pH_{initial} = 8.3$
Model parameters:	$\alpha_c = 1.08$	$h_m = 0.029$ cm

Figure 5.43. Comparison of experiment results and model predictions for Flume Run 9. The ± value represents one standard deviation.

5.2.2.10. Flume Run 10

In Flume Run 10, the exchange of bromide and DTMA with a flat bed was observed under conditions similar to Flume Run 2 in all of the hydraulic and chemical parameters but not in the bed geometry. The initial concentration was 179 μM for both compounds. The bromide concentration profiles at Station 2 are shown in Figure 5.44. The penetration depth of Bromide after 53 hours is only 4 cm whereas the penetration depth of lithium in Flume Run 2 after the same time is about 16 cm (Figure 5.24a). The DTMA concentrations in the porewater samples were not detectable.

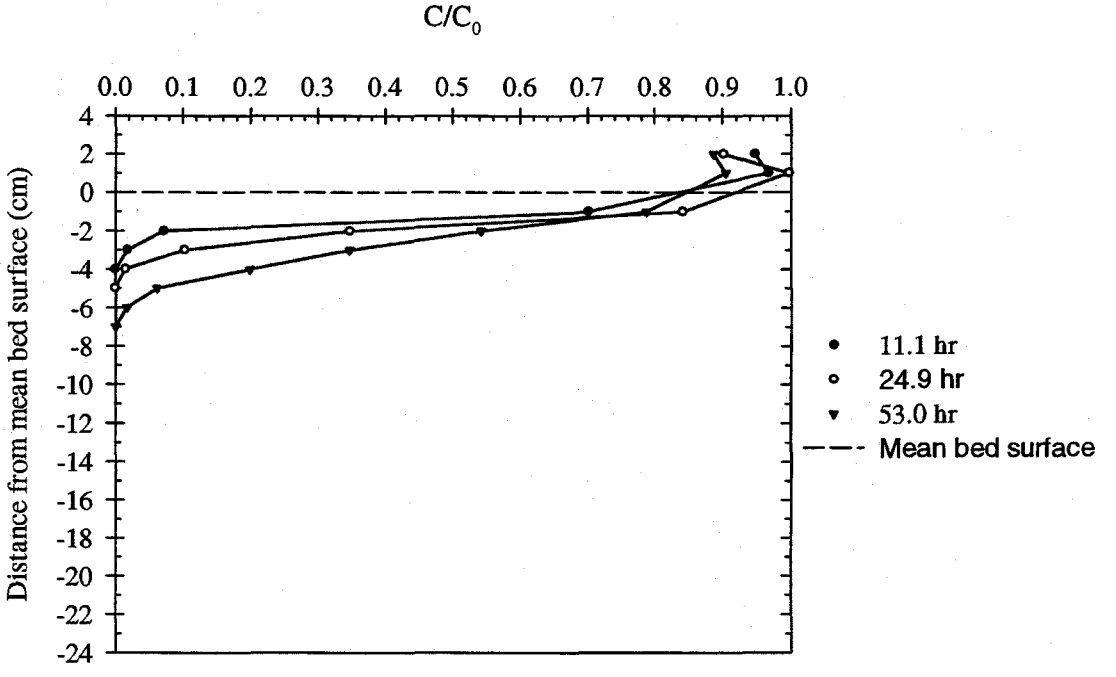

Figure 5.44. Porewater concentration profiles for bromide at Station 2 in Flume Run 10.

Figure 5.45 compares the exchange of bromide and DTMA with a flat bed. Only 10 percent of the bromide and 20 percent of the DTMA was transferred to the bed. The bromide exchange can be modeled as a diffusion process. The details of the model are presented in

Chapter 6, Section 6.1. The exchange with the flat bed is compared to the exchange with a rippled bed in Chapter 6, Section 6.1.

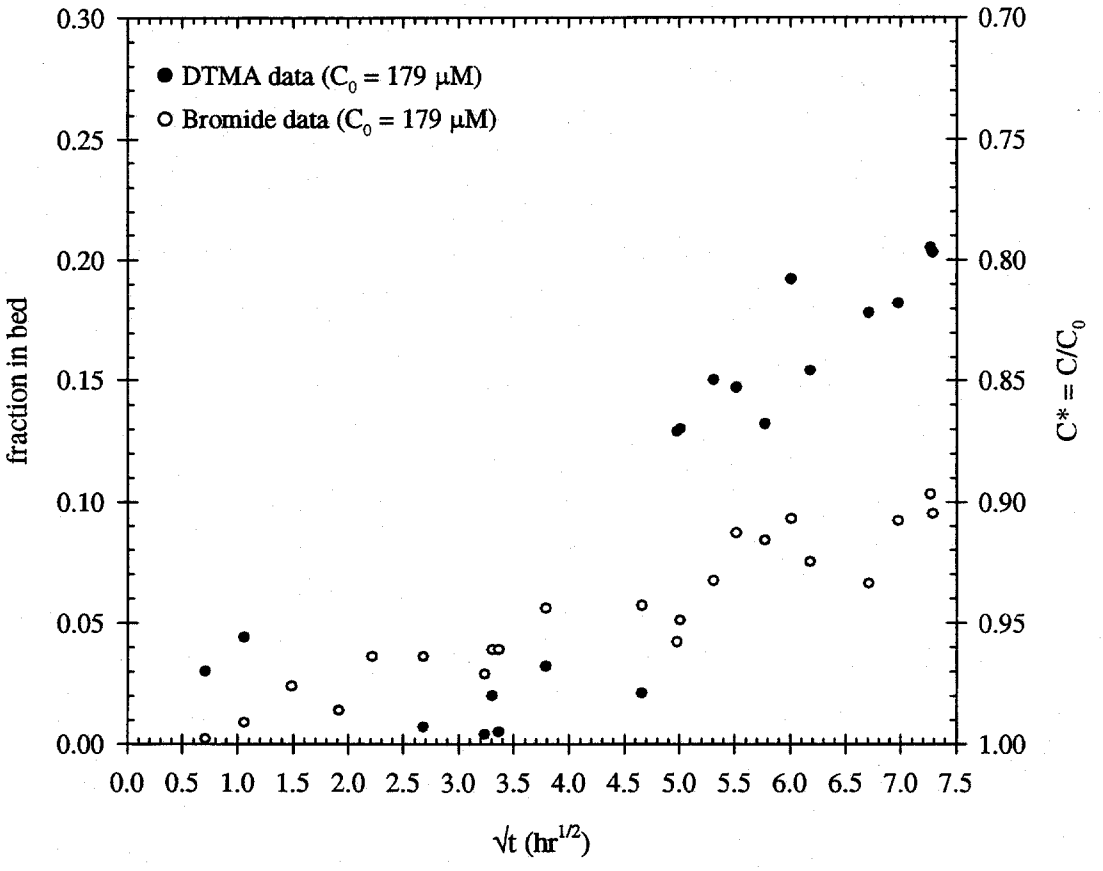

Figure 5.45. Transport of DTMA and bromide into flat bed in Flume Run 10.

The bed/stream exchange observations from Flume Run 10 suggest that with a flat bed, the mass exchange of adsorbing compounds is greater than nonsorbing compounds. This is in contrast with Eylers' (1994) observation that the mass exchange of lithium and calcium (R = 3) with a flat quartz sand bed was the same. The effective retardation coefficient for DTMA is 3.5 (using the Langmuir isotherm from the experiments conducted in April 1998, see Table 5.5). The difference in the results cannot be attributed to different sorption affinities because the retardation

coefficients association with calcium and DTMA are not significantly different. Further flume experiments with a flat bed are required to explain the different results.

5.2.3. General observations and discussion

With the exception of Flume Runs 5 and 8, the bed exchange model simulations for the surfactants agreed very well with the observed mass transfer. The deviation between the model and flume data for Run 4 is due to turnover caused by the moving bedforms. The possible errors in the NTMA adsorption parameters that result from the scatter in the adsorption data may contribute to the difference between the model and observations in Flume Run 8. The sensitivity of the model to the errors in the sorption parameters is examined in Chapter 6, Section 6.8. The success of the model indicates that the partitioning of nonlinearly adsorbing compounds in large flume experiment can be predicted by characterizing the adsorption at the batch scale.

The exchange models for the nonsorbing and weakly adsorbing compounds tend to under-predict the mass transfer for long times ($t^*/\theta > 100$). The bedforms in the flume were irregular and exhibited a distribution of heights and wavelengths with large standard deviations (see Table 5.10). Elliott's dye studies showed that the variability of the bed surface was reflected in the front patterns for nonsorbing compounds (see Figure 2.3 in Chapter 2). Initially, the fronts reflect the smaller bedforms because the porewater velocity is higher for short wavelengths ($u_m \propto 1/\lambda$). As time progressed, the smaller front patterns merged into larger deeper fronts that reflected the longer bedforms, which can induce flow deeper into the bed. Elliott (1997b, page 146) found that this phenomenon could result in a 30 percent increase in the mass exchange.

6. DISCUSSION AND SENSITIVITY ANALYSIS

This chapter contains a discussion of the general results and implications for the stream/bed exchange of nonsorbing and nonlinearly adsorbing compounds. First, Section 6.1 presents a comparison of the mass transfer into a bed covered with bedforms and into a flat bed. Errors that are generated from the linear adsorption assumption are examined in Section 6.2. Because of the large number of variables in the exchange model and the long time required for each flume experiment (13-20 days including preparation and analysis time), it was not possible to conduct flume experiments that spanned the entire range of variables for all of the compounds studied. Therefore, sensitivity analyses are performed using model simulations. The sensitivity of the model to hydraulic, bed and chemical parameters is studied in Sections 6.3 through 6.9. The relative importance of these parameters is summarized in Chapter 7. In Sections 6.10 and 6.11, the applicability the approximate models, which are developed in Chapter 3, Sections 3.5 and 3.6, to the bed/stream exchange of the surfactants in the flume experiments is discussed. The applications of the detailed and approximate exchange models for nonlinearly adsorbing compounds are described with examples in Section 6.12.

6.1. EXCHANGE WITH A FLAT BED

The mass exchange of DTMA in Flume Runs 2 and 10 is compared in Figure 6.1a. These flume runs have similar hydraulic and chemical conditions except the bed surface contains bedforms in Run 2 but is flat in Run 10. After 50 hours, 73 percent of DTMA is transported into the rippled bed and only 20 percent into the flat bed. Figure 6.1b compares the mass exchange of a hypothetical conservative tracer into a rippled bed (modeled using the parameters of Flume Run

2) and the measured mass exchange of bromide with the flat bed in Run 10. After 50 hours, 28 percent of the conservative tracer is transferred into the rippled bed while only 10 percent of the bromide is transported into the flat bed. These comparisons of the mass transfer in Runs 2 and 10 show that the mass exchange of both nonsorbing and adsorbing compounds is significantly greater with a rippled bed than a flat bed.

The amount of bromide contained in the bed increases linearly with the square root of time. Therefore, the bromide exchange into the flat bed can be modeled, over the time of the experiment, as a diffusion process with an effective diffusion coefficient which is constant with depth (Elliott, 1990). The effective diffusion coefficient is estimated using the equivalent penetration depth d_q, defined by Equation (6.1), at the end of the flume experiment.

$$d_q = \frac{d'}{\theta}\left(\frac{1-C^*}{C^*}\right) \tag{6.1}$$

The effective penetration depth of bromide at the end of Flume Run 10 is about 3.1 cm. Then the effective diffusion coefficient D is approximately

$$D = \frac{\pi}{4}\frac{(3\text{ cm})^2}{53\text{ hr}} = 0.14\text{ cm}^2/\text{hr} = 4.0\times10^{-5}\text{ cm}^2/\text{s}$$

The effective diffusion coefficient for the bromide exchange is only four times the estimated molecular diffusion coefficient of 10^{-5} cm^2/s. The effective diffusion coefficients for the dye used in Elliott's flat bed experiments range from 1.5×10^{-5} cm^2/s to 5.4×10^{-5} cm^2/s, which are at least an order of magnitude larger than the dye's molecular diffusion coefficient ($\sim10^{-6}$). The transport that occurrs in excess of molecular diffusion may result from dispersion due to small porewater flows induced by turbulent pressure fluctuations on the bed surface or small variations in the temporally-averaged pressure distribution from slight irregularities and bumps on the bed and on the flume walls.

a) DTMA comparison

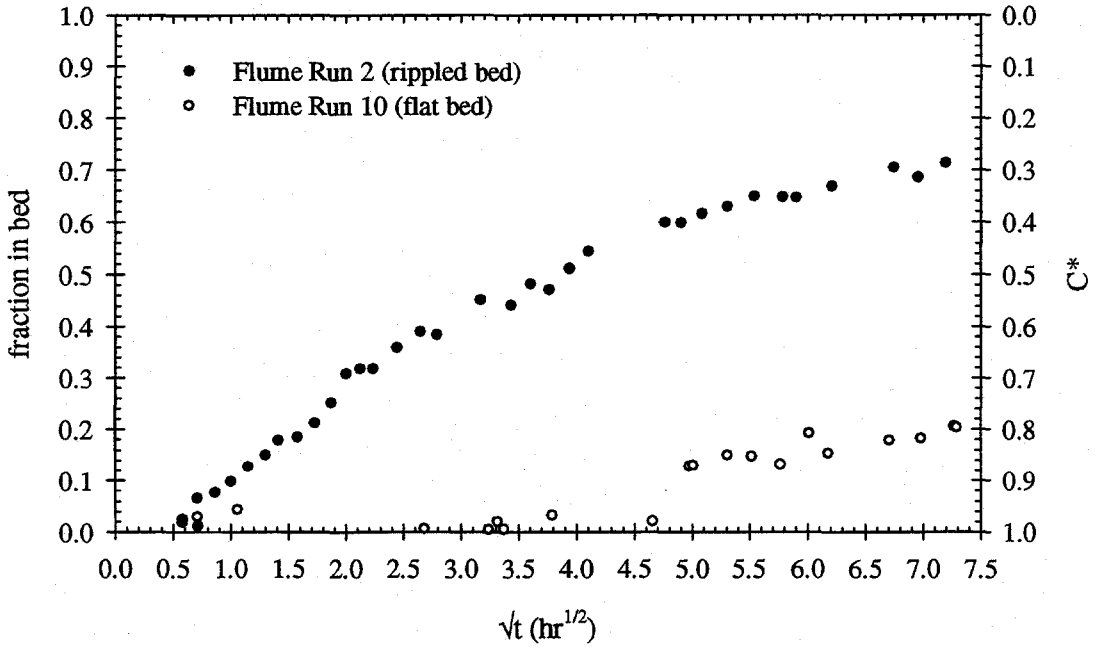

b) Bromide comparison

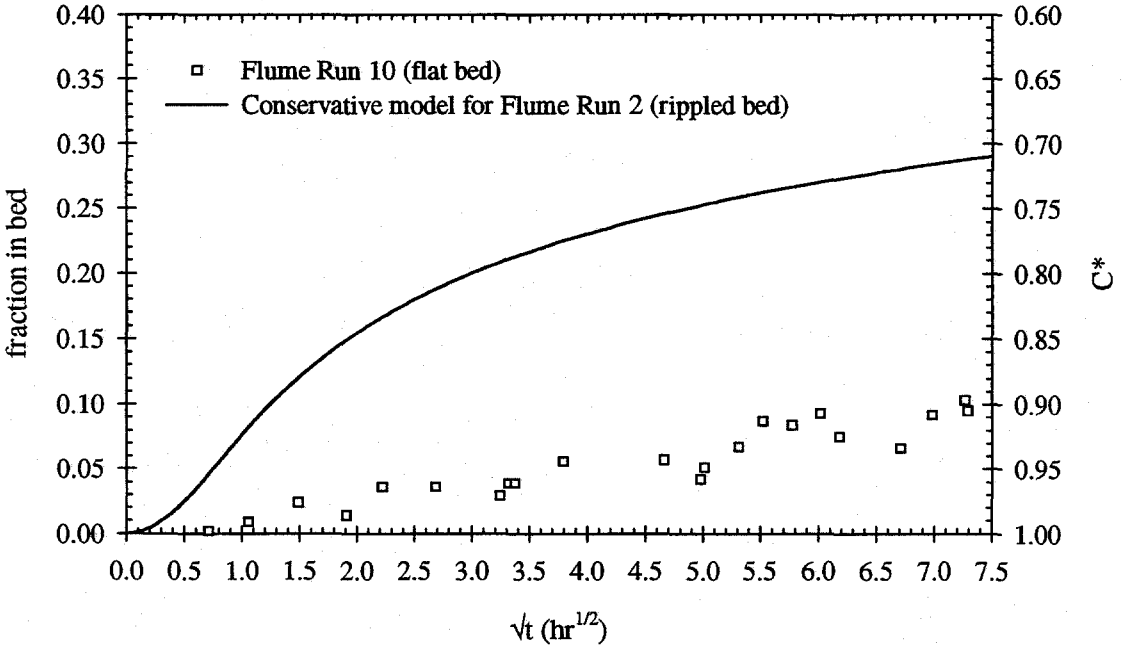

Figure 6.1. Comparison of the mass exchange of (a) DTMA and (b) bromide (different scale) with a flat bed (Flume Run 10) and a rippled bed (Flume Run 2).

6.2. COMPARISON TO BED EXCHANGE WITH LINEAR ADSORPTION

In many field applications, linear adsorption reactions are often assumed because they are easily incorporated into larger transport models. The error resulting from the linear adsorption assumption for the bed/stream exchange of nonlinearly adsorbing compounds in the flume is examined in this section. The mass exchange predictions from Eylers' model (Chapter 3, Section 3.3), which assumes linear adsorption, are compared to the exchange data for lithium, DTMA, MTMA and OTMA from flume experiments presented in Chapter 5. The two retardation coefficients used in the linear adsorption models for the surfactants are the effective retardation coefficients R_{eff} calculated using the initial and final concentrations, yielding minimum and maximum values of R_{eff}, respectively. The effective retardation coefficients are calculated by

$$R_{eff}(C) = 1 + \frac{\rho_b}{\theta}\frac{S_T K_L}{1 + K_L C} \tag{6.2}$$

where ρ_b is the bulk density of the sediment bed, θ is the porosity and S_T and K_L are the Langmuir sorption parameters.

The data and model comparisons illustrate that the assumption of linear adsorption can lead to significant errors in the predicted mass exchange of nonlinearly adsorbing compounds in the flume, even when the adsorption is weak (i.e., lithium on garnet sand). The linear adsorption model is valid for (1) small time when $t^*/\theta < R_{eff}(C_0)$ and (2) large time when the changes in the aqueous concentration in the overlying water column are small and the aqueous concentration of the compound approaches C_{final}. Eylers' linear adsorption model can be used to estimate the upper and lower bounds of the mass exchange of nonlinearly adsorbing compounds in the flume.

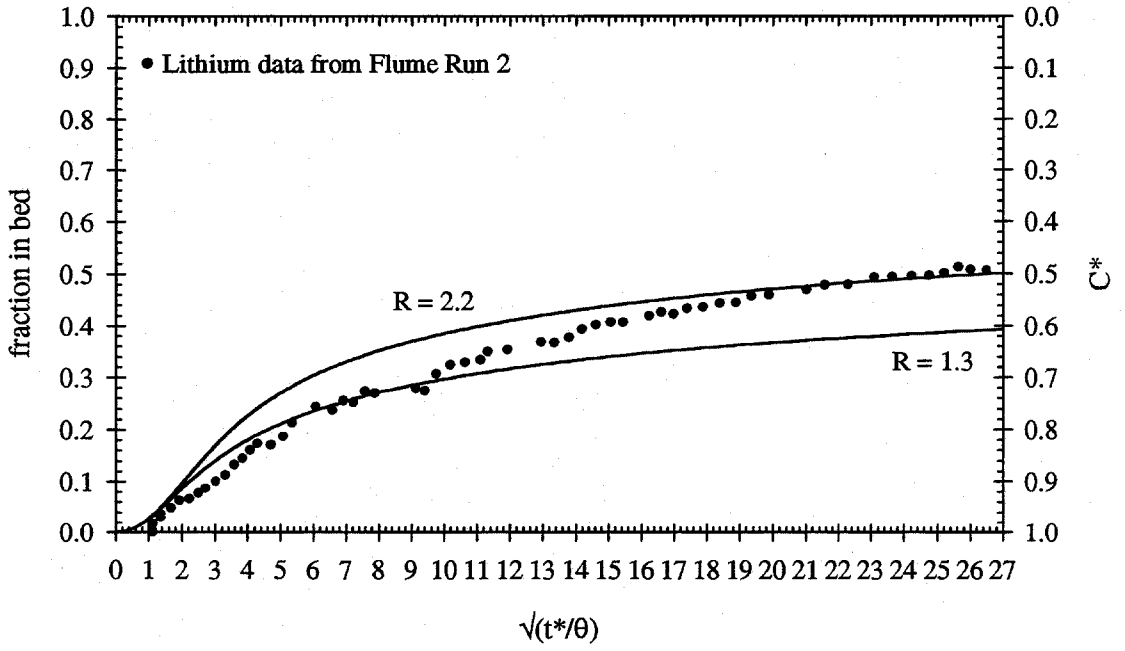

Figure 6.2. Comparison of Eylers' bed/stream exchange model for linearly adsorbing compounds with lithium data from Flume Run 2 (C_0 = 90 μM).

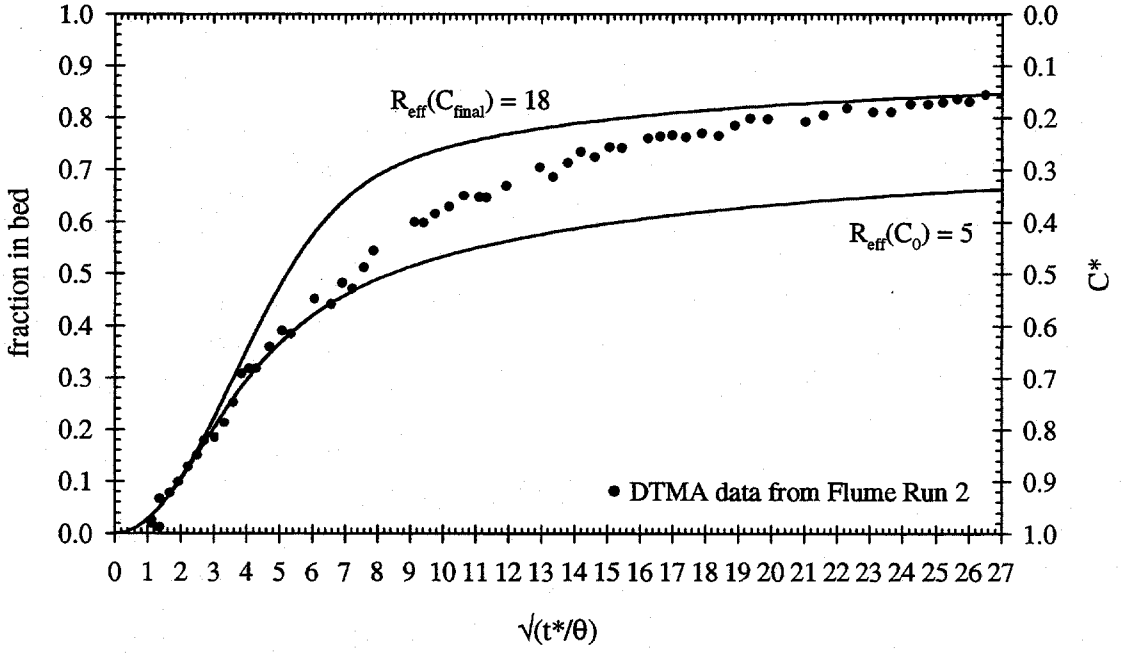

Figure 6.3. Comparison of Eylers' bed/stream exchange model for linearly adsorbing compounds with DTMA data from Flume Run 2 (C_0 = 182 μM).

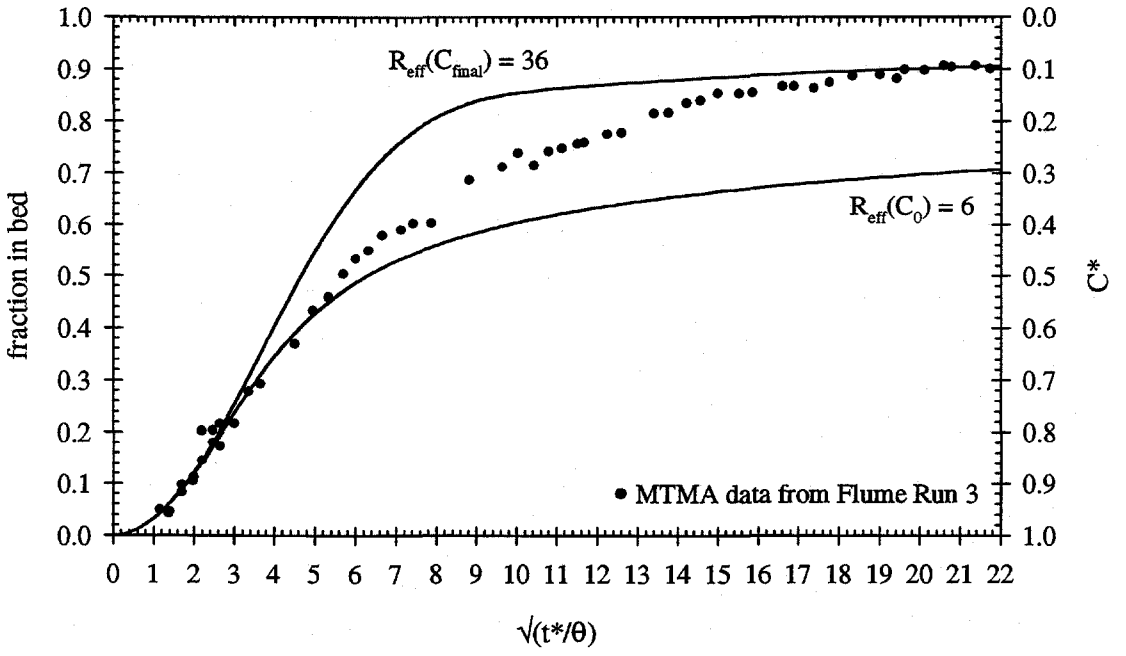

Figure 6.4. Comparison of Eylers' bed/stream exchange model for linearly adsorbing compounds with MTMA data from Flume Run 3 (C_0 = 196 μM).

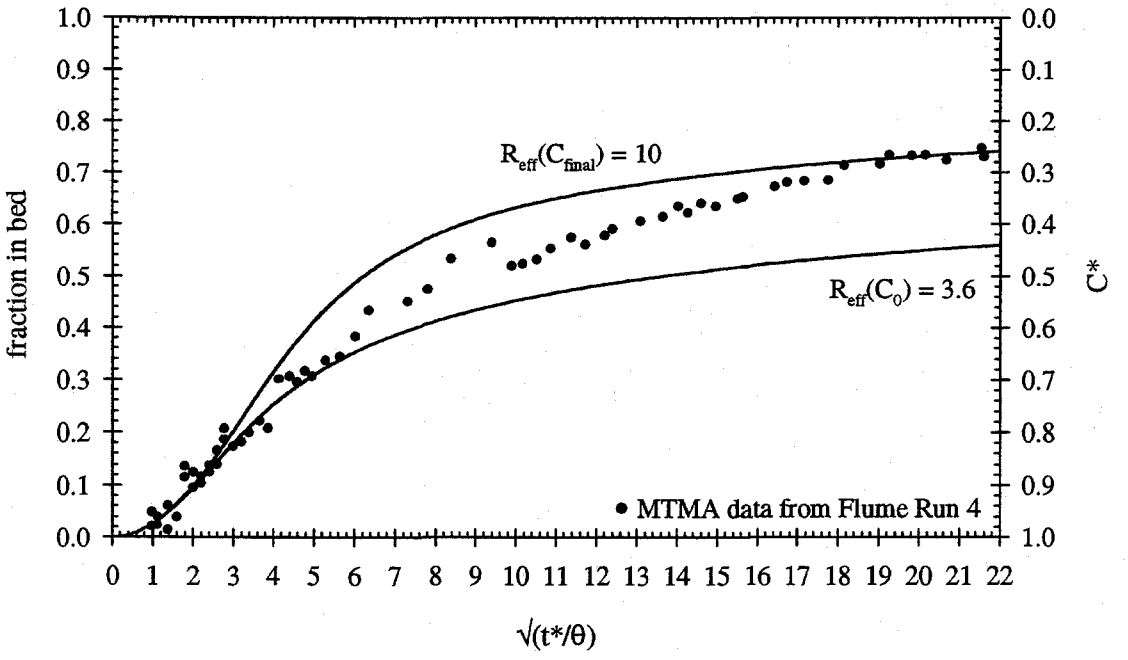

Figure 6.5. Comparison of Eylers' bed/stream exchange model for linearly adsorbing compounds with MTMA data from Flume Run 4 (C_0 = 395 μM).

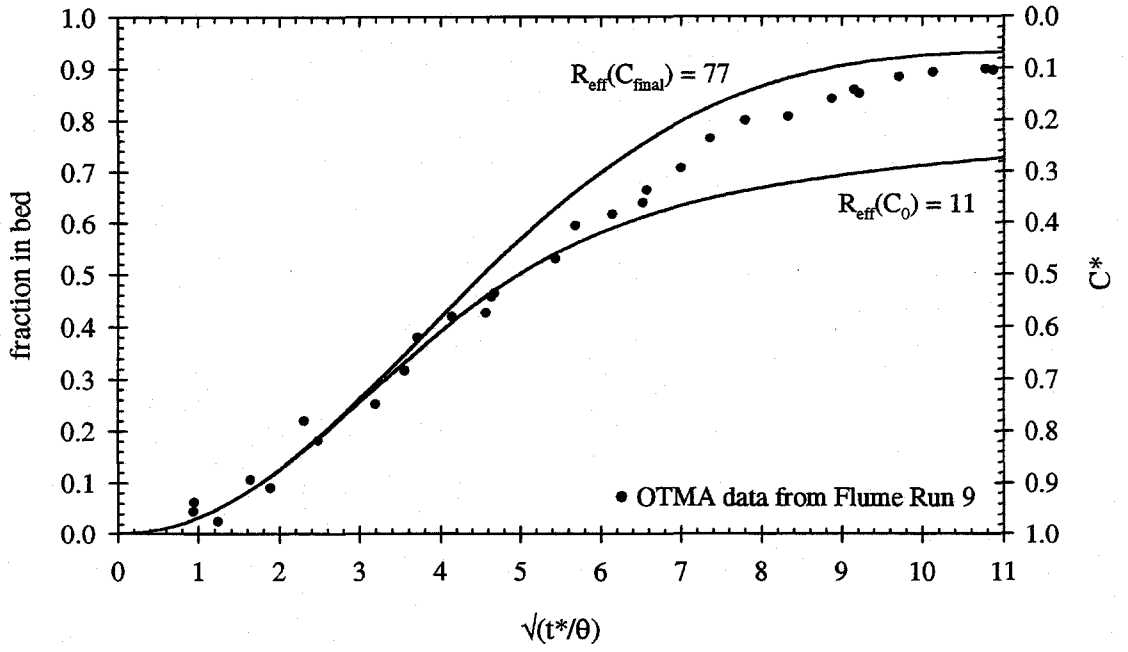

Figure 6.6. Comparison of Eylers' bed/stream exchange model for linearly adsorbing compounds with OTMA data from Flume Run 9 (C_0 = 182 μM).

6.3. SENSITIVITY TO AMPLITUDE OF PRESSURE VARIATIONS

The amplitude of the piezometric head variation (h_m) over the bedforms is the only physical parameter that is not directly measured in the flume. Consequently, in some experiments, h_m is calibrated using the mass exchange data from the flume experiments (see Chapter 5, Section 5.2.1.4 for more details). In this section, the sensitivity of the mass exchange predictions to changes in the value of h_m is evaluated for nonsorbing, linearly adsorbing and nonlinearly adsorbing compounds. The base case for the sensitivity analysis is Flume Run 2 (see Chapter 5, Tables 5.9 through 5.12) where h_m is the calibrated parameter ($h_{m,c} = \alpha_c h_m$).

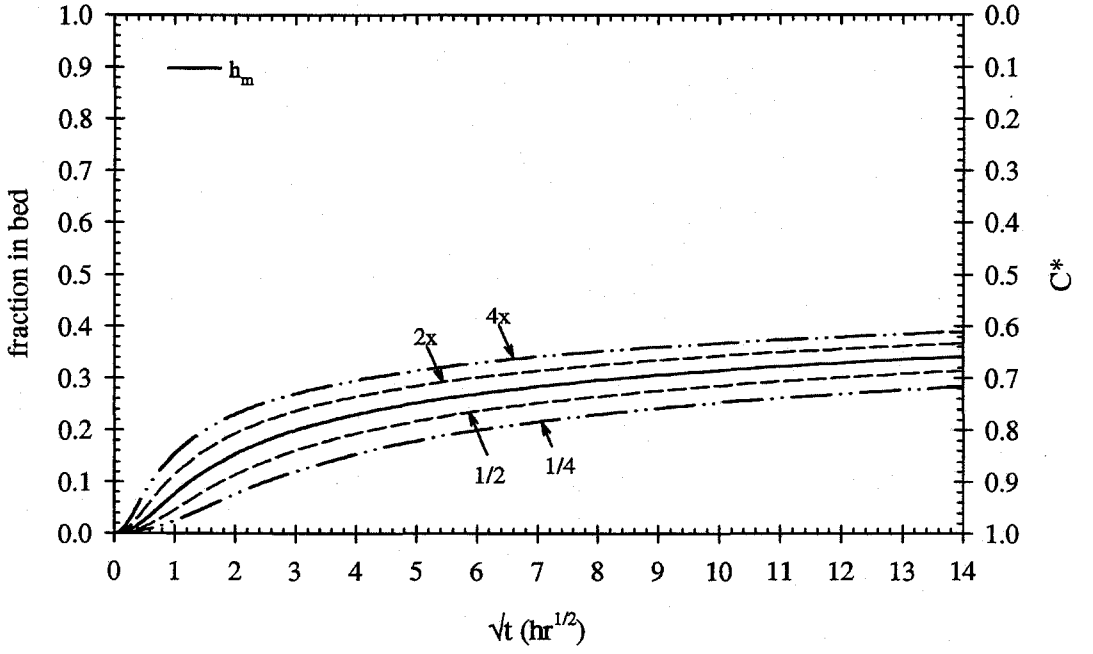

Figure 6.7. Sensitivity of the mass exchange of a nonsorbing compound to changes in the amplitude of the pressure variations over the bedforms. Flume Run 2 is used as the base case.

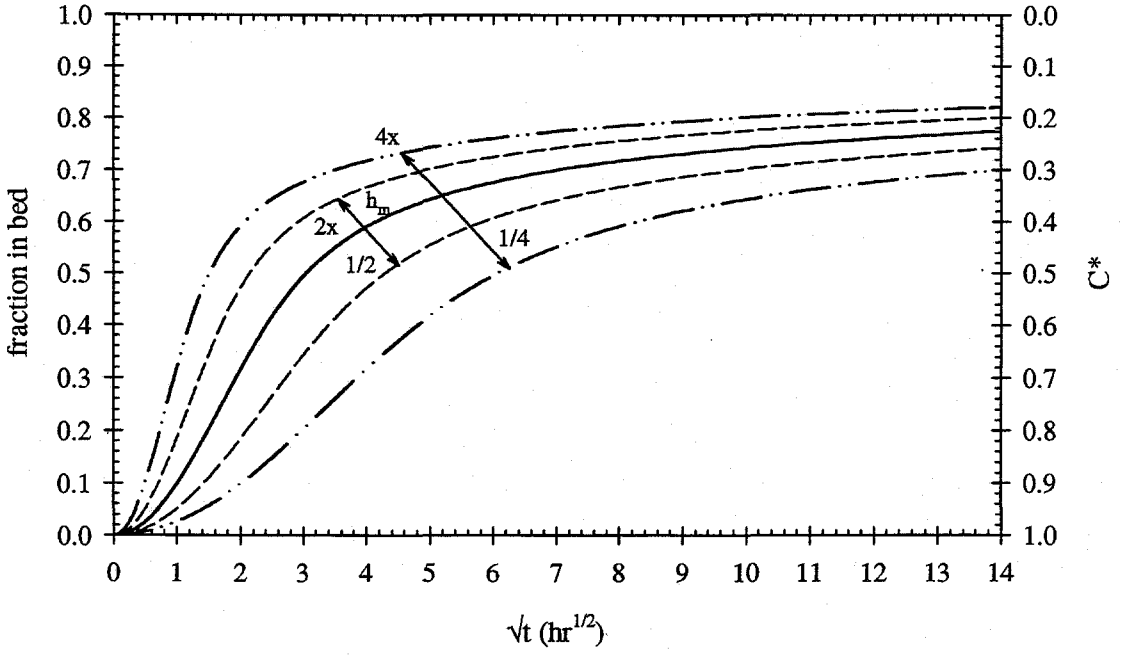

Figure 6.8. Sensitivity of the mass exchange of a linearly adsorbing compound with R = 10 to changes in the amplitude of the pressure variations over the bedforms. Flume Run 2 is used as the base case.

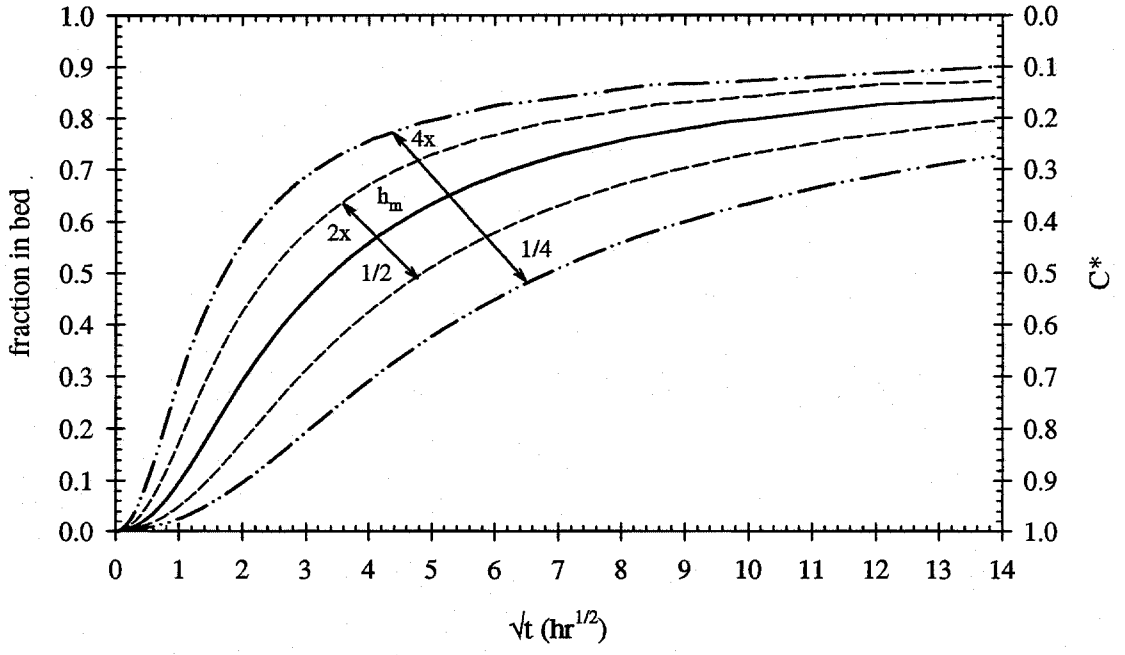

Figure 6.9. Sensitivity of the mass exchange of a nonlinearly adsorbing compound (DTMA C_0 = 182 μM) to changes in the amplitude of the pressure variations over the bedforms. Flume Run 2 is used as the base case.

The effect of h_m on the mass exchange of nonsorbing compounds is illustrated in Figure 6.7, linearly adsorbing compounds in Figure 6.8 and nonlinearly adsorbing compounds in Figure 6.9. The fraction of the compound in the bed is plotted against the square root of time in hours. If the models simulations were plotted with respect to non-dimensional time, the lines would collapse into one because time is scaled by h_m.

The porewater velocity is proportional to h_m, and therefore h_m affects the rate of mass flux into and out of the bed. The adsorbing compounds are more sensitive to h_m than nonsorbing compounds because more mass of the linearly adsorbing compound is retained in the bed, which then increases the sensitivity of the exchange to the rate of mass transport (determined by h_m) into the bed. For both linearly and nonlinearly adsorbing compounds, the mass exchange at short times is more strongly affected by the value of h_m than at long times. At long times, the magnitude of the difference in the model predictions of C* for the adsorbing compounds

approaches the value of difference for nonsorbing compounds. The following figures illustrate the effect of using the predicted and calibrated values of h_m in the model simulations for the mass exchange of the surfactants in Flume Runs 2, 3, 4, 8 and 9. The difference between the NTMA data and model predictions for Flume Run 8 cannot be attributed to the uncertainty of h_m.

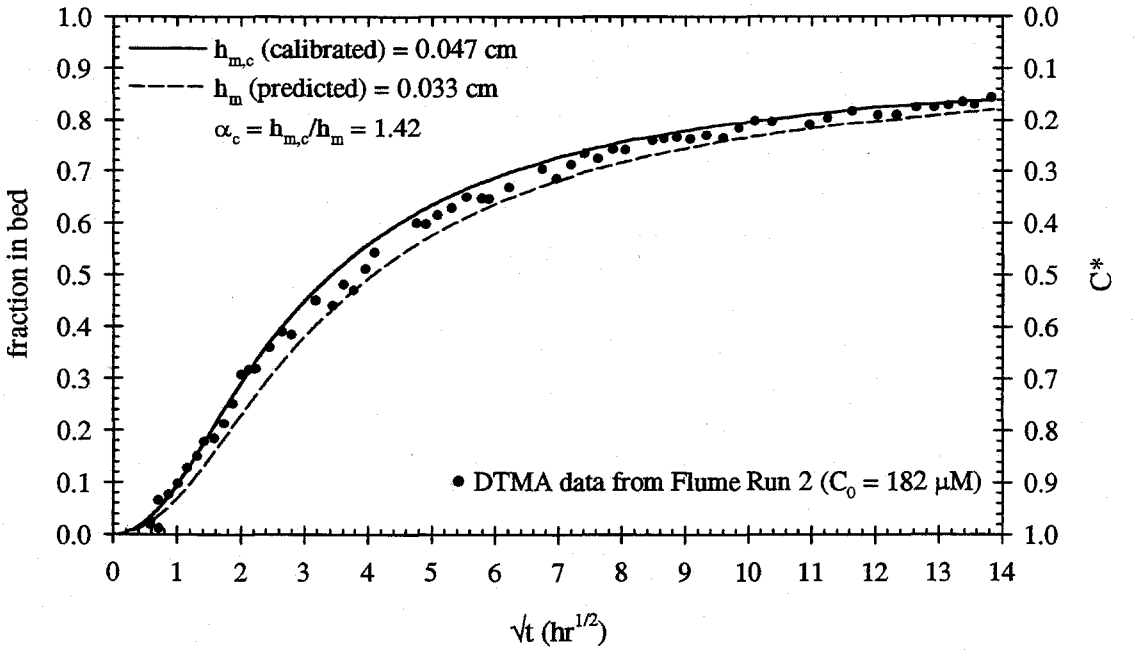

Figure 6.10. Comparison of model simulations with predicted and calibrated values of the amplitude of the pressure variations over the bedforms for DTMA in Flume Run 2.

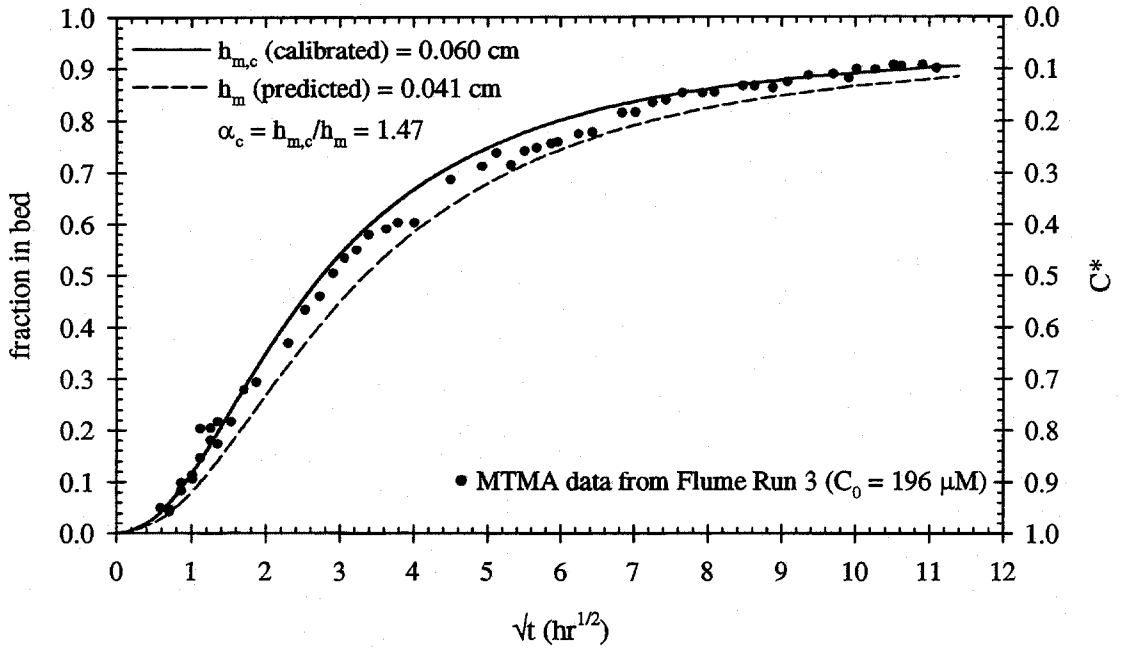

Figure 6.11. Comparison of model simulations with predicted and calibrated values of the amplitude of the pressure variations over the bedforms for MTMA in Flume Run 3.

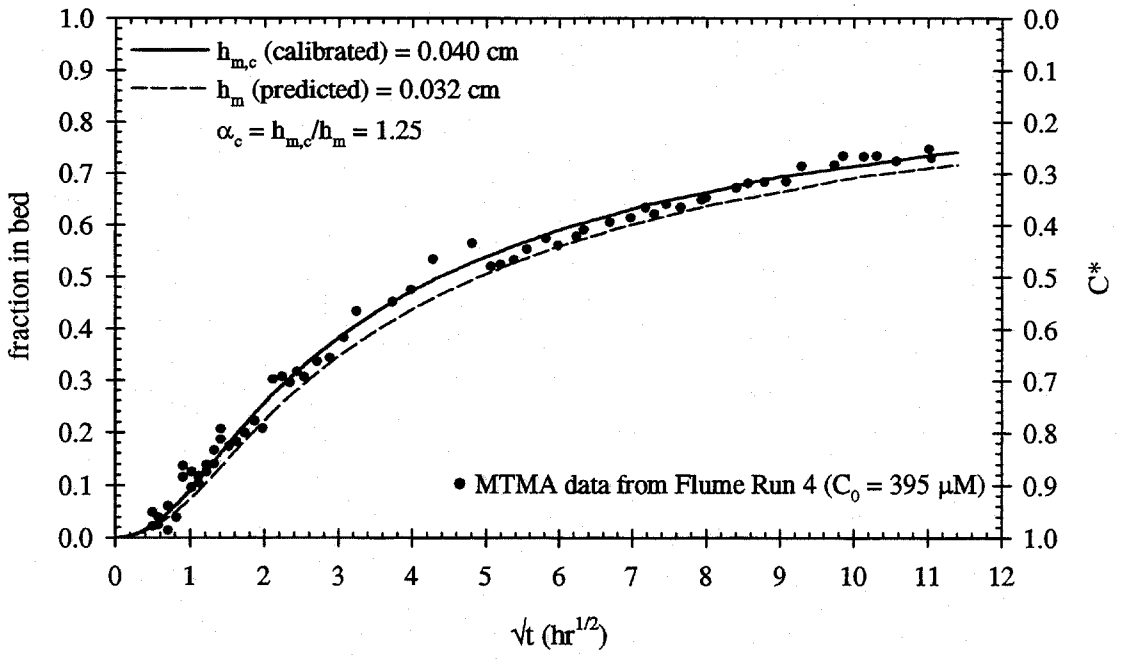

Figure 6.12. Comparison of model simulations with predicted and calibrated values of the amplitude of the pressure variations over the bedforms for MTMA in Flume Run 4.

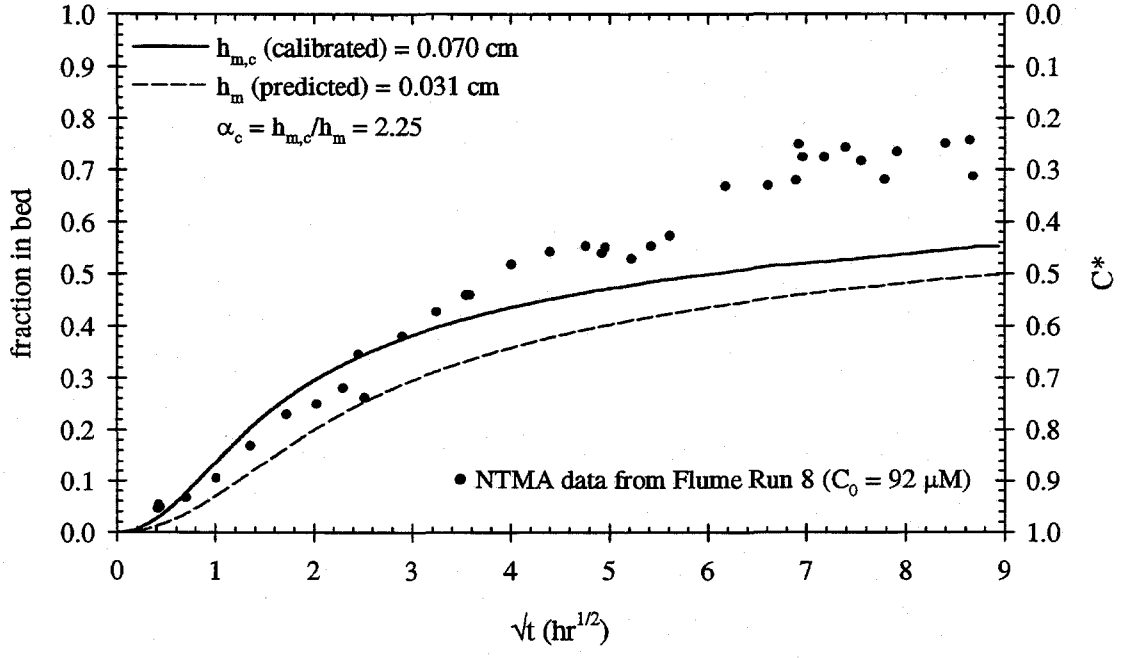

Figure 6.13. Comparison of model simulations with predicted and calibrated values of the amplitude of the pressure variations over the bedforms for NTMA in Flume Run 8.

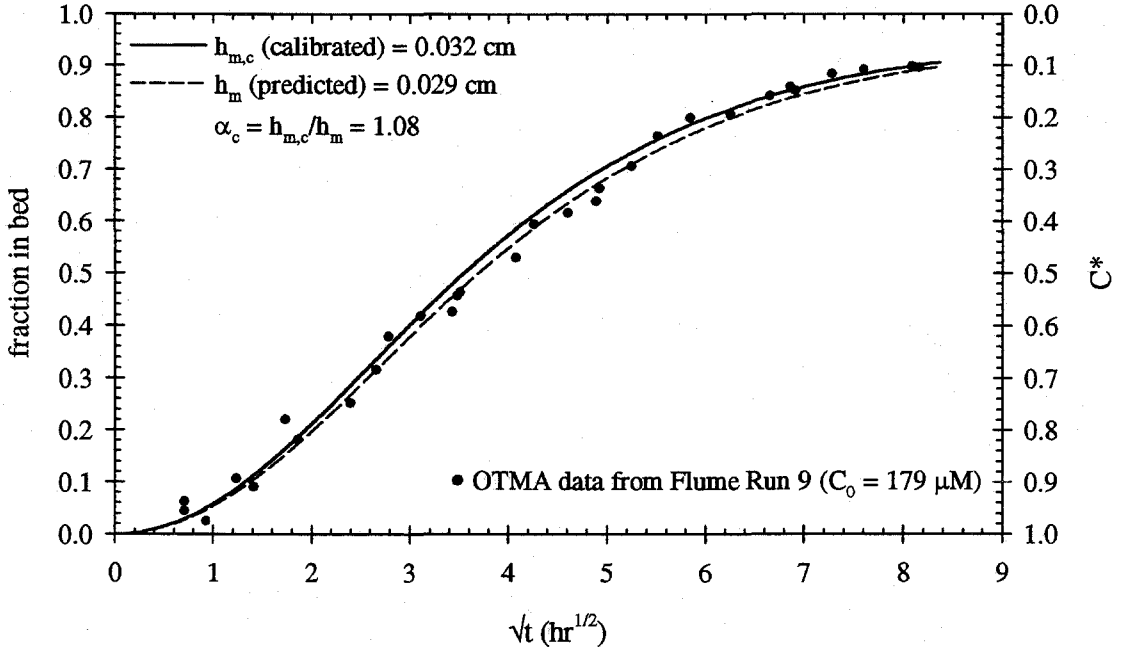

Figure 6.14. Comparison of model simulations with predicted and calibrated values of the amplitude of the pressure variations over the bedforms for OTMA in Flume Run 9.

6.4. SENSITIVITY TO HYDRAULIC PARAMETERS

The bed/stream exchange is influenced by the flow velocity in the channel (U) and the depth of the water column (d). The amplitude of the pressure distribution over a bedform is proportional to the square of the flow velocity ($h_m \propto U^2$). When the velocity increases/decreases by a factor of two, h_m increases/decreases by a factor of four. The shifts in the mass exchange caused by a four-fold increase/decrease in h_m for nonsorbing, linearly adsorbing and nonlinearly adsorbing compounds are shown in Figure 6.7, Figure 6.8 and Figure 6.9, respectively.

The magnitude of h_m is also affected by the depth of the water column (d). The MTMA data from Flume Runs 5 and 6, which are plotted in Figure 6.15, illustrate the change of the bed/stream exchange in response to an increase in the water depth.

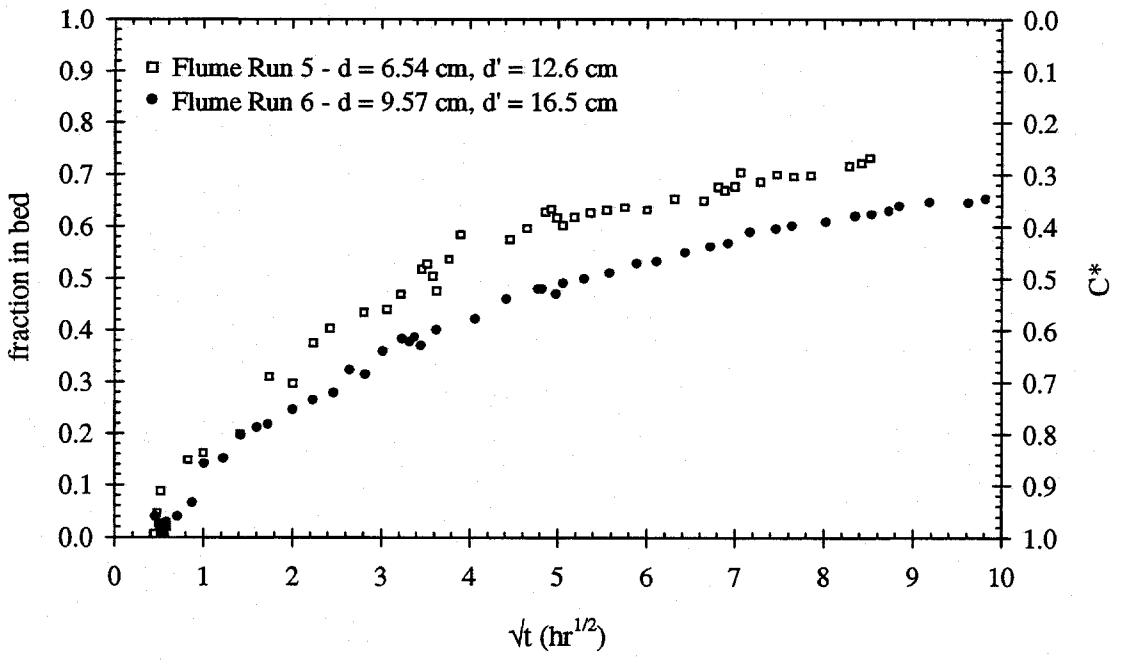

Figure 6.15. Comparison of MTMA mass exchange data from Flume Runs 5 and 6 to illustrate the effect of increasing the water depth in the channel.

For the flume experiments presented in Chapter 5, h_m is inversely proportional to $d^{3/8}$. When the water depth decreases by a factor of two, h_m increases by a factor of 1.3. Conversely, the magnitude of h_m decreases by 23 percent when the water depth increases by a factor of two.

In the flume, the effective water depth d' is also related to d:

$$d' = \frac{1}{A_b}\left(V_{\text{return system}} + b \cdot \text{Length of flume} \cdot d\right) \tag{6.3}$$

where A_b is the plan area of the bed and b is the width of the channel. When d increases, the effective water depth also increases. The total mass of a compound available for the bed/stream exchange is C_0d', where C_0 is the initial concentration. As d' increases for a fixed C_0, the total mass of the compound increases, and thus the same mass transfer to the bed causes smaller decreases in the concentration of the compound in the overlying water column.

The sensitivity of the mass exchange of nonsorbing and nonlinearly adsorbing compounds to the overlying water depth is illustrated in Figure 6.16 and Figure 6.17, respectively. Flume Run 6 is used as the base case. The sensitivity analyses show that the water depth has a major impact on the mass exchange of both nonsorbing and adsorbing compounds. A larger fraction of the total mass is transported into the bed as the water depth decreases. At small times, the total mass retained in the sediment bed is greater for shallower depths because h_m is larger, thus increasing the rate of mass transfer into the bed. However, at long times, the total mass of the compound in the bed becomes greater for deeper water columns because the total mass available for the exchange (C_0d') is larger.

a) fraction of mass transferred to the bed

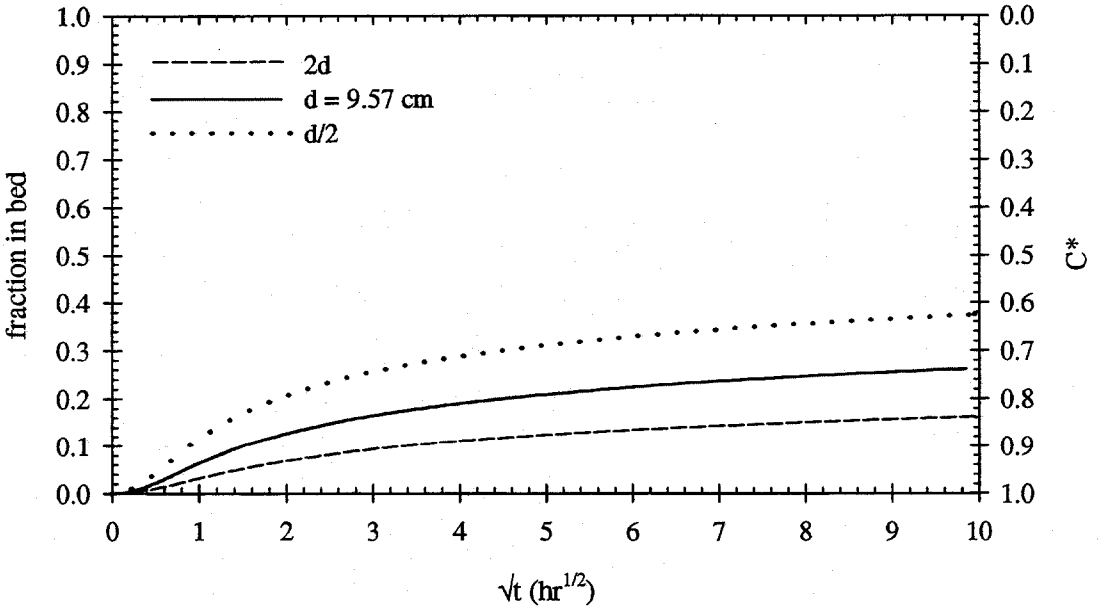

b) accumulated mass per unit plan area of the bed divided by C_0

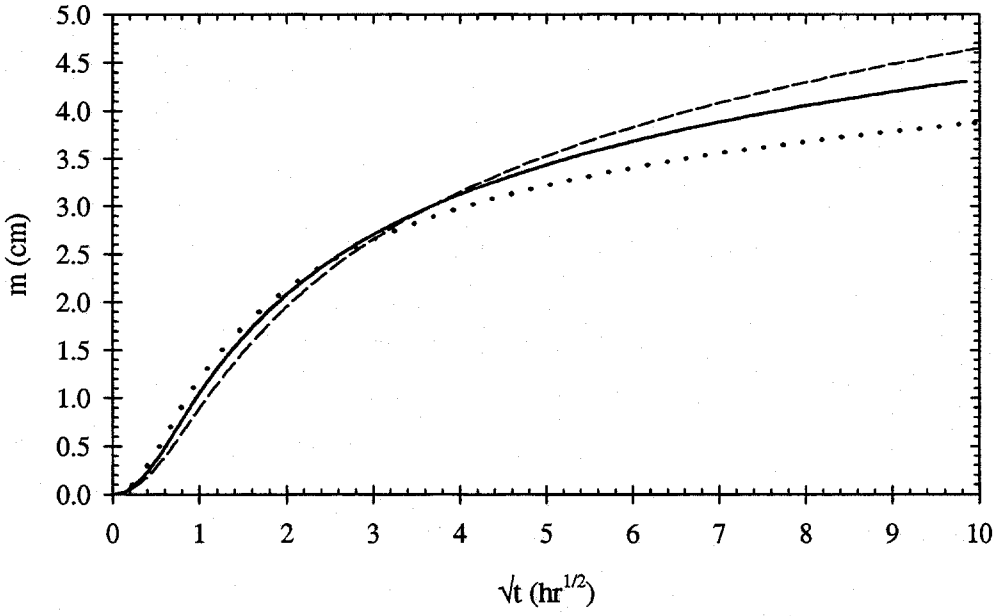

Figure 6.16. Sensitivity of the mass exchange of nonsorbing compounds to water depth. Flume Run 6 is used as the base case.

a) fraction of mass transferred to the bed

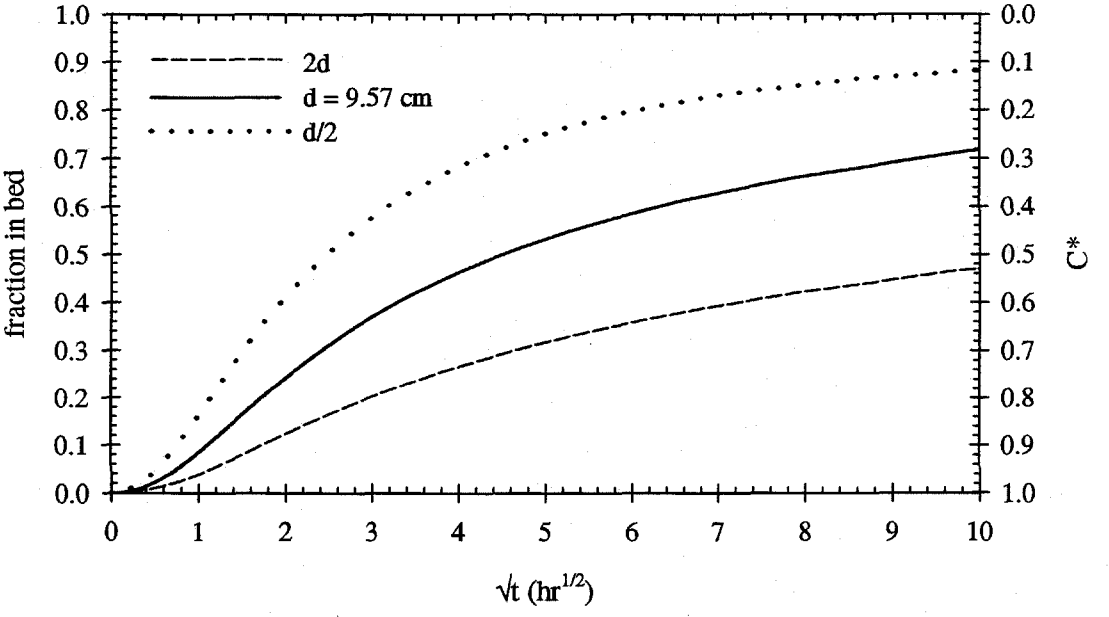

b) accumulated mass per unit plan area of the bed divided by C_0

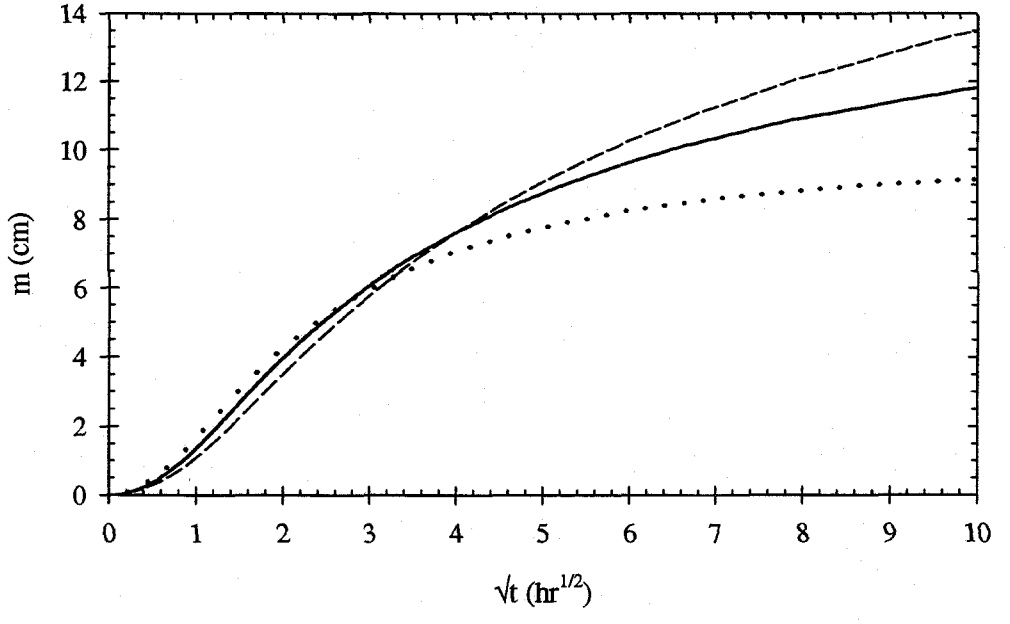

Figure 6.17. Sensitivity of the mass exchange of a nonlinearly adsorbing compound (MTMA C_0 = 295 μM) to water depth. Flume Run 6 is used as the base case.

6.5. SENSITIVITY TO BEDFORM DIMENSIONS

Since the mass exchange is driven by the pressure disturbance caused by the bedforms, the sensitivity of the exchange to the bedform height (H) and wavelength (λ) will be examined. The amplitude of the pressure fluctuation (h_m) is proportional to $H^{3/8}$. Therefore, taller bedforms induce larger pressure variations and porewater velocities ($u_m \propto h_m$). The sensitivity of the mass exchange to h_m is discussed in Section 6.3.

The bedform wavelength does not affect the amplitude of the pressure disturbance over the bedform. For the same hydraulic conditions and bedform height, a longer bedform has the same pressure disturbance applied over a greater distance. The maximum porewater velocity u_m is inversely proportional to the bedform wavelength. Hence, longer bedforms result in slower porewater velocities, but the compounds are pumped deeper into the sediment bed.

The bedforms observed in the flume experiments have wavelengths between 5 and 40 cm. Figure 6.18, Figure 6.19 and Figure 6.20 show the sensitivity of the mass exchange to the bedform wavelength for nonsorbing and linearly adsorbing compounds with retardation coefficients of 2 and 20, respectively. The hydraulic parameters from Flume Run 3 are used. In order to demonstrate the affect of bedform wavelength on the mass exchange, the model simulations for different wavelengths are plotted against time in hours rather than t*. The hydraulic conductivity and h_m are the same in the simulations. Since non-dimensional time ($t^* = (2\pi/\lambda)Kh_m$ where K is the hydraulic conductivity) is scaled by the wavelength, differences in the model simulations would not be accurately illustrated if the results were plotted against t*.

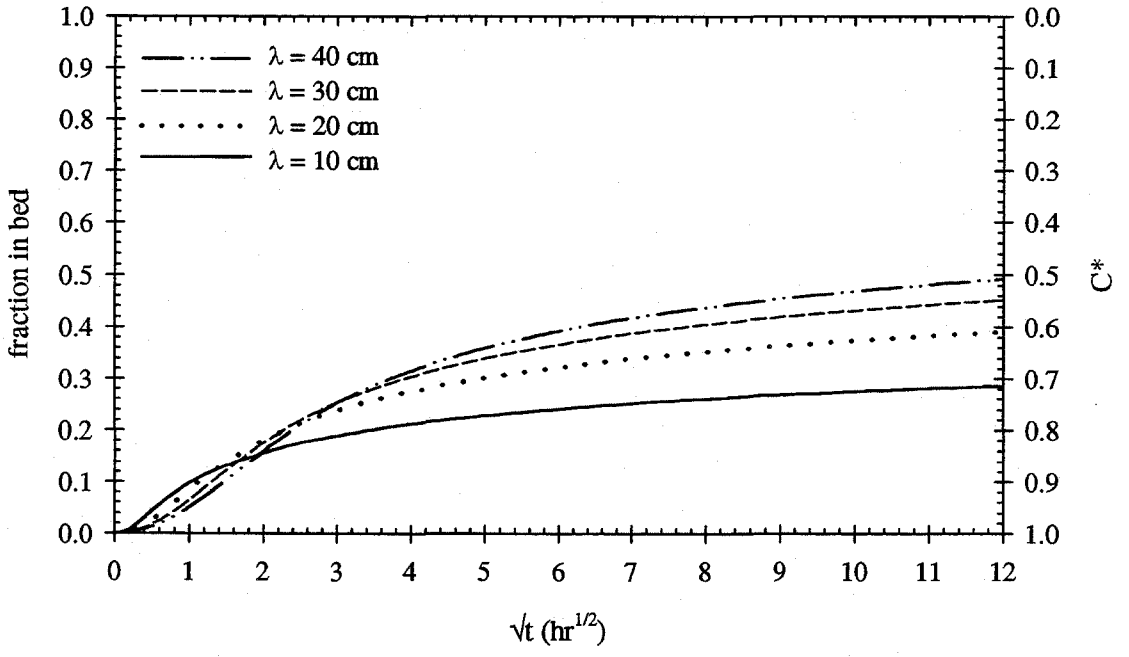

Figure 6.18. Comparison of the mass exchange of a nonsorbing compound for different bedform wavelengths. The hydraulic parameters from Flume Run 3 are used.

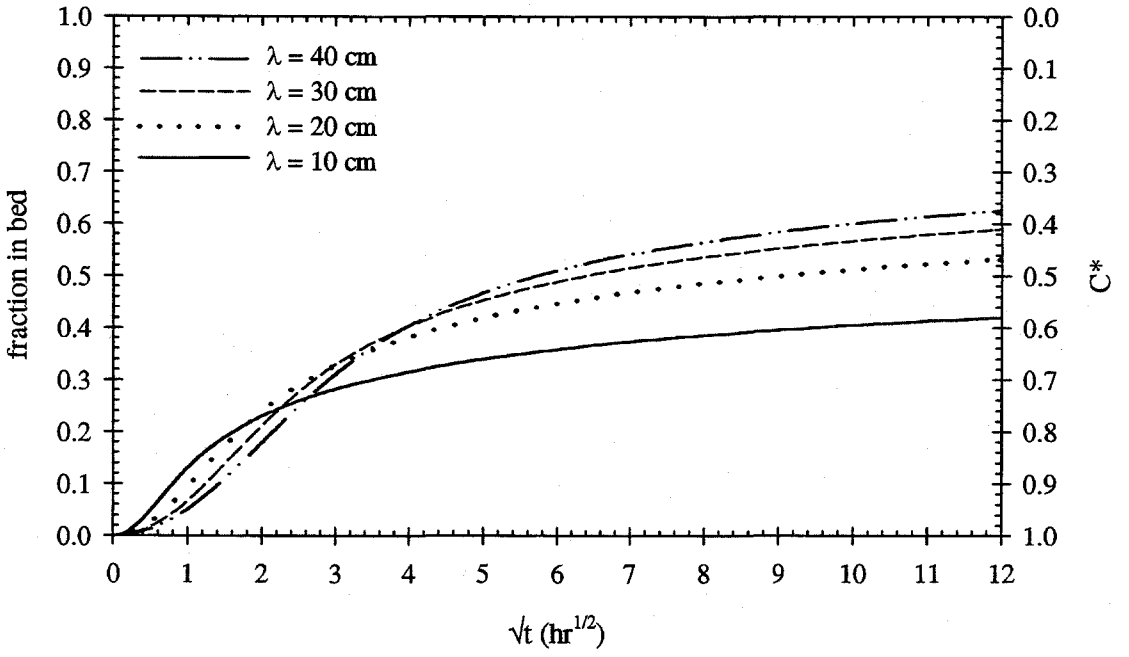

Figure 6.19. Comparison of the mass exchange of a linearly adsorbing compound with R = 2 for different bedform wavelengths. The hydraulic parameters from Flume Run 3 are used.

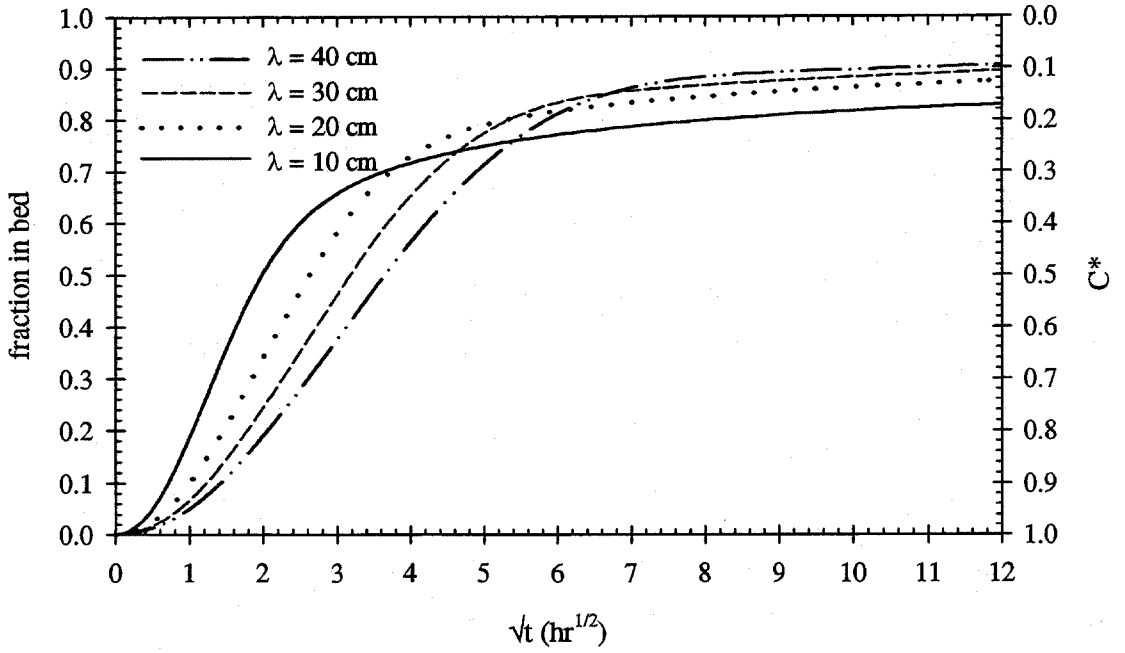

Figure 6.20. Comparison of the mass exchange of a linearly adsorbing compound with R = 20 for different bedform wavelengths. The hydraulic parameters from Flume Run 3 are used.

At small times, the mass transfer to the bed is greater for the smaller wavelengths because their porewater velocities are faster. At large times, the exchange is greater for the longer bedforms because the penetration depth of the compound into the bed is deeper. At short times, the difference in the mass exchange associated with the different bedform wavelengths is small for nonsorbing and weakly adsorbing compounds. The longer bedforms have a more significant impact on the mass exchange at large times. Conversely, the mass exchange for strongly adsorbing compounds is sensitive to the bedform wavelength at small times.

The exchange model for lithium and bromide, which is based on the average bedform wavelength, under-predicted the mass transfer in some of the flume experiments. These differences were attributed to the influence of the longer bedforms in the system. This hypothesis will now be verified.

The average bedform wavelength for Flume Run 6 is 14.9 cm with a standard deviation of 4.0 cm. There are 7 out of the 28 bedforms that are larger than 18.9 cm ($\lambda_{avg} + \sigma_\lambda$). Figure 6.21 compares the bed exchange models using the average wavelength and longer wavelengths, which were observed in the flume, to the bromide data from Flume Run 6. The exchange model based on the longest bedform best fits the observed Bromide data better.

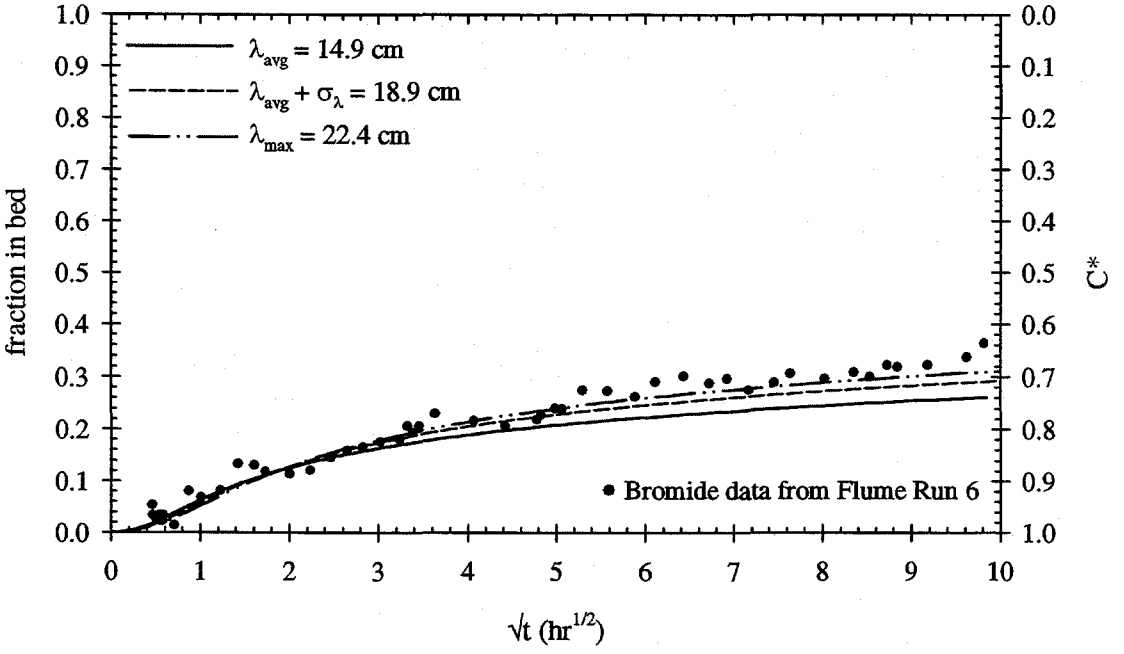

Figure 6.21. Comparison of model simulations based on different bedform wavelengths to the bromide data of Flume Run 6.

The lithium data from Flume Runs 2, 3, 4 and 6 are compared to model simulations derived from different bedform wavelengths in Figure 6.22 through Figure 6.25. The model predictions from the longer wavelengths agree with the lithium exchange during the latter part of the flume experiments. Therefore, after long times, the transport of nonsorbing and weakly adsorbing compounds into a sediment bed covered with random, natural stationary bedforms is significantly influenced by the porewater flows induced by the larger bedforms.

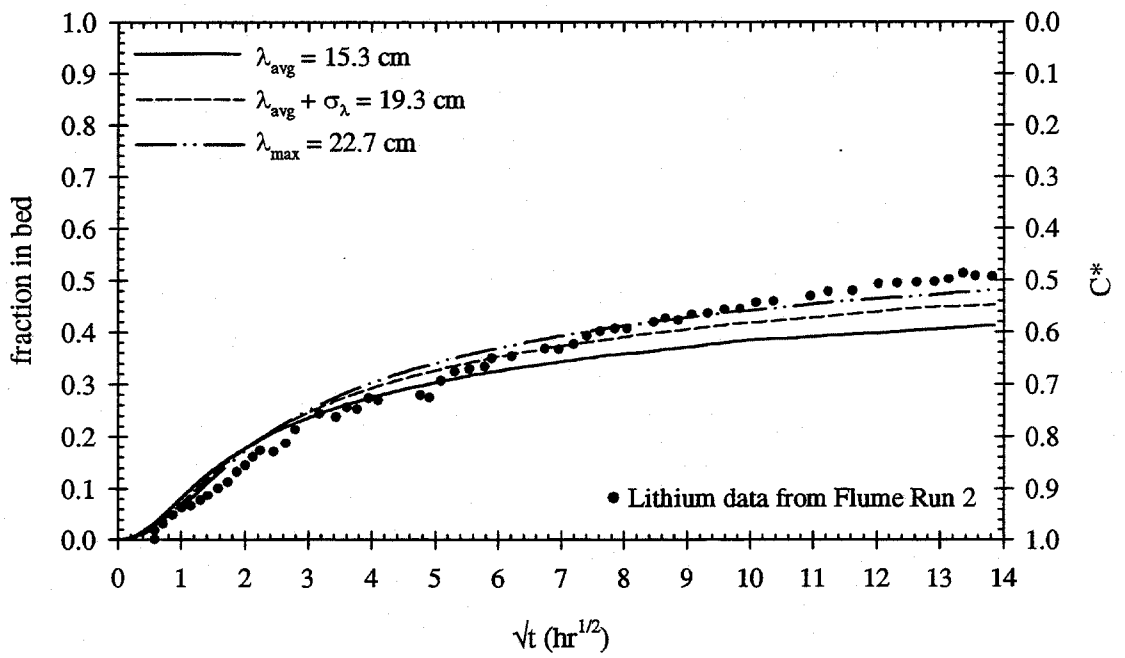

Figure 6.22. Comparison of model simulations based on different bedform wavelengths to the lithium data of Flume Run 2.

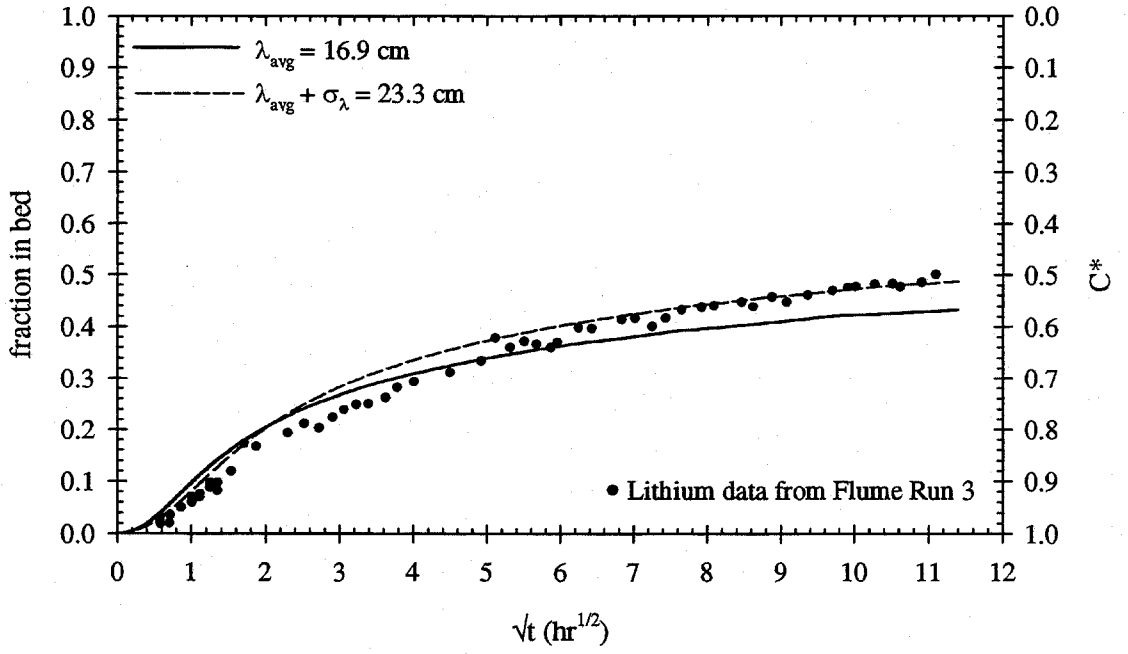

Figure 6.23. Comparison of model simulations based on different bedform wavelengths to the lithium data of Flume Run 3.

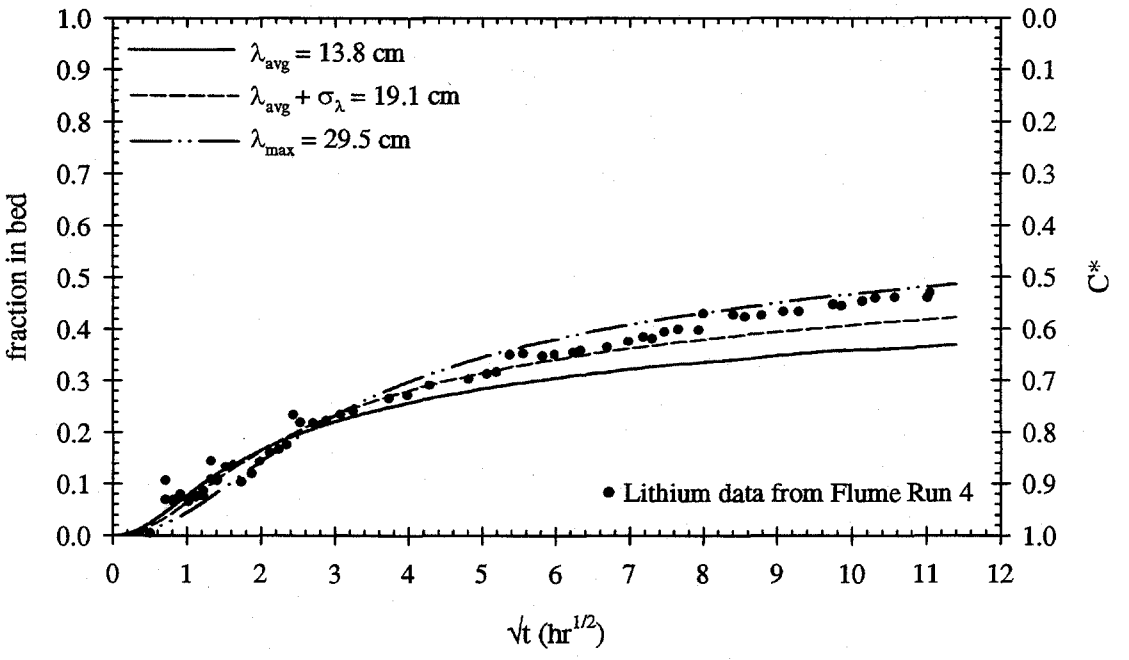

Figure 6.24. Comparison of model simulations based on different bedform wavelengths to the lithium data of Flume Run 4.

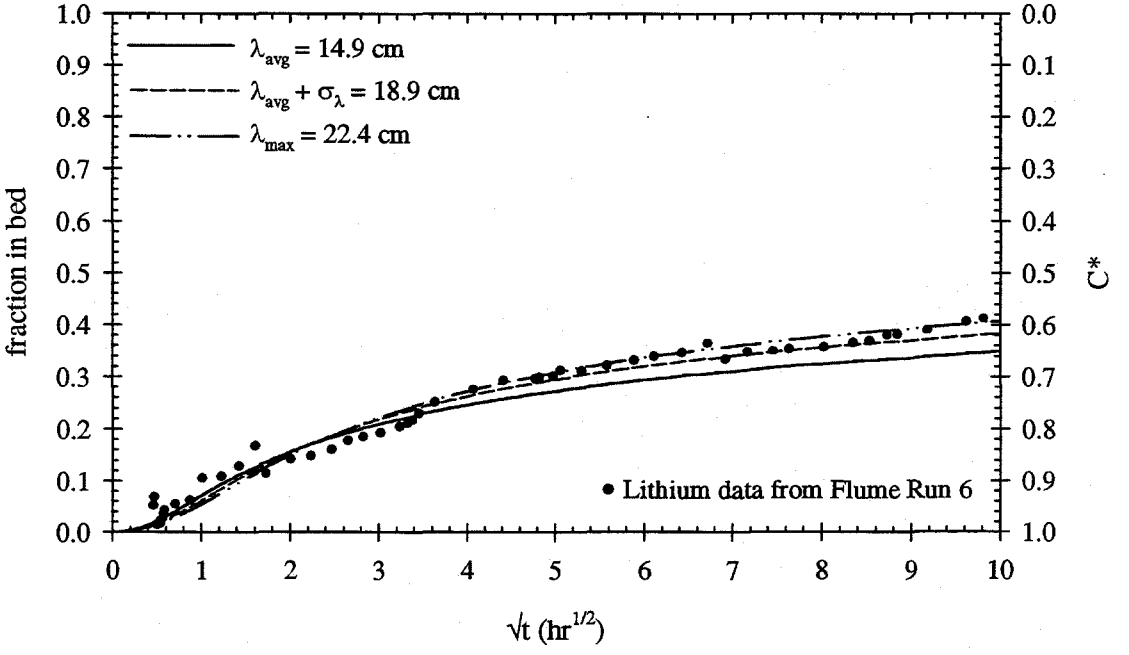

Figure 6.25. Comparison of model simulations based on different bedform wavelengths to the lithium data of Flume Run 6.

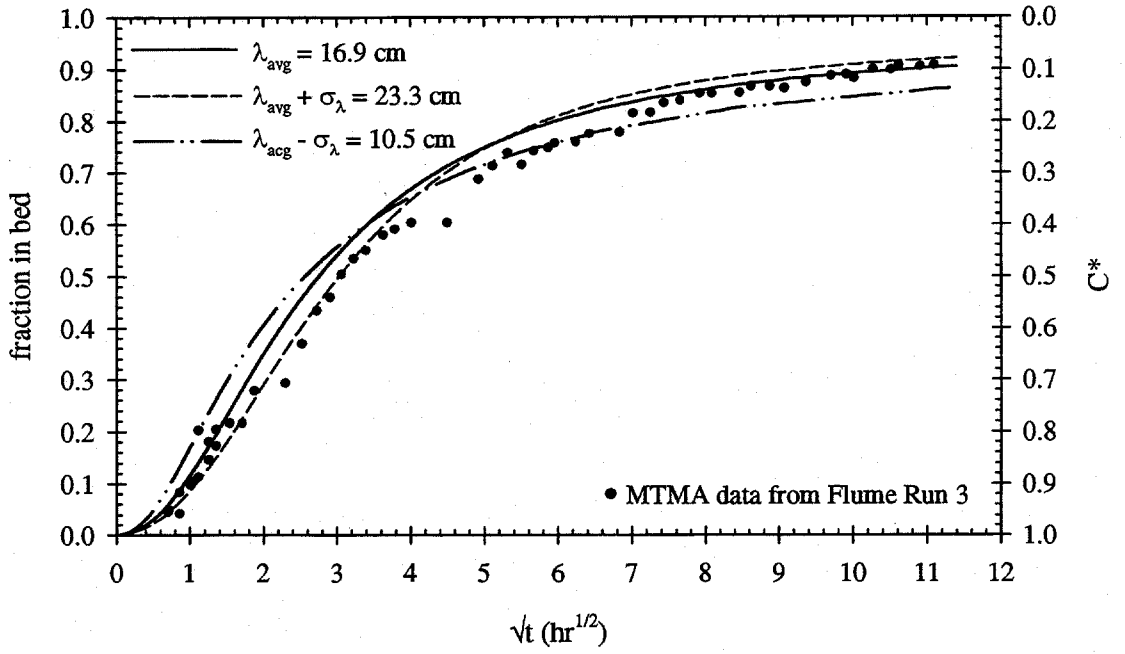

Figure 6.26. Comparison of model simulations based on different bedform wavelengths to the MTMA data of Flume Run 3.

Figure 6.26 compares the MTMA data of Flume Run 3 to model simulations based on short, average and long bedform wavelengths. Early in the experiment, the transport of MTMA into the bed is best modeled using the shorter bedform wavelength. The model predictions derived from the average bedform wavelength agree with the MTMA later in the experiment. The MTMA exchange is not notably affected by the bedforms with longer wavelengths.

The NTMA data from Flume Run 8 is compared to model simulations based on different bedform wavelengths in Figure 6.27. Even the model using the maximum bedform wavelength under-predicts the exchange of NTMA. Since the exchange model based on the average bedform wavelength fits the bromide data well (Chapter 5, Figure 5.41) and bromide moves deeper into the bed than NTMA (because bromide is not retarded), the enhanced NTMA exchange cannot be attributed to the longer bedforms.

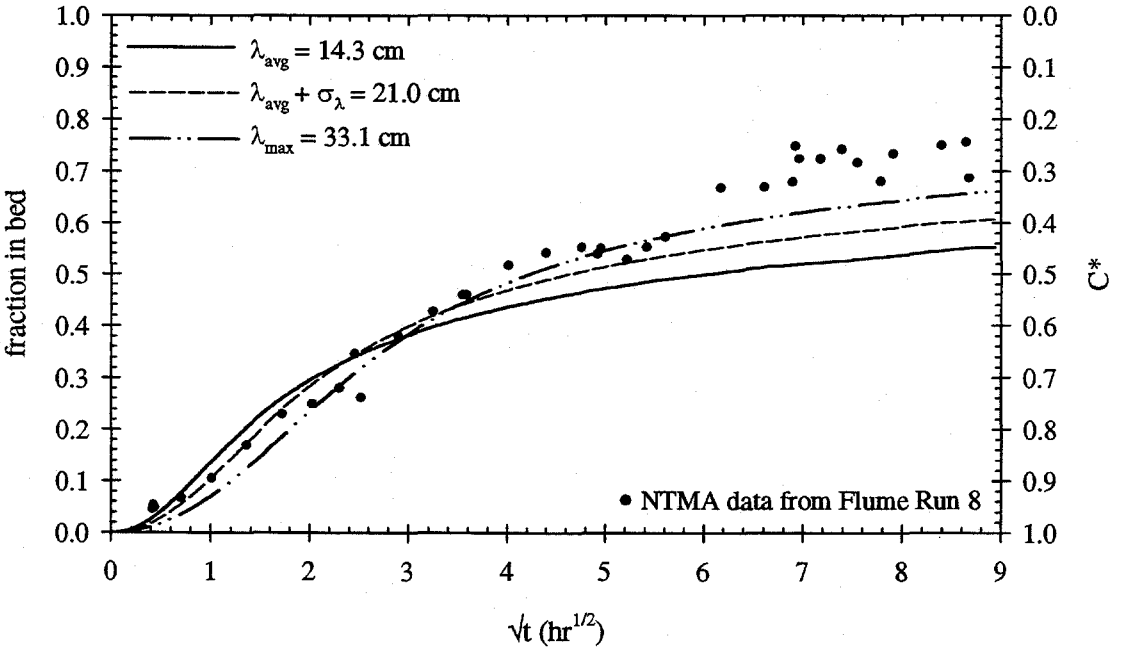

Figure 6.27. Comparison of model simulations based on different bedform wavelengths to the NTMA data of Flume Run 8.

In summary, the bedform wavelength significantly affects the transport of both nonsorbing and adsorbing compounds into the sediment bed. When the bedform wavelengths are highly variable, model studies should examine the sensitivity of the system to the different wavelengths. The transport at short times is controlled by the short bedforms while the transport at large times is driven by the long bedforms. For strongly adsorbing compounds, the length of time for which the short bedforms influence the exchange is long. The exchange of nonsorbing and weakly adsorbing compounds is significantly affected by the presence of long bedforms at longer times.

6.6. SENSITIVITY TO INITIAL CONCENTRATION

6.6.1. Measurement of initial concentration

The initial concentrations of the compounds used in the flume experiments are determined by averaging the measured concentrations of samples collected during the first 20 minutes of the flume run. Some mass exchange occurs during this time and the actual initial concentration may be slightly higher than the "measured" concentration.

The effect of a 5 percent error in the initial concentration C_0 is illustrated for Flume Run 3 in Figure 6.28 and for Flume Run 4 in Figure 6.29. The underestimation of C_0 results in an underestimation of the mass exchange, and the error is larger at small times. The parameter h_m is calibrated using the mass exchange data. If the reported exchange data is underestimated, then the value of h_m will also be underestimated. The sensitivity of the mass exchange to h_m is discussed in Section 6.3.

6.6.2. Effect of changing the initial concentration of the surfactant

The impact of different initial concentrations on the stream/bed exchange of a surfactant is examined in this section. Figure 6.30 compares the mass exchange of MTMA in Flume Run 3 (C_0 = 196 μM) and Flume Run 4 (C_0 = 395 μM). The initial concentration of MTMA in Run 4 is a factor of two greater than the initial concentration in Run 3. The hydraulic and bed conditions are similar.

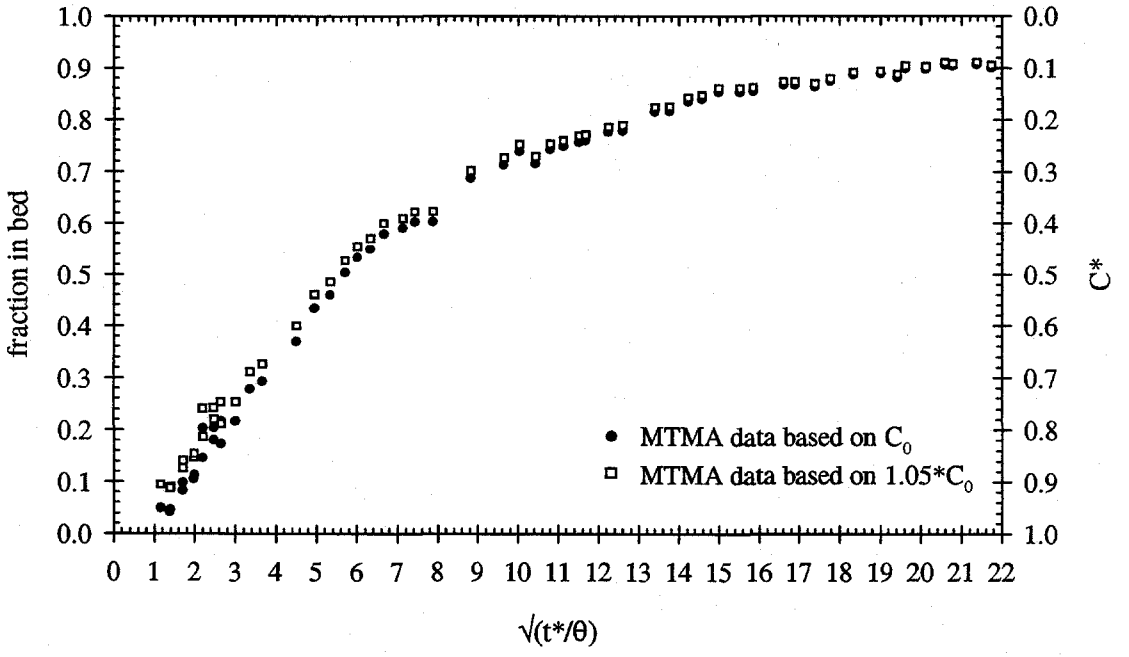

Figure 6.28. The effect of a 5 percent error in the initial concentration C_0 on the measured mass exchange of MTMA in Flume Run 3 (C_0 = 196 μM).

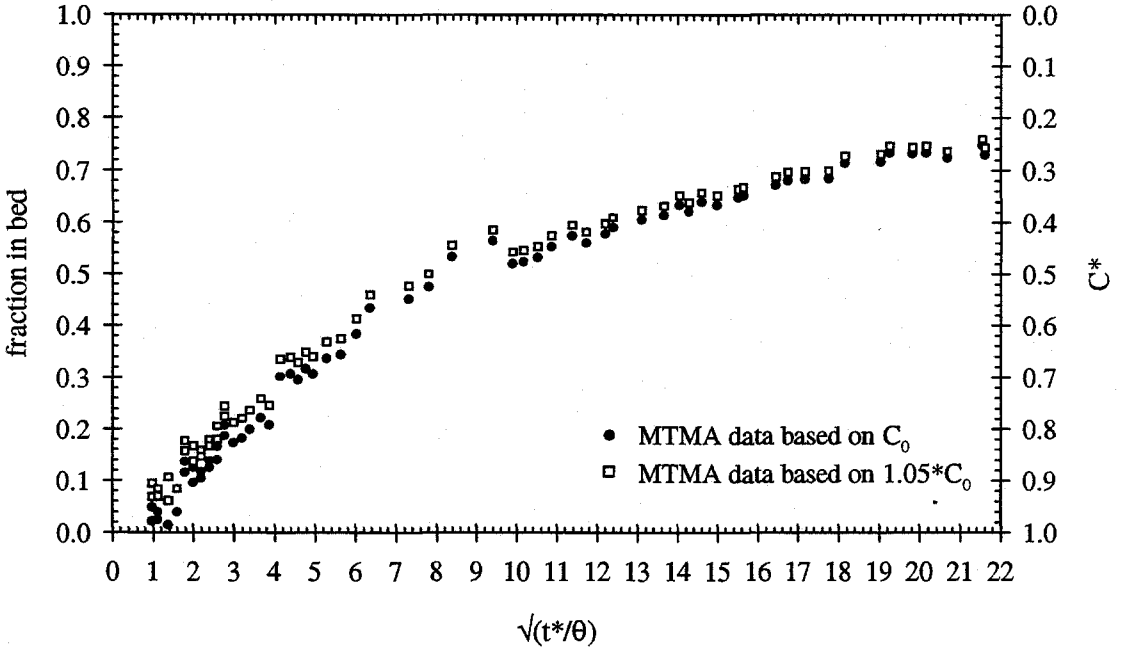

Figure 6.29. The effect of a 5 percent error in the initial concentration C_0 on the measured mass exchange of MTMA in Flume Run 4 (C_0 = 395 μM).

a) fraction of mass transferred to the bed

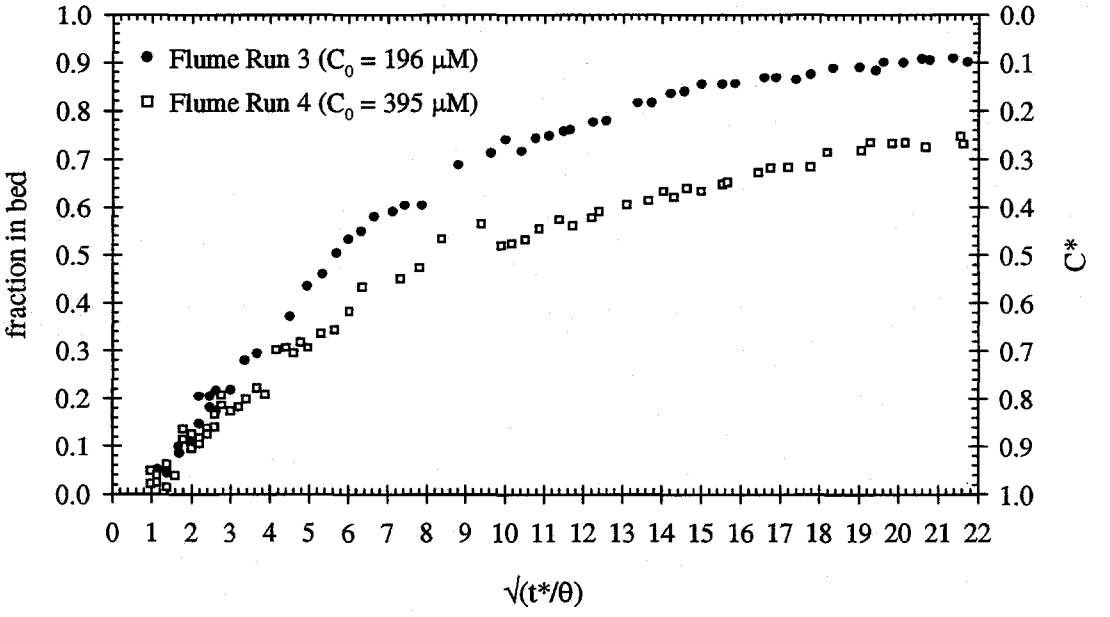

b) normalized accumulated mass per unit plan area of the bed

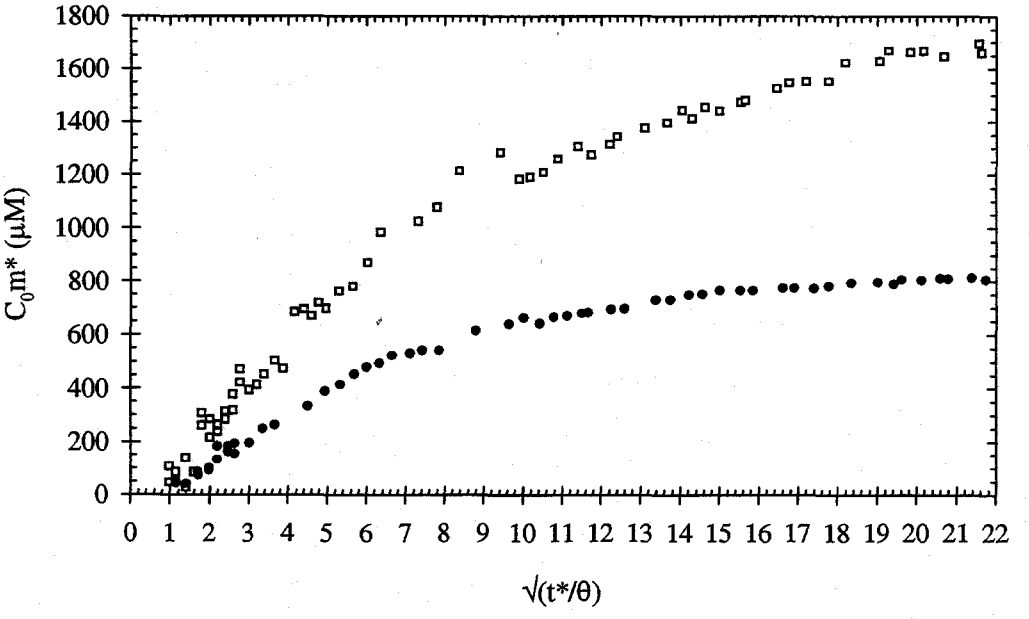

Figure 6.30. Comparison of the exchange of MTMA in the flume at different initial concentrations.

Figure 6.30a shows the fraction of the total mass transferred to the bed with respect to non-dimensional time. The data are plotted against the non-dimensional time to eliminate the differences in the exchange that result from small differences in the hydraulic and bed parameters. A larger fraction of the total mass is retained in the bed for smaller initial concentrations because a higher fraction adsorbs to the sand.

Figure 6.30b shows that the rate of mass transfer and the total mass transferred to the bed are greater at higher initial concentrations. The rate of mass transfer increases with the initial concentration because the effective retardation coefficient decreases as the concentration increases. Since the total mass available for the bed exchange increases with the initial concentration, the total mass transfer to the bed also increases.

6.7. Effect of Surfactant Hydrocarbon Chain Length

In the batch adsorption experiments, the mass of the surfactant adsorbed on the garnet sand increased with the hydrocarbon chain length (Chapter 5, Figure 5.17). Figure 6.31 illustrates the effect of the hydrocarbon chain length on the transport of the surfactants into the sediment bed. In Figure 6.31, the mass exchange of DTMA (12 carbons), MTMA (14 carbons) and OTMA (18 carbons) with the bed is compared for Flume Runs 2, 3 and 9, respectively. The hydraulic parameters, chemical conditions and initial surfactant concentrations are similar for these runs. The mass of the surfactant retained in the bed increases with the hydrocarbon chain length, which agrees with the results of the batch experiments.

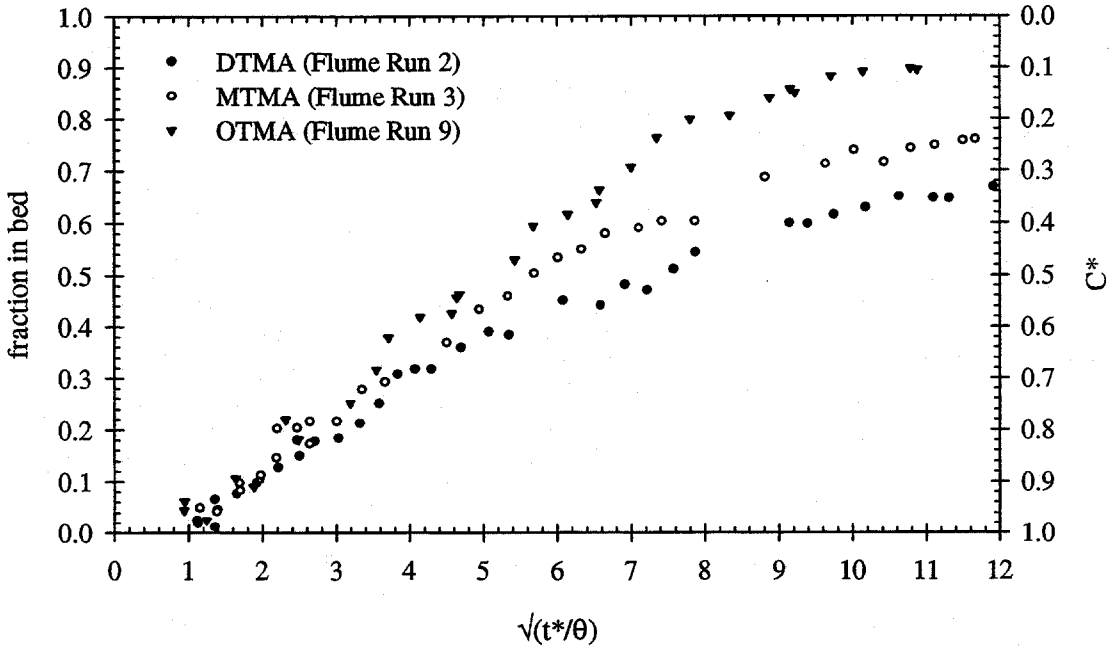

Figure 6.31. The effect of the surfactant hydrocarbon chain length on the stream/bed exchange is illustrated through a comparison of the flume data for DTMA (Flume Run 2, C_0 = 182 μM), MTMA (Flume Run 3, C_0 = 196 μM) and OTMA (Flume Run 9, C_0 = 182 μM).

6.8. SENSITIVITY TO THE LANGMUIR ADSORPTION PARAMETERS

The batch adsorption data from which the isotherms were derived exhibit a considerable amount of scatter, which results in relatively high uncertainties in the adsorption constants. The sensitivity of the exchange models for lithium and the cationic surfactants to changes in the Langmuir sorption parameters K_L (adsorption coefficient) and S_T (sorption capacity) are presented in this section. The values of K_L and S_T that are used in the sensitivity analyses are the upper and lower bounds of the 95 percent confidence limits determined from the isotherm fits.

6.8.1. Sensitivity to lithium sorption parameters

The 95 percent confidence limits of K_L and S_T for the lithium are ± 50 percent and ± 20 percent of the best-fit value, respectively. The sensitivity of the bed exchange model to K_L and

S_T for Flume Run 2 is illustrated in Figure 6.32 and Figure 6.33, respectively. The changes in the model predictions associated with the changes in K_L and S_T are relatively small because the effective retardation coefficient is only about 1.5, indicating weak adsorption. Therefore, the difference between the model and the data cannot be attributed to the error associated with the adsorption parameters.

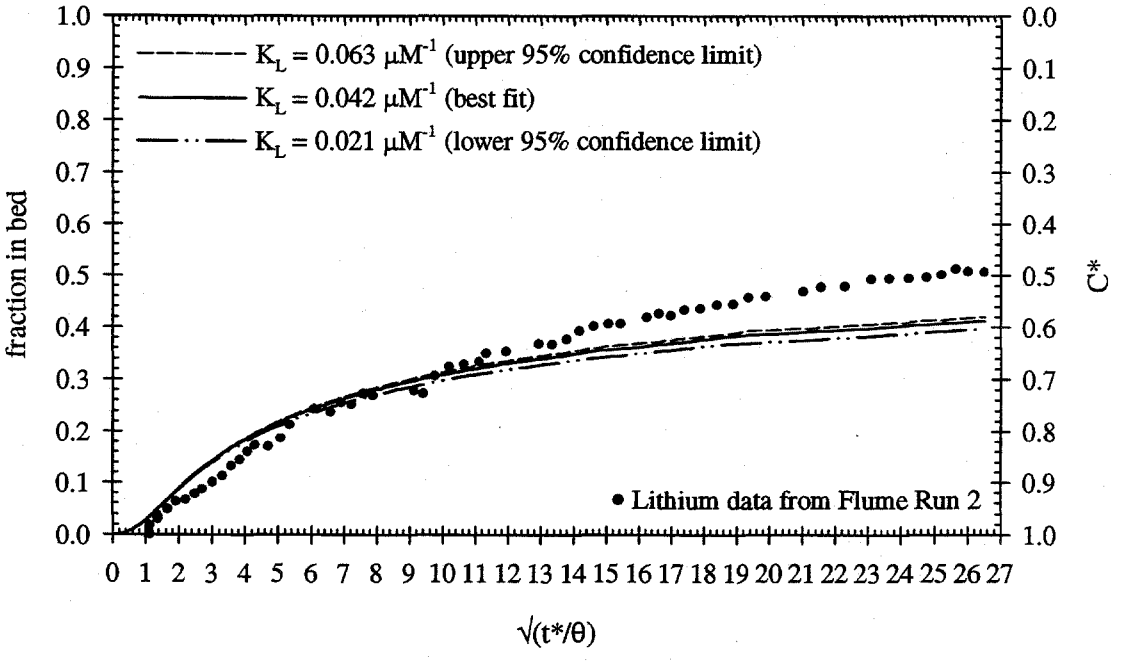

Figure 6.32. Sensitivity of the lithium bed/streamexchange model for Flume Run 2 to the Langmuir adsorption constant K_L.

6.8.2. Sensitivity to DTMA sorption parameters

The sensitivity of the DTMA bed/stream exchange model to K_L and S_T is illustrated in Figure 6.34 and Figure 6.35, respectively, for Flume Run 2. For DTMA, the 95 percent confidence limits are ±47 percent and ±11 percent of the best-fit values of K_L and S_T, respectively. The model results do not differ significantly from the best-fit case. The model simulations coincide for $t^*/\theta < 16$ because they represent total capture by the bed up to that time.

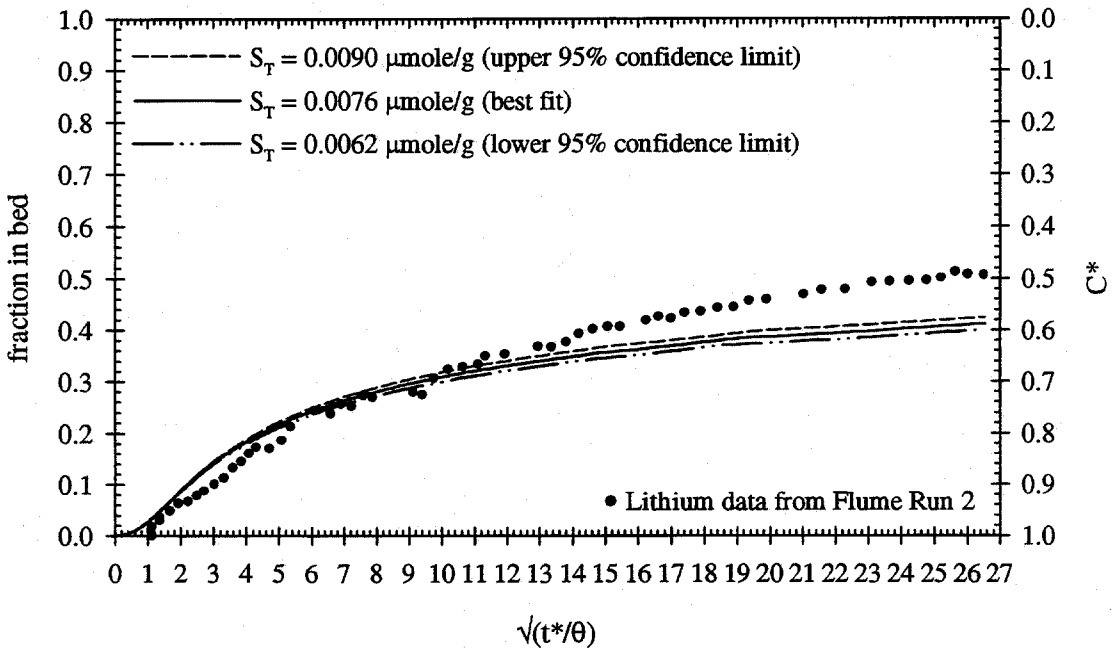

Figure 6.33. Sensitivity of the lithium bed/stream exchange model for Flume Run 2 to the Langmuir adsorption constant S_T.

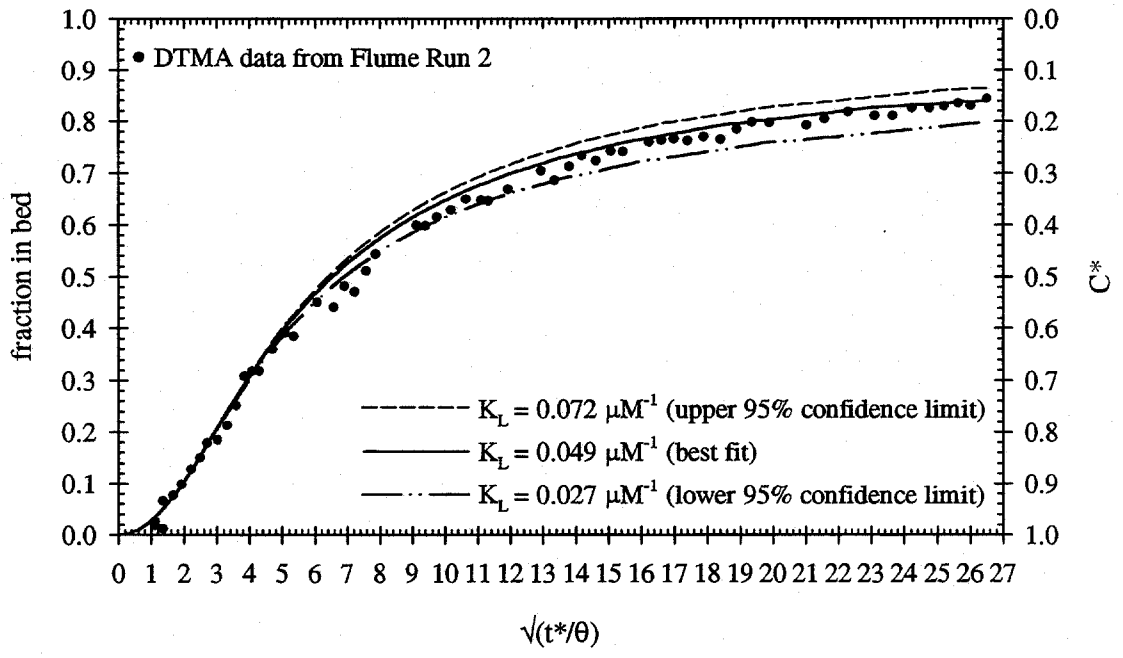

Figure 6.34. Sensitivity of the DTMA bed/stream exchange model for Flume Run 2 to the Langmuir adsorption constant K_L.

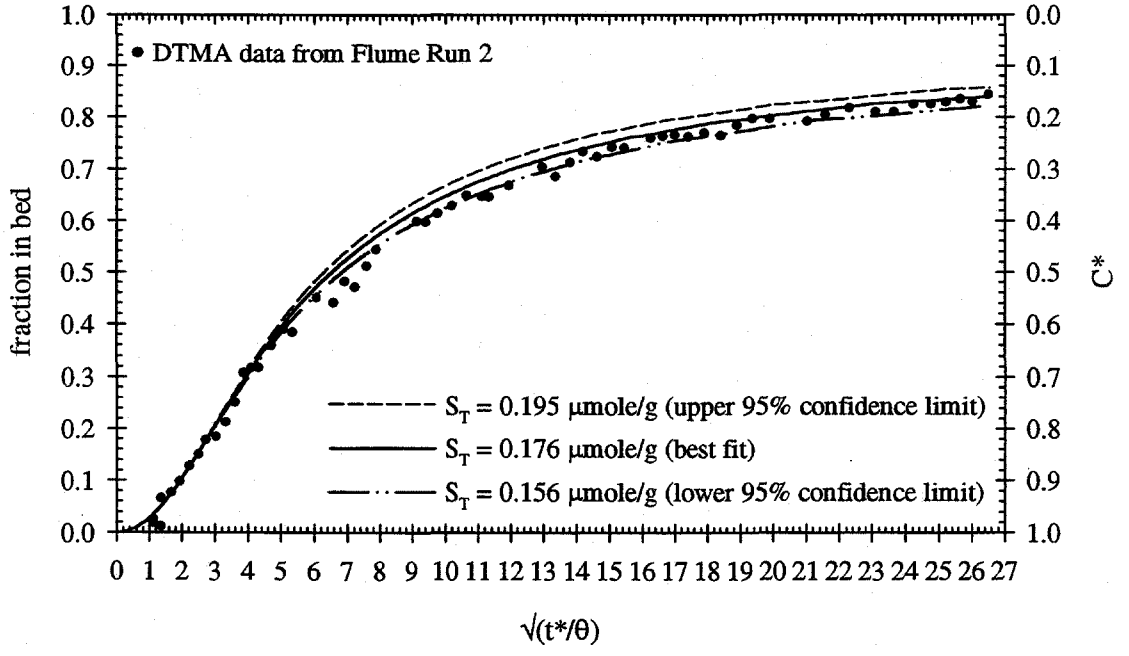

Figure 6.35. Sensitivity of the DTMA bed/stream exchange model for Flume Run 2 to the Langmuir adsorption constant S_T.

6.8.3. Sensitivity to MTMA sorption parameters

The sensitivity of the MTMA bed/stream exchange model simulations to K_L and S_T for Flume Run 6 is illustrated in Figure 6.36 and Figure 6.37, respectively. The 95 percent confidence limits for K_L and S_T are ±30 and ±6 percent of the best-fit values, respectively. The model is more sensitive to the small change in S_T than the larger change of K_L. However, the overall effect on the model predictions is relatively small in both cases.

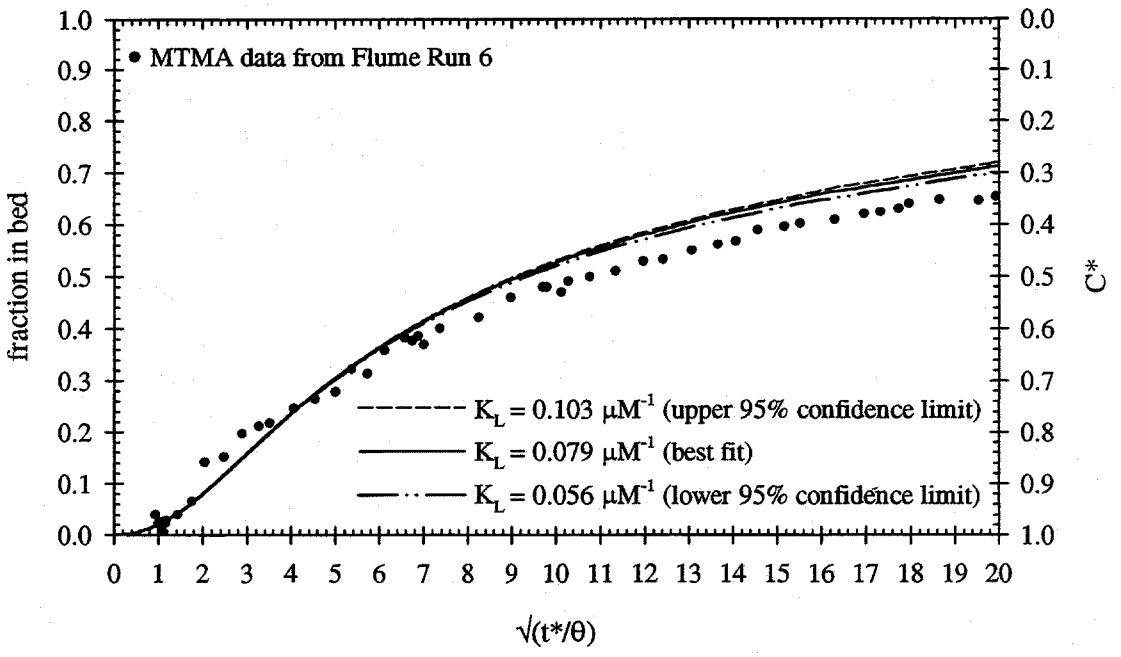

Figure 6.36. Sensitivity of the MTMA bed/stream exchange model for Flume Run 6 to the Langmuir adsorption constant K_L.

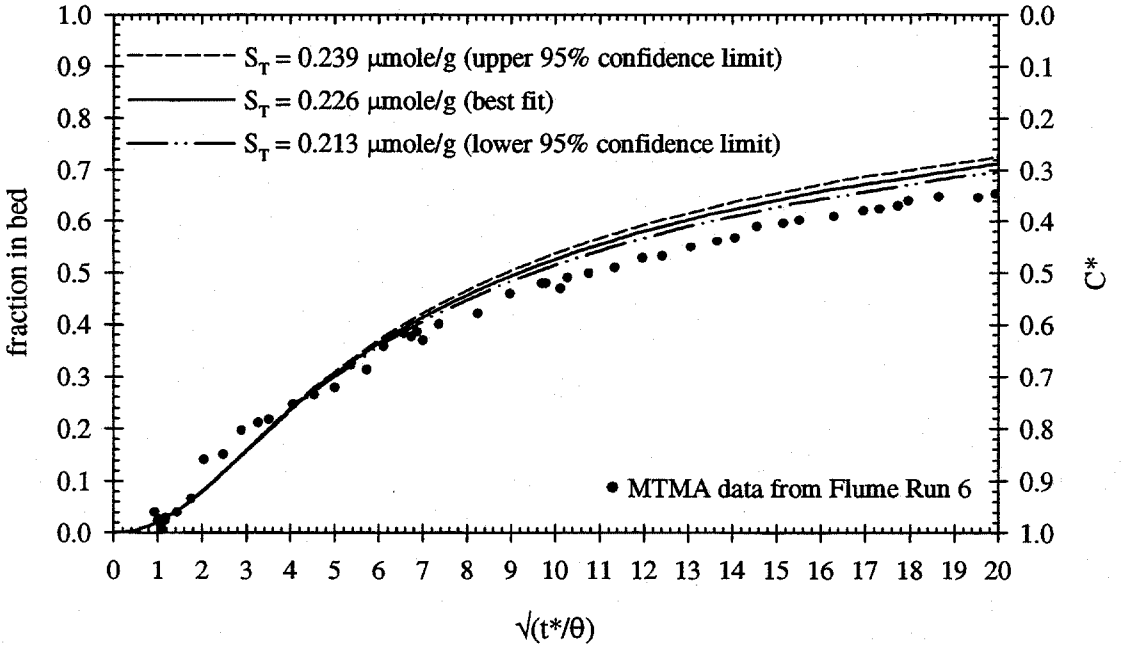

Figure 6.37. Sensitivity of the MTMA bed/stream exchange model for Flume Run 6 to the Langmuir adsorption constant S_T.

6.8.4. Sensitivity to NTMA sorption parameters

The error associated with the NTMA adsorption data is relatively large and the isotherm fits are poor ($R^2 = 0.368$ for the Langmuir fit). The 95 percent confidence limits increase to ±110 percent and ±72 percent of the best-fit values for K_L and S_T, respectively. The following figures show that the NTMA model simulations for Flume Run 8 are strongly influenced by the changes in the sorption parameters. The model simulations using the upper limits for K_L and S_T are closest to the observed exchange data. These simulations suggest that the difference between the flume data and the model for NTMA exchange in Flume Run 8 may be for the most part a result of the uncertainty associated with the sorption parameters.

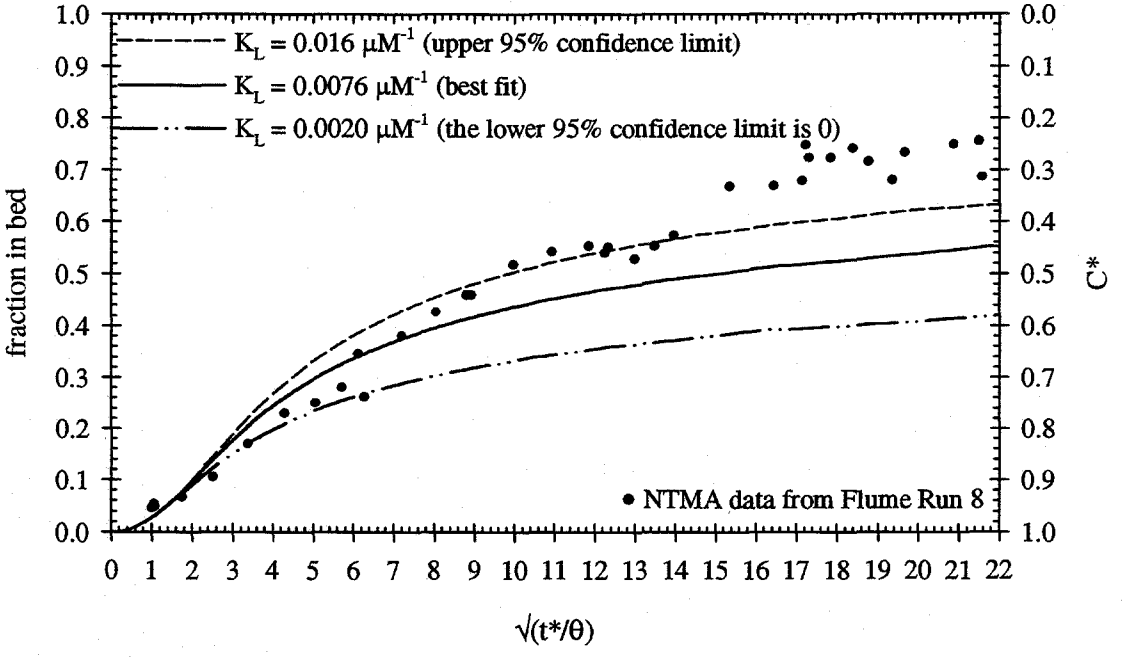

Figure 6.38. Sensitivity of the NTMA bed/stream exchange model for Flume Run 8 to the Langmuir adsorption constant K_L.

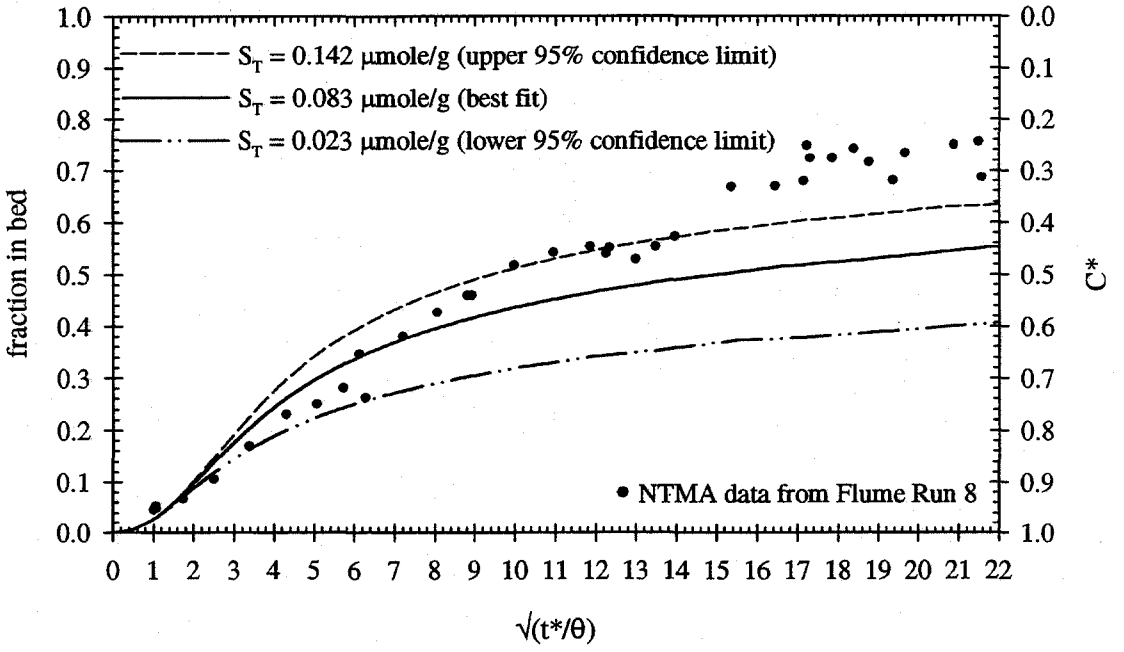

Figure 6.39. Sensitivity of the NTMA bed/stream exchange model for Flume Run 8 to the Langmuir adsorption constant S_T.

6.8.5. Sensitivity to OTMA sorption parameters

The 95 percent confidence limits of K_L and S_T for the OTMA Langmuir fit are ±35 and ±7 percent of the best-fit values, respectively. The sensitivity of the OTMA model simulations for Flume Run 9 is illustrated in Figure 6.40 and Figure 6.41. The model predictions are not significantly affected by the changes in K_L and S_T.

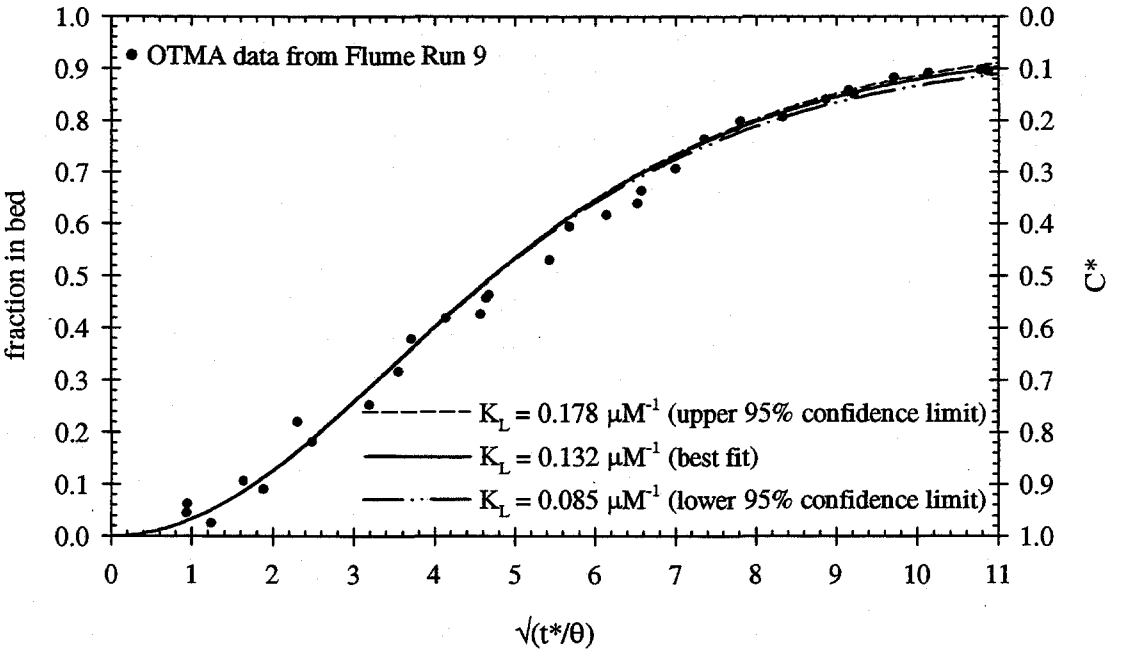

Figure 6.40. Sensitivity of the OTMA bed/stream exchange model for Flume Run 9 to the Langmuir adsorption constant K_L.

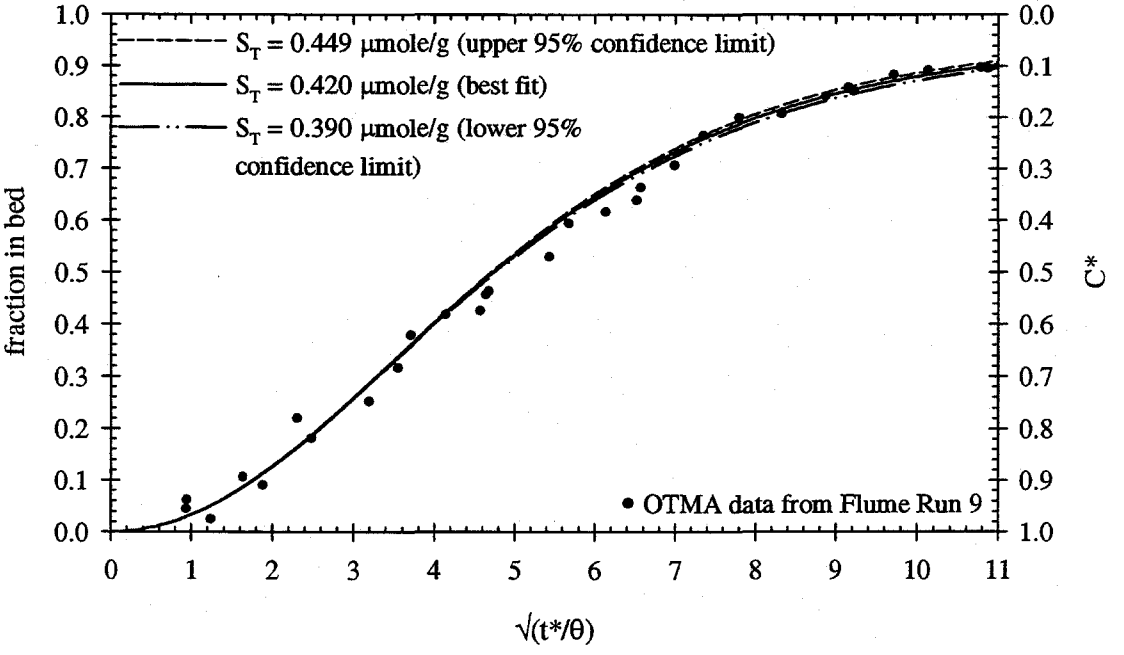

Figure 6.41. Sensitivity of the OTMA bed/stream exchange model for Flume Run 9 to the Langmuir adsorption constant S_T.

6.9. EFFECT OF ISOTHERM TYPE

Four nonlinear isotherm equations – Langmuir, Freundlich, Tóth, Langmuir-Freundlich – were fit the batch adsorption data for lithium and the cationic surfactants (Chapter 5, Section 5.1). The Langmuir isotherm was used in the model simulations to minimize the computation time (Chapter 3, Section 3.4.3); and furthermore, the Langmuir isotherm fit the data as well or better than the other isotherms. In this section, it is demonstrated that the isotherm type does not significantly affect the exchange model predictions for the flume experiments.

The lithium concentrations observed in the flume experiments were between 20 and 100 μM. The isotherms having the best to worst fit are Langmuir > Tóth > Langmuir-Freundlich > Freundlich. The Langmuir, Tóth and Langmuir-Freundlich isotherm fits fall on the same line when the aqueous concentration is between 20 and 100 μM, and therefore their lithium exchange model simulations for the flume runs do not differ. Figure 6.42 compares the lithium exchange model predictions using the Langmuir and Freundlich isotherms to the data from Flume Run 2. The Freundlich exchange model does not differ from the Langmuir model.

The DTMA concentrations in Flume Run 2 are between 20 and 200 μM. In this concentration range, the Tóth and Langmuir-Freundlich isotherm fits are the same. The ranking of the isotherm fits based on the degree of freedom adjusted R^2 is Freundlich > Tóth > Langmuir-Freundlich > Langmuir. For Flume Run 2, Figure 6.43 illustrates that the bed exchange models based on the different adsorption isotherms are not substantially different.

The Tóth and Langmuir-Freundlich isotherm fits for MTMA coincide for the aqueous concentration range observed in the batch adsorption experiments. The isotherms from best to worst fit are Tóth = Langmuir-Freundlich > Langmuir > Freundlich. For Flume Run 3, the isotherm type does not significantly affect the exchange model predictions (see Figure 6.44).

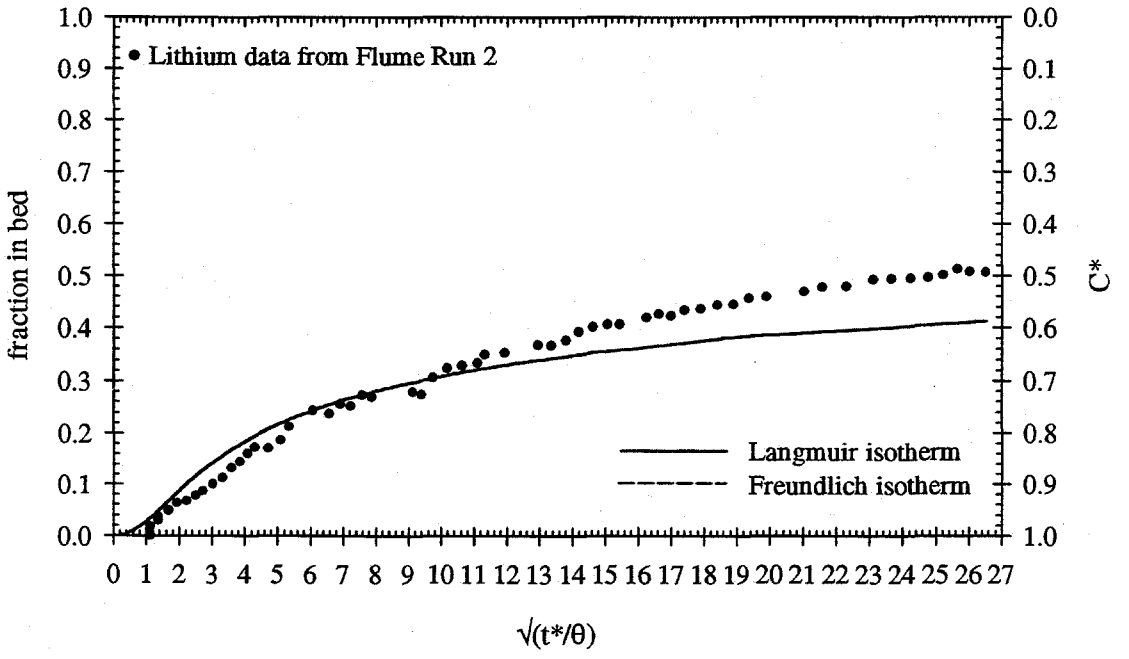

Figure 6.42. Effect of isotherm type on the bed/stream exchange model predictions for lithium in Flume Run 2.

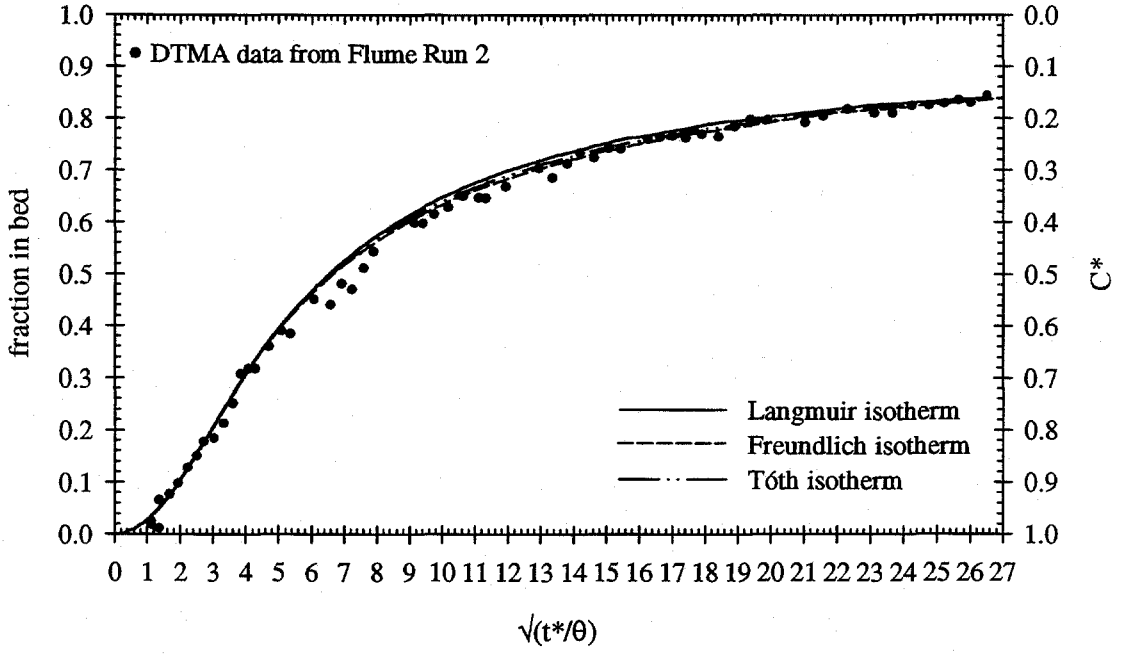

Figure 6.43. Effect of isotherm type on the bed/stream exchange model predictions for DTMA in Flume Run 2.

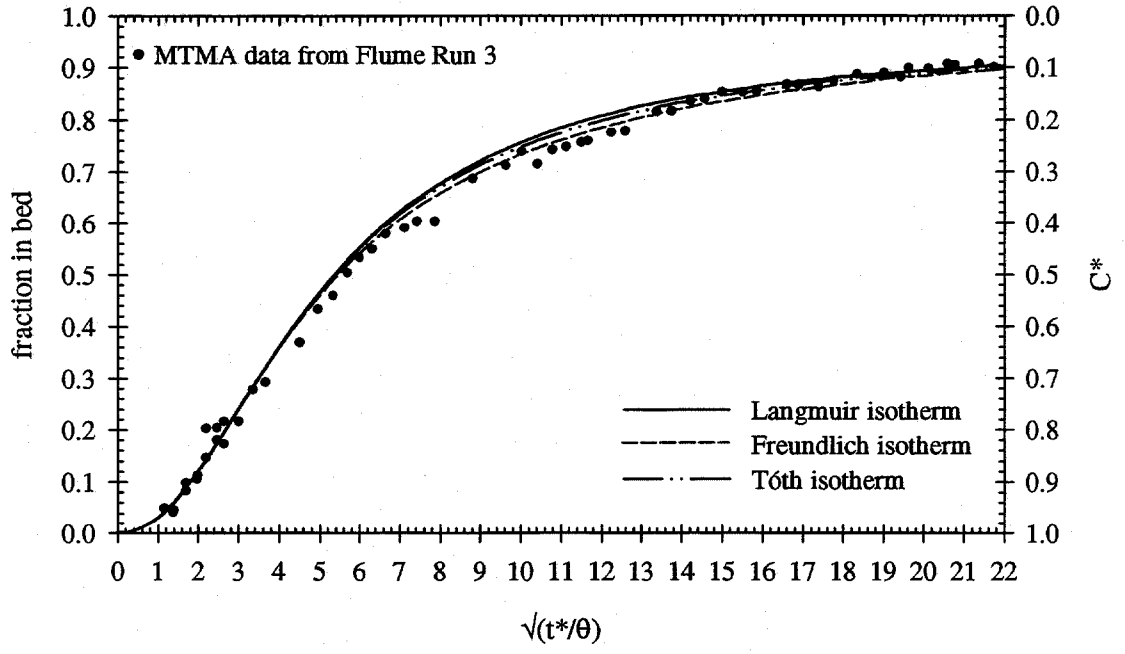

Figure 6.44. Effect of isotherm type on the bed/stream exchange model predictions for MTMA in Flume Run 3.

The Langmuir and Freundlich isotherm fits for NTMA adsorption on the garnet sand are essentially the same for aqueous concentrations greater than 30 μM. The Tóth and Langmuir-Freundlich fits coincide with the Langmuir fit. The Freundlich fit the data slightly better than the Langmuir isotherm, but both isotherms have an R^2 on the order of 0.4. Since the NTMA concentrations in Flume Run 8 are between 20 and 100 μM, the exchange model simulations using the Langmuir and Freundlich isotherms are almost the same (see Figure 6.45).

The order of the isotherm fits for OTMA adsorption on garnet from best to worst is Langmuir > Tóth = Langmuir-Freundlich > Freundlich. The Langmuir, Tóth and Langmuir-Freundlich isotherms coincide throughout the aqueous concentration range observed in the batch adsorption and flume experiments, and therefore their bed exchange model predictions do not differ. The Freundlich isotherm is significantly different from the Langmuir isotherm. However, this difference does not substantially affect the exchange model simulations for Flume Run 9 (Figure 6.46).

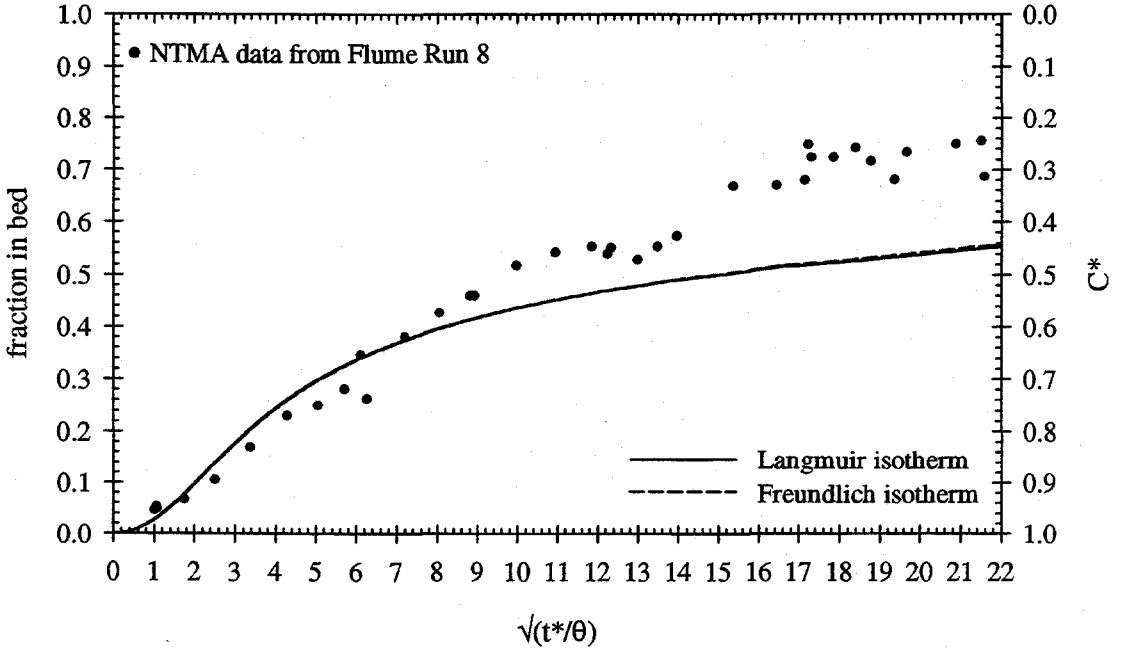

Figure 6.45. Effect of isotherm type on the bed/stream exchange model predictions for NTMA in Flume Run 8.

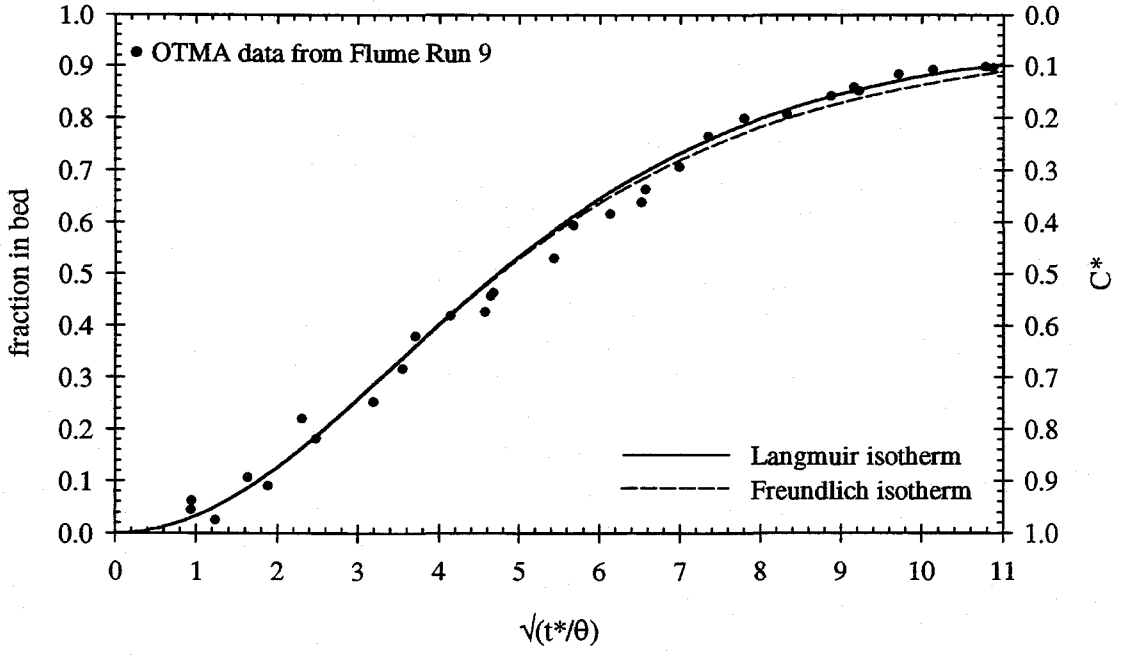

Figure 6.46. Effect of isotherm type on the bed/stream exchange model predictions for OTMA in Flume Run 9.

6.10. APPLICABILITY OF THE MODEL USING THE WELL-MIXED APPROXIMATION

Because of the computational rigor of the detailed exchange model for nonlinearly adsorbing compounds, it would be too costly to include the model into a larger river transport model. Therefore, a simpler approximate model for the bed/stream exchange has been developed. The model is based on the assumption that the bed is well-mixed down to a certain depth with the overlying water column. The details of the model are presented in Chapter 3, Section 5.5. The well-mixed model is applicable in situations where 1) the sediment bed is initially uncontaminated and 2) the concentration in the stream water changes gradually. The computation time of the well-mixed model is on the order of one to two minutes whereas the time required for the detailed model with Langmuir adsorption is one to two hours on a PC with a Pentium processor.

The simulations of the well-mixed model are compared to the surfactant data and detailed model predictions for Flume Runs 2, 3, 4, and 9 in Figure 6.47, Figure 6.48, Figure 6.49 and Figure 6.50, respectively. The well-mixed model slightly under-predicts the mass transport into the bed. The maximum difference in C* is 0.08. The well-mixed and detailed models agree when $t^*/\theta < 1$. Then the difference between the models increases while $dC^*/d(t^*/\theta)$ increases. When C* changes gradually with time, the magnitude of the difference between the models decreases. The error of the well-mixed model is smallest in Flume Run 4 because the change in C* is more gradual than in the other flume runs. The largest error occurs in the well-mixed model for OTMA in Flume Run 9 because the change of C* with time is more drastic than in the other flume runs.

The well-mixed model is best suited to estimate the mass exchange of nonlinearly adsorbing compounds at long times. However, the savings in the computation time may offset the error of the well-mixed model earlier in the experiment.

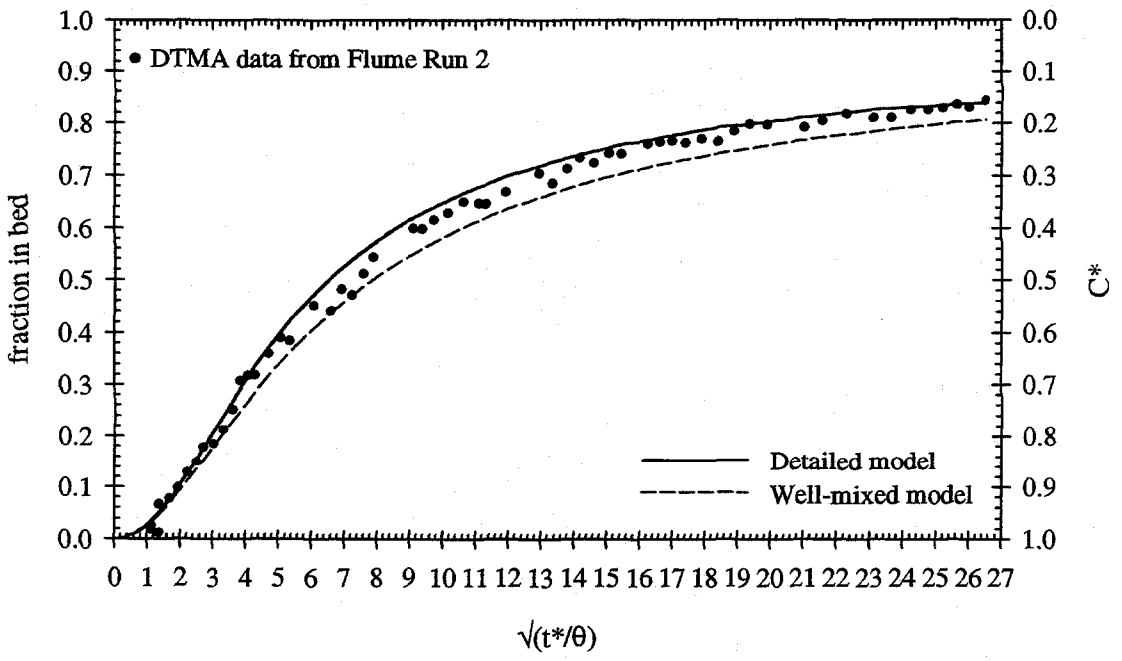

Figure 6.47. Comparison of the well-mixed and detailed bed/stream exchange models for DTMA in Flume Run 2.

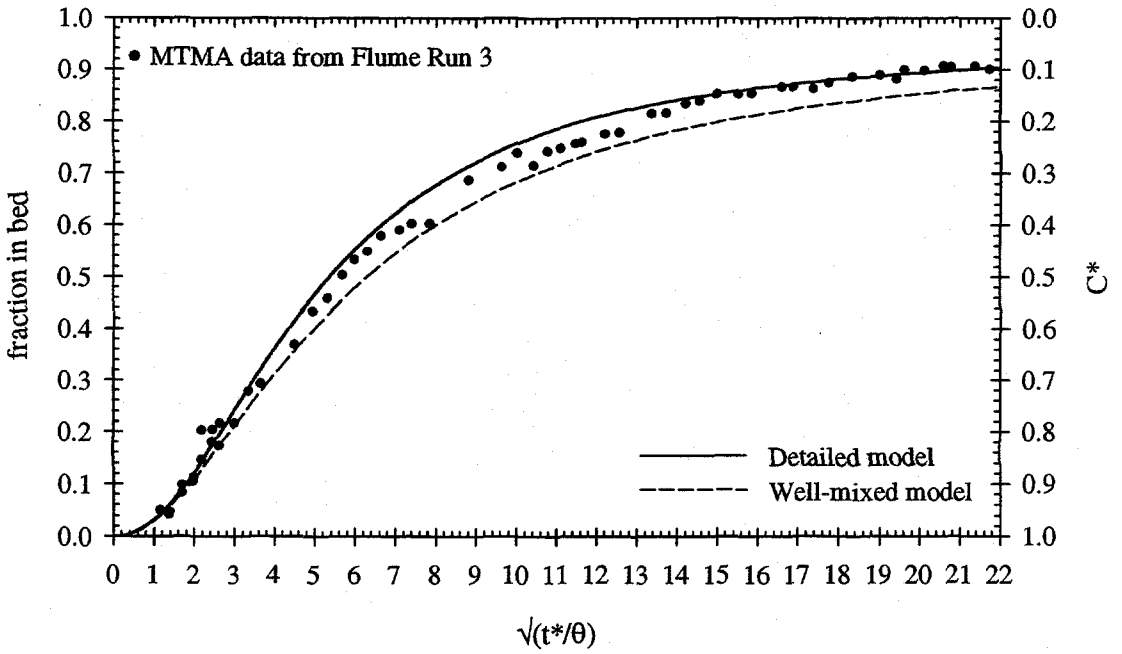

Figure 6.48. Comparison of the well-mixed and detailed bed/stream exchange models for MTMA in Flume Run 3.

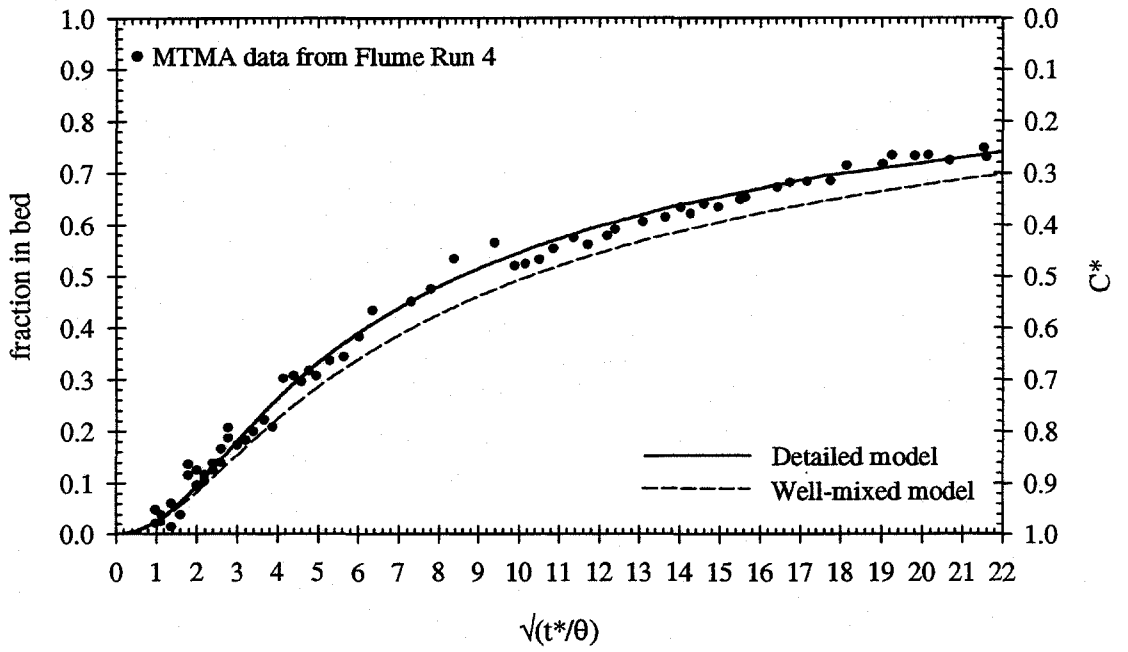

Figure 6.49. Comparison of the well-mixed and detailed bed/stream exchange models for MTMA in Flume Run 4.

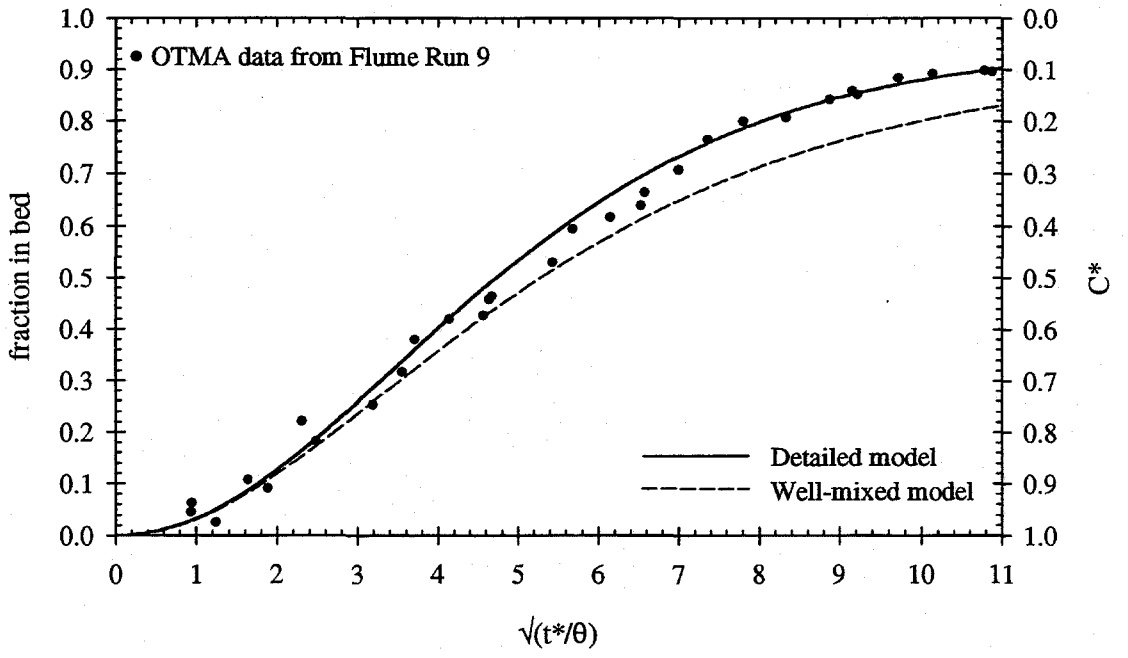

Figure 6.50. Comparison of the well-mixed and detailed bed/stream exchange models for OTMA in Flume Run 9.

6.11. APPLICABILITY OF COMPLETE CAPTURE MODEL

At small times, almost all of the chemical which enters the bed remains in the bed. This process is referred to as complete capture. The complete capture model is presented in Chapter 3, Section 5.6. The detailed model and complete capture model simulations are compared to the flume data from Runs 2, 3 and 9 in Figure 6.51, Figure 6.52 and Figure 6.53, respectively. The effective retardation coefficients R_{eff} associated with the initial concentration C_0 are 5, 6 and 11 for Flume Runs 2, 3 and 9, respectively. The complete capture model describes the mass transfer to the bed for $t^*/\theta < R_{eff}(C_0)$.

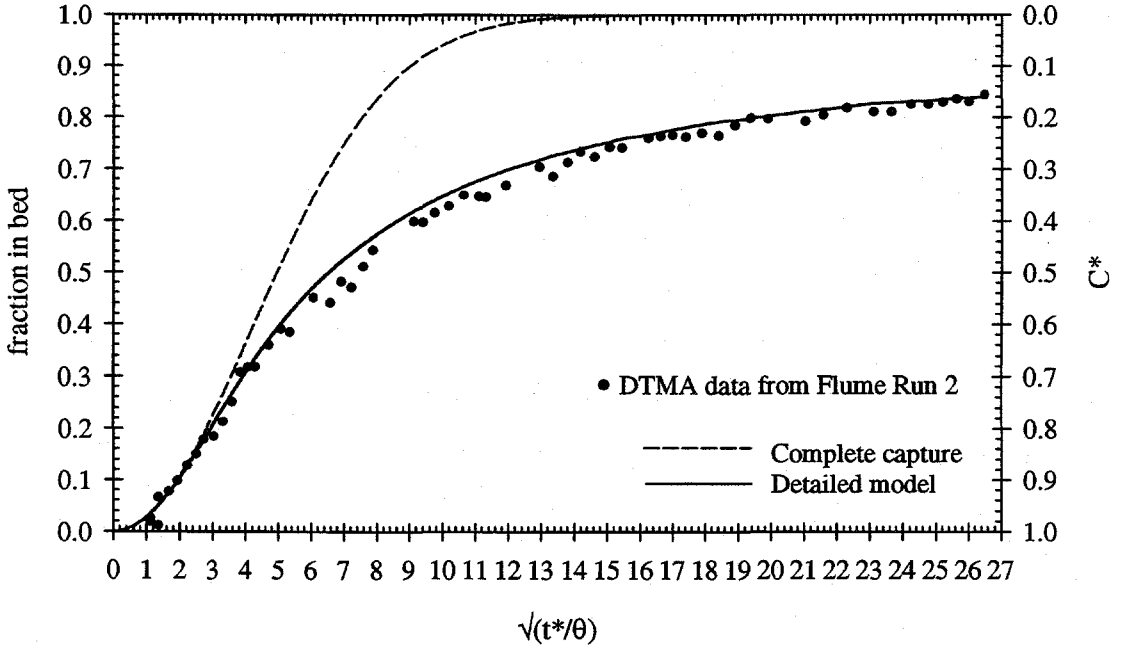

Figure 6.51. Comparison of the complete capture and detailed bed/stream exchange models for DTMA in Flume Run 2 with $R_{eff}(C_0) = 5$.

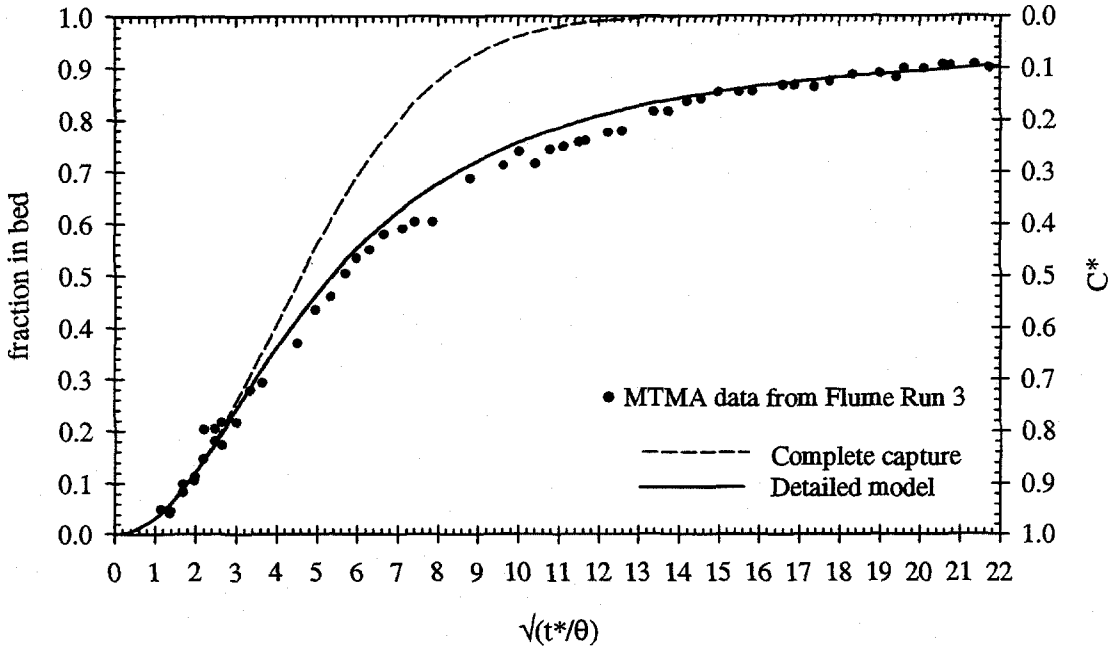

Figure 6.52. Comparison of the complete capture and detailed bed/stream exchange models for MTMA in Flume Run 3 with $R_{eff}(C_0) = 6$.

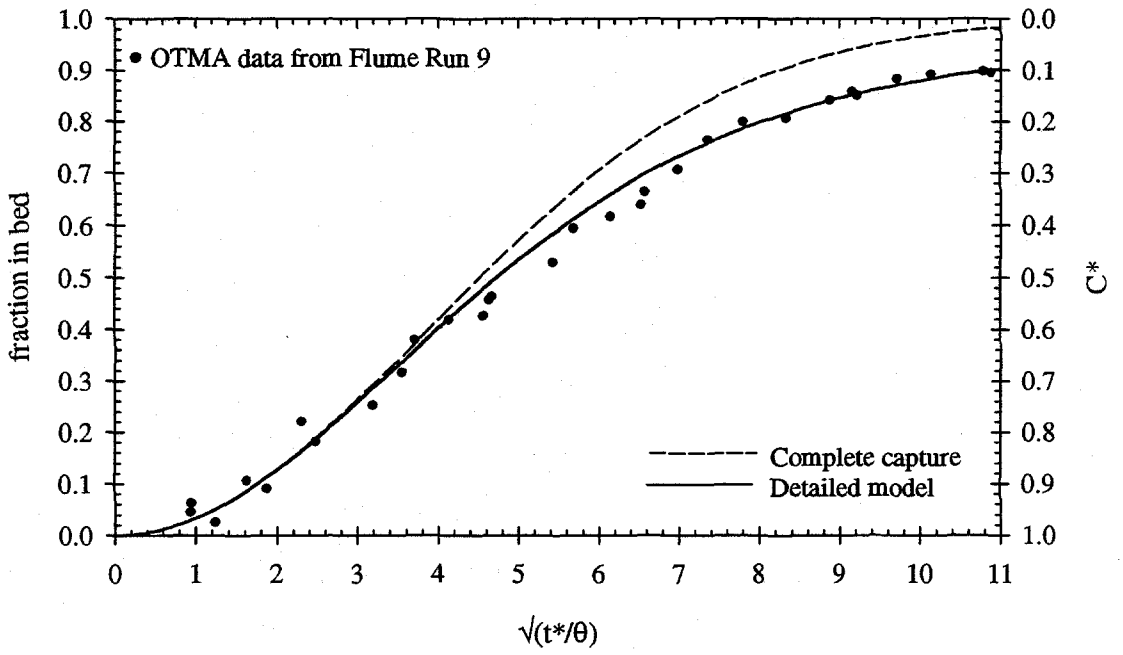

Figure 6.53. Comparison of the complete capture and detailed bed/stream exchange models for OTMA in Flume Run 9 with $R_{eff}(C_0) = 11$.

6.12. Model Application to Natural Streams

6.12.1. General discussion of the detailed exchange model application to natural streams

Although the flume experiments were performed under simplified conditions, the results give some insight into the relevance and magnitude of the mass exchange of nonlinearly adsorbing compounds by porewater advection in a natural stream. Considerably more exchange occurs with a bed covered with ripples and dunes than for a flat bed. The detailed bed/stream exchange model simulations for nonlinearly adsorbing pollutants can be calculated from the flow conditions (flow velocity and depth), bed characteristics (bedform size, bed hydraulic conductivity and porosity) and measured adsorption isotherms. An adsorption isotherm can be determined from batch adsorption experiments using the actual bed sediment as the adsorbent. The parameters can be determined directly and calibration should not be required, except to account for geometric irregularities and bed heterogeneities that are not included in the model. The rate of removal of a nonlinearly adsorbing pollutant to the bed by porewater advection can be calculated using the detailed model for known initial concentrations in the bed and prescribed stream concentration as a function of time. Then the removal rate of the pollutant by porewater advection can be compared to the values expected for other processes that occur in a natural stream.

The sensitivity analysis performed earlier in this chapter for the bed/stream model parameters in the flume system may not be representative of the sensitivity of the model to the same parameters in the field. The finite mass of solute in the flume system suppresses the range of deviations at long times, so the long-time sensitivity conclusions from the flume may not be completely true in the field. Furthermore, the type and extent of variability of the parameters differ from the laboratory to the field. The results of the bed/stream exchange study are most

relevant for determining the net mass exchange for small non-dimensional time, which may be on the order of days to weeks in a natural river, such as for chemical spills. Mass exchanges due to long-term changes in the stream parameters such as seasonal flow variations leading to changes in the morphology of the bed are expected to dominate the mass exchange caused by the bedforms.

For a stream with a wide rectangular channel that is well-mixed laterally and vertically, the transport of a non-volatile contaminant is modeled using the following one-dimensional longitudinal advection-dispersion equation:

$$\frac{\partial C}{\partial t} + U\frac{\partial C}{\partial x} = E\frac{\partial^2 C}{\partial x^2} - \frac{1}{d}\left(F_{b,in} - F_{b,out}\right) - \text{Chemical transformations} \qquad (6.4)$$

where U is the average velocity in the stream channel, E is the longitudinal dispersion coefficient, d is the water depth, and $F_{b,in}$ and $F_{b,out}$ are the fluxes of the contaminant into and out of the bed, respectively. "Chemical transformations" refer to in situ rate of loss of the chemical per unit volume and time; for linear processes, the simplest expression would be $-\kappa C$ where κ is the decay constant.

When the streambed is initially uncontaminated and there is a step increase in the pollutant concentration from zero to C_0 in the stream, the bed/stream exchange of a nonlinearly adsorbing pollutant can be modeled using Eylers' (1994) exchange model based on linear adsorption, with the modified residence time function (Chapter 3, Section 3.3). This is the only special case where a nonlinearly adsorbing compound can be treated by the linear equation because of the sharp contaminant fronts and steady $C = C_0$ in the river at a given location (example in Figure 6.55). The value of the retardation coefficient used to determine the residence time function $\overline{R}_T$ equals the effective retardation coefficient, which is given in Equation (6.2), evaluated at C_0. Eylers (1994) derived the following advection-dispersion equation, which incorporates the residence time function, that can be used to model the pollutant transport in a river with bed/stream exchange neglecting chemical transformations and losses through the air/water interface:

$$\frac{\partial C(x,t)}{\partial t} + U\frac{\partial C(x,t)}{\partial x} = E\frac{\partial^2 C(x,t)}{\partial x^2} - \frac{\bar{v}(0)}{d}C(x,t) + \frac{\bar{v}(0)}{d}\int_0^t \left(-\frac{d\bar{R}_T}{d\tau}\right) C(x,t-\tau)\,d\tau \qquad (6.5)$$

This differential equation has to be solved numerically to determine the value of the pollutant concentration in space and time.

6.12.2. Stream parameters for sample calculations

In Sections 6.12.3 through 6.12.5, the detailed and approximate models are used to simulate the bed/stream exchange in a small river. First, the conditions for which the approximate models (complete capture and well-mixed approximations) are valid are discussed, and sample calculations for simple cases of pollutant loading are performed. Then the importance of nonlinear adsorption effects is demonstrated in Section 6.12.5. The calculations and model simulations in the following sections are performed for a hypothetical small river with the hydraulic and bed parameters listed in Table 6.1.

6.12.3. Application of complete capture model to natural streams for small times

When a streambed is initially uncontaminated, the flux of the pollutant out of the bed is negligible for nonsorbing compounds when $t^*/\theta < 1$; for linearly adsorbing compounds when $t^*/\theta < R$; and for nonlinearly adsorbing compounds when $t^*/\theta < R_{eff}$. In the small river characterized in Table 6.1, complete capture of a nonsorbing solute entering the bed occurs at times less than 0.45 hours ($t^*/\theta < 1$). The time for which complete capture is valid increases proportionally with R and R_{eff}; for example, when R or R_{eff} for an adsorbing compound equals 10, the time of complete capture of influx extends to 4.5 hours.

Table 6.1. Hydraulic and bed parameters for a hypothetical small river.

Parameter	Symbol	Value
Stream water depth	d	50 cm
Flow velocity in the channel	U	40 cm/s
Bedform height	H	18 cm
Bedform wavelength	λ	100 cm
Bedform wavenumber	$k = 2\pi/\lambda$	0.063 cm^{-1}
Hydraulic conductivity in bed	K	0.2 cm/s
Porosity of sediment bed	θ	0.32
Particle density	ρ_s	2.65 g/cm^3
Amplitude of piezometric head	h_m	0.25 cm
Normalization factor for time	$\theta t/t^* = \theta/(k^2 K h_m)$	0.45 hr
Darcy velocity into the bed averaged over the bed surface	$\bar{v}(0) = \frac{kKh_m}{\pi}$	3.61 cm/hr

The bed exchange model based on complete capture in a closed system (similar to the laboratory flume setup) is presented in Chapter 3, Section 3.6. The model is extended to an open system in this section. The flux of a pollutant into the bed surface is given by

$$F_{b,in} = \bar{v}(0)C \tag{6.6}$$

and the accumulated mass transfer per unit area of the bed is

$$\frac{\text{mass}}{\text{area}} = \bar{v}(0)\int_0^t C(\tau)\,d\tau \tag{6.7}$$

With complete capture, the advection-dispersion equation for the pollutant in the river becomes

$$\frac{\partial C(x,t)}{\partial t} + U\frac{\partial C(x,t)}{\partial x} = E\frac{\partial^2 C(x,t)}{\partial x^2} - \frac{\bar{v}(0)}{d}C(x,t) \tag{6.8}$$

The complete capture of a pollutant in the bed is similar to a linear decay process.

For a finite initial pollutant pulse in a river (i.e., a toxic chemical spill), the solution to Equation (6.8) is

$$C(x,t) = \Phi(x,t)\exp\left(-\frac{\bar{v}(0)}{d}t\right) \tag{6.9}$$

where $\Phi(x,t)$ is the solution to the same problem without the mass transfer into the bed. This solution is independent of the adsorption behavior of the pollutant. For the sample river, the decay constant is 0.072 hr^{-1}. Since the bed/exchange with complete trapping is modeled as a linear decay process, the bed/stream exchange is easily incorporated into the larger pollutant fate-and-transport models. However, the maximum time for which the solution is valid is determined by the adsorption behavior. For the sample river, the transport of the pollutant can be described by Equation (6.9) for all x when $t < 0.45R_{eff}(C_0)$ where C_0 is the initial concentration of the pollutant ($t < 0.45R$ for linearly adsorbing compounds). Furthermore, the application of the complete capture model is limited to situations where the riverbed is initially uncontaminated. For longer times, complete trapping model can be used to give an upper bound on the mass transfer to the riverbed.

As a second case, consider a continuous source at x = 0 with $C(0,t) = C_0$. Neglecting longitudinal dispersion, Equation (6.8) reduces to

$$U\frac{\partial C(x)}{\partial x} = -\frac{\bar{v}(0)}{d}C(x) \tag{6.10}$$

with the solution

$$C(x) = C_0\exp\left(-\frac{\bar{v}(0)}{Ud}x\right) \tag{6.11}$$

For the example,

$$C(x) = C_0\exp(-0.050\,x) \tag{6.12}$$

for x in kilometers. Therefore, there is a 5 percent loss of contaminant per kilometer of the flow channel, or a drop to e^{-1} of the initial concentration 20 km downstream.

6.12.4. Application of the well-mixed model to natural streams

When the riverbed is initially uncontaminated, the mass transfer to the bed can be modeled by assuming that the bed, down to a certain depth, is well-mixed with the overlying water column. The mass transfer is modeled by assuming that a pollutant concentration front is driven down into the bed by pumping (Packman, 1997). The details of the model are included in Chapter 3, Section 3.5. The well-mixed model can be applied only when the riverbed is initially uncontaminated. The errors in the well-mixed model are minimized when the model is applied to situations where the pollutant concentration in the river water changes gradually.

The flux of the pollutant into the bed is given by

$$F_{b,in} = \bar{v}\left(d_q(t)\right) C(t) \tag{6.13}$$

where d_q is the depth of concentration front and $\bar{v}\left(d_q\right)$ is the average downward vertical velocity at d_q. The values of d_q and $\bar{v}\left(d_q\right)$ are determined by the adsorption behavior of the contaminants. The formulas for d_q, $\bar{v}\left(d_q\right)$, and the accumulated mass transfer into the bed are given for nonsorbing, linearly adsorbing and nonlinearly adsorbing compounds in Chapter 3, Sections 3.5.1, 3.5.2 and 3.5.3, respectively.

For a step increase in the pollutant concentration from zero to C_0 at t = 0, the mass exchange with the sediment bed is the same for linearly and nonlinearly adsorbing compounds that have the same "effective" retardation coefficients. In this case, the accumulated mass transfer into the bed is found from Equations (3.112) and (3.114) with $C(t) = C_0$ and $R = R_{eff}$ to be:

$$\frac{\text{mass}}{\text{area}} = \theta R_{eff}(C_0) C_0 \left[\frac{1}{k} \ln\left(1 + \frac{k^2 K h_m}{\pi R_{eff}(C_0)} \left(\frac{t}{\theta} \right) \right) \right] \tag{6.14}$$

where the term in [ ] represents d_q. With the well-mixed approximation to the bed/stream exchange, the advection-dispersion equation for pollutant transport in a river is

$$\frac{\partial C(x,t)}{\partial t} + U\frac{\partial C(x,t)}{\partial x} = E\frac{\partial^2 C(x,t)}{\partial x^2} - \frac{\overline{v}(d_q(t))}{d} C(x,t) \tag{6.15}$$

For the well-mixed model, there is an explicit formula relating the mass transfer and time, whereas the residence time function in Eylers' model is solved using an implicit equation (Chapter 3, Section 3.3). Therefore, the well-mixed model is not as computationally rigorous and can be more easily incorporated into the larger river transport models than the residence time model.

The model simulations from the complete capture model, the well-mixed model and Eylers' residence time model are compared in Figure 6.54 for the small river described in Table 6.1 with a step increase in the pollutant concentration from zero to C_0 (R_{eff} = 10) at t = 0 and with an initially uncontaminated bed. The model simulations span 2.7 days (64 hours). The parameter m, which is the accumulated mass transfer per unit plan area of the bed divided by C_0, is plotted against the square root of time in hours. After 64 hours, the riverbed is contaminated to a depth equal to the bedform wavelength (100 cm). For the well-mixed model, the parameter m is equivalent to d_q. The well-mixed model underestimates the mass transfer into the bed for t > 4 hours. The error in m for the well-mixed model is about 13 percent. The error in m decreases when R_{eff} decreases and increases when R_{eff} is larger.

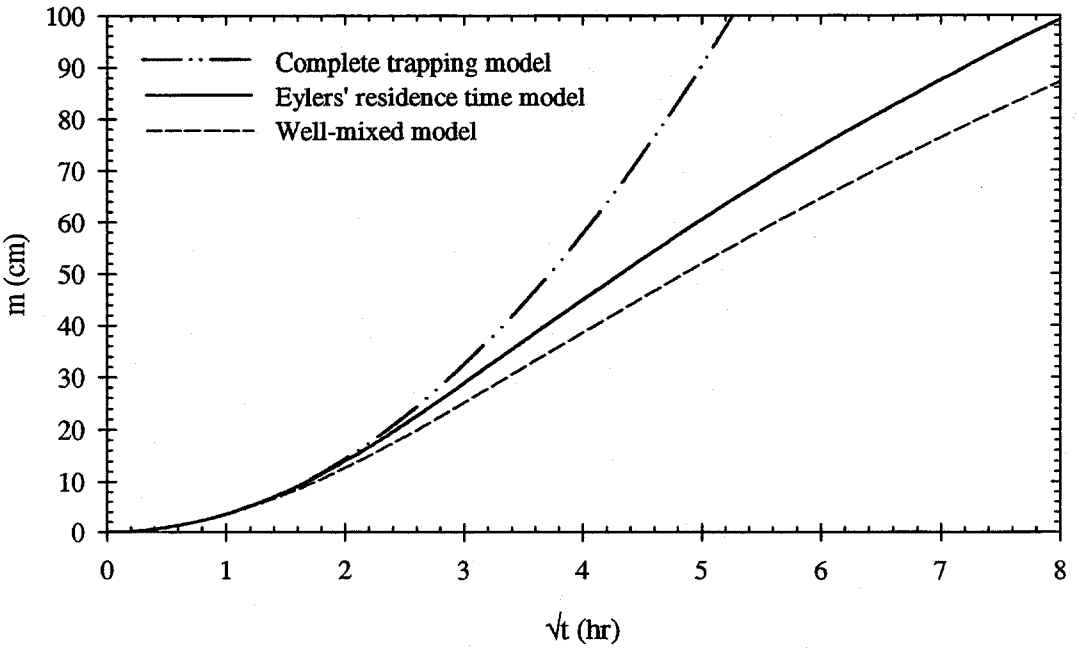

Figure 6.54. Comparison of the complete trapping model, Eylers' residence time model and the well-mixed model for the mass transfer of a nonlinearly adsorbing pollutant with $R_{eff}(C_0) = 10$ after a step increase in the pollutant concentration.

6.12.5. Importance of nonlinear adsorption effects in a natural river

One important aspect of this thesis is that the conditions for which nonlinearly adsorption effects become important have been identified. Nonlinear adsorption effects are important 1) when the sediment bed is already contaminated and 2) when the pollutant concentration in the overlying water fluctuates. The importance of nonlinear adsorption effects is demonstrated for the case of a chemical spill. For the small river described in Table 6.1, the pollutant concentration jumps from zero to C_0 at t = 0 and then drops back to zero at time T. Figure 6.55 shows a comparison of the calculated values of m (the accumulated mass transfer to the bed divided by C_0) for the detailed bed/stream exchange models based on linear and Langmuir adsorption isotherms at two different pulse durations (T = 1 hour and T = 12 hours). The DTMA Langmuir adsorption parameters from Chapter 5, Table 5.4 are used, and the initial concentration

C_0 is 100 μM. The retardation coefficient used in the linear adsorption model is $R_{eff}(C_0)$, which equals 9.2. Figure 6.55 shows that the bed is contaminated to a depth of 3.6 cm for the 1-hour spill and 36 cm for the 12-hour spill. Therefore, the mass transfer to the bed can be considerable, even for chemical spills that last for short time periods.

For nonlinear isotherms that are convex upward, the nonlinear adsorption reactions prolong the recovery time of the river because small pollutant concentrations are highly retarded in the bed. For both spills in Figure 6.55, the ratio $m_{Langmuir}/m_{linear}$ is greater than 2.5 after 10 days. The exchange model based on the linear adsorption assumption under-estimates the recovery time for the riverbed after a chemical spill of a nonlinearly adsorbing pollutant.

The predicted release of the pollutant from the bed differs with the choice of isotherm (Chapter 3, Figure 3.11). Since the Freundlich and Langmuir-Freundlich isotherms have retardations approaching infinity as the aqueous concentration approaches zero, the corresponding exchange models predict infinitely long recovery times. Caution should be exercised when applying these isotherms to situations where small concentrations are modeled.

a) DTMA pulse duration of 1 hour (different scale for m)

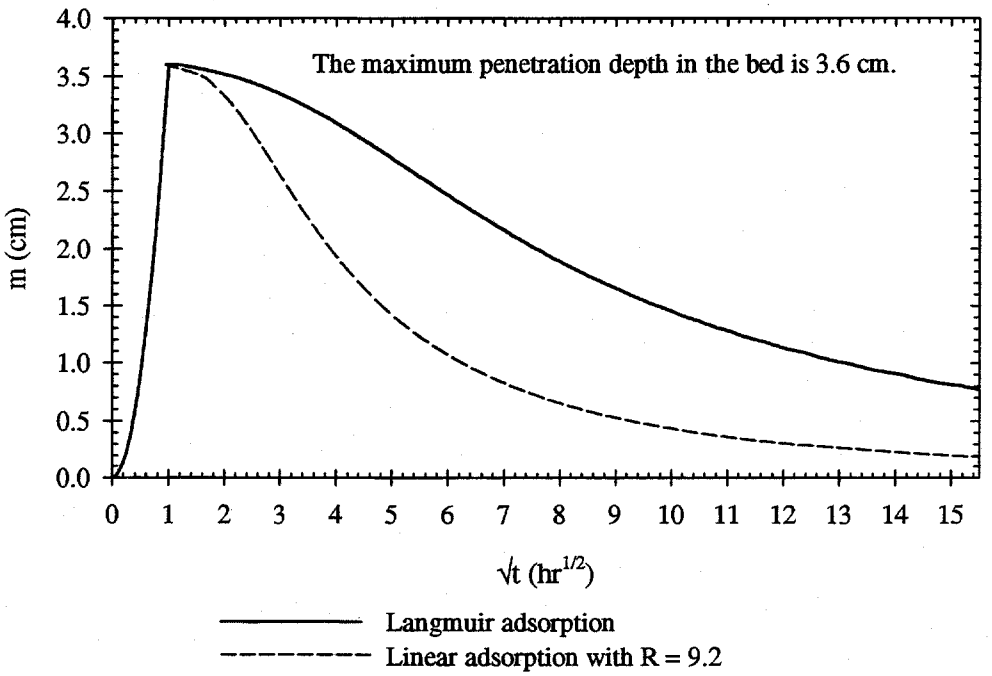

b) DTMA pulse duration of 12 hours

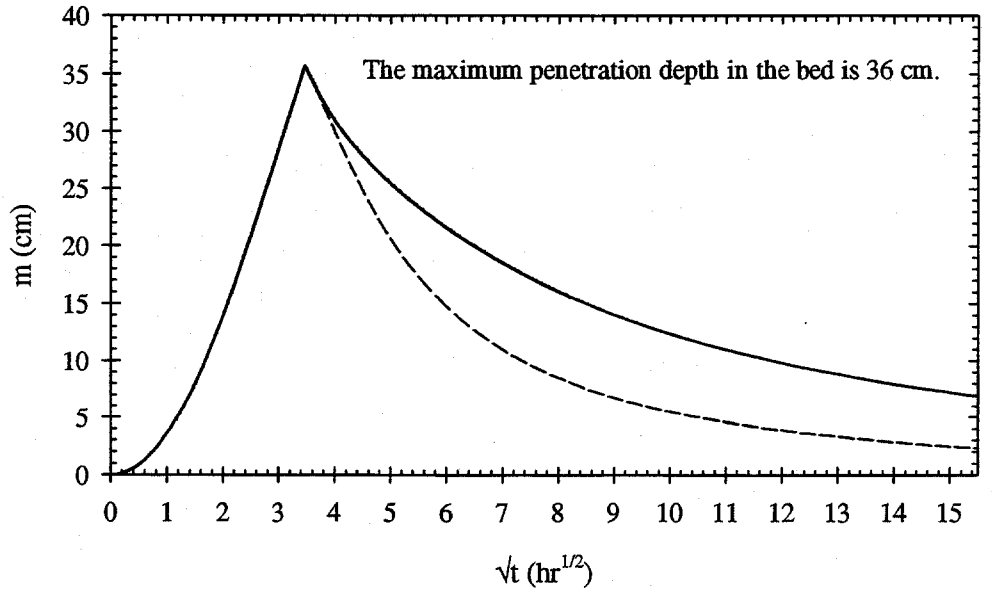

Figure 6.55. Comparison of the predicted recovery time from a chemical spill in a small river for linearly and nonlinearly adsorbing compounds (note different scales for m). The curves are identical on the rising limb.

7. SUMMARY AND CONCLUSIONS

The objective of this thesis was to develop a model that predicts the exchange, due to porewater advection (i.e., pumping), of nonlinearly adsorbing compounds between stream water and a sediment bed covered with stationary bedforms. The mass exchange of the compounds was observed in flume experiments. Batch adsorption experiments were conducted to measure the adsorption coefficients used in the nonlinear isotherms that were incorporated into the pumping model. The exchange results of the flume experiments were used to test the model. This chapter summarizes the experiments and model results in Sections 7.1, 7.2, and 7.3. Suggestions for future research are given in Section 7.4 and the main conclusions follow in Section 7.5.

7.1. SUMMARY OF EXPERIMENTS

Batch and flume experiments were performed using bromide, lithium and four cationic surfactants having hydrocarbon chain lengths of 9 (NTMA), 12 (DTMA), 14 (MTMA) and 18 (OTMA) (Chapter 4, Table 4.2). Garnet sand was used as the model sediment. The properties of the sand are summarized in Chapter 4, Table 4.1. The garnet sand is a mixture of minerals that have high iron, aluminum and silica contents, and more closely resembles natural sediments than the quartz sand used in the previous exchange studies by Elliott (1990), Elliott and Brooks (1997b), Eylers (1994) and Packman (1997).

7.1.1. Batch adsorption experiments

Bromide did not exhibit adsorption to the garnet sand and was therefore used as a conservative (i.e., non-reactive) tracer in the flume experiments. In previous studies at Caltech, lithium was used as the conservative tracer in the bed/stream exchange experiments with quartz sand. However, lithium was not a suitable conservative tracer in this work because the ion adsorbed onto the garnet sand ($R_{eff} \sim 1.5$).

The adsorption of the cationic surfactants on the garnet sand increased with hydrocarbon chain length and with pH; and adsorption decreased with an increase in the ionic strength. Adsorption occurs primarily through hydrophobic and electrostatic interactions. The data indicate that hemi-micelles do not form on the garnet sand surface.

The adsorption isotherms for the cationic surfactants were nonlinear and convex upward. The Langmuir, Freundlich, Tóth and Langmuir-Freundlich isotherm fits to the same adsorption data did not significantly differ in the concentration ranges observed in the flume experiments.

The adsorption data exhibit a considerable amount of scatter for all of the compounds studied. The batch adsorption data for the surfactants are plotted with error bars in Appendix B. The sorbed concentrations are determined by the mass depletion method, which can carry significant errors over to the sorbed concentration calculations when the difference between the initial and final concentrations of the solution is small (see Chapter 5, Section 5.1). The garnet sand experiences mechanical abrasion during the batch adsorption experiments. The production of fines may affect the extent of adsorption and introduce more error into the adsorption data. The error associated with the NTMA aqueous concentration measurements is large (~10 to 50 percent) because NTMA does not form a one-to-one complex with the anionic Orange II dye. Thus, the Orange II dye extraction method is less sensitive for NTMA.

7.1.2. Flume experiments

The exchange of the compounds between the overlying water column and sediment bed was studied in a 5-meter-long tilting recirculating flume. The typical water depth was 6.5 cm with an average flow velocity of 17 cm/s and a bed depth of 23 cm. The net mass transfer to the bed was determined by measuring the depletion of the compound in the overlying water column as the contaminated flume water mixed with the clean porewater displaced from the bed. Porewater concentration profiles were acquired to monitor the penetration depth of the compounds in the bed. Nine experiments were conducted with naturally-created bedforms, and one experiment was conducted with a flat bed to assess the effect of the bedforms on the bed/stream exchange. The bedforms were irregular and exhibited a distribution of heights (0.5 to 2.5 cm) and wavelengths (5 to 40 cm). The bedforms were stationary in all but three of the runs in which the bedforms propagated slowly down the flume (0.04 to 0.1 cm/min). The duration of the exchange experiments in the flume varied from 3 to 8 days (not including preparation and analysis time).

7.2. FLUME EXPERIMENT RESULTS AND MODEL COMPARISONS

7.2.1. Detailed model for the exchange of nonlinearly adsorbing compounds

A new model was developed to predict the exchange of nonlinearly adsorbing compounds between stream water and a sediment bed covered with stationary bedforms. The exchange model solves the advection equation for the transport of nonlinearly adsorbing compounds through a series of streamtubes in the sediment bed and then calculates the resulting flux of the compound into and out of the bed surface. The model neglects of effects of pore-scale

dispersion. Porewater advection defines the surface flux and flow field within the bed. The model can be used to model the exchange with both clean and contaminated beds with arbitrary pollutant loadings in the overlying water column. For contaminated beds, an estimate of the initial distribution of the contaminant concentration within the bed must be input into the model. The application of the model is restricted to compounds with nonlinear isotherms that are convex upward, which is the usual case. All of the parameters used in the model are based on measurable physical and chemical quantities, which do not require calibration.

The sorption parameters used in the model are determined from isotherm equations fitted to the equilibrium batch adsorption data. Equilibrium nonlinear adsorption is modeled using the Langmuir, Freundlich, Langmuir-Freundlich and Tóth isotherm equations. These isotherms are used strictly to provide a mathematical relation to describe the nonlinear adsorption for modeling purposes. The isotherms are not used to define adsorption mechanisms.

The hydraulic and bed parameters used in the model are: the amplitude of the piezometric head variation over the bedform (h_m), the average flow velocity in the channel (U), the depth of the water column (d), the effective water depth (d'), the hydraulic conductivity (K), the porosity of the sediment bed (θ), the average bedform height (H) and the average bedform wavelength (λ). All of these parameters except h_m are measured directly. The value of h_m is estimated using the empirical relation given in Equation (3.3).

7.2.2. Comparison of model simulations to exchange in the flume

The detailed bed/stream exchange model for nonlinearly adsorbing compounds agreed well with the observed mass transfer of the cationic surfactants for seven of the nine flume experiments with bedforms. The maximum difference in the predictions of C* (the ratio of the pollutant concentration in the flume water and the initial concentration C_0) was 0.06 which corresponds to a maximum of 15 μM. The error in the predicted value of C* reduced to less than

0.02 when a correction factor α_c was applied to h_m for each flume experiment, with α_c ranging from 1 to 2. In general, the observed partitioning of the contaminants to the sediment in the flume experiments agreed with the batch adsorption results. Therefore, batch adsorption experiments are useful tools in predicting the exchange of pollutants with riverbeds.

In one flume experiment where the model predictions were significantly different from the flume data ($\Delta C^* \sim 0.18$), the bedforms propagated down the flume at a velocity (0.1 cm/min), fast enough to reducing the pumping exchange; consequently, the model over-predicted the mass transfer of the surfactant into the bed. For the flume experiment with NTMA, the model under-predicted the mass transfer to the bed; the maximum difference between the predicted and observed values of C^* was 0.25. The deviation between the model and the data probably resulted from errors due to the high uncertainty associated with the adsorption parameters used in the model and the errors in the NTMA concentration measurements for the flume water.

The model simulations for the flume experiments are not significantly affected by the use of different nonlinear adsorption isotherms because the isotherm equation representations of the adsorption data do not differ significantly in the range of concentrations observed in the flume experiments. However, the isotherms are considerably different for smaller concentrations (< 10 μM). This difference would be reflected in the exchange simulations for smaller concentrations.

For similar hydraulic and bed parameters, chemical conditions (pH and ionic strength) and initial surfactant concentrations, the mass of the cationic surfactant retained in the bed increased with the hydrocarbon chain length, which agrees with the batch adsorption results. In general, the stronger the adsorption of the compound to the sediment, the larger the mass of pollutant that can be stored in the sediment bed. Because of the partitioning, the penetration depth of adsorbing compounds in the bed is less than the nonsorbing compound at that time.

7.2.3. Comparison to the exchange with a flat bed

The mass transfer of both nonsorbing and nonlinearly adsorbing compounds into a bed covered with stationary bedforms is much greater than the transfer into a flat bed. The bromide exchange with the flat bed can be modeled by a diffusion process with an effective diffusion coefficient of 4.0×10^{-5} cm^2/s. The exchange mechanisms associated with the flat bed are believed to be a combination of molecular diffusion and dispersion due to small porewater flows induced by turbulent pressure fluctuations on the bed surface.

7.2.4. Approximate exchange models

The detailed model for the exchange of nonlinearly adsorbing compounds is computationally intensive, and it would not be practical to incorporate it into a larger river transport model. Therefore, simpler, approximate models were developed.

At small times in the flume experiments, almost all of the pollutant that entered the bed remained in the bed. Therefore, the bed/stream exchange could be modeled assuming complete capture (Chapter 3, Section 3.6). This approximation is valid when $t^*/\theta < R_{eff}(C_0)$, where t^* is non-dimensional time and R_{eff} is the effective retardation coefficient defined by Equation (3.119).

An approximate model based on a well-mixed assumption was developed in Chapter 3, Section 3.5. The model assumes that the overlying water column is well-mixed down to a certain depth with the porewater in the bed. This approach was proposed by Packman (1997). The well-mixed model under-predicted the mass exchange of cationic surfactants in the flume experiments. The maximum difference in C^* between the well-mixed and detailed exchange models was 0.08. The magnitude of the error increased with the strength of adsorption.

Simulations from Eylers' exchange model for linearly adsorbing compounds were compared to the observed mass exchange of the cationic surfactants in the flume experiments.

The linear adsorption model could be used to estimate the lower and upper bounds of the mass exchange of nonlinearly adsorbing compounds in the flume by using the minimum and maximum values of the effective retardation coefficient R_{eff} calculated using the initial and final concentrations of the surfactants in the flume water.

7.3. MODEL APPLICATIONS

7.3.1. Sensitivity analysis at the flume scale

Because of the large number of variables in the exchange model and the time required for each flume experiment (13-20 days including preparation and analysis time), it was not possible to conduct flume experiments that spanned the full range of hydraulic and bed parameters for all of the cationic surfactants. Therefore, sensitivity analyses for the various parameters were performed primarily by model simulations.

7.3.1.1. Sensitivity to hydraulic parameters

The bed/stream exchange in the flume system is sensitive to the hydraulic and bed parameters. The amplitude of the piezometric head h_m affects the rate of mass transfer into and out of the bed. Larger values of h_m generate faster porewater velocities, which in turn increase the rate of mass transfer into the bed. The magnitude of h_m is controlled by the flow velocity U, the bedform height H and the water depth d; h_m is proportional to U^2, $H^{3/8}$ and $d^{-3/8}$ (Equation 3.3).

In the flume system, when the water depth d increases, the effective water depth d' also increases. For the same initial contaminant concentration C_0, when d' increases, the total mass of the compound in the flume increases, and thus the same mass transfer to the bed causes a smaller decrease in the concentration of the compound in the overlying water column. However, at long

times, the total mass of the compound retained in the bed is greater for deeper water columns because the total mass available for the exchange (C_0d') is larger.

The bedform wavelength does not affect the amplitude of the piezometric head. However, for the same hydraulic conditions and bedform height, a longer bedform has the same piezometric head disturbance applied over a greater distance. The porewater velocity is inversely proportional to the bedform wavelength. Hence, longer bedforms result in lower porewater velocities, which reduce the rate of mass transfer, but the compounds are pumped deeper into the bed. The pumping exchange of nonsorbing and weakly adsorbing compounds with the sediment bed is controlled at large time by bedforms having long wavelengths. The exchange of strongly adsorbing compounds is dominated by the shorter bedforms.

7.3.1.2. Sensitivity to adsorption isotherm parameters

Since the model simulations for the flume experiments did not significantly differ for the different isotherms and the computation time was minimized when the Langmuir adsorption isotherm was used, most of the exchange model simulations were based on the Langmuir isotherm. The sensitivity of the exchange model predictions to the errors associated with the Langmuir sorption parameters K_L and S_T was studied using the 95 percent confidence limits of the best-fit values. The 95 percent confidence limits were within 50 percent of the best-fit values of K_L and S_T for DTMA, MTMA and OTMA and 110 percent of the best-fit values for NTMA. The model simulations for the flume experiments with DTMA, MTMA and OTMA were not sensitive to the changes in the Langmuir sorption parameters. However, the simulations of the exchange of NTMA using the 95 percent limits of the sorption parameters were drastically different.

7.3.2. Application to natural streams

The exchange models developed in this thesis were applied to a hypothetical natural stream in Chapter 6, Section 6.12, with numerical examples. Since the model variables are based on physical and chemical parameters that can be measured directly, the exchange models can be applied to different river systems. In general, the effects of changes in the various model parameters follow the same trends that were illustrated in the sensitivity analyses for the flume experiments. However, since the finite mass in the flume suppresses the range of deviations at long times, the long-time sensitivity conclusions from the flume may not be completely true in the field.

The complete capture and well-mixed approximate exchange models can be applied to natural streams when the streambed is initially uncontaminated. The bed/stream exchange with complete capture can be modeled as a linear decay process. The well-mixed model can be used when there is a step increase in the pollutant concentration in the river water, which either remains constant or varies gradually over time.

Nonlinear adsorption effects become important in natural streams when the streambed is initially contaminated or when the pollutant concentration in the river water is variable. In the case of a chemical spill, nonlinear adsorption reactions (with isotherms that are convex upward) increase the recovery time and prolong pollutant exposure compared to linear adsorption reactions as illustrated in Figure 6.55.

7.4. SUGGESTIONS FOR FUTURE STUDIES

The understanding of the bed/stream exchange could be enhanced by developing a better understanding of the hydraulics associated with bedforms, by conducting further experiments and expanding the exchange models for reactive compounds and colloids, and by incorporating the

exchange models into larger river transport models. Detailed suggestions are given in the following sections.

7.4.1. Hydraulics of bed exchange

The piezometric head variation over the bedform controls the rate of exchange by porewater advection. The amplitude of the head variations is estimated from an empirical formula derived from pressure measurements taken over a single, artificial triangular bedform. The effects of neighboring bedforms, different bedform dimensions and shapes, and variations of the wavelength-to-depth ratio need to be quantified. Data should also be collected from the range of bedform sizes observed in the field.

The hydraulics of the exchange with flat beds has been studied, but the mechanisms of the exchange have not been identified. The exchange has been estimated using a diffusion model that required calibration. Further experiments are needed to develop useful predictive models for the exchange with a flat bed.

The models developed for the exchange of nonsorbing compounds with moving bedforms (Elliott, 1990; Packman, 1997) are applicable for fast bedform propagation velocities. The exchange with slowly moving bedforms has not been modeled successfully because the competing effects of pumping and turnover have not been resolved. Further experimental and modeling studies need to be conducted to develop a better understanding of the exchange in the presence of slowly moving bedforms.

7.4.2. Exchange of reactive compounds

The pumping exchange models developed for reactive substances are limited to equilibrium adsorption reactions. Eylers (1994) modeled the simultaneous exchange of adsorbing metal ions. Each metal ion was modeled separately with a constant retardation coefficient

determined from batch experiments. Further studies and models should be conducted to investigate the simultaneous exchange of compounds that co-adsorb on the bed material. Another interesting problem that could be studied is the exchange of compounds that undergo other chemical and biological transformations in the bed and their transformation products.

The kinetic adsorption effects have not been incorporated into the pumping bed-exchange models. Groundwater studies have demonstrated that the adsorption is kinetically controlled in many situations. It follows that similar behavior would occur in the riverbed. Therefore, exchange models that incorporate kinetic effects would be useful. Kinetic effects also become important during bedform turnover.

The exchange of adsorbing compounds and colloidal particles has been studied separately. Contaminants in the water column tend to adsorb to clay and silt-sized particles because these particles have large specific surface areas. The study of the simultaneous exchange of adsorbing compounds and colloidal particles would provide more insight into the ultimate fate of contaminants in a riverbed.

7.4.3. Bed exchange in larger river transport models

It has been demonstrated that the bed/stream exchange of aqueous compounds and small particles is an important process, and detailed models that describe the exchange have been developed. The parameters required by the bed/stream exchange submodels can be measured directly and should not require calibration. Therefore, the exchange model can be applied to different situations. This feature would improve the effectiveness of the larger river transport model.

In order to model the bed/stream exchange in natural rivers, the bed exchange models will have to be incorporated in larger river transport models. For small times, the exchange can be modeled as a linear decay process (i.e., complete capture). Further work is required to optimize the detailed models so that they can be incorporated into the larger river transport

models without unreasonably increasing the computation time. This task will become more feasible as computer performance improves.

7.5. Main Conclusions

1. A new detailed bed/stream exchange model for nonlinearly adsorbing compounds was developed and then verified by flume experiments. Within experimental error, the model simulations agreed with the observed mass exchange in the flume experiments. The error in the model simulations was reduced when a correction factor α_c (ranging from 1 to 2) was applied to h_m (the amplitude of the piezometric head) for each flume experiment.

2. The model incorporated the results of batch adsorption experiments to predict the mass exchange of the nonlinearly adsorbing compounds in the flume. The success of the model indicates that the use of batch scale adsorption experiments can be a powerful tool to predict the behavior of adsorbing pollutants in a river.

3. Sensitivity analyses were performed to demonstrate the changes in the model predictions for the flume experiments in response to variations in the hydraulic and bed parameters. The amplitude of the piezometric head over the bedform primarily controlled the overall rate of the exchange, while the bedform wavelength determined the total mass transfer into the bed.

4. The adsorption of alkyltrimethylammonium cationic surfactants on garnet sand increases with hydrocarbon chain length of the surfactant from 9 to 18 (Figure 5.17) and with pH (Figures 5.4 and 5.12). An increase in ionic strength reduces the adsorption of the surfactants at pH 8

(Figure 5.5). The total mass of the surfactant retained in the sediment bed of the flume increased with the hydrocarbon chain length.

5. The isotherm equation representations of the adsorption data did not statistically differ in the range of cationic surfactant concentrations observed in the flume experiments. Therefore, the model simulations for the flume experiments were not noticeably affected by the use of different adsorption isotherms.

6. Approximate models, which required less computational effort than the detailed exchange model, were developed to predict the exchange of nonlinearly adsorbing compounds for several limiting cases. For the flume experiments, the complete capture model was valid at short times, while the well-mixed model estimated the exchange at long times. The exchange model based on linear adsorption can be used to find the upper and lower bounds on the mass exchange of nonlinearly adsorbing compounds for the entire duration of the flume experiment.

7. The mass transfer of both nonsorbing and nonlinearly adsorbing compounds into a bed covered with stationary bedforms is much greater than the transfer into a flat bed. The exchange of bromide with a flat bed could be modeled as a diffusion process using an effective diffusion coefficient about four times greater than the molecular diffusion coefficient.

8. All of the models developed in this thesis can be extended to predict the mass exchange of nonlinearly adsorbing pollutants in a natural river. The detailed exchange model developed for nonlinearly adsorbing compounds (Chapter 5, Section 5.4) is versatile and can be applied to rivers with contaminated beds and arbitrary pollutant loadings. The model is applicable for

predicting the bed/stream exchange of compounds that have isotherms that are convex upward. Because the detailed model is computationally intensive, two approximate, more restrictive models, which can more easily be incorporated into larger river transport models, were developed. The parameters for the models developed in this thesis can be measured directly and should not require calibration. Therefore, these exchange models can be applied to different river systems.

REFERENCES

A. D. Little Co. (1977), *Human Safety and Environmental Aspects of Major Surfactants*, NTIS PB301-193.

Ambrose, R. B., Jr., S. I. Hill, and L. A. Mulkey (1983), *User's Manual for the Chemical Transport and Fate Model (TOXIWASP), Version 1*, Report EPA-600/3-83-005, U. S. Environmental Protection Agency, Athens, GA.

ASCE (1975), *Sedimentation Engineering*, ASCE, New York.

Basmadjian, D. and F. Quan (1987), "Distribution of Chemicals in Rivers During Contamination and Recovery," *J. Environ. Eng.*, **113**, pp. 1185-1201.

Bear, J. (1972), *Dynamics of Fluids in Porous Media*, American Elsevier, New York.

Bencala, K. E., V. C. Kennedy, G. W. Zellweger, A. P. Jackman, and R. J. Avanzino (1984), "Interactions of Solutes and Streambed Sediment. 1. An Experimental Analysis of Cation and Anion Transport in a Mountain Stream," *Water Resour. Res.*, **20**, pp. 1797-1803.

Bencala, K. E. (1984), "Interactions of Solutes and Streambed Sediment. 2. A Dynamic Analysis of Coupled Hydrologic and Chemical Processes That Determine Solute Transport," *Water Resour. Res.*, **20**, pp. 1804-1814.

Bencala, K. E., D. M. McKnight, and G. W. Zellweger (1990), "Characterization of Transport in an Acidic and Metal-Rich Mountain Stream Based on a Lithium Tracer Injection and Simulations of Transient Storage," *Water Resour. Res.*, **26**, pp. 989-1000.

Berglund, S. (1995), "The Effect of Langmuir Adsorption on Pump-and-Treat Remediation of a Stratified Aquifer," *J. Contam. Hydrol.*, **18**, pp. 199-220.

Berglund, S. and V. Cvetkovic (1996), "Contaminant Displacement in Aquifers: Coupled Effects of Flow Heterogeneity and Nonlinear Adsorption," *Water Resour. Res.*, **32**, pp. 23-32.

Beveridge, A. and W. F. Pickering (1983), "The Influence of Surfactants on the Adsorption of Heavy-Metal Ions by Clays," *Water Res.*, **17**, pp. 215-225.

Bijsterbosch, B. H. (1974), "Characterization of Silica Surfaces by Adsorption from Solution. Investigations into the Mechanism of Adsorption of Cationic Surfactants," *J. Colloid Interface Sci.*, **47**, pp. 186-198.

Blake, G. R. (1965), "Particle Density," in *Methods of Soil Analysis. Part 1. Physical and Mineralogical Properties, Including Statistics of Measurement and Sampling* (Black, C. A., ed.), Agronomy, American Society of Agronomy, Inc., Madison: pp. 371-373.

Boethling, R. S. (1984), "Environmental Fate and Toxicity in Wastewater Treatment of Quaternary Ammonium Surfactants," *Water Res.*, **18**, pp. 1061-1076.

Bosma, W. J. P. and S. E. A. T. M. van der Zee (1993), "Transport of Reacting Solute in a One-Dimensional Chemically Heterogeneous Porous Medium," *Water Resour. Res.*, **29**, pp. 117-131.

Bosma, W. J. P., S. E. A. T. M. van der Zee, A. Bellin, and A. Rinaldo (1994), "Instantaneous Injection of a Nonlinearly Adsorbing Solute in Heterogeneous Porous Formations," in *Transport and Reactive Processes in Aquifers* (Dracos, T. H. and F. Stauffer eds.), A. A. Balkema, Brookfield: pp. 411-417.

Bouchard, D. C., R. M. Powell, and D. A. Clark (1988), "Organic Cation Effects on the Sorption of Metal and Neutral-Organic Compounds on Aquifer Material," *J. Environ. Sci. Health, Part A, Environ. Sci. Eng.*, **23**, pp. 585-601.

Boyle, J. D. (1984), "Effects of Biological Films on BOD Decay Rates in Rivers," *Water Sci. Technol.*, **16**, pp. 643-651.

Böhmer, M. R. and L. K. Koopal (1992a), "Adsorption of Ionic Surfactants on Constant Charge Surfaces. Analysis Based on a Self-Consistent Field Lattice Model," *Langmuir*, **8**, pp. 1594-1602.

Böhmer, M. R. and L. K. Koopal (1992b), "Adsorption of Ionic Surfactants on Variable-Charge Surfaces. 1. Charge Effects and Structure of Adsorbed Layer," *Langmuir*, **8**, pp. 2649-2659.

Böhmer, M. R. and L. K. Koopal (1992c), "Adsorption of Ionic Surfactants on Variable-Charge Surfaces. 2. Molecular Architecture and Structure of the Adsorbed Layer," *Langmuir*, **8**, pp. 2660-2665.

Brown, M. J. and D. R. Burris (1996), "Enhanced Organic Contaminant Sorption on Soil Treated With Cationic Surfactants," *Ground Water*, **34**, pp. 734-744.

Brownawell, B. J., H. Chen, J. M. Collier, and J. C. Westall (1990), "Adsorption of Organic Cations to Natural Materials," *Environ. Sci. Technol.*, **24**, pp. 1234-1241.

Burns, L. A., D. M. Cline, and R. R. Lassiter (1982), *Exposure Analysis Modelling System (EXAMS): User Manual and System Documentation*, Report EPA-600/3-82-023, U. S. Environmental Protection Agency, Athens, GA.

Burns, L. A. and D. M. Cline (1985), *Exposure Analysis Modeling System Reference Manual for EXAMS II*, Report EPA-600/3-85-038, U. S. Environmental Protection Agency, Athens, GA.

Burris, D. R. and C. P. Antworth (1992), "In-Situ Modification of an Aquifer Material by a Cationic Surfactant to Enhance Retardation of Organic Contaminants," *J. Contam. Hydrol.*, **10**, pp. 325-337.

Cameron, D. R. and A. Klute (1977), "Convective-Dispersive Solute Transport With a Combined Equilibrium and Kinetic Adsorption Model," *Water Resour. Res.*, **13**, pp. 183-188.

Cases, J. M. (1970), "On the Normal Interaction Between Adsorbed Species and Absorbing Surface," *Trans. AIME*, **247**, pp. 123-127.

Cases, J. M. and F. Villieras (1992), "Thermodynamic Model of Ionic and Nonionic Surfactant Adsorption-Abstraction on Heterogeneous Surfaces," *Langmuir*, **8**, pp. 1251-1264.

Cerling, T. E., S. J. Morrison, and R. W. Sobocinski (1990), "Sediment-Water Interaction in a Small Stream: Adsorption of ^{137}Cs by Bed Load Sediments," *Water Resour. Res.*, **27**, pp. 1165-1176.

Chander, S., D. W. Fuerstenau, and D. W. Stigter (1983), "On Hemimicelle Formation at Oxide/Water Interfaces," in *Adsorption From Solution* (Ottewill, R. H., R. H. Rochester, and C. H. Smith eds.), Academic Press, New York: pp. 197-210.

Charbeneau, R. J. (1981), "Groundwater Contaminant Transport With Adsorption and Ion Exchange Chemistry: Method of Characteristics for the Case Without Dispersion," *Water Resour. Res.*, **17**, pp. 705-713.

Clarke, G. K. C. and E. D. Waddington (1991), "A Three-Dimensional Theory of Wind Pumping," *J. Glaciol.*, **37**, pp. 89-96.

Colbeck, S. C. (1989), "Air Movement in Snow Due to Windpumping," *J. Glaciol.*, **35**, pp. 209-213.

Connolly, J. P. and R. P. Winfield (1984), *A User's Guide for Wastox, A Framework for Modeling the Fate of Toxic Chemicals in Aquatic Environments*, Report EPA-600/3-84-077, U. S. Environmental Protection Agency, Gulf Breeze, FL.

Cvetkovic, V. and G. Dagan (1994), "Effect of Nonlinear Adsorption on Contamination/Remediation of Heterogeneous Aquifers," in *Transport and Reactive Processes in Aquifers* (Dracos, T. H. and F. Stauffer eds.), A. A. Balkema, Brookfield: pp. 405-409.

Di Toro, D. M., D. J. O'Connor, R. V. Thomann, and J. P. St. John (1982), "Simplified Model of the Fate of Partitioning Chemicals in Lakes and Streams," in *Modeling the Fate of Chemicals in the Aquatic Environment* (Dickson, K. L., A. W. Maki, and J. Cairns, Jr. eds.), Ann Arbor Science, Ann Arbor: pp. 165-190.

Dobiás, B. (1984), "Surfactant Adsorption on Minerals Related to Flotation," in *Structure and Bonding 56 - New Developments* (Clarke, M. J., J. B. Goodenough, J. A. Ibers, C. K. Jorgensen, J. B. Neilands, D. Reinen, R. Weiss, and R. J. P. Williams eds.), Springer-Verlag, New York: pp. 91-147.

Edwards, D. A., Z. Liu, and R. G. Luthy (1992), "Interactions Between Nonionic Surfactant Monomers, Hydrophobic Organic Compounds and Soil," *Water Sci. Technol.*, **26**, pp. 147-158.

Edwards, M. and M. M. Benjamin (1989), "Adsorptive Filtration Using Coated Sand: A New Approach for Treatment of Metal-Bearing Wastes," *J. Wat. Pollut. Control Fed.*, **61**, pp. 1523-1533.

Elliott, A. H. (1990), *Transfer of Solutes Into and Out of Streambeds*, Report KH-R-52, W. M. Keck Laboratory of Hydraulics and Water Resources, California Institute of Technology, Pasadena, CA.

Elliott, A. H. and N. H. Brooks (1997a), "Transfer of Nonsorbing Solutes to a Streambed With Bed Forms: Theory," *Water Resour. Res.*, **33**, pp. 123-136.

Elliott, A. H. and N. H. Brooks (1997b), "Transfer of Nonsorbing Solutes to a Streambed With Bed Forms: Laboratory Experiments," *Water Resour. Res.*, **33**, pp. 137-151.

Esumi, K., T. Nagahama, and K. Meguro (1991), "Characterization of Cationic Surfactant Adsorbed Layer on Silica," *Colloids Surf.*, **57**, pp. 149-160.

Esumi, K., M. Goino, and Y. Koide (1996), "Adsorption and Adsolubilization by Monomeric, Dimeric, or Trimeric Quaternary Ammonium Surfactant at Silica/Water Interface," *J. Colloid Interface Sci.*, **183**, pp. 539-545.

Eylers, H. (1994), *Transport of Adsorbing Metal Ions Between Stream Water and Sediment Bed in a Laboratory Flume*, Report KH-R-56, W.M. Keck Laboratory of Hydraulics and Water Resources, California Institute of Technology, Pasadena, CA.

Eylers, H., N. H. Brooks, and J. J. Morgan (1995), "Transport of Adsorbing Metals From Stream Water to a Stationary Sand-Bed in a Laboratory Flume," *Mar. Freshwater Res.*, **46**, pp. 209-214.

Favoriti, P., V. Monticone, and C. Treiner (1996), "Coadsorption of Naphthalene Derivatives and Cetyltrimethylammonium Bromide on Alumina/Water, Titanium Dioxide/Water and Silica/Water Interfaces," *J. Colloid Interface Sci.*, **179**, pp. 173-180.

Fehlman, H. M. (1985), *Resistance Components and Velocity Distributions of Open Channel Flows Over Bedforms*, M.S. Thesis, Colorado State University, Fort Collins, CO.

Few, A. V. and R. H. Ottewill (1956), "A Spectrophotometric Method for the Determination of Cationic Detergents," *J. Colloid Sci.*, **11**, pp. 34-38.

Finlayson, B. A. (1992), *Numerical Methods for Problems With Moving Fronts*, Ravenna Park Publishing, Inc., Seattle.

Fuerstenau, D. W. (1956), "Streaming Potential Studies on Quartz in Solutions of Aminium Acetates in Relation to the Formation of Hemi-Micelles at the Quartz-Solution Interface," *J. Phys. Chem.*, **60**, pp. 981-985.

Fuerstenau, D. W., T. W. Healy, and P. Somasundaran (1964), "The Role of Hydrocarbon Chain of Alkyl Collectors in Flotation," *Trans. AIME*, **229**, pp. 321-325.

Fuerstenau, D. W. and S. Raghavan (1978), "The Surface and Crystal Chemistry of Silicate Minerals and Their Flotation Behavior," in *Freiberger Forschungshefte A593* (Rektor der Bergakademie Freiberg, ed.), VEB Deutscher Verlag fur Grundstoffindustrie, Leipzig: pp. 75-109.

Gaudin, A. M. and D. W. Fuerstenau (1955), "Quartz Flotation With Cationic Collectors," *Trans. AIME*, **202**, pp. 958-962.

Giles, C. H. and A. S. Trivedi (1969), "A Rapid Semi-Micro Method for Determination of Specific Surface of Solids by Dye Adsorption," *Chem. Ind.*, pp. 1426-1427.

Gillion, R. J. and D. G. Clifton (1990), "Organochloride Pesticide Residues in Bed Sediments of the San Joaquin River," *Water Resour. Bull.*, **26**, pp. 11-24.

Grimm, N. B. and S. G. Fisher (1984), "Exchange Between Interstitial and Surface Water: Implications for Stream Metabolism and Nutrient Cycling," *Hydrobiologia*, **111**, pp. 219-228.

Gschwend, P. M., S. Wu, O. S. Madsen, R. B. Ambrose, Jr., and S. C. McCutcheon (1986), *Modelling the Benthos-Water Column Exchange of Hydrophobic Chemicals*, Report EPA-600/3-86-044, U. S. Environmental Protection Agency, Athens, GA.

Halfon, E. and R. Brueggemann (1990), "Simulation of Disulfoton Fate in the River Rhine With the TOXFATE Model," *Sci. Total Environ.*, **97/98**, pp. 385-394.

Hankins, N. P., J. H. O'Haver, and J. H. Harwell (1996), "Modeling the Effects of pH and Counterions on Surfactant Adsorption at the Oxide/Water Interface," *Ind. Eng. Chem. Res.*, **35**, pp. 2844-2855.

Harwell, J. H., J. C. Hoskins, R. S. Schechter, and W. H. Wade (1985), "Pseudophase Separation Model for Surfactant Adsorption - Isomerically Pure Surfactants," *Langmuir*, **1**, pp. 251-262.

Hayes, K. F., C. Chen, and D. C. McAvoy (1995), "Quaternary Ammonium Surfactant Effects on Sorption of Trace Metals Onto Quartz and Aluminosilicates," *Soil Sci. Soc. Am. J.*, **59**, pp. 380-387.

Hayworth, J. S. and D. R. Burris (1996), "Modeling Cationic Surfactant Transport in Porous Media," *Ground Water*, **34**, pp. 274-282.

Hinz, C., L. A. Gaston, and H. M. Selim (1994), "Effect of Sorption Isotherm Type on Prediction of Solute Mobility in Soil," *Water Resour. Res.*, **30**, pp. 3013-3021.

Holloran, M. (1982), "Model for Instream Regulation of Radioisotopes and Heavy Metals in Riverine Waters Subjected to a Uranium Mill Discharge," *Hydrobiologia*, **91**, pp. 175-188.

Huang, L., C. Maltesh, and P. Somasundaran (1996), "Adsorption Behavior of Cationic and Nonionic Surfactant Mixtures at the Alumina-Water Interface," *J. Colloid Interface Sci.*, **177**, pp. 222-228.

Iler, R. K. (1955), *The Colloid Chemistry of Silica and Silicates*, Cornell University Press, Ithaca.

Jackman, A. P., R. A. Walters, and V. C. Kennedy (1984), "Transport and Concentration Controls for Chloride, Strontium, Potassium and Lead in Uvas Creek, a Small Cobble-Bed Stream in Santa Clara Country, California, U.S.A. 2. Mathematical Modelling," *J. Hydrol.*, **75**, pp. 111-141.

Kennedy, J. F. (1963), "The Mechanics of Dunes and Antidunes in Erodible-Bed Channels," *J. Fluid Mech.*, **16**, pp. 521-544.

Kiefer, J. E. and D. Wilson (1980), "Characterization of Aqueous Colloids by Their Electrical Double-Layer and Intrinsic Surface Chemical Properties," *Sep. Sci. Technol.*, **15**, pp. 57-74.

Kinniburgh, D. G. (1986), "General Purpose Adsorption Isotherms," *Environ. Sci. Technol.*, **20**, pp. 895-904.

Koopal, L. K., E. M. Lee, and M. R. Böhmer (1995), "Adsorption of Cationic and Anionic Surfactants on Charged Metal Oxide Surfaces," *J. Colloid Interface Sci.*, **170**, pp. 85-97.

Lai, R. W. (1970), *Surface Charge, Adsorption of Ionic Surfactants and the Wettability of Oxide Minerals*, Ph.D. Thesis, University of California, Berkeley.

Larsson, P. L., L. Olka, S. O. Ryding, and B. Westoo (1990), "Contaminated Sediment As a Source of PCBs in a River System," *Can. J. Fish. Aquat. Sci.*, **47**, pp. 746-754.

Lawrence, C. A. (1970), "Germicidal Properties of Cationic Surfactants," in *Cationic Surfactants* (Jungermann, E., ed.), Marcel Dekker, New York: pp. 491-526.

Lee, E. M. and L. K. Koopal (1996), "Adsorption of Cationic and Anionic Surfactants on Metal Oxide Surfaces: Surface Charge Adjustment and Competition Effects," *J. Colloid Interface Sci.*, **177**, pp. 478-489.

Lee, J. F., J. R. Crum, and S. A. Boyd (1989), "Enhanced Retention of Organic Contaminants by Soils Exchanged With Organic Cations," *Environ. Sci. Technol.*, **23**, pp. 1365-1372.

Lewis, M. A. and V. T. Wee (1983), "Aquatic Safety Assessment for Cationic Surfactants," *Environ. Toxicol. Chem.*, **2**, pp. 105-118.

Lewis, M. A. (1991), "Chronic and Sublethal Toxicities of Surfactants to Aquatic Animals. A Review and Risk Assessment," *Water Res.*, **25**, pp. 101-113.

Mukerjee, P. and K. J. Mysels (1970), *Critical Micelle Concentrations of Aqueous Surfactant Systems*, National Standard Reference Data Series, U.S. Department of Commerce, Washington, D.C.

Myers, D. (1988), *Surfactant Science and Technology*, VCH Publishers, New York.

Nagaokai, H. and A. J. Ohgaki (1990), "Mass Transfer Mechanism in a Porous Riverbed," *Water Res.*, **24**, pp. 417-425.

Newman, B. D., H. R. Fuentes, and W. L. Polzer (1991), "An Evaluation of Lithium Sorption Isotherms and Their Application to Ground-Water Transport," *Ground Water*, **29**, pp. 818-824.

Nichols, N. M. (1990), "Sedimentologic Fate and Cycling of Kepone in an Estuarine System: Example From the James River Estuary," *Sci. Total Environ.*, **97/98**, pp. 407-440.

O'Connor, D. J., J. A. Mueller, and K. J. Farley (1983), "Distribution of Kepone in the James River Estuary," *J. Environ. Eng.*, **109**, pp. 396-413.

O'Connor, D. J. (1988), "Models of Sorptive Toxic Substances in Freshwater Systems. III: Streams and Rivers," *J. Environ. Eng.*, **114**, pp. 552-574.

Onishi, Y. (1981), "Sediment-Contaminant Transport Model," *J. Hydraul. Div. ASCE*, **107**, pp. 1089-1107.

Ottewill, R. H. and M. C. Rastogi (1960), "The Stability of Hydrophobic Sols in the Presence of Surface Active Agents," *Trans. Faraday Soc.*, **56**, pp. 880-892.

Packman, A. I. (1997), *Exchange of Colloidal Kaolinite Between Stream and Sand Bed in a Laboratory Flume*, Ph.D. Thesis, California Institute of Technology, Pasadena, CA.

Paul, A. C. and K. C. Pillai (1991), "Natural Radionuclides in a Tropical River Subjected to Pollution," *Water Air Soil Pollut.*, **55**, pp. 305-319.

Poulain, C. A. and B. A. Finlayson (1993), "A Comparison of Numerical Methods Applied to Non-Linear Adsorption Columns," *Int. J. Numer. Methods Fluids*, **17**, pp. 839-859.

Press, W. H., B. P. Flannery, S. A. Teukolsky, and W. T. Vetterling (1989), *Numerical Recipes (Fortran)*, Cambridge University Press, New York.

Rabideau, A. J. and C. T. Miller (1994), "Two-Dimensional Modeling of Aquifer Remediation Influenced by Sorption Nonequilibrium and Hydraulic Conductivity Heterogeneity," *Water Resour. Res.*, **30**, pp. 1457-1470.

Reible, D. D. and S. A. Savant-Malhiet (1993), "Comparison of Physical Transport Processes in Noncohesive River Sediments," *J. Environ. Eng.*, **119**, pp. 90-102.

Rhee, H. K., R. Aris, and N. R. Amundson (1986), *First-Order Partial Differential Equations: Volume I. Theory and Application of Single Equations*, Prentice-Hall, Englewood Cliffs.

Richardson, C. P. and A. D. Parr (1988), "Modified Fickian Model for Solute Uptake by Runoff," *J. Environ. Eng.*, **114**, pp. 792-809.

Rosen, M. J. (1989), *Surfactants and Interfacial Phenomena*, 2nd ed., John Wiley & Sons, New York.

Ross, G. J. and C. Wang (1993), "Extractable Al, Fe, Mn, and Si," in *Soil Sampling and Methods of Analysis* (Carter, M. R., ed.), Lewis Publishers, Boca Raton: pp. 239-246.

Rutherford, J. C., J. D. Boyle, A. H. Elliott, T. O. J. Hatherell, and T. W. Chiu (1995), "Modeling Benthic Oxygen Uptake by Pumping," *J. Environ. Eng.*, **121**, pp. 84-95.

Savant, S. A., D. D. Reible, and L. J. Thibodeaux (1987), "Convective Transport Within Stable River Sediments," *Water Resour. Res.*, **23**, pp. 1763-1768.

Scamehorn, J. F., R. S. Schechter, and W. H. Wade (1982), "Adsorption of Surfactants on Mineral Oxide Surfaces From Aqueous Solutions," *J. Colloid Interface Sci.*, **85**, pp. 463-478.

Scheidegger, A., M. Borkovec, and H. Sticher (1993), "Coating of Silica Sand With Goethite: Preparation and Analytical Identification," *Geoderma*, **58**, pp. 43-65.

Schnoor, J. L. (1996), *Environmental Modeling: Fate and Transport of Pollutants in Water, Air, and Soil*, John Wiley & Sons, New York.

Schwarz, R., K. Heckmann, and J. Strnad (1988), "Adsorption Model of Pyridium Salts on Quartz," *J. Colloid Interface Sci.*, **124**, pp. 50-56.

Schwarzenbach, R. P., P. M. Gschwend, and D. M. Imboden (1993), *Environmental Organic Chemistry*, John Wiley & Sons, New York.

Selim, H. M., J. M. Davidson, and R. S. Mansell (1976), "Evaluation of a Two-Site Adsorption-Desorption Model for Describing Solute Transport in Soils," *Proceedings Summer Computer Simulation Conference*, Washington, D.C.

Shen, H. W., H. M. Fehlman, and C. Mendoza (1990), "Bed Form Resistance in Open Channel Flows," *J. Hydraul. Eng.*, **116**, pp. 799-815.

Sips, R. (1950), "On the Structure of a Catalyst Surface," *The Journal of Chemical Physics*, **18**, pp. 1024-1026.

Smith, J. A., P. R. Jaffe, and C. T. Chiou (1990), "Effect of Ten Quaternary Ammonium Cations on Tetrachloromethane Sorption to Clay From Water," *Environ. Sci. Technol.*, **24**, pp. 1167-1172.

Somasundaran, P., T. W. Healy, and D. W. Fuerstenau (1964), "Surfactant Adsorption at the Solid-Liquid Interface - Dependence of Mechanism on Chain Length," *J. Phys. Chem.*, **68**, pp. 3562-3566.

Somasundaran, P. and D. W. Fuerstenau (1966), "Mechanisms of Alkyl Sulfonate Adsorption at the Alumina Water Interface," *J. Phys. Chem.*, **70**, pp. 90-96.

Sposito, G. (1984), *The Surface Chemistry of Soils*, Oxford University Press, New York.

Stahl, R. S. and B. R. James (1991), "Zinc Sorption by Iron-Oxide-Coated Sand As a Function of pH," *Soil Sci. Soc. Am. J.*, **55**, p. 1290.

Stone, A. T., A. Torrents, J. Smolen, D. Vasudevan, and J. Hadley (1993), "Adsorption of Organic Compounds Possessing Ligand Donor Groups at the Oxide/Water Interface," *Environ. Sci. Technol.*, **27**, pp. 895-909.

Streitwieser, A., Jr. and C. H. Heathcock (1981), *Introduction to Organic Chemistry*, 2nd ed., Macmillan Publishing Co., Inc., New York.

Stumm, W. (1992), *Chemistry of the Solid-Water Interface*, John Wiley & Sons, New York.

Stumm, W. and J. J. Morgan (1996), *Aquatic Chemistry. Chemical Equilibria and Rates in Natural Waters*, 3rd ed., John Wiley & Sons, New York.

Takeda, S. and S. Usui (1987), "Adsorption of Dodecylammonium Ion on Quartz in Relation to Its Flotation," *Colloids Surf.*, **23**, pp. 15-28.

Thibodeaux, L. J. and J. D. Boyle (1987), "Bedform-Generated Convective Transport in Bottom Sediment," *Nature*, **322**, pp. 341-343.

Thurman, E. M., L. B. Barber, Jr., and D. LeBlanc (1986), "Movement and Fate of Detergents in Groundwater," *J. Contam. Hydrol.*, **1**, pp. 143-161.

Tóth, J., W. Rudzinski, A. Waksmundski, M. Jaroniec, and S. Sokolowski (1974), "Adsorption of Gases on Heterogeneous Solid Surfaces: The Energy Distribution Function Corresponding to a New Equation for Monolayer Adsorption," *Acta Chim. Hung.*, **82**, pp. 11-21.

van der Zee, S. E. A. T. M. (1990), "Analytical Traveling Wave Solutions for Transport With Nonlinear and Nonequilibrium Adsorption," *Water Resour. Res.*, **26**, pp. 2563-2578.

van Duijn, C. J. and P. Knabner (1992), "Travelling Waves in the Transport of Reactive Solutes through Porous Media: Adsorption and Binary Ion Exchange - Part 1," *Transp. Porous Media*, **8**, pp. 167-194.

Van Genuchten, M. Th., J. M. Davidson, and P. J. Wierenga (1974), "An Evaluation of Kinetic and Equilibrium Equations for the Prediction of Pesticide Movement Through Porous Media," *Soil Sci. Soc. Am. J.*, **38**, pp. 29-35.

Van Genuchten, M. Th. and P. J. Wierenga (1976), "Mass Transfer Studies in Sorbing Porous Media. I. Analytical Solutions," *Soil Sci. Soc. Am. J.*, **40**, pp. 473-480.

Van Genuchten, M. Th. and W. J. Alves (1982), *Analytical Solutions of the One-Dimensional Convective-Dispersive Transport Equation*, U.S.D.A. Technical Bulletin 1661, U. S. Department of Agriculture, Washington D.C.

Vanjara, A. K. and S. G. Dixit (1996), "Adsorption of Cationic Surfactants on Rutile," *Adsorption Science and Technology*, **13**, pp. 397-407.

Vanoni, V. A. and N. H. Brooks (1957), *Laboratory Studies of the Roughness and Suspended Load of Alluvial Streams*, MRD Sediment Series No. 11, U.S. Army Corps of Engineering, Missouri River Div., Omaha, Nebraska.

Vittal, N., K. G. Ranga Raju, and R. J. Garde (1977), "Resistance of Two Dimensional Triangular Roughness," *J. Hydraul. Res.*, **15**, pp. 19-36.

Wagner, J., B. J. Chen, B. J. Brownawell, and J. C. Westall (1994), "Use of Cationic Surfactants to Modify Soil Surfaces to Promote Sorption and Retard Migration of Hydrophobic Organic Compounds," *Environ. Sci. Technol.*, **28**, pp. 231-237.

Wakamatsu, T. and D. W. Fuerstenau (1968), "The Effect of Hydrocarbon Chain Length on the Adsorption of Sulfonates at the Solid/Water Interface," in *Adsorption From Aqueous Solution* (Gould, R. F., ed.), Advances in Chemistry Series 79, American Chemical Society, Washington D.C.: pp. 161-172.

Wängnerud, P. and B. Jönsson (1994), "Adsorption of Ionic Amphiphiles As Bilayers on Charged Surfaces," *Langmuir*, **10**, pp. 3268-3278.

Webb, J. E. and J. L. Theodor (1972), "Wave-Induced Circulation in Submerged Sands," *J. Mar. Biol. Assn. U. K.*, **52**, pp. 903-914.

Weber, W. J., Jr., P. M. McGinley, and L. E. Katz (1991), "Sorption Phenomena in Subsurface Systems: Concepts, Models and Effects on Contaminant Fate and Transport," *Water Res.*, **25**, pp. 499-528.

Weiss, C. S., J. S. Hazlett, M. H. Datta, and M. H. Danzer (1992), "Determination of Quaternary Ammonium Compounds by Capillary Electrophoresis Using Direct and Indirect UV Detection," *J. Chromat.*, **608**, pp. 325-332.

Wilson, D. J. and K. R. Moffat (1979), "Electrical Aspects of Adsorptive Colloid Flotation. IX. Effects of Surfactant Overdosing," *Sep. Sci. Technol.*, **14**, pp. 319-332.

Yeskie, M. A. and J. H. Harwell (1988), "On the Structure of Aggregates of Adsorbed Surfactants: The Surface Changes Density at the Hemimicelle/Admicelle Transition," *J. Phys. Chem.*, **92**, pp. 2346-2352.

Zhang, H., F. W. Schwartz, W. W. Wood, S. P. Garabedian, and D. R. LeBlanc (1998), "Simulation of Variable-Density Flow and Transport of Reactive and Nonreactive Solutes During a Tracer Test at Cape Cod, Massachusetts," *Water Resour. Res.*, **34**, pp. 67-82.

APPENDIX A – Additional Flume Experiment Data

The following figures are the measured bed profiles from each of the flume experiments. The average bedform heights and wavelengths are determined from the bed profiles. The time history of pH and water temperature for each experiment is also included.

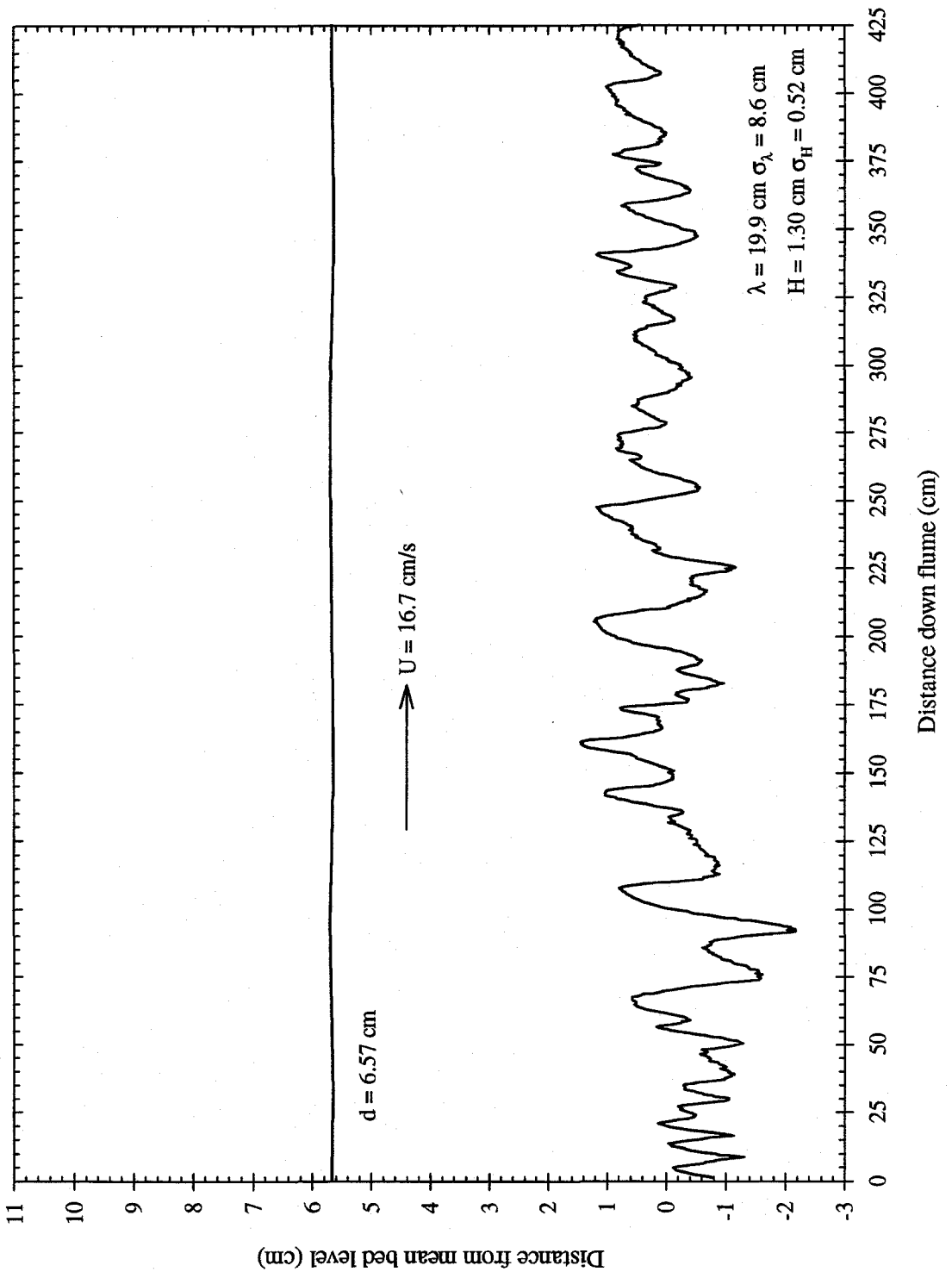

Figure A.1. Bed and water surface profiles from Flume Run 1.

a) pH

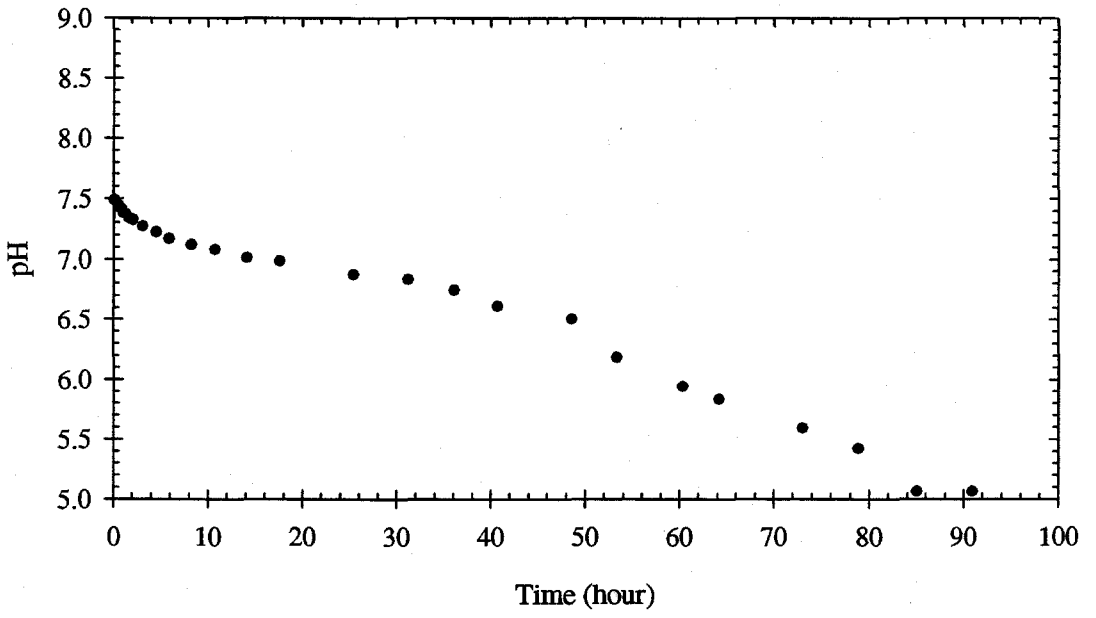

b) Water temperature

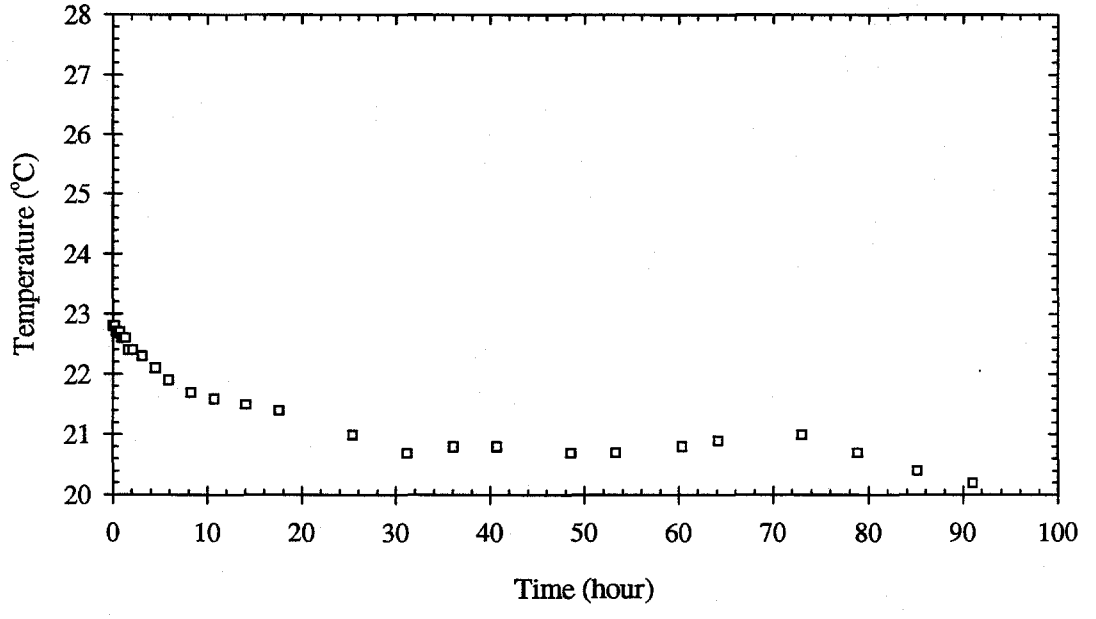

Figure A.2. Time history of a) pH and b) water temperature in Flume Run 1.

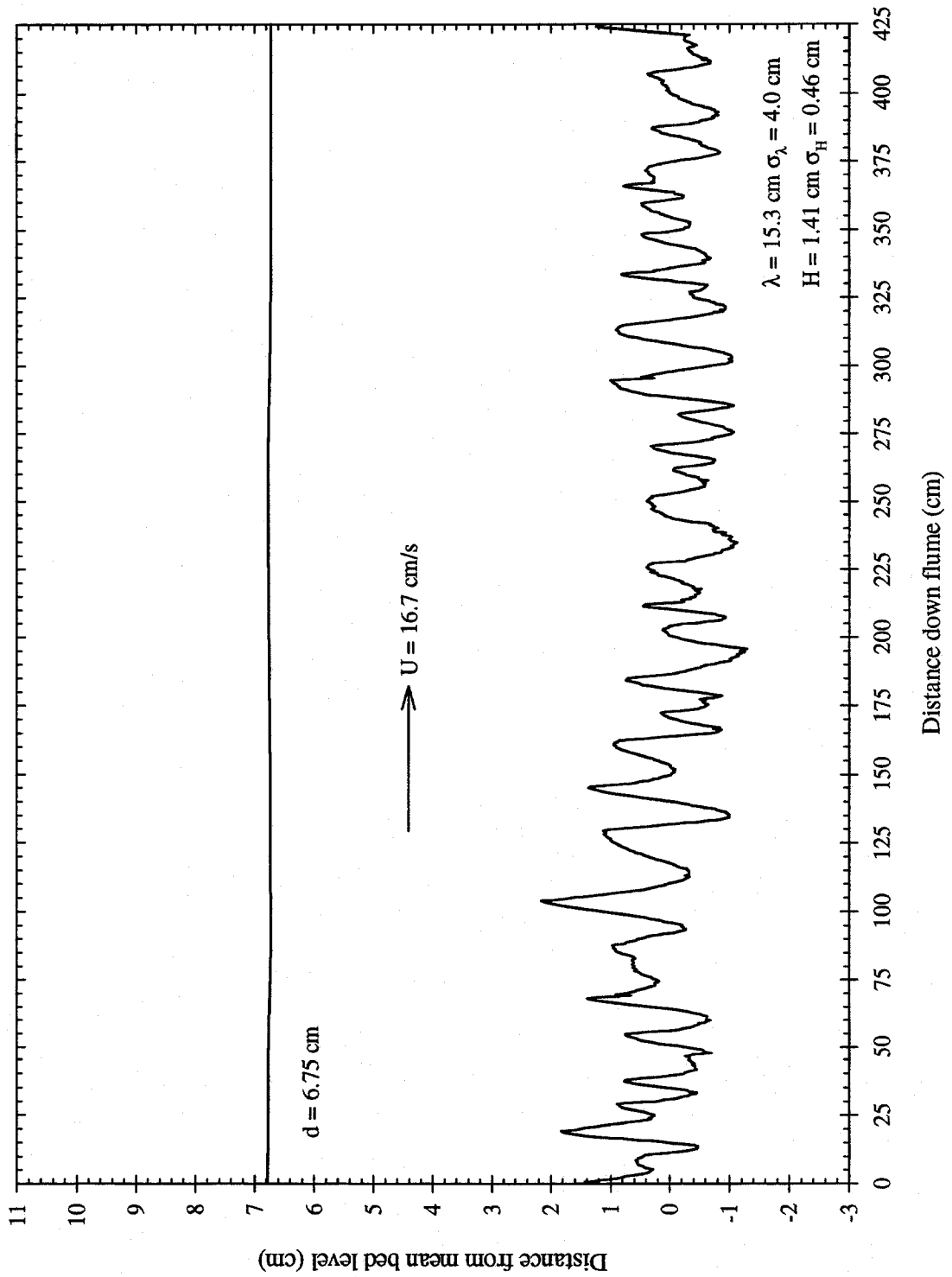

Figure A.3. Bed and water surface profiles from Flume Run 2.

a) pH

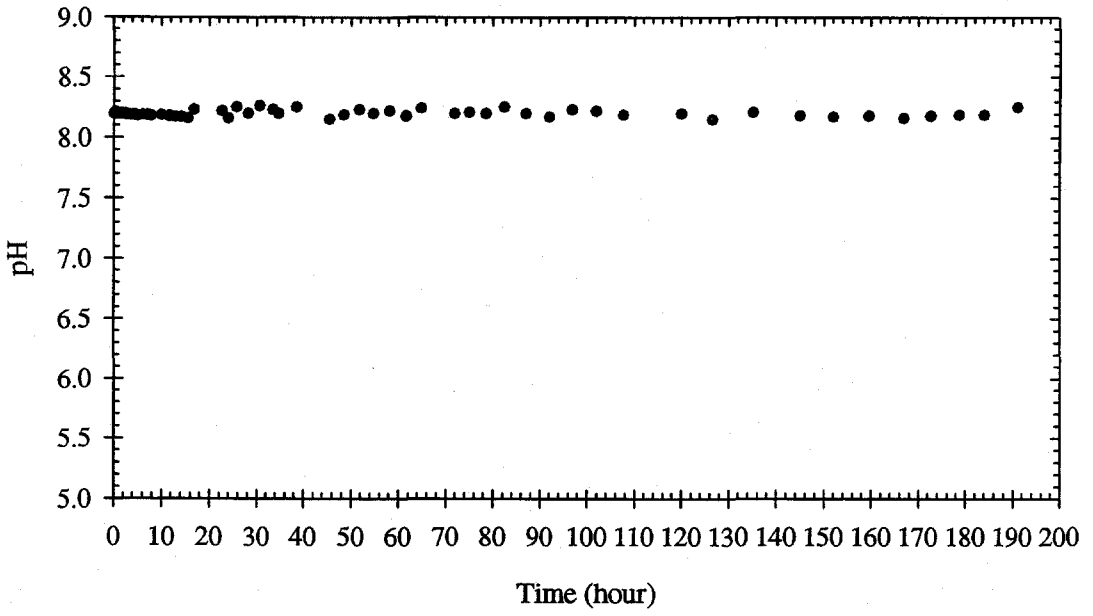

b) Water temperature

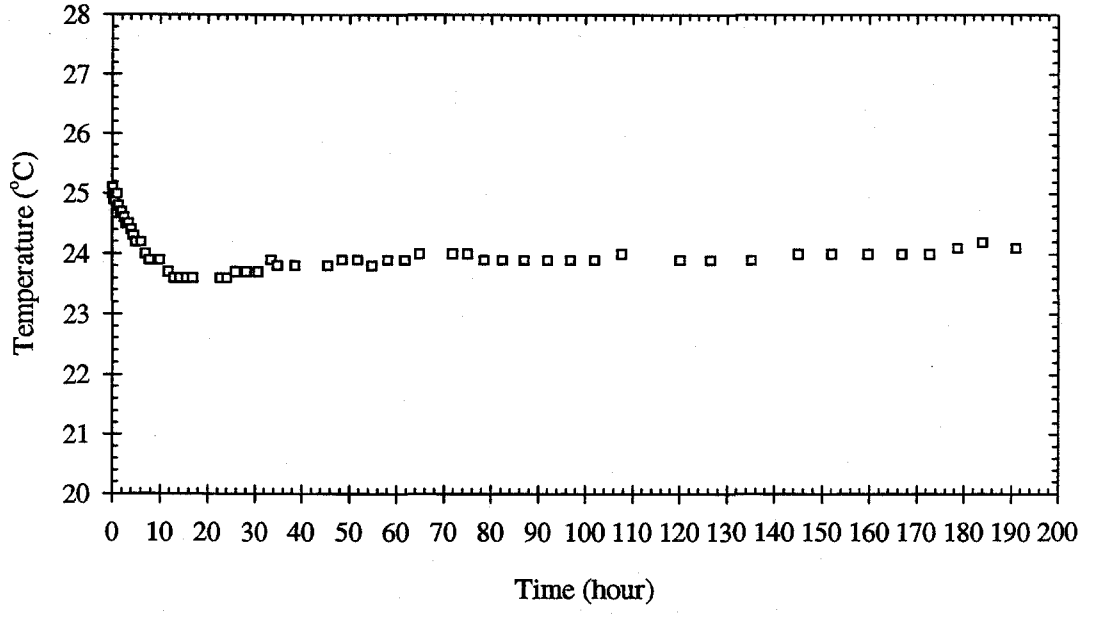

Figure A.4. Time history of a) pH and b) water temperature in Flume Run 2.

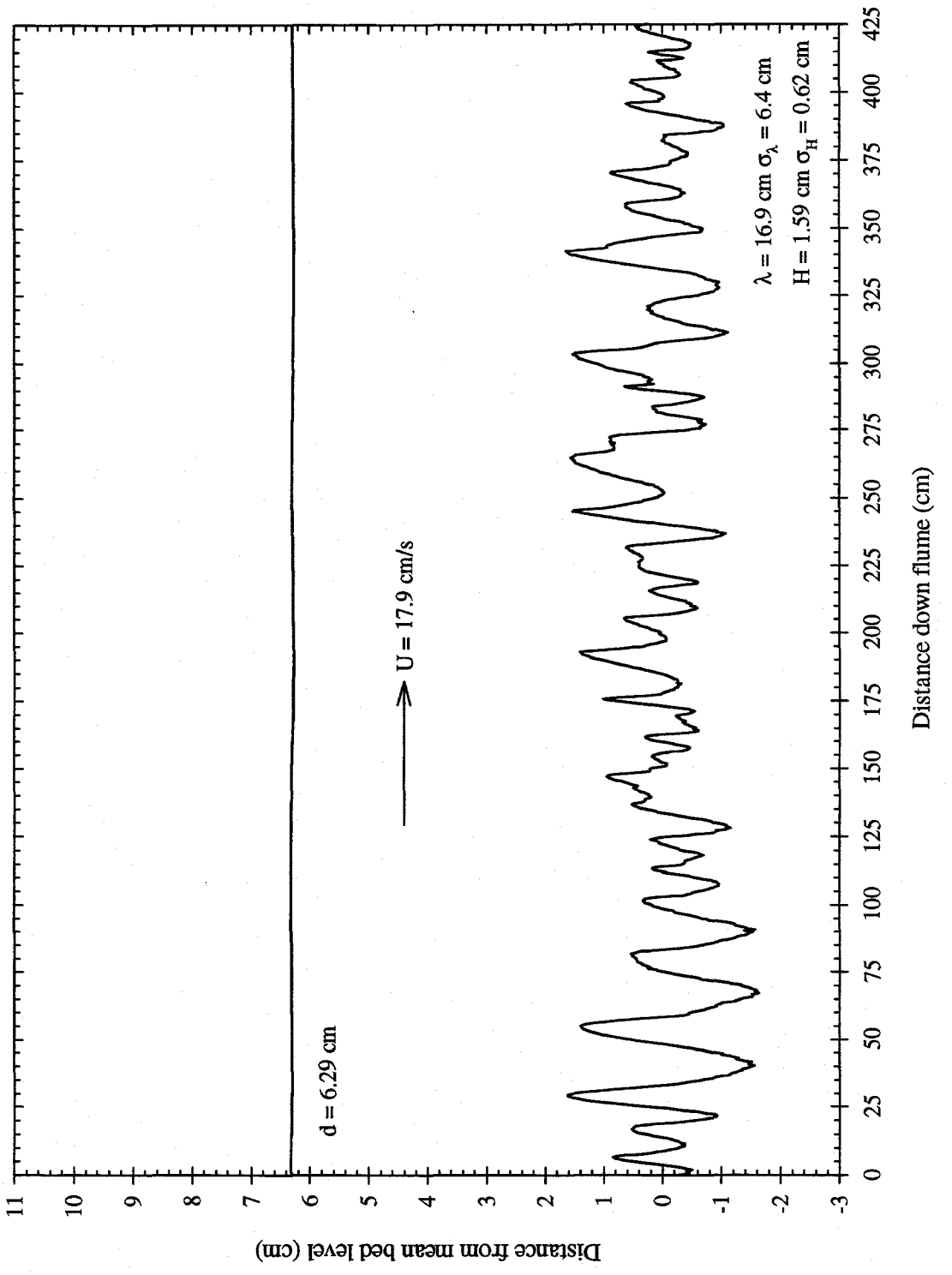

Figure A.5. Bed and water surface profiles from Flume Run 3.

a) pH

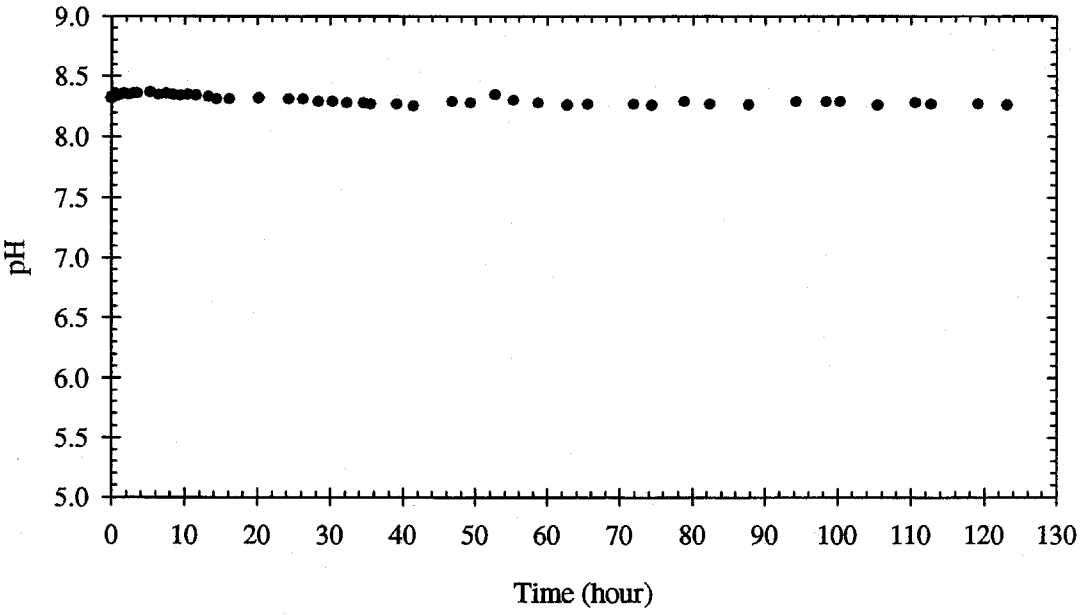

b) Water temperature

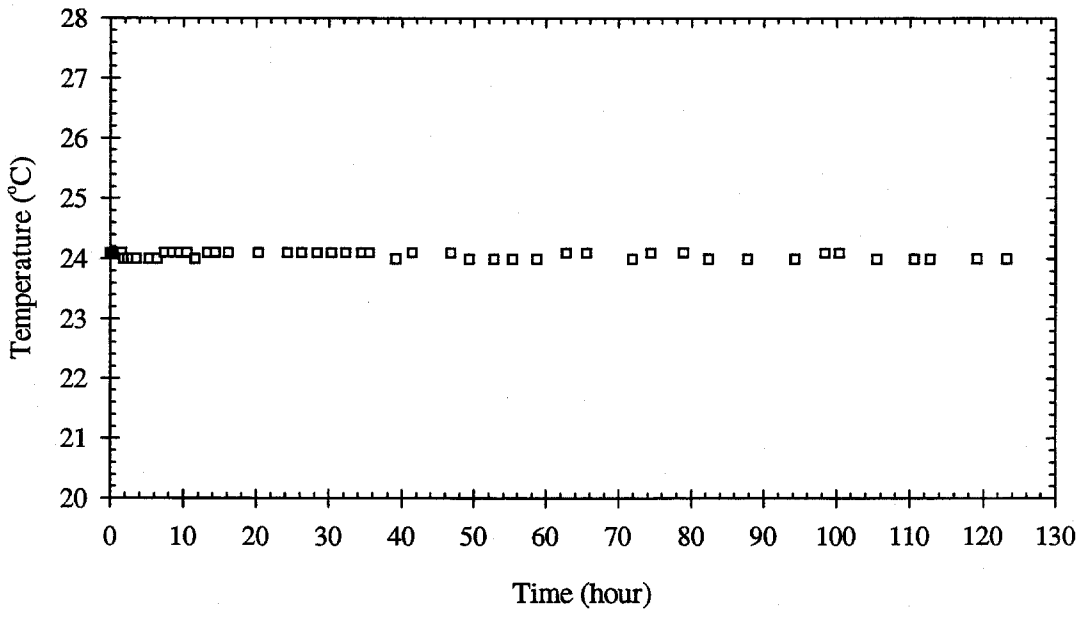

Figure A.6. Time history of a) pH and b) water temperature in Flume Run 3.

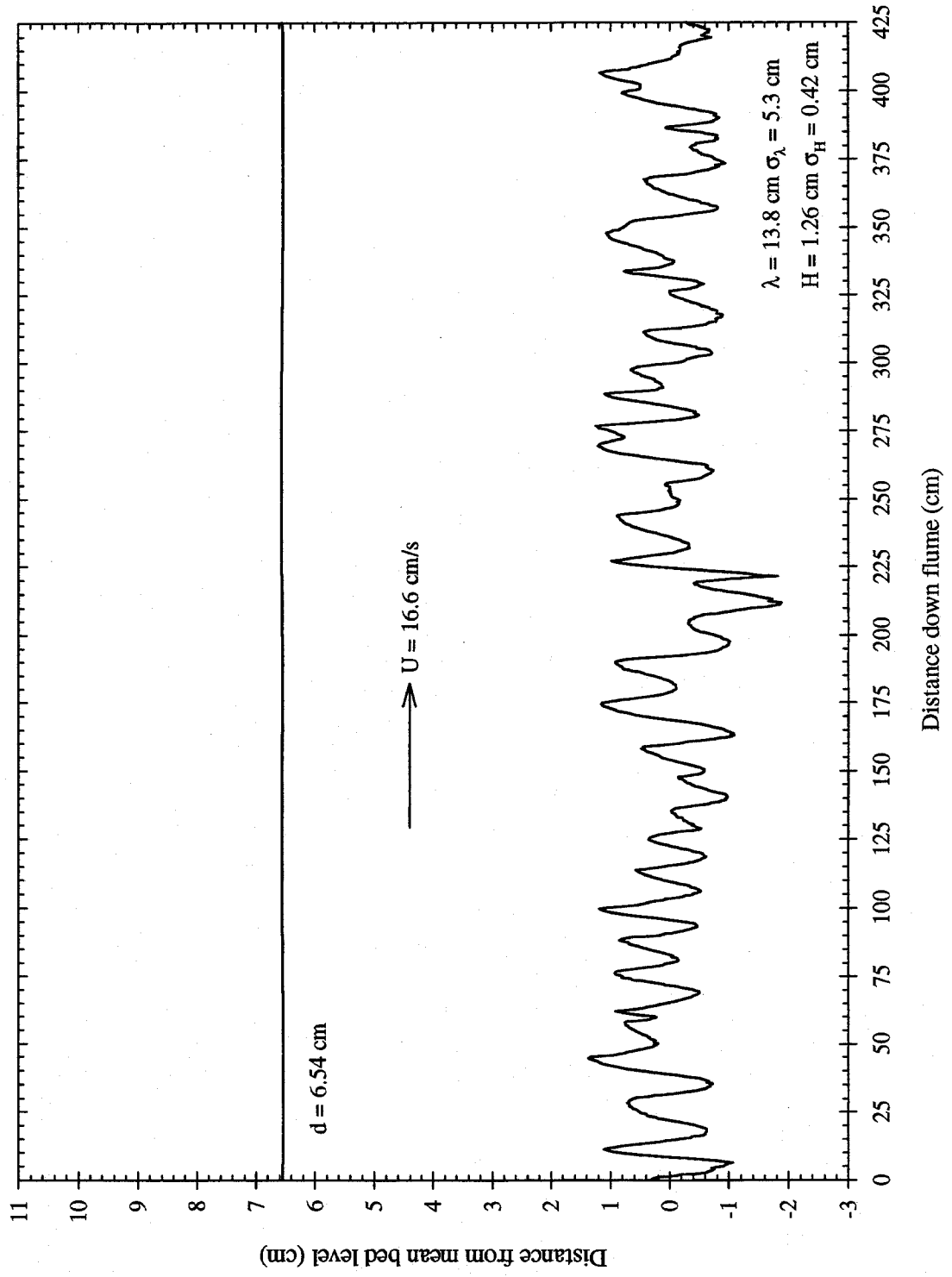

Figure A.7. Bed and water surface profiles from Flume Run 4.

a) pH

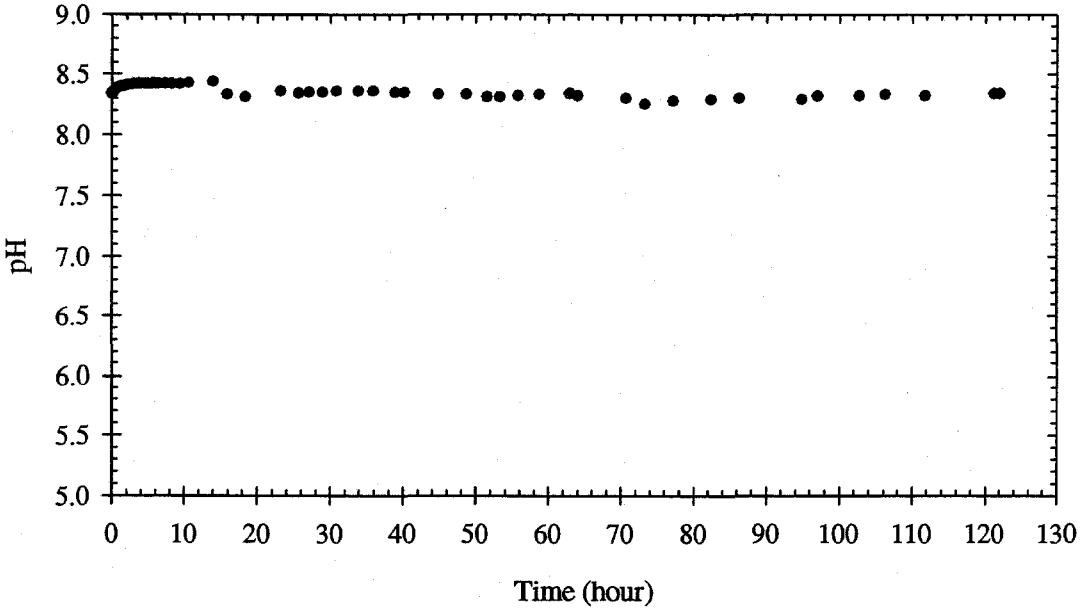

b) Water temperature

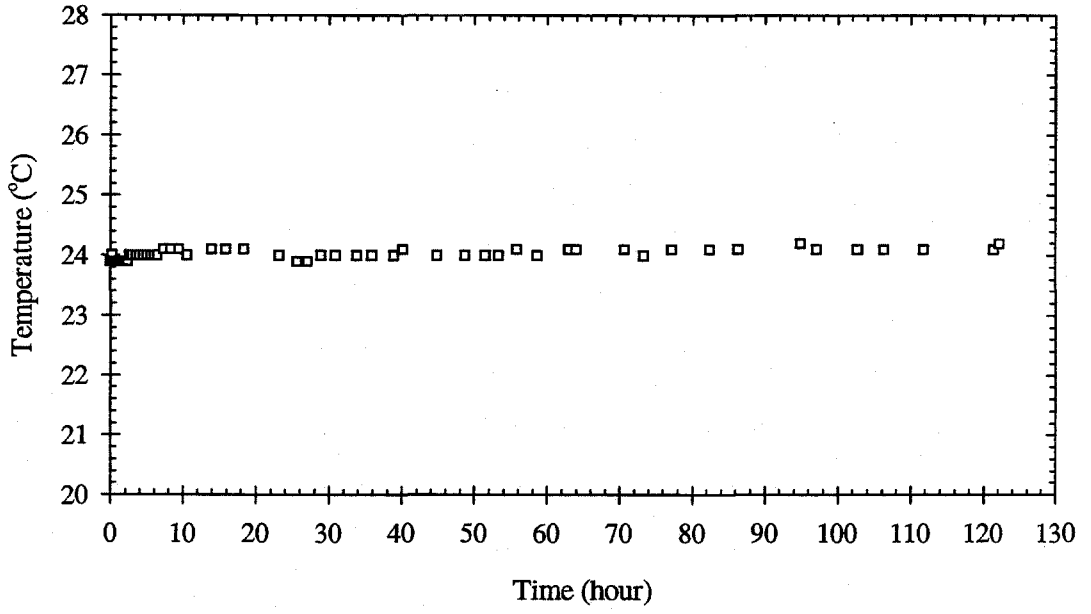

Figure A.8. Time history of a) pH and b) water temperature in Flume Run 4.

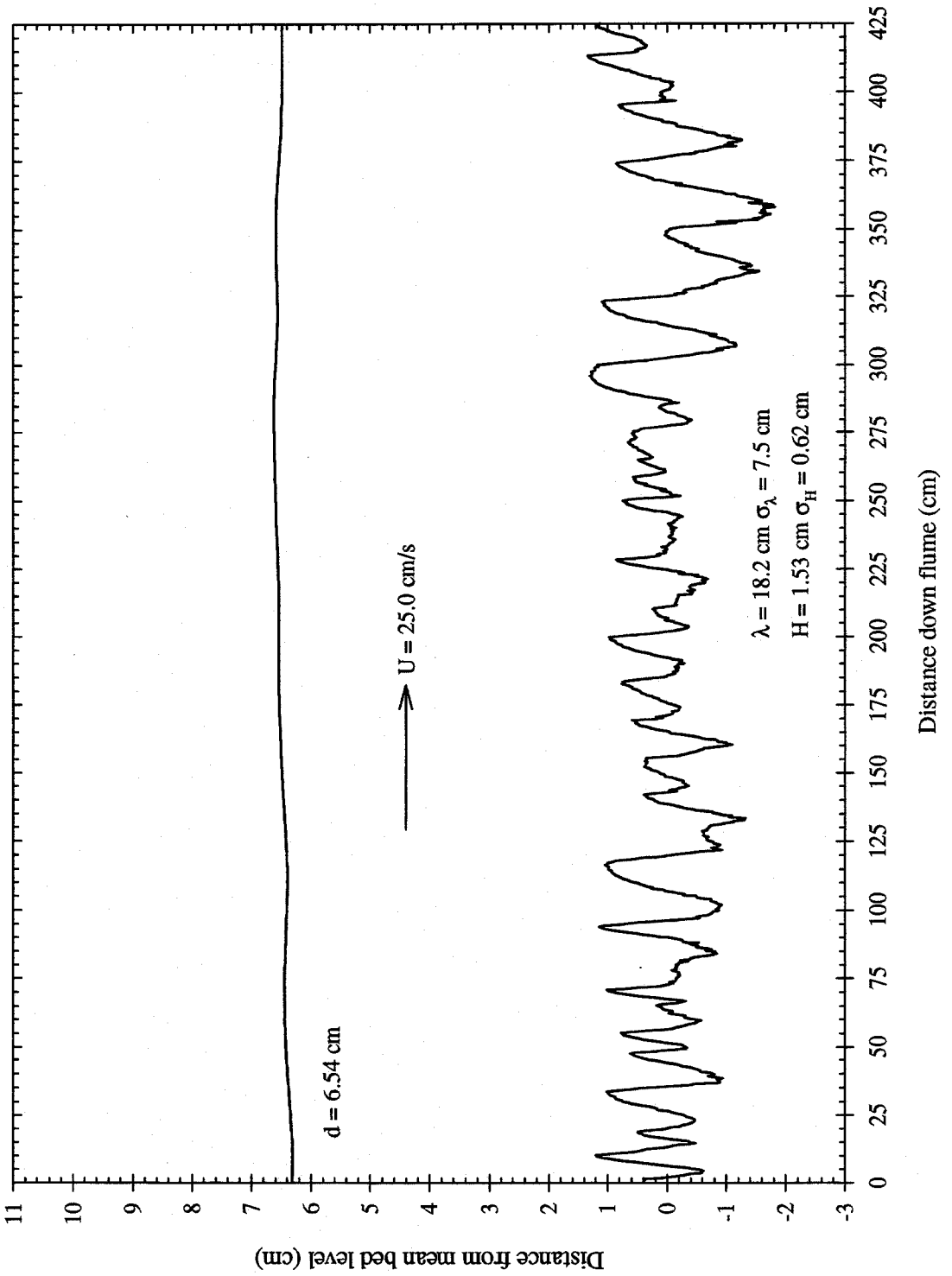

Figure A.9. Bed and water surface profiles from Flume Run 5.

a) pH

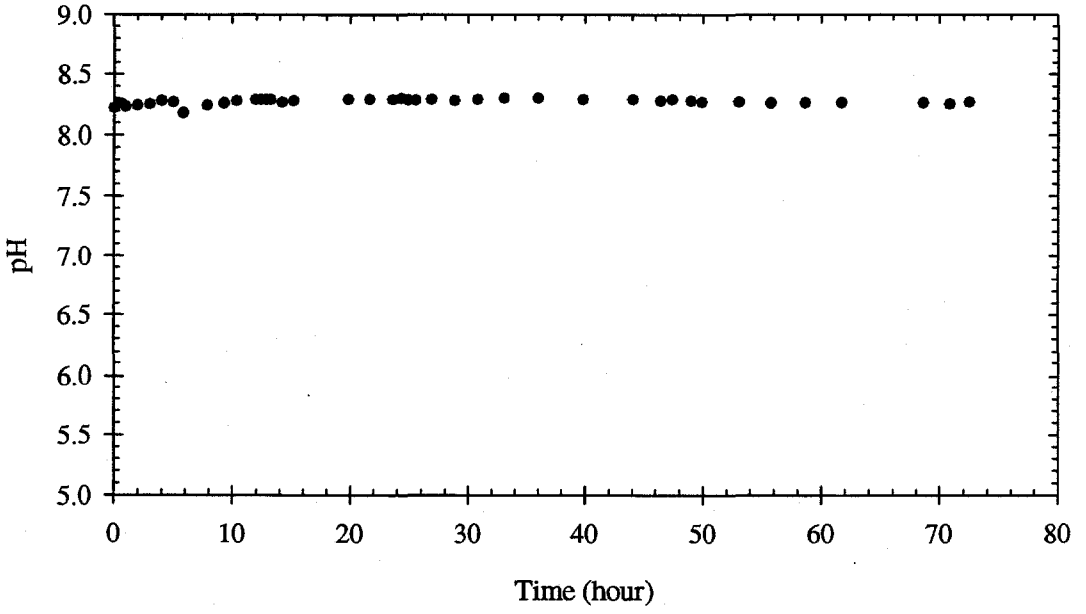

b) Water temperature

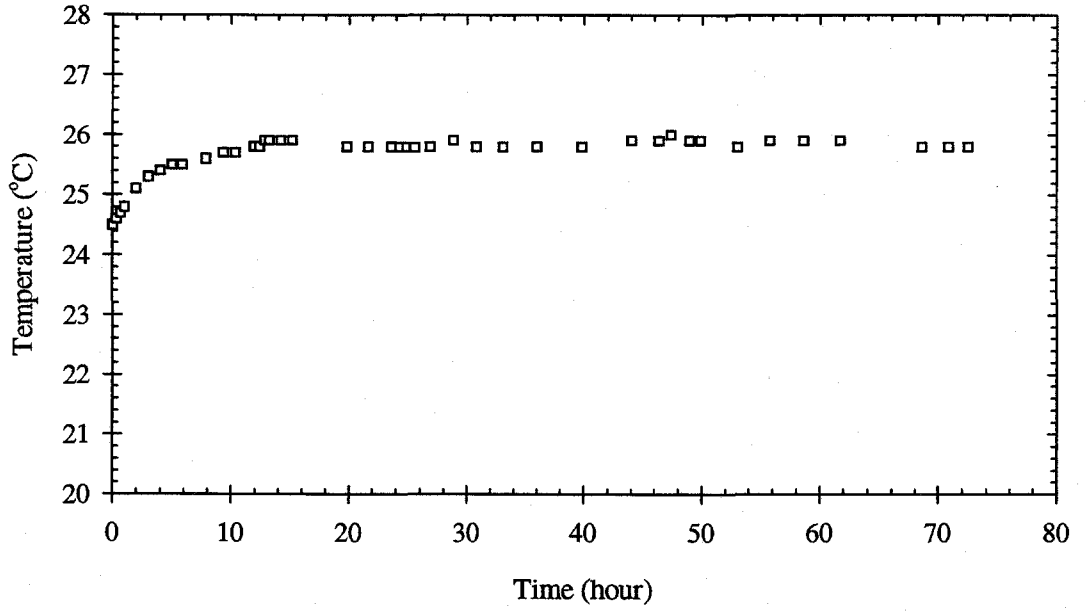

Figure A.10. Time history of a) pH and b) water temperature in Flume Run 5.

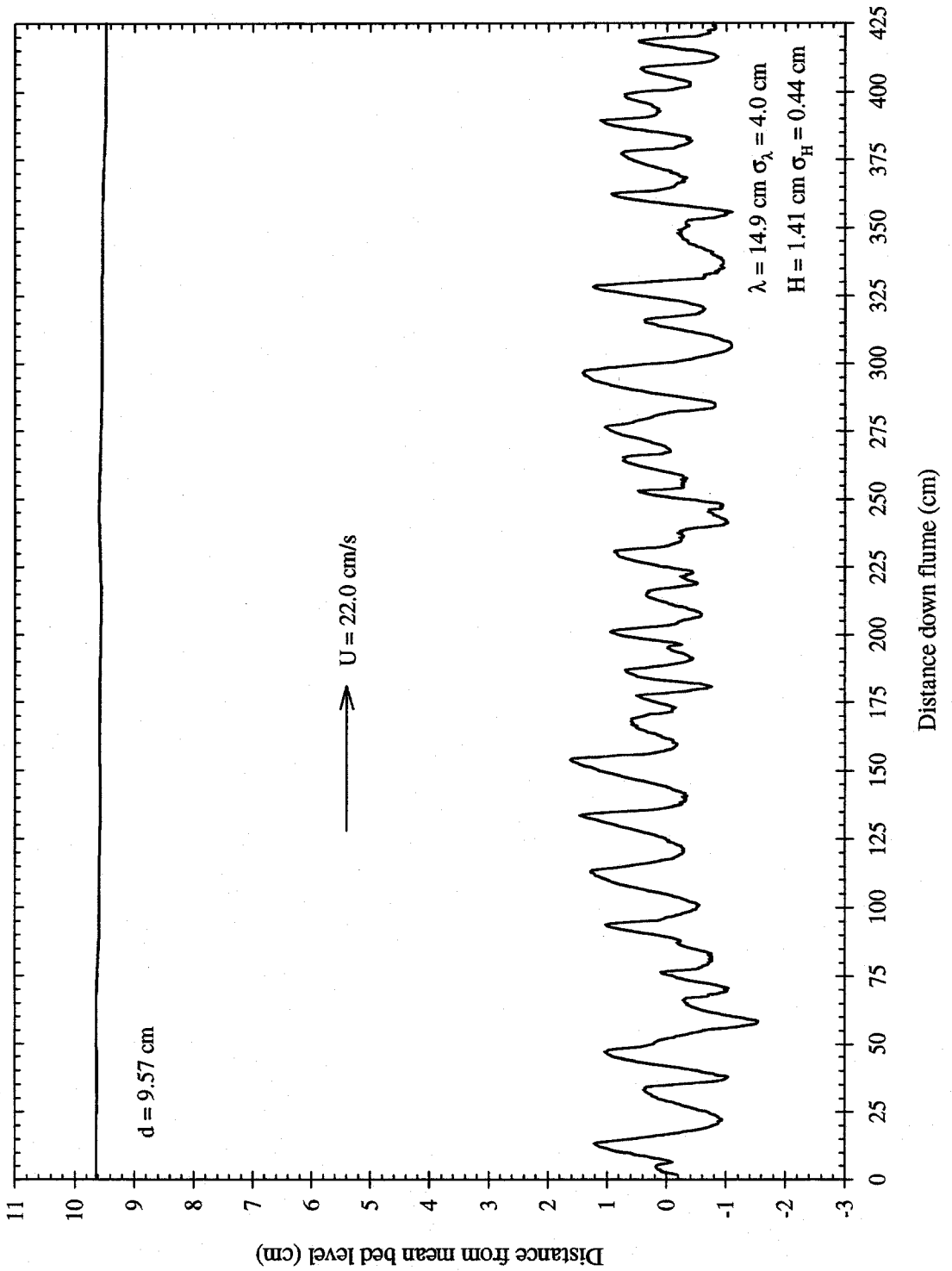

Figure A.11. Bed and water surface profiles from Flume Run 6.

a) pH

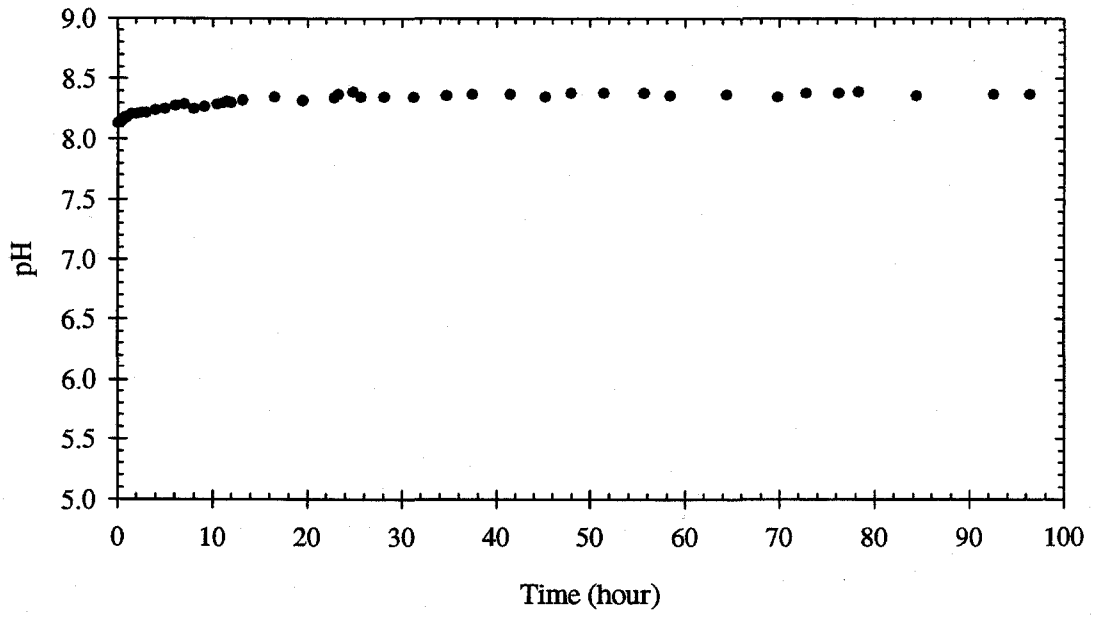

b) Water temperature

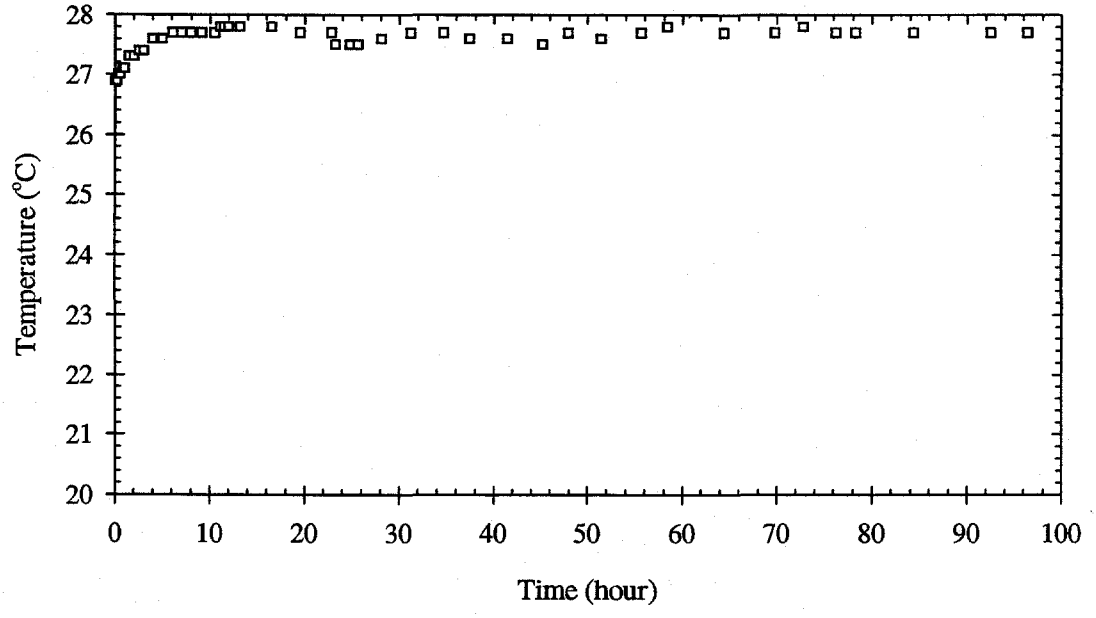

Figure A.12. Time history of a) pH and b) water temperature in Flume Run 6.

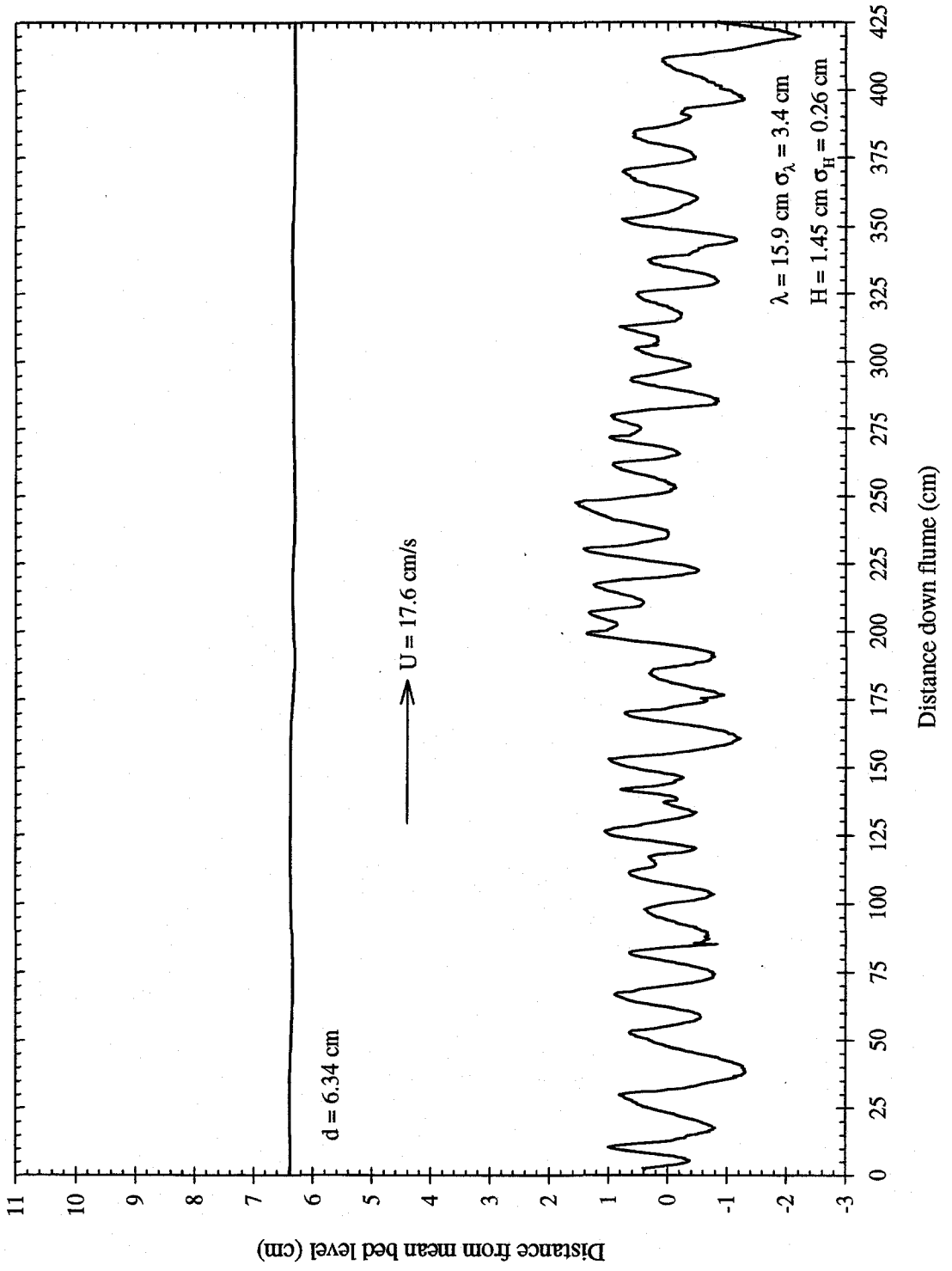

Figure A.13. Bed and water surface profiles from Flume Run 7.

a) pH

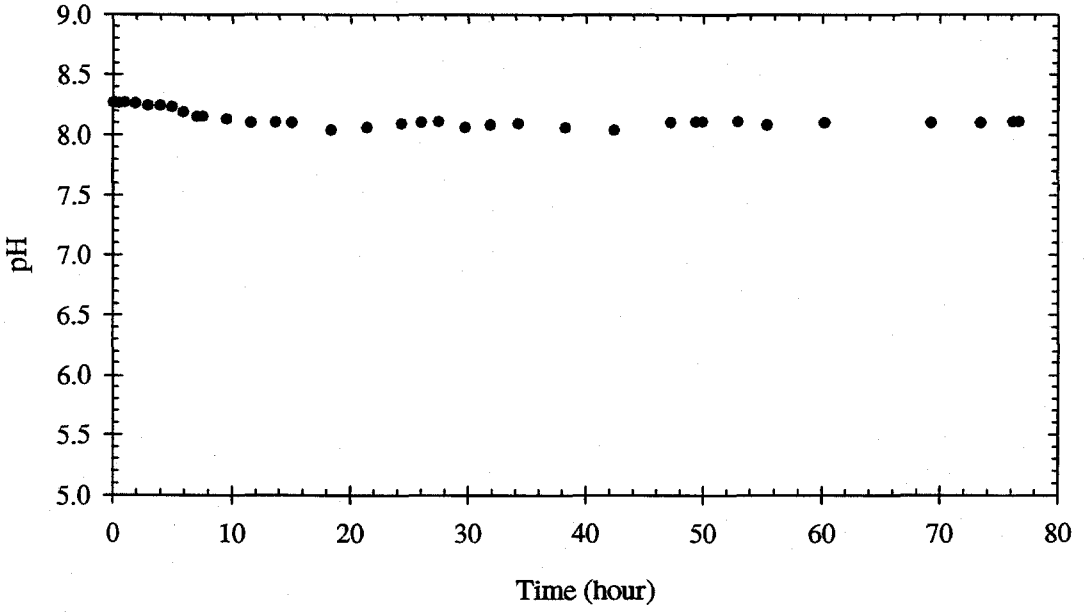

b) Water temperature

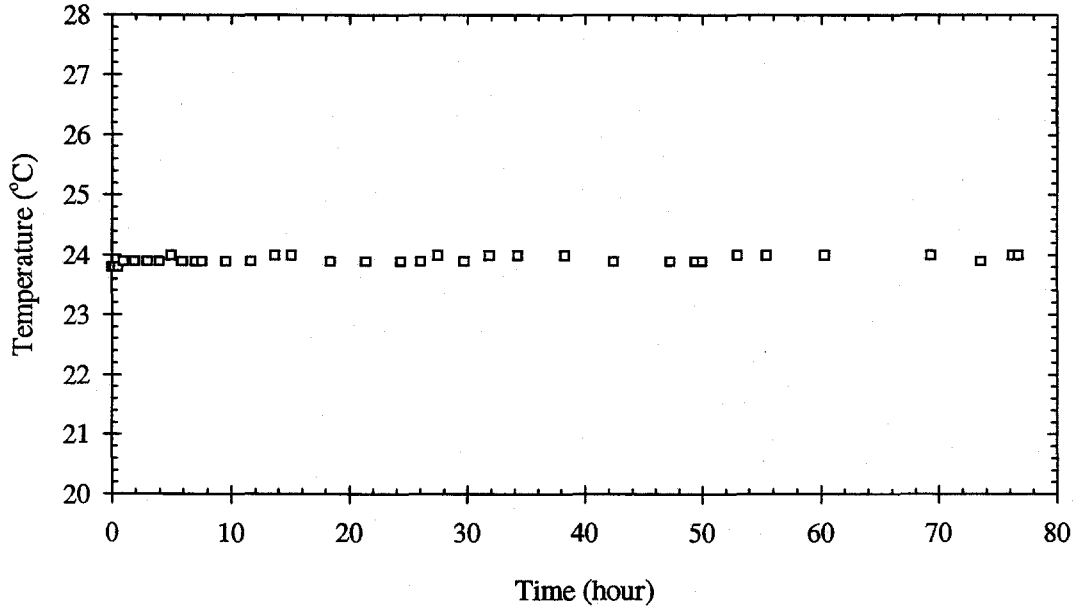

Figure A.14. Time history of a) pH and b) water temperature in Flume Run 7.

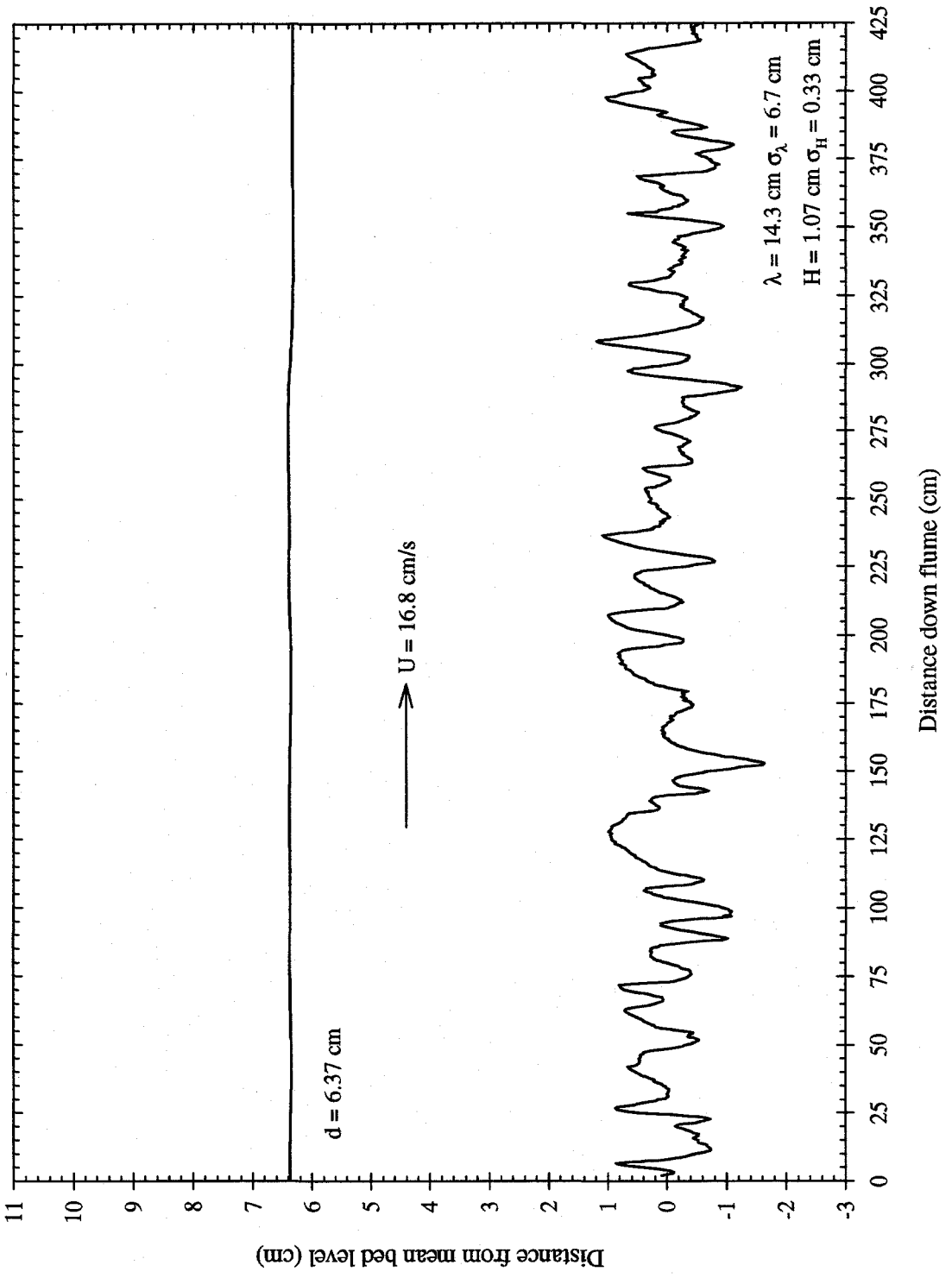

Figure A.15. Bed and water surface profiles from Flume Run 8.

a) pH

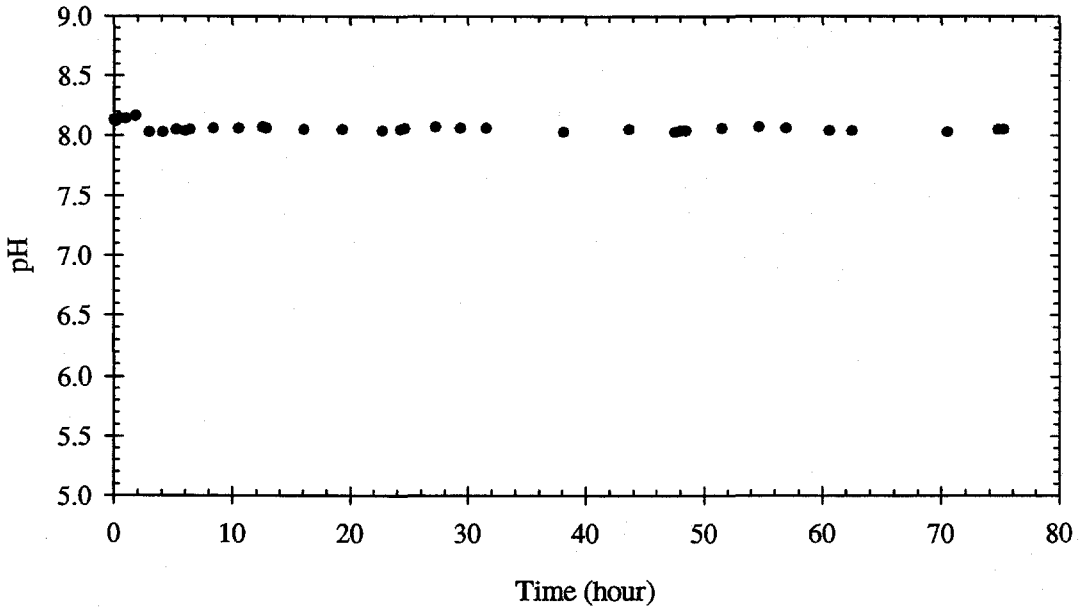

b) Water temperature

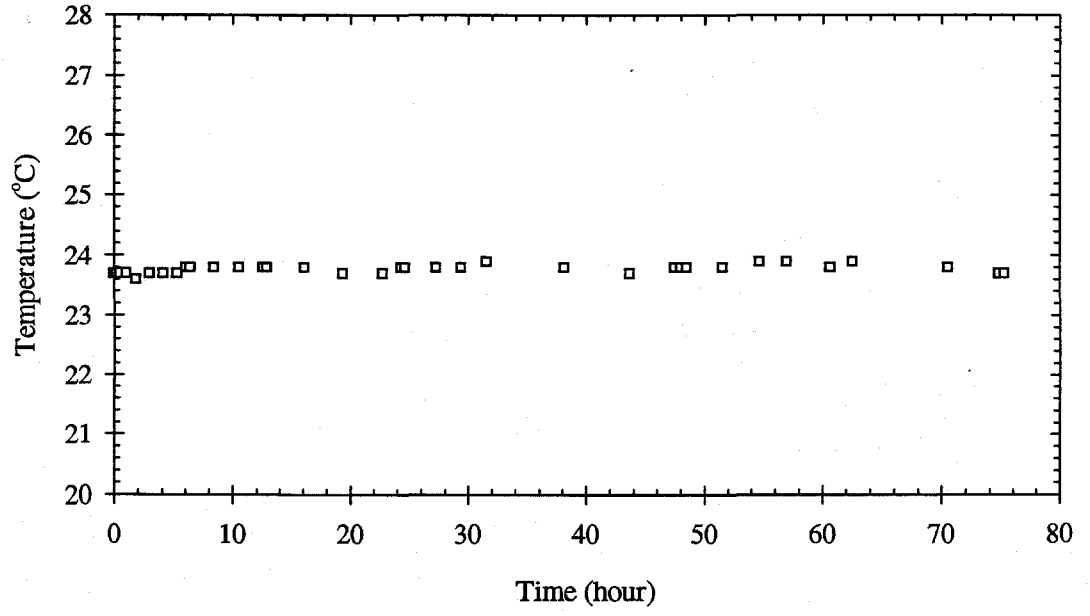

Figure A.16. Time history of a) pH and b) water temperature in Flume Run 8.

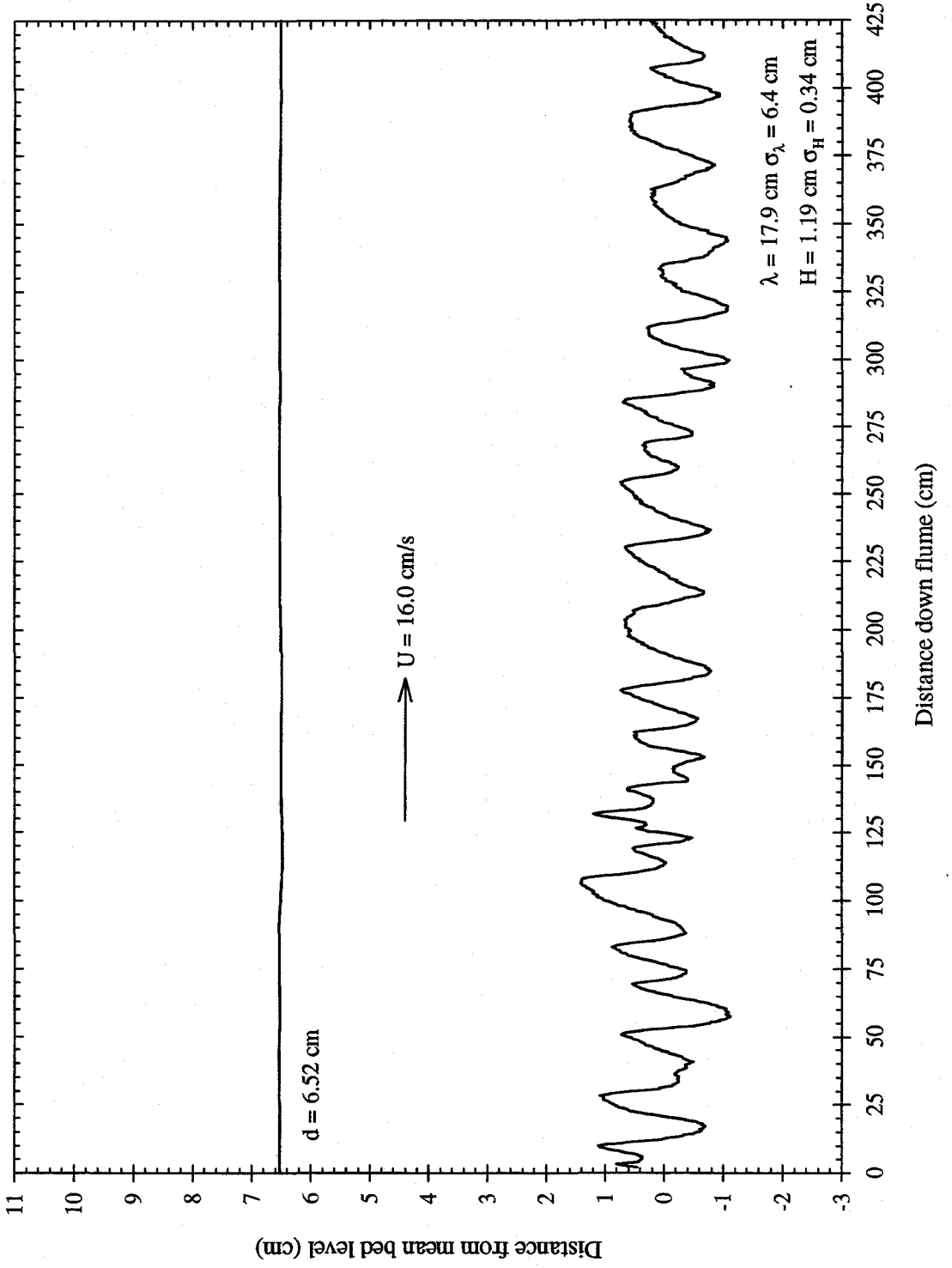

Figure A.17. Bed and water surface profiles from Flume Run 9.

a) pH

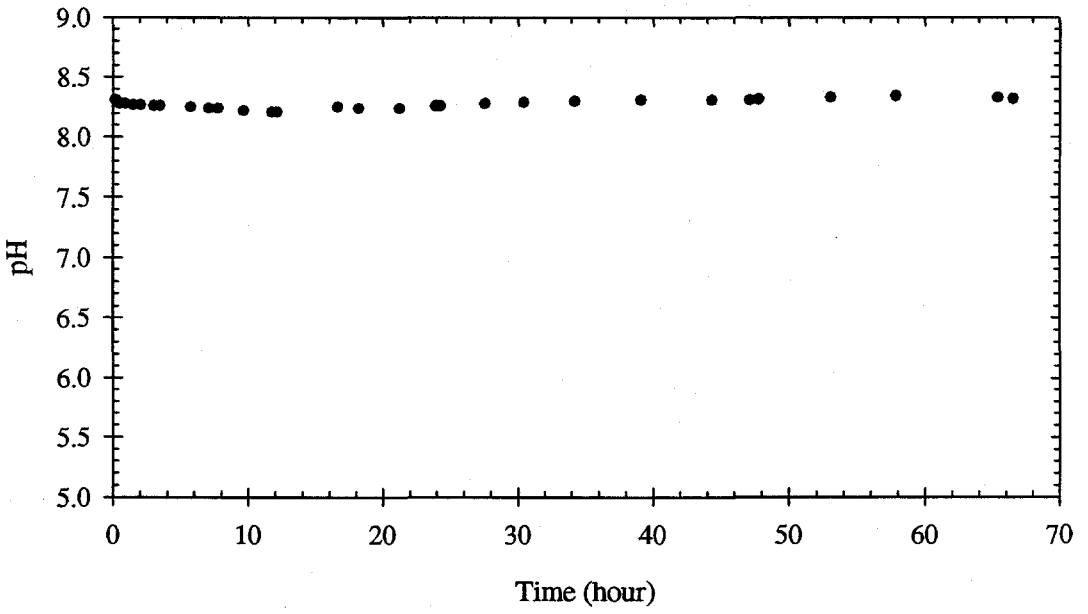

b) Water temperature

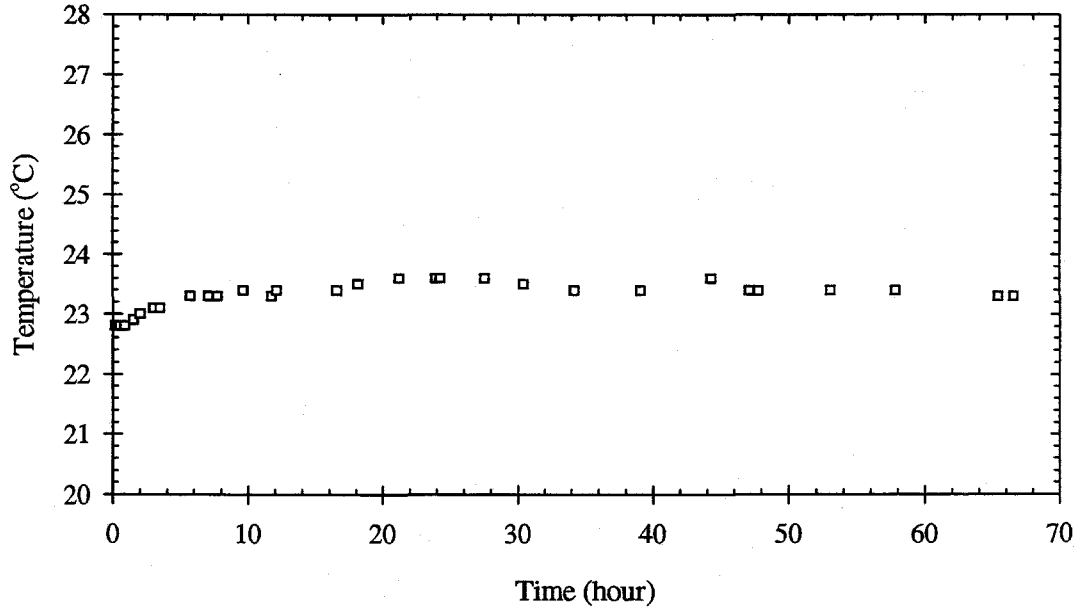

Figure A.18. Time history of a) pH and b) water temperature in Flume Run 9.

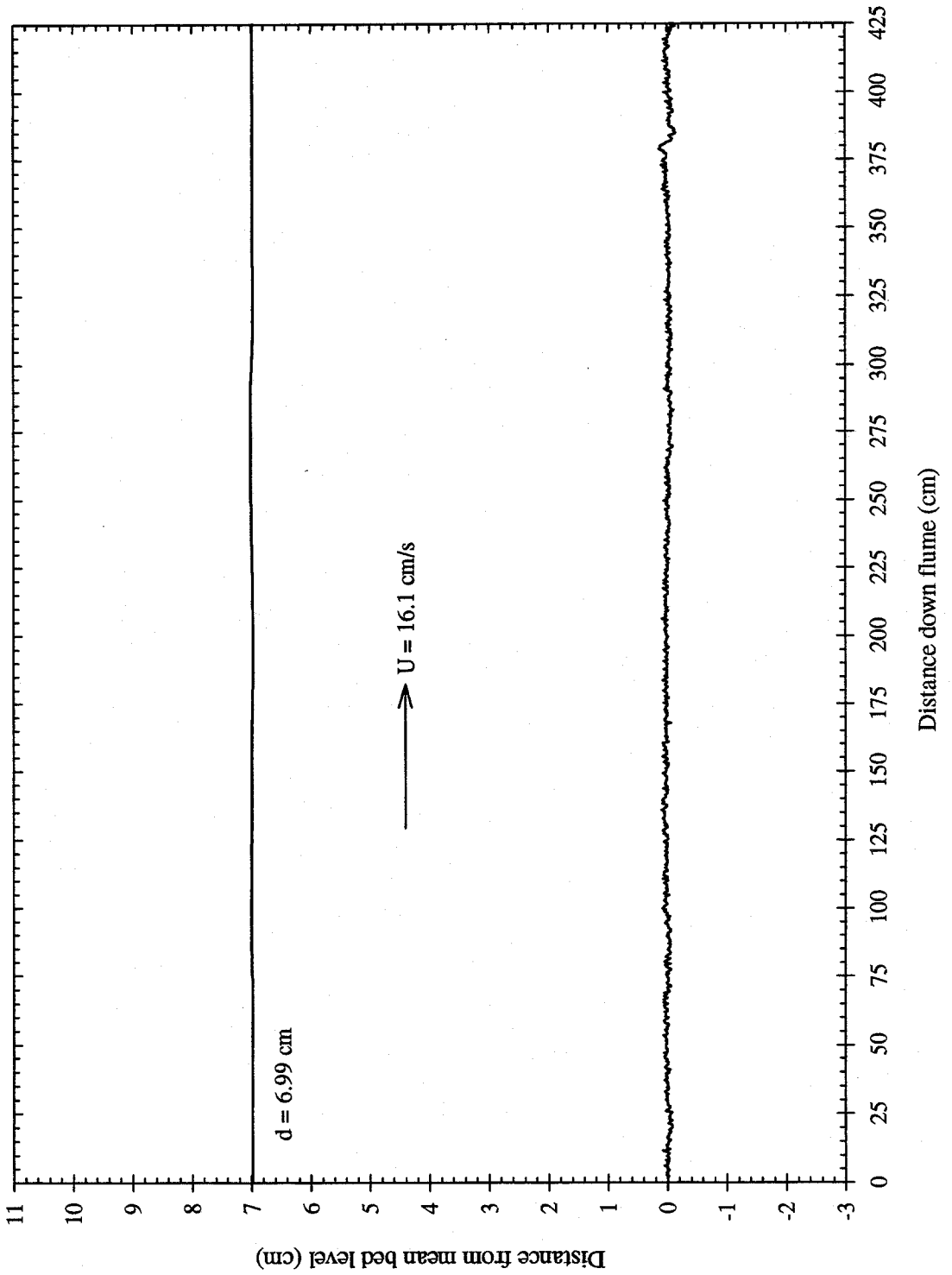

Figure A.19. Bed and water surface profiles from Flume Run 10.

a) pH

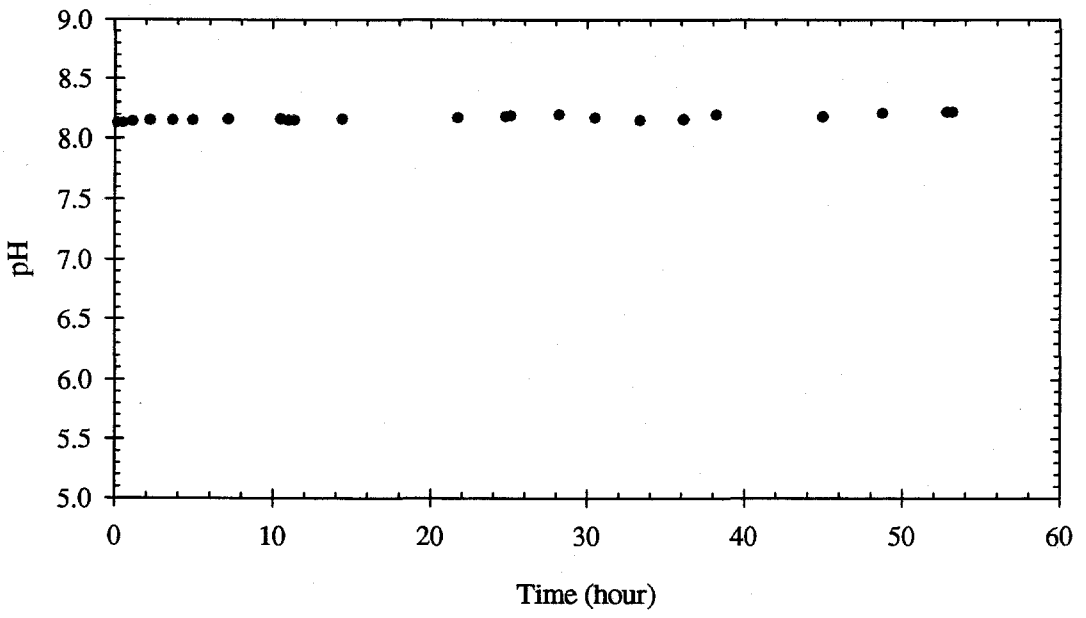

b) Water temperature

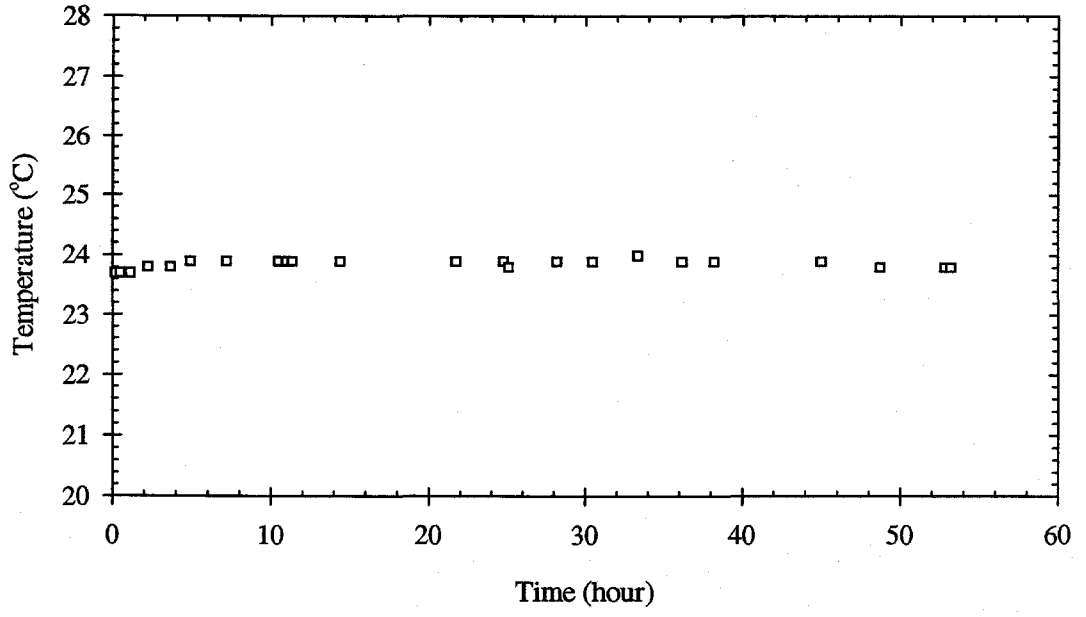

Figure A.20. Time history of a) pH and b) water temperature in Flume Run 10.

APPENDIX B – Errors in Adsorption Data

The following figures show the equilibrium adsorption data with error bars for the cationic surfactants on garnet sand. The supporting text is included in Chapter 5, Section 5.1.

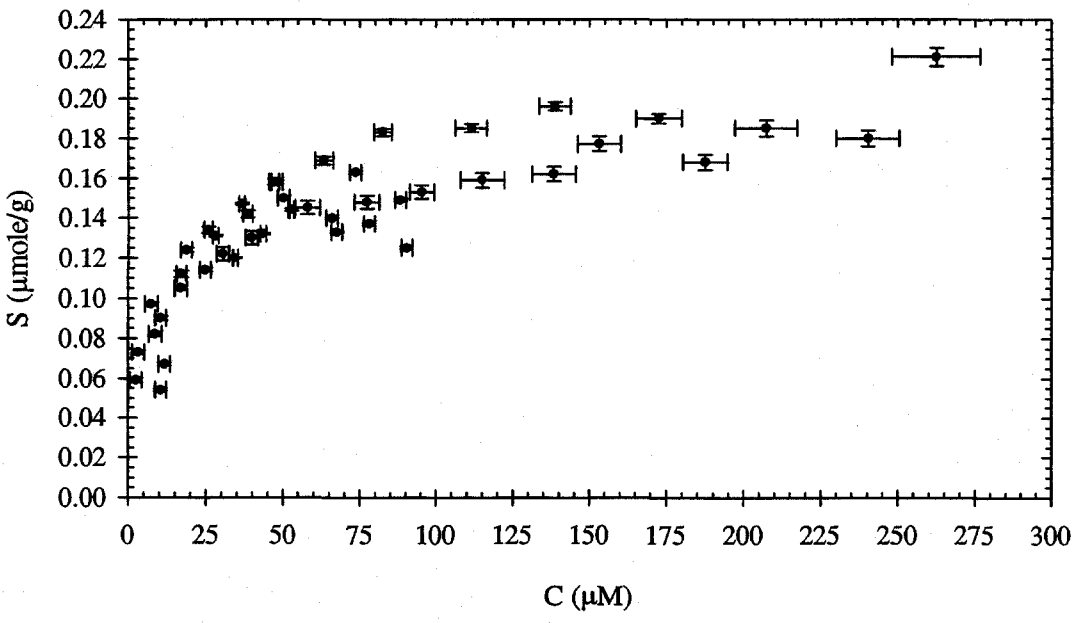

Figure B.1. DTMA adsorption on garnet sand at pH 7 in 1 mM NaCl.

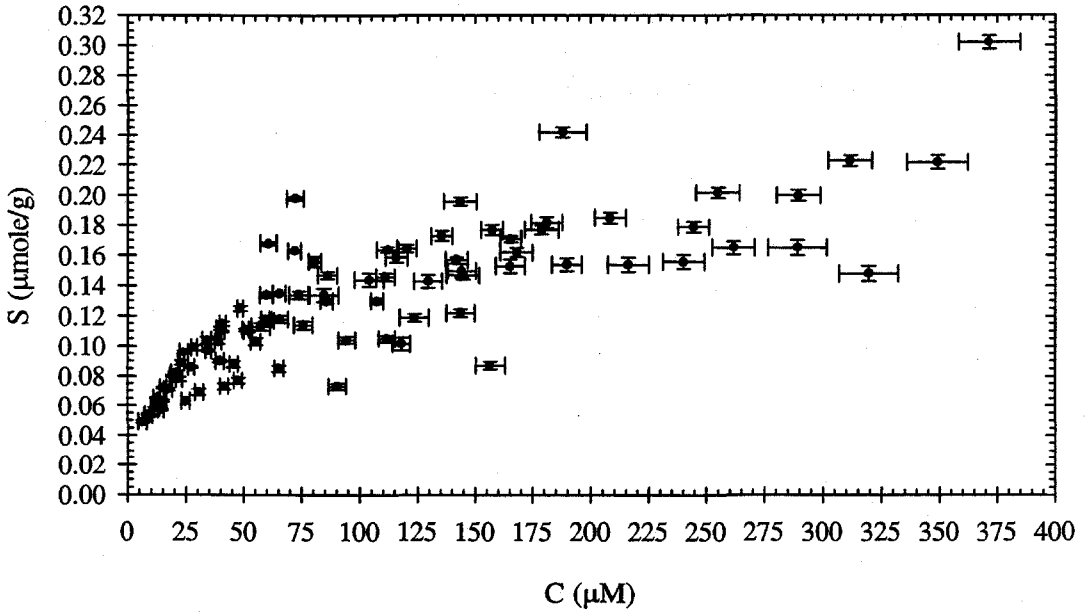

Figure B 2. DMTA adsorption on garnet sand at pH 7 in 10 mM NaCl.

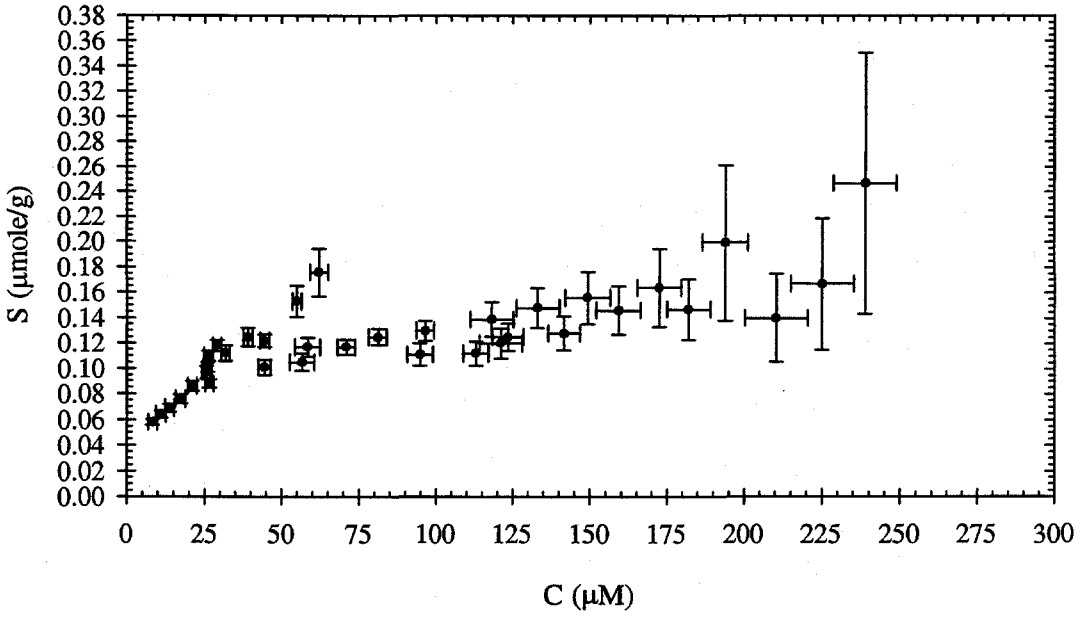

Figure B.3. DTMA adsorption on garnet sand at pH 8 in 10 mM NaCl for data acquired January 1997.

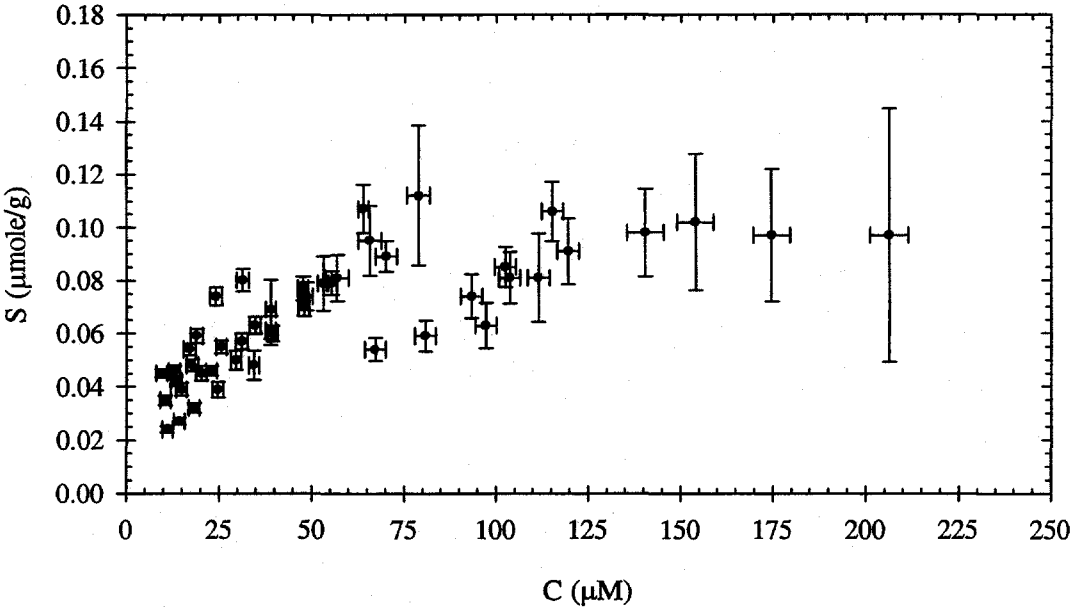

Figure B.4. DTMA adsorption on garnet sand at pH 8 in 10 mM NaCl for data acquired April 1998.

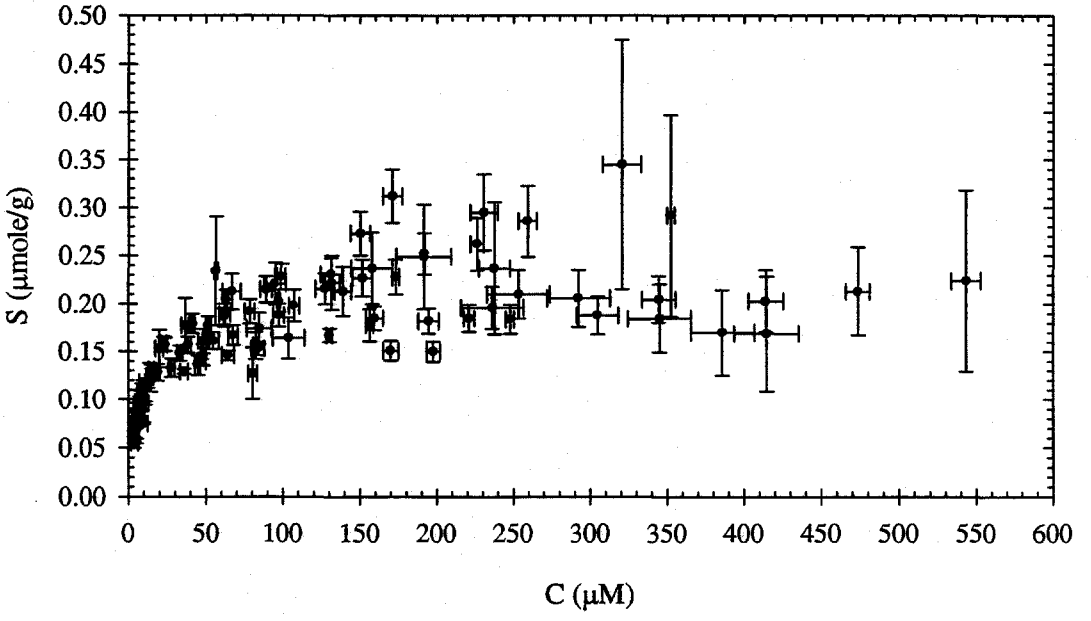

Figure B.5. MTMA adsorption on garnet sand at pH 8 in 10 mM NaCl

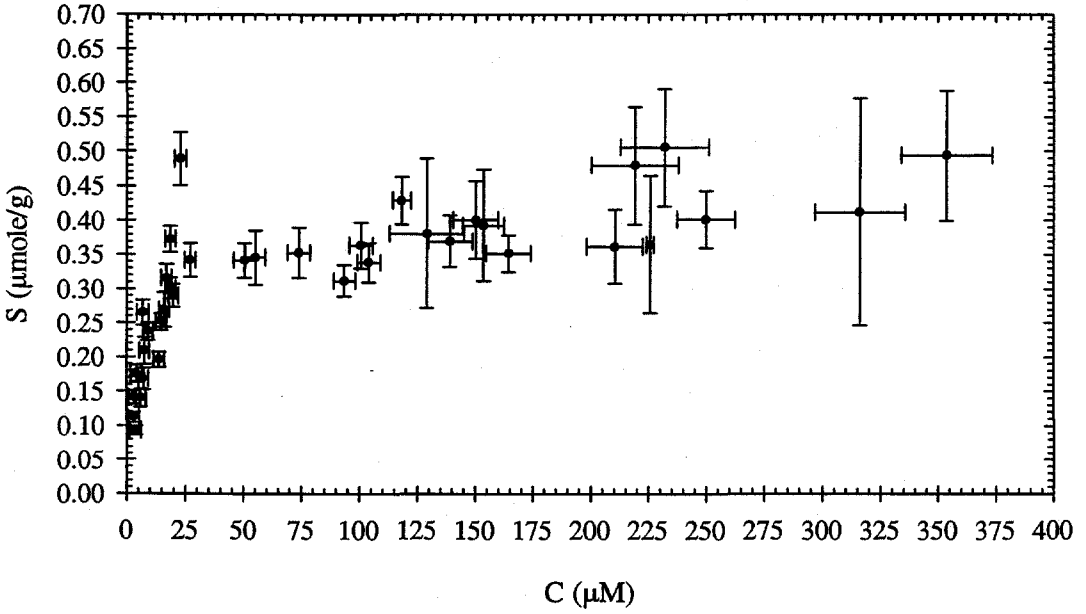

Figure B.6. OTMA adsorption on garnet sand at pH 8 in 10 mM NaCl.

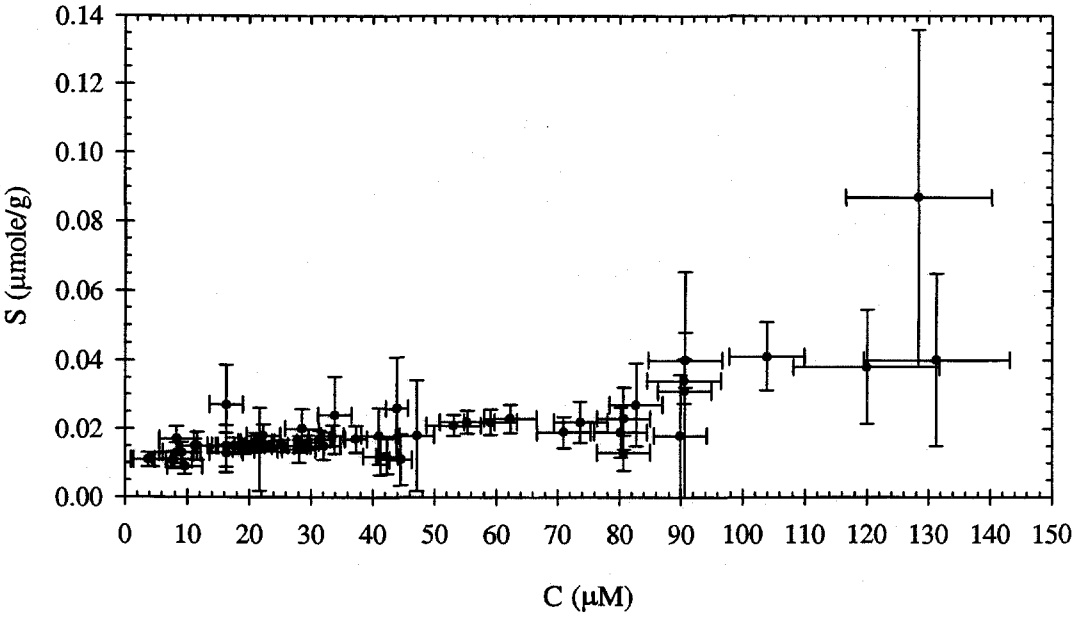

Figure B.7. NTMA adsorption on garnet sand at pH 8 in 10 mM NaCl.

APPENDIX C – Detailed Model Code and Verification

This appendix contains comparisons of the simulations from the finite difference models and the analytical models. The Fortran code for the detailed bed/stream exchange model based on the Langmuir isotherm is included at the end of the appendix.

In order to verify the finite difference method used to solve the advection equation (Chapter 3, Section 3.4.3.1), Figure C.1 compares the numerical solution to the analytical solution for the pulse injection of a contaminant into an initially clean column, which was presented in Chapter 3, Section 3.4.2.2. The column has a length L of 9.0 cm and a seepage velocity w_s of 3.41 cm/hr. It is assumed that the column is packed with garnet sand with a porosity of 0.47. The Langmuir sorption parameters for dodecyltrimethylammonium bromide are used (Chapter 5, Table 5.4). The feed concentration C_0 is 200 μM, and the pulse duration equals 3 hours. The differences between the numerical and analytical solutions are small and decrease with time.

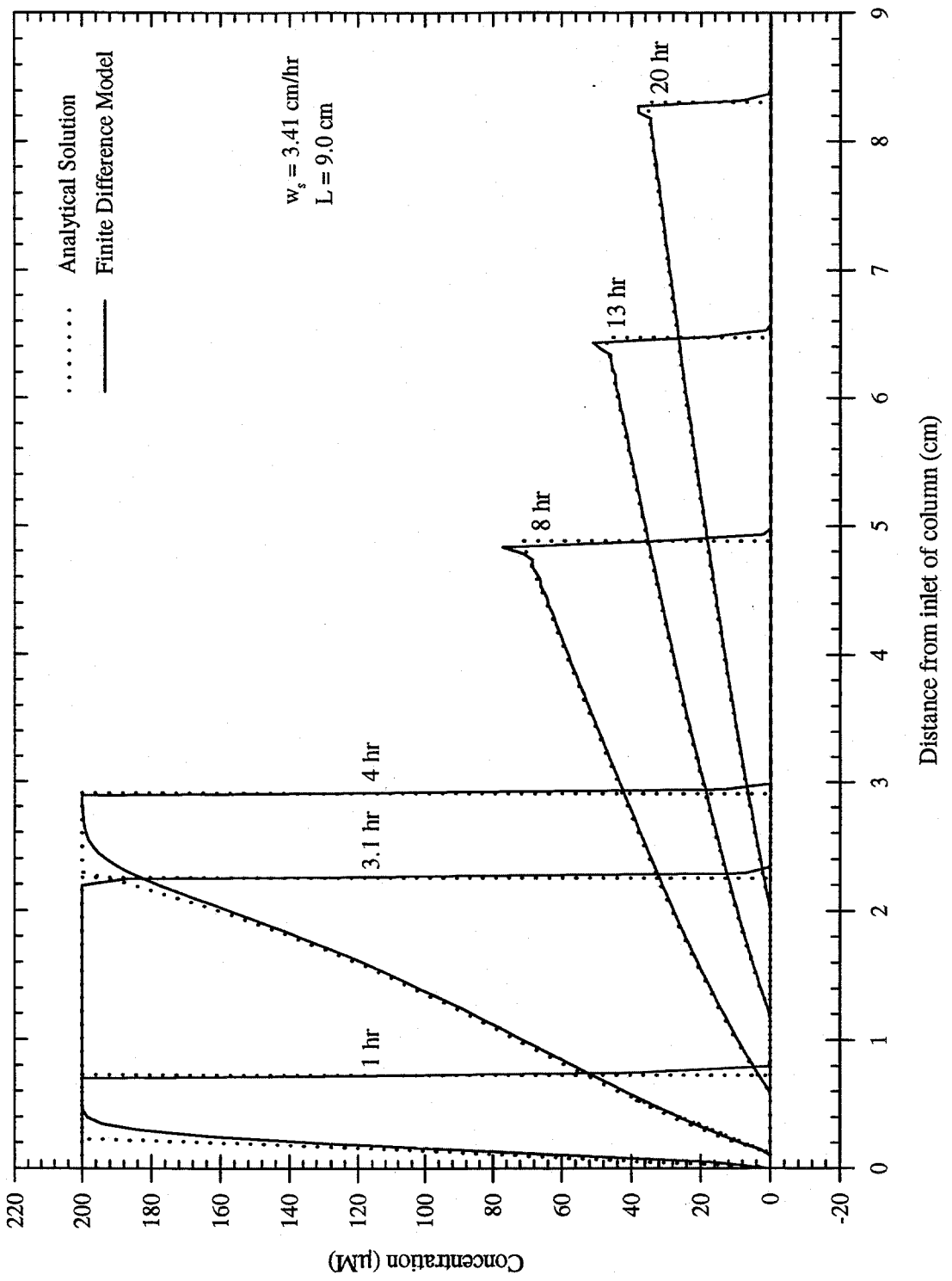

Figure C.1. Comparison of the finite difference solution to the analytical solution for a pulse injection of a DTMA into an initially clean column. The duration of the pulse is 3 hours. The feed concentration is 200 μM. The concentration profiles are compared at 1 hr, 3.1 hr, 4 hr, 8 hr, 13 hr and 20 hr.

Figure C.2 compares the bed/stream exchange simulations for a linearly adsorbing compound, with a retardation coefficient of 10, from Eylers' model, which is based on a modified residence time function, and the finite difference model using a linear isotherm (Chapter 3, Section 3.4.3). The hydraulic and bed parameters from Flume Run 2 are used (Chapter 5, Tables 5.10 through 5.12). The model predictions do not differ. Therefore, the numerical method does not introduce noticeable errors into the bed/stream exchange calculations.

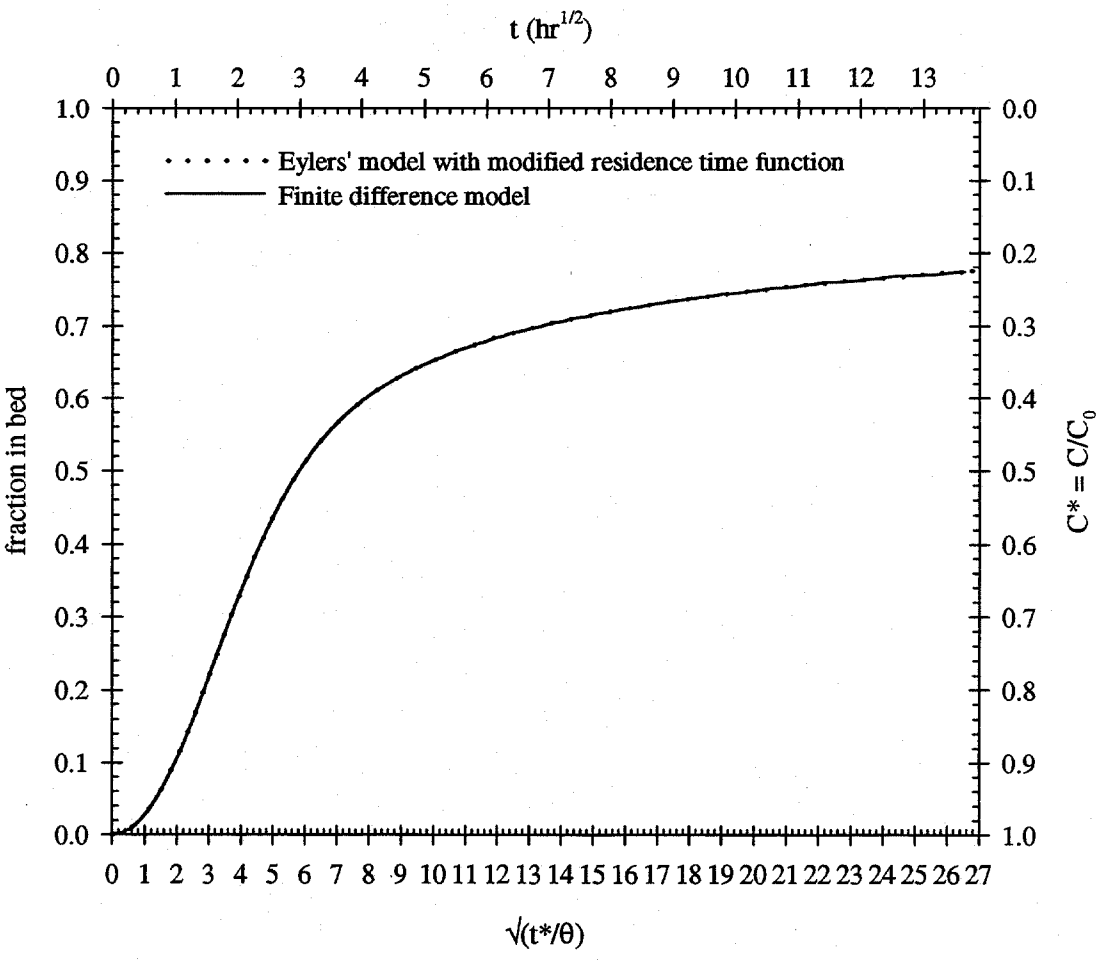

Figure C.2. Comparison of the predicted bed/stream exchange of a linearly adsorbing compound (R=10) from Eylers' model and the finite difference model. The hydraulic and bed parameters from Flume Run 2 are used.

The Fortran code for the bed/stream finite difference exchange model with Langmuir adsorption is listed on the following pages.

```
PROGRAM Exact_FlumeFD_Langmuir
!
!**********************************************************************
!  PROGRAM DESCRIPTION
!**********************************************************************
!  This program calculates the mass transfer of an adsorbing compound in to
!  a sand bed in the flume.  The Langmuir adsorption isotherm is used.  The
!  advection equation is solved along 65 streamlines.  The flux into and out
!  of the stream tubes is calculated and the concentration in the flume water
!  is computed.
!
!  The advection equation is solved using a finite difference method with the
!  flux correction.
!
!  Required inputs are the density of the solid, Kh, porosity, wavelength, d',
!  hm, C0, Klangmuir, Cs_max, thr_max.
!
!  The user has the opportunity to get bed concentration profiles at user
!  specified times.
!
!**************************************************************************
!  VARIABLE DESCRIPTIONS
!--------------------------------------------------------------------------
!  INPUTS:
!   InFile = name of input file (character, length 15)
!   OutFile = name of output file for overlying water results (character,
!             length 15)
!   PFile = name of output file for bed concentration profiles (character,
!           length 15)
!   SG = specific gravity in g/cm^3 (real)
!   Kh = hydraulic conductivity in cm/s (real)
!   theta = porosity (real)
!   wvl = bedform wavelength in cm (real)
!   dprime = effective water depth in cm (real)
!   hm = amplitude of the dynamic pressure head in cm (real)
!   C0 = initial concentration in uM (real)
!   Klg = Langmuir constant K in uM^-1 (real)
!   Smax = Langmuir maximum surface coverage in umole/g (real)
!   thr_max = maximum run time in hours (real)
!   TP_hr = time in hours at which bed concentrations will be written to PFile
!           (real)
!
!  CONSTANTS:
!   PI =
!   dratio = maximum allowable Courant number used in finite difference
!            solution (real)
!   N_tube = number of stream tubes (integer)
!
!  OUTPUTS:
!    Cw() = concentration in overlying flume water in uM (real array)
!    Cb() = concentration in streamtube in uM (real array)
!    time_hr = (real)
!    tstar = dimensionless time (real)
!    Cstar = Cw()/C0 (real)
!    fbed = fraction of mass in bed (real)
!    db_eq = equivalent mixing depth in bed in cm (real)
!
!
!  INTERMEDIATE VARIABLES:
!   kwn = bedform wavenumber in cm^-1 (real)
!   um = maximum Darcy velocity in cm/hr (real)
!   nu = bulk density of bed divided by porosity (real)
!   gamma = product of Langmuir parameters Klg and Smax
```

```
!    dtime = tstar increments (real)
!    mass_in = mass transport into bed per unit area (umole/cm^2) (real)
!    mass_out = mass transport out of bed per unit area (umole/cm^2) (real)
!    Dmass_bed = change of mass in bed per unit area (umole/cm^2) (real)
!
!   STREAMTUBE VARIABLES
!   dX_0() = width of streamtube (real array)
!   Length() = length of streamtube (real array)
!   Darcy_v() = Darcy velocity in streamtube (real array)
!   dL() = distance increment along streamtube used in finite difference calcs
!          (real array)
!   Nodes() = number of distance increments in streamtube (integer array)
!
!   FINITE DIFFERENCE VARIABLES
!   Gb()
!   A_p()
!   A_n()
!   G_L()
!   G_a()
!   G_b()
!   R_p()
!   R_n()
!   Cs()
!   Gs
!   FL_p
!   FL_n
!   FH_p
!   FH_n
!   G_max
!   G_min
!   P_p
!   P_n
!   Q_p
!   Q_n
!   U_p
!   U_n
!   Ac_p
!   Ac_n
!
!   Miscellaneous programming variables:
!    DtAr = array needed for numeric output of date and time function (real)
!    Date = character variable for date and time function (length 8)
!    Tmfile = " (length 10)
!    Zone  =  " (length 5)
!    Ans  = user y/n response to questions (character, length 1)
!    Cdiff = difference in C* used to determine whether or not to write the
!            result
!    LastC = last C* written to the output file (real)
!    S_star = streamline coordinate used in velocity calculations (real)
!    X_star = x-coordinate corresponding to S_star (real)
!
!-------------------------------------------------------------------------------

IMPLICIT NONE

INTEGER, PARAMETER :: N_tube = 65

INTEGER :: I,J, N, P, T, Nodes(1:N_tube), DtAr(8), P_dim

REAL :: SG, Kh, theta, wvl, dprime, hm, C0, Klg, Smax, thr_max, &
        kwn, um, nu, gamma, dX_0, time_hr, tstar, Cstar, fbed, db_eq, &
        LastC, Cdiff, FL_p, FL_n, Gs, FH_p, DMass_bed, S_star, X_star, &
        FH_n, G_max, G_min, P_p, P_n, Q_p, Q_n, U_p, U_n, Ac_p, Ac_n, Retard, &
```

```
        X_0(1:N_tube), Length(1:N_tube), Darcy_v(1:N_tube,0:200),&
        dL(1:N_tube), dratio(1:N_tube), Cs(-1:0), &
        Cb(1:N_tube,0:200,2), Gb(1:N_tube,0:200,2), A_p(0:200), A_n(0:200), &
        G_L(0:200), G_a(0:200), G_b(0:200), R_p(0:200), R_n(0:200)

REAL, PARAMETER :: PI = 3.141592653589793, dtime = 0.01

REAL, ALLOCATABLE :: Cw(:), TP_hr(:)

CHARACTER (LEN = 15) :: InFile, OutFile, Ans*1, Date*8, Tmfile*10, Zone*5
CHARACTER (LEN = 15), ALLOCATABLE :: PFile(:)

COMMON/Tube_info/ Nodes, X_0, Length, Darcy_v, dL, dratio
COMMON/FD_soln_var/ Cb, Gb, A_p, A_n, G_L, G_a, G_b, R_p, R_n

!-------------------------------------------------------------------------------
    InFile = "f2in_hcn.txt"
    OutFile = "f2lg_hcn.out"

    P = 0
    P_dim = 1
    ALLOCATE(TP_hr(1:P_dim), PFile(1:P_dim))
    TP_hr(1) = 5.0
    PFile(1) = " "

!-------------------------------------------------------------------------------
!-------------------------------------------------------------------------------
! GET INPUTS:


   open (UNIT = 13, FILE = InFile, ACTION = "READ", position = "REWIND")

   read (13,*) SG
   read (13,*) Kh
   read (13,*) theta
   read (13,*) wvl
   read (13,*) dprime
   read (13,*) hm
   read (13,*) C0
   read (13,*) Klg
   read (13,*) Smax
   read (13,*) thr_max

   close (13)

!-------------------------------------------------------------------------------
!  INQUIRE ABOUT BED CONCENTRATION PROFILES

   if (P > 0) then

     open (UNIT = 14, FILE = PFile(P), STATUS = "REPLACE", ACTION = "WRITE", &
         position = "REWIND")

     WRITE(14,*) "Bed concentration output from program 'EFD_Lang.f90'."

     CALL date_and_time(Date, Tmfile, Zone, DtAr)
     WRITE(14, FMT="('Date: ',I2,'/',I2,'/',I4)") DtAr(2), DtAr(3), DtAr(1)
     write(14, FMT="('Time: ',I2,':',I2,':',I2)") DtAr(5), DtAr(6), DtAr(7)
     write(14,*)

     write (14,*) "Bed concentration profiles"
     write (14,*)
```

```
   end if

!-------------------------------------------------------------------------------
!  OPEN OUTPUT FILE and WRITE inputs to it


   open (UNIT = 12, FILE = OutFile, STATUS = "REPLACE", ACTION = "WRITE", &
         position = "REWIND")

   PRINT *, "Writing inputs"

   WRITE(12,*) "Output from program 'EFD_Lang.f90'."

   CALL date_and_time(Date, Tmfile, Zone, DtAr)
   WRITE(12, FMT="('Date: ',I2,'/',I2,'/',I4)") DtAr(2), DtAr(3), DtAr(1)
   write(12, FMT="('Time: ',I2,':',I2,':',I2)") DtAr(5), DtAr(6), DtAr(7)
   write(12,*)

   write(12,*) "Specific gravity (g/cm^3),,,", SG
   write(12,*) "Hydraulic conductivity (cm/s),,,", Kh
   write(12,*) "Porosity,,,", theta
   write(12,*) "Bedform wavelength (cm),,,", wvl
   write(12,*) "d' (cm),,,", dprime
   write(12,*) "hm (cm),,,", hm
   write(12,*) "C0 (uM),,,", C0
   write(12,*) "Langmuir K (uM)^-1,,,", Klg
   write(12,*) "Langmuir Smax (umole/g),,,", Smax
   write(12,*) "Maximum time (hr),,,", thr_max
   write(12,*)
   write(12,*) "Time increment in hours = ,,,", dtime

   PRINT *, "Finished writing inputs"

!-------------------------------------------------------------------------------
!  PRELIMINARY CALCULATIONS & ARRAY ALLOCATIONS & VARIABLE INITIALIZATION

kwn = 2.*PI/wvl
um = kwn*(Kh*60.*60.)*hm
nu = SG*1000.*(1-theta)/theta
gamma = Klg*Smax

!  Streamtube characterization

dX_0 = (PI/2.0)/REAL(N_tube)
PRINT *, "calculating streamtube parameters ...."

DO T = 1, N_tube

  X_0(T) = (REAL(T)*dX_0) - 0.5*dX_0

  Length(T) = LOG(TAN((PI/4.0) + (0.5*X_0(T)))) - LOG(TAN((PI/4.0) -
(0.5*X_0(T))))

  dratio(T) = 0.5

  dL(T) = dtime/dratio(T)

  Nodes(T) = INT(Length(T)/dL(T))

  if (Nodes(T) < 100) then

    dL(T) = dtime/0.9
    Nodes(T) = INT(Length(T)/dL(T))
```

```
    dL(T) = Length(T)/REAL(Nodes(T))
    dratio(T) = dtime/dL(T)

    if ( dratio(T) > 0.999 .or. Nodes(T) < 2) then
      PRINT *, "Tube = ", T, " X_0 = ", X_0(T)
      PRINT *, "Length = ", Length(T), " Nodes = ", Nodes(T)
      PRINT *
      PRINT *, "WARNING:  Ratio EXCEEDS 1.  It's value is ", dratio(T)
      PRINT *, "Is this acceptable (y/n)? "
      read *, Ans
      PRINT *
      IF (Ans == "n" .or. Ans == "N") THEN
        PRINT *, "Program TERMINATED"
        STOP
      END IF

    end if

  else if (Nodes(T) < 200) then

    dL(T) = Length(T)/REAL(Nodes(T))
    dratio(T) = dtime/dL(t)

  else

    Nodes(T) = 200
    dL(T) = Length(T)/REAL(Nodes(T))
    dratio(T) = dtime/dL(t)

    if ( dratio(T) > 0.9) then
      PRINT *, "Tube = ", T, " X_0 = ", X_0(T)
      PRINT *, "Length = ", Length(T), " Nodes = ", Nodes(T)
      PRINT *
      PRINT *, "WARNING:  Ratio EXCEEDS 1.  It's value is ", dratio(T)
      PRINT *, "Is this acceptable (y/n)? "
      read *, Ans
      PRINT *
      IF (Ans == "n" .or. Ans == "N") THEN
        PRINT *, "Program TERMINATED"
        STOP
      END IF
    end if

  end if

  do N = 0, Nodes(T)

    S_star = REAL(N)*dL(T)
    X_star = (2.0*ATAN(EXP(-S_star)*TAN((PI/4.0) + (X_0(T)/2.0)))) - (PI/2.0)
    Darcy_v(T,N) = COS(X_0(T))/COS(X_star)

  end do

END DO

PRINT *,"finished calculating streamtube parameters"
PRINT *

!  Initialize Bed Concentrations
  PRINT *, "initializing bed parameters...."
  DO T = 1, N_tube
    do J = 1,2
```

```
      DO N = 0, Nodes(T)

        Cb(T,N,J) = 0.0
        Gb(T,N,J) = 0.0

      END DO
    end do
  END DO
PRINT *, "finished initializing bed."
PRINT *
!  Initialize Variables

ALLOCATE(Cw(0:(INT((thr_max*kwn*um/theta)/dtime)+2)))

time_hr = 0.0
tstar = 0.0
I = 0
Cw(0) = C0
Cstar = 1.0
fbed = 0.0
db_eq = 0.0

write (12,200)
write (12,*)

write (12,201) time_hr, tstar, Cstar, fbed, db_eq, Cw(0)

LastC = Cstar
!-------------------------------------------------------------------------------
!  SOLVE AND INCREMENT OVER TIME
!
!  Loop over I = Loop over time
DO

  !Mass flux into and out of bed during dtime
  DMass_bed = 0.0
  do T = 1, N_tube
    DMass_bed = DMass_bed + (SIN(X_0(T))*(Cw(I) - Cb(T,Nodes(T),1)))
  end do
  DMass_bed = (theta/(PI*kwn))*DMass_bed*(dX_0*dtime)


  !Bed concentrations at bed surface
  DO T = 1, N_tube
    Cb(T,0,2) = Cw(I)
    Gb(T,0,2) = Cw(I)*(1.*(nu*gamma)/(1.+(Klg*Cw(I))))
  END DO


  !Calculate concentration profiles in bed after dtime
  PRINT *, "time (hr) = ", time_hr + (theta/(um*kwn))*dtime
  PRINT *, "Started bed calculations ...."

  DO T = 1, N_tube     !loop over streamtubes

    do N = 0, Nodes(T)    !loop to calculate low-order and high-order flows

      !low-order flows
      if (N > 0) then

        FL_p = dratio(T)*Darcy_v(T,N)*Cb(T,N,1)
        FL_n = dratio(T)*Darcy_v(T,N)*Cb(T,N-1,1)
```

```
  end if

  !high-order flows
  if (N == 0) then
    Gs = Gb(T,N,2)
  else if (N == Nodes(T)) then
    Gs = Gb(T,N,1)
  else
    Gs = Gb(T,N,1) - dratio(T)*Darcy_v(T,N)*(Cb(T,N+1,1) - Cb(T,N,1))
  end if

  if (Gs > 0.0) then

    Cs(0) = (0.5/Klg)*((Klg*Gs) - 1.0 - (nu*gamma) + &
            SQRT( ((1.0 + (nu*gamma) - (Klg*Gs))**2.0) + (4.0*Klg*Gs)))

  else

    Cs(0) = 0.0
    Gs = 0.0

  end if

  if (N > 0) then

    IF (N == Nodes(T)) THEN
      FH_p = (0.5*dratio(T))*Darcy_v(T,N)*(Cb(T,N,1) + Cs(0))
    ELSE
      FH_p = (0.5*dratio(T))*Darcy_v(T,N)*(Cb(T,N+1,1) + Cs(0))
    END IF

    FH_n = (0.5*dratio(T))*Darcy_v(T,N)*(Cb(T,N,1) + Cs(-1))

    !Anti-diffusion terms
    A_p(N) = FH_p - FL_p
    A_n(N) = FH_n - FL_n

    !Low-order solution
    G_L(N) = Gb(T,N,1) - (FL_p - FL_n)

  end if

  Cs(-1) = Cs(0)

end do

!Intermediate terms need to calculate flux correction
do N = 0, Nodes(T)

  if (N == 0) then

    G_a(N) = Gb(T,N,2)
    G_b(N) = Gb(T,N,2)

  else

    G_a(N) = MAX( Gb(T,N,1), G_L(N))
    G_b(N) = MIN( Gb(T,N,1), G_L(N))

  end if

end do
```

```
!Calculate R+- need for flux correction
do N = 0, Nodes(T)

  if (N == 0) then

    G_max = MAX( G_a(N+1), G_a(N))
    G_min = MIN( G_b(N+1), G_b(N))

  else if (N == Nodes(T)) then

    G_max = MAX( G_a(N-1), G_a(N))
    G_min = MIN( G_b(N-1), G_b(N))

  else

    G_max = MAX( G_a(N-1), G_a(N+1), G_a(N))
    G_min = MIN( G_b(N-1), G_b(N+1), G_b(N))

  end if

  if (N == 0) then

    R_p(N) = 0.0
    R_n(N) = 0.0

  else

    P_p = MAX(0.0,A_n(N)) - MIN(0.0,A_p(N))
    Q_p = G_max - G_L(N)
    IF (P_p > 0.0) THEN
      R_p(N) = MIN(1.0 , Q_p/P_p)
    ELSE
      R_p(N) = 0.0
    END IF

    P_n = MAX(0.0,A_p(N)) - MIN(0.0,A_n(N))
    Q_n = G_L(N) - G_min
    IF (P_n > 0.0) THEN
      R_n(N) = MIN(1.0, Q_n/P_n)
    ELSE
      R_n(N) = 0.0
    END IF

  end if

end do

!FINAL bed concentration calcs
do N = 1, Nodes(T)

  if (N < Nodes(T)) then

    IF (A_p(N) < 0.0) THEN
      U_p = MIN(R_n(N+1), R_p(N))
    ELSE
      U_p = MIN(R_n(N), R_p(N+1))
    END IF

  else

    IF (A_p(N) < 0.0) THEN
      U_p = R_p(N)
    ELSE
```

```
        U_p = R_n(N)
      END IF

    end if

    if (A_n(N) < 0.0) then
      U_n = MIN(R_n(N), R_p(N-1))
    else
      U_n = MIN(R_n(N-1), R_p(N))
    end if

    Ac_p = U_p*A_p(N)
    Ac_n = U_n*A_n(N)

    Gb(T,N,2) = G_L(N) - (Ac_p - Ac_n)

    if (Gb(T,N,2) > 0.0) then

      Cb(T,N,2) = (0.5/Klg)*( (Klg*Gb(T,N,2)) - 1.0 - (nu*gamma) + &
                  SQRT( ((1.0 + (nu*gamma) - (Klg*Gb(T,N,2)))**2.0) + &
                  (4.0*Klg*Gb(T,N,2)) ) )

    else

      Cb(T,N,2) = 0.0
      Gb(T,N,2) = 0.0

    end if

    if (Cb(T,N,2) < 0.0) then

      Cb(T,N,2) = 0.0
      Gb(T,N,2) = 0.0

    end if

  end do

  !Reset Gb & Cb concentrations
  do N = 0, Nodes(T)

    Gb(T,N,1) = Gb(T,N,2)
    Cb(T,N,1) = Cb(T,N,2)

  end do

END DO          !Loop over streamtubes

PRINT *, "Finished bed concentration calcs!"
PRINT *

time_hr = time_hr + (theta/(kwn*um))*dtime

Cw(I+1) = ((Cw(I)*dprime)-DMass_bed)/dprime

PRINT *, time_hr, Cw(I+1), DMass_bed

!Write outputs of overlying water column results
Cstar = Cw(I+1)/C0
Cdiff = LastC - Cstar

if (ABS(Cdiff) > 0.001 .or. time_hr > thr_max) then
```

```
      tstar = kwn*um*time_hr/theta
      fbed = 1.0 - Cstar
      Retard = 1.0 + (nu*gamma)/(1.0 + Klg*Cw(I+1))
      db_eq = (dprime/(theta*Retard))*((1.0/Cstar) - 1.)

      write (12,201) time_hr, tstar, Cstar, fbed, db_eq, Cw(I+1)

      LastC = Cstar

    end if

    !Write bed concentration profiles if needed
    if (P > 0) then

      IF (time_hr >= TP_hr(P)) THEN


        PRINT *, "Writing bed concentration profiles ....."
        PRINT *

        write (14,*) "Time of profile in hours = ,,,", time_hr
        write (14,*)

        do T = 1, N_tube

          write (14,*) "Tube = ", T
          write (14,*) "X_0 =,,,", X_0(T)
          write (14,*) "Streamtube length =,,,", Length(T)
          write (14,*) "Nodes ,,,", Nodes(T)

          write (14,202)
          write (14,*)

          DO N = 0, Nodes(T)
            write (14,203) N, Darcy_v(T,N),(REAL(N)*dL(T)/Length(T)), &
                           (REAL(N)*dL(T)), Cb(T,N,2)
          END DO

          write (14,*)
          write (14,*)

        end do

        write (14,*)  "um (cm/hr) =,", um
        write (14,*) "wavelength (cm) =,", wvl
        WRITE (14,*) "k =,", kwn
        write (14,*) "dX_0,", dX_0
        write (14,*)  "dtime,", dtime

        write (14,*) "Tube, Nodes, Cb(0), Cb(N)"
        do T = 1, N_tube
          write (14,*) T,",",Nodes(T),",", Cb(T,0,1),",", Cb(T,Nodes(T),1)
        end do

        CLOSE(14)

        if (P < P_dim) then
          P = P + 1

          open (UNIT = 14, FILE = PFile(P), STATUS = "REPLACE", ACTION = "WRITE",
&
            position = "REWIND")
```

```
        WRITE(14,*) "Bed concentration output from program 'EFD_Lang.f90'."

        CALL date_and_time(Date, Tmfile, Zone, DtAr)
        WRITE(14, FMT="('Date: ',I2,'/',I2,'/',I4)") DtAr(2), DtAr(3), DtAr(1)
        write(14, FMT="('Time: ',I2,':',I2,':',I2)") DtAr(5), DtAr(6), DtAr(7)
        write(14,*)

        write (14,*) "Bed concentration profiles"
        write (14,*)


      else

        P = 0

      end if

    END IF
  end if   !end of writing bed concentration profiles

  if (time_hr > thr_max) EXIT

  I = I + 1


END DO        !Loop over time

CLOSE(12)

PRINT *, "Calculations finished SUCCESSFULLY"

200 FORMAT(//,"Time (hr),","t*/theta,","C*,","fbed,,","deq (cm),","C (uM)")
201 FORMAT(F10.4,",",F10.4,",",F10.7,",",F10.7,",,",F10.5,",",F10.5)
202 FORMAT(/,"Node,", "Darcy v*,", "s/L,", "s (cm),", "Concentration (uM)")
203 FORMAT(I5, ",", F10.7, ",", F10.7, ",", F10.5, ",", F10.5)

PRINT *, "Calculations finished SUCCESSFULLY"


END PROGRAM
```

APPENDIX D – Sample Streamtube Concentration Profiles

Sample DTMA porewater concentration profiles, which are determined from the detailed exchange model, from Flume Run 2 (Chapter 5, Tables 5.10 through 5.11) at different times are illustrated in the following figures for streamtubes with inlets located at the following values of X_0^* : 0.205, 0.906, 1.196 and 1.55. The concentration profiles were recorded at 1 hour (t^*/θ = 3.7), 6 hours (t^*/θ = 22), 12 hours (t^*/θ = 44), 24 hours (t^*/θ = 88), 48 hours (t^*/θ = 176), 72 hours (t^*/θ = 265), 120 hours (t^*/θ = 441) and 192 hours (t^*/θ = 706).

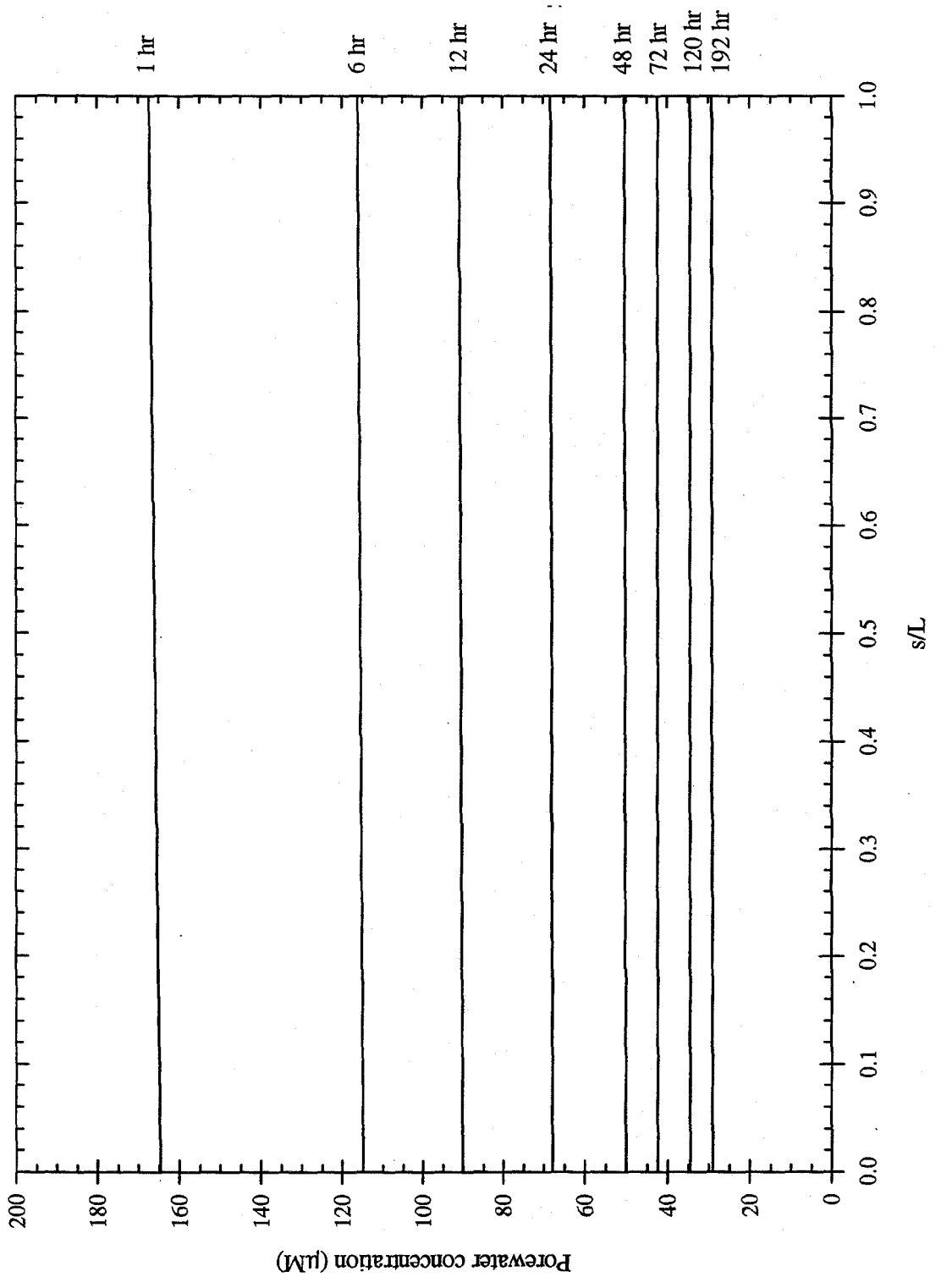

Figure D.1. Simulations of the DTMA porewater concentration profiles for a streamtube with its inlet located at $X_0^* = .205$.

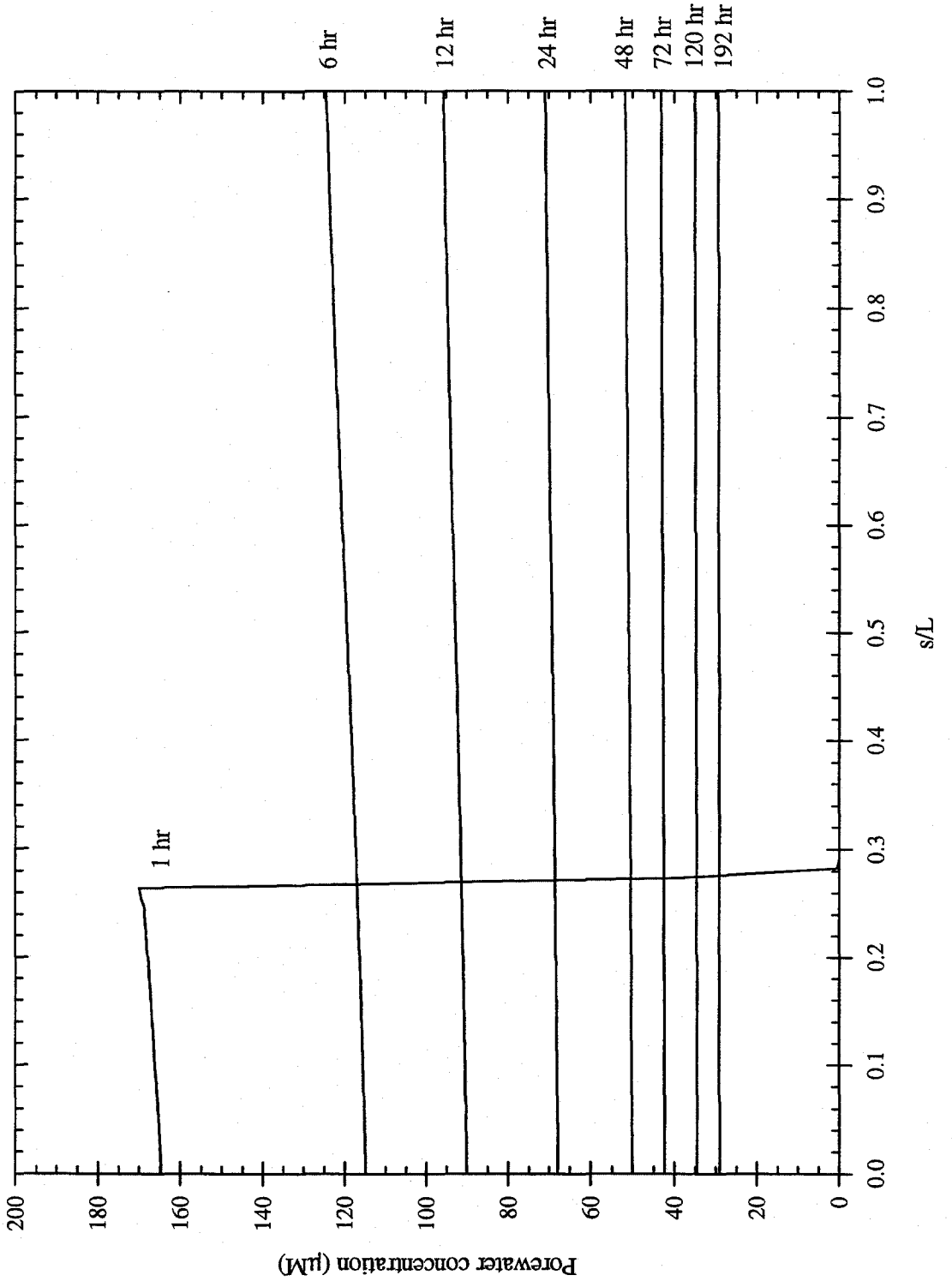

Figure D.2. Simulations of the DTMA porewater concentration profiles for a streamtube with its inlet located at $X_0^* = .906$.

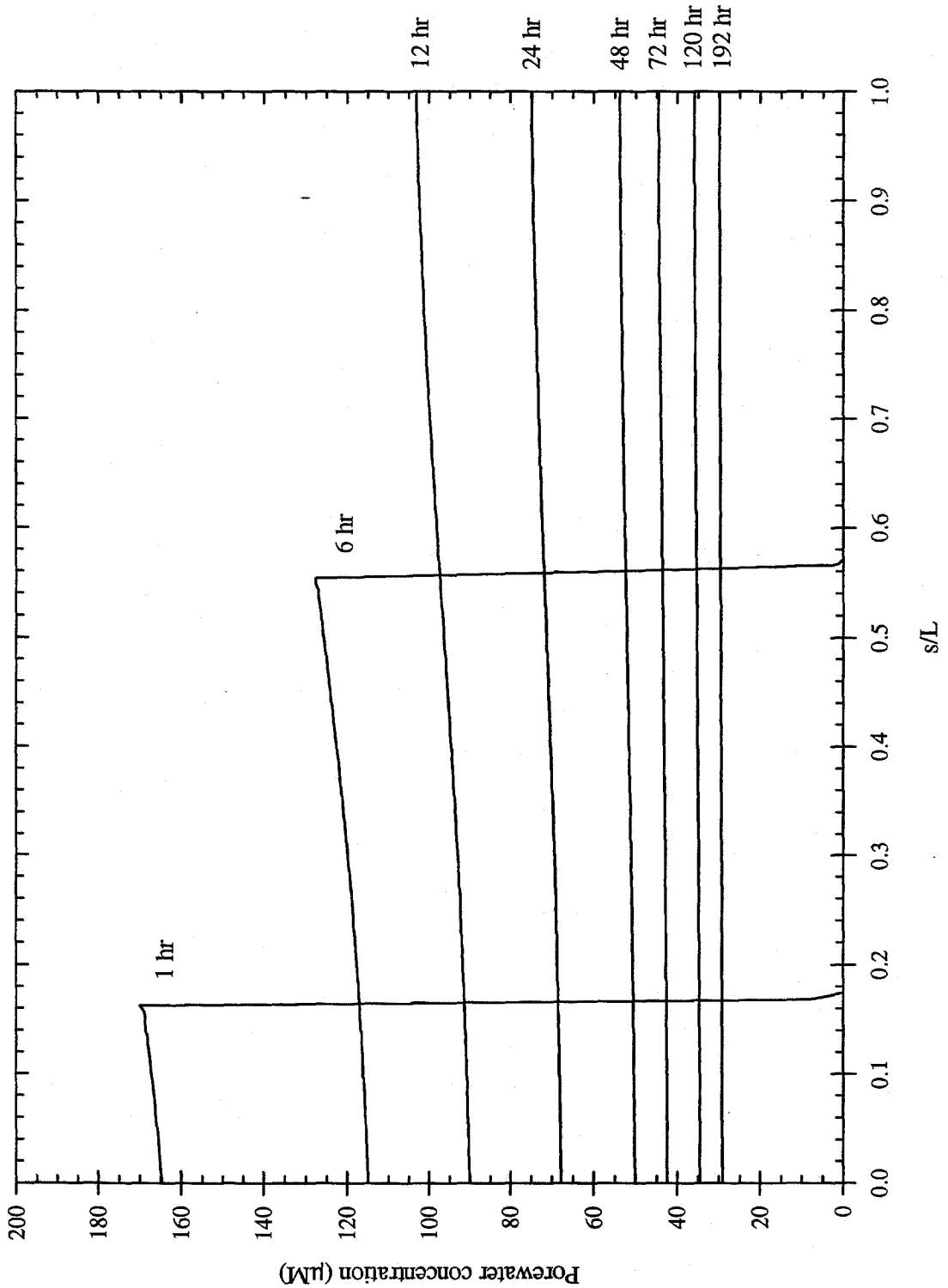

Figure D.3. Simulations of the DTMA porewater concentration profiles for a streamtube with its inlet located at $X_0^* = 1.196$.

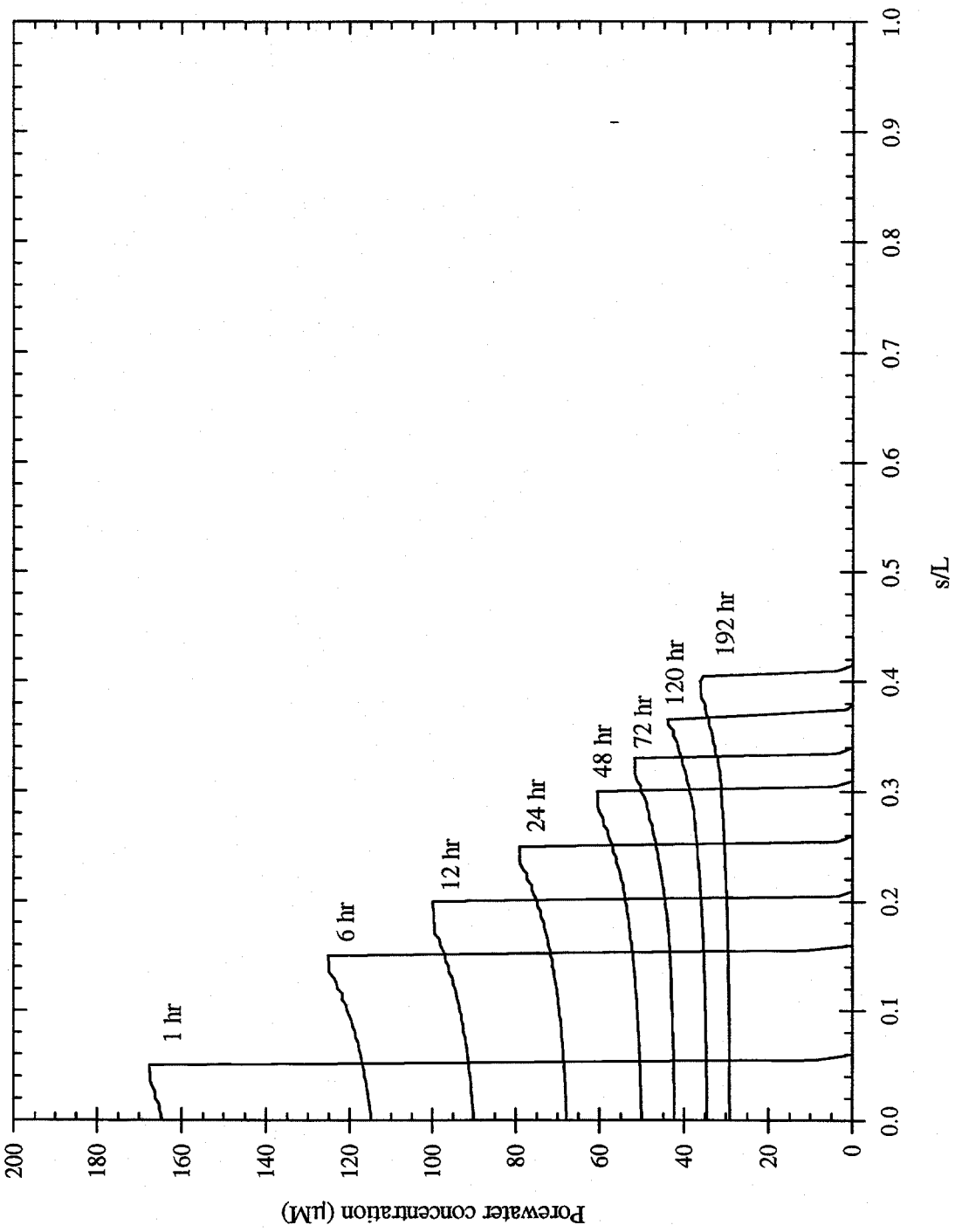

Figure D.4. Simulations of the DTMA porewater concentration profiles for a streamtube with its inlet located at $X_0^* = 1.55$.

APPENDIX E – Additional Lithium Adsorption Calculations

The following table compares the measured lithium adsorption on garnet sand to the adsorption expected from long-range coulombic interactions with the charged garnet sand surface (Stone, 1993). The adsorption experiments were conducted in 10 mM NaCl solutions at pH 8 and 25°C. The Debye parameter κ is 3.29×10^6 cm^{-1}, and an estimated surface potential Ψ_0 of –60 mV is assumed. The observed adsorption of lithium onto garnet sand exceeds the amount that expected to accumulate in the double layer as a diffuse swarm.

Table E.1. (continued on the next page) Comparison of the measured lithium adsorption to the amount of adsorption expected from coulombic interactions.

Sample	Sand (g)	Solution volume (ml)	Li^+ $f_{a,measured}$	I	J	INTEG	$f_{a,coul}$
L10-10	10.327	30.03	0.073	8.00	6.00	1.000004	3.65E-06
L10-20	20.397	30.03	0.141	8.00	6.00	1.000004	3.65E-06
L10-30	30.122	30.08	0.215	8.00	6.00	1.000004	3.65E-06
L10-50	49.865	30.07	0.295	8.00	6.00	1.000004	3.65E-06
L10-60	60.186	30.04	0.245	8.00	6.00	1.000004	3.65E-06
L10-70	70.427	30.05	0.298	8.00	6.00	1.000004	3.65E-06
L20-10	10.319	30.08	0.062	8.00	6.00	1.000004	3.65E-06
L20-20	20.398	30.03	0.098	8.00	6.00	1.000004	3.65E-06
L20-30	30.277	30.04	0.132	8.00	6.00	1.000004	3.65E-06
L20-40	40.528	30.05	0.177	8.00	6.00	1.000004	3.65E-06
L20-50	50.353	30.06	0.229	8.00	6.00	1.000004	3.65E-06
L20-60	60.031	30.03	0.182	8.00	6.00	1.000004	3.65E-06
L20-70	70.166	30.03	0.242	8.00	6.00	1.000004	3.65E-06
L30-10	10.065	30.13	0.063	8.00	6.00	1.000004	3.65E-06
L30-20	20.42	30.05	0.118	8.00	6.00	1.000004	3.65E-06
L30-30	29.971	30.04	0.152	8.00	6.00	1.000004	3.65E-06
L30-40	39.936	30.06	0.197	8.00	6.00	1.000004	3.65E-06
L30-50	49.993	30.07	0.267	8.00	6.00	1.000004	3.65E-06
L30-70	70.013	30.08	0.286	8.00	6.00	1.000004	3.65E-06

Table E.1 continued.

Sample	Sand (g)	Solution volume (ml)	Li^+ $f_{a,measured}$	I	J	INTEG	$f_{a,coul}$
L40-10	10.011	30.02	0.051	8.00	6.00	1.000004	3.65E-06
L40-20	20.265	30.02	0.108	8.00	6.00	1.000004	3.65E-06
L40-30	30.114	30.00	0.126	8.00	6.00	1.000004	3.65E-06
L40-40	40.219	30.01	0.149	8.00	6.00	1.000004	3.65E-06
L40-50	49.918	30.01	0.151	8.00	6.00	1.000004	3.65E-06
L40-60	60.027	30.03	0.227	8.00	6.00	1.000004	3.65E-06
L40-70	69.995	30.02	0.241	8.00	6.00	1.000004	3.65E-06
L50-10	10.06	30.00	0.046	8.00	6.00	1.000004	3.65E-06
L50-20	20.045	30.00	0.091	8.00	6.00	1.000004	3.65E-06
L50-30	30.124	30.00	0.140	8.00	6.00	1.000004	3.65E-06
L50-60	60.014	30.00	0.187	8.00	6.00	1.000004	3.65E-06
L50-70	69.923	30.00	0.254	8.00	6.00	1.000004	3.65E-06
L60-10	10.024	30.01	0.030	8.00	6.00	1.000004	3.65E-06
L60-20	20.208	30.01	0.060	8.00	6.00	1.000004	3.65E-06
L60-30	30.263	30.02	0.122	8.00	6.00	1.000004	3.65E-06
L60-40	40.091	30.00	0.123	8.00	6.00	1.000004	3.65E-06
L60-50	50.126	30.01	0.128	8.00	6.00	1.000004	3.65E-06
L60-60	60.024	30.00	0.145	8.00	6.00	1.000004	3.65E-06
L60-70	70.107	30.11	0.275	8.00	6.00	1.000004	3.65E-06

Table E.1 continued.

Sample	Sand (g)	Solution volume (ml)	Li^+ $f_{a,measured}$	I	J	INTEG	$f_{a,coul}$
L70-10	10.479	30.00	0.030	8.00	6.00	1.000004	3.65E-06
L70-20	20.216	30.05	0.089	8.00	6.00	1.000004	3.65E-06
L70-30	30.486	30.00	0.094	8.00	6.00	1.000004	3.65E-06
L70-40	40.362	30.00	0.116	8.00	6.00	1.000004	3.65E-06
L70-50	49.978	30.01	0.143	8.00	6.00	1.000004	3.65E-06
L70-60	59.832	30.01	0.137	8.00	6.00	1.000004	3.65E-06
L80-10	10.377	30.00	0.029	8.00	6.00	1.000004	3.65E-06
L80-20	20.055	30.00	0.059	8.00	6.00	1.000004	3.65E-06
L80-30	30.141	30.00	0.085	8.00	6.00	1.000004	3.65E-06
L80-40	40.15	30.00	0.099	8.00	6.00	1.000004	3.65E-06
L80-50	50.082	30.00	0.115	8.00	6.00	1.000004	3.65E-06
L80-60	59.997	30.00	0.143	8.00	6.00	1.000004	3.65E-06
L90-10	10.32	30.00	0.017	8.00	6.00	1.000004	3.65E-06
L90-20	20.334	30.00	0.050	8.00	6.00	1.000004	3.65E-06
L90-30	30.165	30.00	0.072	8.00	6.00	1.000004	3.65E-06
L90-40	40.075	30.00	0.079	8.00	6.00	1.000004	3.65E-06
L90-50	50.265	30.00	0.101	8.00	6.00	1.000004	3.65E-06
L90-60	60.322	30.00	0.112	8.00	6.00	1.000004	3.65E-06

Table E.1 continued.

Sample	Sand (g)	Solution volume (ml)	Li^+ $f_{a,measured}$	I	J	INTEG	$f_{a,coul}$
100-10	10.243	30.05	0.031	8.00	6.00	1.000004	3.65E-06
100-20	20.243	30.05	0.081	8.00	6.00	1.000004	3.65E-06
100-35	35.08	30.05	0.062	8.00	6.00	1.000004	3.65E-06
100-50	49.924	30.05	0.099	8.00	6.00	1.000004	3.65E-06
100-60	60.015	30.05	0.102	8.00	6.00	1.000004	3.65E-06
100-70	70.431	30.05	0.113	8.00	6.00	1.000004	3.65E-06